24

Thermodynamics and Dynamics of Micellization and Micelle-Solute Interactions in Block-Copolymer and Reverse Micellar Systems

by

Paschalis Alexandridis

Diploma in Chemical Engineering
National Technical University, Athens, Greece (1989)

Master of Science in Chemical Engineering Practice
Massachusetts Institute of Technology, Cambridge, MA (1990)

Submitted to the Department of Chemical Engineering
in partial fulfillment of the requirements for the degree of

Doctor of Philosophy

at the

Massachusetts Institute of Technology

September, 1994

Author .....
Department of Chemical Engineering
June 6, 1994

Certified by .....
Professor T. Alan Hatton
Thesis Supervisor

Accepted by .....
Professor Robert E. Cohen
Chairman, Committee for Graduate Students

Thermodynamics and Dynamics of Micellization and Micelle-Solute Interactions in Block-Copolymer and Reverse Micellar Systems

by

Paschalis Alexandridis

Submitted to the Department of Chemical Engineering
on June 6, 1994, in partial fulfilment of the requirements for the degree of
Doctor of Philosophy

Abstract

Poly(ethylene oxide)-*block*-poly(propylene oxide)-*block*-poly(ethylene oxide) (PEO-PPO-PEO) copolymers are commercially available nonionic macromolecular surfactants that find widespread industrial applications in detergency, dispersion stabilization, foaming, emulsification, lubrication, etc., along with more specialized applications in, e.g., drug solubilization and controlled release, protecting microorganisms against mechanical damage, and solubilization of organics.

The phase diagram of aqueous PEO-PPO-PEO copolymer solutions was established by determining the critical micellization temperature (CMT) and concentration (CMC) values. Twelve PEO-PPO-PEO copolymers, covering a wide range of molecular weights (2900 - 14600) and PPO/PEO ratios (0.19 - 1.79), were studied. Very good agreement was observed between CMCs and CMTs obtained from dye solubilization and differential scanning calorimetry, surface tension, density, light scattering intensity, and fluorescence spectroscopy experiments. A closed association model was used to derive the standard free energies (ΔG°), enthalpies (ΔH°), and entropies (ΔS°) of micellization. The micellization process is entropy-driven and has an endothermic micellization enthalpy. An empirical correlation was developed for the estimation of CMC and CMT for PEO-PPO-PEO copolymers in aqueous solutions.

Information on the structure of micelles formed by PEO-PPO-PEO copolymers was obtained from light scattering and fluorescence spectroscopy experiments. The hydrodynamic radii of PEO-PPO-PEO micelles remained constant over the temperature range investigated; the polydispersity of the micelle size decreased with temperature. The micropolarity and microviscosity in aqueous PEO-PPO-PEO micellar solutions was probed as a function of temperature using the fluorescence emission spectra of pyrene and bis(1-pyrenylmethyl)ether, respectively. The composition of the micelle core was estimated from pyrene fluorescence data, indicating approximately 30 % PEO content. The microviscosity in the micelle core was found to be similar to that in bulk PPO homopolymer.

The surface tension of aqueous solutions of seven PEO-PPO-PEO copolymers was determined over a wide concentration range, at 25 and 35 °C. Two breaks (changes in slope) were observed in the surface tension vs log concentration curve for most of the copolymers. The low-concentration break is believed to originate from rearrangement of the copolymer molecules on the surface, whereas the high-concentration break corresponded to the CMC. The surface area per copolymer molecule, A, increased as a function of the number of EO units, N_{EO}, obeying a scaling law ($A \sim N_{EO}^{1/2}$) similar to that of lower molecular weight C_iE_j nonionic surfactants. The presence of the PPO block in the center of the copolymer molecule resulted in a copolymer headgroup (PEO) surface area

smaller than that of PEO homopolymers of comparable molecular weight, indicating desorption of PEO segments from the air/water interface.

Following the study on micellization, we investigated the partitioning (solubilization) of hydrophobic solutes in the micelles, and the kinetics of micelle formation and solute uptake/release. The solubilization of 1,6-diphenyl-1,3,5-hexatriene in PEO-PPO-PEO micellar solutions was influenced by both the relative and absolute size of the hydrophobic PPO block. The solubilization process is entropy-driven and has an endothermic enthalpy; a correlation between micellization and solubilization enthalpy was observed. Temperature and concentration jump experiments indicated that the micelle association and dissociation process in PEO-PPO-PEO solutions had a characteristic time of 5 minutes; solubilization of molecularly dispersed solute in the micelles took place over the same time range; dissolution of DPH microcrystalline aggregates could be slower and constituted the rate limiting step in the solubilization process; DPH that has been solubilized in micelles can remain long in solution, even below the CMC.

Reverse micelles or water-in-oil microemulsions are thermodynamically-stable complex fluids that can be envisaged as distinct, nanometer-size water droplets maintained dispersed in an apolar solvent with the aid of a surfactant monolayer that reduces unfavorable oil-water contact. Micelle interactions and cluster formation, and dynamics of surfactant monolayers and solute interfacial association were studied in reverse micellar systems formulated with dioctyl sulfosuccinate (AOT) in various alkanes.

The free energy (ΔG°_{cl}), enthalpy (ΔH°_{cl}), and entropy (ΔS°_{cl}) associated with the formation of droplet clusters in percolating (high-conductivity) water-in-oil microemulsions were estimated utilizing an association model, similar to that used in describing the micellization of amphiphiles. While the microemulsion droplets assembled spontaneously into clusters during percolation ($\Delta G^\circ_{cl} < 0$), ΔH°_{cl} values were found to be positive, indicating that the transfer of microemulsion droplets from solution to the percolating cluster was an enthalpically-unfavorable endothermic process. A positive entropic contribution, related to the attractive interactions known to exist between microemulsion droplets, was the driving force for clustering. Both ΔH°_{cl} and ΔS°_{cl} increased with droplet size and molecular weight of the apolar solvent constituting the continuous phase. The values for ΔH°_{cl} (~ 100 kJ/mol) estimated from the association model are comparable to the activation energies observed in microemulsion droplet coalescence and solubilizate exchange, providing evidence that the latter process is occurring during percolation.

The dynamic response of AOT microemulsion droplets to perturbations caused by rapid energy transfer has been interpreted in terms of the surfactant interface bending rigidity. The Iodine Laser Temperature Jump (ILTJ) technique was used to increase the microemulsion temperature rapidly (within 1 μs) and thus disturb the system equilibrium. The observed characteristic relaxation times of 2 to 10 μs were attributed to the relaxation of the surfactant interface. A bending modulus of approximately 0.4 kT was derived for the AOT monolayer, based on published models for the shape perturbation of a spherical interface. Addition of NaCl to the aqueous pools resulted in a decrease of the bending modulus, in agreement with published theoretical predictions. The time scales of p-nitrophenol (pNP) association at the curved surfactant interface in a AOT microemulsion system were identified and measured to be in the 0.1 - 1 ms time range using ILTJ.

Thesis supervisor: T. Alan Hatton
Title: Chevron Professor of Chemical Engineering

Acknowledgements

I want to express my sincere gratitude and thanks to my thesis advisors, Professors Alan Hatton and Josef Holzwarth; their stimulating, insightful, and guiding comments have always been greatly appreciated. They were both instrumental in shaping my perspective in science and research. Furthermore, Alan taught me how to write papers and prepare presentations, and also how to meet deadlines on the date due; Josef taught me about lasers and optics, and how to troubleshoot and fix misbehaving scientific instrument. It has been a great pleasure to work with them. I look forward to a continuing exchange of ideas in the future.

I have greatly enjoyed and benefitted by the contributions of my thesis committee, Professors Daniel Blankschtein, Bill Deen, Jonathan Harris, and Ken Smith. I particularly want to thank Daniel Blankschtein for his interest in my work, advice on my career plans, and for giving me access to his lab.

During the last year of my thesis work I had the pleasure of collaborating with Dr. Thierry Nivaggioli on fluorescence spectroscopy (and also sharing office and lab space, UROPs, job-search tips, etc.) - thanks a lot Thierry. Thanks are due to Dr. Patricia Hurter for contributing to Chapter 7 of my Thesis.

Vassiliki Athanassiou, Shinya Fukuda, Naoko Munakata, Wendy Yeh, Alexis Black, and Bryan Poltilove participated in this research program under the MIT Undergraduate Research Opportunities Program (UROP), and provided valuable assistance in conducting some of the measurements reported in this Thesis; special thanks are due to Vicky and Shinya for their diligence and friendly attitude.

The microemulsion work was supported by the U.S. National Science Foundation under Grant No. CTS-8902349, with additional financial assistance from the NATO Scientific Commission in the form of a Travel Grant. The block copolymer work was supported by the U.S. Department of Energy under Grant No. DE-FG02-92ER14262 and the Emission Reduction Research Center (ERRC), Newark, NJ. Financial support from the M.I.T. David H. Koch School of Chemical Engineering Practice in the form of Fellowships, and subsistence support by the Fritz-Haber-Institut der Max-Planck-Geselschaft during my stay in Berlin, are gratefully acknowledged.

Drs. Minos Leontidis, Andreas Bommarius, Nick Abbott, and Costas Patrickios, former students in our group, introduced me to many aspects of science and research and interacted with me over the course of my thesis. All my colleagues in Alan's group have been essential in creating a friendly working environment. I would like to mention Ed Brown, for brightening up my day when I was spending hours in front of the Mac in 66-321, Colleen Vandevoorde, Fred von Gottberg, Joachim Howald, and Kristina Kohler for their interest in my work. Carol Phillips has been most helpful and added a personal touch to the sometimes impersonal MIT; I shall always remember her with love. I also want to acknowledge Dieter Bauer, Ron Clarke, and Joachim Frank, members of the JoHo group in Germany.

Maria Athanassiou, Stathis Avgoustiniatos, Constantinos Boussios, Evangelos Goggolidis, Peter Kofinas, Alexandros Koulouris, Angelos Kyrlidis, Dimitris Maroudas, Antonis Mikos, Marios Papaethymiou, Dimitris Petridis, Thanasis Tjavaras, Kostas Tsiveriotis, and other friends at syllogos@mit formed my "support group" and made me feel "at home" many thousand miles away from home.

My gratitude goes to my family for unconditional love, support, and patience with my endeavors. Last, but not least, I want to thank my wife Marina for her love, companionship, and much more. This thesis is dedicated to her and our new family.

Preface

This Thesis is organized in two parts, A and B, reflecting the two micellar systems (aqueous block copolymer solutions and water-in-oil microemulsions) studied here. The various aspects of the investigation are presented in 15 Chapters; each Chapter is autonomous in its presentation of pertinent scientific concepts and discussion of the results, however, connection is always made to related results in other Chapters of the Thesis.

Part A, consisting of Chapters 1 - 9, encompasses the research on thermodynamics of micellization and solubilization, and micelle-solute interactions in aqueous solutions of amphiphilic poly(ethylene oxide)-*block*-poly(propylene oxide)-*block*-poly(ethylene oxide) (PEO-PPO-PEO) copolymers. Chapter 1 is an up-to-date overview of the research conducted on this system; some of the important findings of the present investigation are blended in the literature review of Chapter 1, when appropriate. The micellization behavior of PEO-PPO-PEO copolymers in aqueous solutions and the thermodynamics of copolymer association are discussed in Chapter 2, while a correlation for the estimation of Critical Micellization Concentrations and Temperatures of PEO-PPO-PEO copolymers is presented in Chapter 3. Chapter 4 contains results on the surface activity of PEO-PPO-PEO and related copolymers, and Chapter 5 outlines the effects of temperature on the structural properties of Pluronic P104 and F108 PEO-PPO-PEO copolymer solutions. The use of fluorescence probes to study the microenvironment in PEO-PPO-PEO micelles is presented in Chapter 6. Chapter 7 is a review on solubilization studies conducted in amphiphilic copolymer solutions; the use of PEO-PPO-PEO micelles for solubilization of hydrophobic molecules is one of the motivations of the current investigation. Some new findings on solubilization are also presented in Chapter 7. Chapter 8 is a study on micellization and solubilization kinetics in PEO-PPO-PEO copolymer micellar systems. The contributions of this Thesis to the study of block copolymer micellar systems are summarized in Chapter 9; future work along these lines is also suggested.

Part B includes Chapters 10 - 15 and is a presentation of the research on thermodynamics of micelle clustering and interfacial dynamics in reverse micellar (water-in-oil microemulsion) systems formulated with dioctyl sulfosuccinate (AOT) in various alkanes. Chapter 10 is a review of the various dynamic processes taking place in reverse micellar systems. Heating-induced conductivity percolation in AOT water-in-oil microemulsions is described in Chapter 11, while the thermodynamics of droplet clustering in percolating AOT microemulsions are discussed in Chapter 12. The interfacial dynamics of water-in-oil microemulsion droplets, and, more specifically, the determination of the surfactant monolayer bending modulus is presented in Chapter 13. Chapter 14 deals with the dynamics of interfacial association of p-nitrophenol in an AOT water-in-oil microemulsion.

Thermodynamics and Dynamics of Micellization and Micelle-Solute Interactions in Block-Copolymer and Reverse Micellar Systems

Part B

Thermodynamics of Micelle Clustering and Interfacial Dynamics in Reverse Micellar (Water-in-Oil Microemulsion) Systems

Part A

Thermodynamics of Micellization and Solubilization, and Micelle-Solute Interactions in Aqueous Amphiphilic Block-Copolymer Systems

Chapter 1
Poly(ethylene oxide)-*block*-poly(propylene oxide)-*block*-poly(ethylene oxide) Copolymer Surfactants in Aqueous Solutions and at Interfaces: An Overview

1.1 Introduction

Copolymers are synthesized by the simultaneous polymerization of more than one type of monomer. The result of such synthesis is called a block copolymer if the individual monomer segments occur as blocks of various lengths in the copolymer molecule. The different types of blocks within the copolymer are usually incompatible with one another and, as a consequence, block copolymers self assemble in melts and in solutions. In the case of amphiphilic copolymers in aqueous solutions, the copolymers can assemble in microstructures that resemble micelles formed by low molecular weight surfactants.

Water-soluble triblock copolymers of poly(ethylene oxide) (PEO) and poly(propylene oxide) (PPO), often denoted PEO-PPO-PEO or $(EO)_{m1}(PO)_n(EO)_{m2}$, are commercially available nonionic macromolecular surface active agents. Variation of the molecular characteristics (PPO/PEO ratio, molecular weight) of the copolymer during the synthesis allows the production of molecules with optimum properties that meet the specific requirements in different areas. As a result, PEO-PPO-PEO block copolymers are an important class of surfactants and find widespread industrial applications in detergency, dispersion stabilization, foaming, emulsification, lubrication, etc. [Schmolka, 1977; Bahadur & Riess, 1991], along with more specialized applications in, e.g., pharmaceutics (drug solubilization and controlled release [Lin & Kawasima, 1985; Yokoyama, 1992; Guzman et al., 1992; Kabanov et al., 1992]), bioprocessing (protecting microorganisms against mechanical damage [Murhammer & Goochee, 1990; Zhang et al., 1992; Orton, 1992]), and separations (solubilization of organics in aqueous solutions [Nagarajan et al, 1986; Hurter & Hatton, 1992; Hurter et al., 1994]). Commercial names for these

surfactants are Poloxamers (manufactured by ICI) and Pluronics (manufactured by BASF).

1.2 Synthesis, Nomenclature, and Physical Properties

The PEO-PPO-PEO block copolymers are synthesized by the sequential addition first of propylene oxide (PO) and then ethylene oxide (EO) to a low molecular weight water-soluble propylene glycol, a poly(propylene oxide) oligomer (propylene glycol changes from water soluble to water-insoluble as the molecular weight increases beyond approximately 740). The oxyalkylation steps are carried out in the presence of an alkaline catalyst, generally sodium or potassium hydroxide. The catalyst is then neutralized and removed from the final product. The equations representing the synthesis are shown below [Schmolka, 1977]:

addition of PO to form the PPO middle block

$$HOC(CH_3)HCH_2OH + (m\text{-}1)CH_3CHOCH_2 \rightarrow HO(C(CH_3)HCH_2O)_mH$$

addition of EO to form the PEO side blocks

$$HO(C(CH_3)HCH_2O)_mH + (2n)CH_2OCH_2 \rightarrow$$
$$HO(CH_2CH_2O)_n(C(CH_3)HCH_2O)_m(CH_2CH_2O)_nH$$

The Pluronic PEO-PPO-PEO block copolymers are available in a range of molecular weights and PPO/PEO ratios [Schmolka, 1977; Bahadur & Riess, 1991; BASF Corp., 1989]. Figure 1.1 presents the copolymers arranged in the so-called "Pluronic grid" [Bahadur & Riess, 1991; BASF Corp., 1989]. The copolymers along the vertical lines have the same PPO/PEO composition, while the copolymers along the horizontal lines have PPO block of the same length. The notation for the Pluronic triblock copolymers starts with the letters L (for liquid), P (for paste), or F (for flakes). The first two numbers are indicative of the molecular weight of the PPO block, and the last number signifies the weight fraction of the PEO block. For example, P103 and P104 have the same molecular weight of PPO (on the order of 3000) but P103 has 30 wt % PEO and P104 40 wt % PEO. The notation of Figure 1.1 will be used in the ensuing discussion.

Table 1.1 lists some of the physical properties (average molecular weight, melt/pour

point, viscosity, surface tension, foam height, cloud point and hydrophilic-lipophilic-balance) of the Pluronic PEO-PPO-PEO copolymers (data supplied by the manufacturer [BASF, 1989]). The cloud point, the temperature at which the copolymers phase separate, ranges from a low of ~ 10 °C for copolymers with low PEO content to a high above 100 °C for copolymers with high PEO content. The PEO content also influences the rate of dissolution: this rate decreases as the relative proportion of the PEO block increases. The dissolution rate also decreases as the copolymer molecular weight increases for copolymer groups with the same PPO/PEO ratio [Schmolka, 1997]. This has probably to do with the degree of hydrogen bonding between the copolymer molecules which is also reflected in the physical form of the copolymers (liquid for low molecular weight, low PEO content, solid for high molecular weight, high PEO content copolymers). The Pluronics exhibit maximum foam height at a PPO:PEO ratio of 40:60; foam properties of each copolymer series increase and then decrease slightly as the molecular weight of the PPO segment increases; copolymers with high PPO content are effective defoamers [Schmolka, 1977]. Attempts to correlate the emulsification properties with PPO/PEO ratios and PPO molecular weight have not been very successful; copolymers with PPO blocks of high molecular weight are generally better emulsifiers than the lower molecular weight homologs [Schmolka, 1977]. The thickening power of each series of copolymers increases as the PPO block molecular weight increases and as the PPO/PEO ratio decreases.

1.3 Micelle formation in PEO-PPO-PEO block copolymer aqueous solutions

1.3a Techniques for detecting CMC and CMT

The critical micellization concentration, CMC, the amphiphile concentration at which micelles (thermodynamically stable polymolecular aggregates) start forming, is a parameter of great fundamental value [Hunter, 1987]. The micellization of block copolymers (which depends strongly on their composition) is inherently more complex than that of conventional, low molecular weight amphiphiles. The composition polydispersity could be appreciable even for a copolymer with a narrow distribution of molecular weight, and accordingly, no sharp CMC or CMT (critical micellization temperature, the copolymer solution temperature at which micelles form) has been observed

for block copolymers. In practice, a certain CMC range with some notable uncertainty is usually detected. A large difference is often noted between the CMC values determined by different methods because their sensitivity to the quantity of molecularly dispersed copolymers (unimers) present may vary [Zhou & Chu, 1988]. For common surfactants, a considerable amount of CMC data have been collected and summarized by Mukerjee and Mysels [1971], whereas for block copolymers so far only scarce CMC data (e.g. Sikora and Tuzar [1983], Price [1983]) are available in the literature. Furthermore, the values reported in the literature differ substantially; the lack of sufficient temperature control, in conjunction with batch-to-batch variations, may be responsible for the observed variations [Linse & Malmsten, 1992].

Recent light scattering and fluorescence spectroscopy experiments have shown that PEO-PPO-PEO block copolymers of suitable composition and molecular weight do indeed form polymolecular aggregates in solution. As we show below, the CMC of aqueous PEO-PPO-PEO block copolymer solutions decreases with increasing temperature [Zhou & Chu, 1988; Reddy et al., 1991; Brown et al., 1991; Alexandridis et al., 1994a]. Micellar growth was observed for L64 with an increase in polymer concentration at 25 °C, but the micelle radius remained constant at 35 °C [Al-Saden et al., 1982]. Micelle formation by P85 was investigated by Brown et al. [1991] using static and dynamic light scattering. It was found that monomers, micelles, and micellar aggregates coexist, the relative proportions of each species depending strongly on temperature and polymer concentration. Micellar growth was found to occur with increasing temperature; the increase of scattering intensity at a certain temperature signified the formation of micelles (see also Chapter 5). A significant temperature dependence of the micellization behavior of F68 was also observed [Zhou & Chu, 1988]. Using static and dynamic light scattering, Zhou and Chu [1988] detected three temperature regions, which they called the unimer, transition and micelle regions, respectively. At room temperatures, "particles" with a hydrodynamic radius of around 2.3 nm and a broad polydispersity were detected. Above 50 °C, micelle molecular weights were found to increase linearly with temperature, while the hydrodynamic radius remained constant, at about 8 nm. Wanka et al. [1990] confirmed the finding of Zhou and Chu, that aggregation numbers increase with temperature, while the micelle radius remains approximately constant. More information on Pluronic micelle size and aggregation numbers, determined by scattering techniques, is presented in Section 1.5a.

Spectroscopic techniques, based either on optical absorption or on emission of light from some "probe" molecule, are now well established for investigating a wide range of physical properties of micellar solutions [Hunter, 1987; Grieser & Drummond, 1988]. Photoluminescent probes were employed by Turro and Chung [1984] to study the behavior of a poly(ethylene oxide)-poly(propylene oxide) block copolymer in water. The polymer they used had a total molecular weight of 3000, with a molar ratio of PEO to PPO of 0.8:1.0; it was not specified in the paper whether it was a di- or tri-block copolymer. Regions of no aggregation, monomolecular micelles (resulting from a change of the copolymer segment conformation to a more compact structure), and polymolecular micelles were identified with increasing polymer concentration. The aggregation number of the micelles formed at high polymer concentration was determined to be 52. With an increase in temperature, a hydrophobic fluorescence probe, which would be expected to reside in the micelle core, experienced a more hydrophilic environment, whereas a hydrophilic probe, expected to reside in the interfacial region, experienced a more hydrophobic environment. This observation was attributed to a greater mixing of PEO chains into the hydrophobic micelle core at higher temperatures (due to increased thermal agitation).

A hydrophobic fluorescence probe (diphenylhexatriene, DPH) was used by Alexandridis et al. [1994a] to determine the onset of micellization for a number of Pluronic block copolymer aqueous solutions. The fluorescence efficiency of the DPH is zero in a hydrophilic environment and unity in a hydrophobic environment (such as the core of a micelle), thus providing a sensitive indicator of micelle formation with increasing solution temperature and copolymer concentration. Critical micelle concentration and critical micelle temperature data were derived and correlated to the Pluronic molecular weight and PPO/PEO ratio [Alexandridis et al., 1994a]. Chattopadhyay and London [1984] used fluorescence from DPH to determine the CMC of various surfactants, obtaining values that were within 10% of those determined by other methods. Surface tension results showed that probe molecules, at the levels used to determine the CMC by fluorescence ($<10^{-6}$ kmol m^{-3}), did not noticeably affect the surfactant properties, viz., surface tension, nor the surface tension-derived CMC value [Ananthapadmanabhan et al., 1985]. Edwards et al. [1985] reported that, in general, the CMC values they obtained from the surface tension data for solutions of deionized water and nonionic surfactants showed fairly close agreement with the CMC values inferred from polyaromatic hydrocarbon solubilization data. Similar values for the CMC of the PEO-PPO-PEO block copolymers measured by

surface tension and dye solubilization methods have been reported by Schmolka and Raymond [1965]. The use of surface tension measurements for the determination of CMC in Pluronic copolymer solutions is discussed in detail in Section 7a.

1.3b Effect of copolymer composition and molecular weight on micelle formation

It is apparent from the experimental studies that PEO-PPO-PEO copolymers which are relatively less hydrophobic (more hydrophilic), either due to a high PEO content or a low molecular weight, do not form micelles at room temperature, but do start to aggregate at higher temperatures. This can be explained by the fact that water becomes a poorer solvent for both ethylene oxide and propylene oxide segments at higher temperatures. As shown by Alexandridis et al. [1994a], the micellization process is strongly driven by entropy, and the free energy of micellization is mainly a function of the PPO block, the hydrophobic part of the copolymer.

For groups of copolymers with the same molecular weight PEO and varying PPO block, the CMC values for the Pluronic solutions (at a given solution temperature) decreased as a function of the number of PO segments, indicating that polymers with a larger hydrophobic domain (PPO) form micelles at lower concentrations [Alexandridis et al., 1994a]. Higher temperatures resulted in lower CMC values, with the slope of the log(CMC) vs PO-number curve increasing with temperature. The CMT values for the Pluronic copolymer solutions (at a given copolymer concentration) also decreased with increasing number of PO segments indicating that polymers with a larger hydrophobic domain form micelles at lower temperatures. The CMC and CMT values for groups of Pluronics with the same hydrophobic block and hydrophilic block of varying length, e.g., with 30 (L64, P65, F68), 40 (P84, P85, F88), and 60 (P104, P104, F108) PO segments showed a small increase in the CMC and CMT with increasing number of EO units. This would indicate that the micelle formation becomes more difficult the more hydrophilic the molecules, although the effect of PEO on the CMC and CMT is less pronounced than that of PPO, intimating that PPO is a primary factor in the micellization process. The CMC and CMT values for copolymers of constant PPO/PEO ratio decreased with increasing molecular weight. The CMT values were influenced more by molecular weight, the lower the relative EO content, and the lower the copolymer concentration, as is evidenced by the

steeper slopes for the curves for these conditions [Alexandridis et al., 1994a].

1.4 Micellization thermodynamics

1.4a Association model, differential scanning calorimetry

It is well established that block copolymers of the A-B or A-B-A type form micelles in selective solvents which are thermodynamically good solvents for one block and precipitants for the other. In general, micellization of block copolymers, as in the case of conventional surfactants, obeys the closed association model, which assumes an equilibrium between molecularly dispersed copolymer (unimer) and multimolecular aggregates (micelles) [Price, 1983; Tuzar & Kratochvil, 1976]. There are two main approaches to the thermodynamic analysis of the micellization process: the phase separation model, in which the micelles are considered to form a separate phase at the CMC, and the mass-action model that considers micelles and unassociated unimers to be in an association-dissociation equilibrium [Attwood & Florence, 1983]. In both approaches, the standard free energy change for the transfer of 1 mol of amphiphile from solution to the micellar phase, ΔG° (the free energy of micellization), in the absence of electrostatic interactions (the Pluronic copolymers are nonionic) is given by [Attwood & Florence, 1983; Hunter, 1987] (see also Chapter 2, Appendix B of this Thesis)

$$\Delta G^\circ = R\,T \ln (X_{CMC}) \qquad (1)$$

where R is the gas law constant, T is the absolute temperature, and X_{CMC} is the critical micellization concentration in mol fraction units. It has been assumed here that the concentration of free surfactant in the presence of micelles is constant and equal to the CMC value, in the case of the phase separation model, or that the micelle aggregation number is large for the mass-action model. Applying the Gibbs-Helmholtz equation, we can express the standard enthalpy of micellization, ΔH°, as [Attwood & Florence, 1983; Hunter, 1987]

$$\Delta H^\circ = - R\,T^2 \left[\partial \ln(X_{CMC}) / \partial T \right]_P = R \left[\partial \ln(X_{CMC}) / \partial (1/T) \right]_P \qquad (2)$$

Finally, the standard entropy of micellization per mole of surfactant, ΔS°, can be obtained from:

$$\Delta S^\circ = (\Delta H^\circ - \Delta G^\circ) / T \qquad (3)$$

It has been shown for block copolymer micellization [Yu et al., 1992] that, within experimental error,

$$\partial \ln(X_{CMC}) / \partial (1/T) = \partial \ln(X) / \partial (1/T_{CMT}) \qquad (4)$$

where X is the concentration expressed as mole fraction, and T_{CMT} is the critical micellization temperature; thus Equation 2 becomes

$$\Delta H^\circ = R [\partial \ln(X) / \partial (1/T_{CMT})]_P \qquad (5)$$

In accordance with Equation 5, the inverse CMT values were presented as a function of the logarithm of copolymer concentration (mol-fraction units) for a number of Pluronic copolymers in Alexandridis et al. [1994a]. The CMT data, plotted in this manner, were generally described well by a straight line; the use of a closed association model appeared well justified based on the good fit, and Alexandridis et al. [1994a] consequently employed such a model for estimating ΔH° and ΔS° of the micellization process. Note, that the major assumption involved in deriving Equations 1-5 is based on the micelle aggregation number (N) being large enough so that the terms $RTN^{-1}\ln N$ and $RTN^{-1}\ln X_{mic}$ (where X_{mic} is the mol fraction of micelles) can be omitted from the right-hand-side of Equation 1 [Hunter, 1987]. For a typical aggregation number of 50, $N^{-1}\ln N \approx 0.08$, indeed negligible compared to the value of $|\ln X_{CMC}|$ (in the range 10 - 15). Using the same aggregation number and concentrations $X_{CMC}=6\times10^{-6}$ and $X_{mic}=6\times10^{-10}$, the magnitude of the $|N^{-1}\ln(X_{mic})|$ term is 0.4, approximately 3% of the $|\ln X_{CMC}|$ ($\approx$12) term; the temperature derivatives of the $RTN^{-1}\ln N$ and $RTN^{-1}\ln X_{mic}$ terms that would appear in Equation 2 are also negligible.

The standard enthalpy of micellization, ΔH°, was calculated from the inverse slope of the linear fit to the $1/T_{CMT}$ vs ln(mol fraction) data, in accordance with Equation 5. ΔH° values, together with ΔG° and ΔS° (calculated from Equations 1 and 3, respectively, at the

critical micellization temperature for 1% copolymer solutions) are listed by Alexandridis et al. [1994a] for various Pluronics. The values for the tabulated ΔH°, ΔG°, and ΔS° ranged between 169 and 339 kJ/mol, -24.5 and -28.8 kJ/mol, and 0.638 and 1.244 kJ/(mol K), respectively. The higher values of ΔH°, ΔG°, and ΔS° were observed for P103 and L64 (relatively hydrophobic copolymers), while the lower values were observed for the relatively hydrophilic copolymers F68 and F88. The standard enthalpy of micellization, ΔH°, is positive, indicating that the transfer of unimers from solution to the micelle is an enthalpically-unfavorable endothermic process. The free energy, ΔG°, is negative, since thermodynamically stable micelles are formed spontaneously. Thus, it becomes clear that a negative entropy contribution must be the driving force for micellization of the block copolymers.

The traditional view of micelle formation [Hiemenz, 1986; Hunter, 1987] has been based on the study of the solubility of hydrocarbons in water and what has come to be known as the hydrophobic effect [Tanford, 1980]. The presence of hydrocarbon molecules in water causes a significant decrease in the water entropy, suggesting that it induces an increase in the degree of structuring of the water molecules, owing to cavity formation. When hydrocarbon residues aggregate in aqueous solution to form a micelle, the hydrogen bonding structure in the water is, to a large extent, restored and the water entropy increases; this overcomes the loss of entropy due to the localization of the hydrocarbon chains in the micelles The magnitude of hydrophobic interactions increases with temperature [Ben-Naim, 1980] (note that, although ΔH° and ΔS° were assumed independent of temperature in the simple association model described above, the enthalpy and entropy assigned to the hydrophobic interactions generally decrease with temperature). An additional factor affecting the temperature dependence of micellization in the Pluronic copolymers is the decrease in polarity of both PEO and PPO with increasing temperature [Karlstrom, 1985]; this phenomenon, which eventually leads to macroscopic phase separation, may manifest itself in the micelle formation as a "microscopic phase separation". The entropy contribution usually dominates the micellization process in aqueous surfactant solutions, with the enthalpy playing a minor role. In the Pluronic copolymers, the unfavorable enthalpy component is significant but is, nevertheless, overcome by an even stronger entropy effect. In contrast to the entropy-driven micellization in water, the micellization of copolymers in nonpolar solvents originates from enthalpy interactions between the copolymer segments and the solvent [Price, 1983].

Another method for obtaining estimates of the enthalpy of micellization, ΔH°, is differential scanning calorimetry (DSC). DSC measurements for aqueous Pluronic solutions show endothermic peaks [Wanka et al., 1990; Armstrong et al., 1993], typical for a first-order phase transition, at concentration-dependent characteristic temperatures (see also Chapter 5 of this Thesis). The peaks yield rather high enthalpy values and are broad, extending more than 10 °C. The latter observation has been attributed to the fact that the copolymers are not pure compounds but show a broad molar weight distribution; it is known that melting peaks become broad in the presence of impurities [Wanka et al., 1990]. It should be pointed out that the enthalpy change measured by the peak area in DSC is not the standard enthalpy change but depends upon the real states of the copolymer molecules before and after micellization. The standard state enthalpy change is defined for transfer of 1 mol of copolymers from the ideally dilute solution to the solvated micellar state. In the ideally dilute solution, copolymer segments interact only with solvent, whereas in real solutions segments also interact with each other, and this may cause discrepancies between micellization enthalpies obtained from DSC and the ones derived from an analysis similar to that of Alexandridis et al. [1994a]. It has also been reported by Hiemenz [1986] that ΔH° values calculated by a micellization thermodynamics model generally show poor agreement with those determined calorimetrically, at least for ionic surfactants.

From a rather limited set of data (P123, F127, and P104), Wanka et al. [1990] observed no proportionality between the DSC enthalpy values and the size of the PEO block of the molecules, but they noted that there was proportionality between these values and the number of PO segments, to a first approximation. They concluded from this that the transition was probably due to the dehydration or "melting" of the PO segments. Similar trends were observed in the ΔH° data of Alexandridis et al. [1994a]; it appears from their data set, though, that there is a weak effect of PEO block size on ΔH°. For Pluronics with the same size hydrophobic (PPO) block and varying size hydrophilic (PEO) block (i.e., P103, P104, P105, and F108) ΔH° decreased by ~15% as the number of EO segments increased from 2x7 to 2x132. For Pluronic copolymers with the same size hydrophilic (PEO) block and varying size hydrophobic (PPO) block (i.e., P65, P84, and P123) ΔH° increased by ~100% as the number of PO segments increased from 30 to 70. The PPO effect was more significant, leading to the conclusion that PPO is mainly responsible for the micellization of Pluronics. Differential scanning calorimetry was also

used by Beezer et al. [1992] and Mitchard et al. [1992] to study PEO-PPO-PEO block copolymer solutions. The observed "phase transitions" were in the 100 - 300 kJ/mol range and were initially thought to result from changes in the polymer solvation as the temperature changed. Beezer et al. [1992] and Mitchard et al. [1992] claimed that, at the concentration used (5 g/L), only monomeric species were present in solution. In a more recent paper from the same group, however, Armstrong et al. [1993] concluded that the observed enthalpy change is indicative of an aggregation process, accompanied by desolvation and change in conformation of the hydrophobe. Although direct comparison between the calorimetry ΔH values of Beezer et al. [1992], Mitchard et al. [1992], Armstrong et al. [1993] and the ΔH° of Alexandridis et al. [1994a] cannot be made as the copolymers used were not the same, the data of the latter paper strongly suggest that the micellization process is the major contribution to the calorimetrically-observed enthalpy change.

1.4b Effect of copolymer composition and molecular weight on micellization thermodynamics

Free energies of micellization per mol of copolymer in solution, ΔG° (calculated at the CMT for the various copolymers at different solution concentrations) exhibited some scatter when plotted as a function of Pluronic molecular weight, but they indicated the tendency for higher molecular weight copolymers to have more negative free energies of micellization [Alexandridis et al., 1994a]. The ΔG° data collapsed into a single smooth curve, independent of copolymer composition ratio PPO/PEO, when normalized with respect to the total number of monomer units in the polymer, $N_{EO} + N_{PO}$ [Alexandridis et al., 1994a]. The lower molecular weight Pluronics yielded more negative ΔG° values per monomer unit. The dependence of the thermodynamic parameters ΔH° and ΔG° on the PPO/PEO composition ratio was also examined. The normalized ΔH° (expressed in kJ / mol of average monomer unit) approached zero as the PPO/PEO ratio went to zero [Alexandridis et al., 1994a]. It can thus be inferred that the micellization process is dominated by the PPO (hydrophobic) part of the copolymer. A similar trend was observed by Armstrong et al. [1993] based on DSC enthalpy changes of ICI Poloxamer solutions, and by Williams et al. [1985] using the increment in apparent molar volume on "thermal transition" of PolySciences PEO-PPO copolymers as a function of PPO/PEO. The fact that

the normalized ΔH° values are approximately the same for Pluronics of a constant PPO/PEO ratio and different molecular weights would indicate that the micellization enthalpy per monomer unit is independent of molecular weight.

In contrast to the trend of decreasing ΔG° with increasing Pluronic molecular weight, there is no definite dependence of ΔH° on molecular weight over the range covered in the study of Alexandridis et al. [1994a]. The ΔH° data presented in Alexandridis et al. [1994a] revealed two main groups of copolymers, the relatively hydrophobic P103, P104, P105, and P123 with ΔH° in the 300-350 kJ/mol range and the relatively hydrophilic L64, P65, P84, and P85 with ΔH° in the 180-230 kJ/mol range, while ΔH° for the other four copolymers ranged between 170 and 270 kJ/mol. A plot of ΔG° of micellization (expressed in kJ / mol of average monomer unit) as a function of PPO/PEO, showed the ΔG°/unit values approaching zero as the PPO/PEO ratio goes to zero [Alexandridis et al., 1994a]. The unit free energy, however, decreases (becomes more negative) with a decrease in molecular weight for Pluronics with a constant PPO/PEO ratio. In a different investigation Reddy et al. [1991] estimated the ΔG° of micellization at -20 kJ/mol and the ΔH° of micellization at 200 kJ/mol for a solution of purified L64, utilizing ln(CMC) vs 1/T data (only three data points, though). The same group [Yu et al., 1992] reported the ΔH° of micellization at 316 ± 20 kJ/mol for a solution of purified F127 (from ln(concentration) vs 1/CMT data). These values vary approximately 20% from the ΔG° = -24.5 kJ/mol and ΔH° = 230 kJ/mol for L64 and ΔH° = 253 for F127 reported by Alexandridis et al. [1994a].

1.5 Structure of block copolymer micelles

1.5a Aggregation number, micelle size and shape

The association of PEO-PPO-PEO block copolymers into micelles and the structure of these micelles have been investigated by a number of research groups [Al-Saden et al., 1982; Zhou & Chu, 1987; Zhou & Chu, 1988; Brown et al., 1991; Reddy et al., 1991; Brown et al., 1992; Almgren et al., 1992; Malmsten & Lindman, 1992; Mortensen, 1992; Mortensen et al., 1992; Mortensen & Brown, 1993; Mortensen & Pedersen, 1993;

Fleischer, 1993; Pandya et al., 1993b]. We present below information for micelles formed by Pluronics L64, P85, F88, F68, and F127, for which a considerable number of studies have been published. Significant information has been obtained from light and neutron scattering studies. In general, the monomer size is found to be approximately 1 nm and the micelle size 10 nm, independent of concentration (although, the concentrations used were usually above ~ 5% to allow good signal to noise ratio in the scattering experiments). The effect of temperature is interesting: an increase in the aggregation number with temperature has been observed, while the micellar radius remained constant. The conclusions are complicated by the the rather broad CMT transition, and the fact that dynamic light scattering detects hydrodynamic radius which includes hydration water.

L64 showed detectable aggregates at 25 °C only at concentrations above about 6%, with micelle size increasing with concentration (10 nm at 8% - 12.5 nm at 20%) and with significant polydispersity, probably indicating a multiple association process [Al-Saden et al., 1982]. At 35 °C, however, essentially invariant values for the hydrodynamic radius were found over a wide concentration range and the systems were essentially monodisperse; these systems are more likely represented by a closed association model [Al-Saden et al., 1982]. Zhou and Chu [1987] found the micellar molecular weight to increase exponentially with increasing temperature; composition heterogeneity (presence of impurities) caused strong angular asymmetry of scattered light by L64 solutions. The mode of association of a purified L64 sample in aqueous solutions has been examined by Reddy et al. [1991]; association at 34.5 and 40 °C was described by a cooperative association model which assumes aggregate growth by stepwise addition of unimers; note that this is in contrast to the results reported by Al-Saden et al. [1982]. Almgren et al. [1992] calculated (from static light scattering data) the aggregation numbers at the temperatures 21.0, 25.9, 40.0, and 60.0 °C to be 2, 4, 19, and 85 respectively, indicating a smooth increase with temperature. More recently, the temperature effect in aqueous solutions of L64 was examined by means of viscosity, sedimentation, scattering and sound velocity measurements [Pandya et al., 1993b]. The micelles grew large, particularly at temperatures near the cloud point. The viscosity data for L64 were analyzed to estimate various parameters, including the hydrated micellar volume, hydration number, hydrodynamic radius, etc.

Dynamic light scattering experiments indicated the coexistence of unimers

(hydrodynamic radius 1.8 nm), micelles (hydrodynamic radius 8 nm), and micellar aggregates, at P85 concentrations smaller than 10% and at low temperatures (25 °C) [Brown et al., 1991]. Micelles were formed at 25 °C at a copolymer concentration of approximately 5%; at temperatures 40 °C and higher, micelles were present at all concentrations used (C > 0.3%). The hydrodynamic radius of the micelles (calculated at infinite dilution) was approximately constant (8 nm) over the temperature range 15 - 50 °C (aggregation number 20 - 40). At finite concentrations the apparent micellar radius increased with increasing temperature. The hard sphere radius of a copolymer molecule of M_w = 4500 would be 1.15 nm; thus, from the 1.8 nm radius one may conclude that the unimer is highly compact, possibly with the PEO chains forming a tight shell about the nonhydrated PPO core [Brown et al., 1991]. Intrinsic viscosity measurements (capillary viscometry) were made on dilute P85 solutions in order to obtain more information on the molecular dimensions. The intrinsic viscosity decreased from 16 mL g^{-1} at 15 °C to 6.5 mL g^{-1} at 50 °C. The intrinsic viscosity of 6.5 mL g^{-1} at 50 °C suggested a very compact particle (although with some dissymmetry and/or solvation); the radius of gyration, R_g, was estimated at 8.3 nm. Values for the hydrodynamic radii of the micellar component from self-diffusion coefficients (measured by pulsed-field-gradient NMR and extrapolated to infinite dilution) varied between 6.2 an 9.0 nm in the temperature range 21.3 - 35.7 °C, with an average value of 7.7 nm. The trend with temperature contrasted with the constant micelle radius detected using dynamic light scattering. This was possibly the result of polydispersity since the number-average quantity obtained with NMR would be very sensitive to even small amounts of monomer [Brown et al., 1991]; the difference between the hydrodynamic radii determined from pulsed field gradient (PFG) NMR and dynamic light scattering was smaller at the higher temperatures at which the suspension is nearly monodisperse. The self-diffusion of P85 in aqueous solutions was investigated with PFG-NMR [Fleischer, 1993; Fleischer et al., 1993]. The hydrodynamic radii of the unimer and the micelles were determined to be 1.5 and 4.5 nm, respectively, and found to be independent of temperature and concentration in the concentration range 1 - 10 %. Mortensen [Mortensen, 1992; Mortensen et al., 1992] studied the structure of P85 aqueous solutions using neutron scattering. The radius of gyration of the free copolymer was 1.7 nm. The micellar sizes (micelle core radius and hard-sphere interaction radius) appeared to be independent of polymer concentration, but showed a small temperature dependance reflecting changes in aggregation number. The micelle core radius and hard-sphere interaction radius were 3.8 nm and 6.0 nm at 20 °C, respectively, and increased to 5.1 nm

and 7.5 nm at 50 °C; the aggregation number was 37 at 20 °C, increasing to 78 at 40 °C [Mortensen & Pedersen, 1993].

Brown et al. [1992] and Mortensen and Brown [1993] published studies comparing P85, F87, and F88 copolymers. Relaxation time distributions obtained by Laplace inversion of the dynamic light scatting (DLS) correlation functions demonstrated complex states of aggregation in solution [Brown et al., 1992]. Monomer, micelles, and larger aggregates coexisted in proportions that depend sensitively on temperature and concentration [Brown et al., 1991]. The monomers had hydrodynamic radii in the size range 1.5 - 3.0 nm and micelles were 8 - 13 nm (in sequence of increasing PEO block length); the clusters were 80 nm and larger. The micelle aggregation number for F88 was 17 at 40 °C, and the hydrodynamic radius 13 nm (40 °C) and 10.5 nm (50 °C). Molecular weights, gyration radii, etc., could not be determined from static light scattering measurements owing to the highly polydisperse character of the solutions. The inverse osmotic compressibility was evaluated from the absolute scattering intensity at zero angle, providing a measure of the relative strengths of solute/solvent and solute/solute interactions; formation of micelles and aggregates was consistent with low values of the inverse osmotic compressibility.

Pluronics P85, F87, and F88 had approximately the same tendency for micelle formation when compared at the same molar concentration; for the same weight concentration, P85 formed micelles more readily [Brown et al., 1992]. From a plot of the critical micellization temperature of L81, P85, P87 and F88 vs the concentration of PPO in solution, it appeared that the PPO concentration is the relevant parameter decisive for determination of the CMT [Mortensen and Brown, 1993]. L81 formed aggregates at temperatures below the common curve, presumably due to the much more hydrophobic nature of L81; there was also some deviation from the curve for P85 at low PPO concentrations. The micellar core radius, R_c, and to some extent also the hard-sphere interaction radius, R_{hs}, appeared to be essentially independent of polymer concentration but showed a significant increase with temperature (radii were obtained by fitting to the experimental scattering data). The difference between R_c and R_{hs} remained practically unaffected by the temperature. When R_c was plotted against the reduced temperatures $T - T_{CMT}$, the data for solutions of P85, P87, and F88 followed a common master curve. A double logarithmic plot of R_c vs $T - T_{CMC}$, gave the empirical scaling relation $R_c \sim (T -$

$T_{CMT})^{0.2}$ [Mortensen & Brown, 1993]. Close to T_{CMT} the aggregation number is very small and increases continuously following a $N \sim (T - T_{CMT})^{0.6}$ relationship (assuming the micellar core to consist mainly of PO segments, the aggregation number scales with the third power of the core radius, R_c) to approximately N ~ 200 at the highest temperature, where spherical micellar aggregates are present.

From the hard-sphere data analysis, it appeared that the main difference between P85, P87, and F88 micelles at a given temperature is the size of the micelles; the larger the PEO block, the smaller the core and the aggregation number [Mortensen & Brown, 1993]. The dependence of the core radius and the aggregation number on the degree of polymerization of both EO and PO [Mortensen & Brown, 1993] was in contrast to the Halperin [1987] star model of polymeric micelles which was recently shown to be valid for the system PEO-PS-PEO [Xu et al., 1992]. The relationship of increasing micellar core with decreasing number of EO units would lead to a limitation in the formation of spherical micelles, namely if the number of EO units is so small that the core radius extends the length of a stretched PPO chain. Extrapolating the core radii data for P85, F87, and F88 to the EO unit number corresponding to L81, would predict a value for the core that approaches or exceeds the maximum value given by the length of a fully extended PPO chain; this was probably the reason why L81 did not form spherical micellar aggregates [Mortensen & Brown, 1993].

Static and dynamic light scattering experiments on F68 solutions revealed three temperature regions, those of unimer, transition, and micelle, respectively [Zhou & Chu, 1988]. A transition corresponding to the CMT was observed; below the CMT, low scattering intensity and small particle size (2.3 nm) were detected, showing little temperature dependence. Only unimers were present below the CMT; micelle formation became appreciable above CMT. In the micelle region, the micellar weights measured were of the order of 10^5 g mol^{-1} (average aggregation number was 65) and increased linearly with increasing temperature, while the hydrodynamic radius of the micelles remained nearly constant (8.0 nm) [Zhou & Chu, 1988] (note, though, that Al-Saden et al. [1982] reported the average hydrodynamic radius to increase with temperature for given concentration). Such a dual effect of temperature was interpreted in terms of enhanced dehydration with temperature [Zhou & Chu, 1988]. In static light scattering measurements the scattered light field is a measure of the polarizability difference between the dispersed particle and the

surrounding medium, thus providing useful information concerning the "dry" dispersed particles. In the dynamic light-scattering experiments, the Brownian motion of the "wet" dispersed particles is monitored to provide the size information on the solvated particles. It is well established that dehydration of nonionic surfactants gradually occurs with increasing temperature, which results in an enhanced tendency to separate from the solvent environment and, consequently, in an increase in the aggregation number [Zhou & Chu, 1988].

The hydrodynamic F127 micellar radius in water, as calculated from diffusion (DLS) data at the CMC, remained constant at 10.2 nm, over the temperature range 35 - 45 °C [Attwood et al., 1985]. Viscometric studies, however, showed a progressive dehydration of the micelles with temperature increase; the aggregation number was 3 at 35 °C, 9 at 40 °C, and 12 at 45 °C [Attwood et al, 1985]. The hydration and microviscosity in the solution and gel form of F127 have been studied using the fluorescent probe molecules pyrene and 8-anilino-1-naphthalene sulfonic acid (ANS). The results indicate that the microviscosity decreases with increasing temperature [Gilbert et al., 1987a]. Malmsten and Lindman [1992a] used NMR to study diffusion of molecules in F127 solutions. The diffusion of the polymer molecules was slow ($D_p = 10^{-11}$ - 10^{-12} m^2/s), decreasing with increasing polymer concentration (roughly as $D_p \sim c^{-1}$) up to 20 wt%; the diffusion coefficent of water was $D_w = 10^{-9}$ m^2/s [Malmsten & Lindman, 1992a]. Water self-diffusion decreased monotonically with increasing polymer concentration, giving $D/D_o = 0.5$ at 40 wt%. The decrease in D/D_o with increasing polymer concentration could be reproduced by taking into account the obstruction due to excluded volume and the hydration of the polymer molecules. The analysis yielded that somewhere between two and five water molecules per EO group were perturbed. On increasing the temperature, the water diffusion increased. The data of Malmsten and Lindman [1992] are consistent with a gradual dehydration of the polymer molecules with increasing temperature, in agreement with Attwood et al [1985]. The dehydration, however, was uncorrelated with the occurrence of the gel region [Malmsten & Lindman, 1992b].

1.5b Phase diagram

The phase behavior of PEO-PPO-PEO triblock copolymers dissolved in water has been studied by Mortensen and coworkers using small-angle neutron scattering and

dynamic light scattering [Mortensen, 1992; Mortensen & Pedersen, 1993; Mortensen & Brown, 1993]. The structural properties have been studied as a function of polymer concentration and temperature for a series of copolymers with the same PPO block and varying size PEO block. At low temperature ($T \leq 15$ °C) and low polymer concentrations, the unimers were fully dissolved Gaussian chains with radius R_g=1.7 nm. Close to ambient temperature, the hydrophobic nature of PPO caused aggregation of the polymers into spherical micelles with core sizes of the order of 4 - 5 nm, somewhat temperature dependent. According to the data analysis, the core size increased with decreasing PEO block size and with increasing temperature. The copolymer with the largest PEO block aggregated in micelles with a core diameter which, within the whole temperature regime, was smaller than the length of a stretched PPO chain. Micelles formed by copolymers of intermediate PEO size had a core diameter which at high temperature approached the size of a fully stretched PPO chain, thus causing an abrupt change from spherical to rodlike structure (as observed both by neutron scattering and depolarized light scattering). It appeared from the hard-sphere data analysis that the micelle-forming polymers could all be scaled to a common phase behavior where the critical micellization temperature is determined by the PPO concentration, whereas the crystallization (gelation) temperature is determined by the total copolymer concentration [Mortensen & Brown, 1993]. The concentration of micelles increased roughly linearly with temperature, until either a saturation was reached, where all polymers were part of a micelle, or the volume density of micelles was so high that they "locked" into a crystalline structure of hard spheres. In the 60 - 70 °C temperature range, the micellar structure changed from spherical form to prolate ellipsoid, leading to a decreasing intermicelle interaction. At high concentration this caused melting of the cubic lattice and led successively to the formation of a rodlike structure with hexagonal symmetry. Close to 95 °C, large aggregates of polymers ordered in lamellae structure were formed, leading to an opaque suspension [Mortensen & Pedersen, 1993]. Figure 1.2 shows the phase diagram for Pluronic P85, depicting the concentration-temperature regions where the different aggregates exist [Mortensen, 1992]. The micellization boundary (phase diagram) for a number of aqueous PEO-PPO-PEO solutions is presented in Figure 1.3 (the CMC-CMT data are from Chapter 2 of this Thesis).

1.5c Effect of additives on micellization

The phase behavior of L64 in the presence of various additives was studied by

Pandya et al. [1993a] using cloud point and phenol index (amount of added phenol resulting in a turbid solution) measurements. Addition of electrolytes, having anions and cations of different sizes and polarizabilities, resulted in either increase or decrease in cloud point; the effect of salts was discussed in terms of "salting in" and "salting out" and followed the Hofmeister series. The effect of various nonelectrolytes (e.g., hydroxy compounds and amides) on the cloud point of L64 was also examined and discussed in terms of their influence on water structure [Pandya et al., 1993a]. The aggregation behavior of P85 and L64 in aqueous solution has been investigated in the presence of added salts (KCNS, KI, KBr, KCl and KF) by viscosity, cloud point, light scattering, pulse gradient spin echo NMR, and solubilization measurements [Bahadur et al., 1993]. The salts have a strong effect on the cloud points of the Pluronics. A slight linear increase in cloud point was observed with an increase in copolymer concentration in the case of L64, following an initial decrease up to a polymer concentration of ~2%. KCNS, which is known to increase the cloud point, showed a similar trend in both L64 and P85 solutions. KBr, KCl, and KF decreased the cloud point. A linear increase or decrease in cloud point with increasing salt concentration was observed. Both P85 and L64 formed micelles which increase in size and change into elongated shapes when the cloud point was approached. The changes of size and shape of the micelles, revealed by the intrinsic viscosity and rheological properties, seem to occur at the same temperature relative to the cloud point, independent of the nature of the salt. The onset of micelle formation was also shifted in the same direction as the cloud point by the salts, but to a lesser degree [Bahadur et al., 1993]. The cloud point of F68 was reduced by 50 °C when 1.0 M KF was added to the aqueous solution [Bahadur et al., 1992]. The size of the unimers and micelles in the solution, as estimated from diffusion coefficients (determined by dynamic light scattering and NMR self-diffusions measurements) or micelle molecular weights (from static light scattering), were similar in the presence and absence of salts, but the growth of the micelles started at a lower temperature (25 °C in 1.0 M KF, 44 °C in water) and continued over a wider temperature range in the salt solution [Bahadur et al., 1992]. The influence of temperature on F127 micellar size and hydration was less pronounced in the presence of 0.5 mol dm^{-1} NaCl in the aqueous solution [Attwood et al, 1985].

Sodium dodecylsulfate (SDS) increased the cloud point of L64 which, otherwise, decreased in the presence of small amounts of electrolytes. The clouding behavior of a mixed L64/SDS system in the absence and presence of salt was discussed by Pandya et al.

[1993a], primarily in terms of electrical charge on the micelle surface. NMR chemical shift measurements and fluorescence quenching have been combined in a study of the aggregation behavior and properties of L64 and F68 in the presence of sodium dodecyl sulfate, at 20 and 40 °C [Almgren et al., 1991]. While the copolymers did not form micelles at 20 °C, they formed mixed micelles with SDS, at SDS concentrations as low as 1mM. The aggregation numbers obtained from fluorescence quenching studies indicate that about 3 SDS molecules per copolymer molecule are needed to "glue" together the PPO blocks into a hydrophobic core at 20 °C [Almgren et al., 1991]. The micelles formed at low SDS concentrations were small (15 SDS molecules associated with 4 - 5 copolymer molecules); at high SDS concentrations the micelles consisted mainly of SDS. L64 formed micelles at 40 °C that were large but decreased rapidly in size upon addition of SDS. The ^{13}C chemical shifts for the methyl carbons in the PPO block were indicative of a change from a coiled conformation in small micelles, unimers, as well as in the bulk PPO liquid, to a more extended PPO conformation in the large micelles. The change of the shifts of the individual carbons in the alkyl chain of SDS on addition of the copolymers to SDS micelles followed a similar pattern for both L64 and F68 [Almgren et al., 1991].

Recently, Hecht and Hoffmann [1994] reported the influence of SDS on the aggregation behavior of F127. For block copolymer solutions in the concentration range of 1-5% and increasing SDS concentration, the light scattering intensity passed through a deep minimum, the electric birefringence passed over a maximum, and the endothermic peak of the DSC signals (due to the micellization of the block copolymer) disappeared. The results indicated that SDS binds to unimers of F127 and thereby suppresses completely the formation of F127 micelles. At saturation, approximately six SDS molecules bind to one F127 molecule. The birefringence data indicated that the F127/SDS complex exists in a more or less extended conformation and not as a coil. The binding of SDS on F127 was also confirmed by surface tension measurements, that showed the surface active block copolymers to be replaced from the interfaces by SDS molecules. The binding of SDS on F127 commenced at concentration far below the CMC of SDS. Addition of CTAB (N-cetyl-N,N,N-trimethylammonium bromide) to F127 solutions decreased the magnitude of the DSC peak, showing that CTAB (a cationic surfactant) also suppresses the micellization of F127. The zwitterionic surfactant C_{14}DMAO (N,N-dimethyl-1-tetradecanamine N-oxide) suppresses F127 micellization at concentrations 10 times above its CMC, suggesting a different mode of association than SDS; perhaps, F127 molecules bind to the surface of

C_{14}DMAO micelles.

1.6 Modelling of block copolymer micellization and micelle structure

Theories of micelle formation in solutions of block copolymers have been advanced by a number of researchers over the past decade. Leibler et al. [1983], Noolandi and Hong [1983], Munch and Gast [1988], and Nagarajan and Ganesh [1989] computed the free energy of micelle formation assuming uniform copolymer segment concentrations in the core and corona regions, respectively. Scaling theories for polymeric micelles with an insoluble core and an extended corona were developed by Halperin [1987], Marques [1988], Semenov [1985], and Zhulina and Birsthein [1986]. In a third approach, van Lent and Scheutjens [1989], Linse [1993], and Hurter et al. [1993] used a self-consistent mean field theory to determine the detailed segment density profiles within a micelle, making no a priori assumptions as to the locations of the micellar components. The micelle structures determined from this model have been confirmed recently by Monte Carlo simulations (e.g., Wang et al. [1993]) and show that the interfacial region between the core and corona of the micelle is diffuse, and not sharp as is assumed in the other modelling approaches.

1.6a Phenomenological models

Munch and Gast [1988] applied the theory of Leibler et al. [1983], which treated micelle formation in mixtures of block copolymers and homopolymers, to describe the micellization of diblock copolymers in solution. The micelle core was assumed to be a melt of B chains, while the corona contained A chains with solvent S. The interaction between the solvent S and the B segment was described by the χ_{BS} interaction parameter, whereas athermal interactions between the A segment and solvent was assumed (χ_{AS}=0). The energy of a single micelle was expressed as a contribution of core-solvent interfacial energy, energy due to deformation of the copolymer chains in the micelle, and free energy of mixing solvent molecules with the A monomers in the corona (ϕ_o: volume fraction of A in the corona). The total free energy of the system included the energy of the micelles, the free energy of mixing individual diblock copolymers with solvent molecules (ϕ_1: volume

fraction of copolymers outside the micelles), and an energy contribution arising from the translational entropy of the gas of micelles. The total free energy was minimized with respect to the micelle aggregation number p, ϕ_1, and ϕ_o.

One useful feature of the theory of Leibler et al. [1983] is that, for high degree of incompatibility between B and S, the free energy minimization with respect to ϕ_1 results in an analytical estimate for CMC as $\phi_1 \rightarrow 0$ [Munch and Gast, 1988]:

$$\phi_1 \approx \exp (f/kT + N - \chi_{BS}N_B) \qquad (13)$$

where f/kT is the energy per chain in an isolated micelle, N is the total number of segments in the copolymer molecule, N_B is the number of B (core) segments, and $\chi_{BS}N_B$ is the total effective interaction per chain (since the A chain is in an athermal environment). The leading order terms in f/kT are [Munch and Gast, 1988]:

$$f/kT \approx (6\pi^2 N_B)^{1/6} (\chi_{BS}N_B)^{1/2} p^{-1/3} + N (1+N_B/N_A)^{-1} (1-\phi_o) \phi_o^{-1} \ln(1-\phi_o) \qquad (14)$$

The first term in the right side of Eq 14 comes from the energy of forming the micelle core - solvent interface and opposes the formation of micelles, whereas the second term, which originates from the configurational entropy of mixing solvent molecules with A monomers in the corona, favors micellization. As χ_{AS} was assumed to be to zero, no effect of block A on micellization could be seen in the model of Munch and Gast, other than the configurational entropy of mixing solvent molecules with A monomers in the corona. The model of Nagarajan and Ganesh [1989] took into account A-solvent interactions at the expense, though, of an analytical expression for ϕ_{CMC}.

In the micellization theory developed by Nagarajan and Ganesh [1989] the micelles were also assumed to have a completely segregated core region, consisting of only the B block, and a corona region consisting of the solvent S and the solvent compatible A block. The free energy of micellization was expressed in terms of changes in the state of dilution of blocks A and B, changes in the state of deformation of blocks A and B, localization of the copolymer molecules at the micelle interface, and formation of the micellar core - solvent interface. The hydrophobic interactions, which strongly influence the micellization

in water as discussed above, were implicitly accounted for in the experimentally determined χ values used for the PEO-water and PPO-water interaction free energy terms. The micellization parameters were obtained from minimization of the free energy expression with respect to the radius of the micelle core and the corona thickness. The most important contribution favoring micellization arises from the change in state of dilution of block B as it goes from solvent S into the micelle core (note that the mutual incompatibility of blocks A and B is also essential for micellization, otherwise the incompatibility of the solvent for the polymer blocks will give rise to macroscopic phase separation; the incompatibility of blocks A and B was implicitly taken into account by the completely segregated core structure assumed for the micelle). The most important contribution opposing micellization originates from the formation of the micelle core - solvent interface. The optimal aggregation number is determined primarily by balancing the free energy contributions due to change in state of dilution and deformation of the A (more important in the case of the PEO-PPO/water system) and B blocks, favoring low aggregation numbers, and the free energy contributions due to formation of the micelle core - solvent interface that favor high aggregation numbers.

The theory of Nagarajan and Ganesh, developed for diblock copolymers, succeeds in predicting qualitatively the contributions of the copolymer composition and molecular weight on the micellization of triblock copolymers. Predictions of Nagarajan's model for $\ln\phi_{CMC}$ are compared to experimentally determined [Alexandridis et al., 1994a] $\ln\phi_{CMC}$ values in Chapter 3 of this Thesis. The trends are the same in both theory and experiment, although the theory overpredicts the experimentally obtained free energies of micellization by a factor of eight, resulting in unrealistically low CMC values. Part of the numerical discrepancy could be eliminated by adding extra terms in the expression for the free energy of micellization to account for the entropy penalty involved in joining two AB diblock copolymer molecules to create a A(2B)A triblock, and in having loops in the micelle core.

Prochazka et al. [1991] modified Nagarajan's model to treat association of A-B-A block copolymers in solvents selective for A blocks by inroducing two additional terms in the free energy expression. These terms accounted for reduction in entropy due to loop formation of the middle (B) block, and localization of the two A-B joints of the copolymer in the interface between the core and the corona of the micelle. The result was less negative ΔG° (in the correct direction with respect to agreement between experiment and theory) but

the decrease in the absolute value of the predicted ΔG° was ~ 10% and not enough to account for the 8-fold overprediction of the experimental ΔG°s. A comparison of the model calculations by Nagarajan and Ganesh [1989] for a diblock copolymer with the results of Prochazka et al. [1991] obtained for a triblock copolymer (of the same molecular weight and composition as the diblock) showed the aggregation number of the diblock copolymer micelles to be more than three to five times higher than the one for the triblock micelles. Linse [1993] concluded, using a mean-field lattice micellization model, that there is a 5-fold increase in CMC and a 4-fold decrease in aggregation number in going from a diblock to a triblock PEO-PPO copolymer. Prochazka et al. [1991] also made an interesting observation regarding the effect of the deformation energy contribution to the model ΔG° expression: model calculations using the deformation energy term used by Nagarajan and the term used by Leibler et al. [1983] result in different aggregation number (note that both terms are based on Flory's [1953] approach).

Recently, Izzo and Marques [1993] studied theoretically (using scaling concepts) the formation of dilute phases of spherical, cylindrical, and planar aggregates of diblock A-B and triblock A-B-A copolymer chains in solvents selective to B. They treated the micelle formation of the triblock copolymers in the same way as the diblocks, the only difference being that the core was composed of twice as many chains of length B/2. This resulted in $\Delta G^\circ_{triblock} \sim 2\ \Delta G^\circ_{diblock}$, which is counterintuitive and opposite to the micellization theories examined above. It thus appears that the entropy loss associated with the formation of loops is essential for describing the micellization of triblock copolymers. The loop (backfolding) entropy term was first introduced by ten Brinke and Hadziioannou [1987] in their model of B-A-B copolymer micelle formation in A-homopolymer, and modified by Balsara et al. [1991] in a similar model. Balsara et al. [1991] comment on the applicability of the theory of Leibler et al. [1983], originally proposed for micellization of A-B block copolymer in A-homopolymer, in the theories of Munch and Gast [1988] and Nagarajan and Ganesh [1989], that treat micellization in selective solvents. They note that, in the presence of solvents, the description of the core-corona interface is complicated owing to the three-component (presence of solvent on interface) nature of the problem [Balsara et al., 1991]. These points, in addition to the hydrogen bonding interactions between both PEO and PPO with water, may account for the quantitative discrepancy between predictions of phenomenological block-copolymer micellization theories and the experimental results of Alexandridis et al. [1994a] for the system PEO-PPO-PEO/water.

1.6b Mean field lattice models

Another approach in modelling block copolymer micelles has been through the Scheutjens - Fleer theory [Scheutjens & Fleer, 1979], an extension of the Flory-Huggins analysis of homogeneous polymer solutions [Flory, 1953], in which the polymer chains are allowed to assume different conformations on a lattice. A first-order Markov approximation (the position of a segment depends only on that of the preceding segment in the chain) is used in the Flory-Huggins analysis and, as a result, the chain conformation follows the path of a random walk. In addition, a mean field assumption is invoked to describe the interactions between unlike segments. The free energy of the system is minimized in order to calculate the equilibrium thermodynamic properties of the polymer solution. For spatially inhomogeneous systems such as those containing interfaces, Scheutjens and coworkers [van Lent & Scheutjens, 1989; Scheutjens & Fleer, 1979; Leermakers et al., 1989] restricted the mean field approximation to two dimensions, i.e., within parallel or concentric lattice layers, and applied a step-weighted random walk to account for the inhomogeneities normal to the layers. The polymer and solvent molecules are assumed to be distributed over a lattice, such that solvent molecules and polymer segments occupy one lattice site each. Each polymer chain can assume a large number of possible conformations, defined by the layer numbers in which successive segments are found. There can be many different arrangements for each conformation; if the number of polymer chains in each conformation is specified, the configurational entropy contribution to the system free energy can be evaluated, the other contributions to this free energy being due to the interactions between the polymer molecules, solvent molecules and the surface, which are characterized by Flory-Huggins χ-parameters. If the free energy of the system is minimized with respect to the number of polymer chains in each conformation, it is possible to calculate the equilibrium segment density profiles.

The self-consistent field theory can be used to calculate the segment density profiles in a micelle once the aggregation number of the micelle is known [van Lent & Scheutjens, 1989; Leermakers et al., 1989; Leermakers & Scheutjens, 1989]. To find this aggregation number, small system thermodynamics can be used [Hall & Pethica, 1967; Hill, 1963; Hill, 1964], in which the change in the free energy due to the change in the number of micelles (at constant temperature, pressure and number of molecules) must be zero at

equilibrium. This "excess free energy" is the sum of the energy required to create micelles, and the energy due to the translational entropy of the micelles. Since the segment density profiles are required in order to calculate the energy of micelle formation, an iterative process is followed. The self-consistent mean field lattice theory of Scheutjens and Fleer [1979] has been used to study many colloidal systems, including homopolymer and block copolymer adsorption on surfaces [Evers et al., 1990], interactions between adsorbed polymer layers [Scheutjens & Fleer, 1985] and the formation of micelles [Leermakers et al., 1989], vesicles [Leermakers & Scheutjens, 1989] and membranes [Scheutjens et al., 1989].

Recently, the Scheutjens and Fleer theory has been extended to study the formation of micelles by linear PEO-PPO-PEO and branched, star-like, amphiphilic block copolymers, and the solubilization of naphthalene in these micelles has been analyzed as a function of polymer structure, composition and molecular weight by Hurter at al. [1993a; 1993b]. The detailed segment density profiles in the micelles were obtained, and macroscopic quantities such as critical micelle concentration, aggregation number and micelle size were calculated. The calculations show that higher molecular weight polymers form larger micelles. The addition of the solute causes the micelle to become larger, with a lower core concentration of water, and a higher concentration of PPO in the core. The simple lattice theory for flexible chain molecules, however, cannot capture effects such as the phase behavior of PEO and PPO in water, where a lower critical solution temperature is observed. To predict such behavior, the gauche and trans bond orientations of the polymer chain must be accounted for. Leermakers [1988] used the rotational isomeric state scheme, which accounts for the gauche-trans orientations in a chain, and eliminates backfolding, combined with the self-consistent field theory, to predict the formation of lipid bilayer membranes and lipid vesicles. An approach which is computationally more simple than the rotational isomeric state scheme, but which accounts for the temperature and composition dependence of the interaction parameter χ in a physically acceptable manner, has recently been presented by Karlstrom [1985]. This model for PEO recognized that certain sequences of the gauche-trans orientations in an EO monomer would lead to a polar conformation, while others would be essentially nonpolar; the probability of the nonpolar conformations increased with temperature making the polymer more hydrophobic. Using this model, the solubility gap in PEO-water and PPO-water phase diagrams could be reproduced.

A model for block copolymer micelles has been developed [Hurter at al., 1993a; Linse, 1993], which incorporates Karlstrom's ideas to account for the conformational distribution in PEO and PPO. An increase in temperature caused the model-predicted aggregation number of the micelles to increase, and the critical micelle concentration to decrease. The aggregation number increased rapidly with polymer concentration in the dilute regime, but was approximately invariant to polymer concentration at concentrations far from the CMC. Raising the PPO content or the molecular weight of the polymer increased the aggregation number, and decreased the CMC. The model predicts that the most hydrophobic polymer, P103, does not form spherical micelles at higher polymer concentrations, owing to phase separation or formation of aggregates of structure different than spherical. An increase in PEO block size resulted in a smaller micelle core, while the corona became more extended. This was also reflected in a decreasing predicted aggregation number for the micelles. The conformation of the polymer was affected by both the temperature and the composition of the surrounding solution; both PEO and PPO had a lower fraction of polar segments in the core of the micelles, and the polar fraction decreased with an increase in temperature. The micelle aggregation number was found to increase with an increase in the solute bulk concentration. This is in agreement with the experimental results of Al-Saden et al. [1982], who found that the increase in the hydrodynamic radius of L64 aggregates with hexane uptake was greater than could be explained by the additional volume of the solute. It was postulated that the increase in hydrodynamic radius resulted from a combination of an increase in the aggregation number and the incorporation of solute.

The phase behavior of aqueous solutions of polymers containing PEO and PPO has been modeled by Linse [1993b] on the basis of a mean-field lattice theory (similar to the one used by Hurter at al. [1993]) for multicomponent mixtures of copolymers with internal states occurring in heterogeneous systems. The regions for monomeric solution, spherical micelles, and elongated rods have been examined for three PEO-PPO-PEO triblock copolymers. A semiquantitative description of the strong temperature dependence of the phase behavior was obtained. At low polymer concentrations and at low temperatures a monomeric solution was found, whereas at either higher temperatures or higher concentrations a solution of spherical micelles was present. At even higher temperatures, there was a transition from spherical to infinitely long rod-like aggregates, and eventually

the system separated into two phases.

A comparison of the phase diagrams for P105, P95, and P104 (as predicted by the model of Linse [1993b]) indicated that a reduction of the molecular weight by ~ 20% with constant PPO/PEO ratio (P105 to P95) led to an increase in the CMC for a given temperature, a smaller micellar region, and a region of rods of similar extension but slightly shifted to lower temperature. Decreasing the PEO block size, while keeping constant the PPO block (P105 to P104), resulted in a shift of the CMC curve to lower copolymer concentration at a given temperature, a smaller micellar region, and a smaller region of rod-like aggregates which was considerably shifted to lower temperatures [Linse, 1993b]. Comparison of the modelling predictions for the phase diagram of Linse [1993b] to the experimentally determined phase diagram of Mortensen [1992] reveals qualitative agreement with respect to the number of phases occurring and their relative location. However, the calculated CMC curve occurred at temperatures 20 - 30 K higher, and the calculated region for the hexagonal phase occurred at lower temperature, thus leading to a too narrow temperature range for the micellar solution phase. Segment density profiles indicated that, at a given concentration, the radial extension increased whereas the headgroup area decreased on increasing temperature for both micelles and rods. At the transition from micelles to rods the radial extension was reduced abruptly by ca. 10% [Linse, 1993b]. In addition to the phase behavior, Linse [1993a] used the model to predict micellization properties (i.e., CMC, aggregation number, hydrodynamic radius) and their temperature dependence for Pluronic copolymer solutions. Both the PPO/PEO ratio and the total molecular weight influence micellization, in qualitative agreement with experimental CMC data [Alexandridis et al., 1994a]. For polymers with the same PPO/PEO composition, increasing the molecular weight resulted in increasing the aggregation number. The model predicted "infinite" aggregation number for P103, similarly to the predictions of Hurter et al. [1993].

The self-consistent mean-field theory used by Hurter et al. [1993] and Linse [1993] was able to reproduce the anomalous phase behavior of PEO and PPO homopolymers, predict the micellization behavior of PEO-PPO-PEO block copolymers, and provide detailed information on the microstructure of the micelles. Copolymers of varying blockiness and block sequence could be handled, and no apriori assumptions with respect to the core/corona interface were necessary. The model calculations showed qualitative

agreement with experimental predictions on the effect of temperature, concentration, hydrophobicity, and molecular weight of the polymer; quantitative agreement was also good, considering that all the model input parameters were obtained from independent experiments. The phenomenological theory of Nagarajan and Ganesh [1989], developed originally for diblock copolymers and extended to triblocks by Prochazka et al. [1991], was also successful in predicting qualitatively the contributions of the copolymer composition and molecular weight on the micellization of triblock copolymers (although the predicted CMCs were unreasonably low). A sharp interface had to be assumed, though, between the core and the corona, and variation of the number of blocks or block sequence was not straightforward. Furthermore, the effects of temperature on micellization were not examined. An advantage of the Nagarajan and Ganesh theory is that the various contributions to the micellization free energy were easily quantified leading to a better appreciation of their magnitude and influence to the micellization.

1.7 Surface activity of PEO-PPO copolymers

1.7a Adsorption at the air-water interface

Surface tension data for various Pluronic copolymer aqueous solutions at two temperatures, 25 and 35 °C, have been reported by Alexandridis et al. [1994b]. At low concentrations the surface tension decreased with increasing concentration for all copolymers, in accord with the Gibbs' adsorption isotherm [Chattoraj & Birdi, 1984]. A change in slope (break) was observed in the surface tension curve at a characteristic concentration, after which the surface tension values continued to decrease until a plateau was reached (second break); the surface tension values remained constant with further increase of copolymer concentration [Alexandridis et al., 1994b]. This behavior (two breaks) was observed for most copolymers studied and was very reproducible. The first (low concentration) break occurred at a copolymer concentration of approximately 0.001 %, which was roughly the same for both temperatures studied and for different copolymers. The surface tension value at the onset of this break varied from 40 to 50 mN/m.

The presence of two breaks has led to some confusion in the literature on Pluronic

copolymers regarding the interpretation of the surface tension dependance on concentration, and the extraction of the CMC from such a set of data [Wanka et al., 1990; Prasad et al., 1979; Anderson, 1972]. In most cases it has been assumed that the first change in slope signified the CMC [Anderson, 1972; Bahadur & Pandya, 1992], although other interpretations, such as formation of "unimolecular" micelles [Prasad et al., 1979], have been given. The region of decreasing surface tension that follows the break at 0.001%, and the second break have often been ignored [Prasad et al., 1979; Anderson, 1972], but it has been suggested that they were due to broad copolymer molecular weight distribution and to the presence of impurities [Wanka et al., 1990].

Alexandridis et al. [1994b] showed that there is good agreement between the CMCs determined from dye solubilization [Alexandridis et al., 1994a] and the concentration at the second break of the surface tension curve, and therefore reached the conclusion that the higher-concentration break corresponds to the CMC and signifies the formation of polymolecular micelles having a well defined hydrophobic interior (i.e. able to solubilize organic solutes). It should be noted that the copolymer concentrations at the second break, extracted from the surface tension data of Wanka et al. [1990] (0.3% for F127, and 0.01% for P104, both at 25 °C) and Prasad et al. [1979], are also comparable to the CMC values found in the dye solubilization study of Alexandridis et al. [1994a]. Two other observations supporting the conclusion that the higher-concentration break is the CMC are (i) the plateau observed in the surface tension values after the high-concentration break, and (ii) the effect of temperature on the copolymer concentration at which the second break occurs. Attainment of a constant surface tension value is an indication of micelle formation (CMC) in solutions of typical surfactants [Chattoraj & Birdi, 1984]. While the surface tension of Pluronic solutions keeps decreasing with increasing copolymer concentration after the first low-concentration break, it remains constant after the second break (a dip in the surface tension after the break observed for Pluronic P85 is most likely due to impurities [Reddy et al., 1991; Yu et al., 1992; Mysels, 1986]). Regarding the effect of temperature, the copolymer concentration at which the second change in slope occurs decreased significantly with increasing temperature, in good agreement with CMCs obtained from dye solubilization [Alexandridis et al., 1994a] and observations in other studies of Pluronics [Brown et al., 1991; Mortensen & Pedersen, 1993], whereas the concentration at the first break did not vary significantly [Alexandridis et al., 1994b].

Having attributed the high-concentration break (change in the slope) of the surface tension curve to the formation of micelles in the bulk (CMC), we examine below the origin of the first (low-concentration) break. The wide molecular weight distribution of the copolymers studied, and the presence of hydrophobic impurities, have been singled out in the past as possible factors that caused differences in the CMC values obtained by surface tension and dye solubilization methods. The effect of molecular weight distribution on surface tension of nonionic surfactants has been nicely demonstrated by Crook et al. [1963], who studied the surface tension of normal (Poisson) distribution and single species octylphenoxy-ethoxyethanols ($OPE_{1\text{-}10}$, 1-10 is the number of ethylene oxide segments), and mixtures of single species and normal distribution OPE_4 and OPE_{10}. The authors found preferential adsorption of molecules with shorter PEO-chain length ($OPE_{3\text{-}5}$) at the air/water interface; this was demonstrated by a less sharp (but still, only one) break in the surface tension curve, and a dip in the surface tension values in the vicinity of the break. Such a behavior was attributed to the replacement of highly surface active, short-PEO-chain-length, molecules (contributing to a low surface tension value) on the interface by the major component, when these highly surface active molecules were solubilized in micelles formed by the major component. No manifestations of the above were seen in the surface tension curves for Pluronics [Alexandridis et al., 1994b]. As for the influence of impurities, a decrease in surface tension with time, observed in some experiments at low copolymer concentrations, would indicate the presence of hydrophobic impurities that adsorb slowly on the surface [Mysels, 1986]. However, the presence of such impurities should result in a lowering of the surface tension (described above as a "dip") below the steady value obtained after the CMC. Such a "dip" was not observed in the vicinity of the low-concentration break in the surface tension curve, but can be seen in some of our experiments (e.g., P85) at the high-concentration break. It can thus be concluded that neither polydispersity of the copolymer size nor hydrophobic impurities are causing the low-concentration break observed in the surface tension curves of Pluronic solutions.

It has been proposed that the low-concentration break in the surface tension vs copolymer concentration curves is due to a change in configuration (structural transition) of the copolymer molecules at the air-water interface [Alexandridis et al., 1994b]. Constant surface coverage has been attained at bulk copolymer concentrations ranging from 10^{-6} to 10^{-3} %, with the PEO-PPO-PEO copolymer molecules adsorbed at the interface possibly as an inverted "U" (this is one of the proposed orientations for homopolymer PEO at the

interface [Gallaugher & Hibbert, 1937]) and the PEO chains located at the air/water interface. At a bulk concentration of approximately 10^{-3} %, a structural transition occurs and the copolymer layer becomes more compact; water is expelled [Lo Nostro & Gabrielli, 1993] and PEO segments protrude into the aqueous solution [Phipps et al., 1993] or fold around PPO. More copolymer molecules can fit at the interface (causing it to become thicker [Rennie et al., 1989]) and the surface tension continues to decrease with increasing bulk copolymer concentration but at a slower rate (note also that a bulk concentration of 10^{-3} % is comparable to the bulk PEO concentration required for full coverage of the air/water interface according to Glass [1969] and the bulk PPO concentration at which phase separation occurs [Schwuger, 1973]). Upon the formation of micelles in the bulk, further increase in the number of copolymer molecules in the bulk is accommodated by an increase in the number of micelles, the activity of the copolymer in the bulk remains approximately constant, and the surface tension attains a steady value that does not change with further increase in the bulk copolymer concentration.

The values for surface area per copolymer molecule calculated through the Gibbs adsorption isotherm [Prasad et al., 1979; Alexandridis et al., 1994b] are generally small compared to those of nonionic surfactants with an aliphatic chain and PEO headgroup (of comparable size to the PEO block of Pluronics) [Nikas et al., 1992; Kronberg et al., 1984], indicating that there is considerable folding of the polymers at the air/water interface [Prasad et al., 1979] and/or desorption of PEO segments in the water phase [Aston et al., 1990; Santos Magalhaes et al., 1991]. The area per copolymer molecule increased with the number of EO segments in the molecule for a family of Pluronic copolymers with the same PPO and varying PEO block length [Alexandridis et al., 1994b]. An increase in the length of the hydrophobic (PPO) block, for a group of copolymers that have the same PEO block size, resulted in a decrease in the area that each molecule occupies at the air/water interface, in agreement with Prasad et al. [1979]. This finding suggests a more compact interfacial layer for larger PPO segment size, with the copolymer molecules oriented on the surface in a coiled manner having PPO out of the aqueous phase, and the hydrophilic PEO units at the extremities of the copolymer partly anchoring the polymer in the aqueous phase and partly folding around PPO. Yeates et al. [1986] reported areas per molecule higher for $C_1E_8C_i$ than for $C_iE_{15}C_i$ (C: methyl groups, i = 5-12, E: ethylene oxide groups) indicating again that the hydrophobic moiety makes the interfacial layer more compact.

Phipps et al. [1993] studied the conformation of Pluronic F127 at the hexane/water interface employing a neutron reflectivity technique. Use of hexane was necessary to achieve contrast variation, however the authors report indications that the presence of hexane had little effect on either the adsorbed amount or the conformation of the copolymer on the water side of the interface; in this respect, their findings should also be applicable for copolymers adsorbed at air/water interfaces. F127 was found to adopt a conformation that extended beyond the micellar radius in water and, thus, appeared quite stretched. The estimated (unperturbed) radius of gyration of a PEO block is 2.0 nm and that of the PPO block 1.6 nm; the volume fraction profile of F127 at the interface (fitted from the neutron scattering data) showed the PEO segments to protrude 9 nm into the water subphase and PPO to extent 4 nm in hexane [Phipps et al., 1993]. On the contrary, a random copolymer of poly(vinyl alcohol-*co*-acetate) was found to adopt a very flat conformation at the interface, forming a dense layer of ~2 nm. The experimental findings regarding the conformation of the Pluronic copolymer at the interface were borne out by a Scheutjens-Fleer simulation (similar to the one used to model block copolymer micelles [Linse, 1993; Hurter et al., 1993]) that showed the copolymer attached to the interface by the hydrophobic PPO block and the PEO blocks having a "parabolic" segment density profile, similar to a polymer chain grafted at a solid surface. Both the protrusion of PEO in the water subphase and the resemblance of PEO to a grafted chain agree with the findings of the surface tension study of Alexandridis et al. [1994b].

1.7b Adsorption at solid-water interfaces

The adsorption of several Pluronic copolymers (L61, L62, L64, F38, F68, F88, and F108) onto polystyrene latex particles was described by Kayes and Rawlins [1979]. Langmurian isotherms were obtained, and, in general, maximum adsorption occurred after the measured apparent CMC. The areas occupied by a molecule at the interface in the plateau region of the adsorption isotherm were found to be greater than those observed at the air/water interface [Prasad et al., 1979; Alexandridis et al., 1994b] and considerable less than those at a quartz/water interface (reported in an early study by Heydegger and Dunning [1959]), indicating the importance of the nature of the interface on adsorption. The area-per-molecule values measured were 2.85, 3.20, 5.90, 6.51, 15.10, 17.52, and 24.26 nm^2 for L61, L62, L64, F38, F68, F88, and F108, respectively. Examination of the molecular areas at the interface showed that the adsorbed PPO blocks formed small

loops or were tightly coiled on the surface; this was confirmed by determination of the adsorbed layer thickness from light scattering and electrophoresis experiments [Kayes and Rawlins, 1979].

Baker and Berg [1988] investigated the adsorption configuration of PEO and its copolymers with PPO (Pluronic triblock copolymers P75, P85, F68, F98, F108, and random copolymers 50-HB-260, 50-HB-2000, 50-HB-5100) on model polystyrene latex dispersions. The adsorption isotherms exhibited the expected behavior, with both adlayer thickness and specific adsorption increasing with the PEO block size and the bulk polymer concentration. The thickness isotherms have essentially the same shape as conventional high affinity specific adsorption isotherms, rising rapidly at low concentrations and levelling off at bulk polymer concentrations corresponding to the plateau adsorption coverage. The specific adsorption values for Pluronics reach their plateau values at bulk copolymer concentrations slightly higher than their critical micellization concentrations. In addition, the concentration corresponding to the adsorption plateau is well above the concentration required to create a monolayer of polymer segments at the particle surface (assuming all particles are in contact with the surface). These data suggest that the polymers adsorb in the extended configuration, with thin PPO loops and trains attached to the surface and longer PEO tails extending away from the surface [Baker & Berg, 1988].

Lee et al. [1989] investigated the effect of surface modification of polystyrene latex particles on subsequent protein adsorption; the surface modifiers used were Pluronic copolymers. The hydrodynamic thickness δ_h of the adsorbed (on the particles) copolymers was plotted against the number of EO units [Lee et al., 1989]. The scaling exponent of the fit to the experimental points suggested a coil-like chain conformation for the PEO blocks of the adsorbed copolymers. The dimensions of the adsorbed Pluronic copolymers were smaller than those of the extended rod-like chain, but larger than those of the adsorbed PEO homopolymer. These δ_h values were also larger than the corresponding free surfactant unimer dimensions, suggesting that the picture of "loops and trains" for the hydrophobic PPO block and "loops and tails" for the hydrophilic PEO blocks is a suitable description for the adsorbed copolymers [Lee et al., 1989] in agreement with Baker and Berg [1988].

Killmann et al. [1988] reported the hydrodynamic layer thickness of PEO homopolymer and PEO-PPO-PEO copolymers adsorbed on polystyrene latex and

precipitated silica particles. The conformation of the adsorbed polymer was determined by the surface-polymer interactions; hydrophobic interactions exist on the apolar latex surface, whereas hydrogen bonds dominate on the polar silica surface. PEO-PPO-PEO copolymers adhered to the latex by the hydrophobic PPO segments; the PEO blocks extended into the solution as tails, and the layer thickness depended on the molar mass of the PEO blocks. The adsorption mechanism of PEO-PPO-PEO copolymers on silica resembled that of PEO homopolymer; the adlayer thicknesses of the block copolymers were very small and comparable to the thickness of PEO adlayers on silica [Killmann et al., 1988].

The adsorption of PEO-PPO-PEO block copolymers on silica, as well as the adsorption of PEO homopolymer, has been studied by Tiberg et al. [1991] and Malmsten et al. [1993]. For a number of polymers of a total molecular weight of ~ 15000, it was found that the adsorbed amount is rather low (0.35 - 0.40 mg/m^2) and independent of the PPO content in the range 0 - 30 % PPO. For a copolymer of a total molecular weight of 4000 and 50% PPO content, the adsorbed amount was approximately 0.20 mg/m^2. All polymers investigated formed thin adsorbed layers, with hydrodynamic thicknesses of approximately 2 - 5 nm. The pH dependence of the adsorbed amount and the hydrodynamic thickness was similar to that displayed by PEO homopolymers. Ellipsometry experiments provided information on both adsorption and desorption kinetics, both of which are fast processes in these systems, occurring over minutes. Finally, ellipsometry experiments showed that an abrupt increase in the adsorbed amount occurred prior to micelle formation in the solution. At temperatures above the CMT, the adsorbed amount remained independent of temperature (in the temperature range studied). The hydrodynamic thickness was much smaller than the hydrodynamic diameter of the solution micelles for all temperatures [Malmsten et al., 1993]. No abrupt increase in the adsorbed amount was observed on hydrophobic surfaces, although a strong increase in the adsorbed amount was observed as the system approached the phase boundary. The qualitative aspects of this finding were predicted theoretically as being a consequence of a partial phase separation phenomenon due to elevated copolymer concentration in the surface zone [Tiberg et al., 1991]. The experimental findings were interpreted with a modified mean-field theory which takes the reversed temperature phase behavior of the system into account [Tiberg et al., 1991; Malmsten et al., 1993].

1.8 Gels formed by PEO-PPO-PEO block copolymers

Pluronic copolymer solutions of high polymer concentration exhibit a dramatic change in viscosity at temperatures close to ambient, revealing a "thermoreversible gelation" [Wanka et al., 1990; Brown et al., 1991; Yu et al., 1992; Wang & Johnston, 1991; Schmolka, 1991]. Several mechanisms have been proposed as driving forces for this thermal gelation: Rassing and Attwood [1983] related the gel transition to intrinsic changes in the micellar properties, Vadnere et al. [1984] discussed the gelation in terms of entropic changes involving locally ordered water molecules close to the hydrophobic units, whereas Wanka et al. [1990] and Wang and Johnston [1991] speculated on the possibility of an ordered three-dimensional structured state or network. Recently, neutron scattering studies showed that the observed change in viscosity is due to a "hard-sphere crystallization" as the micelle concentration approaches the critical volume fraction of 0.53 (micelles close-pack) [Mortensen, 1992; Mortensen & Pedersen, 1993]. At even higher temperatures the gel "dissolves" again. The PEO chains in the micellar mantle interpenetrate extensively in the gel, yielding a dynamic correlation length of magnitude 0.8 nm at the highest concentration used (about 0.35 g/mL) [Brown et al., 1992]. Oscillatory shear measurements show that the gelation onset temperature and the thermal stability range of the gel increase with increasing PEO length [Brown et al., 1992].

Ultrasonic relaxation- and ^{13}C-NMR spectra were reported for F127 dissolved in water and D_20, respectively, by Rassing et al. [1984]. The polymer solution exhibited reverse thermal behavior; a 20% w/w solution formed a gel at room temperature. The ultrasonic relaxation, as well as the methyl carbon resonance, of the PPO block showed distinct anomalies over the temperature range where the gel formation takes place. Such anomalies, however, were also observed in dilute solutions where a gel is not being formed. On the basis of the results obtained, it was deduced that observed relaxations arose predominantly from conformational changes related to alternations in the orientation of the methyl group side chains in the PPO block of the polymer. These conformational changes were thought to be induced by extrusion of hydrated water with increasing temperature from the existing micelles, the interiors of which consist of the PPO blocks. It was further proposed that the dehydration causing a higher friction between the end groups in the polymer chain was responsible for the reverse thermal behavior of the viscosity and, hence, for the gel formation in concentrated copolymer solutions [Rassing et al., 1984].

The temperature induced gelation in F127 Pluronic copolymer solutions was reflected in the rapid increase of the storage modulus by two or more orders of magnitude [Wanka et al., 1990]. The storage modulus G' approached a steady value after the gel formation; that value increased with increasing copolymer concentration. The gel formation temperature decreased with increasing polymer concentration. The copolymer gels exhibited a characteristic yield stress at which they flow when stress is applied. The yield value was zero for solutions below the gel temperature, and increased above the gel temperature with further increase in the temperature. The yield value increased with polymer concentration; the highest yield values were above 1000 Pa. Wanka et al. [1990] noted also that the gels were not birefringent, indicating that they were not anisotropic liquid crystalline phases. Brown et al. [1991; 1992] measured the viscoelastic properties of P85, P87, and F88 as a function of temperature. They defined the gelation temperature as the temperature where the storage molulus, G', equaled the loss shear modulus, G''. P85, P87, and F88 showed qualitatively similar gelling behavior, but important quantitative differences were observed [Brown et al., 1992]. P85 formed a gel at 35 °C at copolymer concentration of 20 %; P85 formed a gel over a rather narrow temperature interval (up to 48 °C), whereas P87 and F88 remained gels till 80 °C. The maximum values of G' were similar for F87 and F88 and somewhat smaller for P85. Brown et al. [1992] concluded that the gelation onset temperature and the thermal stability range of the gel increased with increasing PEO block length.

The sol-gel transition temperature was measured as a function of polymer concentration for nine Pluronic copolymers by Vadnere et al. [1984]. The enthalpy of gelation, ΔH°_{gel}, was estimated from a relationship similar to the one used for obtaining ΔH° of micellization from CMC vs temperature data. A positive enthalpy change between 5 and 10 kcal per mol of copolymer was observed in all cases. Unlike gelation of gelatine, where the large enthalpy change (-67 kcal/mol) favors the gelation process, the enthalpy in the case of Pluronics is unfavorable to gelation. The following trends were noted when the polymer concentration required to give a gel transition temperature of 25 °C were plotted as a function of PPO/PEO ratio: the concentration needed for gel formation was approximately the same for copolymers with the same size PPO block; for given PPO/PEO ratio, the polymer concentration required to form a gel (at a given temperature) decreased with increasing molecular weight; a linear relationship was found between $\log M_w$ and 1/T for

copolymers with the same PPO/PEO composition ratio. The presence of NaCl, KCl, and $NaSO_4$ decreased the gel transition temperature, whereas the opposite effect was observed with urea, alcohol and sodium dodecylsulfate. The enthalpy of gel formation was not significantly altered by the added substances, suggesting that entropy plays the major role in the gelation process [Vadnere et al., 1984].

Gilbert et al. [1987a] studied the potential of using F127 gels for controlled drug delivery; they reported the effect of solutes and polymers on the gelation properties. The gelation temperature was determined for a range of F127 concentrations (24 - 34 %) with benzoic acid loading increasing from 0 to 2% w/v. The gel-sol transition temperature decreased as the benzoic acid concentration increased [Gilbert et al., 1987a]. The homologous series of para-hydroxybenzoate esters, methyl, ethyl, propyl, and butyl, were also considered: the more lipophilic compounds resulted in a greater decrease in the gel-sol temperature for all copolymer concentrations studied. Addition of PEO homopolymer increased the gelation temperature, the extent of increase depending on the PEO chain length and concentration.

The effect of additives on gel formation in aqueous F127 solutions has also been reported by Malmsten and Lindman [1992b; 1993]. The stability range of the gel phase depended strongly on the presence of salts. NaCl, which is often referred to as a typical "salting out" cosolute, displaced the whole gel region, as well as the cloud point, to lower temperatures [Malmsten & Lindman, 1992b]. NaSCN, a typical "salting-in" cosolute displaced the whole gel region and the cloud point to higher temperatures [Malmsten & Lindman, 1992b]. The effects of added PEO and PPO homopolymers were also investigated. It was found that PEO of intermediate molecular weight caused the gel to "melt", at an amount of homopolymer which depended on the copolymer concentration. The efficiency of PEO in inducing the gel melting increased with its molecular weight, but at very high PEO molecular weights, phase separation (rather than gel melting) occurred. The gel melting behavior was also observed upon addition of a cationic polyelectrolyte, poly(diallyldimethylammonium chloride) (PDADMAC). Addition of PPO homopolymer, on the other hand, tended to increase the stability region of the gel, depending, however, on the PPO molecular weight [Malmsten & Lindman, 1993].

1.9 Comparison of PEO-PPO copolymers to other nonionic copolymers and surfactants

1.9a PEO-PBO block copolymers

A significant amount of information on the synthesis and solution behavior of block copolymers composed of poly(ethylene oxide) (PEO) and poly(butylene oxide) (PBO) has been reported in the last few years from the group of Attwood, Price, and Booth at the University of Manchester. According to this group, the PEO-PBO-PEO copolymers have the advantage of greater composition and chain length uniformity over comparable PEO-PPO-PEO copolymers. Luo et al. [1992] note that the preparation of PEO-PPO-PEO copolymers involves the anionic polymerization of propylene oxide (PO) to form difunctional PPO, followed by polymerization of ethylene oxide to form the outer blocks; the anionic polymerization of PO is complicated by a side reaction, involving hydrogen abstraction from the methyl group of PO to form allyl alcohol, which leads to initiation of additional monofunctional PPO chains and, in turn, to diblock copolymers with a different PPO content. The anionic polymerization of butylene oxide is more straightforward, since transfer does not occur and difunctional PBO can be exclusively produced.

Luo et al. [1992] prepared by sequential anionic copolymerization a poly(ethylene oxide)-poly(butylene oxide)-poly(ethylene oxide) triblock copolymer, denoted $EO_{58}BO_{17}EO_{58}$, where EO represents ethylene oxide and BO represents butylene oxide, and determined its micellar and gelation properties in aqueous solution. Surface tension, light scattering intensity, photon correlation spectroscopy, and gelation measurements were made at various temperatures over a full concentration range from dilute solution into the gel (> 20 %). Surface tension measurements at 30 °C over the 10^{-3} to 10 g/L concentration range showed a single break at 0.3 g/L, indicative of the CMC. The CMC of the PEO-PBO-PEO copolymer was lower that the CMC of F68, a PEO-PPO-PEO copolymer of comparable molecular weight and PEO composition. The micelle radius was approximately 6 nm, while the micelle "molecular" weight increased with temperature; the aggregation number was 13 at 30 °C and 20 at 55 °C. ΔH° of micellization was estimated to 34 kJ/mol from analyzing CMC vs temperature. The lower and upper temperature boundaries for the gel region were identified, and the occurrence of syneresis (separation of water from the

gel) was noted. Nicholas et al. [1993] compared the micellar and gelation properties of $EO_{58}BO_{17}EO_{58}$, $EO_{71}BO_{28}EO_{71}$, and $EO_{132}BO_{53}EO_{132}$ copolymers in aqueous solutions; the copolymers had similar PEO composition (75-80 wt % PEO) but different chain lengths (molecular weights: 7000, 8800, and 17500, respectively). Measurements were made at 30 °C over the full concentration range from dilute solution into the gel. Critical micelle and gel concentrations decreased markedly as chain length increased, and micellar weights and sizes increased. The CMCs for $EO_{71}BO_{28}EO_{71}$ and $EO_{132}BO_{53}EO_{132}$ were 0.16 and <0.02 g/L, respectively; the aggregation numbers were 40 and 600 for $EO_{71}BO_{28}EO_{71}$ and $EO_{132}BO_{53}EO_{132}$, respectively. Phase separation was observed in dilute solutions of the copolymer of higher molecular weight ($E_{132}B_{53}E_{132}$). The micellar, gelation and drug release properties of aqueous $EO_{40}BO_{15}EO_{40}$ solutions were investigated by Luo et al. [1993]. A brief investigation of the rate of release of salicyclic acid from the gel served to illustrate useful sustained release. The gelation behavior, interpreted via the hard-sphere model, was consistent with the measured micellar sizes.

Diblock PEO-PBO copolymers have also been synthesized and characterized by the Manchester group. Sun et al. [1991] reported preliminary results on the preparation of $EO_{135}BO_{33}$ and its micellization and surface properties in dilute aqueous solutions. Six PEO-PBO diblock copolymers ($EO_{92}BO_7$, $EO_{50}BO_{13}$, $EO_{49}BO_8$, $EO_{50}BO_4$, $EO_{24}BO_{10}$, and $EO_{27}BO_5$) have been prepared by Beddels et al. [1993], and their micellisation in aqueous solution was investigated. Surface tension, static and dynamic light scattering and gel permeation chromatography techniques were used to study solutions at temperatures in the range 20 to 50 °C over a wide concentration range (up to 100 g/L). CMCs, micellar molar masses and radii were reported [Beddels et al. 1993]. The thermodynamics of micellisation of EO_mBO_n diblock copolymers was discussed in relation to that of related triblock copolymers ($EO_mBO_nEO_m$ and $EO_mPO_nEO_m$). Tanodekaew et al. [1993] prepared a series of diblock copolymers $EO_{30}BO_n$ (with n in the range 3 to 16) by sequential anionic polymerization, and investigated the association behavior of the copolymers in aqueous soluiton and the gelation of their concentrated micellar solutions. At temperatures in the range 30 - 50 °C, a minimum PBO-block length of 4 to 5 was required for micellization. Gelation of micellar solutions of the copolymers was observed for copolymers with PBO-block lengths of 6 to 7 units or more. The relationships between (i) standard Gibbs energy of micellization and molecular characteristics and (ii) critical gelation concentration and

micellar characteristics were explored.

1.9b PEO-PS block copolymers

Evidence for the formation of micelles in aqueous solutions of poly(styrene)-poly(ethylene oxide) (PS-PEO) block copolymers has been reported by Bahadur and Sastry [1987], and Riess and Rogez [1982]. The polymers were synthesized with ethylene oxide as the major component in order to make the copolymers water soluble, the polystyrene being extremely hydrophobic. The apparent molecular weight of PS-PEO micelles was found by Riess and Rogez [1982] and Xu et al. [1991; 1992] to increase with increasing copolymer molecular weight and decreasing PEO content. Diblock copolymers formed larger micelles than triblock copolymers. Bahadur and Sastry [1987] found the micelle size to decrease with an increase in PS content, which shows that the micelle size also depends on the insoluble block. Increasing the temperature resulted in the formation of micelles with a smaller hydrodynamic radius. This is probably because water becomes a poorer solvent for ethylene oxide at higher temperatures, so that the corona becomes less swollen with water, resulting in a decrease in the hydrodynamic radius. Critical micelle concentrations of these PS-PEO block copolymers were estimated from the increase of the fluorescence intensity of pyrene with an increase in polymer concentration, and found to be of the order of 1-5 mg/L [Wilhelm et al., 1991]. The micelle/water partition coefficient of pyrene was found to be of the order of 3×10^5, based on the polystyrene volume [Wilhelm et al., 1991].

Gallot et al. [1982] investigated micelle formation in methanol/water mixtures, for several series of PEO-PS block copolymers each having a constant PS chain length, and varying lengths of the PEO block. Light scattering and small angle neutron scattering measurements carried out in methanol showed that the critical micelle concentrations were primarily dependent on the molecular weight of the PS block and that, for a given molecular weight of the PS block, the aggregation number decreased with an increase in the PEO chain length. Despite the decrease in aggregation number, the hydrodynamic radius of the micelles was found to increase with PEO chain length. The SANS results showed the polystyrene core to be compact and small compared to the overall dimensions of the micelles and the micelles to be spherical.

1.9c CiEj surfactants

It is interesting to compare the micellization of Pluronic block copolymers to that of C_iE_j (j-ethyleneglycol-i-alkyl ethers) low molecular-weight nonionic surfactants, which has been more widely studied [Barry & El-Eini, 1976; Meguro et al., 1981]. In the latter systems, it was found that the CMC decreased and that the micellar size increased strongly, both with increasing temperature. Thus, in these respects, the analogy between Pluronics and C_iE_j seems valid. However, the pronounced sensitivity of the CMC to temperature, or of the CMT to concentration, as found here for many Pluronics, is not evident with the n-alkyl poly(ethylene glycol) ethers, C_iE_j [Meguro et al., 1987]. The decrease of the hydrophilicity of the PEO blocks with increasing temperature has comparatively little effect on the CMC for C_iE_j [Meguro et al., 1987]; in the case of Pluronic copolymer solutions, a 10 °C decrease in temperature resulted in changes of the CMC by more than an order of magnitude [Alexandridis et al., 1994a]. The number of EO units has also a small effect on the CMC of C_iE_j surfactants [Meguro et al., 1987; Barry & El-Eini, 1976]; the change in CMC per EO-unit for Pluronic copolymers was smaller than an equivalent change for the C_iE_j, indicating that the influence of PEO block on CMC diminishes as the size of the surfactant increases. The main determinant of the CMC for C_iE_j was found to be the length of the alkyl (hydrophobic) chain. The logarithm of CMC for the C_iE_8, i = 10 - 15, series decreased linearly with increasing carbon number in the alkyl chain (CMC varied by approximately 2.5 orders of magnitude over the carbon number range studied) [Meguro et al., 1981].

The free energy of micellization, ΔG°, decreased with increasing number of carbon atoms in the alkyl chain, and with increasing temperature for j-ethyleneglycol-i-alkyl ethers with the same headgroup (PEO) and varying hydrophobic tail [Meguro et al., 1981; Nandi & Basumallick, 1993]. Free energy changes for micelle formation per methylene group were equal to -0.69 kcal/mol, or -2.887 kJ/mol, to be compared with ΔG°_{-PO-} of approximately -0.45 kJ/mol for the Pluronics. ΔH° decreased with increasing carbon number, while T ΔS° increased, indicating that ΔS° contributes mainly to micellization, while ΔH° counteracts micellization. The headgroup contribution to ΔG° decreased with increasing temperature, attributed to dehydration of the PEO chain. For j-ethyleneglycol-i-alkyl ethers with the same hydrophobic tail and varying PEO headgroup (e.g for the system $C_{16}E_j$, j = 17, 32, 44, 63 [Barry & El-Eini, 1976]) ΔG° increased

(became less negative) with increasing number of EO units in the hydrophilic headgroup, and decreased with increasing temperature. ΔH° and ΔS° decreased with increasing number of EO units, while the headgroup contribution to ΔG° increased with increasing number of EO units.

1.10 Select applications of block copolymer solutions

1.10a Solubilization of organics

An interesting property of aqueous micellar systems is their ability to enhance the solubility in water of otherwise water-insoluble hydrophobic compounds. This occurs because the core of the micelle provides a hydrophobic microenvironment, suitable for solubilizing such molecules. The phenomenon of solubilization forms the basis for many practical applications of amphiphiles. The enhancement in the solubility of lyophobic solutes in solvents afforded by amphiphilic copolymer micelles has shown promise in many industrial and biomedical applications [Hurter et al., 1994].

The solubilization of para-substituted acetanilides in a series of Pluronic PEO-PPO-PEO triblock copolymers depended on both the polymer composition and the nature of the solubilizate [Collett & Tobin, 1979]. The more hydrophobic halogenated acetanilides exhibited a decrease in solubility with an increase in the PEO content, whereas the opposite trend was noted with less hydrophobic drugs such as acetanilide and the hydroxy, methoxy, and ethoxy substituted compounds. The solubility of indomethacin in aqueous solutions of Pluronic copolymers was studied by Lin and Kawashima [1985]. This hydrophobic anti-inflammatory drug was solubilized in significant amounts only above a certain threshold copolymer concentration, most likely related to the CMC. The solubilizing capacity increased with polymer molecular weight, and with temperature. Approximately 0.5 moles indomethacin per mole of surfactant could be solubilized in copolymer solutions [Lin & Kawashima, 1985].

Nagarajan et al. [1986] studied the solubilization of aromatic and aliphatic hydrocarbons in solutions of PEO-PPO and poly(N-vinylpyrrolidone-styrene) (PVP-PS) copolymers. A 10 wt % solution of 12500 molecular weight PEO-PPO (70:30) copolymer

(of undefined blockiness), and a 20% solution of poly(N-vinylpyrrolidone-styrene) (40:60) were used. For both aromatic and aliphatic hydrocarbons, more hydrocarbon was solubilized per gram of polymer in the PVP-PS copolymer than in the PEO-PPO copolymer. This is probably due to the fact that the PEO-PPO copolymer contained only 30% of the hydrophobic PPO constituent, whereas the PVP-PS copolymer contained 60% PS, and that the PS is more hydrophobic than PPO. Nagarajan et al. [1986] also noted that aromatic hydrocarbons were solubilized in larger amounts than the aliphatic hydrocarbons. A Flory-Huggins type interaction parameter between the solubilizate and the polymer block constituting the core, χ_{sc}, was estimated using Hildebrand-Scatchard solubility parameters. It was found that the aromatic hydrocarbons, which had smaller values of χ_{sc}, were solubilized to a greater extent than the aliphatic molecules, which had larger values of χ_{sc}. However there was not a direct correlation between χ_{sc} and the amount solubilized, particularly for the aliphatic molecules which had large χ_{sc} values. For binary mixtures of benzene and hexane, it was shown that the micelles selectively solubilized the aromatic benzene.

An extensive study on the effect of copolymer structure on the solubilization of naphthalene in a range of PEO-PPO-PPO block copolymers has been reported by Hurter and Hatton [1992]. Enhanced solubility of naphthalene in Pluronic copolymer solutions can be achieved. As the PPO/PEO ratio increases, at a given total polymer concentration, the solubility of naphthalene is enhanced. For the majority of the copolymers studied by Hurter and Hatton [1992], the partition coefficient was found to be constant over the entire polymer concentration range probed. A linear relationship between the polymer concentration and the amount of naphthalene solubilized was observed, an indication that the micellar structure did not change significantly in this concentration range, and that increasing the polymer concentration led to an increase in the number of micelles rather than micellar growth [Hurter and Hatton, 1992]. The solubilization of 1,6-diphenyl-1,3,5-hexatriene (DPH), a fluorescence dye, in Pluronic copolymer micelle solutions was investigated by Alexandridis et al. [1994c]. DPH partitioned favorably in the micellar phase, with the partition coefficient higher for P123 (a Pluronic copolymer with 70% PPO), and decreasing in the order of P123 > P103 > P104 = P105 > F127 > P84 > P85 = F108 > F88 > F68 > P65. It can be concluded from these data that the solubilization was influenced form both the relative (with respect to PEO) and absolute size of the hydrophobic PPO block.

1.10b Protection of microorganisms

Insect and mammalian cells are becoming important in the biotechnology industry for the production of complex proteins. These cells are sensitive to shear, and are thus difficult to grow to high cell concentrations such as the ones found in fermentation for the production of antibiotics. Cell death occurs during sparging because of high shear. Copolymers of the Pluronic family have been shown to protect mammalian cells from such damage.

Murhammer and Goochee [1990a; 1990b] examined the structural features of nonionic polyglycol copolymer molecules responsible for the protective effect in sparged animal cell bioreactors. It was shown that the same Pluronics that did not inhibit cell growth were the ones that provided protection from sparging in the bioreactors used in this study. The protective ability of Pluronics was found to correlate with the hydrophilic-lipophilic balance (HLB); the copolymers with the largest HLB (higher PEO content) were the protective agents. The PEO-PPO-PEO copolymers studied were more effective than homopolymer PEO in protecting the microorganisms. Supplementing the medium with 0.2% Pluronic L35 provided significantly more protection to cells growing in a Kontes airlift bioreactor than does 0.2% F68 [Murhammer & Goochee, 1990a]. It was also demonstrated that increasing the Pluronic F68 concentration to 0.5%, which results in a molar concentration comparable to that of 0.2% L35, provided significant cell protection; L35 and F68 appear to be comparable protective agents on a molar basis [Murhammer & Goochee, 1990b].

Zhang et al. [1992] measured the mechanical properties of hybridoma cells taken from a continuous culture in the presence or absence of Pluronic F68 in the medium. The mean bursting membrane tension and the mean elastic area compressibility modulus of the cells were significantly greater in a medium with 0.05% F68, compared to that without Pluronic. The short-term effect of Pluronic was also tested by its addition at various levels up to 0.2% immediately before the mechanical property measurements; a significant short-term effect could only be detected above a threshold concentration of 0.1 % [Zhang et al., 1992]. Orton [1992] found F68 to provide significant protection in mammalian cells in a sparged bubble column reactor. It was observed that when F68 was present in the

medium, cells no longer attached to bubbles and tended to aggregate less among themselves. Orton has also visualized a shedding effect: on a bubble formed in medium without F68, the cells were found to be associated with the bubble surface. In the presence of F68, cells were quickly shed from the gas-liquid interface.

1.10c Medical applications of PEO-PPO-PEO copolymers

Kabanov et al. [1992] prepared "microcontainers" for drug targeting using Pluronic block copolymers. In order to achieve targeting of such microcontainers to a certain cell, the copolymer molecules were conjugated with antibodies against a target-specific antigen or with protein ligands selectively interacting with target cell receptors (proteins were attached to aldehyde-group containing Pluronic molecules using the reductive alkylation reaction). The obtained conjugates were then incorporated into micelles containing solubilized drugs (such as fluorescein isothiocyanate (FITC) and haloperidol) by simple mixing of the corresponding components. It was found that solubilization of FITC in Pluronic micelles considerably influenced its distribution in animal (mouse) tissues, resulting in the drastic increase of FITC fluorescence in lung. The penetration efficienty of FITS in lung tissues increased witn increasing Pluronic hydrophobicity in the series F68, P85, L64. Such behavior was attributed to either different partitioning properties of Pluronics in tissue membranes (recall the study of Atkinson et al. [1988]) or differences in micelle size. Conjugation of FITC-containing micelles with insulin vector resulted in increase of FITC penetration in all tissues, including the brain. Specific targeting of the solubilized FITC in brain was observed when a Pluronic conjugate with antibodies to the antigen of brain glial cell (a_2-glycoprotein) was incorporated into the micelles. A considerable increase of FITC fluorescence in the brain and decrease of its fluorescence in the lungs had been registered under these conditions. The possibility of using micellar microcontainers for targeting of neuroleptics (haloperidol) in brain was also studied. Incorporation of antibodies to a_2-glycoprotein into haloperidol-containing micelles resulted in a drastic increase of drug effect, indicating that vector-containing Pluronic micelles can provide an effective transport of solubilized neuroleptics across blood-brain barrier. The same research group also demonstrated that a low-molecular weight compound (ATP), solubilized in Pluronic micelles acquires the ability to penetrate withion an intact cell in vitro [Slepnev et al., 1992].

Guzman et al. [1992] evaluated Pluronic copolymers gels as a vehicle for subcutaneous administration of drugs using a phenolsulfophthalein (PR) as a tracer. The type of Pluronic copolymer (F108 or F127), their concentrations, and the effect of solutes (NaOH, NaCl or PR) on gelation properties were studied; sodium hydroxide and sodium chloride decreased the gel-sol transition temperature, whereas the opposite effect was observed with PR. The "in vitro" release rates obtained for PR were inversely proportional to the concentration of Pluronic used and a zero-order release rate was observed in all preparations assayed. The amount released at a given time was smaller at high polymer concentrations; this was attributed to the gel matrix being more rigid. Pluronic F127/PR preparations were administered subcutaneously (SC) to Wistar rats; PR plasma levels were compared with those reached after SC or intravenous administration of a PR aqueous solution. The gel formulation produced a sustained plateau level within 15 min that lasted 8-9 h. Good fits for experimental in vivo data from Pluronic gels were obtained using a zero-order input and first-order output two-compartment pharmacokinetics model; the fitted parameters of the model indicate that release of PR from the gel controlled the PR absorption process. The results obtained suggest that F127 aqueous gels may be of practical use as a vehicle for SC administration of drugs.

The adsorption of PPO-PEO copolymers at surfaces as a means of preventing protein adsorption at these surfaces has been explored by Lee et al. [1989] and Amiji and Park [1992]. Proteins adsorb to almost all surfaces during the first few minutes of blood exposure. There has been much effort in minimizing or eliminating protein adsorption, because surfaces showing minimal protein adsorption are important in many applications, including devices that come in contact with blood, membranes for separation processes, contact lenses [Lee et al., 1989]. Lee et al. [1989] found adsorption of human albumin on low density polyethylene (LDPE) surfaces treated with copolymer to be significantly decreased as compared with the untreated surface. The protein resistance to the copolymer-treated surface was highly dependent on the amount of copolymer adsorbed and on the mobility of the PEO segments. Starlike PEO-PPO block copolymers were found to have better adsorption properties than triblocks. Despite the favorable results, the authors voice concern over the stability of the adsorbed copolymer layer and the possible desorption of the copolymers into the treated medium [Lee et al., 1989].

Amiji and Park [1992] examined adsorption of fibrinogen and platelet adhesion

onto dimethyldichlorosilane-treated glass and LDPE surfaces treated with PEO homopolymer and various PEO-PPO-PEO block copolymers. PEO could not prevent platelet adhesion and activation, even when the bulk PEO concentration for adsorption was increased to 10 mg/ml. Pluronics containing 30 PO segments could not prevent platelet adhesion and activation, although the number of EO segments varied up to 76. Pluronics containing 56 PO segments inhibited platelet adhesion and activation, although the number of EO segments was as small as 19. Fibrinogen adsorption on the Pluronic-coated surfaces was reduced by more than 95% compared to adsorption on control surfaces. The ability of Pluronics to prevent platelet adhesion and activation was mainly dependent on the number of PO segments, rather than the number of EO segments [Amiji & Park, 1992]. This was contrary to the findings of Lee et al. [1992] who suggested that copolymer with large PPO block do no adsorb well because they form micelles in solution; it should be noted though, that the number of Pluronic copolymers studied by Lee et al. was rather limited. According to Amiji and Park [1992], the PO segments were responsible for attaching the copolymer to the surface and the EO segments for repelling fibrinogen and platelets by a steric repulsion mechanism.

1.11 Dynamics of micelle and gel formation

The kinetics of micelle formation in aqueous solutions of low-molecular-weight surfactants have attracted considerable attention. In general, two relaxation processes have been observed: a fast process (μs - ms time range) attributed to a surfactant molecule entering or exiting a micelle, and a slower process (ms - s time range) due to micelle assembly or dissociation [Aniansson et al., 1976]. The large molecular weight and chain-like structure of block copolymer molecules is expected to complicate the processes of micelle formation and exchange of copolymer molecules between micelles and the bulk solution; disentanglement of copolymer molecules from the micelles should result in time scales slower than the ones observed in conventional surfactants. Linse and Malmsten [1992] and Malmsten and Lindman [1992a] followed the temperature dependence of the F127 micellization process by performing gel-permeation chromatography (GPC) experiments at different temperatures. The micelle fraction appeared as a separate peak in the chromatogram; this led the authors to the conclusion that the residence time of the polymer molecules in the F127 micelles is extremely long (~hours). However, Fleischer

[1993] reported that the lifetime of a copolymer molecule within the micelle was shorter that the minimum observation time of the experiments (≈ 3 ms). He reached this conclusion from PFG-NMR measurements of F127 copolymer self-diffusion: since unimers and micelles coexist in the solution, Fleischer expected to observe two self-diffusion coefficients, one for the unimers, and one for the micelles, if there were no exchange of the molecules between the two states within the diffusion time. A single diffusion coefficient was, nevertheless, observed, and thus Fleischer [1993] inferred that the copolymer solution was in the dynamic range of fast exchange.

Kinetics of gelation for aqueous solutions of Pluronic F98 and F127 copolymers were investigated by Wang and Johnston [1991] using pulse shearometry. The pulse shearometer was designed to measure the propagation velocity (and from this the dynamic shear modulus) of a shear wave through a viscoelastic material that has been subjected to conditions of non-steady shear. Three distinct linear phases were observed for the log dynamic shear modulus (G') vs time profiles as copolymer solutions of varying concentrations were allowed to passively warm at room temperature to a temperature exceeding the sol-to-gel transition temperature, T_m. The initial exponential phase was due to warming, while the beginning of the second exponential phase coincided with the onset of the gelation process as determined by visual observation. The third exponential phase was attributed to the rate of formation of the polymer network (gelation appeared to be complete at the beginning of this phase). A comparison of F127 (30%, T_m =10.9 °C) and F98 (37%, T_m=11.1 °C) would suggest that the concentration of copolymer required to achieve a certain gelation temperature decreases with increasing molecular weight of the PPO block of the copolymer. Characteristic times for gelation were 17 and 9 mins for 20 and 30 % F127, respectively, and 43, 30 mins for 20, 30 % F98, respectively; the gelation process was more rapid for F127 (at a given concentration) and the times decreased with increasing concentration for a given copolymer. Wang and Johnston [1991] suggested that the rate of gelation for the Pluronic solutions studied was dependent on the rate of heat transfer through the polymer solution (copolymer solutions were allowed to passively warm at room temperature). If this statement is true then the attribution by the authors of the time-dependent results to "kinetics of gelation" is erroneous, and the time-scales the reported were actually kinetics of heat transfer. It becomes obvious from the above, that the dynamics of block copolymer micelle and gel formation, although important from a theoretical and practical point of view, are still unexplored and not well understood.

1.12 Conclusions

The phase behavior and aggregation properties of poly(ethylene oxide)-*block*-poly(propylene oxide)-*block*-poly(ethylene oxide) (PEO-PPO-PEO) copolymers in solution, as affected by the polymer molecular composition and concentration, additives, and solution temperature, are important in understanding the mechanism of copolymer action underlying the various applications. While the PEO-PPO-PEO copolymers exist in solution as individual coils (unimers) at low temperatures and/or concentrations, micelles are formed with increasing the copolymer concentration and/or solution temperature, as revealed by light scattering and dye solubilization experiments. The unimer-to-micelle transition is not sharp, but spans a concentration decade or 10 °C. The critical micellization concentrations (CMC) and temperatures (CMT) decrease with increase in the copolymer PPO content or molecular weight, and in the presence of salts. The dependence of CMC on temperature and differential scanning calorimetry indicate that the micellization process is endothermic and driven by the entropy gain in water when unimers aggregate to form micelles (hydrophobic effect) and the decrease in polarity of EO and PO as temperature increases. The free energy and enthalpy of micellization can be correlated to the number of EO and PO segments in the copolymer and its molecular weight. The micelles have hydrodynamic radii of approximately 10 nm and aggregation numbers in the order of 50. The aggregation number is thought to be independent of concentration and to increase with temperature, although there is no clear consensus for the latter. Phenomenological and mean-field lattice models for the formation of micelles can capture qualitatively the trends observed experimentally. A self-consistent mean-field theory was able to reproduce the anomalous phase behavior of PEO and PPO homopolymers, predict the micellization behavior of PEO-PPO-PEO block copolymers, and provide detailed information on the distribution of the copolymer segments in the micelles. The model calculations showed qualitative agreement with experimental predictions on the effect of temperature, concentration, hydrophobicity, and molecular weight of the polymer; quantitative agreement was also good, considering that all the model input parameters were obtained from independent experiments. The PEO-PPO-PEO copolymers adsorb on air-water and solid-water interfaces; for copolymers adsorbed at hydrophobic interfaces, the PPO block is located at the interface while the PEO block extends into the solution. Gels are formed

by certain PEO-PPO-PEO block copolymers at high concentrations, while the micelles remain apparently intact in the form of a "crystal". The gelation onset temperature and the thermal stability range of the gel increase with increasing PEO block length.

1.13 References Cited in Chapter 1

1. Alexandridis, P.; Holzwarth, J. F.; Hatton, T. A. *Macromolecules* **1994**, *27*, 2414; Chapter 2 of this Thesis.
2. Alexandridis, P.; Athanassiou, V.; Fukuda, S.; Hatton, T. A. *Langmuir* **1994b**, in press; Chapter 4 of this Thesis.
3. Alexandridis, P.; Holzwarth, J. F.; Hatton, T. A. Manuscript in preparation, 1994c; Chapter 7 of this Thesis.
4. Almgren, M.; Stam, J. v.; Lindblad, C.; Li, P.; Stilbs, P.; Bahadur, P. *J. Phys. Chem.* **1991**, *95*, 5677.
5. Almgren, M.; Bahadur, P.; Jansson, M.; Li, P.; Brown, W.; Bahadur, A. *J. Colloid Interface Sci.* **1992**, *151*, 157.
6. Al-Saden, A. A.; Whateley, T. L.; Florence, A. T. *J. Colloid Interface Sci.* **1982**, *90*, 303.
7 Amiji, M.; Park, K. *Biomaterials* **1992**, *13*, 682.
8. Ananthapadmanabhan, K. P.; Goddard, E. D.; Turro, N. J.; Kuo, P. L. *Langmuir* **1985**, *1*, 352.
9. Anderson, R. A. *Pharm. Acta Helv.* **1972**, *47*, 304.
10 Aniansson, E. A. G.; Wall, S. N.; Almgren, M.; Hoffmann, H.; Ulbricht, W.; Zana, R.; Lang, J.; Tondre, C. *J. Phys. Chem.* **1976**, *80*, 905.
11. Armstrong, J. K.; Parsonage, J.; Chowdhry, B.; Leharne, S.; Mitchell, J.; Beezer, A.; Lohner, K.; Laggner, P. *J. Phys. Chem.* **1993**, *97*, 3904.
12. Aston, M. S.; Herrington, T. M.; Tadros, T. F. *Colloids and Surfaces* **1990**, *51*, 115.
13. Attwood, D., Florence, A. T. *Surfactant Systems: Their Chemistry, Pharmacy and Biology*; Chapman and Hall: London, 1983.
14. Attwood, D.; Collet, J. H.; Tait, C.J. *Int. J. Pharm.* **1985**, *26*, 25.
15. Bahadur, P.; Sastry, N. V. *Eur. Polym. J.* **1987**, *24*, 285.
16. Bahadur, P.; Riess, G. *Tenside Surf. Det.* **1991**, *28*, 173.

17. Bahadur, P.; Pandya, K. *Langmuir* **1992**, *8*, 2666.
18. Bahadur, P.; Li, P.; Almgren, M.; Brown, W. *Langmuir* **1992**, *8*, 1903.
19. Bahadur, P.; Pandya, K.; Almgren, M., Li, P.; Stilbs, P. *Colloid Polym. Sci* **1993**, *271*, 657.
20. Baker, J. A.; Berg, J. C. *Langmuir* **1988**, *4*, 1055.
21. Balsara, N. P.; Tirrell, M.; Lodge, T. P. *Macromolecules* **1991**, *24*, 1975.
22. Barry, B. W.; El-Eini, D. I. D. *J. Colloid Interface Sci.* **1976**, *54*, 339.
23. Beddels, A. D.; Arafeh, R. M.; Yang, Z.; Attwood, D.; Heatley, F.; Padget, J. C.; Price, C.; Booth, C. *J. Chem. Soc. Faraday Trans.* **1993**, *89*, 1235.
24. Beezer, A.; Mitchard, N.; Mitchell, J. C.; Armstrong, J. K.; Chowdhry, B.; Leharne, S.; Buckton, G. *J. Chem. Res. (S)* **1992**, 236.
25. Ben-Naim, A. *Hydrophobic Interactions*, Plenum Press, New York, NY, 1080.
26. Brown, W.; Schillen, K.; Almgren, M.; Hvidt, S.; Bahadur, P. *J. Phys. Chem.* **1991**, *95*, 1850.
27. Brown, W.; Schillen, K.; Hvidt, S. *J. Phys. Chem.* **1992**, *96*, 6038.
28. Chattopadhyay, A.; London, E. *Anal. Biochem.* **1984**, *139*, 408.
29. Chattoraj, D. K.; Birdi, K. S. *Adsorption and the Gibbs Surface Excess*, Plenum Press, New York, NY, 1984.
30. Colett, J. H.; Tobin, E. A. *J. Pharm. Pharmacol.* **1979**, *31*, 174.
31. Crook, E. H.; Fordyce, D. B.; Trebbi, G. F. *J. Phys. Chem.* **1963**, *67*, 1987.
32. Edwards, D. A.; Luthy, R. G.; Liu, Z. *Environ. Sci. Technol.* **1991**, *25*, 127.
33. Evers, O. A.; Scheutjens, J. M. H. M.; Fleer, G. J. *Macromolecules* **1990**, *23*, 5221.
34. Fleischer, G. *J. Phys. Chem.* **1993**, *97*, 517.
35. Fleischer, G.; Bloss, P.; Hergerth, W. D. *Colloid Polym. Sci.* **1993**, *271*, 217.
36. Flory, P. *Principles of Polymer Chemistry*; Cornell University : Ithaca, NY, 1953.
37. Gallaugher, A. F.; Hibbert, H. *J. Am. Chem. Soc.* **1937**, *59*, 2514.
38. Gallot, Y.; Selb, J.; Marie, P.; Rameau, A. *ACS Polym. Prepr.* **1982**, *23*, 16.
39. Gilbert, J. C.; Washington, C.; Davies, M. C.; Hadgraft, J. *Int. J. Pharm.* **1987**, *40*, 93.
40. Gilbert, J. C.; Richardson, J. L.; Davies, M. C.; Palin, K. J.; Hadgraft, J. *J. Controlled Release* **1987**, *5*, 113.
41. Glass, J. E. *J. Phys. Chem.* **1969**, *72*, 4459.
42. Grieser, F.; Drummond, C. J. *J. Phys. Chem.* **1988**, *92*, 5580.

43. Guzman, M.; Garcia, F. F.; Molpeceres, J.; Aberturas, M. R. *Int. J. Pharm.* **1992**, *80*, 119.
44. Halperin, A. *Macromolecules* **1987**, *20*, 2943.
45. Hall, D. G.; Pethica, B. A., Chapter 16 in *Nonionic Surfactants*, Schick, M.J. (Ed.), Marcel Dekker, 1967.
46. Hecht, E.; Hoffmann, H. *Langmuir* **1994**, *10*, 86.
47. Heydegger, H. R.; Duning, H. N. *J. Phys. Chem.* **1959**, *63*, 1613.
48. Hiemenz, P. C. *Principles of Colloid and Surface Chemistry*, 2nd ed.; Marcel Dekker, Inc.: New York, 1986; p 446.
49. Hill, T. L. *Thermodynamics of Small Systems, Vol. 1*, Benjamin, 1963.
50. Hill, T. L. *Thermodynamics of Small Systems, Vol. 2*, Benjamin, 1964.
51. Hunter, R. J. *Foundations of Colloid Science*; Oxford University Press: New York, 1987; Vol. 1.
52. Hurter, P. N.; Hatton, T. A. *Langmuir* **1992**, *8*, 1291.
53. Hurter, P. N.; Scheutjens, J. M. H. M.; Hatton, T. A. *Macromolecules* **1993**, *26*, 5030.
54. Hurter, P. N.; Scheutjens, J. M. H. M.; Hatton, T. A. *Macromolecules* **1993**, *26*, 5592.
55. Hurter, P. N.; Alexandridis, P.; Hatton, T. A. in *Solubilization*, Christian, S. D.; Scamehorn, J. F. (Eds.), Marcel Dekker, 1994, in press.
56. Izzo, D.; Marques, C. M. *Macromolecules* **1993**, *26*, 7189.
57. Kabanov, A. V.; Batrakova, E. V.; Melik-Nubarov, N. S.; Fedoseev, N. A.; Dorodnich, T. Yu.; Alakhov, V. Yu.; Chekhonin, V. P.; Nazalova, I. R.; Kabanov, V. A. *J. Controlled Release* **1992**, *22*, 141.
58. Kabanov, A. V.; Slepnev, V. I.; Kuznetsova, L. E.; Batrakova, E. V.; Alakhov, V. Yu.; Melik-Nubarov, N. S.; Sveshnikov, P. G.; Kabanov, V. A. *Biochem. Int.* **1992**, *26*, 1035.
59. Karlstrom, G. *J. Phys. Chem.* **1985**, *89*, 4962.
60. Kayes, J. B.; Rawlins, D. A. *Colloid Polym. Sci.* **1979**, *257*, 622.
61. Killmann, E.; Maier, H.; Baker, J. A. *Colloids Surfaces* **1988**, *31*, 51.
62. Kronberg, B.; Stenius, P.; Thorssell, Y. *Colloids and Surfaces* **1984**, *12*, 113.
63. Lee, J.; Martic, P. A.; Tan, J. S. *J. Colloid Interface Sci.* **1989**, *131*, 252.
64. Lee, J.-H.; Kopecek, J.; Andrade, J. D. *J. Biomed. Mat. Res.* **1989**, *23*, 351.
65. Leermakers, F. A. M. *Ph.D. Thesis*, Wagenigen Agricultural University,

Wagenigen, 1988.

66. Leermakers, F. A. M.; van der Schoot, P. P. A. M.; Scheutjens, J. M. H. M.; Lyklema, J. in *The Equilibrium Structure of Micelles* Mittal, K. L. (Ed.), Plenum, 1989.
67. Leermakers, F. A. M.; Scheutjens, J. M. H. M. *J. Phys. Chem.* **1989**, *93*, 7417.
68. Leibler, L.; Orland, H.; Wheeler, J. C. *J. Chem. Phys.* **1983**, *79*, 3550.
69. Lin, S.-Y.; Kawashima, Y. *Pharm. Acta Helv.* **1985**, *60*, 339.
70. Linse, P. *Macromolecules* **1993**, *26*, 4437.
71. Linse, P. *J. Phys. Chem.* **1993**, *97*, 13896.
72. Linse, P.; Malmsten, M. *Macromolecules* **1992**, *25*, 5434.
73. Lo Nostro, P.; Gabrielli, G. *Langmuir* **1993**, *9*, 3132.
74. Luo, Y.-Z.; Nicholas, C. V.; Attwood, D.; Collet, J. H.; Price, C.; Booth, C. *Colloid Polym. Sci.* **1992**, *270*, 1094.
75. Luo, Y.-Z.; Nicholas, C. V.; Attwood, D.; Collet, J. H.; Price, C.; Booth, C.; Chu, B.; Zhou, Z.-K. *J. Chem. Soc. Faraday Trans.* **1993**, *89*, 539.
76. Malmsten, M.; Lindman, B. *Macromolecules* **1992**, *25*, 5440.
77. Malmsten, M.; Lindman, B. *Macromolecules* **1992**, *25*, 5446.
78. Malmsten, M.; Lindman, B. *Macromolecules* **1993**, *26*, 1282.
79. Malmsten, M.; Linse, P.; Cosgrove, T. *Macromolecules* **1992**, *25*, 2474.
80. Malmsten, M.; Linse, P.; Zhang, K.-W. *Macromolecules* **1993**, *26*, 2905.
81. Marques, C. M. *Macromolecules* **1988**, *21*, 1051.
82. Meguro, K.; Takasawa, Y.; Kawahashi, N.; Tabata, Y.; Ueno, M. *J. Colloid Interface Sci.* **1981**, *83*, 50.
83. Meguro, K.; Ueno, M.; Esumi, K. in *Nonionic Surfactants: Physical Chemistry*; Schick, M.J., Ed. Marcel Dekker Inc.: New York, 1987, p109.
84. Mitchard, N. M.; Beezer, A. E.; Mitchell, J. C.; Armstrong, J. K.; Chowdhry, B. Z.; Leharne, S.; Buckton, G. *J. Phys. Chem.* **1992**, *96*, 9507.
85. Mortensen, K. *Europhys. Lett.* **1992**, *19*, 599.
86. Mortensen, K.; Brown, W.; Norden, B. *Phys. Rev. Lett.* **1992**, *68*, 3240.
87. Mortensen, K.; Brown, W. *Macromolecules* **1993**, *26*, 4128.
88. Mortensen, K.; Pedersen, J. S. *Macromolecules* **1993**, *26*, 805.
89. Mukerjee, P.; Mysels, K. J. *Critical Micelle Concentrations of Aqueous Surfactant Systems*, NSRDS-NBS 36, Government Printing Office, Washington, DC, 1971.
90. Munch, M. R.; Gast, A. P. *Macromolecules* **1988**, *21*, 1360.

91. Murhammer, D. W.; Goochee, C. F. *Biotechnol. Prog.* **1990**, *6*, 142.
92. Murhammer, D. W.; Goochee, C. F. *Biotechnol. Prog.* **1990**, *6*, 391.
93. Mysels, K. J. *Langmuir* **1986**, *2*, 423.
94. Nagarajan, R.; Barry, M.; Ruckenstein, E. *Langmuir* **1986**, *2*, 210.
95. Nagarajan, R.; Ganesh, K. *J. Chem. Phys.* **1989**, *90*, 5843.
96. Nagarajan, R.; Ganesh, K. *Macromolecules* **1989**, *22*, 4312.
97. Nandi, N.; Basumallick, I. N. *J. Phys. Chem.* **1993**, *97*, 3900.
98. Nicholas, C. V.; Luo, Y.-Z.; Deng, N.-J.; Attwood, D.; Collet, J. H.; Price, C.; Booth, C. *Polymer* **1993**, *34*, 138.
99. Nikas, Y. J.; Puvvada, S.; Blankschtein, D. *Langmuir* **1992**, *8*, 2680.
100. Noolandi, J.; Hong, K. M. *Macromolecules* **1983**, *16*, 1443.
101. Orton, D. E. *Quantitative and Mechanistic Effects of Bubble Aeration on Animal Cells in Culture*, Ph.D. Thesis, Massachusetts Institute of Technology, Cambridge, MA, 1992.
102. Pandya, K.; Lad, K.; Bahadur, P. *J. Macromolec. Sci.-Pure Appl. Chem.* **1993**, *A30*, 1.
103. Pandya, K.; Bahadur, P.; Nagar, T. N.; Bahadur, A. *Colloids and Surfaces* **1993**, *70*, 219.
104. Phipps, J. S.; Richardson, R. M.; Cosgrove, T.; Eaglesham, A. *Langmuir* **1993**, *9*, 3530.
105. *Pluronic and Tetronic Surfactants*, Technical Brochure, BASF Corp., Parcippany, NJ, 1989.
106. Prasad, K. N.; Luong, T. T.; Florence, A. T.; Paris, J.; Vaution, C.; Seiller, M.; Puisieux, F. *J. Colloid Interface Sci.* **1979**, *69*, 225.
107. Price, C. *Pure Appl. Chem.* **1983**, *55*, 1563.
108. Prochazka, O.; Tuzar, Z.; Kratochvil, P. *Polymer* **1991** *32*, 3038.
109. Rassing, J.; Attwood, D. *Int. J. Pharm.* **1983**, *13*, 47.
110. Rassing, J.; McKenna, W. P.; Bandyopadhyay, S.; Eyring, E. *J. Mol. Liq.* **1984**, *27*, 165.
111. Reddy, N. K.; Fordham, P. J.; Attwood, D.; Booth C. *J. Chem. Soc., Faraday Trans.* **1991**, *86*, 1569.
112. Rennie, A. R.; Crawford, R. J.; Lee, E. M.; Thomas, R. K.; Crowley, T. L.; Roberts, S.; Qureshi, M. S.; Richards, R. W. *Macromolecules* **1989**, *22*, 3466.
113. Riess, G.; Rogez, D. *ACS Polym. Prepr.* **1982**, *23*, 19.

114. Santos Magalhaes, N. S.; Benita, S.; Baszkin, A. *Colloids Surfaces* **1991**, *52*, 195.
115. Scheutjens, J. M. H. M., Fleer, G. J. *J. Phys. Chem.* **1979**, *83*, 1619.
116. Scheutjens, J. M. H. M.; Fleer, G. J. *Macromolecules* **1995**, *18*, 1882.
117. Scheutjens, J. M. H. M.; Leermakers, F. A. M.; Besseling, N. A. M.; Lyklema, J. in *Surfactants in Solution, Vol 7*, Mittal, K.L. (Ed.), Plenum, 1989.
118. Schmolka, I. R., Raymond, A. J. *J. Am. Oil Chem. Soc.* **1965**, *42*, 1088.
119. Schmolka, I. R. *J. Am. Oil Chem. Soc.* **1977**, *54*, 110.
120. Schmolka, I. R. *J. Am. Oil Chem. Soc.* **1991**, *69*, 206.
121. Schwuger, M. J. *J. Colloid Interface Sci.* **1973**, *43*, 491.
122. Semenov, A. N. *Sov. Phys. JETP* **1985**, *61*, 733.
123. Sikora, A.; Tuzar, Z. *Makromol. Chem.* **1983**, *184*, 2049.
124. Slepnev, V. I.; Kuznetsova, L. E.; Gubin, A. N.; Batrakova, E. V.; Alakhov, V. Yu.; Kabanov, A. V. *Biochem. Int.* **1992**, *26*, 587.
125. Sun, W.-B.; Ding, J.-F.; Mobbs, R. H.; Heatley, F.; Attwood, D.; Booth, C. *Colloids Surfaces* **1991**, *54*, 103.
126. Tanford, C. *The Hydrophobic Effect: Formation of Micelles and Biological Membranes*, 2nd ed.; J. Wiley & Sons: New York, 1980.
127. Tanodekaew, S.; Deng, N.-J.; Smith, S.; Yang, Y.-W.; Attwood, D.; Booth, C. *J. Phys. Chem.* **1993**, *97*, 11847.
128. ten Brinke, G.; Hadziioannou, G. *Macromolecules* **1987**, *20*, 486.
129. Tiberg, F.; Malmsten, M.; Linse, P.; Lindman, B. *Langmuir* **1991**, *7*, 2723.
130. Turro, N. J.; Chung, C. *Macromolecules* **1984**, *17*, 2123.
131. Tuzar, Z.; Kratochvil, P. *Adv. Colloid Interface Sci.* **1976**, *6*, 201.
132. Vandere, M.: Amidon, G. L.; Lindenbaum, S.; Haslam, J. L. *Int. J. Pharm.* **1984**, *22*, 207.
133. van Lent, B.; Scheutjens, J. M. H. M. *Macromolecules* **1989**, *22*, 1931.
134. Wang, P.; Johnston, T. P. *J. Appl. Polym. Sci.* **1991**, *43*, 283.
135. Wang, Y.; Mattice, W. L.; Napper, D. H. *Langmuir* **1993**, *9*, 66.
136. Wanka, G.; Hoffmann, H.; Ulbricht, W. *Colloid Polym. Sci.* **1990**, *266*, 101.
137. Wilhelm, M.; Zhao, C.-L.; Wang, Y.; Xu, R.; Winnik, M.A.; Mura, J.-L.; Riess, G.; Croucher, M. D. *Macromolecules* **1991**, *24*, 1033.
138. Williams, R. K.; Simard, M. A.; Jolicoeur, C. *J. Phys. Chem.* **1985**, *89*, 178.
139. Xu, R.; Winnik, M. A.; Hallett, F. R.; Riess, G.; Croucher, M. D.

Macromolecules **1991**, *24*, 87.

140. Xu, R.; Winnik, M. A.; Riess, G.; Chu, B.; Croucher, M. D. *Macromolecules* **1992**, *25*, 644.
141. Yeates, S. G.; Craven, J. R.; Mobbs, R. H.; Booth, C. *J. Chem. Soc. Faraday Trans. 1* **1986**, *82*, 1865.
142. Yokoyama, M. *Crit. Rev. Therapeutic Drug Carrier Systems* **1992**, *9*, 213.
143. Yu, G.-E.; Deng, Y.; Dalton, S.; Wang, Q.-G.; Attwood, D.; Price, C.; Booth C. *J. Chem. Soc., Faraday Trans.* **1992**, *88*, 2537.
144. Zhang, Z.; Al-Rubeai, M; Thomas, C. R. *Enzyme Microb. Technol.* **1992**, *14*, 980.
145. Zhou, Z.; Chu, B. *J. Colloid Interface Sci.* **1988**, *126*, 171.
146. Zhou, Z.; Chu, B. *Macromolecules* **1987**, *21*, 2548.
147. Zhulina, Y. B.; Birshtein, T. M. *Polym. Sci. USSR (Engl. Transl.)* **1986**, *12*, 2880.

Chapter 1: List of Tables and Figures

Table 1.1 Properties of the Pluronic PEO-PPO-PEO copolymers.

A	B	C	D	E	F	G	H	I
L35	1900	50	7	375	49	25	73	18-23
F38	4700	80	48	260	52	35	>100	>24
L42	1630	20	-26	280	46	0	37	7-12
L43	1850	30	-1	310	47	0	42	7-12
L44	2200	40	16	440	45	25	65	12-18
L62	2500	20	-4	450	43	25	32	1-7
L63	2650	30	10	490	43	30	34	7-12
L64	2900	40	16	850	43	40	58	12-18
P65	3400	50	27	180	46	70	82	12-18
F68	8400	80	52	1000	50	35	>100	>24
L72	2750	20	-7	510	39	15	25	1-7
P75	4150	50	27	250	43	100	82	12-18
F77	6600	70	48	480	47	100	>100	>24
P84	4200	40	34	280	42	90	74	12-18
P85	4600	50	34	310	42	70	85	12-18
F87	7700	70	49	700	44	80	>100	>24
F88	11400	80	54	2300	48	80	>100	>24
F98	13000	80	58	2700	43	40	>100	>24
P103	4950	30	30	285	34	40	86	7-12
P104	5900	40	32	390	33	50	81	12-18
P105	6500	50	35	750	39	40	91	12-18
F108	14600	80	57	2800	41	40	>100	>24
L122	5000	20	20	1750	33	20	19	1-7
P123	5750	30	31	350	34	45	90	7-12
F127	12600	70	56	3100	41	40	>100	18-23

A: Copolymer
B: Average molecular weight
C: PEO wt.%
D: Melt/pour point (°C)
E: Viscosity (Brookfield) (cps; liquids at 25 °C, pastes at 60 °C, solids at 77 °C)
F: Surface tension at 0.1%, 25 °C (dynes/cm)
G: Foam height (mm) (Ross Miles, 0.1% at 50 °C)
H: Cloud point in aqueous 1% solution (°C)
I: HLB (hydrophilic-lipophilic balance)

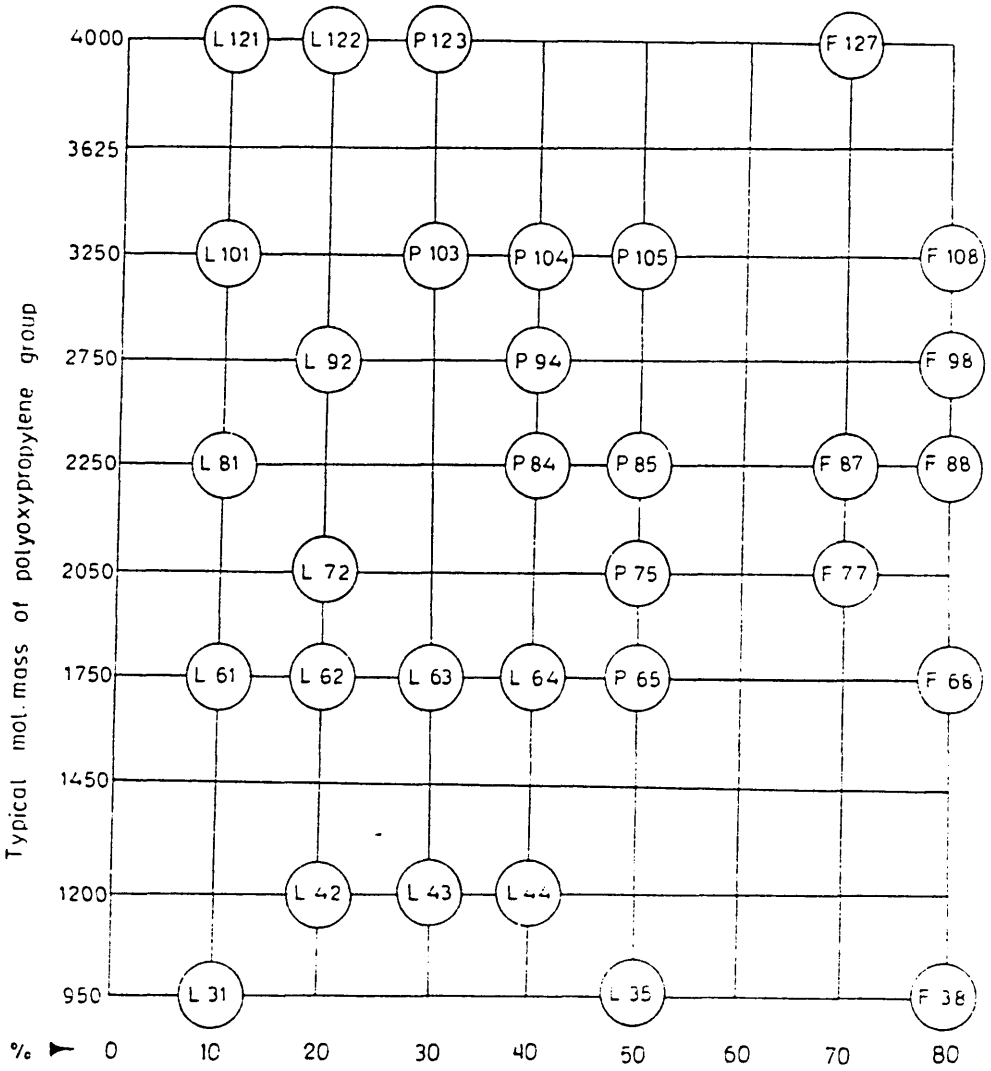

Percentage of ethylene oxide in a molecule - the Pluronic grid

Figure 1.1 Pluronic copolymers arranged in the "Pluronic grid". The copolymers along the vertical lines have the same PPO/PEO composition, while the copolymers along the horizontal lines have PPO block of the same length. [Bahadur & Riess, 1991; BASF Corp., 1989]

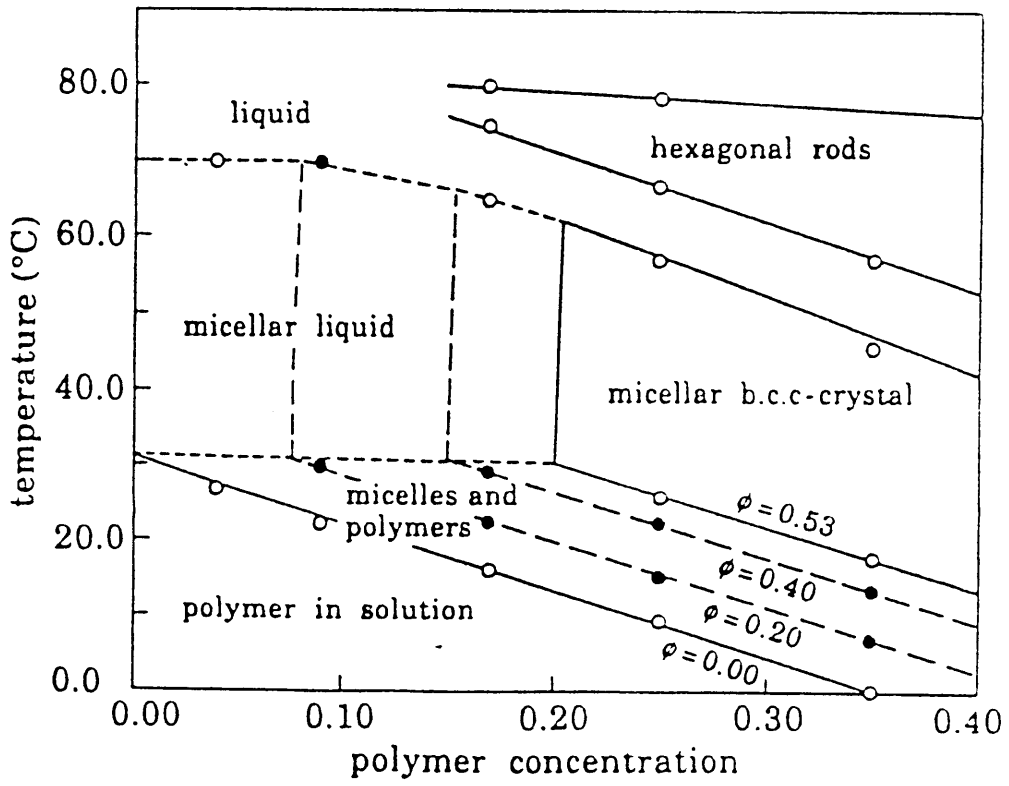

Figure 1.2 Phase diagram of aqueous P85 solution, showing the fully dissolved polymers at low temperature and concentrations, the CMC-CMT line (ϕ=0), the ϕ_c=0.53 transition to b.c.c. micellar crystal, and the high-temperature hexagonal phase (ϕ is the hard-sphere micelle volume fraction). At T ≈ 60 °C a liquid phase appears between the crystalline b.c.c. and hexagonal phases. [Mortensen, 1992]

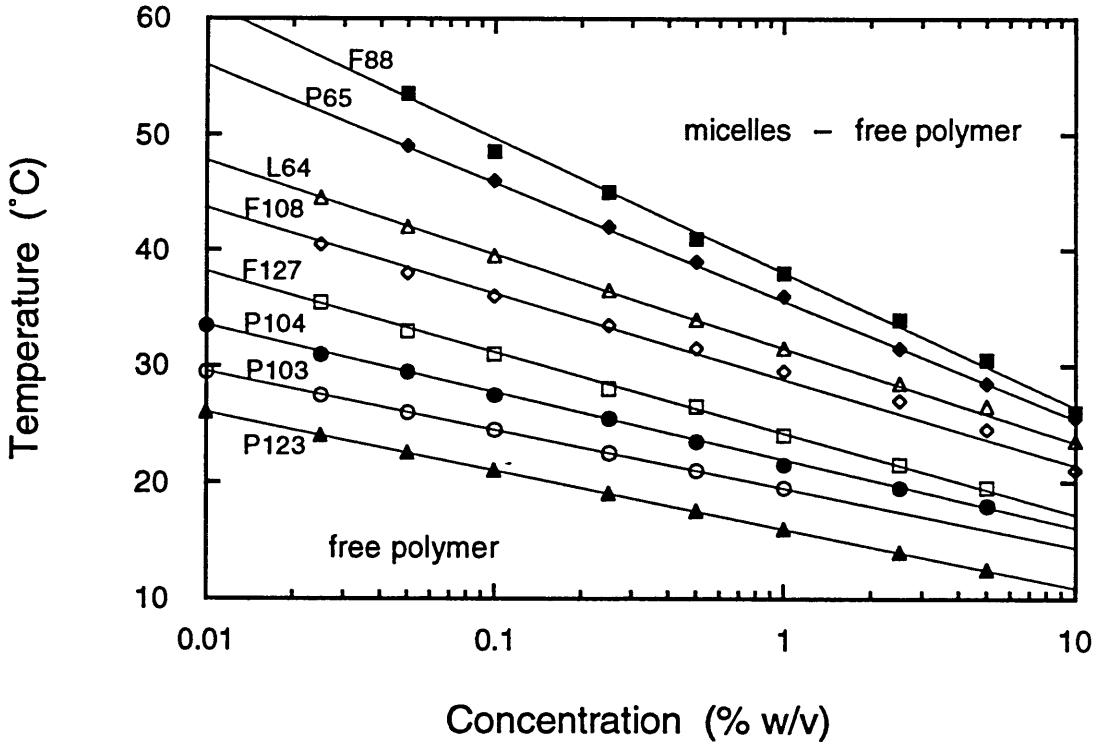

Figure 1.3 Phase diagram of aqueous PEO-PPO-PEO solutions, showing the CMC-CMT line.

Chapter 2
Micellization Behavior of PEO-PPO-PEO Triblock Copolymers in Aqueous Solutions and Thermodynamics of Copolymer Association

2.1 Introduction

Temperature-dependent micellization and gel formation are two of the most characteristic properties of aqueous poly(ethylene oxide)-*block*-poly(propylene oxide)-*block*-poly(ethylene oxide) (PEO-PPO-PEO) block copolymer solutions. Owing to the marked change in water solubility of the center poly(propylene oxide) block at elevated temperatures, the block-copolymers form various aggregates, depending on the degree of polymerization (m1, m2, and n). A number of triblock copolymers have been shown to aggregate in the form of micelles [Zhou & Chu, 1988; Wanka et al., 1990; Reddy et al., 1991; Brown et al., 1991; Malmsten & Lindman, 1992; Mortensen & Pedersen, 1993], with a core presumably dominated by PPO and a corona dominated by hydrated PEO blocks [Mortensen, 1992]. It is also known that, at temperatures close to ambient, high-concentration copolymer solutions exhibit a dramatic change in viscosity, revealing a "thermoreversible gelation" [Wanka et al., 1990; Brown et al., 1991; Yu et al., 1992; Wang & Johnston, 1991]. Several mechanisms have been proposed as driving forces for this thermal gelation: Rassing and Attwood [1983] related the gel transition to intrinsic changes in the micellar properties and Vadnere et al. [1984] discussed the gelation in terms of entropic changes involving locally ordered water molecules close to the hydrophobic units, whereas Wanka et al. [1990] and Wang and Johnston [1991] speculated at the possibility of an ordered three-dimensional structured state or network. Recently, neutron scattering studies showed that the observed change in viscosity is due to a "hard-sphere crystallization" as the micelle concentration approaches the critical volume fraction of 0.53 [Mortensen, 1992].

The critical micellization concentration (CMC), the fraction of polymer molecules in

micellar form, and the size and the aggregation number of the micelles, as well as the temperature dependence of these parameters, are of great interest for aqueous PEO-PPO-PEO block copolymer micellar solutions. Perhaps the parameter of greatest fundamental value is the critical micellization concentration, the copolymer concentration at which micelles start forming [Hunter, 1987, p 565]. As we show below, and as has previously been observed, the CMC of aqueous PEO-PPO-PEO block copolymer solutions decreases with increasing temperature [Zhou & Chu, 1988; Wanka et al., 1990; Brown et al., 1991].

In comparison with conventional, low molecular weight amphiphiles there is some inherent complexity in the micellization of block copolymers, which depends strongly on their composition. The composition polydispersity could be appreciable even for a copolymer with a narrow distribution of molecular weight, and accordingly, no sharp CMC or CMT (critical micellization temperature, the copolymer solution temperature at which micelles form) has been observed for block copolymers. In practice, a certain CMC range with some notable uncertainty could be detected. A large difference is often noted between the CMC values determined by different methods because their sensitivity to the quantity of molecularly dispersed copolymers (unimers) present may vary [Zhou & Chu, 1988]. For common detergents, a considerable amount of CMC data have been collected and summarized by Mukerjee and Mysels [1971], whereas for block copolymers so far only scarce CMC data (see e.g. Sikora and Tuzar [1983] and Price [1983]) are available in the literature. Furthermore, the values reported in the literature differ substantially; the lack of sufficient temperature control, in conjunction with batch-to-batch variations, may be responsible for the observed variations [Linse & Malmsten, 1992].

The need for a systematic study of the CMC and CMT for the PEO-PPO-PEO block copolymers becomes apparent from the discussion in the preceding paragraph, both from an applications point of view (mapping the micellization/solubilization regime for a given copolymer) and from theoretical considerations (determining the origin of micellization and the effects of hydrophilic PEO and hydrophobic PPO). Furthermore, the thermodynamic parameters of copolymer micellization can be derived from CMC data at different temperatures, given a copolymer association mechanism [Attwood & Florence, 1983; Hunter, 1987, p 583], providing further insight on the energetics of the micellization.

In a recent study that explored the potential for using PEO-PPO-PEO block copolymer micelles in the treatment of water contaminated with polycyclic aromatic hydrocarbons, it was shown that solubilization efficiency depended strongly on the molecular structure, composition, and molecular weight of the copolymer used [Hurter & Hatton, 1992]. Some speculation was made as to the reasons for this behavior, but verification of these arguments, which requires either structural experimental characterization or detailed theoretical analysis of the association and solubilization behavior of these polymer systems, is still lacking. In an attempt to address this issue, we undertook a detailed theoretical (using a self-consistent mean-field theory [Hurter, 1987]) and experimental investigation on the micellization and solubilization in the aqueous PEO-PPO-PEO block copolymer solutions. We report here experimental results on block copolymer micelle formation and micellization thermodynamics.

The solubilization of a dye (1,6-diphenyl-1,3,5-hexatriene, DPH) in copolymer solutions, detected by its fluorescence and UV-visible spectra, was employed in our investigation for the determination of the solution CMT and CMC values. Spectroscopic techniques, based either on optical absorption or on emission of light from some "probe" molecule, are now well established for investigating a wide range of physical properties of micellar solutions [Hunter, 1987, p 600; Grieser & Drummond, 1988]. The fact that micelles can solubilize relatively large amounts of sparingly water-soluble compounds has been used to determine the onset of micelle formation [Mukerjee & Mysels, 1971; Yekta et al., 1979] by measuring the concentration of a chosen sparingly soluble substance, possessing a convenient UV-visible absorbing chromophore, in the presence of increasing amounts of surfactant. Below the CMC, the concentration of the solubilizate in solution is the same as in aqueous solution in the absence of surfactant. Above the CMC, the total amount of the additive in solution increases sharply as the total micelle concentration increases.

Chattopadhyay and London [1984] used fluorescence from DPH to determine the CMC of various surfactants, obtaining values that were within 10% of the ones determined by other methods. Surface tension results showed that probe molecules, at the levels used to determine the CMC by fluorescence ($<10^{-6}$ kmol m^{-3}), did not noticeably affect the surfactant properties, viz., surface tension, nor the surface tension derived CMC value [Ananthapadmanabhan et al., 1985]. Edwards et al. [1991] reported that, in general, the

CMC values they obtained from the surface tension data for solutions of deionized water and nonionic surfactants showed fairly close agreement to the CMC values inferred from polyaromatic hydrocarbon solubilization data. Similar values for the CMC of the PEO-PPO-PEO block copolymers measured by surface tension and dye solubilization methods have been reported by Schmolka and Raymond [1965]. The following are an example: L64 CMC value at 25 °C is 0.0016 g/dL or 5.6 μM (measured with dye absorption) and 4.2 μM (measured with surface tension); CMC value at 40 °C is 0.0033 g/dL or 11.5 μM (measured with dye absorption) and 13.9 μM (measured with surface tension) [Schmolka & Raymond, 1965]. However, different values for the CMC of the PEO-PPO-PEO block copolymers measured by surface tension and dye (benzopurpurine) solubilization methods have been reported by Anderson [1972]. It becomes apparent though, from a closer inspection of his data, that Anderson misinterpreted the dye solubilization vs copolymer concentration curve. Such a curve is usually sigmoidal, with the first inflection indicating the micelle formation and the second inflection the complete solubilization of the dye. Anderson based his conclusions on the second inflection; the CMC value obtained from the first inflection of the dye solubilization vs copolymer (F68) concentration curve is actually very close to the CMC value derived from his surface tension measurements (~2 x 10^{-3} %).

We measured the CMT and CMC values of 12 Pluronic PEO-PPO-PEO block copolymers, covering a wide range of molecular weights (2900 - 14600) and PPO/PEO ratios (0.19 - 1.79). A closed association model was found to describe adequately the copolymer micellization process for the majority of the Pluronics. Using such a model, we obtained the standard free energies (ΔG°), enthalpies (ΔH°), and entropies (ΔS°) of micellization and correlated them to the copolymer molecular weight and composition. We also compared the PEO-PPO-PEO block copolymers to PPO-PEO-PPO block and PEO-PPO random copolymers, in an attempt to probe the effect of molecular architecture on the formation of micelles.

2.2 Materials and Methods

Copolymers: The Pluronic PEO-PPO-PEO block copolymers were obtained from

BASF Corp., Parsippany, NJ, and used as received. These polymers are available in a range of molecular weights and PPO/PEO ratios [Schmolka, 1977; Bahadur & Riess, 1991; BASF, 1989]. Table 2.1 lists the physical properties of the polymers studied (data supplied by the manufacturer). To facilitate analysis of the results, a brief description of the system of nomenclature for the BASF Pluronics follows. The notation for the Pluronic triblock copolymers starts with the letters L (for liquid), P (for paste), or F (for flakes). The first two numbers are indicative of the molecular weight of the PPO block, and the last number signifies the weight fraction of the PEO block. For example, P103 and P104 have the same molecular weight of PPO (on the order of 3000) but P103 has 30 wt % and P104 40 wt % PEO. The random PEO/PPO copolymer, UCON 50HB-3520 (50% PEO, 3520 molecular weight), was purchased from Union Carbide Chemicals and Plastics Company Inc., South Charleston, WV; the PPO-PEO-PPO Pluronic-R block copolymer, 25R4 (40% PEO), was obtained from BASF Corp.

Spectroscopic probe: 1,6-diphenyl-1,3,5-hexatriene (DPH) (CA # 1720-32-7) was obtained from Molecular Probes Inc., Eugene, OR, and used as received. The DPH dye used for the determination of the CMT and CMC in the present study is a well known probe of membrane interiors. The primary application of DPH has been to estimate membrane "fluidity", based on fluorescence depolarization measurements [Haugland, 1992]. Solvent and temperature effects on the fluorescence of DPH have been studied by Cehelnic et al. [1975]. The fluorescence of DPH is minimal in water and is substantially enhanced by association with lipids and other surfactants. This property has been exploited to determine the CMC's of anionic, uncharged, zwitterionic, and cationic detergents [Chattopadhyay & London, 1984]. DPH has also been used in probing micelles of tetradecyl-trialkylammmonium bromides [Lianos & Zana, 1982], and didodecyl-dimethylammonium bromide (DDAB) / alkane / water microemulsions [Chen et al., 1988].

Sample preparation: Aqueous copolymer solutions were prepared by dissolving the polymer in Milli-Q water (18 MΩ·cm) and diluting to the desired concentration (ranging from 0.001% to 20% w/v). The experiments on the Pluronic solutions were performed within a few days of the solution preparation. A dye solubilization technique [Chattopadhyay & London, 1984] was employed to determine the onset of copolymer micellization (CMC, CMT). Sample preparation was similar to that of Chattopadhyay and London [1984]: a stock solution of 0.4 mM DPH in methanol was prepared; 25 μL

(measured with a Hamilton microsyringe) of the DPH/methanol solution was added to 2.5 mL of copolymer solution, so that the final copolymer solution contained 1% v/v methanol and 0.004 mM DPH. The solutions were left in the dark to equilibrate for at least 3 h (and no more than 24 h) before the spectroscopic measurement. A single DPH concentration was used (0.004 mM), as no effect of DPH concentration on the CMC was observed (for DPH concentration range 0.0025 - 0.025 mM) by Chattopadhyay and London [1984].

Effect of methanol: The aqueous block copolymer solutions used for the determination of the CMC and CMT contained approximately 1% methanol; methanol was used to dissolve DPH, the latter being sparingly soluble in water. Methanol was also used in the preparation of a solution of high-concentration polycyclic aromatic hydrocarbons (PAHs), employed in PAH solubilization experiments from aqueous solutions by Edwards et al. [1991]. They found that methanol was a preferred solvent, as their tests showed no effect on surfactant solubilization; most higher alcohols could not be utilized since they affected the CMC values significantly [Rosen, 1989]. Measured apparent PAH solubilities at zero surfactant concentration in the presence of 1% by volume methanol appear to be enhanced by ~20-30% relative to reported solubilities in pure water. The presence of methanol did not shift the CMC or the slope of the solubilization curve for a solution of pyrene and octylphenol PEO surfactant [Edwards et al., 1991]. Bedo et al. [1992] studied the effect of methanol, ethanol and isopropyl alcohol on the micellization of ethoxylated nonylphenols and their data suggest that 1% methanol increased the CMC by approximately 40%; isopropyl alcohol had a far more pronounced effect on the CMC. The sample preparation for the CMC determination of Chattopadhyay and London [1984] involved dissolving DPH in THF and adding 1 μL to 2 mL of surfactant solution. These authors found that up to 1-2% (v/v) THF had little effect on the CMC for several detergents.

Spectroscopy: Emission fluorescence spectra of the copolymer/DPH/water samples were obtained with a Shimadzu RF-5000 recording spectrofluorophotometer, using an excitation wavelength of 350 nm and emission wavelength range 350-650 nm. The emission intensity peak used to observe the DPH solubilization in the copolymer micelles was at 457 nm. UV-vis absorption spectra of the copolymer/DPH/water samples were recorded in the 300-500 nm range using a Perkin-Elmer Lambda 3B UV/vis spectrophotometer, controlled by the Perkin-Elmer Computerized Spectroscopy Software (PECSS). The main absorption intensity peak, characteristic of DPH, was at 356 nm. For

both fluorescence and absorption spectroscopy experiments, the samples were placed in Teflon-stoppered quartz cuvettes. Temperature control within 0.05 °C was achieved using a Neslab RTE-110 refrigerated bath/circulator. The temperature range employed was 15 - 55 °C, as measured in the thermostated photometer reference cell. At least 1 h was allowed for the sample temperature equilibration. After establishing that emission fluorescence spectroscopy gave the same results as visible absorption spectroscopy, we used the latter to obtain the data reported here (the absorption spectrum of a molecule is, in principle, the same as the fluorescence excitation spectrum, which, in turn, is the mirror image of the fluorescence emission spectrum [Birks, 1970, p 85]).

2.3 Results and Discussion

UV-vis spectra of aqueous Pluronic solutions with concentrations from 0.001 to 20% w/v containing DPH were taken at 5 °C temperature intervals over the range 15 - 55 °C. At low concentrations and/or low temperatures, the Pluronics did not associate in aqueous solution, DPH was not solubilized in a hydrophobic environment, and, as a result, the fluorescence and UV-vis intensities due to DPH were very low. At higher concentrations and/or temperatures the Pluronics formed micelles, and DPH was solubilized in the hydrophobic micelle interior, giving a characteristic spectrum. Figure 2.1a shows the UV-Vis absorption spectra of a typical DPH/Pluronic/water solution (P104, 0.5% w/v) at different temperatures and Figure 2.1b the absorption intensity at 356 nm of the previous sample, as a function of temperature. The CMT values for Pluronics of various concentrations were obtained from the first inflection of the absorption intensity at 356 nm vs temperature plot.

2.3a Critical micellization temperature data

Figure 2.2 shows the dependence of the intensities at 356 nm (spectral maximum due to DPH) on temperature, for various concentrations of a typical Pluronic (P104) aqueous solution. The critical micellization temperature values were obtained from the first inflection of the intensity vs temperature sigmoidal curve (or alternatively from the first appearance of a well defined peak in the sample spectrum) that indicated the formation of a hydrophobic domain. This domain appears to be the result of aggregation of many

Pluronic molecules to form a micelle, rather than the coiling of a single molecule. Dye solubilization experiments with random PEO-PPO copolymers of similar PPO/PEO composition and block PPO-PEO-PPO copolymers of comparable PEO and PPO block sizes showed no increase in the absorption intensity due to the DPH, indicating that the existence of hydrophobic (PPO) patches in a single molecule are not sufficient for solubilization of DPH. The second inflection of the intensity vs temperature sigmoidal curve was indicative of the complete solubilization of DPH in the block copolymer micelles. The use of DPH solubilization to determine CMT proved to be a reliable and reproducible method; the uncertainty in the CMT values reported here is less than ±1 °C (the uncertainties in the CMT values arose mainly from the use of lines tangent to parts of the intensity vs temperature curve for deriving the temperature corresponding to the CMT). There was some difficulty involved in the CMT determination only for L64, as the samples became turbid in the vicinity of micelle formation [Zhou & Chu, 1988].

The CMT values obtained for various Pluronic copolymers are listed in Table 2.2 as a function of copolymer concentration, expressed in both percent w/v and mM concentration units. To the best of our knowledge, this is the first comprehensive compilation of CMT data for aqueous Pluronic solutions, and the only one available for F123, P103, P104, P105, F108, P84, and P65; such a data set should prove to be useful for the numerous applications of Pluronics that depend on their micelle forming abilities. The few CMT values available in the literature agree well with our data: 15 °C CMT for 10% F127 solution reported by Gilbert et al. [1987] compared to our 16 °C; 25 °C CMT for 5% P85 solution reported by Brown et al. [1991] compared to our 25 °C; 25 °C CMT for 6% L64 solution reported by Al-Saden et al. [1982] compared to our 26 °C. Furthermore, the CMT values obtained from the DPH solubilization method compare very well to the onset of pyrene and naphthalene solubilization in L64, P104, and F108 [Hurter et al., 1993, p 1663]. The agreement between our CMT data (from dye solubilization experiments) and CMT data from light scattering intensity is not as good for F68; Zhou and Chu [1988] obtained CMT values of 42.3, 39.0, and 36.3 °C for 1.25, 2.50, and 5.17% polymer concentrations, respectively, compared to our 46 and 40 °C for 2.5 and 5.0%, respectively. F68 is fairly hydrophilic (80% PEO) and may form premicellar aggregates discernible with light scattering, but with no well-defined hydrophobic core to allow for DPH solubilization.

2.3b Critical micellization concentration data

Figure 2.3 shows the dependence of the intensities at 356 nm (spectral maximum due to DPH) on Pluronic P104 concentration, at various temperatures. The critical micellization concentration was estimated again from the first inflection of the intensity vs log concentration sigmoidal curve; the uncertainty in the CMC values reported is less than ±15% (the uncertainties in the CMC values arose similarly to those discussed for CMT). Table 3 lists the CMC values for various Pluronics as a function of solution temperature.

Given the number of publications dealing with aqueous solutions of Pluronics, there are surprisingly few reliable CMC data for Pluronics. The CMC values we obtained are generally 1 order of magnitude higher than the values reported by Schmolka and Raymond [1965] for F68, P84, P85, F88, P104, and F108. Prasad et al. [1979] measured the surface tension of aqueous Pluronic solutions (L64, F68, P85, and F88) and detected in several systems two points of inflection in the surface tension vs log concentration plots. They interpreted this as due to the formation of so-called "monomolecular" aggregates in dilute solution, and multimolecular aggregates in more concentrated solutions. Wanka et al. [1990] found that the surface tension of P104, P123, and F127 decreased linearly with the logarithm of the copolymer concentration according to the Gibbs isotherm of adsorption over several concentration decades. At a characteristic concentration, there was a break in the curve; the surface tension kept decreasing with further increase in concentration, but with a smaller slope, until a second concentration was reached above which the surface tension remained constant. This transition region extended approximately 1 concentration decade. According to Wanka et al. the two breaks in the curves could be interpreted as being due to the existence of two critical concentrations; taking other types of measurements into account, however, it seemed more conceivable that the transition region could be related to the fact that the block copolymers were not well defined samples but had a broad molecular weight distribution [Wanka et al., 1990]. In addition, any trace impurities (originating from the manufacturing process) in the polymer solutions would have a significant effect on surface tension measurements. Interestingly enough, the concentrations at the second inflection point from Wanka et al., [1990] (0.3% for F127 and 0.01% for P104, both at 25 °C) and Prasad et al. [1979] are comparable to the CMC values found in our study. Two breaks can also be observed in a surface tension data set for P94 published by Bahadur and Pandya [1992], who derived the

CMC from the first break. In detailed surface tension measurements with the same copolymers used for the dye solubilization experiments (to avoid inconsistency due to different polymer batches), we have also observed the two inflection points in the surface tension curves [Alexandridis et al. 1994; see also Chapter 4 of this Thesis].

The ambiguities in the different ways of measuring the CMC in Pluronic solutions point to the need to define clearly the applications for which the data are intended. The dye solubilization method for determining the CMC is ideal for determining the range of solubilization enhancement of otherwise sparingly soluble organics in the presence of Pluronic copolymers, provided the molecules to be solubilized are of comparable hydrophobicity and size to DPH. In fact, the partition coefficient for DPH in the copolymer micelles can be estimated from the same set of data used to obtain the CMC values. The molar solubilization ratio (MSR), defined as the number of moles of organic compound solubilized per mole of surfactant added to solution, is a measure of the effectiveness of a particular surfactant in solubilizing a given solubilizate [Attwood & Florence, 1983]. The increase in solubilizate concentration per unit increase in micellar surfactant concentration is equivalent to the MSR. In the presence of excess hydrophobic organic compound, the MSR may be obtained from the slope of the curve that results when the solubilizate concentration is plotted against surfactant concentration [Edwards et al., 1991]. The effect of copolymer PPO/PEO composition, molecular weight, solution concentration, and temperature on the molar solubilization ratio of DPH in aqueous block copolymer solutions will be presented in detail elsewhere [see Chapter 7 of this Thesis].

2.3c CMC and CMT values as a function of copolymer composition and molecular weight

The CMC and CMT values listed in Tables 2.2 and 2.3 are discussed in this section in terms of the number of propylene oxide (PO) and ethylene oxide (EO) segments in the Pluronic block copolymer molecules. This enables estimation of the effect of the polymer structure and molecular weight on micellization behavior.

PPO effect: The CMC values for Pluronics P65, P84 and P123, which have the same hydrophilic (PEO) block and varying hydrophobic (PPO) block, are plotted semilogarithmically in Figure 2.4a as a function of the number of PO segments in the

Pluronic molecule, for different solution temperatures (25, 35, and 45 °C). The log(CMC) values for the Pluronics solutions (at a given solution temperature) decreased in a roughly linear fashion ($R^2 > 0.99$) with increasing number of PO segments, indicating that polymers with a larger hydrophobic (PO) domain form micelles at lower concentrations. Higher temperatures resulted in lower CMC values, with the slope of the log(CMC) vs PO number curve increasing with temperature. The CMT values for the Pluronics solutions (at a given copolymer concentration) decreased as a function of PO units, as shown in Figure 2.4b, indicating that polymers with a larger hydrophobic domain form micelles at lower temperatures.

PEO effect: The CMC and CMT values for groups of Pluronics with the same hydrophobic segment and varying hydrophilic segment, e.g., with 30 (L64, P65, F68), 40 (P84, P85, F88), and 60 (P104, P104, F108) PO segments, plotted as a function of EO segments (plot not shown), show a small increase in the CMC and CMT with increasing number of EO units. This would indicate that the micelle formation becomes more difficult the more hydrophilic the molecules, although the effect of PEO on the CMC and CMT is less pronounced than that of PPO, intimating that PPO is a primary factor in the micellization process.

Molecular weight effect: The CMC and CMT values for copolymers of constant PPO/PEO ratio but varying molecular weight decrease with increasing number of EO segments (at a given copolymer solution temperature and concentration for the CMC and CMT respectively). It can thus be concluded that, for given PPO/PEO ratio, Pluronics of higher molecular weight form micelles more readily, e.g. at lower concentrations and temperatures. Parts a and b of Figure 2.5 show the CMC and CMT values, respectively, for various Pluronics as a function of the number of EO segments, for groups of copolymers with 40% (L64, P84, P104), 50% (P65, P85, P105), and 80% (F68, F88, F108) PEO content and at various copolymer solution temperatures (in Figure 2.5a) and concentrations (in Figure 2.5b). The CMT values were influenced more by molecular weight the lower the relative PEO content, and the lower the copolymer concentration, as is evidenced by the steeper slopes for the curves for these conditions. A linear fit was found to describe adequately the CMC and CMT dependence on the number of EO units for copolymers of constant relative PEO content and varying molecular weight ($R^2 > 0.98$ for Figure 2.5a while $R^2 > 0.94$ for 40% PEO and $R^2 > 0.99$ for 50 and 80% PEO in Figure

2.5b).

Comparison of Pluronic CMC and CMT values to those of C_iE_j nonionic surfactants: It is interesting to compare the micellization of Pluronic block copolymers to that of C_iE_j (j-ethyleneglycol-i-alkyl ethers) low molecular-weight nonionic surfactants, which has been more widely studied [Barry & El-Eini, 1976; Meguro et al., 1981]. In the latter systems, it was found that the CMC decreased and that the micellar size increased strongly, both with increasing temperature. Thus, in these respects, the analogy between Pluronics and C_iE_j seems valid. However, the pronounced sensitivity of the CMC to temperature, or of the CMT to concentration, as found here for many Pluronics, is not evident with the n-alkyl poly(ethylene glycol) ethers, C_iE_j [Meguro et al., 1987]. The decrease of the hydrophilicity of the PEO blocks with increasing temperature has comparatively little effect on the CMC for C_iE_j: for $C_{12}E_8$ the CMC is reported as 9.7 x 10^{-5} M at 15 °C and 5.8 x 10^{-5} M at 40 °C (~40% decrease in the CMC for 25 °C increase in temperature) [Meguro et al., 1987]. In the case of Pluronic copolymer solutions, a 10 °C decrease in temperature results in changes of the CMC by more than an order of magnitude (see Figure 2.5a).

Also, the number of EO units has little effect, at least for short EO headgroups: the CMC is given as 6.5 x 10^{-5} M for $C_{12}E_5$ and 7.2 x 10^{-5} M for $C_{12}E_8$ [Meguro et al., 1987]. For longer EO chains ($C_{16}E_j$, j = 17, 32, 44, 63), log(CMC) increased linearly as a function of EO weight fraction, the CMC varying by up to an order of magnitude over the EO range studied, the slope being steeper at higher temperatures [Barry & El-Eini, 1976]. Although the increase in the CMC with increasing EO may appear significant for the $C_{16}E_j$, j = 17, 32, 44, 63, surfactant series, the change in the CMC per EO unit in this case is less pronounced than the CMC change between $C_{12}E_5$ and $C_{12}E_8$. In the case of Pluronics, the change in CMC per EO-unit was found to be even smaller, indicating that the influence of PEO on CMC diminishes as the size of the surfactant increases. This can be observed in Figure 2.5a where, for the same change of CMC, it takes 50 EO units for Pluronics of high molecular weight (80% EO group) but only 10 EO units for the lower molecular weight Pluronics. The main determinant of the CMC for C_iE_j was found to be the length of the alkyl (hydrophobic) chain. The logarithm of CMC for the C_iE_8, i = 10 - 15, series decreased linearly with increasing carbon number in the alkyl chain (CMC varied by approximately 2.5 orders of magnitude over the carbon number range studied) [Meguro et

al., 1981]. For the Pluronics, an increasing hydrophobicity of the PO block with increasing temperature, in combination with the size polydispersity of the PO blocks, has been advanced as the reason for the strong temperature dependence of the CMC [Almgren et al., 1992].

2.3d Thermodynamics of block copolymer micelle formation

It is well established that block copolymers of the A-B or A-B-A type form micelles in selective solvents which are thermodynamically good solvents for one block and precipitants for the other block. In general, micellization of block copolymers, as in the case of conventional detergents, obeys the closed association model, which assumes an equilibrium between molecularly dispersed copolymer (unimer) and multimolecular aggregates (micelles) [Price, 1983; Tuzar & Kratochvil, 1976]. There are two main approaches to the thermodynamic analysis of the micellization process: the phase separation model, in which the micelles are considered to form a separate phase at the CMC, and the mass-action model that considers micelles and unassociated monomers in association-dissociation equilibrium [Attwood & Florence, 1983]. In both approaches, the standard free energy change for the transfer of 1 mol of amphiphile from solution to the micellar phase (free energy of micellization), ΔG°, in the absence of electrostatic interactions (nonionic surfactants) is given by [Attwood & Florence, 1983; Hunter , 1987, p 583]

$$\Delta G^\circ = R\,T \ln (X_{CMC}) \qquad (1)$$

where R is the gas law constant, T is the absolute temperature, and X_{CMC} is the critical micellization concentration in mole fraction units. It is assumed here that the concentration of free surfactant in the presence of micelles is constant and equal to the CMC value, in the case of the phase separation model, or that the micelle aggregation number is large for the mass-action model. Applying the Gibbs-Helmholtz equation, and assuming the aggregation number to be independent of temperature in the case of the mass-action model, we can express the standard enthalpy of micellization, ΔH°, as [Attwood & Florence, 1983; Hunter , 1987, p 583]

$$\Delta H^\circ = - R\,T^2 [\, \partial \ln(X_{CMC}) / \partial\, T\,]_P = R [\, \partial \ln(X_{CMC}) / \partial\, (1/T)\,]_P \qquad (2)$$

Finally, the standard entropy of micellization per mole of surfactant, ΔS°, can be obtained from:

$$\Delta S^\circ = (\Delta H^\circ - \Delta G^\circ) / T \qquad (3)$$

It has been shown for block copolymer micellization [Yu et al., 1992; Stainsby & Alexander, 1950; Price et al., 1989; Quintana et al., 1993; Deng et al., 1963; Booth, 1992; Yang et al., 1992] that, within experimental error,

$$\partial \ln(X_{CMC}) / \partial (1/T) = \partial \ln(X) / \partial (1/T_{CMT}) \qquad (4)$$

where X is the concentration expressed as mole fraction, and T_{CMT} is the critical micellization temperature; thus eq (2) becomes

$$\Delta H^\circ = R [\partial \ln(X) / \partial (1/T_{CMT})]_P \qquad (5)$$

2.3e 1/TCMT vs ln(X) plot: mode of copolymer association

In accordance with Equation 5, the inverse CMT values were plotted as a function of the logarithm of copolymer concentration (mole-fraction units) for a number of Pluronics, as shown in Figure 2.6. We chose to use this representation (CMT for a given concentration) instead of Equation 2 (CMC for a given temperature) as it more closely reflects our experimental procedures, where the temperature of a sample of given polymer concentration was varied. The CMT data, plotted in this manner, are generally described well by a straight line. Exceptions to the linear fit are F68, F88, and F108, for which the slopes appear to increase at high concentrations (>5% w/v). These three polymers are all hydrophilic and of high molecular weight; it may be that for them the simple assumptions of the thermodynamic analysis do not hold well at high polymer concentrations. The hydrated PEO chains of the micelle coronas will overlap and entangle with increasing polymer concentration, up to the formation of a gel-like structure (F108 of 20% w/v forms a gel at room temperature).

One of the assumptions involved in deriving Equations 1 - 5 is that the micelle

aggregation number is independent of temperature. Although there are some studies (e.g., Zhou and Chu [1988] for F68, Mortensen and Pedersen [1993] for P85, Almgren et al. [1992] for L64 and Attwood et al. [1987] for F127) indicating an increase in the aggregation number with temperature, Equation 5, based on a closed association model, correlated the CMT data in a satisfactory way. The temperature dependent terms (that could come into the association model) would contribute less that 3% of the ΔG° value. Reddy et al. [1991] examined the mode of association of a purified L64 sample in aqueous solutions by measuring the light scattering intensity as a function of temperature and concentration. The association at 34.5 and 40 °C was described by a cooperative association model which assumed aggregate growth by stepwise addition of unimers. Deviation of the experimental curves from the computed curves was observed at high concentrations and attributed to solution nonideality [Reddy et al., 1991]. It should be noted, though, that the data set used for the analysis of Reddy et al. [1991] was relatively limited. A concentration-independent diffusion coefficient and micelle weight-average molecular weight have been explained by a closed association model for hexa(oxyethylene glycol) monoether micelles [Corkill & Walker, 1972]. The use of a closed association model in the case of the copolymer we studied appears well justified based on the good fit of the data to Equation 5; we consequently employed such a model for estimating ΔH° and ΔS° of the micellization process.

2.3f ΔG°, ΔH° and ΔS° as a function of copolymer composition and molecular weight

The standard enthalpy of micellization, ΔH°, was calculated from the inverse slope of the linear fit to the $1/T_{CMT}$ vs ln(mole fraction) data, in accordance with Equation 5. ΔH° values, together with ΔG° and ΔS° (calculated from Equations 1 and 3, respectively, at the critical micellization temperature for 1% copolymer solutions) are listed in Table 2.4 for various Pluronics. It is emphasized that these data are for a constant CMC, and not constant temperature (for any given concentration, there is a unique CMT; conversely, for any given temperature, there is a unique CMC). The values for the tabulated ΔH°, ΔG°, and ΔS° range between 169 and 339 kJ/mol, -24.5 and -28.8 kJ/mol, and 0.638 and 1.244 kJ/(mol K), respectively. The higher values of ΔH°, ΔG°, and ΔS° were observed for P103 and L64 (relatively hydrophobic copolymers), while the lower values were observed

for the relatively hydrophilic copolymers F68 and F88.

The standard enthalpy of micellization, ΔH°, is positive, indicating that the transfer of unimers from solution to the micelle is an enthalpically-unfavorable endothermic process. The free energy, ΔG°, is negative, since thermodynamically stable micelles are formed spontaneously. Thus, it is clear that a negative entropy contribution must be the driving force for micellization of the block copolymers. The traditional view of micelle formation [Hunter, 1987, Vol. 1, p 567; Hiemenz, 1986, p 447] has been based on the study of the solubility of hydrocarbons in water and what has come to be known as the hydrophobic effect [Tanford, 1980]. The presence of hydrocarbon molecules in water causes a significant decrease in the water entropy, suggesting that it induces an increase in the degree of structuring of the water molecules, owing to cavity formation. When hydrocarbon residues aggregate in aqueous solution to form a micelle, the hydrogen bonding structure in the water is, to a large extent, restored and the water entropy increases; this overcomes the loss of entropy due to the localization of the hydrocarbon chains in the micelles. The entropy contribution usually dominates the micellization process in aqueous surfactant solutions, with the enthalpy playing a minor role. In the Pluronic copolymers, the unfavorable enthalpy component is significant but is, nevertheless, overcome by an even stronger entropy effect. In contrast to the entropy-driven micellization in water, the micellization of copolymers in nonpolar solvents originates from enthalpy interactions between the copolymer segments and the solvent [Price, 1983].

Free energies of micellization per mole of polymer in solution, ΔG°, calculated at the critical micellization temperatures for the various copolymers at different solution concentrations, are shown as a function of Pluronic molecular weight in Figure 2.7a. Although the data exhibit some scatter, presumably because of the widely varying composition ratios of the polymers used in this study, they do indicate the tendency for higher molecular weight copolymers to have more negative free energies of micellization, indicating a greater propensity to form micelles with increasing polymer chain length. This is despite the fact that the larger polymers are generally more hydrophilic, as they are composed predominantly of ethylene oxide groups.

The data shown in Figure 2.7a collapse into a single smooth curve, independent of copolymer composition ratio PPO/PEO, when normalized with respect to the total number

of monomer units in the polymer, $N_{EO} + N_{PO}$, as shown in Figure 2.7b. It can be seen clearly that the lower molecular weight, more hydrophobic Pluronics correspond to more negative ΔG° per monomer unit values. These data were correlated as a function of molecular weight M_W and concentration, C, by the empirical equation

$$\Delta G^\circ / (N_{EO} + N_{PO}) = A_1 \tan^{-1}(M_W) + A_2 \quad (6)$$

where A_1, A_2 are concentration dependent constants, given by

$$A_1 = 1263 - 360.5 \log(C) \quad (7)$$

and

$$A_2 = -1985 + 566.3 \log(C) \quad (8)$$

respectively. The fit is good ($R^2 > 0.997$) and the predictions of the correlation for $\Delta G^\circ / (N_{EO} + N_{PO})$ (kJ / monomer unit) differ at most by 2.5% from the experimentally determined values. Since this correlation holds for PEO-PPO-PEO copolymers covering a wide range of molecular weights and PPO/PEO compositions, it can be used for predicting ΔG° for copolymers that have not yet been studied experimentally. Once ΔG° is known, the critical micellization concentrations and temperatures can also be estimated (see also Chapter 3 of this Thesis). The normalization of the data in this fashion enables the composition ratio effects to be decoupled from the effects of overall molecular weight and copolymer concentration on the micellization process.

To further probe the origin of micelle formation in Pluronic copolymer solutions, the dependence of the thermodynamic parameters ΔH° and ΔG° on the PPO/PEO composition ratio was examined. Figure 2.8a shows that the normalized ΔH° (expressed in kJ / mol of average monomer unit) approaches zero as the PPO/PEO ratio goes to zero. It can thus be inferred that the micellization process is dominated by the PPO (hydrophobic) part of the copolymer. A similar trend was observed by Armstrong et al. [Armstrong et al., 1993] based on DSC enthalpy changes of ICI Poloxamer solutions and by Williams et al. [Williams et al., 1985] using the increment in apparent molar volume on "thermal transition" of PolySciences PEO-PPO copolymers as a function of PPO/PEO. The fact that

the normalized ΔH° values are approximately the same for different Pluronics of a constant PPO/PEO ratio would indicate that the micellization enthalpy per monomer unit is independent of molecular weight. In contrast to the trend of decreasing ΔG° with increasing Pluronic molecular weight, there is no definite dependence of ΔH° on molecular weight over the range covered in this study. The ΔH° data presented in Table 4.4 reveal two main groups of copolymers, the relatively hydrophobic P103, P104, P105, and P123 with ΔH° in the 300-350 kJ/mol range and the relatively hydrophilic L64, P65, P84, and P85 with ΔH° in the 180-230 kJ/mol range, while ΔH° for the other four copolymers ranges from 170 to 270 kJ/mol. The dependence of the normalized ΔH° on the copolymer composition is far more instructive and is presented in Figure 2.8a. A plot of ΔG° of micellization (expressed in kJ / mol of average monomer unit) as a function of PPO/PEO (Figure 2.8b), again shows the ΔG°/unit values approaching zero as the PPO/PEO ratio goes to zero. The unit free energy, however, decreases (becomes more negative) with a decrease in molecular weight for Pluronics with a constant PPO/PEO ratio.

The compilation of ΔG°, ΔH°, and ΔS° data for a wide range of Pluronic block copolymers presented in this paper is, to the best of our knowledge, the most complete in the literature. In a previous investigation Reddy et al. [1991] estimated the ΔG° of micellization at -20 kJ/mol and the ΔH° of micellization at 200 kJ/mol for a solution of purified L64, utilizing ln(CMC) vs 1/T data (only three data points, though). The same group [Yu et al., 1992] reported the ΔH° of micellization at -316 ± 20 kJ/mol for a solution of purified F127 (from ln(concentration) vs 1/CMT data). These values are close to our estimates of ΔG° = -24.5 kJ/mol and ΔH° = 230 kJ/mol for L64 and ΔH° = 253 for F127 (the copolymers we used were not purified).

ΔH° from Differential Scanning Calorimetry: Another method for obtaining estimates of the free enthalpy of micellization, ΔH°, is differential scanning calorimetry (DSC). DSC measurements for aqueous Pluronic solutions show endothermic peaks, typical for a first-order phase transition, at concentration-dependent characteristic temperatures [Wanka et al., 1990; Armstrong et al., 1993]. The peaks have rather high enthalpy values (almost 3 orders of magnitude larger than typical enthalpy values for phase transitions in lyotropic liquid crystals [Wanka et al., 1990]) and are rather broad, extending more than 20 °C. The latter can be due to the fact that the copolymers are not pure

compounds but show a broad molar weight distribution; it is well known also that melting peaks become broad in the presence of impurities [Wanka et al., 1990]. It should be pointed out here that the enthalpy change measured by the peak area in DSC is not the standard enthalpy change but depends upon the real states of the chains before and after micellization. The standard state enthalpy change is defined for transfer of 1 mol of chains from the ideally dilute solution to the solvated micellar state. In the ideally dilute solution, copolymer segments interact only with solvent, whereas in real solutions segments also interact with each other, and this may cause discrepancies between micellization enthalpies obtained from DSC and the ones derived from an analysis similar to ours [Deng et al., 1992]. It has also been reported by Hiemenz [1986] that ΔH° values calculated by a micellization thermodynamics model generally show poor agreement with those determined calorimetrically, at least for ionic surfactants.

From a very limited set of data (P123, F127, and P104 studied with DSC), Wanka et al. [1990] observed no proportionality between the enthalpy values and the size of the EO portion of the molecules, but they noted that there was proportionality between these values and the PO groups, to a first approximation. From this they concluded that the transition is probably due to the dehydration or "melting" of the PO groups [Wanka et al., 1990]. Similar trends were observed in our ΔH° data. It appears, though, from our data set that there is a weak effect of EO on ΔH°. For Pluronics with the same size hydrophobic (PPO) segment and varying size hydrophilic (PEO) segment, i.e., P103, P104, P105, and F108, ΔH° decreased by ~15% as the number of EO segments increased from 2 x 7 to 2 x 132. On the contrary, for Pluronics with the same size hydrophilic (PEO) block and varying size hydrophobic (PPO) block, i.e., P65, P84, and P123, ΔH° increased by ~100% as the number of PO segments increased from 30 to 70. The PPO effect was more significant and, together with the data of Figure 2.8, leads to the conclusion that PPO is mainly responsible for the micellization of Pluronics.

Differential scanning calorimetry was also used by Beezer et al. [1992] on PEO-PPO-PEO block copolymer solutions. The observed "phase transitions" were in the 100 - 300 kJ/mol range and were initially thought to result from changes in the polymer solvation as the temperature changed. The authors claimed that, at the concentration used (5 g/L), only monomeric species were present in solution [Beezer et al., 1992]. In a more recent paper from the same group, Armstrong et al. [1993] concluded that the observed enthalpy

change is indicative of an aggregation process, accompanied by desolvation and change in conformation of the hydrophobe. Although direct comparison between the calorimetry ΔH values of Armstrong et al. [1993] and Beezer et al. [1992] and our ΔH° cannot be made as the copolymers used were not the same, our data strongly suggest that the micellization process is the major contribution to the calorimetrically-observed enthalpy change.

2.3g Molecular mechanism of temperature effects on PEO-PPO-PPO aqueous solutions

The "molecular-level" mechanism behind the temperature dependence of PEO-PPO-PEO micellization, and particularly the effect of PEO, is still a matter of some controversy. In principle, models in the literature are based on either the solute-solvent [Kjelander & Florin, 1981; Goldstein, 1984], or the solute-solute interactions [Karlstrom, 1985]. Kjelander and Florin [1981] attempted to reproduce the negative entropy and enthalpy of water-PEO mixing, and the phase diagram of the PEO-water system assuming a zone with increased structuring of water to exist around the PEO chain. The phase separation that takes place at high temperatures was attributed to a breakdown of the zones of enhanced water structure. The chain length dependence was mainly determined from the combinatorial entropy of the chains. The water solubility of PEO could be explained in terms of a good structural fit between the water and the polymer. While PPO also has negative entropy and enthalpy of mixing with water, they are less negative than those for PEO-water. Kjelander and Florin [1981] claim that when PPO is introduced into water it also develops a hydration shell with an enhanced structure of water, but since the methyl groups of PPO constitute a steric hinderance, the water structure is weak and leads to phase separation. It should be noted here that, while PPO is practically insoluble in water at room temperature, it can be soluble at low temperatures (e.g., up to -7 °C for PPO with degree of polymerization = 20, reported by Kjelander & Florin [1981]).

A weak point to the above theory, according to Karlstrom [1985], is the highly disorderd state of PEO in aqueous solutions that is incompatible with an ordered water hydration shell. Karlstrom [1985] predicted (with semiquantitative agreement) the phase diagram of PEO-water using Flory-Huggins theory and assuming that each segment of the PEO chain may exist in two forms due to the rotations around the C-C and C-O bonds. From quantum mechanical calculations, corroborated by ^{13}C NMR chemical shift

measurements, the conformation of the OCCO segment was divided into two classes, one being polar, having a low energy and a low statistical weight, and one being less polar, or nonpolar, having a higher energy and a higher statistical weight [Malmsten & Lindman, 1992]. At low temperatures, the former class of states dominates and the solute-solvent interaction is favorable, whereas at higher temperature, the latter class of states becomes increasingly populated, rendering the solute-solvent interaction less favorable. Malmsten and Lindman [1992] used a similar model, assuming temperature dependent EO-EO, PO-PO, and EO-PO interactions, to predict the micellization behavior of PEO-PPO-PEO block copolymer solutions. They found that both PO and EO blocks repel each other progressively less with increasing temperature, until, at some temperature, the effective PO-PO attraction dominates over the EO-EO repulsion, and micelles form. A more comprehensive discussion of the mechanisms of the temperature dependence, and clouding in particular, is presented by Lindman et al. [1990].

The self-consistent mean-field lattice models used for predicting PEO-PPO-PEO block copolymer solution behavior by Hurter et al. [1993] and Linse et al. [Malmsten et al., 1993] also incorporated Karlstrom's ideas and accounted for conformational distributions in PEO and PPO, thus allowing the investigation of temperature effects on the aggregation behavior of these copolymers. The model predictions of Hurter et al. [1993] and Malmsten et al. [1993] (e.g. decrease of CMC and CMT with increasing PPO) agree well with the trends observed experimentally, thus supporting the polar-nonpolar state model as an explanation of the temperature effect on the solution behavior of PEO and PPO.

2.4 Conclusions

The critical micellization temperature (CMT) and critical micellization concentration (CMC) values of 12 Pluronic poly(ethylene oxide)-poly(propylene oxide)-poly(ethylene oxide) (PEO-PPO-PEO) block copolymers, covering a wide range of molecular weights (2900 - 14600) and PPO/PEO ratios (0.19 - 1.79), have been determined employing a dye solubilization method. In general, it is evident that copolymers with a larger hydrophobic (PPO) domain formed micelles at lower concentrations, or, for a given copolymer concentration, have lower CMTs. For copolymer groups with the same PPO/PEO ratio, Pluronics of higher molecular weight form micelles more readily, e.g., at lower

concentrations and temperatures. The hydrophilic group appears to play a smaller role in the micellization process.

A closed association model was found to describe adequately the copolymer micellization process for the majority of the Pluronics and was used to obtain standard free energies (ΔG°), enthalpies (ΔH°), and entropies (ΔS°) of micellization for these Pluronics. The standard enthalpy of micellization, ΔH°, was found to be positive for all Pluronics tested, indicating that the transfer of unimers from solution to the micelle is an enthalpically unfavorable endothermic process. A negative entropy contribution must, therefore, be the driving force for the micellization for the block copolymers.

The comprehensive compilation of CMT and CMC data for aqueous Pluronic solutions presented here is expected to be of value in the numerous applications of Pluronics that depend on their micelle forming abilities. The utility of these results is enhanced by the finding that the free energies of micellization per monomer unit, $\Delta G^\circ / (N_{EO} + N_{PO})$, correlated well with molecular weight and solution concentration over the wide range of polymer composition ratios investigated and can be used for the estimation of the micellization parameters of other polymers in this class.

2.5 Appendix A: Hydrophobic (PPO) contribution to ΔG°

When the CMC values for various Pluronics were plotted semilogarithmically (Figure 2.4) as a function of the number of PO segments in the Pluronic molecule, for various solution temperatures, the log(CMC) was found to decrease in a roughly linear fashion as a function of the number of PO segments, N_{PO}. Since ΔG° is directly proportional to log(CMC), one can derive the dependance of ΔG° on PO from the slope of the log(CMC) vs N_{PO} line using the data set of Figure 2.4. Indeed, ΔG°_{total} could be expressed as the sum of contributions from the PEO hydrophilic headgroup, ΔG°_{PEO}, and the PPO hydrophobic tail, ΔG°_{PPO}, with $\Delta G^\circ_{PPO} = N_{PO}\, \Delta G^\circ_{-PO-}$, as with smaler hydrocarbon-chain surfactants [Meguro et al., 1981]. Then, the slope of the ΔG°_{total} vs N_{PO} curve should give ΔG°_{-PO-}, the micellization free energy contribution per PO segment, and the intercept ΔG°_{PEO}, the PEO contribution to the total micellization free energy.

Fitting the data in this way, we obtained ΔG°_{-PO-} values ranging from -0.330 ± 0.052 kJ/(mole-PO-) at 15 °C, to -0.822 ± 0.112 kJ/(mole-PO-) at 55 °C. The values for ΔG°_{-PO-} became more negative as the temperature increased, indicating that the contribution of PO to the micellization free energy increases with temperature. This is a result of the positive micellization entropy [Ben-Naim, 1980] and is also observed in surfactants with aliphatic chains (reported by Puvvada and Blankschtein [1990]). The micellization free energy per methylene group for C_iE_j nonionic surfactants was, nevertheless, reported to be independent of temperature [Meguro et al, 1981]. Wanka et al. [1990] used their data and data reported by Schmolka and Raymond [1965] to calculate values for ΔG° for the transfer of a PO-group from Pluronic aqueous solution into a micelle and obtained a value of approximately 0.3 kT or 0.73 kJ/mol. The ΔG°_{-PO-} value we obtained is smaller that the one reported by Wanka et al. [1990]; Wanka et al. give no details of their calculation by which we could check this discrepancy. The free energy for transfering a methylene group into micelles of normal hydrocarbon surfactants is known to be 1.2 kT or 2.9 kJ/mol [Klevens, 1953]. Comparing Pluronics to normal hydrocarbon surfactants we estimated that approximately six -PO- groups are needed in order to obtain the same transfer free energy as for one $-CH_2-$ group.

One may argue that correlating ΔG°_{total} vs N_{PO} for Pluronics of different headgroup (PEO) sizes is not well justified. However we have shown that the Pluronics behave in a concerted way with respect to micellization (e.g. see Figure 2.7b). This, in addition to the fact that ΔG°_{-PO-} values obtained from fitting data from P65, P84, and P123 (Pluronics with the same PEO size) are, within the uncertainty of fitting, the same as ΔG°_{-PO-} obtained by correlating data from all the Pluronics, lead us to believe that there is real significance to the ΔG°_{-PO-} values reported above. The intercept of the ΔG°_{total} vs N_{PO} line decreased (became more negative) with increasing temperature. As this intercept loosely corresponds to the PEO contribution to the micellization free energy, ΔG°_{PEO}, its decrease with increasing temperature may be indicative of PEO dehydration at higher temperatures, contributing towards the formation of micelles. Meguro et al. [1981] found for C_iE_j surfactants a decrease in ΔG°_{PEO} with increasing temperature, similar to the Pluronics. However, ΔG°_{PEO} for C_iE_j surfactants had positive values, while for the case of Pluronics ΔG°_{PEO} was negative for temperatures higher than ~ 18 °C.

Comparison of Pluronic ΔG°, ΔH°, ΔS° to those of C_iE_j nonionic surfactants: For j-ethyleneglycol-i-alkyl ethers with the same headgroup and varying hydrophobic tail (e.g. for the groups C_iE_8, i = 10 to 15 [Meguro et al, 1981], and C_iE_6, i = 6, 8, 10, 12, reported by Nandi and Basumallick [1993]) ΔG° decreased with increasing number of carbon atoms in the alkyl chain, and with increasing temperature. Free energy changes for micelle formation per methylene group equal -0.69 kcal/mol, or -2.887 kJ/mol, to be compared with ΔG°_{-PO-} of approximately -0.45 kJ/mol for the Pluronics. ΔH° decreased (became more negative) with increasing carbon number, while $T\Delta S^\circ$ increased, indicating that ΔS° contributes mainly to micellization, while ΔH° counteracts micellization. The headgroup contribution to ΔG° decreased with increasing temperature, due to dehydration of the PEO chain. For j-ethyleneglycol-i-alkyl ethers with the same hydrophobic tail and varying headgroup (e.g for the system $C_{16}E_j$, j = 17, 32, 44, 63 [Barry & El-Eini, 1976]) ΔG° increased (became less negative) with increasing number of EO units in the hydrophilic headgroup, and decreased with increasing temperature. ΔH° and ΔS° decreased with increasing number of EO segments, while the headgroup contribution to ΔG° increased with increasing number of EO segments.

Appendix B: Micellization thermodynamics

The following text is excerpted (with modifications) from the discussion of Hunter [1987] on the thermodynamics of micellization in aqueous solutions. Careful analyses of the thermodynamics of micelle formation have been given by a number of authors, including Hall and Pethika [1967] and Tanford [1980]. Hunter [1987] followed the latter treatment, with some modifications. The aim is to relate the chemical potential of an amphiphile or surfactant in free solution with that of the same molecule in a micelle of arbitrary size. In an isothermal system at equilibrium this chemical potential must be constant throughout the system.

Tanford distinguishes what he calls the "cratic" contribution to the chemical potential from the intrinsic contribution, which is due to local (chemical and physical) interactions. The cratic part is that due to the entropy of mixing and so for any particular

size of micelle, is equal to: RT ln(mole fraction of micelles of size n). This would give the contribution per mole of micelles of size n, assuming ideal behavior [see Note at the end of Appendix B] (the use of mole fractions is connected with the most appropriate choice of standard state). It is more convenient to express this contribution in terms of the concentration of the monomeric surfactant: RT $\ln(X_n/n)$ where X_n is the mole fraction of monomer in micelles of size n. The cratic contribution per mole of monomeric amphiphile is 1/n of this and so:

$$\mu_{mic,\,n} = \mu^{\circ}_{mic,\,n} + (RT/n)\ \ln(X_n/n) \qquad (B.1)$$

Note that in this formulation, each of the micellar sizes is treated as a separate component, with its own standard state chemical potential. Equating $\mu_{mic,\,n}$ with the value for the free surfactant gives:

$$\mu^{\circ}_{mic,\,n} - \mu^{\circ}_{1} = (RT)\ln\alpha_1 - (RT/n)\ \ln(X_n/n) \qquad (B.2)$$

or

$$\ln X_n = -\,n\,(\mu^{\circ}_{mic,\,n} - \mu^{\circ}_{1})\,/\,(RT) + n\,\ln\alpha 1 + \ln n \qquad (B.3)$$

where α_1 is the activity of the monomer.

Equation B.3 gives explicitly the distribution function of micelles of different size, in terms of the quantity $(n\,\mu^{\circ}_{mic,\,n} - n\,\mu^{\circ}_{1})$, which is the value of ΔG°_{n} for the reaction in which an n-mer is formed from monomers. An optimal size n* can be defined as the value of n for which X_n is a maximum at the particular surfactant activity:

$$(\partial \ln X_n / \partial n)_{\alpha 1} = 0 \quad (n = n^*) \qquad (B.4)$$

Tanford [1980] points out that, if the size distribution is reasonably narrow, the value of n* is experimentally indistinguishable from the number average or mass average micellar size. All can then be set approximately equal to a mean size, $\bar{n}$. At this level of approximation, all micelles are treated as the same and lumped together with a standard chemical potential, μ°_{mic}.

$$\ln X_{mic} = - n (\mu^{\circ}_{mic} - \mu^{\circ}_{1}) / (RT) + \tilde{n} \ln\alpha_1 + \ln \tilde{n} \qquad (B.5)$$

The activity of the free surfactant α_1 is given by y_1X_1, where y_1 is the activity coefficient and it is tempting to assume that $y_1 \approx 1$, since X_1 is usually fairly small (even above the CMC the concentration of the free surfactant remains close to the CMC value). For non-ionic surfactants the activity coefficient correction can probably be dispensed with altogether with negligible error [Desnoyers et al. 1983].

The relation between the standard chemical potential change and the CMC (X_o) can be obtained from Equation B.5 by introducing the ratio $\sigma = X_{mic}/X_o$ and recognizing that, at the CMC, $X_1 = X_o - X_{mic}$. We then have:

$$(\mu^{\circ}_{mic} - \mu^{\circ}_{1}) / (RT) = [(\tilde{n}-1)/\tilde{n}] \ln X_o + \ln y_1 + \ln(1-\sigma) + (1/\tilde{n}) \ln(\tilde{n}/\sigma) \qquad (B.6)$$

A knowledge of the CMC (X_o) and the mean aggregation number, $\tilde{n}$, is required to estimate values of $(\mu^{\circ}_{mic} - \mu^{\circ}_{1})$. The value of σ can be taken to be anywhere from 0.01 to 0.1 with negligible effect on the result but, of course, one has to either assume $y_1 = 1$ or make some correction for it. This latter correction should be relatively unimportant if one wishes only to evaluate the change in $(\mu^{\circ}_{mic} - \mu^{\circ}_{1})$ as the chain length changes. Indeed, for many purposes, the following approximation, valid for large $\tilde{n}$ and small σ is sufficiently accurate:

$$\mu^{\circ}_{mic} - \mu^{\circ}_{1} = \Delta G^{\circ} = RT \ln X_o. \qquad (B.7)$$

A further correction is essential in order for Equation B.7 to be applied to ionic surfactants.

From Equation B.5 we can write, for the free energy change on micelle formation:

$$\begin{aligned} \Delta G^{\circ} &= \mu^{\circ}_{mic} - \mu^{\circ}_{1} = RT \ln \alpha_1 - (RT/n) \ln X_{mic} \\ &\approx RT \ln(CMC) - (RT/n) \ln X_{mic} \end{aligned} \qquad (B.8)$$

neglecting the $(n^{-1} \ln n)$ term. The temperature and pressure derivatives of Equation B.8 give the standard enthalpy change ΔH° and volume change ΔV°, per mole of monomer:

$$\Delta H^\circ = -RT^2(\partial \ln(CMC)/\partial T)_P + (RT^2/n)(\partial \ln(X_{mic})/\partial T)_P \quad (B.9)$$

and

$$\Delta V^\circ = RT(\partial \ln(CMC)/\partial P)_T + (RT/n)(\partial \ln(X_{mic})/\partial P)_T \quad (B.10)$$

ΔS° can be obtained from:

$$\Delta S^\circ = (\Delta H^\circ - \Delta G^\circ)/T \quad (B.11)$$

In the neighbourhood of the CMC the value of X_{mic} is small, and since n is not always known, it is common practice to neglect the second term on the right of each of these expressions and to estimate ΔG° from the approximate Equation B.7.

Note on modelling solution entropy in the theory of micellization: Nagarajan [1993] examined the consequences of using various entropy models to predict the properties of solutions in which micelles are present. The four widely used entropy estimates compared by Nagarajan [1993] were based on the ideal solution model (used in the derivation of Appendix B), the gas-like translation model, the Flory-Huggins model, and the translational entropy model. The ideal solution model was found to provide CMC results that were in very good agreement with experimental values for both a non-ionic and an ionic surfactant. Nagarajan [1993] noted that applying the entropy estimate based on the ideal solution model, would result in ignoring all size variations among the species constituting the surfactant solution. The ideal solution model provided predictions of the CMC, the micelle size, its dependence on surfactant concentration and the polydispersity index in good agrement with experiments; however, the model failed in its predictions of the solution phase separation behavior. It can be concluded that, for the applications of this Thesis, the use of the ideal solution model for deriving solution entopy is a very good choice.

2.6 References Cited in Chapter 2

1. Al-Saden, A. A.; Whateley, T. L.; Florence, A. T. *J. Colloid Interface Sci.* **1982**,

90, 303.

2. Alexandridis, P.; Athanassiou, V.; Fukuda, S.; Hatton, T. A. *Langmuir*, **1994**, in press; Chapter 4 of this Thesis.
3. Almgren, M.; Bahadur, P.; Jansson, M.; Li, P.; Brown, W.; Bahadur, A. *J. Colloid Interface Sci.* **1992**, *151*, 157.
4. Ananthapadmanabhan, K. P.; Goddard, E. D.; Turro, N. J.; Kuo, P. L. *Langmuir* **1985**, *1*, 352.
5. Anderson, R .A. *Pharm. Acta Helv.* **1972**, *47*, 304.
6. Armstrong, J. K.; Parsonage, J.; Chowdhry, B.; Leharne, S.; Mitchell, J.; Beezer, A.; Lohner, K.; Laggner, P. *J. Phys. Chem.* **1993**, *97*, 3904.
7. Attwood, D., Florence, A. T. *Surfactant Systems: Their Chemistry, Pharmacy and Biology*; Chapman and Hall: London, 1983.
8. Attwood, D.; Collet, J. H., Tait, C.J. *Int. J. Pharm.* **1987**, *40*, 93.
9. Bahadur, P.; Riess, G. *Tenside Surf. Det.* **1991**, *28*, 173.
10. Bahadur, P.; Pandya, K. *Langmuir* **1992**, *8*, 2666.
11. Barry, B. W.; El-Eini, D. I. D. *J. Colloid Interface Sci.* **1976**, *54*, 339.
12. Bedo, Zs.; Berecz, E.; Lakatos, I. *Colloid Polym. Sci.* **1992**, *270*, 799.
13. Beezer, A.; Mitchard, N.; Mitchell, J. C.; Armstrong, J. K.; Chowdhry, B.; Leharne, S.; Buckton, G. *J. Chem. Res. (S)* **1992**, 236.
14. Ben-Naim, A. *Hydrophobic Interactions*, Plenum Press, New York, 1980, p. 202.
15. Birks, J. B. *Photophysics of Aromatic Molecules*; Wiley-Interscience: New York, 1970, p 85.
16. Brown, W.; Schillen, K.; Almgren, M.; Hvidt, S.; Bahadur, P. *J. Phys. Chem.* **1991**, *95*, 1850.
17. Cehelnic, E. D.; Cundall, R. B.; Lockwood, J. R.; Palmer, T. F. *J. Phys. Chem.* **1975**, *79*, 1369.
18. Chattopadhyay, A.; London, E. *Anal. Biochem.* **1984**, *139*, 408.
19. Chen, V.; Warr, G. G.; Evans, D. F.; Prendergast, F. G. *J. Phys. Chem.* **1988**, *92*, 768.
20. Corkill, J. M.; Walker, T. *J. Colloid Interface Sci.* **1972**, *39*, 620.
21. Deng, Y.; Ding, J.; Stubbersfield, R. B.; Heatley, F.; Attwood, D.; Price, C.; Booth, C. *Polymer* **1992**, *33*, 1963.
22. Deng, Y.; Yu, G. R.; Price, C.; Booth, C. *J. Chem. Soc., Faraday Trans.* **1992**, *88*, 1441.

23. Edwards, D. A.; Luthy, R. G.; Liu, Z. *Environ. Sci. Technol.* **1991**, *25*, 127.
24. Gilbert, J. C.; Washington, C.; Davies, M. C.; Hadgraft, *J. Int. J. Pharm.* **1987**, *40*, 93
25. Goldstein, R. E. *J. Chem. Phys.* **1984**, *80*, 5340.
26. Grieser, F.; Drummond, C. J. *J. Phys. Chem.* **1988**, *92*, 5580.
27. Haugland, R. P. *Handbook of Fluorescent Probes and Research Chemicals*, 5th ed.; Molecular Probes Inc.: Eugene, OR, 1992.
28. Hiemenz, P. C. *Principles of Colloid and Surface Chemistry*, 2nd ed.; Marcel Dekker, Inc.: New York, 1986.
29. Hunter, R. J. *Foundations of Colloid Science*; Oxford University Press: New York, 1987; Vol. 1.
30. Hurter, P. N.; Hatton, T. A. *Langmuir* **1992**, *8*, 1291.
31. Hurter, P. N.; Scheutjens, J. M. H. M.; Hatton, T. A. *Macromolecules* **1993**, *26*, 5030.
32. Hurter, P. N.; Scheutjens, J. M. H. M.; Hatton, T. A. *Macromolecules* **1993**, *26*, 5592.
33. Hurter, P. N.; Anger, L. A.; Vojdovich, L. J., Kelley, C. A.; Cohen, R. E.; Hatton, T. A. in *Solvent Extraction in the Process Industries*; Logsdail, D. H., Slater, M. J., Eds., Elsevier Applied Science: London, 1993, Vol. 3, p 1663.
34. Karlstrom, G. *J. Phys. Chem.* **1985**, *89*, 4962.
35. Kjelander, R.; Florin, E. *J. Chem. Soc., Faraday Trans. 1* **1981**, *77*, 2053.
36. Klevens, H. B. *J. Amer. Oil Chem. Soc.* **1953**, *30*, 74.
37. Lianos, P.; Zana, R. *J. Colloid Interface Sci.* **1982**, *88*, 594.
38. Lindman, B.; Karlstrom, G.; Carlsson, A.; Malmsten, M. *Adv. Colloid Interface Sci.* **1990**, *32*, 183.
39. Linse, P.; Malmsten, M. *Macromolecules* **1992**, *25*, 5434.
40. Linse, P. *Macromolecules* **1993**, *26*, 4437.
41. Linse, P. *J. Phys. Chem.* **1993**, *97*, 13896.
42. Malmsten, M.; Linse, P.; Zhang, K.-W. *Macromolecules* **1993**, *26*, 2905.
43. Meguro, K.; Ueno, M.; Esumi, K. in *Nonionic Surfactants: Physical Chemistry*; Schick, M. J., Ed. Marcel Dekker Inc.: New York, 1987, p109.
44. Meguro, K.; Takasawa, Y.; Kawahashi, N.; Tabata, Y.; Ueno, M. *J. Colloid Interface Sci.* **1981**, *83*, 50.
45. Mitchard, N. M.; Beezer, A. E.; Mitchell, J. C.; Armstrong, J. K.; Chowdhry, B.

Z.; Leharne, S.; Buckton, G. *J. Phys. Chem.* **1992**, *96*, 9507.
46. Mortensen, K.; Pedersen, J. S. *Macromolecules* **1993**, *26*, 805.
47. Mortensen, K. *Europhys. Lett.* **1992**, *19*, 599.
48. Mukerjee, P.; Mysels, K. J. Critical Micelle Concentrations of Aqueous Surfactant Systems. NSRDS-NBS 36, Government Printing Office, Washington, DC, 1971.
49. Nagarajan, R.*Colloids Surfaces A* **1993**, *71*, 39.
50. Nandi, N.; Basumallick, I.N. *J. Phys. Chem.* **1993**, *97*, 3900.
51. *Pluronic and Tetronic Surfactants*. Technical Brochure, BASF Corp., Parcippany, NJ, 1989.
52. Prasad, K. N.; Luong, T. T.; Florence, A. T.; Paris, J.; Vaution, C.; Seiller, M.; Puisieux, F. *J. Colloid Interface Sci.* **1979**, *69*, 225.
53. Price, C. *Pure Appl. Chem.* **1983**, *55*, 1563.
54. Price, C.; Stubbersfield, R. B.; El-Kafrawy, S.; Kendall, K. D. *Br. Polym. J.* **1989**, *21*, 391.
55. Puvvada, S.; Blankschtein, D. *J. Chem. Phys.* **1990**, *92*, 3710.
56. Quintana, J. R.; Villacampa, M.; Katime, I. A. *Macromolecules* **1993**, *26*, 601.
57. Rassing, J; Attwood, D. *Int. J. Pharm.* **1983**, *13*, 47.
58. Reddy, N. K.; Fordham, P. J.; Attwood, D.; Booth C. *J. Chem. Soc., Faraday Trans.* **1991**, *86*, 1569.
59. Rosen, M. J. *Surfactants and Interfacial Phenomena*, 2nd ed.; J. Wiley & Sons: New York, 1989.
60. Schmolka, I. R. *J. Am. Oil Chem. Soc.* **1977**, *54*, 110.
61. Schmolka, I. R., Raymond, A. J. *J. Am. Oil Chem. Soc.* **1965**, *42*, 1088.
62. Sikora, A.; Tuzar, Z. *Makromol. Chem.* **1983**, *184*, 2049.
63. Stainsby, G.; Alexander, A. E. *Trans. Faraday Soc.* **1950**, *46*, 587.
64. Tanford, C. *The Hydrophobic Effect: Formation of Micelles and Biological Membranes*, 2nd ed.; J. Wiley & Sons: New York, 1980.
65. Tuzar, Z.; Kratochvil, P. *Adv. Colloid Interface Sci.* **1976**, *6*, 201.
66. Vadnere, M.: Amidon, G. L.; Lindenbaum, S.; Haslam, J. L. *Int. J. Pharm.* **1984**, *22*, 207.
67. Wang, P.; Johnston, T. P. *J. Appl. Polym. Sci.* **1991**, *43*, 283.
68. Wanka, G.; Hoffmann, H.; Ulbricht, W. *Colloid Polym. Sci.* **1990**, *266*, 101.
69. Williams, R. K.; Simard, M. A.; Jolicoeur, C. *J. Phys. Chem.* **1985**, *89*, 178.
70. Yang, L.; Bedells, A. D.; Attwood, D.; Booth, C. *J. Chem. Soc., Faraday Trans.*

1992, *88*, 1447.

71. Yekta, A.; Aikawa, M.; Turro, N. J. *Chem. Phys. Lett.* **1979**, *63*, 543.
72. Yu, G.-E.; Deng, Y.; Dalton, S.; Wang, Q.-G.; Attwood, D.; Price, C.; Booth C. *J. Chem. Soc., Faraday Trans.* **1992**, *88*, 2537.
73. Zhou, Z.; Chu, B. *J. Colloid Interface Sci.* **1988**, *126*, 171.

Chapter 2: List of Tables

Chapter 2: List of Figures

Figure 2.4 (a) Critical micellization concentrations and (b) critical micellization temperatures of Pluronic copolymers, having the same number of EO segments, as a function of the number of PO segments.

Figure 2.5 (a) Critical micellization concentrations for Pluronic copolymers at various solution temperatures and (b) critical micellization temperatures at various copolymer concentrations, as a function of the number of EO segments, for copolymers of 40, 50, and 80% EO content.

Figure 2.6 Reciprocal T_{CMT} vs copolymer concentration plots for various Pluronics, used for the determination of the micellization enthalpy in terms of the closed association model.

Figure 2.7 Effect of Pluronic molecular weight on the free energies of micellization for various polymer concentrations expressed as (a) ΔG° (kJ/mol), and (b) $\Delta G^{\circ} / (N_{EO} + N_{PO})$ (kJ / mol of monomer segments).

Figure 2.8 Effect of polymer composition ratio, PPO/PEO, on (a) $\Delta H^{\circ} / (N_{EO} + N_{PO})$, and (b) $\Delta G^{\circ} / (N_{EO} + N_{PO})$.

Table 2.1 Properties of the Pluronic copolymers used in this study.

Polymer	Mol.Weight	PPO segm. weight	PO units	EO units	Lot number
L64	2900	1740	30	2x13	WPWN-505A
P65	3400	1700	29	2x18	WPAN-605B
F68	8400	1680	29	2x76	WPON-611B
P84	4200	2520	43	2x19	WPTN-561B
P85	4600	2300	40	2x26	WPAN-628B
F88	11400	2280	39	2x103	WPDN-616B
P103	4950	3465	60	2x17	WPHM-539B
P104	5900	3540	61	2x27	WPAN-503B
P105	6500	3250	56	2x37	WPDI-522A
F108	14600	2920	50	2x132	WPDN-564B
P123	5750	4025	69	2x19	WPYM-569B
F127	12600	3780	65	2x100	WPON-593B
25R4	3600	2500	2x21	25	WPMN-515B

Table 2.2 Critical micellization temperatures for Pluronic PEO-PPO-PEO copolymer aqueous solutions as a function of copolymer concentration.

Concentration (% w/v)	L64 mM	L64 CMT	P65 mM	P65 CMT	F68 mM	F68 CMT
0.01		-		-		-
0.025	0.086	44.5		-		-
0.05	0.172	42	0.147	49		-
0.1	0.345	39.5	0.294	46		-
0.25	0.862	36.5	0.735	42		-
0.5	1.72	34	1.47	39	0.595	52.5
1.0	3.45	31.5	2.94	36	1.19	50
2.5	8.62	28.5	7.35	31.5	2.98	46
5.0	17.2	26.5	14.7	28.5	5.95	40
10	34.5	23.5	29.4	25.5	11.9	33
15		-		-	17.9	27

Concentration (% w/v)	P84 mM	P84 CMT	P85 mM	P85 CMT	F88 mM	F88 CMT
0.01	0.024	46.5	0.022	46.5		-
0.025	0.059	42.5	0.054	43		-
0.05	0.119	39.5	0.109	40	0.044	52.5
0.1	0.238	37	0.217	37.5	0.088	48.5
0.25	0.595	33.5	0.543	33.7	0.219	45
0.5	1.19	31	1.09	32	0.439	41
1.0	2.38	28.5	2.17	29.5	0.877	38
2.5	5.95	25.5	5.43	27	2.19	34
5.0	11.9	23	10.9	25	4.39	30.5
10	23.8	19		-	8.77	26
15		-		-	13.2	21.5

Table 2.2 (continued)

Concentration (% w/v)	P103 mM	P103 CMT	P104 mM	P104 CMT	P105 mM	P105 CMT
0.01	0.02	29.5	0.017	33.5	0.015	32
0.025	0.05	27.5	0.042	31	0.038	30
0.05	0.101	26	0.085	29.5	0.077	28.5
0.1	0.202	24.5	0.169	27.5	0.154	27
0.25	0.505	22.5	0.424	25.5	0.385	25
0.5	1.01	21	0.847	23.5	0.769	23.5
1.0	2.02	19.5	1.69	21.5	1.54	21.7
2.5		-	4.24	19.5	3.85	19.5
5.0		-	8.47	18		-
10		-		-		-
15		-		-		-

Concentration (% w/v)	F108 mM	F108 CMT	P123 mM	P123 CMT	F127 mM	F127 CMT
0.01		-	0.017	26		-
0.025	0.017	40.5	0.043	24	0.02	35.5
0.05	0.034	38	0.087	22.5	0.04	33
0.1	0.068	36	0.174	21	0.079	31
0.25	0.171	33.5	0.435	19	0.198	28
0.5	0.342	31.5	0.87	17.5	0.397	26.5
1.0	0.685	29.5	1.74	16	0.794	24
2.5	1.71	27	4.35	14	1.98	21.5
5.0	3.42	24.5	8.70	12.5	3.97	19.5
10	6.85	21		-		-
15		-		-		-

Table 2.3 Critical micellization concentrations for Pluronic PEO-PPO-PEO copolymer aqueous solutions, as a function of solution temperature.

Temperature (°C)	L64 % w/v	L64 mM	P65 % w/v	P65 mM	F68 % w/v	F68 mM
20	-		-		-	
25	-		-		-	
30	1.5	5.172	4	11.76	-	
35	0.4	1.379	1	2.941	-	
40	0.1	0.344	0.35	1.029	7	8.333
45	0.02	0.069	0.1	0.294	3	3.571
50	-		0.04	0.117	0.9	1.071
55	-		-		0.3	0.357

Temperature (°C)	P84 % w/v	P84 mM	P85 % w/v	P85 mM	F88 % w/v	F88 mM
20	-		-		-	
25	2.6	6.190	4	8.695	-	
30	0.6	1.428	0.9	1.956	-	
35	0.15	0.357	0.2	0.434	1.7	1.491
40	0.04	0.095	0.05	0.108	0.6	0.526
45	0.013	0.031	0.014	0.030	0.24	0.210
50	-		-		0.09	0.079
55	-		-		0.04	0.035

Table 2.3 (continued)

Temperature (°C)	P103 % w/v	P103 mM	P104 % w/v	P104 mM	P105 % w/v	P105 mM
20	0.7	1.414	2	3.389	2.2	3.384
25	0.07	0.141	0.3	0.508	0.3	0.461
30	0.01	0.020	0.04	0.067	0.025	0.038
35	0.002	0.004	0.008	0.013	0.005	0.007
40	-		0.002	0.003	0.001	0.001
45	-		-		-	
50	-		-		-	
55	-		-		-	

Temperature (°C)	F108 % w/v	F108 mM	P123 % w/v	P123 mM	F127 % w/v	F127 mM
20	-		0.18	0.313	4	3.174
25	4.5	3.082	0.03	0.052	0.7	0.555
30	0.8	0.547	0.005	0.009	0.1	0.079
35	0.15	0.103	0.001	0.002	0.025	0.019
40	0.04	0.027	-		0.008	0.006
45	0.008	0.005	-		-	
50	-		-		-	
55	-		-		-	

Table 2.4 Standard free energies (ΔG°), enthalpies (ΔH°), and entropies (ΔS°) of micellization of various Pluronic copolymers at their critical micellization temperature for 1% solutions.

Polymer	Mol.Weight	PPO/PEO	ΔH° kJ/mol	ΔG° kJ/mol	ΔS° kJ/(mol K)
L64	2900	1.155	230	-24.5	0.835
P65	3400	0.766	182	-25.3	0.671
F68	8400	0.190	215	-28.8	0.756
P84	4200	1.149	211	-25.2	0.784
P85	4600	0.764	229	-25.5	0.842
F88	11400	0.190	169	-28.5	0.638
P103	4950	1.791	339	-24.8	1.244
P104	5900	1.146	296	-25.4	1.092
P105	6500	0.763	331	-25.6	1.212
F108	14600	0.190	266	-28.4	0.975
P123	5750	1.788	329	-24.9	1.223
F127	12600	0.326	253	-27.5	0.944

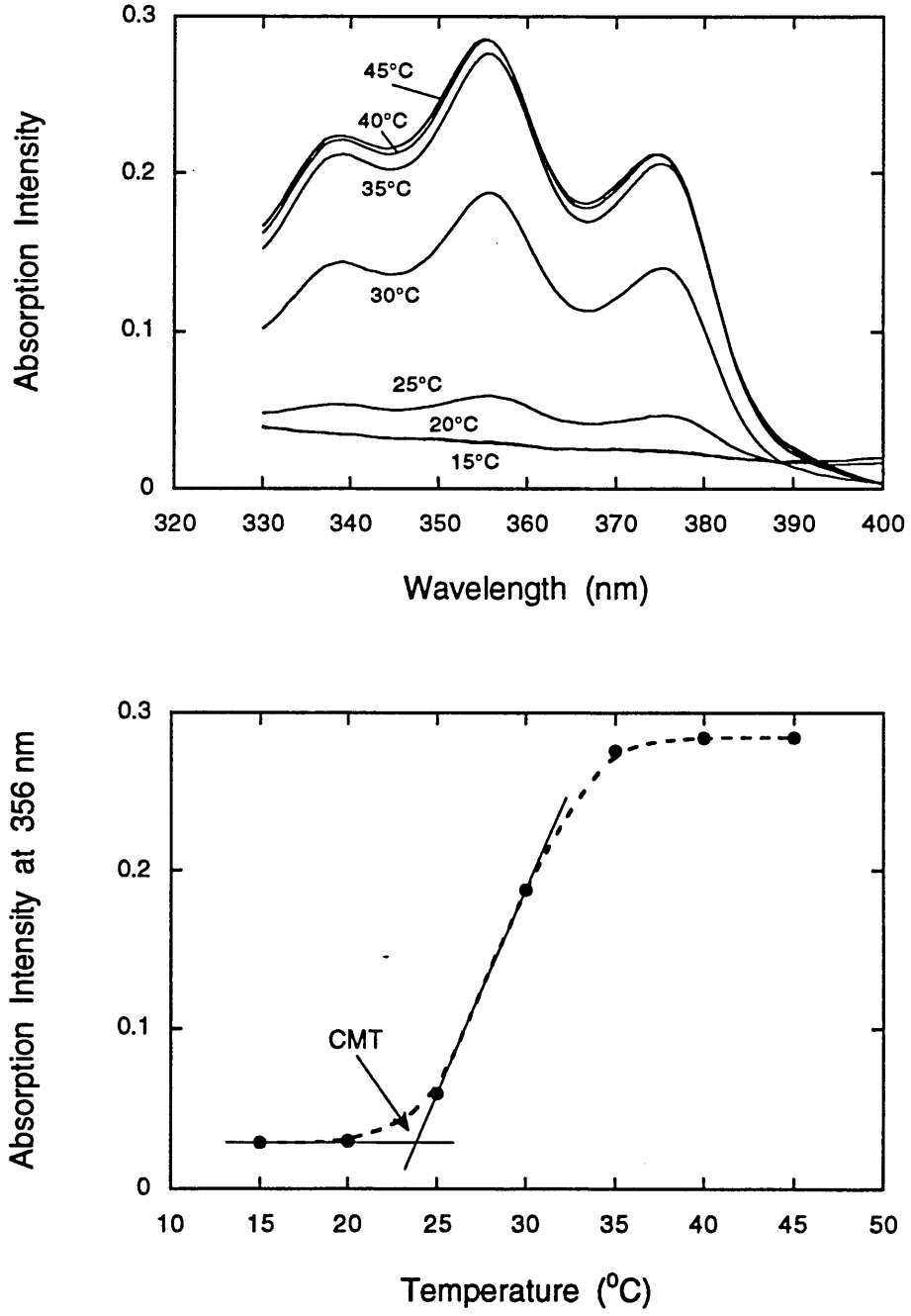

Figure 2.1 Effect of temperature on (a) UV-vis absorption spectra and (b) the absorption intensity at 356 nm for DPH in a 0.5% w/v solution of Pluronic P104. The estimation of the critical micellization temperature from the data is indicated in (b).

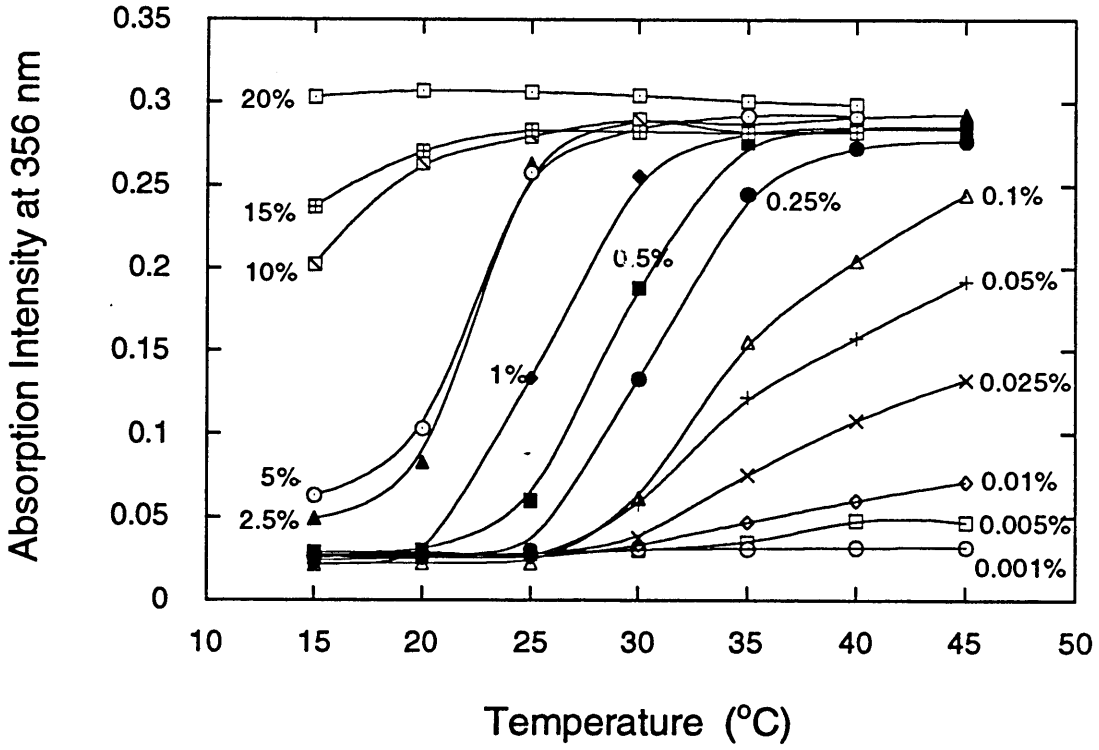

Figure 2.2 Temperature effects on the absorption intensity of DPH at 356 nm in aqueous solutions of Pluronic P104 of various concentrations. The critical micellization temperatures can be estimated from the first break in the curves.

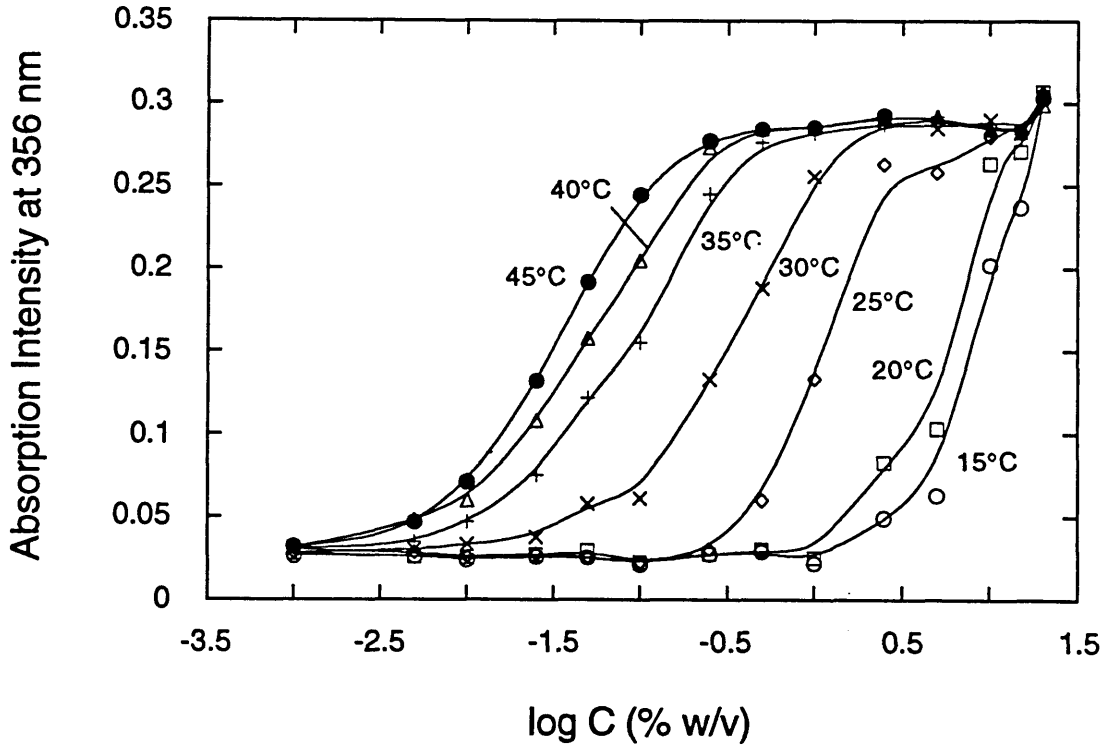

Figure 2.3 Effect of concentration, with temperature as parameter, on the absorption intensity of DPH at 356 nm in aqueous solutions of Pluronic P104. The critical micellization concentrations can be estimated from the first break in the curves.

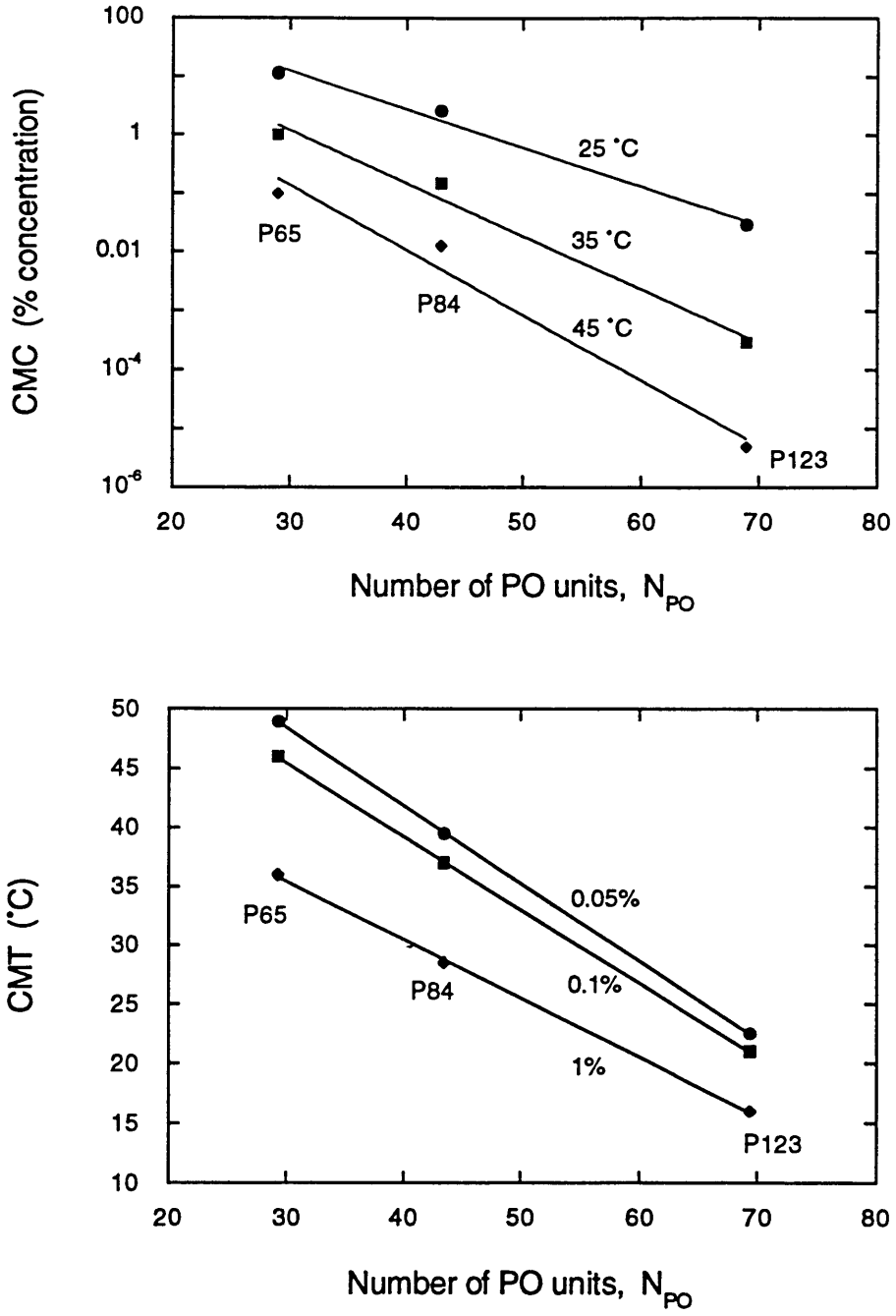

Figure 2.4 (a) Critical micellization concentrations and (b) critical micellization temperatures of Pluronic copolymers, having the same number of EO segments, as a function of the number of PO segments.

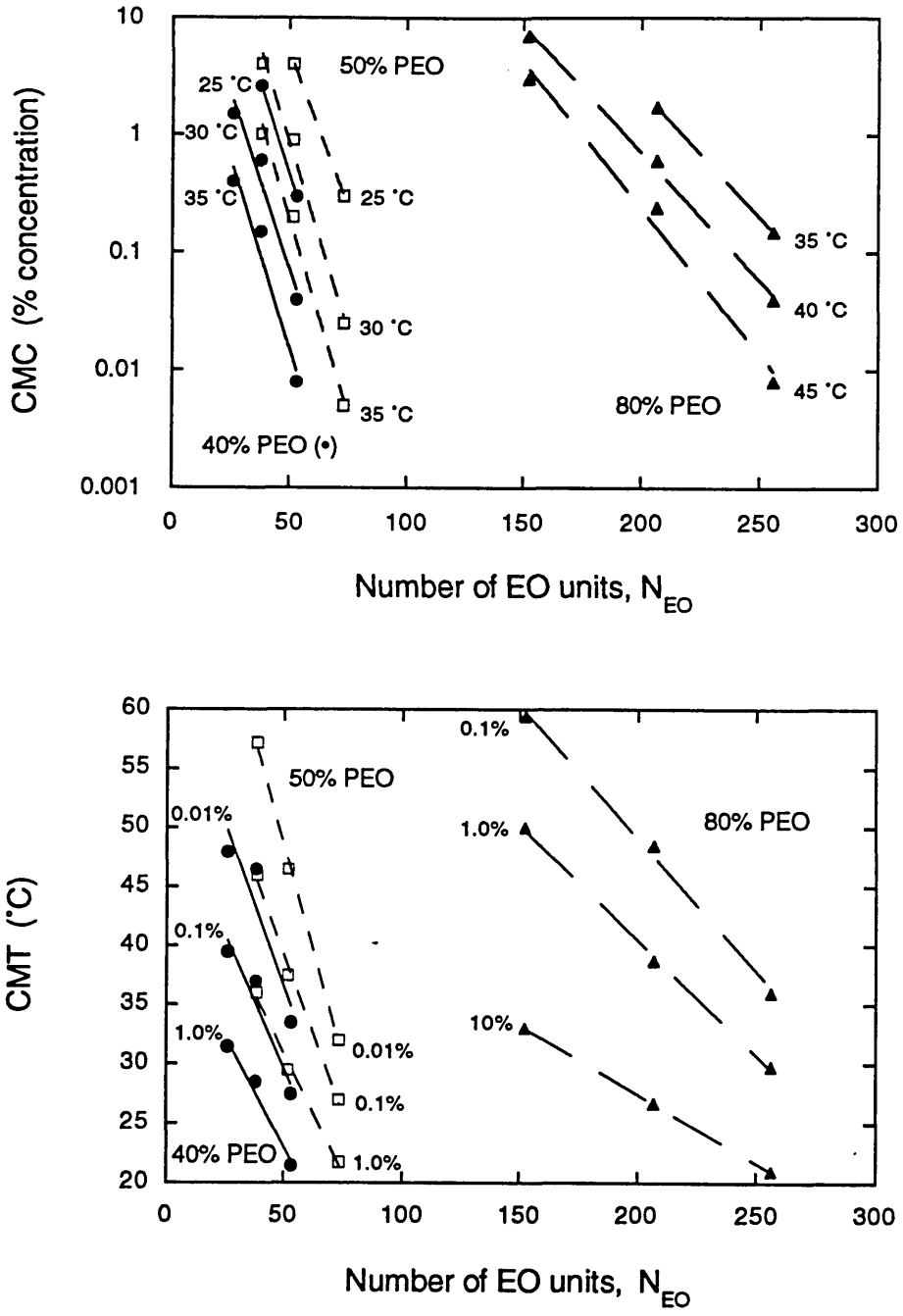

Figure 2.5 (a) Critical micellization concentrations for Pluronic copolymers at various solution temperatures and (b) critical micellization temperatures at various copolymer concentrations, as a function of the number of EO segments, for copolymers of 40, 50, and 80% EO content.

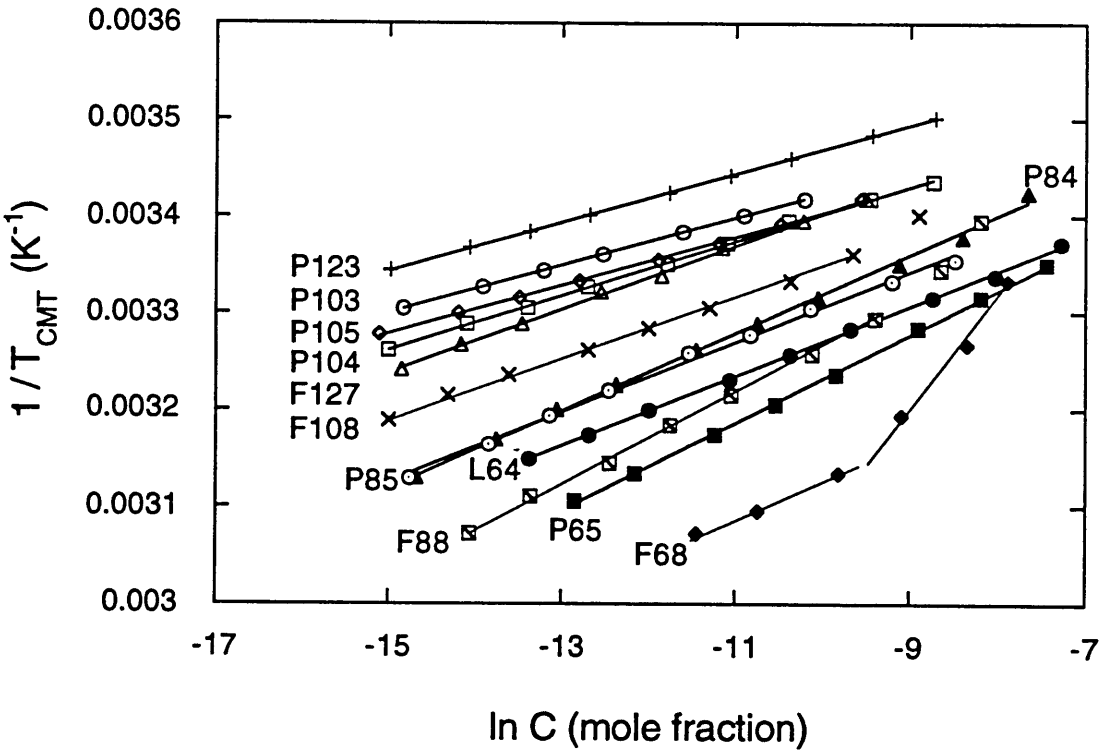

Figure 2.6 Reciprocal T_{CMT} vs copolymer concentration plots for various Pluronics, used for the determination of the micellization enthalpy in terms of the closed association model.

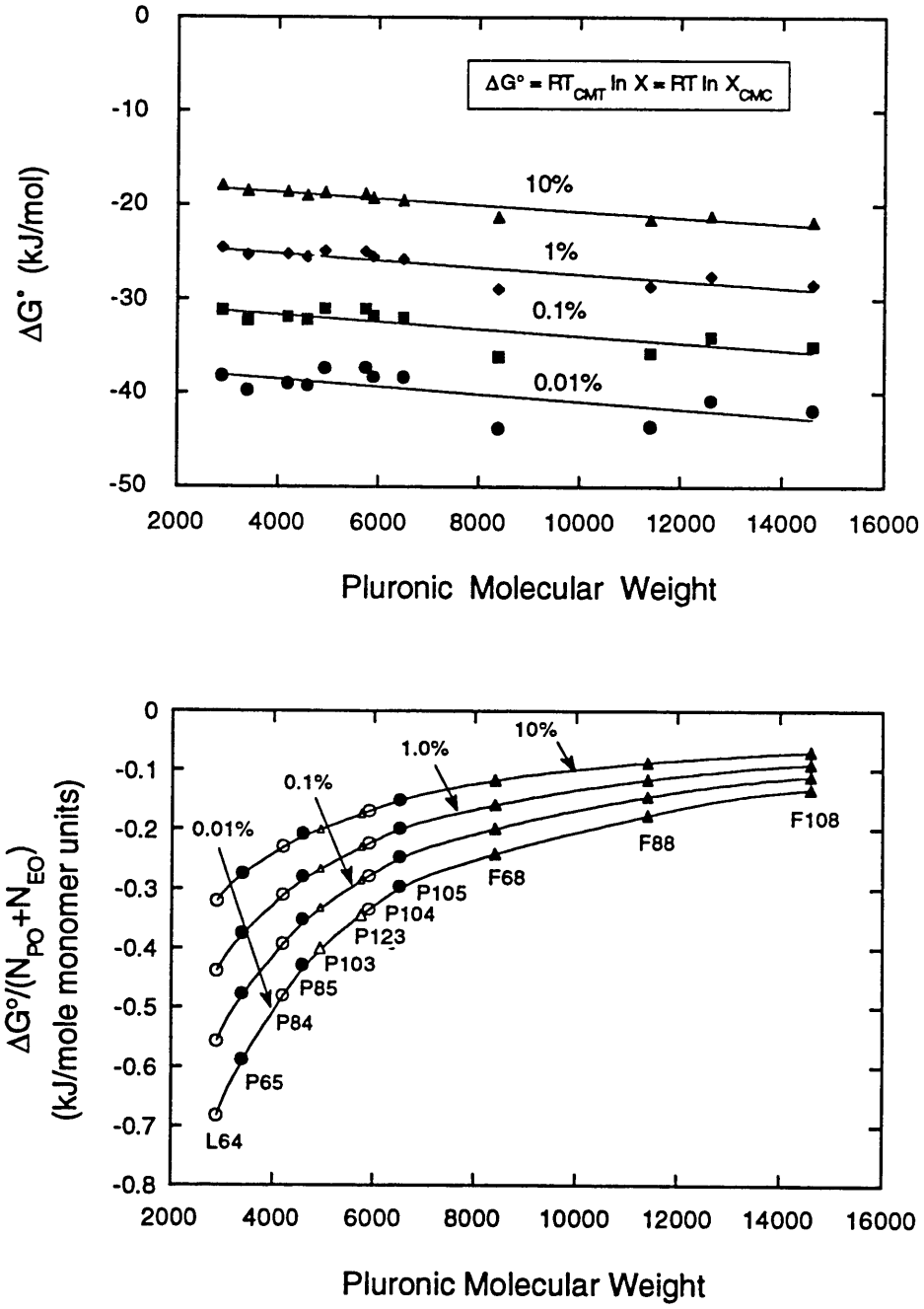

Figure 2.7 Effect of Pluronic molecular weight on the free energies of micellization for various polymer concentrations expressed as (a) ΔG° (kJ/mol), and (b) $\Delta G^{\circ} / (N_{EO} + N_{PO})$ (kJ / mol of monomer segment).

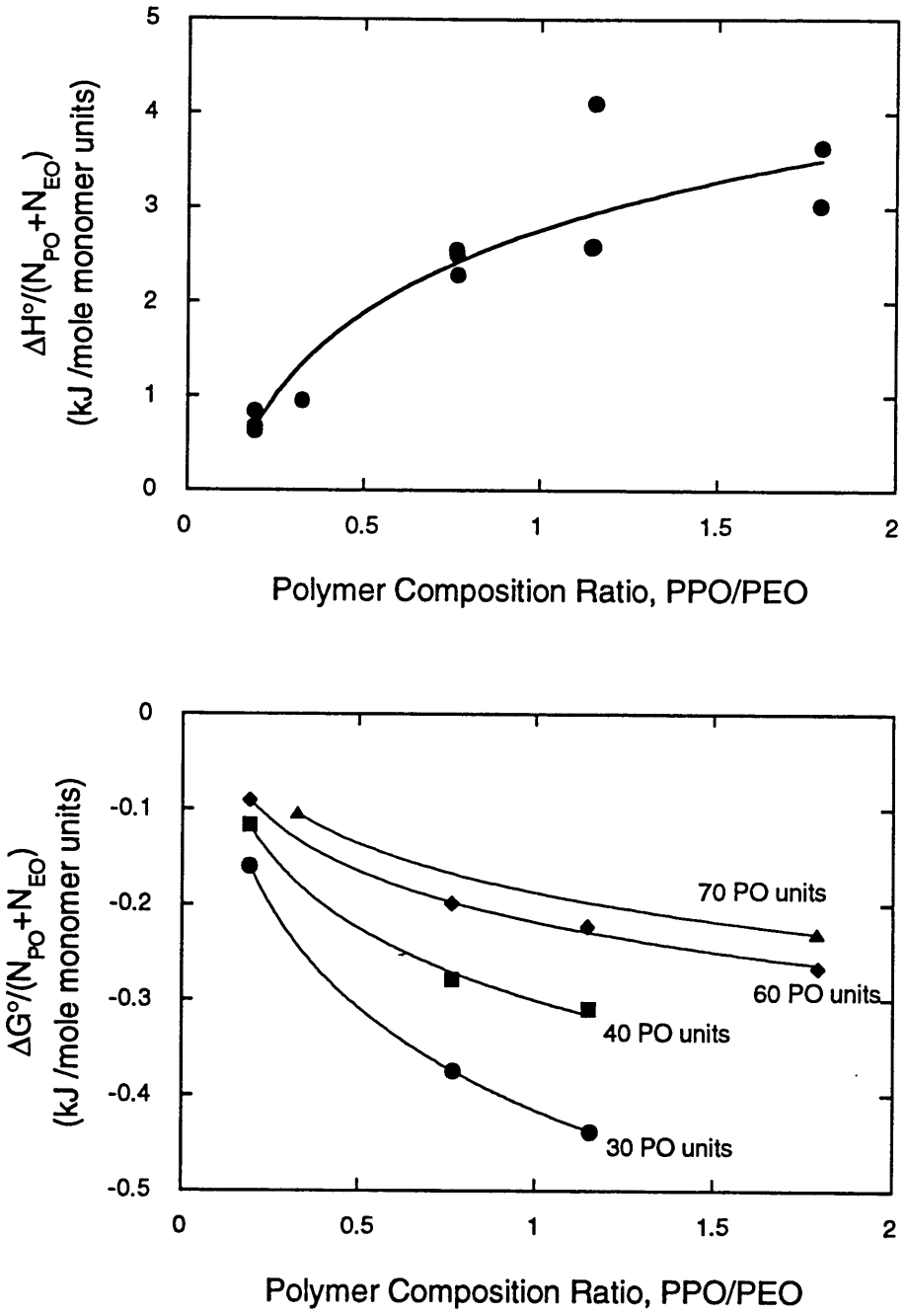

Figure 2.8 Effect of polymer composition ratio, PPO/PEO, on (a) $\Delta H^{\circ} / (N_{EO} + N_{PO})$, and (b) $\Delta G^{\circ} / (N_{EO} + N_{PO})$.

Chapter 3
A Correlation for the Estimation of Critical Micellization Concentrations and Temperatures of Pluronic PEO-PPO-PEO Triblock Copolymers in Aqueous Solutions

3.1 Introduction

Temperature-dependent micellization is a characteristic property of aqueous poly(ethylene oxide)-*block*-poly(propylene oxide)-*block*-poly(ethylene oxide) (PEO-PPO-PEO) copolymer solutions. A number of these copolymers have been shown to aggregate at elevated temperatures in the form of micelles, with a core presumably dominated by PPO and a corona dominated by hydrated PEO segments [Alexandridis & Hatton, 1994]. Considerable effort has been made in modelling the micellization of block copolymers in solvents selective for one block (see Hurter et al. [1993] and references cited therein). One line of research has been the formulation of a phenomenological expression for the system free energy; parameters of interest to the micellization, such as critical micellization concentration (CMC) and aggregation number, are obtained from minimization of the system free energy. While there are theories successful in predicting some of the trends observed experimentally for block copolymer micelles, the contributions to the expressions for the micellization free energy (ΔG°) vary from theory to theory. In fact, some of the free energy contributions considered may be inapplicable in the specific case of PEO-PPO-PEO copolymers, due to the nature of water as a solvent and the finite solubility of PPO in water. Experimentally determined ΔG° data may shed light to the free energy contributions considered in the various theories, and help improve their predictive capabilities for systems of industrial importance like the Pluronic/water.

In the context of an ongoing experimental [Hurter & Hatton, 1992; Alexandridis et al., 1994] and theoretical [Hurter et al., 1993] investigation of the micellization behavior and solubilization efficacy of PEO-PPO-PEO copolymers, we have measured critical

micellization concentrations and critical micellization temperatures (CMT) for 12 Pluronic PEO-PPO-PEO block copolymers, covering a wide range of molecular weights (2900 - 14600) and PPO/PEO ratios (0.19 - 1.79) [Alexandridis et al., 1994]. An empirical correlation for estimating CMC and CMT for aqueous PEO-PPO-PEO copolymer solutions, in which CMC and CMT are expressed as a function of the copolymer molecular weight, PPO/PEO composition, and solution temperature (for CMC determination) or concentration (in the case of CMT), is presented here. The correlation, based on a simple expression for the standard free energy of micellization, is discussed in the light of Flory-Huggins free energy of mixing and phenomenological theories of block copolymer micellization.

3.2 Materials and Methods

The Pluronic poly(ethylene oxide)-*block*-poly(propylene oxide)-*block*-poly(ethylene oxide) copolymers, obtained from BASF Corporation, Parsippany, NJ, are available in a range of molecular weights and PPO/PEO ratios [Alexandridis et al., 1994]. The copolymers considered here are presented in Figure 3.1, arranged in the form of a grid; the relative sizes of the PEO (side) and PPO (middle) blocks are drawn approximately on scale. Experimentally determined CMC and CMT values for a number of Pluronics have been reported by Alexandridis et al. [1994].

3.3 Results and Discussion

3.3a Thermodynamics of micelle formation: association model

In general, micellization of block copolymers, as in the case of conventional detergents, obeys the closed association model, which assumes an equilibrium between molecularly dispersed copolymer (unimer) and multimolecular aggregates (micelles). Based on this model, the standard free energy change for the transfer of one mole of amphiphile from solution to the micellar phase (free energy of micellization), ΔG°, in the absence of electrostatic interactions (the PEO-PPO-PEO copolymers are nonionic) is given

by [Hunter, 1987]

$$\Delta G^{\circ} = R\,T\,\ln X_{CMC} \qquad (1)$$

where R is the gas law constant, T the absolute temperature, and X_{CMC} the critical micellization concentration expressed in mole fraction units. It is assumed that the concentration of unimer in the presence of micelles is constant and equal to the CMC value and that the micelle aggregation number is large (n>100 is usually sufficiently large). Applying the Gibbs-Helmholtz equation we can express the standard enthalpy of micellization, ΔH°, as [Hunter, 1987]

$$\Delta H^{\circ} = -RT^2 \left[\partial \ln X_{CMC} / \partial T \right]_P = R \left[\partial \ln X_{CMC} / \partial (1/T) \right]_P \qquad (2)$$

Equation 2 indicates that there should be a linear relationship between $\ln X_{CMC}$ and 1/T (provided ΔH° is independent of temperature). This was indeed the case when the inverse CMT values were plotted as a function of the natural logarithm of copolymer mole fraction [Note 1] for a number of Pluronics [Alexandridis et al., 1994]. Figure 3.2 shows the inverse CMT values plotted vs concentration expressed in % w/v units, to facilitate ease of use and comparison with concentration data in such units reported elsewhere. The CMT data, plotted in this manner, are described adequately by a straight line [Note 2], as shown in Figure 3.2 where the solid lines are the fit to the experimental data. Detailed analysis and discussion on the influence of copolymer composition and molecular weight on CMCs and CMTs is presented elsewhere [Alexandridis et al., 1994]; the focus here is on using these data to develop tools for predicting the micellization behavior of aqueous Pluronic solutions. As a first step, we present the equations that fitted the data of Figure 3.2:

$$1 / T_{CMT} = S \log C + I \qquad (3)$$

where T_{CMT} is the critical micellization temperature expressed in K, C is the copolymer concentration (% w/v), and S and I are constants whose values are listed in Table 3.1 for various Pluronic copolymers. The molecular weights (M_W) of the copolymers are also listed in Table 3.1, to facilitate conversion from mass concentration to mole fraction units (X). The mole fraction concentration as a function of % w/v is given by (assuming the

density of the copolymer solution to equal the density of pure water)

$$X = C / [\, C + (5.55 - 0.055\, C)\, M_W \,] \qquad (4)$$

Equation 3 allows accurate determination of CMC at a given temperature, or CMT for a given concentration, for each of the 12 PEO-PPO-PEO Pluronic copolymers studied here.

3.3b ΔG° as a function of copolymer molecular weight

Micellization free energy, ΔG°, values, expressed in kJ per mole of copolymer and calculated at the CMT for copolymer solutions of the same mass concentration, exhibited a trend of decrease (became more negative) with increasing copolymer molecular weight, M_w; the ΔG° data, plotted in this manner, showed considerable scatter [Alexandridis et al., 1994]. When ΔG° was expressed in kJ per mole of ethylene-oxide (EO) and propylene-oxide (PO) segments, it could be seen that the lower M_w Pluronic copolymers corresponded to more negative free-energy-per-segment ($\Delta G^{\circ\prime}$) values. Furthermore, the $\Delta G^{\circ\prime}$ data behaved in a remarkably concerted way when examined as a function of copolymer M_w. $\Delta G^{\circ\prime}$ values (kJ per mole of EO and PO segments) for 12 Pluronic copolymers are plotted in Figure 3.3 as a function of $1/M_w$; 3 $\Delta G^{\circ\prime}$ data sets are presented, estimated using Equation 1 at the CMT, for 0.01, 0.1, and 1.0% copolymer solutions. It is worth emphasizing that this normalization reduced the rather scattered ΔG° (kJ/mol) vs M_w data to a straight line for a wide range of PPO/PEO ratios. To enhance the utility of the data set of Figure 3.3, and to allow for interpolation, the $\Delta G^{\circ\prime}$ (kJ/mol segment) values were correlated as a function of M_W and % w/v concentration, C, via the empirical equation:

$$\Delta G^{\circ\prime} = (+ 0.3670 \log C - 1.2547)\, 10^3 / M_W - 0.0045 \log C - 0.0070 \qquad (5)$$

The accuracy of the fit is excellent ($R^2 > 0.999$); the solid lines in Figure 3.3, results of the fit, can attest to this. $\Delta G^{\circ\prime}$ values predicted from Equation 5 differ less than 2.5% from the experimentally determined ones. The validity of a relatively simple relationship (Equation 5) for the determination of the free energy of micellization, ΔG°, for PEO-PPO-PEO copolymers points to the relative importance of the copolymer composition and molecular weight on the micellization process. For a given copolymer concentration, it appears as if

the differences between PEO and PPO are either not important or cancel out at the CMT, and ΔG° depends only on the polymer molecular weight and the total number of EO and PO segments. Note that the intercepts of the $\Delta G^{\circ\prime}$ vs $1/M_W$ lines are approximately zero; the contribution to ΔG° per segment diminishes as the number of segments increases. Theoretical analysis to rationalize such a behavior is presented in the following section. The utility of such a relationship for predicting critical micellization concentrations and temperatures for PEO-PPO-PEO copolymer aqueous solutions is examined below.

Equation 5 can now be used as a tool to estimate the micellization properties for PEO-PPO-PEO copolymers in the 2900 - 14600 M_w range and for PPO/PEO ratios 0.19 - 1.79. The standard free energies (ΔG°) can be determined directly from Equation 5, while enthalpies (ΔH°), and entropies (ΔS°) of micellization for various copolymers can be derived form Equation 2 utilizing CMTs and CMCs obtained from the correlations presented below. Values for the critical micellization temperature (T_{CMT}) in K can be obtained from the $\Delta G^{\circ\prime}$ expression (Equation 5) through Equation 1:

$$T_{CMT} = N_{PO+EO}\,(R\ln X)^{-1} \cdot [\, M_W^{-1}\, 10^3\, (+ 0.3670 \log C - 1.2547\,) - 0.0045 \log C - 0.0070\,] \quad (6)$$

where N_{PO+EO} is the number of propylene-oxide and ethylene-oxide segments in the copolymer molecule and $R = 0.008314$ kJ K^{-1} mol^{-1}. The natural logarithm of the copolymer mole fraction, X, can be expressed in a simplified way as a function of M_W and C (assuming that the value of C is much smaller than 100) as

$$\ln X = 2.302 \log C - \ln M_W - 1.715 \quad (7)$$

The fitting ability of Equation 6 is demonstrated in Figure 3.4a, where the estimated (using Equation 6) T_{CMT} values are plotted as a function of the experimentally determined T_{CMT}s for the 12 copolymers that we studied and for a range of copolymer concentrations. The experimental and predicted values are in good agreement and distribute evenly along the 45° line for the temperature range 20 - 60 °C. A systematic deviation can be seen at the two temperature extremes, a result of the simple (linear) functional form used to fit the data; a quadratic fit to the $\Delta G^{\circ\prime}$ vs $1/M_W$ data set should improve the accuracy of the fit.

A simple expression for the critical micellization concentration, C_{CMC}, expressed in mass units (% w/v), can be also obtained, using Equations 6 and 7.

$$\log C_{CMC} = \frac{R\,T\,(\ln M_W + 1.715) + N_{PO+EO}\,(-1254.7\,M_W^{-1} - 0.0070)}{2.302\,R\,T + N_{PO+EO}\,(-367\,M_W^{-1} + 0.0045)} \qquad (8)$$

The predictive ability of Equation 8 is demonstrated in Figure 3.4b, where the estimated (from Equation 8) C_{CMC} values are plotted as a function of the experimentally determined C_{CMC}s for the copolymers studied and for a range of temperatures. In the cases where the assumption of Equation 7 is not valid a numerical solution is needed for the system of Equations 4 and 6. Equations 6 and 8 were derived from experimental data that fell in the temperature range of 10 - 70 °C and concentration range of 0.01 - 1 %. Concequently the predictions are valid in this range of conditions, which cover most of the applications of PEO-PPO-PEO copolymers.

3.3c Thermodynamics of block copolymer micelle formation: models vs experiment

Most of the theories proposed for the micellizaton of block copolymer use free energy terms that originate from either the Flory-Huggins theory of polymer solutions or polymer scaling concepts. We start our analysis by considering the Flory-Huggins free energy of mixing expression [Flory, 1953]:

$$\Delta G_{mix} = RT\,[\,\ln\phi - (N-1)\,(1-\phi) + \chi N(1-\phi)^2\,] \qquad (9)$$

where ΔG_{mix} is the free energy associated with transferring one mole of polymer from pure liquid polymer into solution, ϕ is the volume fraction of polymer in the solution, N is the degree of polymerization of the polymer chain (number of monomer segments), and χ is the Flory-Huggins interaction parameter between polymer and solvent (χ is zero for athermal mixing, positive for endothermic and negative for exothermal mixing). The first two terms in the ΔG_{mix} expression originate from the configurational entropy (always

favoring mixing), and the last from the enthalpy of mixing (unfavorable when $\chi>0$). In the case of an AB block copolymer, it can be shown [Flory, 1953] that ΔG_{mix} is given again by Equation 9, with χ being the average of χ_A and χ_B (weighted by the number of A and B segments, respectively) and under the assumption that $\chi_{AB}=0$.

The free energy change for the transfer of one mole of copolymer from solution to the micellar phase (free energy of micellization, ΔG°), can be compared to the free energy associated with transferring one mole of polymer from solution into pure liquid polymer, minus ΔG_{mix}. To facilitate the comparison of the experimentally determined ΔG° for Pluronic solutions to ΔG_{mix}, we express the latter per mole of monomer segments:

$$\Delta G_{mix}' = \Delta G_{mix}/N = RT [(\ln\phi)/N - (1-1/N)(1-\phi) + \chi(1-\phi)^2] \quad (10)$$

For constant ϕ, increasing N (and molecular weight) results in less negative $\Delta G_{mix}'$. Substituting $\chi = (1-\phi)^{-1}$ in Equation 10 [Note 3]

$$\Delta G_{mix}' = RT (\ln\phi-\phi+1) / N \quad (11)$$

$\Delta G_{mix}'$ from Equation 11 has the same dependence on M_w (a multiple of N) and ϕ as $\Delta G^{\circ\prime}$ in Equation 5 ($\Delta G_{mix}'$ becomes less negative as M_w or ϕ increase), however, it describes a phenomenon (mixing) which is opposite to that of the micellization (demixing of copolymer from the solvent) of Pluronic copolymers in aqueous solutions. The micellization of PEO-PPO-PEO copolymers is enthalpically unfavorable and driven by entropy [Alexandridis et al., 1994]; the latter was atrributed to the hydrophobic effect, i.e. the excess ordering of water molecules around the polymer chains. One can make the argument that, at the CMC, the configurational entropy that the polymer gains (when dissolved in water) is balanced by the entropy that the water loses due to the hydrophobic effect (i.e. the term $\ln\phi$, which is favoring mixing in the absence of hydrophobic interactions, is favoring demixing / micellization in their presence). In this case, Equations 10 and 11 are suitable for representing ΔG°, and the $\Delta G^{\circ\prime}$ vs M_w^{-1} data (plotted in Figure 3.3) can be fitted to the functional form of Equation 10:

$$\Delta G^{\circ\prime} = M_w^{-1} \{ M_w RT [(\ln\phi)/N - (1-1/N)(1-\phi) + \chi(1-\phi)^2] \} \quad (12)$$

The expression in { } is equal to the slope of the $\Delta G^{\circ\prime}$ vs M_w^{-1} plot (Figure 3.3). Thus χ, which represents the average (over the copolymer segments) copolymer-solvent interaction parameter, can be calculated for the PEO-PPO-PEO/water system as a function of M_w, ϕ, and temperature, using the experimentally determined slopes of Figure 3.4. For constant ϕ, χ scales as M_w^{-1}, and for a given χ, ϕ (which is the CMC) scales as M_w^{-1}. Also, for small ϕ, $\ln\phi >> \phi - 1$ and $\phi/N = X$, and Equation 11 becomes $\Delta G_{mix} = RT \ln X + RT \ln N$, the first term of which is identical to Equation 1.

From the discussion in the above paragraph, it is shown that the simple Flory-Huggins free-energy-of-mixing expression can capture some of the features of the experimentally observed behavior of ΔG°, but entropy loss on the water (solvent) side during polymer/water mixing has to be considered in order to get the correct sign. We examine below micellization models that allow more detailed description of the various contributions involved in micelle formation.

Munch and Gast [1988] modelled the micellization of diblock copolymers in solutions applying the theory of Leibler et al. [1983], who treated micelle formation in mixtures of block copolymers and homopolymers. The micelle core was assumed to be a melt of B chains, while the corona contained A chains with solvent S. The interaction between S and B segments was described by the χ_{BS} interaction parameter, whereas athermal interactions between A and S were assumed (χ_{AS}=0). The energy of a single micelle was expressed as a contribution of core-solvent interfacial energy, energy due to deformation of the copolymer chains in the micelle, and free energy of mixing S molecules with the A segments in the corona (ϕ_o: volume fraction of A in the corona). The total free energy of the system included the energy of the micelles, the free energy of mixing individual diblock copolymers with S molecules (ϕ_1: volume fraction of copolymers outside the micelles), and an energy contribution arising from the translational entropy of the gas of micelles. The total free energy was minimized with respect to the micelle aggregation number (p), ϕ_1, and ϕ_o. For high degree of incompatibility between B and S, the free energy minimization with respect to ϕ_1 resulted in an analytical estimate for CMC

as $\phi_1 \rightarrow 0$ [Leibler et al., 1983]:

$$\phi_1 \approx \exp (f/kT + N - \chi_{BS}N_B) \qquad (13)$$

where f/kT is the energy per chain in an isolated micelle, N is the total number of segments in the copolymer molecule, N_B is the number of B (core) segments, and $\chi_{BS}N_B$ is the total effective interaction per chain (since the A chain is in an athermal environment). The leading order terms in f/kT are [Munch & Gast, 1988]:

$$f/kT \approx (6\pi^2 N_B)^{1/6} (\chi_{BS}N_B)^{1/2} p^{-1/3} + N (1+N_B/N_A)^{-1} (1-\phi_o) \phi_o^{-1} \ln(1-\phi_o) \qquad (14)$$

The first term in the right side of Equation 14 comes from the energy of forming the micelle core - solvent interface and opposes the formation of micelles, whereas the second term, that originates from the configurational entropy of mixing solvent molecules with A monomers in the corona, favors micellization.

Since the free energy of micellization ΔG° is proportional to $\ln \phi_1$ (see Equation 1), the functional form of $\Delta G^{\circ\prime}$ ($=\Delta G^\circ/N$) for the Munch and Gast theory can be obtained from Equations 13 and 14:

$$\Delta G^{\circ\prime} \sim N^{-1}(6\pi^2 N_B)^{1/6}(\chi_{BS}N_B)^{1/2}p^{-1/3} + (1+N_B/N_A)^{-1} (1-\phi_o)\phi_o^{-1} \ln(1-\phi_o) - \chi_{BS}N_B N^{-1} + 1 \qquad (15)$$

After neglecting the first term of Equation 15 (as being much smaller than the other terms) and rearranging we get

$$\Delta G^{\circ\prime} \approx M_w^{-1} \{ M_w RT (1+\alpha)^{-1} [(\phi_o^{-1} - 1) \ln(1-\phi_o) + 1 - \alpha (\chi_{BS}+1)] \} \qquad (16)$$

where $\alpha = N_B/N_A$ (in the case of PEO-PPO copolymers in water, α is the PPO/PEO ratio). The expression in { } (in Equation 16) is equal to the experimentally determined slope of the $\Delta G^{\circ\prime}$ vs M_w^{-1} plot (Figure 3.3) and this allows us to examine the interdependence of χ_{BS}, ϕ_o, M_w and T at the CMC (assuming the validity of the Munch and Gast model for the

PEO-PPO-PEO/water system). For a given total copolymer concentration volume fraction, the term in { } is the same for all copolymers; as a result increase in M_w should be balanced by either a decrease in ϕ_o, or an increase in χ_{BS}. For a given copolymer solution, an increase in concentration could be compensated by decrease in χ_{BS} or increase in ϕ_o. The trends described above are reasonable; note that $\ln\phi_1$ (CMC) varies as $-N_B$, (Eq 13) as was indeed experimentally observed [Alexandridis et al., 1994]. As χ_{AS} was assumed to be to zero, no effect of block A on micellization could be seen in the model of Munch and Gast, other than the configurational entropy of mixing solvent molecules with A monomers in the corona.

We subsequently examine the phenomenological block copolymer micellization theory of Nagarajan and Ganesh [1989] in which A-solvent interactions were taken into account in the expense, though, of an analytical expression for ϕ_{CMC}. The micelles were also assumed to have a completely segregated core region, consisting of only the B block, and a corona region consisting of the solvent S and the solvent compatible A block. The free energy of micellization was expressed in terms of changes in the state of dilution of blocks A and B, changes in the state of deformation of blocks A and B, localization of the copolymer molecules at the micelle interface, and formation of the micellar core - solvent interface. The hydrophobic interactions, that strongly influence the micellization in water as discussed above, were implicitly accounted for in the experimentally determined χ values used for the PEO-water and PPO-water interaction free energy terms. The micellization parameters were obtained from minimization of the free energy expression with respect to the radius of the micelle core and the corona thickness.

The most important contribution favoring micellization arose from the change in state of dilution of block B as it went from solvent S into the micelle core (note that the mutual incompatibility of blocks A and B is also essential for micellization, otherwise the incompatibility of the solvent for the polymer blocks would give rise to macroscopic phase separation; the incompatibility of blocks A and B was implicitly taken into account by the completely segregated core structure assumed for the micelle). The most important contribution opposing micellization originated from the formation of the micelle core - solvent interface. The optimal aggregation number was determined primarily by balancing the free energy contributions due to change in state of dilution and deformation of the A

(more important in the case of the PEO-PPO/water system [Nagarajan & Ganesh, 1989]) and B blocks, favoring low aggregation numbers, and the free energy contributions due to formation of the micelle core - solvent interface that favored high aggregation numbers.

The theory of Nagarajan and Ganesh, developed for diblock copolymers, succeeded in predicting qualitatively the contributions of the copolymer composition and molecular weight on the micellization of triblock copolymers. This is illustrated in Figure 3.5 where predictions of Nagarajan's model for $\ln\phi_{CMC}$ are compared to experimentally determined $\ln\phi_{CMC}$ values from Alexandridis et al. [1994] (the comparison is made between AB and A(2B)A copolymers). The effect of EO on ΔG° is predicted from the theory to be approximately 0.14 kJ/molEO while it was found from experiments in the 0.03 - 0.05 kJ/molEO range (Figure 3.5a); the contribution of PO is predicted from the theory to be -1.73 kJ/molPO while it was found from experiments in the (-0.41) - (-0.28) kJ/molPO range (Figure 3.5b); the effect of copolymer molecular weight was -9.87 kJ/mol(1000 M_w units) from the theory vs -1.16 to -2.69 kJ/mol(1000 M_w units) from experiment (Figure 3.5c); lastly, the contribution of % PPO changes was -3.9 kJ/mol in the theory vs -0.72 in the experiment (Figure 3.5d). As seen in Figure 3.5, the trends are the same in both theory and experiment, however, the theory overpredicts the experimentally obtained free energies of micellization by a factor of four, resulting in unrealistically low predicted CMC values.

Prochazka et al. [1991] modified Nagarajan's model to treat association of A-B-A block copolymers by accounting for reduction in entropy due to loop formation of the middle (B) block, and localization of the two A-B joints of the copolymer in the interface between the core and the corona of the micelle. The result was less negative ΔG° (in the correct direction with respect to agreement between experiment and theory) but the decrease in the absolute value of the predicted ΔG° was ~ 10% and not enough to account for the 8-fold overprediction of the theory the experimental ΔG°s. Balsara et al. [1991] noted that, in the presence of solvents, the description of the core-corona interface using the theory of Leibler et al. [1983] is complicated due to the three-component nature of the problem (presence of solvent on interface). This point, in addition to the hydrogen bonding interactions between both PEO and PPO with water, may account for the quantitative discrepancy between predictions of block-copolymer micellization theories and the experimental results of Alexandridis et al. [1994] for the system PEO-PPO-PEO/water.

3.4 Conclusions

Correlations for the estimation of critical micellization concentrations and critical micellization temperatures of PEO-PPO-PEO triblock copolymer aqueous solutions have been developed. CMC and CMT are expressed as a function of the copolymer molecular weight, PPO/PEO composition, and temperature (for CMC determination) or concentration (in the case of CMT). The correlation was developed from experimental CMT data, and is based on a simple equation for the standard free energy of micellization (ΔG°). Such a correlation should be very useful to the practitioners of the field, as it allows easy prediction of CMC and CMT for a wide range of PEO-PPO-PEO copolymers, with minimal number of input parameters. The correlations developed here can also prove helpful in evaluating published theories of micellization and improving their treatment of PEO-PPO water systems. In order to rationalize the observed trends, the experimentally obtained correlation for the standard free energy of micellization (ΔG°) was compared to the Flory-Huggins free energy of mixing, and theories of block copolymer micellization proposed by Munch and Gast [1988] and Nagarajan and Ganesh [1989]. Simple expressions for ΔG°, that have the same functional form as the experimentaly determined ΔG°, were derived from the Flory-Huggins and Munch and Gast theories, thus providing insight in the interdependence of the micellization parameters χ_{BS}, ϕ, M_w and T for the PEO-PPO-PEO/water system. The theory of Nagarajan and Ganesh was not amenable to similar analysis due to the complexity of the free energy expressions used, but was evaluated by comparing theoretical CMC predictions for PEO-PPO/water systems (presented in their paper) to experimental CMCs. The latter theory succeeds in predicting qualitatively the contributions of the copolymer composition and molecular weight on the micellization of triblock copolymers. The theory, however, overpredicts the experimentally obtained free energies of micellization by a factor of eight; modification in the Nagarajan theory that accounted for triblock copolymers [Prochazka et al., 1991] was not sufficient to reduce the discrepancy between the experimental data and theoretical predictions.

3.5 References and Notes Cited in Chapter 3

1. Alexandridis, P.; Hatton, T. A. *Colloids Surfaces A* **1994**, submitted for publication; Chapter 1 of this Thesis.
2. Alexandridis, P.; Holzwarth, J. F.; Hatton, T. A. *Macromolecules* **1994**, *27*, 2414; Chapter 2 of this Thesis.
3. Balsara, N. P.; Tirrell, M.; Lodge, T. P. *Macromolecules* **1991**, *24*, 1975.
4. Flory, P. *Principles of Polymer Chemistry*; Cornell University : Ithaca, NY, 1953.
5. Hunter, R. J. *Foundations of Colloid Science, Vol. 1*; Oxford University Press, 1987, p. 583.
6. Hurter, P. N.; Hatton, T. A. *Langmuir*, **1992**, *8*, 1291.
7. Hurter, P. N.; Scheutjens, J. M. H. M.; Hatton, T. A. *Macromolecules* **1993**, *26*, 5030.
8. Leibler, L.; Orland, H.; Wheeler, J. C. *J. Chem. Phys.* **1983**, *79*, 3550.
9. Munch, M. R.; Gast, A. P. *Macromolecules* **1988**, *21*, 1360.
10. Nagarajan, R.; Ganesh, K. *J. Chem. Phys.* **1989**, *90*, 5843.
11. Prochazka, O.; Tuzar, Z.; Kratochvil, P. *Polymer* **1991** *32*, 3038.

Note 1 We considered the CMT vs X data set for estimating ΔH°, instead of CMC vs T data, in accordance with the way in which the experiments were conducted, by varying the temperature of a sample of given concentration. Note that, at the point where micelles start forming, a copolymer solution is at both the CMC and the CMT.

Note 2 Exceptions to the linear fit are F68, F88 and F108, for which the slopes appear to increase at high concentrations. These copolymers are all hydrophilic and of high molecular weight and it may be that the simple assumptions of the thermodynamic analysis do not hold well at high polymer concentrations where the hydrated PEO chains of the micelle coronas will overlap and entangle.

Note 3 If Equation 10 were an adequate description of the copolymer micellization, then χ for the Pluronic copolymer - water system would be equal to $(1-\phi)^{-1}$ at infinite copolymer molecular weight ($\Delta G^{\circ\prime} \rightarrow 0$ at $M_w^{-1} \rightarrow 0$, as suggested by the experimental data shown in Figure 3.3). Thus the value of χ (which represents the average χ of the PEO/water and PPO/water interactions) is higher than but approximately equal to 1; this is realistic given that the χ values of the PEO-water

and PPO-water systems are 0.4 and 2.0 respectively [Hurter et al., 1993]. Note that, if χ were equal to $(1-\phi)^{-1}$ (as suggested by Equation 10 and Figure 3.3), ΔG_{mix} (expressed in kJ/mol) would be independent of M_w.

Chapter 3: List of Tables and Figures

Table 3.1 Constants of the $1/T_{CMT}$ vs log(% concentration) correlation for various Pluronic copolymers.

Pluronic	Mol. Weight	Slope, S ($\times 10^5$)	Intercept, I ($\times 10^3$)
L64	2900	8.423	3.283
P65	3400	10.70	3.240
F68	8400	8.919	3.097
P84	4200	9.132	3.315
P85	4600	8.415	3.302
F88	11400	10.96	3.215
P103	4950	5.666	3.418
P104	5900	6.506	3.392
P105	6500	5.782	3.392
F108	14600	7.246	3.307
P123	5750	5.852	3.460
F127	12600	7.629	3.365

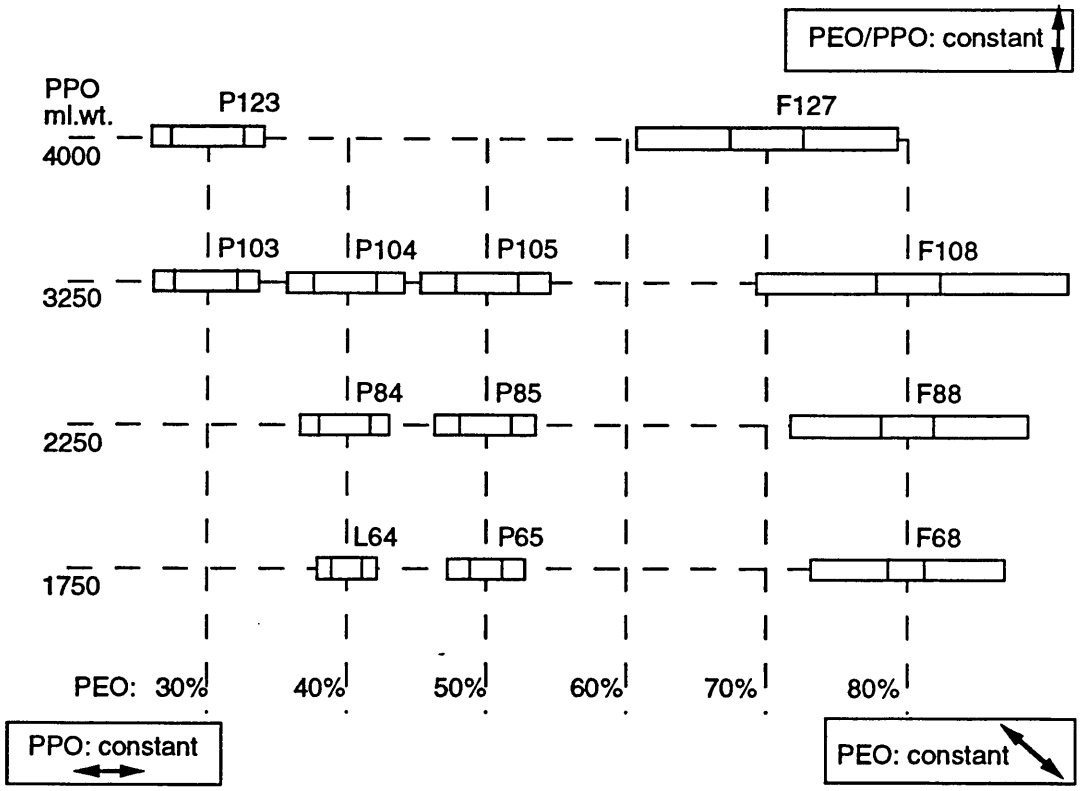

Figure 3.1 The Pluronic grid.

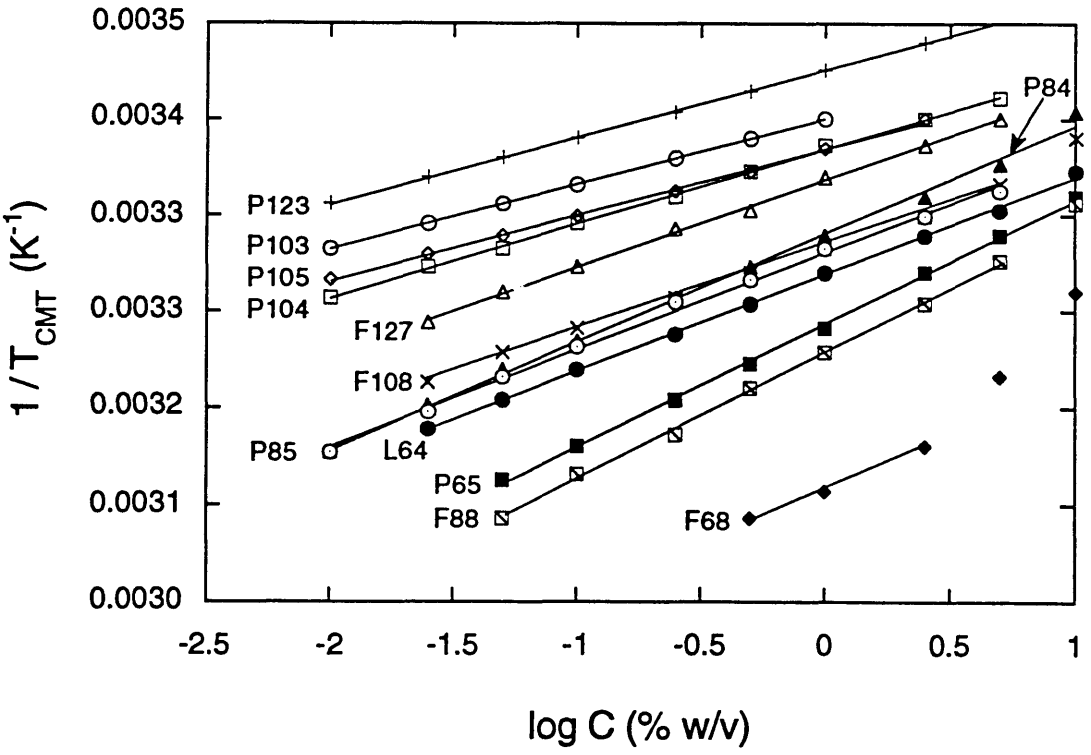

Figure 3.2 $1/T_{CMT}$ vs log(C) plots for various Pluronics.

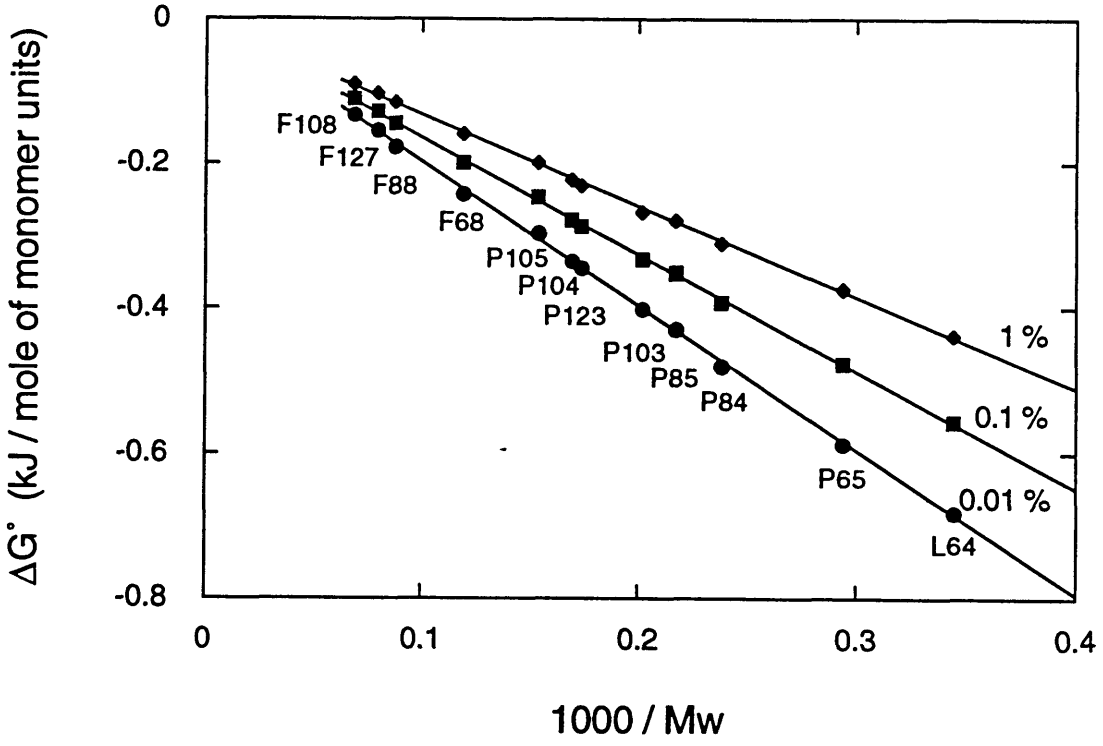

Figure 3.3 $\Delta G^{\circ\prime}$ (expressed in kJ per mole of PO and EO segments) as a function of Pluronic copolymer inverse molecular weight. The solid lines are the results of fit using Equation 5.

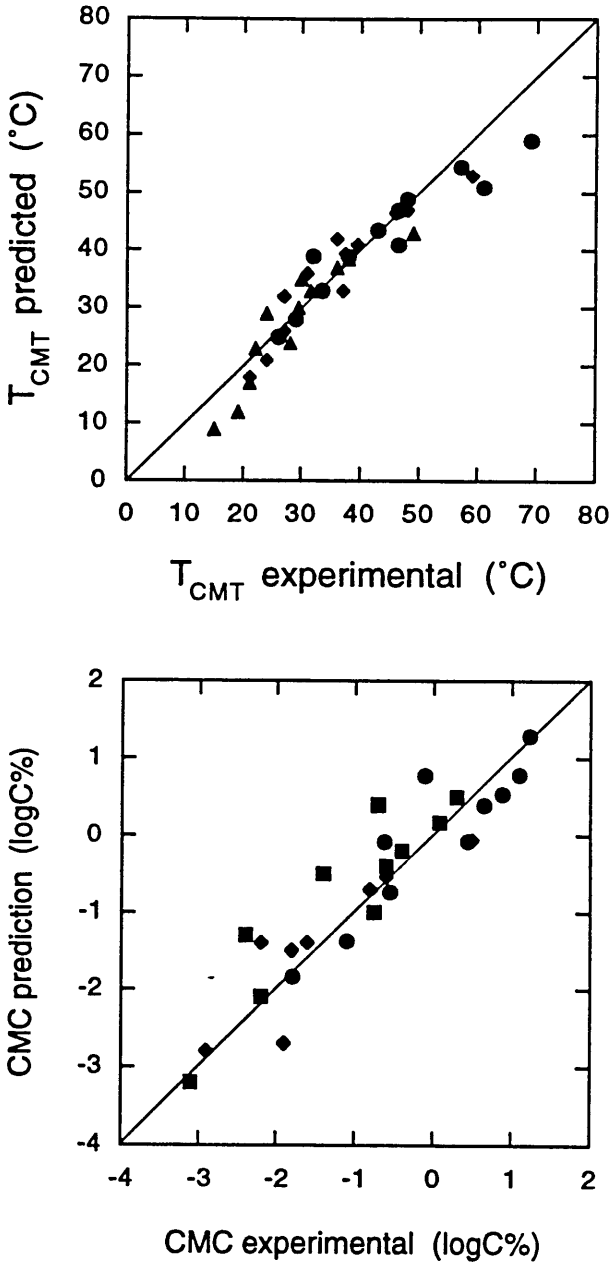

Figure 3.4 (a) T_{CMT} values, predicted from Equation 6, plotted as a function of experimentally determined T_{CMT}. The circles represent data at 0.01%, the squares at 0.1% and the diamonds at 1% copolymer concentration.
(b) C_{CMC} values, predicted from Equation 8, plotted as a function of experimentally determined C_{CMC}. The circles represent data at 25, the squares at 35 and the diamonds at 45 °C.

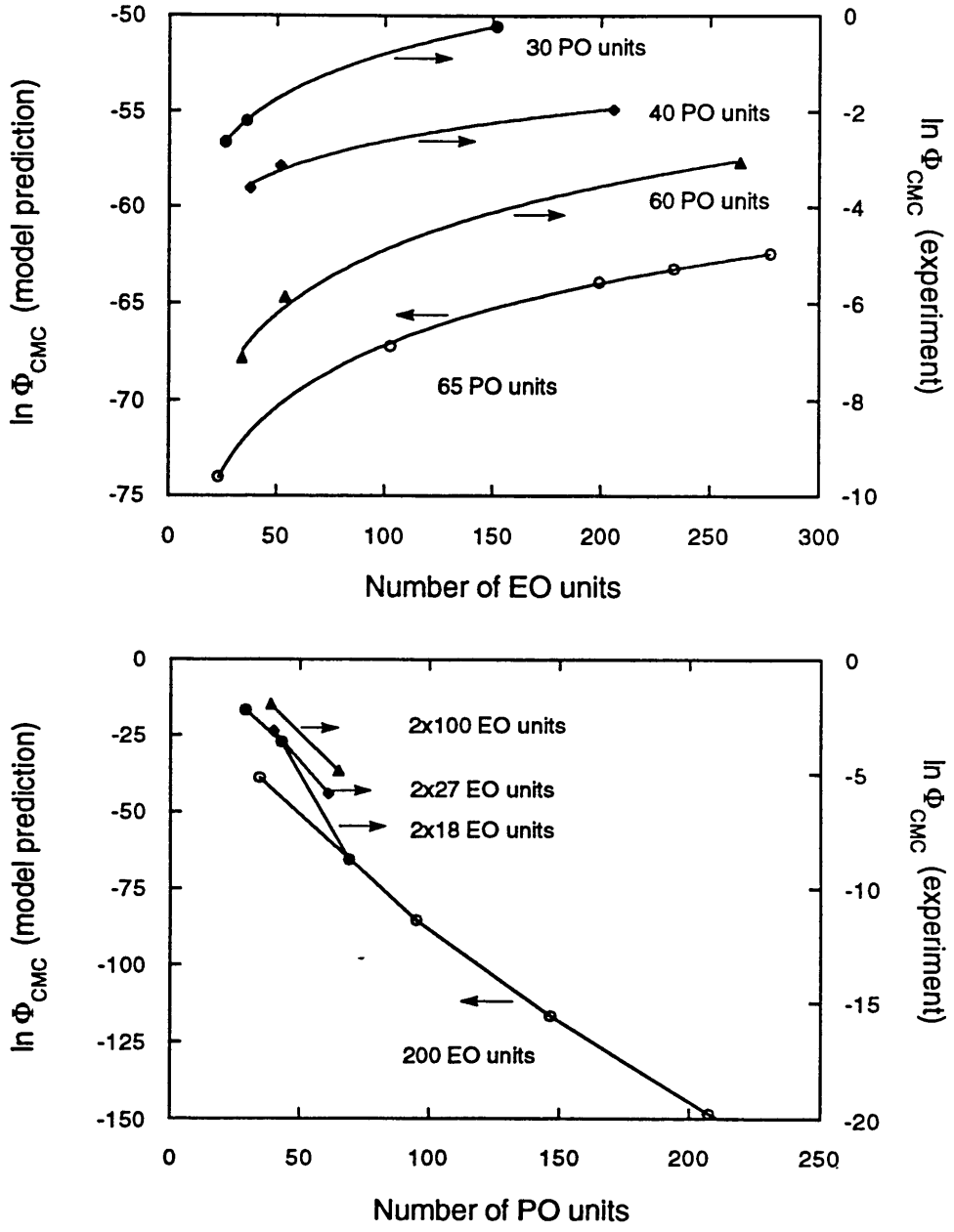

Figure 3.5 Predictions of Nagarajan's model for $\ln\phi_{CMC}$ compared to experimentally determined $\ln\phi_{CMC}$ values: (a) effect of EO segments, (b) effect of PO segments, (c) effect of copolymer molecular weight, (d) effect of PPO content. The filled symbols are experimental data (right Y axis); the open circles are model predictions (left Y axis).

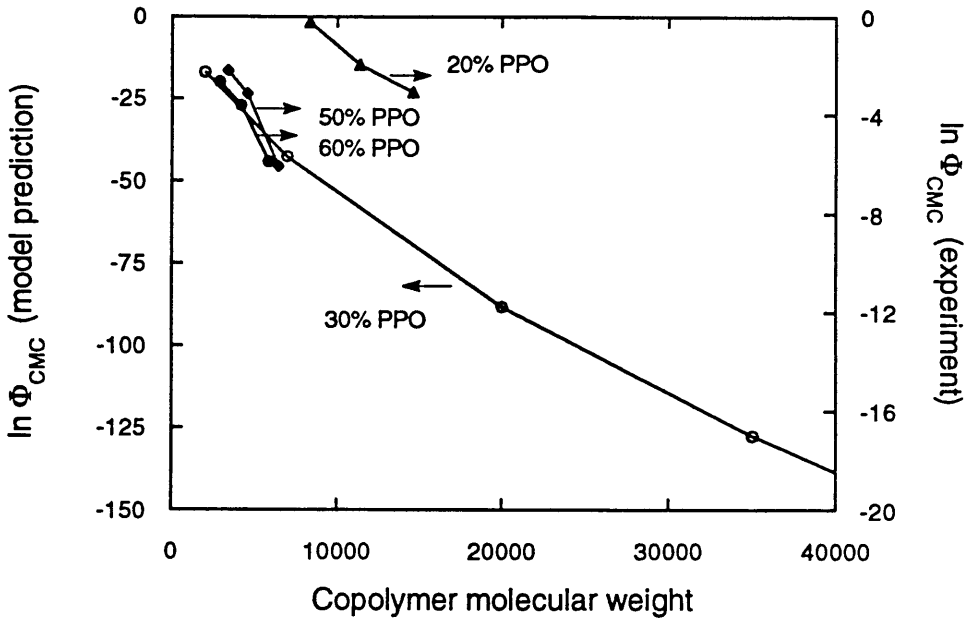

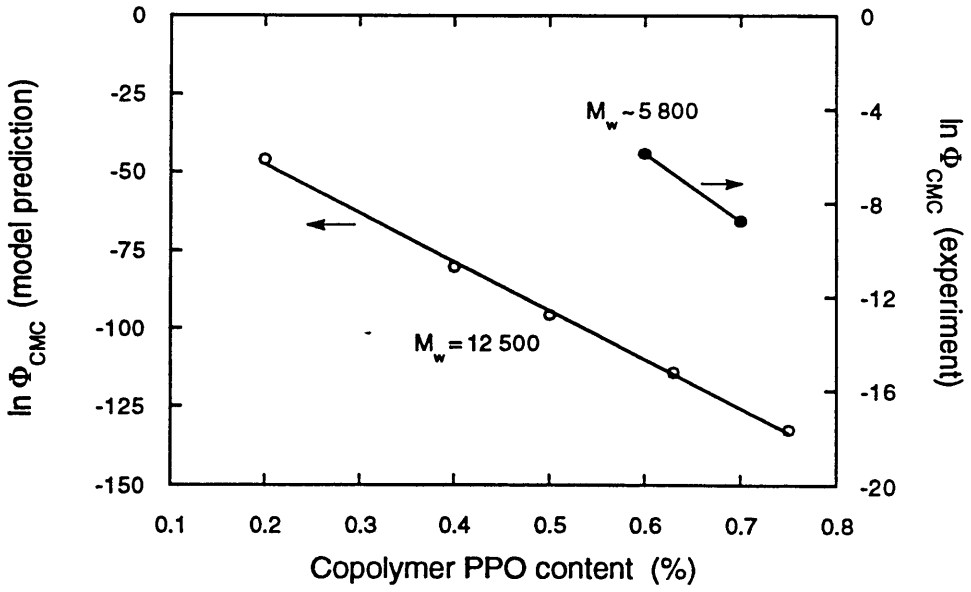

Figure 3.5 Continued

Chapter 4
Surface Activity of PEO-PPO-PEO Triblock Copolymers

4.1 Introduction

The critical micellization concentration, CMC, the amphiphile concentration at which micelles start forming [Hunter, 1987], is a parameter of great fundamental value. In comparison with conventional, low-molecular-weight amphiphiles there is some inherent complexity in the micellization of poly(ethylene oxide)-*block*-poly(propylene oxide)-*block*-ethylene oxide) (PEO-PPO-PEO) copolymers, as it depends strongly on their composition. The composition polydispersity could be appreciable even for a copolymer with a narrow distribution of molecular weight, and could thus result in a broad CMC or CMT (critical micellization temperature, the copolymer solution temperature at which micelles form) transition. A large difference is often noted between the CMC values determined by different methods because their sensitivity to the quantity of unimers (individual copolymer molecules) present in solution may vary [Zhou & Chu, 1988]. Furthermore, the lack of sufficient temperature control, batch variations, or differences in the concentration ranges covered in CMC experiments, may be responsible for the observed variations [Linse & Malmsten, 1992]. Given the number of publications dealing with aqueous solutions of Pluronics, there are surprisingly few reliable CMC data for Pluronic copolymers in the literature.

Two commonly used techniques for the determination of CMC in micellar solutions are surface tension and dye solubilization [Hunter, 1987; Ananthapadmanabhan et al, 1985]. Edwards et al. [1991] reported that, in general, the CMC values they obtained from the surface tension data for solutions of deionized water and nonionic surfactants showed fairly close agreement to the CMC values inferred from polyaromatic hydrocarbon solubilization data. Chattopadhyay and London [1984] used dye solubilization to determine the CMC of various surfactants, obtaining CMC values that were within 10% of the ones determined by other methods, including surface tension. Prasad et al. [1979]

measured the surface tension of aqueous Pluronic copolymer solutions, and found that the break (change in slope) of the surface tension vs log concentration curve, conventionally assigned to CMC, occurred at concentrations different from the ones at which dye solubilization commences. Subsequently, they interpreted this break as due to the formation of so-called "monomolecular" aggregates in dilute solution. Careful inspection of their surface tension plots, however, reveals two incidents of slope change in several systems. Wanka et al. [1990] found that the surface tension of Pluronics P104, P123, and F127 decreased linearly with the logarithm of the copolymer concentration according to the Gibbs' isotherm of adsorption over several concentration decades. At a characteristic concentration there was a break in the curve; the surface tension kept decreasing with further increase in concentration, but with a smaller slope, until a second concentration was reached above which the surface tension remained constant. This transition region, extending approximately one concentration decade, was related to the fact that the block copolymers are not well defined samples but have a broad molar weight distribution, and to the presence of impurities [Wanka et al, 1990]. It appears that interpretation of surface tension measurements, a standard way of determining CMC of surfactants, may be ambiguous in the case of Pluronic copolymers.

In the context of an ongoing investigation on the potential for using PEO-PPO-PEO block copolymer micelles as colloidal extractants [Hurter & Hatton, 1992] we undertook a detailed theoretical [Hurter et al, 1993] and experimental [Alexandridis et al., 1994] investigation on micellization and solubilization in aqueous PEO-PPO-PEO block copolymer solutions. The CMT and CMC values for solutions of several Pluronics were determined using a dye solubilization technique. To investigate the discrepancy between CMCs obtained by the dye solubilization and surface tension measurements, and to gain information on the conformation of the PEO-PPO-PEO copolymers on the air/water interface, surface tension measurements were made using the same copolymers as for the dye solubilization experiments, to avoid inconsistency due to different polymer batches. The surface tensions of aqueous solutions of poly(ethylene oxide)-*block*-poly(propylene oxide)-*block*-poly(ethylene oxide) copolymers were determined over the 10^{-5} - 10 % w/v concentration range, at two temperatures (25 and 35 °C). Seven Pluronic PEO-PPO-PEO block copolymers were investigated, covering a wide range of molecular weights (3400 - 14600) and PPO/PEO ratios (0.19 - 1.79). The surface activity of PEO-PPO-PEO block copolymers was compared to that of a PPO-PEO-PPO block copolymer, a PEO-PPO

random copolymer, and published data for PEO and PPO homopolymers.

4.2 Materials and Methods

The Pluronic PEO-PPO-PEO block copolymers, available in a range of molecular weights and PPO/PEO ratios [Schmolka, 1977; Bahadur & Riess, 1991; BASF, 1989], were obtained from BASF Corp., Parsippany, NJ, and used as received. Table 4.1 lists the composition of those Pluronic polymers studied here. The copolymers considered here are also presented in Figure 4.1, arranged in the form of a grid; the relative sizes of the PEO (side) and PPO (middle) blocks are drawn approximately on scale. The random PEO-PPO copolymer, UCON 50HB-5100 (50% PEO, 3930 molecular weight), was purchased from Union Carbide Chemicals and Plastics Co. Inc., South Charleston, WV; the PPO-PEO-PPO Pluronic-R block copolymer, 25R4 (40% PEO), was obtained from BASF Corp.

The Wilhelmy plate method (Krüs, K10T tensiometer) was employed for measuring the surface tension of the copolymer solutions. Aqueous copolymer solutions were prepared by dissolving the polymer in Milli-Q water and diluting to the desired concentration (ranging from 10^{-5} to 10 % w/v). Temperature control within 0.05 °C was achieved using a Neslab RTE-110 refrigerated bath/circulator. All glassware was washed in a 1N NaOH-ethanol bath, then in a nitric acid bath, and thoroughly rinsed with Milli-Q water before use. The platinum Wilhelmy plate was washed using acetone, rinsed in Milli-Q water, and flamed until red-hot before each measurement [Nikas et al., 1992].

4.3 Results and Discussion

4.3a Surface activity of Pluronic PEO-PPO-PEO copolymers

Surface tension data for various Pluronic copolymer solutions at the two temperatures, 25 and 35 °C, are presented in Figure 4.2, plotted semilogarithmically with respect to copolymer bulk concentration. At low concentrations the surface tension decreased with increasing concentration for all copolymers, in accord with the Gibbs'

adsorption isotherm [Chattoraj & Birdi, 1984]. A change in slope (break) was observed in the surface tension curve at a characteristic concentration, after which the surface tension values continued to decrease until a plateau was reached (second break); the surface tension values remained constant with further increase of copolymer concentration. This behavior (two breaks) was observed for most copolymers studied and was very reproducible. The first (low concentration) break occurred at a copolymer concentration (0.001 %) which is roughly the same for both temperatures studied and for different copolymers (with the exception of F108). The surface tension value at the onset of this break varied from 40 to 50 mN/m. The concentration range between the two breaks was wider for the hydrophilic, low molecular weight, copolymers P65 and P85. The extent of this concentration region decreased with temperature for a given polymer, and almost disappeared at 35 °C for the relatively hydrophobic Pluronics P123, P103, and P105. At the higher temperature (35 °C) surface tension values were lower (for a given copolymer concentration), and the change of slope corresponding to CMC appeared at lower concentrations, compared to the ones at 25 °C.

The presence of two breaks has led to some confusion in the surface tension studies available for Pluronic copolymers regarding the interpretation of the surface tension dependance on concentration, and the extraction of CMC from such a set of data. In the few studies reported to date [Wanka et al., 1990; Prasad et al., 1979; Anderson, 1972], the surface tension data show the same trends as reported here, with the first break occurring in the vicinity of 0.001% concentration. In most cases it has been assumed that this change in slope signified the CMC [Anderson, 1972; Bahadur & Pandya, 1992], although other interpretations, such as formation of "unimolecular" micelles [Prasad et al., 1979], have been given. The region of decreasing surface tension that follows the break at 0.001%, and the second break have often been ignored [Prasad et al., 1979], but it has been suggested that they were due to broad copolymer molecular weight distribution and to the presence of impurities [Wanka et al., 1990]. The most complete (in terms of number of copolymers and concentration range probed) surface tension study is that of Prasad et al. [1979] who investigated L42, L44, L62, L64, F68, P85, and F88 Pluronic copolymer solutions. However the authors were not able to link the CMC to the features of the surface tension vs concentration curve. Anderson [1972] measured the surface tension of L61, L62 and F68 solutions at low concentrations but apparently missed the second break (and the "real" CMC) in the surface tension curve. In the following section we examine the

results of our surface tension measurements in the light of related information aiming at understanding the behavior of the copolymers on the interface and relating it to their bulk behavior.

4.3b Interpretation of the surface tension dependence on concentration

Typically, the surface tension of aqueous surfactant solutions decreases (and the corresponding surface pressure increases) with increasing surfactant concentration, reflecting an increase in the activity of the surfactant in the bulk under constant coverage of the air/water interface with surfactant, and then the surface tension reaches a constant value (at the CMC) that does not change with further increase in the bulk surfactant concentration (surfactant activity at the bulk remains approximately constant) [Chattoraj & Birdi, 1984]. The situation is more complicated in the case of Pluronic copolymer solutions: as shown in Figure 4.2, and in agreement with other studies [Wanka et al., 1990; Prasad et al., 1979], two breaks can be observed in the surface tension vs log copolymer concentration plot. There is good agreement between the CMCs determined from the dye solubilization study of Alexandridis et al. [1994] (indicated by arrows in Figure 4.2) and the concentration at the second break of the surface tension curve. This is exemplified in Figure 4.3 where CMC values obtained from surface tension measurements are plotted versus CMC values obtained from dye solubilization experiments reported by Alexandridis et al. [1994]; there is small scatter of the CMC data around the 45° line. Based on this agreement, we were drawn to the conclusion that the higher-concentration break in the surface tension curve corresponds to the CMC and signifies the formation of polymolecular micelles having a well defined hydrophobic interior (i.e. able to solubilize organic solutes). It should be noted that the copolymer concentrations at the second break, extracted from the surface tension data of Wanka et al. [1990] (0.3% for F127, and 0.01% for P104, both at 25 °C) and Prasad et al. [1979], are also comparable to the CMC values found in our dye solubilization study [Alexandridis et al., 1994].

Two other observations supporting the conclusion that the higher-concentration break is the CMC are (i) the plateau observed in the surface tension values after the high-concentration break, and (ii) the effect of temperature on the copolymer concentration at which the second break occurs. Attainment of a constant surface tension value is an indication of micelle formation (CMC) in solutions of typical surfactants [Chattoraj &

Birdi, 1984]. While the surface tension of Pluronic solutions keeps decreasing with increasing copolymer concentration after the first low-concentration break, it remains constant after the second break as attested to by the horizontal solid lines in the surface tension curves of Figure 4.2 (a dip in the surface tension after the break observed for Pluronic P85 is most likely due to impurities [Reddy et al, 1991; Yu et al., 1992; Mysels, 1986]). Regarding the effect of temperature, the copolymer concentration at which the second change in slope occurs decreased significantly with increasing temperature, in good agreement with CMCs obtained from dye solubilization [Alexandridis et al., 1994] and observations in other studies of Pluronics [Chapter 1 of this Thesis], whereas the concentration at the first break did not vary much (see Figure 4.2). None of the previous surface tension studies was done at more than one temperature to allow such an observation.

Having attributed the high-concentration break (change in the slope) of the surface tension curve to the formation of micelles in the bulk (CMC), we examine below the origin of the first (low-concentration) break. The possibility of an experimental artifact should be ruled out as this change in the slope occurred at surface tension values different for each copolymer, was reproducible, and has been observed by other researchers. The wide molecular weight distribution of the copolymers studied, and the presence of hydrophobic impurities, have been singled out in the past as possible factors that caused differences in the CMC values obtained by surface tension and dye solubilization methods. While the Pluronic copolymers are commercial products and likely to possess both a not-so-narrow molecular weight distribution and impurities originating from the manufacturing process, we show below that neither polydispersity nor impurities should be the origin of first break in the surface tension curve. The effect of molecular weight distribution on surface tension of nonionic surfactants has been nicely demonstrated by Crook et al. [1963], who studied the surface tension of normal (Poisson) distribution and single species octylphenoxy-ethoxyethanols ($OPE_{1\text{-}10}$, 1-10 is the number of ethylene oxide segments), and mixtures of single species and normal distribution OPE_4 and OPE_{10}. The authors found preferential adsorption of molecules with shorter PEO-chain length ($OPE_{3\text{-}5}$) at the air/water interface; this was demonstrated by a less sharp (but still, only one) break at the surface tension curve, and a dip of the surface tension values in the vicinity of the break. Such a behavior was attributed to the replacement of highly surface active, short-PEO-chain-length, molecules (contributing to a low surface tension value) on the interface by the major

component, when these highly surface active molecules were solubilized in micelles formed by the major component. No manifestations of the above were seen in our surface tension curves.

Regarding the influence of impurities, a decrease of surface tension with time, observed in some of our experiments at low copolymer concentrations, would indicate the presence of hydrophobic impurities that adsorb slowly on the surface [Mysels, 1986]. However, the presence of such impurities should result in a lowering of the surface tension (described above as a "dip") below the steady value obtained after the CMC. Such a "dip" was not observed in the vicinity of the low-concentration break in the surface tension curve, but can be seen in some of our experiments (e.g., P85) at the high-concentration break. Furthermore, in the concentration region where both breaks occurred the time needed for the surface tension to reach a constant value (after the Wilhelmy plate touched the surface) was short, indicating no strong influence of impurities. It can thus be concluded that neither polydispersity of the copolymer size nor hydrophobic impurities are causing the low-concentration break observed in the surface tension curves of Pluronic solutions. Reddy et al. [1991] and Yu et al. [1992] measured the surface tension of unpurified and purified samples of L64 and F127, and observed in both studies minima in the surface tension curves for the unpurified samples; purification of the copolymer samples resulted in surface tension curves that showed no evidence of a minimum and exhibited a sharp break corresponding to CMC.

The formation of "monomolecular micelles" in the bulk aqueous phase, accompanied by a change in the activity of the copolymer, was advanced by Prasad et al. [1979] for interpreting their surface tension results. While a change in the dependance of copolymer activity to the bulk concentration can lead to changes in the surface tension [Chattoraj & Birdi, 1984], the formation of monomolecular micelles is not very convincing as an explanation, since the bulk copolymer concentration is very low (10^{-4} g/L) and there seems to be no obvious driving force for changing the conformation of the individual copolymer molecules from an extended to a more compact form. The triblock structure of the PEO-PPO-PEO copolymers should not be the reason for the observed change in the slope of the surface tension curve at low concentrations, since a break in the curve has also been observed at similar concentrations with both PPO-PEO-PPO triblock and random PEO-PPO copolymers (see Figure 4.5 and related discussion). Were the break in the

surface tension a result of changes in behavior of the bulk copolymer activity, the question would arise of the cause of such an activity change.

Recently deGennes [1992] proposed that, under certain circumstances, a dense polymer phase and a very dilute system of swollen chains can coexist in a polymer solution. Based on experimental (light scattering) data from Polik and Burchard [1983], deGennes suggested that the system PEO/water could exhibit such a behavior. Although the PEO used by Polik and Burchard was of high molecular weight and concentration (compared to the Pluronic copolymers that we studied) and the behavior suggesting two coexisting phases occurred at 70 °C, the presence of the hydrophobic PPO could justify the difference in concentration, molecular weight, and temperature between the Pluronic and PEO/water systems, in the case that the coexistence phenomenon was valid for both. Wagner et al. [1993] extended the theoretical treatment by deGennes and predicted that, in the presence of polymer "clusters", a polymer brush would show two layers, one dense (near the wall) and one dilute. It appears that a "phase separation" of the kind proposed by deGennes at low polymer concentration would cause a change in the activity of the polymer, and could possibly lead to an break in the surface tension curve; however there is not sufficient experimental evidence to support such a hypothesis.

We should also mention here an interesting similarity between the surface tension behavior of the Pluronics and the surface tension of polymer - ionic surfactant mixtures. Two breaks are observed in the surface tension vs concentration curve for the later system; the first resulting from complexation of surfactant with the polymer chains, and the second due to micelle formation [Arai et al, 1971; Schwuger, 1973]. One could conceive that, in the case of Pluronics, a hydrophobic minor component (possibly a diblock copolymer or a triblock with short PEO blocks) complexes with the triblock copolymer. Such a scenario would explain the observed trend well and therefore cannot be excluded from consideration. However, it would have required the presence of a large amount of the hydrophobic component and, probably, a copolymer of high molecular weight. Furthermore, Goddard [1986] reports that there is no complexation between nonionic polymer and nonionic surfactant.

It appears from the above that a "phase transition" in the bulk that would lead to changes in the surface tension vs log concentration curve at bulk copolymer concentrations

of 10^{-4} g/L is unlikely (but still possible). On the other hand, a change in the configuration of the copolymer at the air/water interface ("phase transition" on the surface) could lead to a break in the surface tension vs log concentration curve that would occur at low bulk but significant surface copolymer concentrations. Our hypothesis ("scenario") for interpreting the dependance of surface tension on copolymer concentration is as follows:

(i) At very low copolymer bulk concentrations ($<10^{-6}$ %) the polymer molecules adsorb on the air/water interface in an extended configuration and the surface pressure is low (surface "gas"); the surface tension decreases with concentration, with a slope that increases with concentration (this concentration region was not studied here).

(ii) Constant surface coverage has been attained at copolymer bulk concentrations ranging from 10^{-6} to 10^{-3} %, with the PEO-PPO-PEO copolymer molecules adsorbed at the interface possibly as an inverted "U" (this is one of the proposed orientations for homopolymer PEO at the interface [Gallaugher & Hibbert, 1937]) and the PEO chains located at the air/water interface; the Gibbs' law describes well the dependance of surface tension on bulk concentration and the area per molecule can be calculated (see Figure 4 and related discussion).

(iii) At a bulk concentration of approximately 10^{-3} %, with the interface fully covered with copolymer, a change in configuration (structural transition) occurs and the copolymer layer becomes more compact; water is expelled [Lo Nostro & Gabrielli, 1993] and PEO segments protrude into the aqueous solution [Phipps et al., 1993] or fold around PPO. More copolymer molecules can fit on the interface (causing it to become thicker [Rennie et al, 1989]) and the surface tension continues to decrease with increasing bulk copolymer concentration but with a slower rate than in case (ii) (note also that a bulk concentration of 10^{-3} % is comparable to the bulk PEO concentration required for full coverage of the air/water interface according to Glass [1969] and the bulk PPO concentration at which phase separation occurs [Schwuger, 1973]).

(iv) Upon the formation of micelles in the bulk (CMC), further increase in the number of copolymer molecules in the bulk is accommodated by an increase in the number of micelles, the activity of the copolymer in the bulk remains approximately constant, and the surface tension attains a steady value that does not change with further increase in the bulk copolymer concentration.

Critical Micellization Concentration (CMC) values: The PEO-PPO-PEO copolymers investigated here were chosen in such a way as to comprise families having the

same PPO/PEO ratio and differing molecular weight (P123-P103, P105-P85-P65), constant PPO and varying PEO block size (P103-P104-P105-F108), and constant PEO and varying PPO block size (P65-P123, P85-P104) (see Figure 4.1). This allowed us to examine the effect of PPO, PEO, and molecular weight on the micellization of the copolymers. The CMC values for Pluronics with the same size PEO block and varying PPO decreased significantly with increasing number of PO segments (e.g., the CMC values at 25 °C were 5% and 0.2% for P85 and P104, respectively), indicating that polymers with a larger hydrophobic (PPO) domain form micelles at lower concentrations. CMC values for a group of Pluronics with the same hydrophobic block and hydrophilic segment of varying size indicate an increase in CMC with increasing number of EO segments (CMC's for P103 and F108 were 0.1% and 2 %, respectively). However, the effect of PEO on CMC is less pronounced than the effect of PPO (when the changes in CMC are measured per EO or PO segment), alluding to the fact that PPO is mainly responsible for micellization [Alexandridis et al., 1994]. For a given PPO/PEO ratio, Pluronics of higher molecular weight form micelles at lower concentrations (e.g., the CMC values at 25 °C were 5% and 0.2% for P85 and P105, respectively). The CMC values at 35 °C were lower than the CMC's at 25 °C for all copolymers. The CMC data at the two different temperatures are adequate in giving a definite trend (decrease in CMC with increase in temperature), but not sufficient to allow thermodynamic analysis with respect to a copolymer association model. This has been addressed in our earlier study of CMC's, CMT's, and micellization thermodynamics of Pluronic copolymer aqueous solutions [Alexandridis et al., 1994].

CMC/C_{20} ratio values: The CMC/C_{20} ratio, where C_{20} is the concentration of amphiphile in solution that reduces the surface tension by 20 mN/m (dyn/cm) [Rosen, 1989], is a convenient way of measuring the relative effect of some structural or microenvironmental factor on micellization and on adsorption of the amphiphile. An increase in the CMC/C_{20} ratio as result of some factor indicates that micellization is inhibited more than adsorption, or adsorption facilitated more than micellization [Rosen, 1098]. The CMC/C_{20} ratios for the Pluronic PEO-PPO-PEO copolymers studied here are listed in Table 4.2. The ratio values for the Pluronics are generally high when compared to CMC/C_{20} ratios for a large number of surfactants listed by Rosen [1989]; ionic surfactants (both anionic and cationic) with a single straight methyl-chain hydrophobic group exhibit in aqueous solutions low CMC/C_{20} (on the order of 1 - 5) whereas the CMC/C_{20} ratios for

ethoxylated nonionic surfactants range between 10 and 20. The CMC/C_{20} ratios for the more hydrophilic PEO-PPO-PEO copolymers (P65, P85) at room temperature can be as high as 10^4 (adsorption more important than micellization). However, a strong temperature dependence is observed, leading to ratio values of ~20, for the hydrophobic copolymers P103 and P123 at 35 °C (see Table 4.2); the latter values are comparable to those observed for small-molecular-weight nonionic surfactants. The strong temperature effect on the CMC/C_{20} ratio for the Pluronics can be ascribed to the temperature dependence of the CMC [Chapter 1 of this Thesis; Alexandridis et al., 1994], and, in particular, to the increasing hydrophobicity with temperature of both EO and PO segments of the copolymer molecule; the adsorption of the PEO-PPO-PEO copolymers at the air/water interface is less sensitive to temperature. The CMC/C_{20} ratio decreased with increasing number of PO segments for groups of Pluronic copolymers with the same number of EO segments (i.e., P123-P65, and P85-P104), and increased with increasing number of EO segments for groups of Pluronics with the same size PPO block (i.e., P103-P104-P105-F108). Both these trends are in agreement with those observed for ethoxylated nonionic surfactants [Rosen, 1989]. Furthermore, the CMC/C_{20} ratio increased with decreasing molecular weight for the Pluronics P105, P85, and P65 that have the same composition, reflecting again the effect of molecular weight on the CMC [Alexandridis et al., 1994].

4.3c Surface area per copolymer molecule

Block copolymers of the Pluronic family find applications in the preparation of stable oil-in-water emulsions [BASF, 1989]; some of the advantages of the Pluronics are strong adsorption at the interface and the provision of an effective steric barrier that inhibits coalescence and flocculation of emulsion droplets. Information on the packing of copolymer molecules at interfaces is needed for a fundamental understanding of the role of Pluronics in such systems. To this end, areas per molecule were calculated from the surface tension data of Figure 4.2 using the simple form of the Gibbs adsorption isotherm [Chattoraj & Birdi, 1984] that relates the surface (excess) concentration of the surfactant, Γ, to the surface tension and the surfactant chemical potential:

$$\Gamma = -(1 / RT)(d\gamma / d \ln C) \qquad (1)$$

where the area per molecule, A, is equal to $(\Gamma N)^{-1}$, γ is the surface tension, N is

Avogadro's number, R is the molar gas constant, T is the absolute temperature, and an ideal solution is assumed. Note that Equation 1 is valid for a single component adsorbing at the interface. In the case of many components (e.g. polydisperse polymer or presence of impurities) $d\ln C_1 = d\ln C_2 = ... = d\ln C_{total}$ and Equation 1 becomes [Chattoraj & Birdi, 1984]

$$\Sigma_i \Gamma = - (1 / RT) (d\gamma / d \ln C_{total}) \quad (2)$$

The area calculated from $\Sigma_i \Gamma$ (Equation 2) will be the average surface area of the adsorbed species. In the absence of information on the exact composition of the Pluronic samples, one can assume that the area per molecule estimated from the surface tension data will be an average area. The solid lines at low copolymer concentrations shown in Figure 4.2 indicate the bulk concentration range (generally 10^{-6} to 10^{-3} wt %) over which area per molecule values were extracted.

The values for surface area per copolymer molecule calculated in this way (tabulated in Table 4.2) are generally small compared to those of nonionic surfactants with an aliphatic chain and PEO headgroup of comparable size to the PEO block of Pluronics [Nikas et al., 1992; Mysels, 1986; Kronberg et al., 1984], indicating that there is considerable folding of the polymers at the air/water interface [Prasad et al., 1979] and/or desorption of PEO segments in the water phase [Aston et al., 1990]. One would expect that, since two PEO moieties are attached to PPO, the PEO blocks extend horizontally on the interface and occupy more area (per copolymer molecule) than in the case of C_iE_j surfactants, which are anchored to the interface by their hydrocarbon tail. This would result in a slope ($d\gamma/d\ln C$) that is small when the surface occupancy is very low (copolymers spread on the surface), and grows as more and more copolymers come to the surface (copolymers are packed). Indeed this may be the case at very low copolymer concentrations, lower than the ones we studied. Although the same trend (shallow slope followed by steeper slope) is observed between the two breaks of the surface tension vs log concentration curve, it seems unlikely that this is the result of the above process, as that explanation would leave unaccounted for the linear decrease in surface tension at concentrations lower than that of the first break (see also discussion above on the origin of the low-concentration break).

Effect of EO and PO segments on surface area: The area per copolymer molecule

increases with the number of EO segments in the molecule for a family of Pluronic copolymers with the same PPO and varying PEO block length, as seen in Figure 4.4. Also shown on the same plot are areas per molecule for a series of octylphenoxy-ethoxyethanol surfactants (area values were extracted from Crook et al. [1963]). There is some experimental evidence that suggests that the headgroup areas of C_iE_j surfactants adsorbed at air/water interfaces scale with the number of EO units, N_{EO}, as $N_{EO}^{1/2}$; this scaling law can be rationalized by assuming that the environment seen by a polymer chain at the interfacial layer resembles that in a polymer melt near an impenetrable wall [Nikas et al., 1992]. For long polymer chains (which obey scaling laws [deGennes, 1975]) the average thickness, λ, of a PEO layer in the melt scales as $n^{1/2}$ [deGennes, 1975], where n is the number of bonds in the polymer chain. The average area per chain can be estimated as $A=\upsilon/\lambda$, where υ is the dry volume of the chain and $\upsilon \sim n$; as a result, A scales as $n/n^{1/2} = n^{1/2} \sim N_{EO}^{1/2}$ [Nikas et al., 1992]. Although the above derivation is valid in the limit of long polymer chains, it has recently been shown by Sarmoria and Blankschtein [1992] that, in the case of PEO, scaling laws are obeyed even for short ($N_{EO}=10$) chains. The scaling exponent for the surface area dependance on N_{EO} was found to be indeed 0.50 for the data set of Crook et al. [1963] presented in Figure 4.4. The scaling exponent for the Pluronics was estimated from a fit to be 0.433, lower than the exponent in the case of octylphenoxy-ethoxyethanol surfactants.

It is not clear at this time whether the 0.433 exponent is significant or it is, within experimental error, the same as 0.5 (shown with a solid line in Figure 4.4). One reason of this uncertainty is the exact location of the PEO segments; the exponent was derived assuming all were part of the interfacial layer, but some PEO units may fold around the PPO segment or desorb into the aqueous subphase (chain segment desorption of a poly(12-hydroxystearic acid)-PEO block copolymer into the subphase upon compression of the interface at a Langmuir trough was reported by Aston et al. [1990]) and thus not contribute on the interfacial area. Increase in the length of the hydrophobic (PPO) section, for a group of copolymers that have the same PEO segment size, results in a decrease in the area that each molecule occupies at the air/water interface, in agreement with Prasad et al. [1979]. This finding suggests a more compact interfacial layer for larger PPO segment size, with the copolymer molecules oriented on the surface in a coiled manner having PPO out of the aqueous phase, and the hydrophilic PEO units at the extremities of the copolymer partly anchoring the polymer in the aqueous phase and partly folding around PPO. Yeates et al.

[1986] reported areas per molecule higher for $C_1E_8C_i$ than for $C_iE_{15}C_i$ (C: methyl groups, i = 5-12, E: ethylene oxide segments) indicating again that the hydrophobic moiety makes the interfacial layer more compact. The area per molecule for PEO-poly(dimethylsiloxane)-PEO copolymers has also been shown to decrease as the size of the hydrophobic moiety increased [Kanellopoulos & Owen, 1971].

Prasad et al. [1979] obtained areas per molecule for Pluronics L42, L44, L62, L64, F68, P85, and F88, applying the Gibbs adsorption equation to the surface tension values at concentrations below the low-concentration break of the surface tension curve. They found areas ranging from 64 $Å^2$ for L62 to 146 $Å^2$ for L44. When the areas-per-molecule were plotted against the hydrophile/lipophile balance (HLB) number of the copolymers, it became evident that, for a given PPO block, the surface area per molecule increased with increasing size of the PEO blocks attached to the sides of the PPO block. Increasing the size of the central hydrophobic block (PPO) at a given HLB resulted in a marked decrease in the area occupied at the surface that was attributed to folding of the molecules at the surface. Wanka et al. measured surface tension of P104 and P123 solutions at 25 °C and obtained areas per molecule that are approximately 20% higher that the values we obtained; this discrepancy can be attributed to differences in the surface tension values for low copolymer concentrations, where the presence of impurities could alter the surface tension values. Reddy et al. [1991] reported surface area of 180 $Å^2$ for L64. However, the concentration range covered in this study was rather limited (0.01 - 10 %) and the surface tension values reported were only up to 45 mN/m, leaving open the possibility that the surface tension data used for deriving the area per molecule values did not belong to the constant surface coverage region. Indeed, Prasad et al. [1979], who measured the surface tension of L64 over a wide concentration range (10^{-6} - 10 %) derived a value for area per molecule half than that derived from Reddy et al. [1991].

Two simple models have been considered in the literature regarding the configuration of the PEO chain (which influences the area per copolymer molecule) on the air/water interface [Zhou & Chu, 1988; Rosch, 1967]: the "zig zag" model, in which the chain is fully extended and the length and width of the EO monomer unit are 3.6 and 2.5 Å, respectively, and the "meander" model in which the chain is twisted into an expanded helical coil form with the corresponding length and width being 2.0 and 4.5 Å, respectively. The cross-sectional areas would be 28 $Å^2$ for the meander chain and 19 $Å^2$

for the zigzag chain. It has been concluded by some authors that in aqueous solution poly(ethylene oxide) chains with more than 10 EO units are predominantly in the meander configuration rather than in the zigzag form [Rosch, 1967]. From aggregation number and hydrodynamic radius data of Pluronic copolymer micelles, Zhou and Chu [1988] found the meander configuration of PEO to be more reasonable, since fewer kinks are required to fill up the micelle corona region than those needed for the zigzag form.

Phipps et al. [1993] studied the conformation of Pluronic F127 at the hexane/water interface employing a neutron reflectivity technique. Use of hexane was necessary to achieve contrast variation, however the authors report indications that the presence of hexane had little effect on either the adsorbed amount or the conformation of the copolymer on the water side of the interface. In this respect their findings should also be applicable for copolymer at air/water interfaces. F127 was found to adopt a conformation that extended beyond the micellar radius in water, and thus, appeared quite stretched. The estimated (unperturbed) radius of gyration of a PEO block is 20 Å and that of the PPO block 16 Å; the volume fraction profile of F127 at the interface (fitted from the neutron scattering data) shows the PEO segments to protrude 90 Å into the water subphase and PPO to extent 40 Å in hexane [Phipps et al., 1993]. On the contrary, a random copolymer of poly(vinyl alcohol-*co*-acetate) was shown to adopt a very flat conformation at the interface, forming a dense layer of ~20 Å. The experimental findings regarding the conformation of the Pluronic copolymer at the interface were borne out by a Scheutjens-Fleer simulation (similar to the one used by our group and others to model block copolymer micelles [Hurter et al, 1993]) that showed the copolymer attached to the interface by the hydrophobic PPO block and the PEO blocks having a "parabolic" segment density profile, similar to a polymer chain grafted at a solid surface. Both the protrusion of PEO in the water subphase and the resemblance of PEO to a grafted chain agree with the findings of our surface tension study. Note that the study of Phipps et al. [1993] was done at copolymer concentrations above the CMC whereas the surface areas reported here were derived from surface tension data below CMC.

Effect of temperature on surface area: Increasing temperature typically results in expansion (higher surface area per molecule) of monolayers spread at air/water interfaces. This phenomenon originates from higher flexibility of the hydrophobic part of the molecules at higher temperatures (stronger thermal agitation produces stronger repulsion

between the hydrophobic chains) [Lo Nostro & Gabrielli, 1993]. A decrease in the area per copolymer molecule with increase in temperature was observed in our experiments (see Table 4.2). This can be attributed to either less PEO hydration water at the higher temperature, or an increase in hydrophobicity of the PPO core, or both. The former would indicate more compact packing of copolymer molecules at higher temperatures, in agreement with light scattering results that show the hydrodynamic radius of Pluronic copolymer micelles to remain roughly constant while the aggregation number of micelles increased with temperature (see Chapter 1 of this Thesis) and the weakening of hydrogen bonding between PEO and water with increasing temperature [Alexandridis et al., 1994]. The latter would lead to a behavior similar to that discussed in a previous paragraph where increase in the size of the PPO block in copolymers having PEO blocks of similar length results in lower surface areas (PEO partly folds around PPO).

The only surface tension study that has been done so far at more than one temperature was by Reddy et al. [1991], who studied L64 at three temperatures. They obtained areas that increased with temperature, but as discussed above, the bulk concentration range from which these areas were deriv :d was very limited and, perhaps, not representative of the constant surface coverage concentration region from which the values for surface area are estimated [Chattoraj & Birdi, 1984]. Decrease in surface area of aliphatic alcohols (spread monolayers of 1-tetradecanol and 1-hexadecanol) with increasing temperature has been reported by Lo Nostro and Gabrielli [1993]. They interpreted this behavior in terms of squeezing out water molecules from the coordination shells that surround the polar headgroups of the amphiphile.

4.3d Surface activity of PPO-PEO-PPO triblock and PEO-PPO random copolymers

In addition to the Pluronic PEO-PPO-PEO triblock copolymers, we studied the surface activity of two other copolymers, commercially identified as 25R4 and 50HB-5100, that have different structure (25R4 is a PPO-PEO-PPO triblock and 50HB-5100 is a random PEO-PPO copolymer) but are of comparable PPO/PEO composition and molecular weight to some of the Pluronics. As these two polymers do not form micelles in aqueous solutions (as determined by a dye solubilization technique [Alexandridis et al., 1994]; see also the light scattering study of Zhou and Chu [1994]),

they could serve as controls with respect to the influence of the molecule structure on the surface activity. Surface tension data are reported in Figures 4.5a for 25R4 and 4.5b for 50HB-5100, plotted as a function of copolymer concentration for two temperatures (25 and 35 °C). Both copolymers lowered the surface tension significantly (from ~70 to ~50 mN/m) with increasing concentration (for the concentration range 10^{-5} - 10^{-4} %). A break (change of slope) in the surface tension curve was observed at concentrations 10^{-4} - 10^{-3} % for both copolymers, after which a further (but shallow) decrease in surface tension was effected by increase in copolymer concentration. A plateau in the surface tension value was never reached for concentrations up to 10% (note that the high concentration employed for 25R4 is limited by the solubility of 25R4 in water). The occurrence of a break at concentrations of 10^{-4} - 10^{-3} % for these polymers that form no micelles is in support of the argument proposed earlier in the paper that the low-concentration break observed for Pluronics is not connected to micelle formation. One can also argue that the phenomenon behind this break is independent of the blockiness or the block sequence of the copolymers.

Regarding the surface tension values following the change in slope discussed above, 25R4 is more effective than 50HB-5100 in lowering the surface tension. 25R4 has the same number of EO segments as P103, and the surface area per 25R4 molecule (calculated from the surface tension slope at the 2.5×10^{-5} - 10^{-4} % concentration range) is approximately the same as the one for P103. 50HB-5100 is intermediate in composition and molecular weight to P65 and P85 (both are relatively hydrophilic) but appears to form a more compact interface (judging from the slope of the surface tension curve at the 10^{-5}-10^{-4} % concentration range) than P65 and P85.

For comparison purposes, surface tension data for aqueous solutions of PEO and PPO homopolymers, are plotted in Figures 4.6a and 4.6b, respectively. Data for PEO of 1000, 1540, and 4000 molecular weight were taken from Couper and Eley [1948] and data for PEO of molecular weight 2 400 000 were from Glass [1969]. Surface tension values for PPO oligomer (M_w: 620 and 2000) solutions were extracted from Schwuger [1973]; data at high concentrations were not available because the solubility limit of PPO in water was reached. Both PEO and PPO adsorb at the air/water interface and lower the surface tension, the PPO having a much greater effect. Increase in polymer concentration resulted in a smooth decrease of surface tension, as expected for nonassociating solutes [Chattoraj & Birdi, 1984]. An exception is the high-molecular-weight PEO that exhibits a break in the

surface tension, attributed to the attainment of full coverage at the interface [Glass, 1969]; note, however, that this data set was obtained using the pendant drop technique that may be more sensitive to the extent of surface coverage than the ring method used by Couper and Eley [1948].

The area per molecule values obtained from Couper and Eley [1948] indicate that the polymer molecules lie flat on the surface; this is in disagreement with the earlier work of Gallaugher and Hibbert [1937] and Glass [1969] who suggest that portions of the PEO structure are oriented out of the interfacial region. Kawaguchi et al. [1984], who found looping of PEO molecules from the surface into the aqueous subphase to take place above a critical concentration (0.4 mg/m^2), and Kuzmenka and Granick [1988], who noted that at high surface coverage the PEO monolayer "collapsed" to a three-dimensional structure, support the idea of PEO extending into the water subphase. Rennie et al. [1989] studied the adsorption of PEO (M_w~20 000) at the air/water interface using specular reflection of neutrons and found that the surface layer had a thickness comparable to the radius of gyration in solution, the segment density in the layer increased with both increasing concentration and temperature, and that an appreciable quantity of water was present in the surface region. They estimated area per monomer ranging from 28 Å^2 at 0.004 % PEO concentration to 11 Å^2 at 0.1 %. The variation of area per monomer with concentration would suggest that the monolayer is not complete until a bulk concentration of at least 0.1 wt% is reached; this disagrees with the results obtained by Glass [1969] who found that the monolayer was complete at a concentration of approximately 0.002 %.

4.4 Conclusions

The surface tension of aqueous solutions of poly(ethylene oxide)-*block*-poly(propylene oxide)-*block*-poly(ethylene oxide) copolymers was determined for the 10^{-5} - 10 % w/v concentration range, at two temperatures (25 and 35 °C). Seven Pluronic PEO-PPO-PEO block copolymers were investigated, covering a wide range of molecular weights (3400 - 14600) and PPO/PEO ratios (0.19 - 1.79). Two breaks were observed in the surface tension vs log concentration curve for most of the copolymers. Our hypothesis for interpreting the dependance of surface tension on copolymer concentration is adsorption of the PEO-PPO-PEO copolymer at the interface as an inverted "U" with the PEO chains at

the interface (low bulk copolymer concentrations). At a bulk copolymer concentration of approximately 0.001%, a "phase transition" occurs at the interface, the copolymer layer becomes more compact and perhaps PEO segments protrude into the aqueous solution or fold around PPO. This picture agrees with recent neutron reflectivity studies by Phipps et al. [1993]. The surface tension continues to decrease with increasing bulk concentration until the CMC. Upon the formation of micelles the activity of the copolymer in the bulk remains approximately constant and the surface tension attains a steady value that does not change with further increase in the copolymer bulk concentration.

There was good agreement between the CMC values determined from the second break of the surface tension curve and dye solubilization experiments. The surface area per copolymer molecule, A, increased as a function of the number of EO units, N_{EO}, obeying a scaling law ($A \sim N_{EO}^{1/2}$) similar to that followed by lower molecular weight C_iE_j nonionic surfactants. The presence of PPO in the center of the copolymer resulted in a copolymer headgroup (PEO) surface area smaller than that of homopolymer PEO (of comparable molecular weight), indicating desorption of PEO segments from the air/water interface and/or tightly packed segments. The surface activity of PEO-PPO-PEO block copolymers was compared to that of a PPO-PEO-PPO block copolymer and a PEO-PPO random copolymer. A break in the surface tension was observed for the latter, supporting the idea that the low-concentration change of slope observed for Pluronics is not related to micelle formation. Published information on PEO homopolymers at air/water interfaces supports the argument that some EO segments desorb from the interface and are present in the aqueous subphase.

4.5 Appendix: Surface Activity of PEO

Couper and Eley [1948] measured surface tension (using a ring balance) for PEO homopolymers of relatively low molecular weights (1000 - 6000) and derived values for area per molecule which indicated that the polymer molecules lay flat on the surface, in disagreement with the earlier work of Hibbert and coworkers [Gallaugher & Hibbert, 1937; Lovell & Hibbert, 1940]. Gallaugher and Hibbert concluded (from surface tension measurements of pure PEO oligomers) that the PEO molecules at the liquid surface are oriented in the form of an inverted "U" with at least one ethylene oxide group in the

surface, the rest of the chain forming the sides of the "U" in the interior of the liquid. The adsorption of PEO at the air - water interface has been studied by Glass [1969] by means of surface tension measurements using the pendant drop technique. He was able to derive adsorption isotherms for different molecular weights and to follow the rate of adsorption of polymer at the interface. Accodring to Glass, all PEO entities (ranging from oligomers to polymers with 2,400,000 molecular weight) have portions of their structure oriented out of the interfacial region. Glass reported that, below a molecular weight range of 10000, the surface activities of the aqueous solutions exhibited a marked dependence upon molecular weight: the surface tension values decrease with decreasing degree of polymerization

More recently, surface pressure and scattering techniques have been used to probe the organization of PEO on the air - water interface. Ito et al. [1990], using electrocapillary waves diffraction, found PEO of molecular weight 148000 to be highly interface active (water - toluene interface). Kawaguchi et al. [1984] concluded from surface quasi-elastic light scattering results that, above a critical concentration (0.4 mg/m^2), looping of the PEO molecules from the surface into the aqueous subphase takes place. From a study of the influence of temperature on surface pressure isotherms for PEO, Kuzmenka and Granick [1988] noted that at low surface coverage there was a loss of entropy due to the confinement of the molecules in two dimensions. At higher surface coverage there was a gain in entropy as the monolayer "collapsed" to a three-dimensional structure. Additionally they suggested that water ordered at the surface with the PEO subunits.

Rennie et al. [1989] used specular reflection of neutrons to study the adsorption of PEO (~20000) at the air - water interface. Their results indicate that the surface layer has a thickness comparable to the radius of gyration in solution, and that the segment density in the layer increases with both increasing concentration and temperature. There is, however, always an appreciable quantity of water in the surface region. The area per monomer ranged from 28 $Å^2$ at 0.004 % PEO concentration to 11 at 0.1 %. The variation of area per monomer with concentration suggests that the monolayer is not complete until a concentration of at least 0.1 wt%. This disagrees with the results obtained by Glass [1969] who found that the monolayer was complete at a concentration of about 0.002 %. Henderson et al. [1933] investigated the organization of PEO (40000 Da) spread at the air-water interface using surface pressure isotherms and neutron reflectometry. Surface pressure isotherms gave a value of 43 $Å^2$ area per monomer at the dilute limit

(approximately twice as much as the value of Couper and Eley [1948]). Neutron reflectometry results suggest that, at low surface concentrations (< 0.4 mg/m^2), the polymer can be described as a single layer which is much diluted by water. At higher concentrations (up to 1.0 mg/m^2) the polymer penetrates the subphase and the segment distribution normal to the interface is describable by a Gaussian concentration profile. As the deposited surface concentration increases, the polymer penetrates deeper into the subphase and the topmost layer concentration remains approximately constant. The layer thickness of the spread monolayer is considerable thicker than the equilibium excess layer obtained in a solution of PEO.

Bailey et al. [1979] measured the interfacial tension of PEO and PPO oligomers (PEO molecular weight 400 - 4000, PPO molecular weight 1000 - 2000) using the pendant drop method. They found the interfacial tension to increase with increasing PPO molecular weight and to decrease with increasing PEO molecular weight. They explained these results by assuming that the predominant interaction is the adsorption of the PPO -OH end group at the interface with the PEO, by hydrogen bonding to the PEO ether links. An increase in interfacial tension was observed with decrease in temperature.

4.6 References cited in Chapter 4

1. Alexandridis, P.; Holzwarth, J. F.; Hatton, T. A., *Macromolecules* **1994**, *27*, 2414; Chapter 2 of this Thesis.
2. Ananthapadmanabhan, K. P.; Goddard, E. D.; Turro, N. J.; Kuo, P. L. *Langmuir* **1985**, *1*, 352.
3. Anderson, R. A. *Pharm. Acta Helv.* **1972**, *47*, 304.
4. Arai, H.; Murata, M.; Shinoda, K. *J. Colloid Interface Sci.* **1971**, *37*, 223.
5. Aston, M. S.; Herrington, T. M.; Tadros, T. F. *Colloids and Surfaces* **1990**, *51*, 115.
6. Bahadur, P.; Riess, G. *Tenside Surf. Det.* **1991**, *28*, 173.
7. Bahadur, P.; Pandya, K. *Langmuir* **1992**, *8*, 2666.
8. Bailey A. I.; Salem, B. K.; Walsch, D. J.; Zeyntountsian, A. *Colloid Polym. Sci.* **1979**, *257*, 948.
9. Chattopadhyay, A.; London, E. *Anal. Biochem.* **1984**, *139*, 408.

10. Chattoraj, D. K.; Birdi, K. S. *Adsorption and the Gibbs Surface Excess*, Plenum Press, New York, 1984.
11. Couper, A.; Eley, D. D. *J. Polym. Sci.* **1948**, *3*, 345.
12. Crook, E. H.; Fordyce, D. B.; Trebbi, G. F. *J. Phys. Chem.* **1963**, *67*, 1987.
13. deGennes, P. G. *Scaling Concepts in Polymer Physics*, Cornell University Press, Ithaca, NY, 1975.
14. deGennes, P. G. *Pure Appl. Chem.* **1992**, *64*, 1585.
15. Edwards, D. A.; Luthy, R. G.; Liu, Z. *Environ. Sci. Technol.* **1991**, *25*, 127.
16. Gallaugher, A. F.; Hibbert, H. *J. Am. Chem. Soc.* **1937**, *59*, 2514.
17. Garti, N.; Katz, M. *J. Dispersion Sci. Technology* **1985**, *6*, 149.
18. Glass, J. E. *J. Phys. Chem.* **1969**, *72*, 4459.
19. Goddard, E. D. *Colloids and Surfaces* **1986**, *19*, 255.
20. Henderson, J. A.; Richards, R. W.; Penfold, J.; Thomas, R. K.; Lu, J. R. *Macromolecules* **1993**, *26*, 4591.
21. Hunter, R. J. *Foundations of Colloid Science*, Oxford University Press, 1987, Vol. 1.
22. Hurter, P. N.; Hatton, T. A. *Langmuir* **1992**, *8*, 1291.
23. Hurter, P. N.; Scheutjens, J. M. H. M.; Hatton, T. A. *Macromolecules* **1993**, *26*, 5592.
24. Hurter, P. N.; Scheutjens, J. M. H. M.; Hatton, T. A. *Macromolecules* **1993**, *26*, 5030.
25. Ito, K.; Sauer, B. B.; Skarlupka, R. J.; Sano, M.; Yu, H. *Langmuir* **1990**, *6*, 1379.
26. Kanellopoulos, A. G.; Owen, M. J. *J. Colloid Interface Sci.* **1971**, *35*, 120.
27. Kawaguchi, M.; Komatsu, S.; Matsuzumi, M.; Takahashi, A. *J. Colloid Interface Sci.* **1984**, *102*, 356.
28. Kronberg, B.; Stenius, P.; Thorssell, Y. *Colloids and Surfaces* **1984**, *12*, 113.
29. Kuzmenka, D. G.; Granick, S. *Macromolecules* **1988**, *21*, 779.
30. Linse, P.; Malmsten, M. *Macromolecules* **1992**, *25*, 5434.
31. Lo Nostro, P.; Gabrielli, G. *Langmuir* **1993**, *9*, 3132.
32. Lovell, E. L.; Hibbert, H. *J. Am. Chem. Soc.* **1940**, *62*, 2144.
33. Malmsten, M.; Lindman, B. *Macromolecules* **1992**, *25*, 5440.
34. Mysels, K. J. *Langmuir* **1986**, *2*, 423.
35. Nikas, Y. J., Puvvada, S.; Blankschtein, D. *Langmuir* **1992**, *8*, 2680.

36. Phipps, J. S.; Richardson, R. M.; Cosgrove, T.; Eaglesham, A. *Langmuir* **1993**, *9*, 3530.
37. Polik, W. F.; Burchard, W. *Macromolecules* **1983**, *16*, 978.
38. Prasad K. N.; Luong, T. T.; Florence, A. T.; Paris, J.; Vaution, C.; Seiller, M.; Puisieux, F. *J. Colloid Interface Sci.* **1979**, *69*, 225.
39. Reddy, N. K.; Fordham, P. J.; Attwood, D.; Booth, C. *J. Chem. Soc. Faraday Trans.* **1991**, *86*, 1569.
40. Rennie, A. R.; Crawford, R. J.; Lee, E. M.; Thomas, R. K.; Crowley, T. L.; Roberts, S.; Qureshi, M. S.; Richards, R. W. *Macromolecules* **1989**, *22*, 3466.
41. Rosch, H., in *Nonionic Surfactants*, Schick, M.J., Ed., Dekker, New York, 1967.
42. Rosen, M. J. *Surfactants and Interfacial Phenomena*, 2nd Edition, J. Wiley & Sons, New York, 1989.
43. Sarmoria, C.; Blankschtein, D. *J. Phys. Chem.* **1992**, *96*, 1978.
44. Schmolka, I. R. *J. Am. Oil Chem. Soc.* **1977**, *54*, 110.
45. Schwuger, M. J. *J. Colloid Interface Sci.* **1973**, *43*, 491.
46. Wagner, W.; Brochard-Wyart, F.; Hervert, H.; deGennes, P. G. *Colloid Polym. Sci.* **1993**, *271*, 621.
47. Wanka, G.; Hoffmann, H.; Ulbricht, W. *Colloid Polym. Sci.* **1990**, *266*, 101.
48. Yeates, S. G.; Craven, J. R.; Mobbs, R. H.; Booth, C. *J. Chem. Soc. Faraday Trans. 1* **1986**, *82*, 1865.
49. Yu, G.-E.; Deng, Y.; Dalton, S.; Wang, Q.-G.; Attwood, D.; Price, C.; Booth, C. *J. Chem. Soc. Faraday Trans.* **1992**, *88*, 2537.
50. Zhou, Z.; Chu, B. *J. Colloid Interface Sci.* **1988**, *126*, 171.
51. Zhou, Z.; Chu, B. *Macromolecules* **1994**, *27*, 2025.
52. *Pluronic and Tetronic Surfactants*, Technical Brochure, BASF Corp., Parsippany, NJ, 1989.

Chapter 4: List of Tables and Figures

Table 4.1 Composition of the Pluronic PEO-PPO-PEO copolymers studied here.

Polymer	Mol.Weight	PPO segm. weight	PO units	EO units	Lot number
P123	5750	4025	69	2x19	WPYM-569B
P103	4950	3465	60	2x17	WPHM-539B
P104	5900	3540	61	2x27	WPAN-503B
P105	6500	3250	56	2x37	WPDI-522A
F108	14600	2920	50	2x132	WPDN-564B
P85	4600	2300	40	2x26	WPAN-628B
P65	3400	1700	29	2x18	WPAN-605B
25R4	3600	2500	2x21	25	WPMN-515B

Table 4.2 Surface tension for 0.1% Pluronic PEO-PPO-PEO copolymer solutions, CMC/C_{20} ratio, and area-per-molecule values at the air/water interface.

Polymer	γ (mN/m) at 0.1%		CMC / C_{20}		Area/molecule (Å^2)	
	25 °C	35 °C	25 °C	35 °C	25 °C	35 °C
P123	33.4	32.8	125	20	50	40
P103	33.8	33.0	500	20	62	52
P104	35.2	33.6	1500	80	77	67
P105	35.9	34.3	2000	100	99	83
F108	42.2	38.0	2000	200	152	135
P85	39.9	33.2	25000	2000	122	105
P65	43.1	38.4	40000	4000	118	106

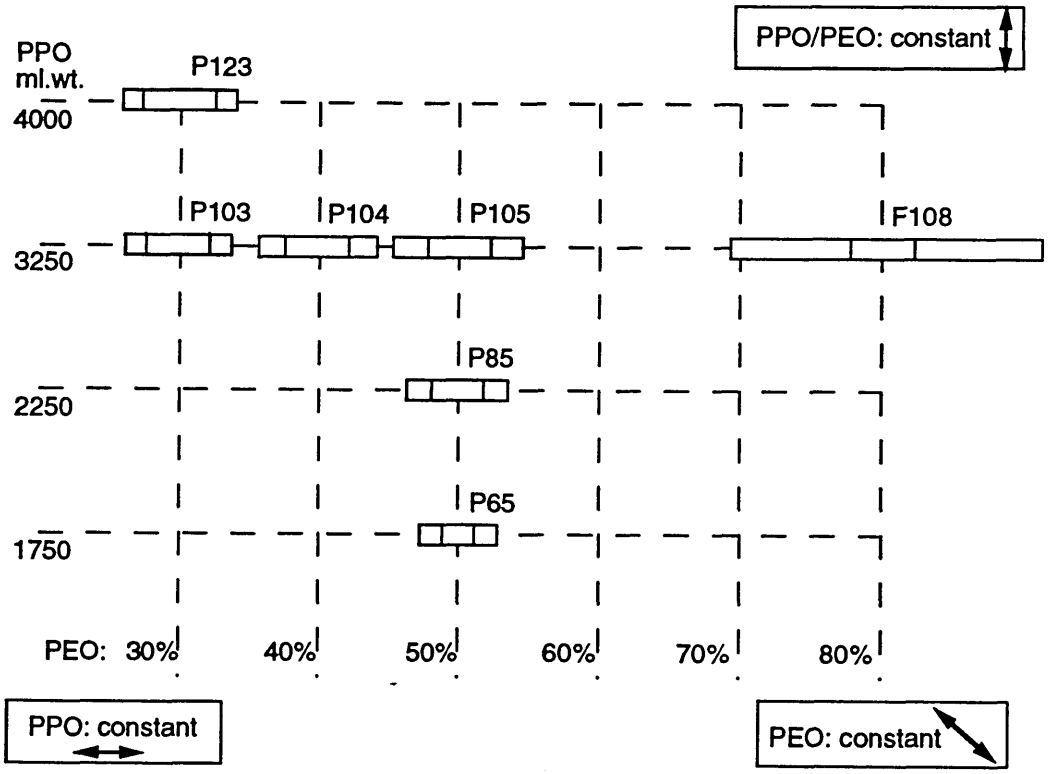

Figure 4.1 Schematic of the Pluronic copolymers used in this study.

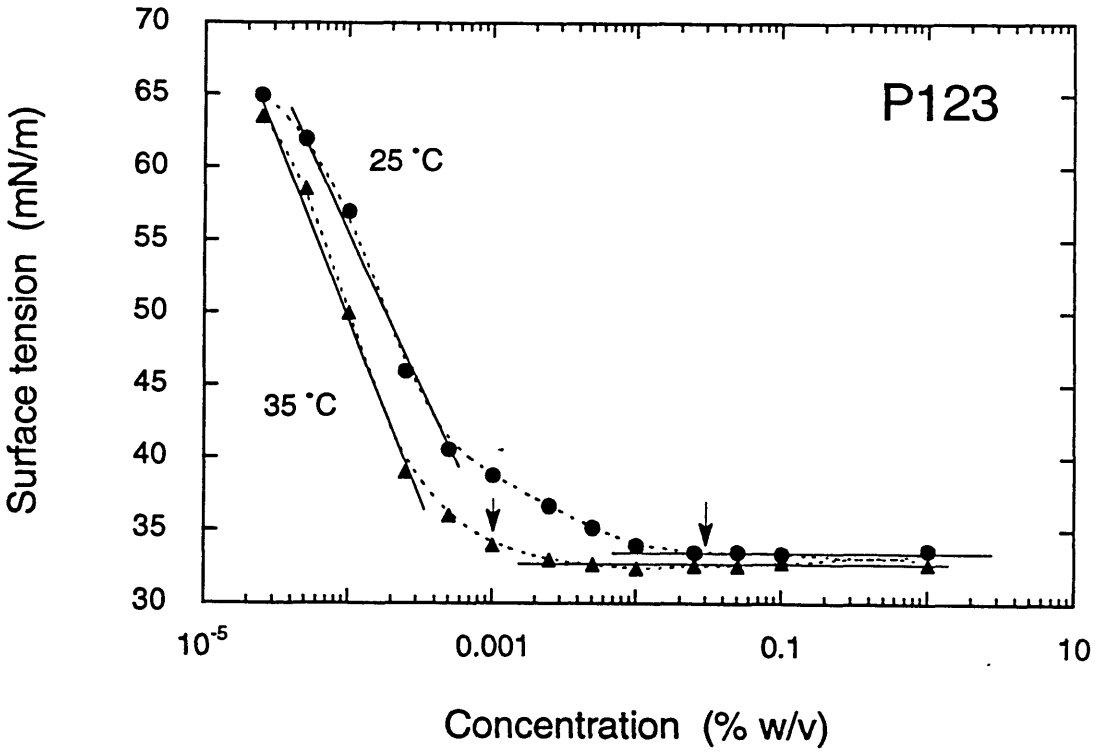

Figure 4.2 Surface tension data for various Pluronic copolymer solutions, plotted as a function of concentration for two temperatures (25 and 35 °C): (a) P123, (b) P103, (c) P104, (d) P105, (e) F108, (f) P85, (g) P65. The solid lines at low copolymer concentrations indicate the range from which area per molecule values were obtained, while the solid lines at high concentrations underline the steady surface tension values attained after the formation of micelles in the bulk. The arrows mark the CMC obtained for the same copolymer using dye solubilization.

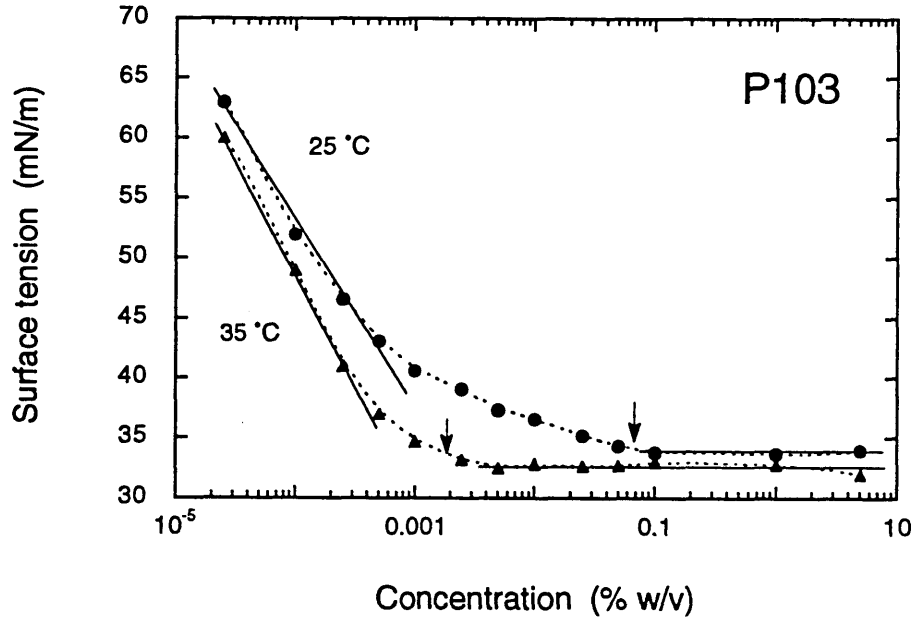
P103
25 °C
35 °C
Surface tension (mN/m)
Concentration (% w/v)
70
65
60
55
50
45
40
35
30
10-5
0.001
0.1
10

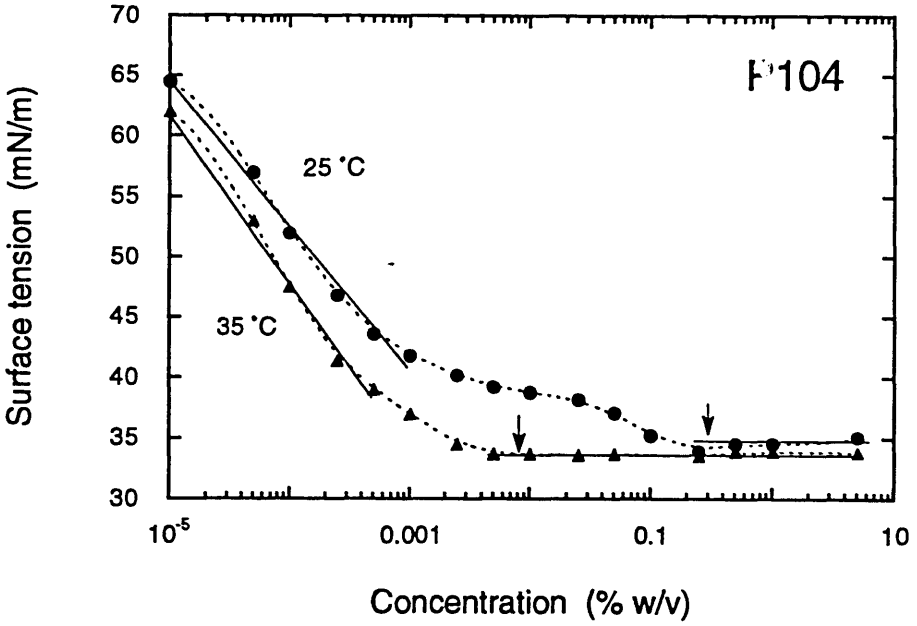
P104
25 °C
35 °C
Surface tension (mN/m)
Concentration (% w/v)
70
65
60
55
50
45
40
35
30
10-5
0.001
0.1
10

Figure 4.2 (b) & (c)

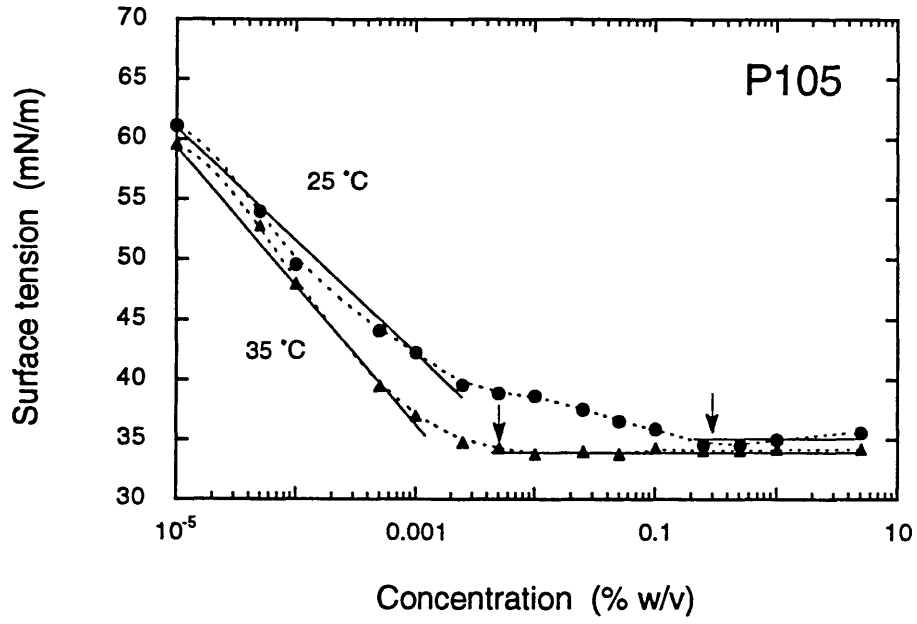
P105
25 °C
35 °C
Surface tension (mN/m)
70
65
60
55
50
45
40
35
30
10-5
0.001
0.1
10
Concentration (% w/v)

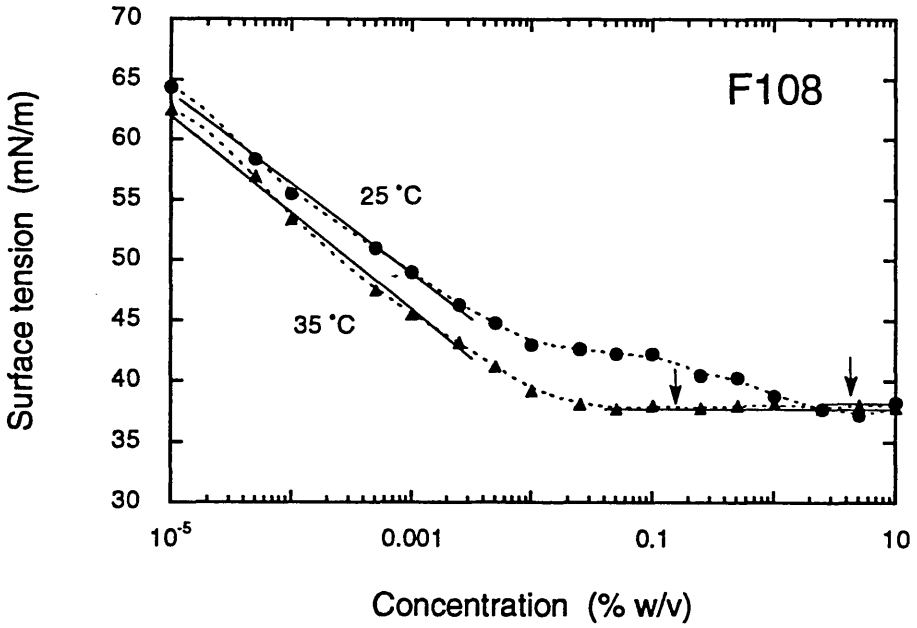
F108
25 °C
35 °C
Surface tension (mN/m)
70
65
60
55
50
45
40
35
30
10-5
0.001
0.1
10
Concentration (% w/v)

Figure 4.2 (d) & (e)

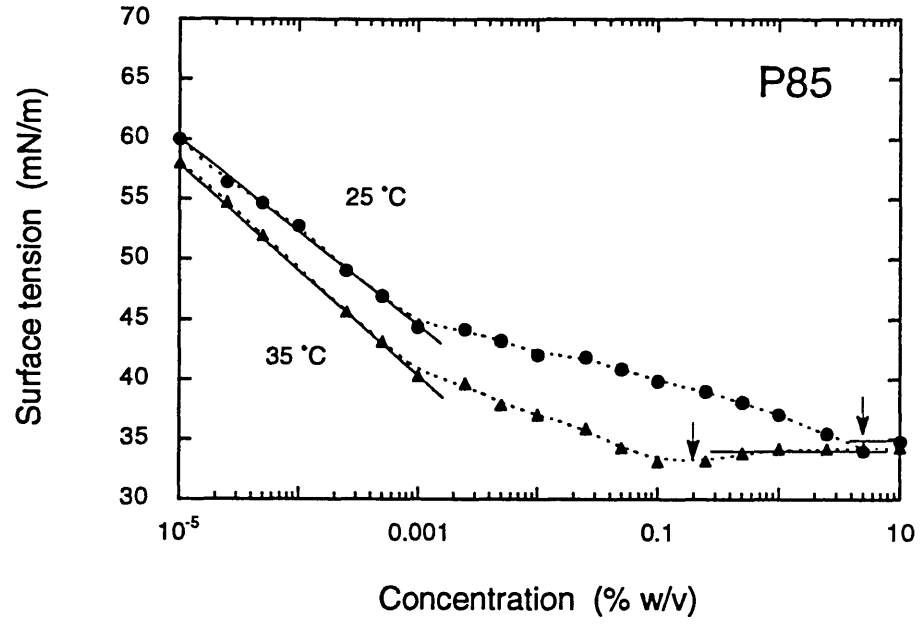
P85
25 °C
35 °C
Surface tension (mN/m)
Concentration (% w/v)
70
65
60
55
50
45
40
35
30
10-5
0.001
0.1
10

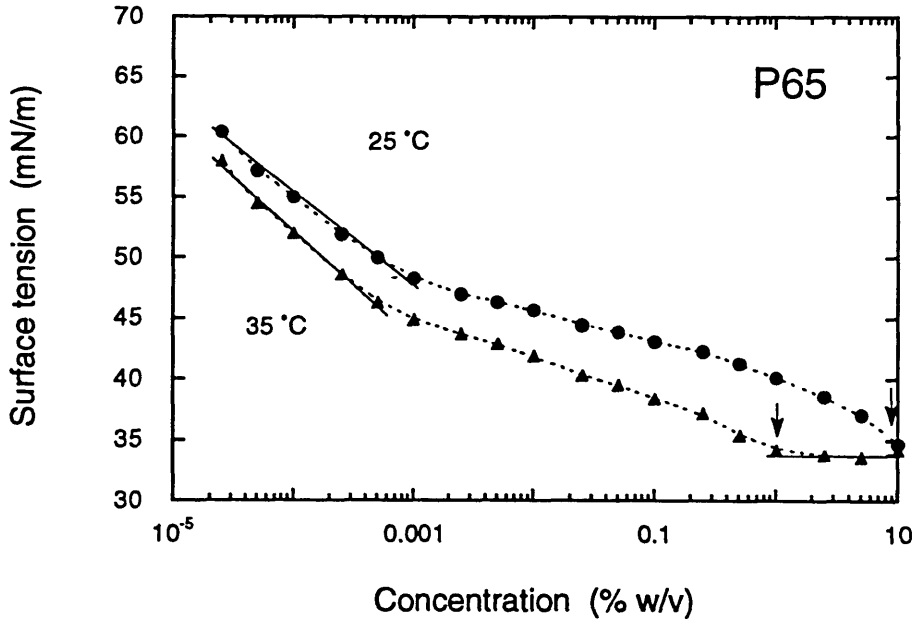
P65
25 °C
35 °C
Surface tension (mN/m)
Concentration (% w/v)
70
65
60
55
50
45
40
35
30
10-5
0.001
0.1
10

Figure 4.2 (f) & (g)

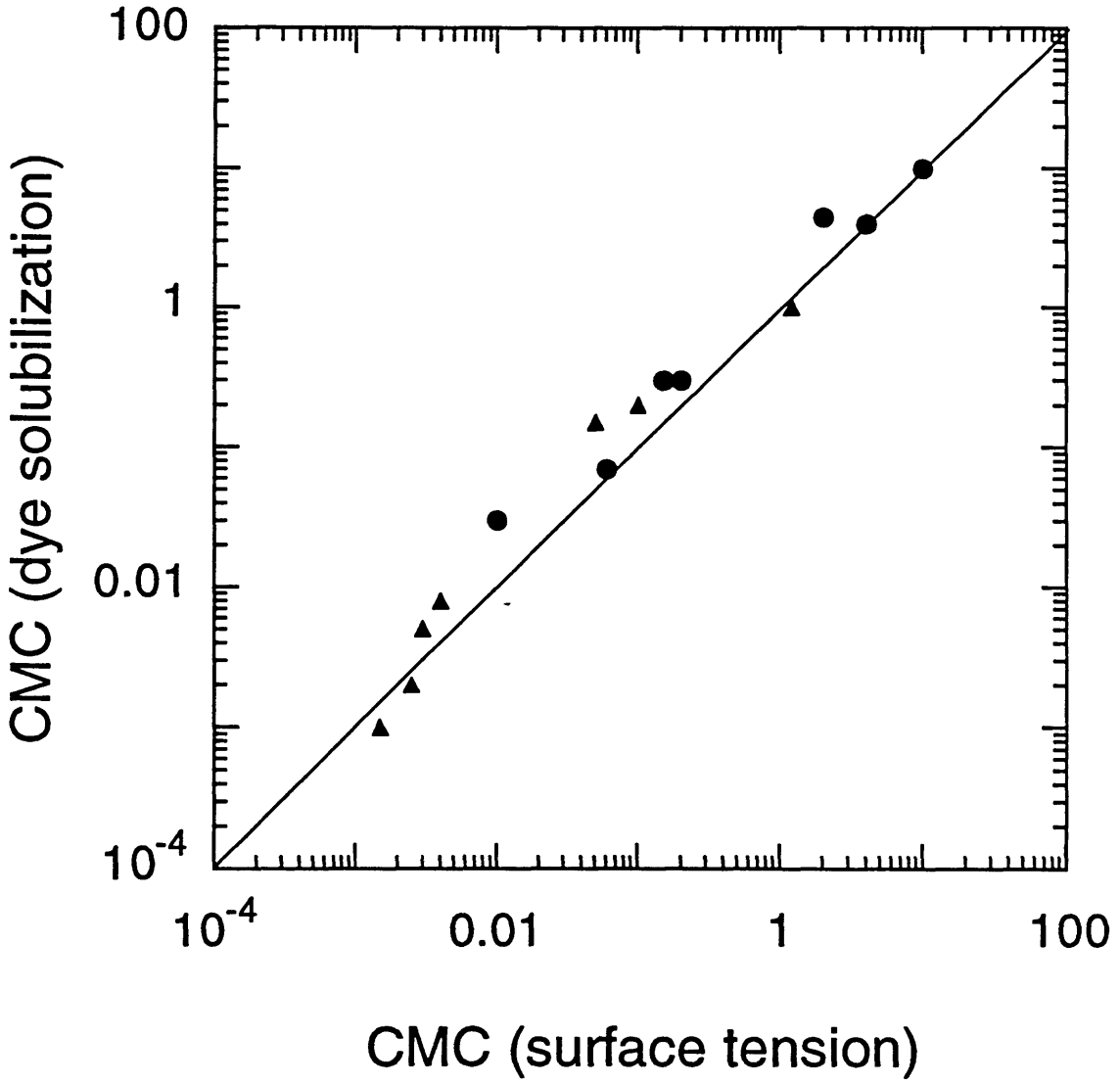

Figure 4.3 CMC values obtained from surface tension measurements relative to CMC values obtained from dye solubilization experiments. The solid line is drawn at 45°.

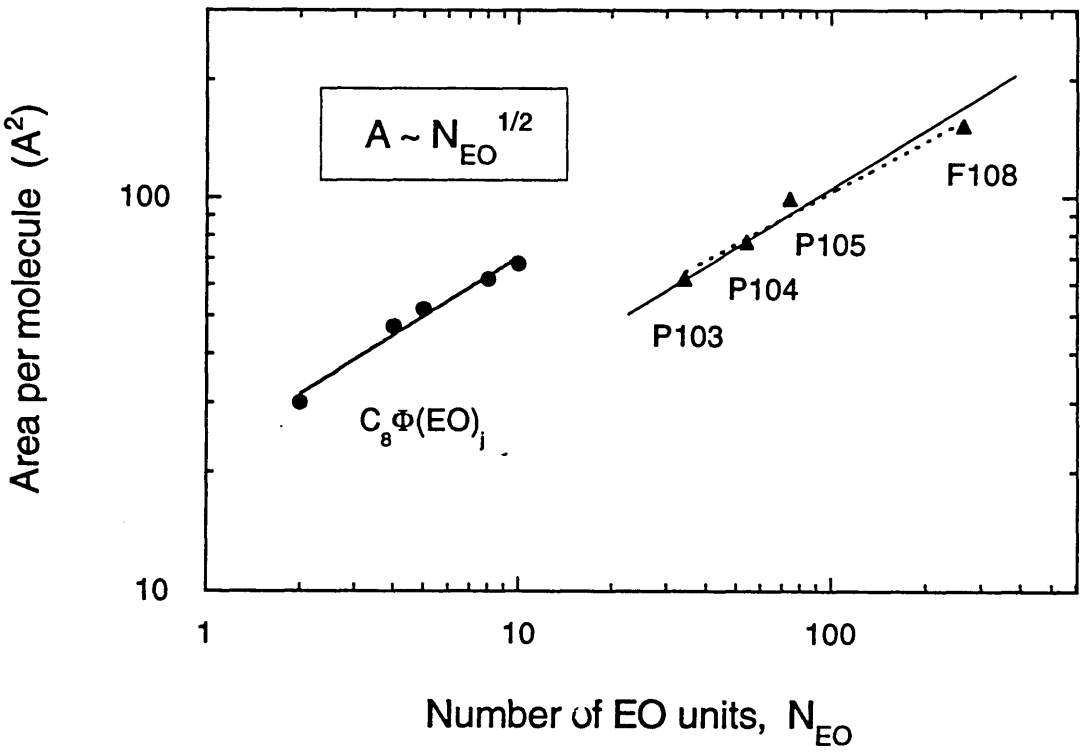

Figure 4.4 Area per molecule as a function of the number of EO monomers in the copolymer molecule, for a family of Pluronics with the same PPO and increasing PEO length. Also shown on the plot are areas per molecule for a series of octylphenoxy-ethoxyethanol surfactants (data from Crook et al., 1963]).

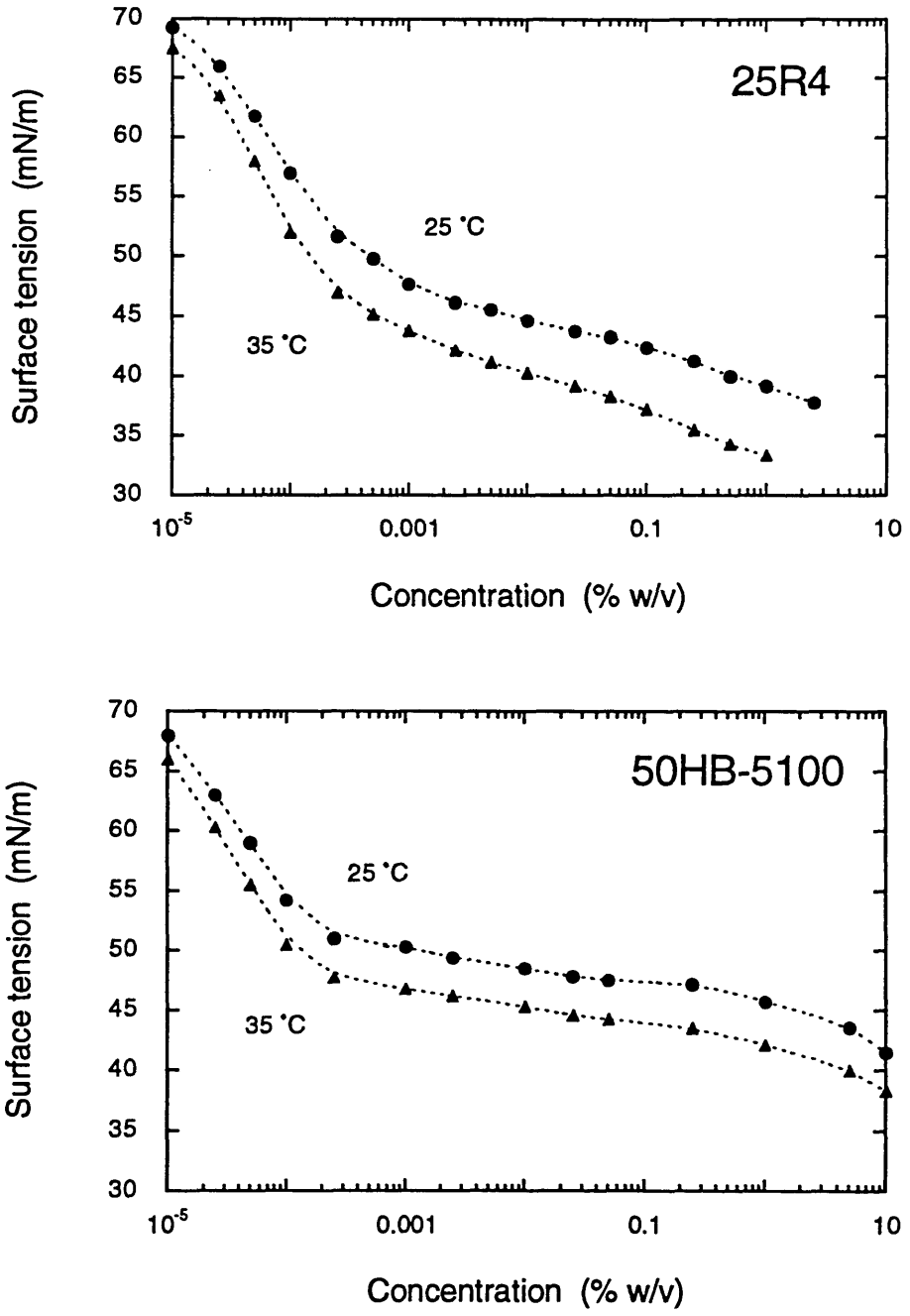

Figure 4.5 Surface tension data for solutions of (a) Pluronic 25R4 PPO-PEO-PPO block copolymer and (b) UCON 50HB-5000 PPO-PEO random copolymer as a function of copolymer concentration at 25 and 35 °C.

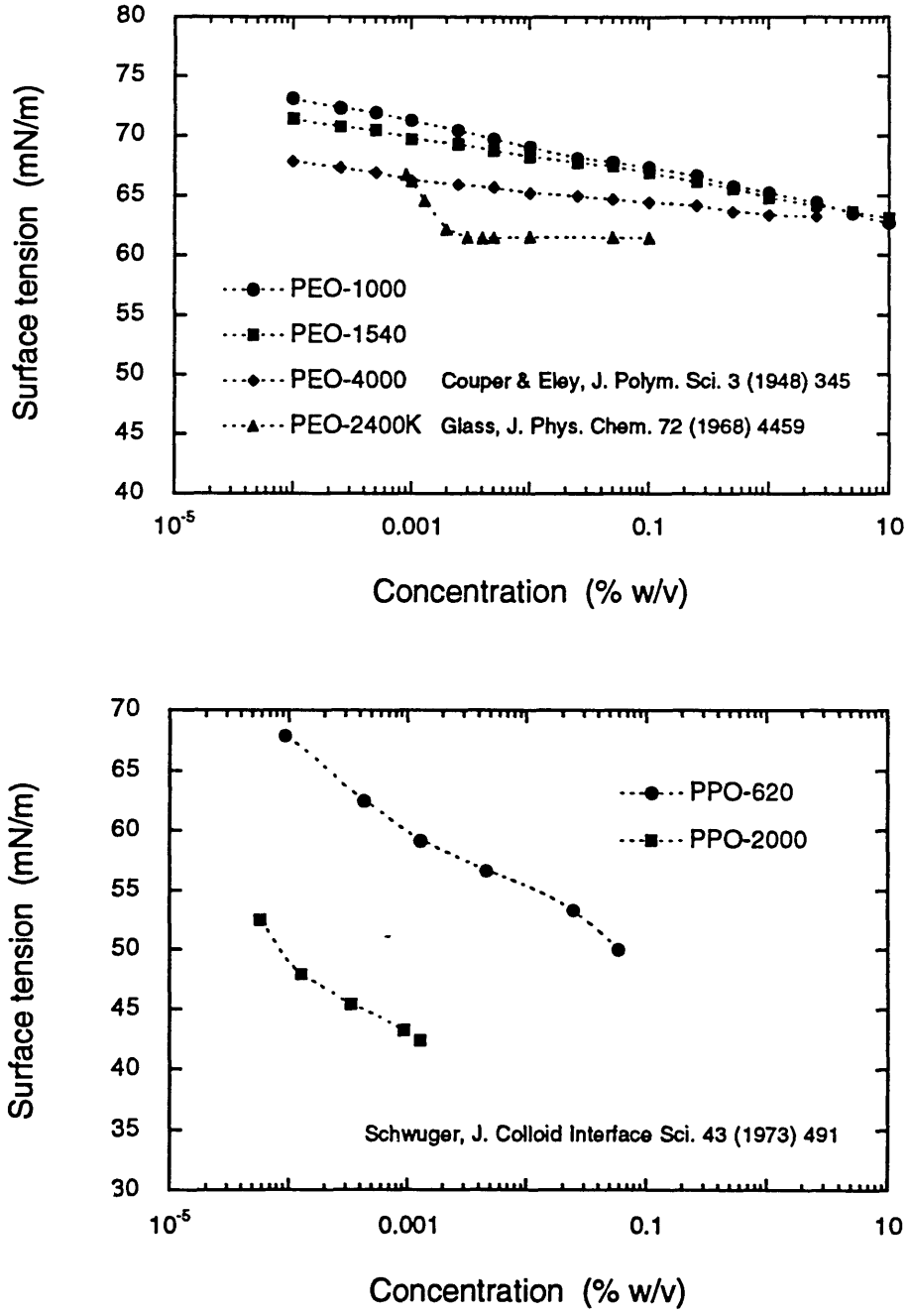

Figure 4.6 Surface tension data for solutions of (a) PEO homopolymer and (b) PPO homopolymer as a function of copolymer concentration.

Chapter 5
Temperature Effects on Structural Properties of Pluronic P104 and F108 PEO-PPO-PEO Copolymer Solutions

5.1 Introduction

Temperature-dependent micellization is a characteristic property of aqueous poly(ethylene oxide)-*block*-poly(propylene oxide)-*block*-poly(ethylene oxide) (PEO-PPO-PEO) copolymer solutions [Alexandridis & Hatton, 1994; Zhou & Chu, 1988; Wanka et al., 1990; Reddy et al., 1991; Brown et al., 1991; Malmsten & Lindman, 1992; Mortensen & Pedersen, 1993; Mortensen, 1992]. The critical micellization concentration (the copolymer concentration at which micelles start forming), CMC, the size and the aggregation number of the micelles, as well as the temperature dependence of these parameters, are of great interest for aqueous PEO-PPO-PEO block copolymer micellar solutions. Significant information has been obtained from light and neutron scattering studies on the structure of micelles formed by Pluronics L64, P85, F88, F68, and F127 [Al-Saden et al., 1982; Zhou & Chu, 1988; Brown et al., 1991; Reddy et al., 1991; Brown et al., 1992; Almgren et al., 1992; Malmsten & Lindman, 1992; Mortensen et al., 1992; Mortensen & Brown, 1993; Mortensen & Pedersen, 1993]. It has been found by Zhou and Chu [1988], Mortensen and Pedersen [1993], and others, that the average aggregation number increases with temperature; the absolute values vary between different copolymers and even between different batches of the same copolymer. For some systems the micelle hydrodynamic radius remains constant while the aggregation number increases with temperature, probably a result of dehydration of the PEO headgroups [Zhou & Chu, 1988]. In general, the monomer and the micelle size are found to be on the order of 1 nm and 10 nm, respectively, independent of concentration (although, the concentrations used in the scattering experiments were usually large to allow for good signal to noise ratio).

In a recent study that explored the potential for using PEO-PPO-PEO block

copolymer micelles in the treatment of water contaminated with polycyclic aromatic hydrocarbons, it was shown that the solubilization efficiency depended strongly on the molecular structure, composition, and molecular weight of the copolymer used, as well as the solution temperature [Hurter & Hatton, 1992; McFann et al., 1993; Hurter et al., 1993; Hurter et al., 1994]. In an attempt to address this behavior and gain a fundamental understanding of the association and solubilization behavior of amphiphilic block polymer systems, we undertook a detailed theoretical [Hurter et al., 1993] and experimental investigation [Alexandridis et al., 1994] on the micellization and solubilization in aqueous PEO-PPO-PEO block copolymer solutions. A self-consistent mean-field lattice theory for block copolymers has been developed, in which the polymer segments were allowed to assume both polar and non-polar conformations [Hurter et al., 1993]. The theory reproduced qualitatively the effect of copolymer composition and molecular weight on micellization and micelle structure, and their temperature dependence. The CMT (critical micellization temperature, the copolymer solution temperature at which micelles start forming) and CMC values of 12 Pluronic PEO-PPO-PEO block copolymers, covering a wide range of molecular weights (2900 - 14600) and PPO/PEO ratios (0.19 - 1.79), were determined employing a dye solubilization method [Alexandridis et al., 1994]. A closed association model was found to describe adequately the copolymer micellization process for the majority of the Pluronics, and used to obtain the standard free energies (ΔG°), enthalpies (ΔH°), and entropies (ΔS°) of micellization. The thermodynamic parameters were correlated to the copolymer composition and molecular weight [Alexandridis et al., in preparation].

In comparison with conventional, low molecular weight amphiphiles, the micellization of block copolymers is inherently more complex, as it depends strongly on their composition. In practice, a certain CMC or CMT range with some notable uncertainty is detected. A large difference has often been noted between the CMC values determined by different methods because their sensitivity to the quantity of unimers present may vary [Zhou & Chu, 1988]. Furthermore, the values reported in the literature differ substantially; the lack of sufficient temperature control, in conjunction with batch variations, may be responsible for the observed variations [Linse & Malmsten, 1992]. Occasionally, surface tension and dye solubilization experiments have been misinterpreted resulting in inaccurate CMC values being reported [Alexandridis et al., 1994]. The use of DPH solubilization to determine CMT [Alexandridis et al., 1994] proved to be a reliable and reproducible method;

as shown in the ensuing discussion, the CMC and CMT values determined from dye solubilization agree very well with CMC and CMTs obtained from other methods.

The effects of temperature on the micellization properties and the structure of the micelles for two PEO-PPO-PEO triblock copolymers (Pluronic P104 and F108), that have the same hydrophobic (PPO) block and different size hydrophilic (PEO) blocks (the number of EO segments of F108 is 5 times that of P104), are reported in this paper. CMT and CMC data, obtained from a dye solubilization method, are corroborated with differential scanning calorimetry, surface tension, density, light scattering intensity, and fluorescence spectroscopy experiments. The hydrodynamic radii of the copolymer micelles and their size distribution are determined as a function of temperature using dynamic light scattering. The experimentally-determined effect of the PEO block size on the micelle structure is compared to the predictions of a mean-field lattice theory. Finally, the molecular mechanism responsible for the temperature effects is discussed.

5.2 Materials and Methods

Materials: The Pluronic PEO-PPO-PEO block copolymers were obtained from BASF Corp., Parsippany, NJ, and used as received. P104 and F108 have a PPO block of similar molecular weight (on the order of 3000) but P104 has 40 wt % and F108 80 wt % PEO [BASF, 1989]. Information on the copolymer composition is presented in Table 5.1. Aqueous copolymer solutions were prepared by dissolving the polymer in Milli-Q water (18 MΩ·cm) and diluting to the desired concentration. The experiments on the Pluronic solutions were performed within a few days of the solution preparation. 1,6-diphenyl-1,3,5-hexatriene (DPH) (CA # 1720-32-7) was obtained from Molecular Probes Inc., Eugene, OR, and used as received. The solubilization of DPH in micelles was used for the determination of the CMT and CMC values of the copolymer solutions [Alexandridis et al., 1994]. Benzo[def]phenanthrene (pyrene) (CA# 129-00-0) was purchased from Sigma Chemical Co., St. Louis, MO, and was recrystallized three times from ethanol.

Calorimetry: Differential scanning calorimetry measurements were done using a Microcal MC-2 instrument (Microcal Inc., Amherst, MA). The reference cell was filled

with triple-distilled water; both reference and sample cell were under nitrogen pressure during the measurements, to prevent formation of bubbles and/or solvent evaporation at high temperatures. Temperature scans were performed at a rate of 30 K/h. Both increasing- and decreasing-temperature scans were carried out for all samples reported here; no difference between the up-and down-scans was observed.

Surface tension: The Wilhelmy plate method was employed for measuring the surface tension of the copolymer solutions. A Krüss K10T tensiometer (Krüss USA, Charlotte, NC) was used. Temperature control within 0.05 °C was achieved using a Neslab RTE-110 refrigerated bath/circulator. All glassware was washed in a 1N NaOH-ethanol bath, then in a nitric acid bath, and thoroughly rinsed with Milli-Q water before use. The platinum Wilhelmy plate was washed using acetone, rinsed in Milli-Q water, and flamed until red-hot before each measurement [Nikas et al., 1992].

Density: A Calculating Digital Density Meter DMA 45 (Anton Paar, Graz, Austria) was employed to measure the densities for aqueous Pluronic solutions; the density is determined by placing the sample in a U-shaped tube and measuring the period of oscillations of this tube electronically. The instrument was calibrated by measuring the density of water and air (over the temprature range of interest) for which precice density values are available in the literature [Kohlrausch, 1968]. Temperature control was achieved using a Neslab RTE-110 refrigerated bath/circulator.

Light scattering: Intensity and dynamic light scattering measurements were performed at a scattering angle of 90° using a Brookhaven Model BI-200SM instrument (Brookhaven Instrument Corp., Holtsville, NY). The light source was a Lexel 8 mW argon ion laser operating at λ = 514 nm (Lexel Laser, Inc., Fremont, CA). The signal analysis was performed using a BI-9000AT Digital Correlator. The scattering cells were first rinsed with a copolymer solution which was filtered through a 0.2 μm filter to remove dust, and then filled with the rest of the solution. Temperature control was achieved using a Neslab RTE-110 refrigerated bath/circulator.

Spectroscopy: UV-vis absorption spectra of the copolymer/DPH/water samples were recorded in the 300-500 nm range using a Perkin-Elmer Lambda 3B UV/vis spectrophotometer (Perkin-Elmer Corp., Norwalk, CT). The main absorption intensity

peak, characteristic of DPH solubilized in a hydrophobic environment, was at 356 nm [Alexandridis et al., 1994]. Fluorescence spectra were recorded on a SPEX FluoroMax spectrofluorometer (SPEX Industries, Inc., Edison, NJ) using a 0.5 nm bandpass in the "s/r" mode (to correct for variations in lamp intensity). Wavelengths of excitation (λ_{ex}) were chosen according to the maximum intensity obtained in the excitation spectra; depending on the solution, $\lambda_{ex} \approx 335$ nm and $\lambda_{em} \approx 372$ nm (sample PM counts were always smaller than 10^5 counts/sec to ensure linear response of the detector). Step increments and integration times were set at 0.5 nm and 0.6 sec respectively. All samples were aerated, magnetically stirred, temperature controlled using a thermostated cuvette holder connected to a circulating water bath, and examined at right-angle geometry. Each spectrum was obtained by averaging 3 scans, corrected for scatter using an equivalent blank solution. In all cases the I_1/I_3 values were averaged over 4 different experiments. The reproducibility of these results was better than 3% and the standard deviation on the I_1/I_3 values was smaller than 0.03. The pyrene concentration was $3x10^{-7}$ M in all samples; no excimer formation was observed, even in the micellar solutions.

5.3 Results and Discussion

5.3a Micellization phase diagram

UV-vis spectra of aqueous Pluronic P104 and F108 solutions containing DPH were taken at regular temperature intervals over the range 15 - 50 °C. At low concentrations and/or low temperatures, the copolymers did not associate, DPH was not solubilized, and, as a result, the UV-vis absorbance intensity due to DPH was very low. At higher concentrations and/or temperatures the Pluronics formed micelles, and DPH was solubilized in the hydrophobic micelle interior, giving a characteristic spectrum [Alexandridis et al., 1994]. Figure 5.1 shows the temperature dependence of the absorbance intensities at the DPH spectral maximum (356 nm), for various concentrations of P104 and F108 aqueous solutions; the amount of DPH solubilized in the micelles is directly proportional to the UV-vis absorption intensity values. The CMT values were obtained from the first break of the intensity vs temperature sigmoidal curve (or alternatively from the first appearance of a well defined peak in the spectrum) that indicated

the formation of a hydrophobic domain. This domain appears to be the result of aggregation of many Pluronic molecules to form a micelle, rather than the coiling of a single molecule [Alexandridis et al., 1994]. The second break of the intensity vs temperature sigmoidal curve was indicative of the complete solubilization of DPH in the block copolymer micelles. The CMT values obtained for Pluronics P104 and F108 are listed in Table 5.2, and CMCs in Table 5.3. The CMT values for F108 solutions of a given concentration were higher than the ones for P104, intimating that the micelle formation becomes more difficult the more hydrophilic the molecules; however, the effect of PEO on the CMT is less pronounced than that of PPO [Alexandridis et al., 1994]. The CMT data are plotted as a function of copolymer concentration in Figure 5.2 in a form of a micellization "phase diagram" for the copolymer solutions. At temperatures below the micellization boundary, the copolymers exist as individual molecules in solution (unimers); micelles coexist in equilibrium with unimers above the micellization boundary.

5.3b Thermodynamics of micellization

Association model: The standard free energy change for the transfer of 1 mol of amphiphile from solution to the micellar phase (free energy of micellization), ΔG°, assuming an equilibrium between unimer and micelles, is given by [Hunter, 1987; Alexandridis et al., 1994]

$$\Delta G^\circ = R\,T \ln (X_{CMC}) \qquad (1)$$

where R is the gas law constant, T is the absolute temperature, and X_{CMC} is the critical micellization concentration (expressed in mol fraction units) at temperature T. ΔG° is given in terms of the standard enthalpy of micellization, ΔH°, and the standard entropy of micellization per mole of surfactant, ΔS° as [Hunter, 1987]

$$\Delta G^\circ = \Delta H^\circ - T\,\Delta S^\circ \qquad (2)$$

ΔG° values for P104 and F108 solutions, calculated at the CMC at various temperatures, are plotted in Figure 5.3 as a function of temperature. The micellization free energy values, ΔG°, are negative, since thermodynamically stable micelles are formed spontaneously;

furthermore, ΔG°s become more negative at higher temperatures, indicating a larger driving force for micellization. The standard enthalpy of micellization, ΔH°, can be calculated from the intercept of a linear fit of the ΔG° vs T data, in accordance with Equation 2. ΔH°, is positive, indicating that the transfer of unimers from solution to the micelle is an enthalpically-unfavorable endothermic process. Thus, it is clear that a positive entropy contribution must be the driving force for micellization of the block copolymers (aggregation of copolymer molecules will lead to an increase of the solution entropy). The origin of such a behavior is discussed in Section 5.3g. The ΔH° and ΔS° values for both copolymers are shown in Figure 5.3.

Differential Scanning Calorimetry: Another method for obtaining estimates of the enthalpy of micellization, ΔH°, is differential scanning calorimetry (DSC). The heat capacity of P104 aqueous solutions (determined from DSC) is plotted in Figure 5.4 as a function of temperature, for various copolymer concentrations. An endothermic "phase transition" is observed, that can be attributed to micelle formation. Indeed, the arrows in Figure 5.4 indicate that the CMTs determined from DPH solubilization coincide with the onset of the endothermic transition. Endothermic peaks, typical for a first-order phase transition, at concentration-dependent characteristic temperatures have also been observed for Pluronic copolymer solutions by Wanka et al. [1990] and Armstrong et al. [1993]. The peaks have rather high enthalpy values (almost 3 orders of magnitude larger than typical enthalpy values for phase transitions in lyotropic liquid crystals [Wanka et al., 1990]) and are rather broad, extending from 10 to 15 K. The latter has been attributed to the fact that the copolymers are not single compounds but show a broad molar weight distribution [Wanka et al., 1990]. In addition to polydispersity, the broad peak can be also due to a gradual increase in the number (and size) of micelles in solution as temperature increases. The enthalpy of micellization can be obtained from the integral of the DSC peak; the ΔH values for P104 were 370 kJ/mol, independent of concentration. There is a 20 % difference between the DSC enthaply and the ΔH° estimated from the association model. It should be pointed out here that the enthalpy change measured by the peak area in DSC is not the standard enthalpy change but depends upon the real states of the copolymer chains before and after micellization. The standard state enthalpy change is defined for transfer of 1 mol of chains from the ideally dilute solution to the solvated micellar state. In the ideally dilute solution, copolymer segments interact only with solvent, whereas in real solutions

segments also interact with each other, and this may cause discrepancies between micellization enthalpies obtained from DSC and the ones derived from an analysis similar to ours [Deng et al., 1992]. It has also been reported by Hiemenz [1986] that ΔH° values calculated by a micellization thermodynamics model generally show poor agreement with those determined calorimetrically, at least for ionic surfactants.

5.3c Surface activity

Surface tension data for aqueous P104 solutions at the two temperatures, 25 and 35 °C, are presented in Figure 5.5, plotted semilogarithmically with respect to copolymer bulk concentration. At low copolymer concentrations the surface tension decreased with increasing concentration, in accord with the Gibbs' adsorption isotherm [Chattoraj & Birdi, 1984]. A change in slope (break) was observed in the surface tension curve at a characteristic concentration (approximately 10^{-3} %), after which the surface tension values continued to decrease until a plateau was reached (second break); the surface tension values remained approximately constant with further increase of copolymer concentration. At the higher temperature (35 °C) surface tension values were lower (for a given copolymer concentration), and the change of slope corresponding to CMC appeared at lower concentrations, compared to the ones at 25 °C. The presence of two breaks has led to some confusion in the surface tension studies available for Pluronic copolymers regarding the interpretation of the surface tension dependance on concentration, and the extraction of CMC from such a set of data. The low-concentration break has been suggested to originate from rearrangement of the copolymer molecules on the surface at complete coverage of the air/water interface [Alexandridis et al., 1994b]. The breaks at the high-concentration part of the surface tension curve occurred at concentrations that correspond to the critical micellization concentration values as determined by the dye solubilization technique; the arrows in Figure 5.5 indicate the CMC obtained from DPH solubilization.

Areas per molecule at the air/water interface for P104 and F108 were calculated from surface tension data using the simple form of the Gibbs adsorption isotherm [Chattoraj & Birdi, 1984] that relates the surface (excess) concentration of the surfactant, Γ, to the surface tension and the surfactant chemical potential:

$$\Gamma = - (1 / RT) (d \gamma / d \ln C) \qquad (3)$$

where the area per molecule, A, is equal to $(\Gamma N)^{-1}$, γ is the surface tension, N is Avogadro's number, R is the molar gas constant, T is the absolute temperature, and an ideal solution is assumed. In the absence of information on the exact composition of the Pluronic samples, the area per molecule estimated from Equation 3 will be an average area. The bulk concentration range over which area per molecule values were extracted was 10^{-6} to 10^{-3} wt %. The values for surface area per copolymer molecule calculated in this way (presented in Table 5.4) are generally small compared to those of nonionic surfactants with an aliphatic chain and PEO headgroup of comparable size to the PEO block of Pluronics [Kronberg et al., 1984; Mysels, 1986; Nikas et al., 1992], indicating that there is considerable folding of the polymers at the air/water interface [Prasad et al., 1979] and/or desorption of PEO segments to the water phase [Aston et al., 1990; Phipps et al., 1993].

Effect of temperature on surface area: Increasing temperature typically results in expansion (larger surface area per molecule) of monolayers spread at air/water interfaces; this phenomenon originates from stronger thermal agitation resulting in increased repulsion between the hydrophobic chains [Lo Nostro & Gabrielli, 1993]. A decrease in the area per copolymer molecule with increase in temperature was observed for both P104 and F108 (see Table 5.4). This can be attributed to either less PEO hydration water at the higher temperature, or an increase in hydrophobicity of the PPO core, or both. The former would indicate more compact packing of copolymer molecules at higher temperatures, in agreement with light scattering results that show the hydrodynamic radius of Pluronic copolymer micelles to remain roughly constant while the aggregation number of micelles increases with temperature, and with the weakening of hydrogen bonding between PEO and water with increasing temperature [Alexandridis & Hatton, 1994]. The latter would lead to a behavior similar to that discussed by Prasad et al. [1979] and Alexandridis et al. [1994b], where an increase in the size of the PPO block in copolymers having PEO blocks of similar length results in lower surface areas as PEO partly folds around PPO. A decrease in surface area of aliphatic alcohols with increasing temperature has been interpreted by Lo Nostro and Gabrielli [1993] in terms of a squeezing out of water molecules from the coordination shells that surround the polar headgroups of the amphiphile.

5.3d Density

The density of Pluronic P104 and F108 aqueous solutions of varying concentrations was investigated as a function of temperature. The density of bulk F108 is higher than that of bulk P104, and the density of both copolymers is higher than the water density [BASF, 1989]. As shown in Figure 5.6a, the density values decreased with increasing temperature. The rate of this decrease increased with temperature, a fact can be related to the CMT (the arrows shown in Figure 5.6 correspond to the CMT values obtained from DPH solubilization experiments). To probe this effect, the partial specific volume values of the copolymers was calculated from the measured densities.

The partial specific volume, υ, of a solute is a characteristic thermodynamic parameter which defines various intermolecular interactions [Williams et al., 1985; Armstrong et al., 1993]. The experimental quantity at a given concentration, c, is the apparent partial specific volume, $\upsilon(c)$, which can be determined from density measurements according to the following relation [Armstrong et al., 1993]:

$$\upsilon(c) = \rho_{solvent}^{-1} \left[1 - (\rho_{solution} - \rho_{solvent}) / C_{solution} \right] \qquad (4)$$

where the values of ρ and c are expressed in g/ml. Partial specific volume values of P104 and F108 in aqueous solutions are plotted as a function of temperature in Figure 5.6b. The abrupt increase in $\upsilon(c)$ is indicative of a heating-induced "phase transition". This phase transition is related to the formation of micelles (the arrows indicate the CMT values obtained from DPH solubilization experiments). The CMT from such a set of data can be obtained from the intersection of the solid lines shown in Figure 5.6b. The observed phase transition becomes broader and less pronounced with increase in the PEO content of the copolymer (compare P104 to F108). As the data indicate, the copolymer chain becomes less dense (more expanded) during micellization. This could be rationalized if one envisions a randomly coiled unimer being transfered to a micelle with a well-defined hydrophobic core and extended hydrophilic corona.

Armstrong et al. [1993] found the experimentally determined partial specific volume values for Poloxamer solutions below the CMT to agree resonably well with those calculated for orthorhombic perpendicular or monoclinic lattice structures. At temperatures

above the CMT, experimental υ values agreed more closely with those calculated for the theoretical α form of hexagonally packed chains based on alkanols, characteristic of a more expanded form. Densitometric studies conducted in aqueous solutions of low-molecular weight (200 - 1000) PEO showed no indication of a thermal phase transition or conformational change (as quoted in Armstrong et al. [1993]).

5.3e Light scattering investigation

The static light scattering intensity (originating from concentration fluctuations) depends on the scattering angle, the solution refractive index increment and the osmotic compressibility, through the Ornstein-Zernike relation; for sufficiently dilute solutions, the scattering intensity is directly proportional to the weight-average aggregation number of the micelles, $<N_w>$ [Hiemenz, 1986]. A large increase in the intensity of scattered light would, therefore, indicate an increase in $<N_w>$, provided critical fluctuations are not significant. Light scattering intensity for 0.5% P104 and F108 aqueous solutions is plotted in Figure 5.7 as a function or temperature. The abrupt increase in the intensity is indicative of micelle size and/or number growth upon heating past the CMT. The arrows in Figure 5.7 indicate the CMT values obtained from DPH solubilization experiments; there is very good agreement between these CMTs and the onset of increased scattering intensity. The rate of intensity increase with respect to temperature after the CMT is higher for P104 than for F108; this can be due to a larger number of molecules (and micelles) present in solution for the same mass concentration.

The exponential decay of the correlation of the intensity fluctuations, originating from the Brownian motion of the micelles, is measured during a dynamic light scattering experiment. The correlation decay depends on the diffusivity of the micelles according to the equation $\Gamma=Dq^2$, where Γ is the relaxation or correlation time, D is the effective translational diffusion coefficient, and q is the scattering vector. Figure 5.8a shows the temperature dependence of the translational diffusion coefficient of P104 and F108 micelles, as determined from dynamic light scattering measurements. The micelle diffusion coefficients were in the range 2.5×10^{-7} - 5.5×10^{-7} cm^2/s, and depended on temperature and copolymer type and concentration. The "effective" hydrodynamic radius of the micelles, R_h, is obtained from D through the Stokes-Einstein equation, $R_h = kT/(6\pi\eta D)$, where k is the Boltzmann constant, T is the absolute temperature, and η is the solvent viscosity

[Hiemenz, 1986]. It is interesting that, when the temperature and viscosity are input in the Stokes-Einstein equation, the calculated hydrodynamic radii (R_h) of the copolymer micelles were found to be independent of temperature as seen in Figure 5.8b (note that the R_h value for 2.5% P104 at 25 °C is higher than R_h at higher temperatures, probably due to the relatively high polydispersity observed at 25 °C - see Figure 5.10a and discussion in the next paragraph). R_h was approximately 8 and 11 nm, for P104 and F108 micelles, respectively (Figure 5.8b).

The constant value of the hydrodynamic radii with respect to temperature does not imply that the micelle aggregation number or "molecular" weight are independent of temperature. Indeed, Zhou and Chu [1988] found the F68 micellar weights (determined from static light scattering) to increase linearly with increasing temperature, while the hydrodynamic radius of the micelles remained nearly constant. Such a dual effect of temperature was interpreted in terms of enhanced dehydration of EO segments with increasing temperature [Zhou & Chu, 1988]; dehydration of EO segments with temperature can also be inferred from the area-per-molecule values obtained from surface tension (see Table 5.4). The intensity measured in static light scattering is a measure of the refractive index difference between the dispersed particle and the surrounding medium, thus providing useful information concerning the compound (other than water) dispersed. On the other hand, the Brownian motion of "hydrated" dispersed particles that is monitored in the dynamic light scattering experiments results in size information on the solvated micelles. A decrease in micelle size with increase in copolymer concentration was observed for both P104 and F108 (the polymer concentrations checked were 0.5 and 2.5%). This may be a result of more hydration water available at the low polymer concentration; in a 25 g/L (2.5%) F108 micellar solution, approximately 125 g/L (12.5%) of water are hydrating the EO segments (assuming 15 water molecules per EO segment [Pandya et al., 1993]).

The experimentally determined effect of the PEO block size on the micelle structure can be compared to the predictions of the mean-field lattice theory of Hurter et al. [1993b]. Figure 5.9a shows the density profiles for EO and PO segments in P104 and F108 micelles, predicted by the model of Hurter et al. [1993b]. An increase in the PEO block size resulted in a decrease in the predicted micelle core, while the corona became more extended. The experimentally determined hydrodynamic radius increased 35% from P104 to F108, while the predicted value increased by 15%. The difference in size between the

micelles formed by the two copolymers was reflected in a smaller aggregation number for the F108 micelles (compared to the P104 micelles) as shown in Figure 5.9b and Table 5.5. For comparison purposes, we estimated the micelle aggregation number from the experimentally determined hydrodynamic radii, using density values for EO and PO segments equal to those of the bulk homopolymers, and assuming a number of water molecules hydrating the corona of the micelles. The aggregation number values (1), (2), and (3) (reported in Table 5.5) were calculated assuming, respectively, 14, 11, and 7 water molecules hydrating each EO segment (these hydration values were reported by Pandya et al. [1993] for L64 micelles at 30, 35, and 40 °C, respectively). The agreement between the predicted and experimental aggregation numbers is good for P104, and could be improved for F108, were the hydration numbers for the F108 PEO chains larger than the ones used here to obtain the aggregation number estimate (a larger hydration number for F108 compared to P104 is reasonable since the F108 EO segments extend further in the solution).

Brown et al. [1992] and Mortensen and Brown [1993] published studies comparing P85, F87, and F88 copolymers that have the same PPO block (M_w = 2300) and 50, 70, and 80 % PEO, respectively. The micellar core radius, R_c appeared to be essentially independent of polymer concentration but showed a significant increase with temperature. A double logarithmic plot of R_c vs $T - T_{CMT}$, gave the empirical scaling relation $R_c \sim (T - T_{CMT})^{0.2}$ [Mortensen & Brown, 1993]. Close to T_{CMT} the aggregation number, N, is very small and increases continuously following the $N \sim (T - T_{CMT})^{0.6}$ relationship to approximately N ~ 200 at the highest temperature, where spherical micellar aggregates are present. From the hard-sphere data analysis of Mortensen and Brown [1993], it appeared that the main difference between P85, P87, and F88 micelles at a given temperature is the size of the micelles; the larger the PEO block, the smaller the core and the aggregation number. These observations compare favorably with the PEO effect on aggregation number and micelle core size for Pluronic copolymers of the P103, P104, P105, F108 series, predicted by the model of Hurter et al. [1993b] (Figure 5.9b).

The scattering intensity fluctuation correlation can also be used to obtain information on the micelle size distribution, by using a fitting procedure. The parameter of interest in this case is the polydispersity, defined as the variance of the z-average diffusion coefficent distribution divided by the square of the average:

$$\text{polydispersity} = (\langle D_z^2 \rangle - \langle D_z \rangle^2) / \langle D_z \rangle^2 \quad (5)$$

The square root of polydispersity is, thus, the relative standard deviation of the intensity-weighted diffusion coefficient distribution. Figure 5.10a shows the micelle polydispersity as a function of temperature for 2.5% P104 and F108 copolymer solutions (the polydispersity values reported here were obtained form the second cumulant [Brown et al., 1975] fitted to the correlation function). The polydispersity of the micelles decreased with increasing temperature and appeared to depend on $T - T_{CMT}$. F108 micelles exhibited larger polydispersity than P104 micelles; the latter were essentialy monodisperse at temperatures higher than 35 °C (according to Brookhaven Instruments Corp. [1992], a sample is essentially monodisperce when the polydispersity value is smaller than 0.02). Apparently the hydrated PEO segments enhance polydispersity as can be inferred from a comparison of P104 and F108 at the same temperature and the effect of temperature for a given copolymer. The size distributions (calculated through the Exponential Sampling fitting routine [Brookhaven Instruments Corp., 1992]) for P104 micelles at various temperatures and F108 micelles at 45 °C are presented in Figure 5.10b. The distribution can be seen to narrow with increasing temperature for P104 micelles. Note that dynamic light scattering measurements yield intensity-weighted quantities, and not the more commonly used number- or volume-weighted ones. In this respect, it would be more instructive to compare the various distributions (estimated through the same fitting procedure), rather than draw solid conclusions regarding the absolute numbers of a given size distribution.

5.3f Fluorescence spectroscopy

Pyrene is a well-characterized spectroscopic probe, sensitive to the polarity of the medium in which it is disolved [Thomas, 1984; Winnik et al., 1990]. Pyrene exhibits a characteristic fluorescence emission spectrum, consisting mainly of five bands that are referred to as, I_1, I_2, ..., I_5 (from shorter to longer wavelengths). The I_1/I_3 intensity ratio of this vibrational fine structure, often referred to as the "Py scale" [Dong & Winnik, 1984], depends strongly on the polarity of the medium: the larger the ratio, the more polar the medium. Electronically excited pyrene is a reporter of the average micropolarity of the environment it visits during its lifetime (ca. 300 ns); in this sense, the probe is attractive for

studying restricted microenvironments such as micellar systems [Thomas, 1984; Ananthapadmanabhan et al., 1985]. The I_1/I_3 ratios of the pyrene fluorescence emission intensity for 0.5% aqueous P104 and F108 solutions are presented in Figure 5.11 (open symbols) as a function of temperature. Also shown in the same graph are DPH solubilization data for the same copolymer solutions (filled symbols). A sharp decrease in I_1/I_3 is observed for the Pluronic copolymer solutions at characteristic temperatures, different for each polymer, followed by a less dramatic linear decrease as temperature increases further. The sharp decrease has been attributed to the formation of micelles composed of a hydrophobic core into which pyrene partitions preferentially [Thomas, 1984; Ananthapadmanabhan et al., 1985]. The temperature dependence of the I_1/I_3 intensity ratio can be used for the determination of the CMT, as has been done using the I_1/I_3 vs. concentration plots for the determination of the CMC [Thomas, 1984; Ananthapadmanabhan et al., 1985]. Judging from the DPH solubilization data (and also from the DSC data of Figure 5.4), CMTs should be determined from the mid-point (inflection) of the I_1/I_3 decrease region. Note, that the I_1/I_3 ratio started decreasing at temperatures where there was no detectable dye solubilization; this may reflect the higher sensitivity of the fluorescence technique (in detecting a few micelles) or it can be due to pyrene associating with premicellar aggregates.

5.3g Molecular mechanism of the temperature effect on PEO-PPO-PPO aqueous solutions

As discussed in Section 5.3b, the enthaply of micellization is positive for Pluronics in aqueous solutions; the unfavorable enthalpy component is significant but is, nevertheless, overcome by an even stronger entropy effect. The traditional view of micelle formation [Hiemenz, 1986; Hunter, 1987] is based on the "hydrophobic effect" [Tanford, 1980; Ben-Naim, 1980]. The presence of hydrocarbon molecules in water causes a significant decrease in the water entropy, suggesting an increase in the degree of structuring of the water molecules. When hydrocarbon residues aggregate in aqueous solution to form a micelle, the hydrogen bonding structure in the water is restored and the water entropy increases, overcoming the entropy loss due to the localization of the hydrophobic chains in the micelles. The entropy contribution usually dominates the micellization process in aqueous surfactant solutions, with the enthalpy playing a minor role [Hunter, 1987]. The magnitude of the hydrophobic effect increases with temperature [Ben-Naim, 1980], in

agreement with the observed increased tendency of micelle formation with increasing temperature. However such an explanation does not take into account the nature of the copolymer.

Other interpretations of the "molecular-level" mechanism behind the temperature dependence of PEO-PPO-PEO micellization are based on either solute-solvent [Kjelander & Florin, 1981; Goldstein, 1984], or solute-solute interactions [Karlstrom, 1985] (note, that the hydrophobic effect outlined above is based on solvent-solvent interactions). Kjelander and Florin [1981] attempted to reproduce the negative entropy and enthalpy of water-PEO mixing and the phase diagram of the PEO-water system assuming a zone with increased structuring of water to exist around the PEO chain. The phase separation that takes place at high temperatures was attributed to a breakdown of the zones of enhanced water structure. Kjelander and Florin [1981] claim that when PPO is introduced into water it also develops a hydration shell with an enhanced structure of water, but since the methyl groups of PPO constitute a steric hinderance, the water structure is weak and leads to phase separation. Karlstrom [1985] predicted the phase diagram of PEO-water using the Flory-Huggins theory and assuming that each segment of the PEO chain can exist in two forms, one being polar with a low energy and a low statistical weight, and one being less polar, or nonpolar, having a higher energy and statistical weight. The polar conformations dominate at low temperatures making the solute-solvent interaction favorable, whereas at higher temperature, the nonpolar class of states becomes increasingly populated, rendering the solute-solvent interaction less favorable [Lindman et al., 1990].

The model for predicting the solution behavior of block copolymer micelles, developed by Hurter at al. [1993a] and Linse [1993], incorporates Karlstrom's ideas to account for the conformational distribution in PEO and PPO, thus allowing the investigation of temperature effects on the aggregation behavior of these copolymers. An increase in temperature caused the model-predicted micelle aggregation number to increase, and the CMC to decrease [Hurter at al., 1993a]. The conformation of the polymer was affected by both the temperature and the composition of the surrounding solution; both PEO and PPO had a lower fraction of polar segments in the core of the micelles, and the polar fraction decreased with an increase in temperature. The model predictions of Hurter et al. and Linse agree with the trends observed experimentally (i.e., temperature effects on copolymer surface area and micropolarity), thus supporting the polar-nonpolar state model

as an explanation of the temperature effect on the solution behavior of PEO and PPO.

5.4 Conclusions

We have investigated the effects of temperature on the micellization behavior and structure of micelles for two poly(ethylene oxide)-*block*-poly(propylene oxide)-*block*-poly(ethylene oxide) copolymers, Pluronic P104 and F108, using an array of techniques. Solubilization of a hydrophobic dye (DPH) was used to determine critical micellization concentration and temperature data for aqueous copolymer solutions, and thus define the micellization phase diagram for P104 and F108. The copolymer concentrations needed to form micelles decreased with increasing solution temperature; for a given mass concentration, F108 formed micelles at higher temperatures than P104 (Figure 5.2). A positive (endothermic) enthalpy of micellization (on the order of 300 kJ/mol) was estimated using a copolymer association model and DSC. CMCs and CMTs obtained from dye solubilization were compared to those estimated from differential scanning calorimetry, surface tension, density, static light scattering intensity, and fluorescence spectroscopy measurements. Best agreement between the different techniques is achieved when the critical micellization data are estimated from (i) the onset of solubilization of a hydrophobic dye (Figure 5.1), (ii) the onset of the endothermic transition observed in DSC (Figure 5.4), (iii) the second break in the surface tension vs. concentration curve (Figure 5.5), (iv) the first break in the partial specific volume vs. temperature curve (Figure 5.6b), (v) the onset of increased light scattering intensity (Figure 5.7), and (vi) the inflection in the pyrene fluorescence intensity I_1/I_3 ratio (Figure 5.11). These guidelines should facilitate the reporting of consistent CMC and CMT data for amphiphilic copolymer solutions.

Structural information on P104 and F108 was obtained through surface tension, density, and dynamic light scattering exeriments. The area-per-molecule values for copolymers adsorbed at the air/water interface (estimated from surface tension measurements) were relatively low, indicating extension of the EO segments in the aqueous subphase and/or coiling around the PO segments. The area values obtained at 35 °C were lower than those at 25 °C (Table 5.4) intimating a decrease in hydration of the EO segments and/or increase in the hydrophobicity of the PO segments, in accord with light scattering and fluorescence findings. The temperature dependence of the partial specific volume of

the copolymers exhibited a "phase-transition" behavior at the CMT (Figure 5.6b), showing the molecules to become more extended as they enter the micelles. The hydrodynamic radii (R_h) of the copolymer micelles (determined using dynamic light scattering) were found to be independent of temperature; R_h was approximately 8 and 11 nm, for P104 and F108 micelles, respectively (Figure 5.8b). The polydispersity of the micelles decreased with increasing temperature and depended on $T - T_{CMT}$. F108 micelles exhibited larger polydispersity than P104 micelles; the latter were esentialy monodisperse at temperatures higher than 35 °C. A decrease in micelle size with increase in copolymer concentration was observed for both P104 and F108. The experimentally determined effect of the PEO block size on the micelle structure was in agreement with the predictions of a mean-field lattice theory (Figure 5.9).

5.5 Reference cited in Chapter 5

1. Alexandridis, P.; Hatton, T. A. *Colloids Surfaces A*, **1994**, submitted for publication; Chapter 1 of this Thesis.
2. Alexandridis, P.; Holzwarth, J. F.; Hatton, T. A. *Macromolecules* **1994**, *27*, 2414; Chapter 2 of this Thesis.
3. Alexandridis, P.; Nivaggioli, T.; Holzwarth, J. F.; Hatton, T. A. *Polym. Prepr. (Am. Chem. Soc., Div. Polym. Chem.)* **1994**, *35(1)*, 604.
4. Alexandridis, P.; Athanassiou, V.; Fukuda, S.; Hatton, T. A. *Langmuir* **1994b**, in press; Chapter 4 of this Thesis.
5. Almgren, M.; Bahadur, P.; Jansson, M.; Li, P.; Brown, W.; Bahadur, A. *J. Colloid Interface Sci.* **1992**, *151*, 157.
6. Al-Saden, A. A.; Whateley, T. L.; Florence, A. T. *J. Colloid Interface Sci.* **1982**, *90*, 303.
7. Ananthapadmanabhan, K. P.; Goddard, E. D.; Turro, N. J.; Kuo, P. L. *Langmuir* **1985**, *1*, 352.
8. Armstrong, J.K.; Parsonage, J.; Chowdhry, B.; Leharne, S.; Mitchell, J.; Beezer, A.; Lohner, K.; Laggner, P. *J. Phys. Chem.* **1993**, *97*, 3904.
9. Aston, M. S.; Herrington, T. M.; Tadros, T. F. *Colloids Surfaces* **1990**, *51*, 115.
10. Ben-Naim, A. *Hydrophobic Interactions*, Plenum Press, New York, NY, 1980.
11. Brown, J. C.; Pusey, P. N.; Dietz, R. *J. Chem. Phys.* **1975**, *62*, 1136.

12. Brown, W.; Schillen, K.; Almgren, M.; Hvidt, S.; Bahadur, P. *J. Phys. Chem.* **1991**, *95*, 1850.
13. Brown, W.; Schillen, K.; Hvidt, S. *J. Phys. Chem.* **1992**, *96*, 6038.
14. Chattoraj, D. K.; Birdi, K. S. *Adsorption and the Gibbs Surface Excess*, Plenum Press, New York, 1984.
15. Deng, Y.; Yu, G. R.; Price, C.; Booth, C. *J. Chem. Soc., Faraday Trans.* **1992**, *88*, 1441.
16. Dong, D. C.; Winnik, M. A. *Can. J. Chem.* **1984**, *62*, 2560.
17. Goldstein, R. E. *J. Chem. Phys.* **1984**, *80*, 5340.
18. Hiemenz, P. C. *Principles of Colloid and Surface Chemistry*, 2nd ed.; Marcel Dekker, Inc.: New York, 1986.
19. Hunter, R. J. *Foundations of Colloid Science*; Oxford University Press: New York, 1987; Vol. 1.
20. Hurter, P. N.; Hatton, T. A. *Langmuir* **1992**, *8*, 1291.
21. Hurter, P. N.; Anger, L. A.; Vojdovich, L. J., Kelley, C. A.; Cohen, R. E.; Hatton, T. A. in *Solvent Extraction in the Process Industries*; Logsdail, D. H., Slater, M. J., Eds., Elsevier Applied Science: London, 1993, Vol. 3, p 1663.
22. Hurter, P. N.; Alexandridis, P.; Hatton, T. A. in *Solubilization*, Christian, S. D.; Scamehorn, J. F., Eds., Marcel Dekker, 1994, in press; Chapter 7 of this Thesis.
23. Hurter, P. N.; Scheutjens, J. M. H. M.; Hatton, T. A. *Macromolecules* **1993a**, *26*, 5030.
24. Hurter, P. N.; Scheutjens, J. M. H. M.; Hatton, T. A. *Macromolecules* **1993b**, *26*, 5592.
25. Karlstrom, G. *J. Phys. Chem.* **1985**, *89*, 4962.
26. Kjelander, R.; Florin, E. *J. Chem. Soc., Faraday Trans. 1* **1981**, *77*, 2053.
27. Kohlrausch, J. *Praktische Physik*, Vol. 3, 22nd Edition, B. G. Treubner, Stuttgart, F.R.G., 1968.
28. Kronberg, B.; Stenius, P.; Thorssell, Y. *Colloids Surfaces* **1984**, *12*, 113.
29. Lindman, B.; Carlsson, A.; Karlstrom, G.; Malmsten, M. *Adv. Colloid Interface Sci.* **1990**, *32*, 183.
30. Linse, P.; Malmsten, M. *Macromolecules* **1992**, *25*, 5434.
31. Linse, P. *Macromolecules* **1993**, *26*, 4437.
32. Linse, P. *J. Phys. Chem.* **1993**, *97*, 13896.
33. Lo Nostro, P.; Gabrielli, G. *Langmuir* **1993**, *9*, 3132.

34. Malmsten, M.; Lindman, B. *Macromolecules* **1992**, *25*, 5440.
35. McFann, G. J.; Johnston, K. P.; Hurter, P. N.; Hatton, T. A. *Ind. Eng. Chem. Res.* **1993**, *32*, 2336.
36. Mortensen, K. *Europhys. Lett.* **1992**, *19*, 599.
37. Mortensen, K.; Brown, W. *Macromolecules* **1993**, *26*, 4128.
38. Mortensen, K.; Pedersen, J. S. *Macromolecules* **1993**, *26*, 805.
39 Mysels, K. J. *Langmuir* **1986**, *2*, 423.
40. Nikas, Y. J., Puvvada, S.; Blankschtein, D. *Langmuir* **1992**, *8*, 2680.
41. Pandya, K.; Bahadur, P.; Nagar, T. N.; Bahadur, A. *Colloids Surfaces A* **1993**, *70*, 219.
42. Phipps, J. S.; Richardson, R. M.; Cosgrove, T.; Eaglesham, A. *Langmuir* **1993**, *9*, 3530.
43. Prasad, K. N.; Luong, T. T.; Florence, A. T.; Paris, J.; Vaution, C.; Seiller, M.; Puisieux, F. *J. Colloid Interface Sci.* **1979**, *69*, 225.
44. Reddy, N. K.; Fordham, P. J.; Attwood, D.; Booth C. *J. Chem. Soc., Faraday Trans.* **1991**, *86*, 1569.
45. Tanford, C. *The Hydrophobic Effect: Formation of Micelles and Biological Membranes*, 2nd ed.; J. Wiley & Sons: New York, 1980.
46. Thomas, J. K. *The Chemistry of Excitation at Interfaces.* ACS Monograph 181. Caserio, M. C., Ser. Ed., Washington, 1984, Chapter 5.
47. Wanka, G.; Hoffmann, H.; Ulbricht, W. *Colloid Polym. Sci.* **1990**, *266*, 101.
48. Williams, R. K.; Simard, M. A.; Jolicoeur, C. *J. Phys. Chem.* **1985**, *89*, 178.
49. Winnik, M. A.; Pekcan, O.; Croucher, M. D. in *Scientific Methods for the Study of Polymer Colloids and their Applications*. Candau, F., Ottewill, R. H., Eds., Kluwer Academic Publishers, 1990. Pages 225-245.
50. Zhou, Z.; Chu, B. *J. Colloid Interface Sci.* **1988**, *126*, 171.
51. *Pluronic and Tetronic Surfactants.* Technical Brochure, BASF Corp., Parcippany, NJ, 1989.
52. *Instruction Manual*, Brookhaven Instruments Corp., Holtsville, NY, 1992.

Chapter 5: List of Tables

Chapter 5: List of Figures

Figure 5.7 Light scattering intensity for P104 and F108 aqueous solutions (0.5% concentration), plotted as a function or temperature. The abrupt increase in the intensity is indicative of micelle growth. The arrows indicate the CMT values obtained from DPH solubilization experiments.

Figure 5.8 (a) Temperature dependence of the translational diffusion coefficient of P104 and F108 micelles, as determined from dynamic light scattering measurements.
(b) Micelle hydrodynamic radius as a function of temperature.

Figure 5.9 (a) Segment density profiles for EO (solid line), PO (broken line) and water (dotted line) in P104 and F108 micelles, predicted by the model of Hurter et al. [1993b]. One lattice site corresponds to approximatelly 0.4 nm.
(b) Effect of PEO content on aggregation number and core and total micelle size for Pluronic copolymers of the P103, P104, P105, F108 series, predicted by the model of Hurter et al. [1993b].

Figure 5.10 (a) Micelle polydispersity (see text for definition) as a function of temperature.
(b) Micelle size distribution for various temperatures.

Figure 5.11 Temperature dependence of the ratio of vibronic band intensities, I_1/I_3, of pyrene (0.3 mM) in P104 and F108 aqueous solutions (open symbols). Also shown in the same graph are the DPH intensity data for the same copolymer solutions (filled symbols).

Table 5.1 Composition of P104 and F108 Pluronic copolymers.

Polymer	Mol.Weight	PPO/ PEO	PPO segm. weight	PO units	EO units	Lot number
P104	5900	1.15	3540	61	2x27	WPAN-503B
F108	14600	0.19	2920	50	2x132	WPDN-564B

Table 5.2 Critical micellization temperatures for Pluronic P104 and F108 copolymer aqueous solutions as a function of copolymer concentration.

Concentration (% w/v)	P104 mM	P104 CMT	F108 mM	F108 CMT
0.01	0.017	33.5		-
0.025	0.042	31	0.017	40.5
0.05	0.085	29.5	0.034	38
0.1	0.169	27.5	0.068	36
0.25	0.424	25.5	0.171	33.5
0.5	0.847	23.5	0.342	31.5
1.0	1.69	21.5	0.685	29.5
2.5	4.24	19.5	1.71	27
5.0	8.47	18	3.42	24.5
10		-	6.85	21

Table 5.3 Critical micellization concentrations for Pluronic copolymer aqueous solutions, as a function of solution temperature.

Temperature (°C)	P104 % w/v	P104 mM	F108 % w/v	F108 mM
20	2	3.389	-	
25	0.3	0.508	4.5	3.082
30	0.04	0.067	0.8	0.547
35	0.008	0.013	0.15	0.103
40	0.002	0.003	0.04	0.027
45	-		0.008	0.005

Table 5.4 Surface tension for 0.1% Pluronic P104 and F108 copolymer solutions and area-per-molecule values at 25 and 35 °C.

Polymer	γ (mN/m)		Area per molecule (nm^2)	
	25 °C	35 °C	25 °C	35 °C
P104	35.2	33.6	0.77	0.67
F108	42.2	38.0	1.52	1.35

Table 5.5 Comparison of experimentally determined micelle size and aggregation number to the model predictions of Hurter et al. [1993b].

	Experiment		Model prediction	
	P104	F108	P104	F108
micelle radius	7.7 nm	10.4 nm	6 nm	7 nm
aggregation number	60 (1) 70 (2) 92 (3)	35 (1) 43 (2) 61 (3)	78	20

Aggregation number values (1), (2), and (3) were calculated from the micelle hydrodynamic radius, assuming, respectively, 14, 11, and 7 water molecules hydrating each EO segment. See text for discussion.

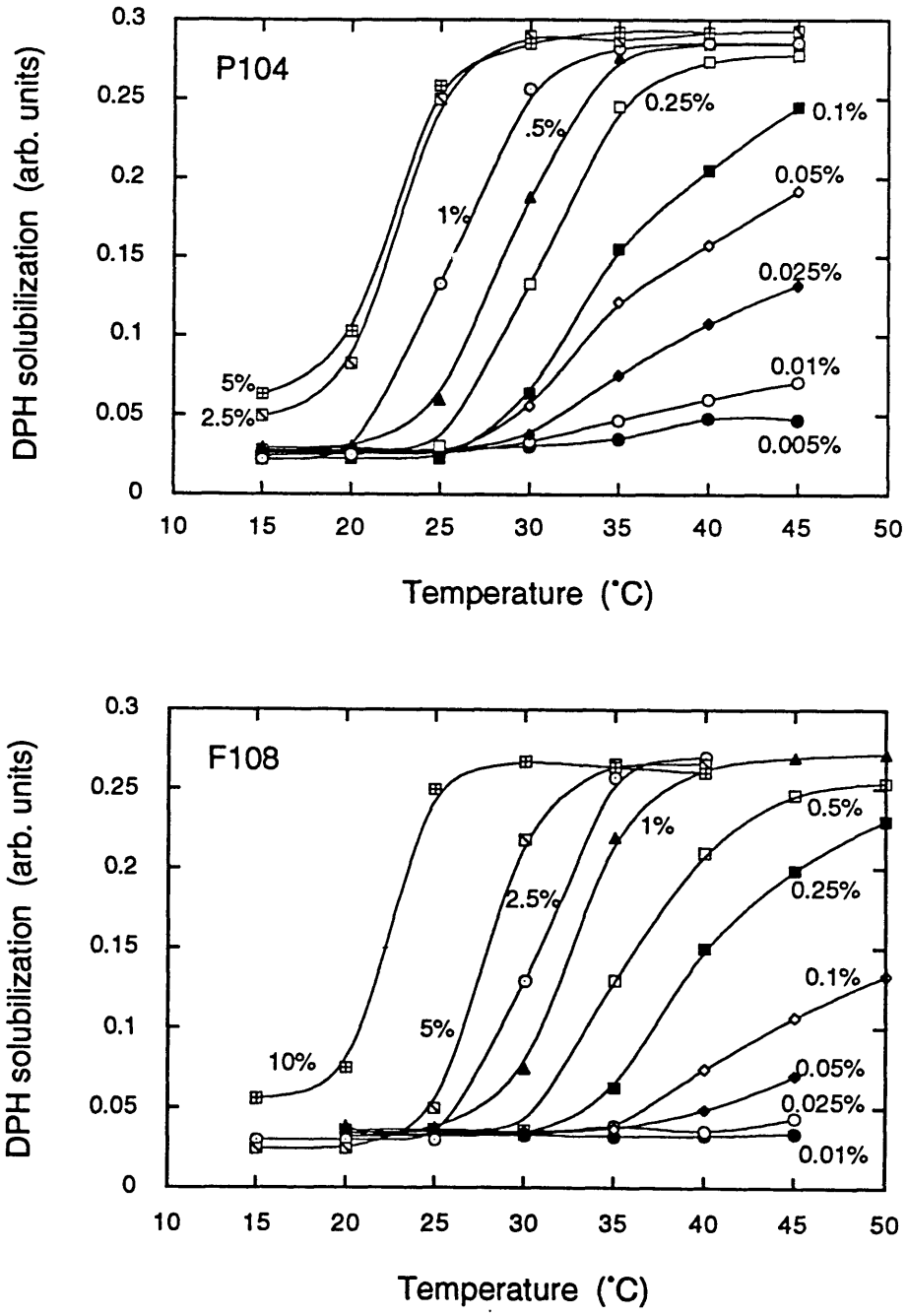

Figure 5.1 Temperature effects on the solubilization of DPH in aqueous solutions of (a) Pluronic P104, and (b) Pluronic F108 of various concentrations. The critical micellization temperatures can be estimated from the first break in the curves.

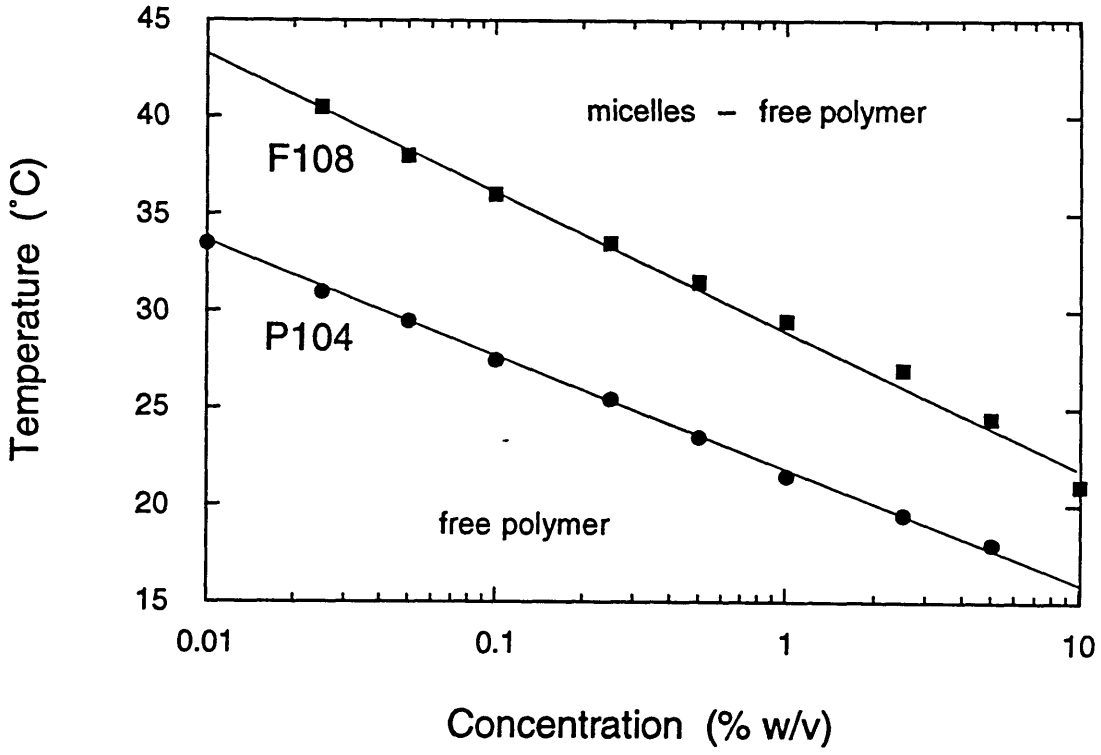

Figure 5.2 Micellization boundary for P104 and F108 copolymer aqueous solutions. At temperatures below the micellization boundary, the copolymers do not associate; micelles coexist in equilibrium with unimers above the micellization boundary.

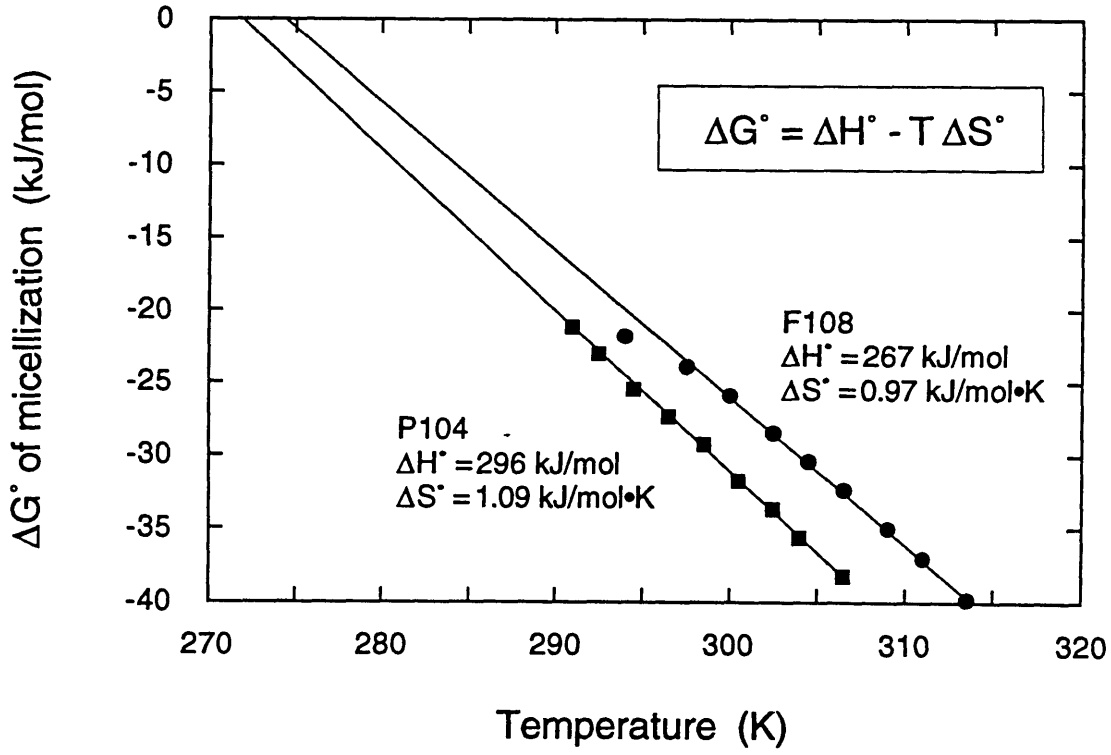

Figure 5.3 Micellization free energy, ΔG°, plotted as a function of temperature, for P104 and F108 copolymer solutions.

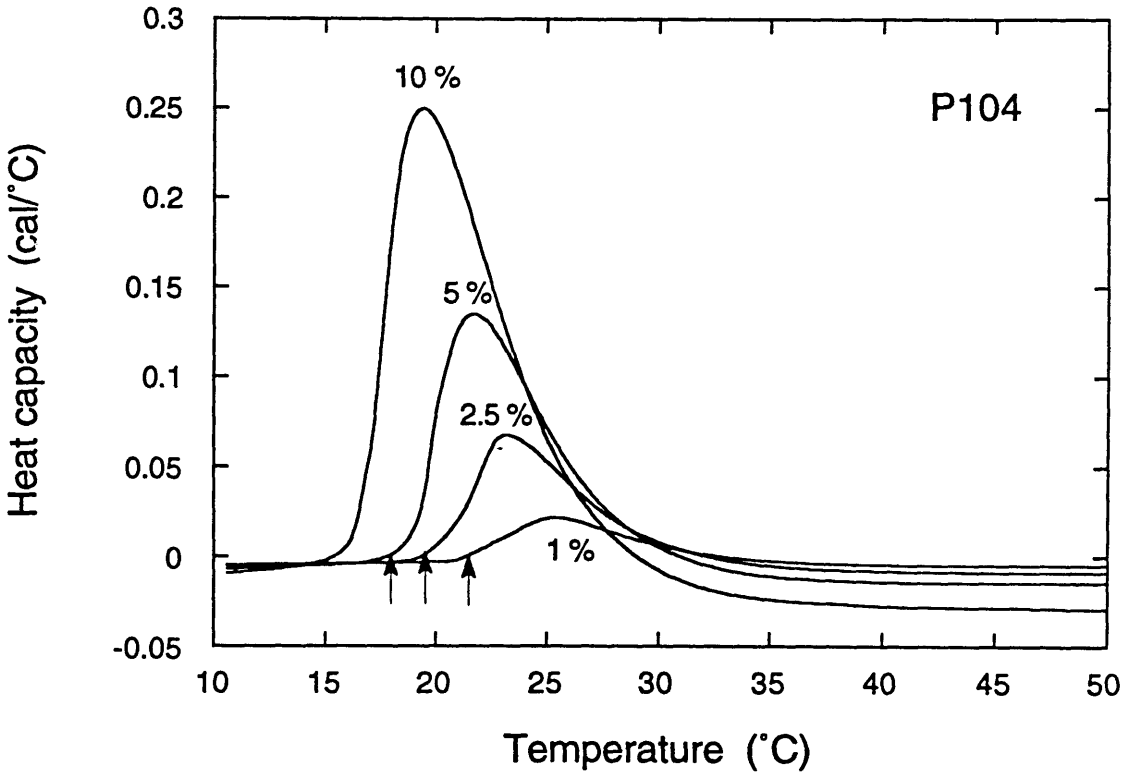

Figure 5.4 Heat capacity of P104 aqueous solutions (determined from DSC) showing the endothermic "phase transition" attributed to micelle formation. The arrows indicate the CMT values obtained from DPH solubilization experiments.

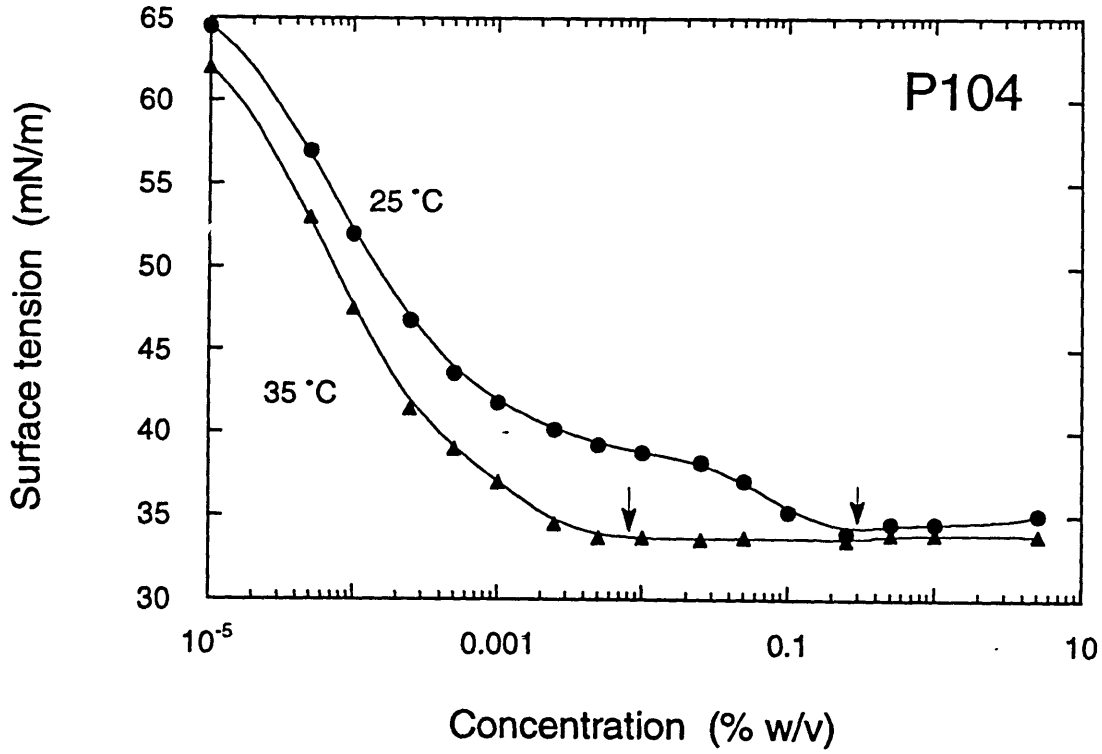

Figure 5.5 Surface tension data for aqueous P104 solutions, plotted semilogarithmically with respect to copolymer bulk concentration at the two temperatures, 25 and 35 °C. The arrows indicate the CMC values obtained from DPH solubilization experiments.

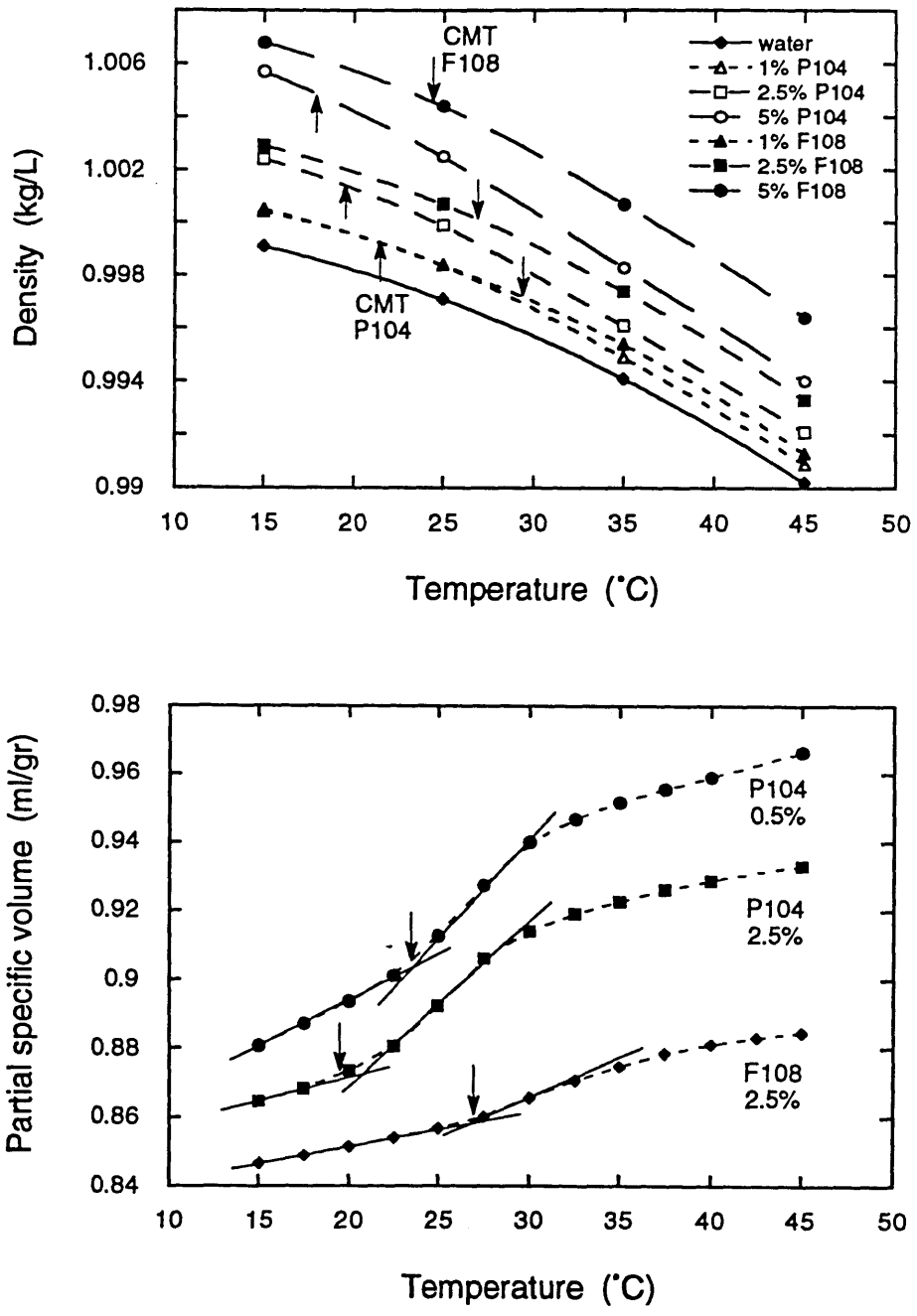

Figure 5.6 (a) Density of P104 and F108 aqueous solutions, plotted as a function of temperature. The arrows indicate the CMT values obtained from DPH solubilization experiments.
(b) Partial specific volume values of P104 and F108 in aqueous solutions, plotted as a function of temperature. The CMT can be obtained from the intersection of the solid lines drawn in the graph. The arrows indicate the CMT values obtained from DPH solubilization experiments.

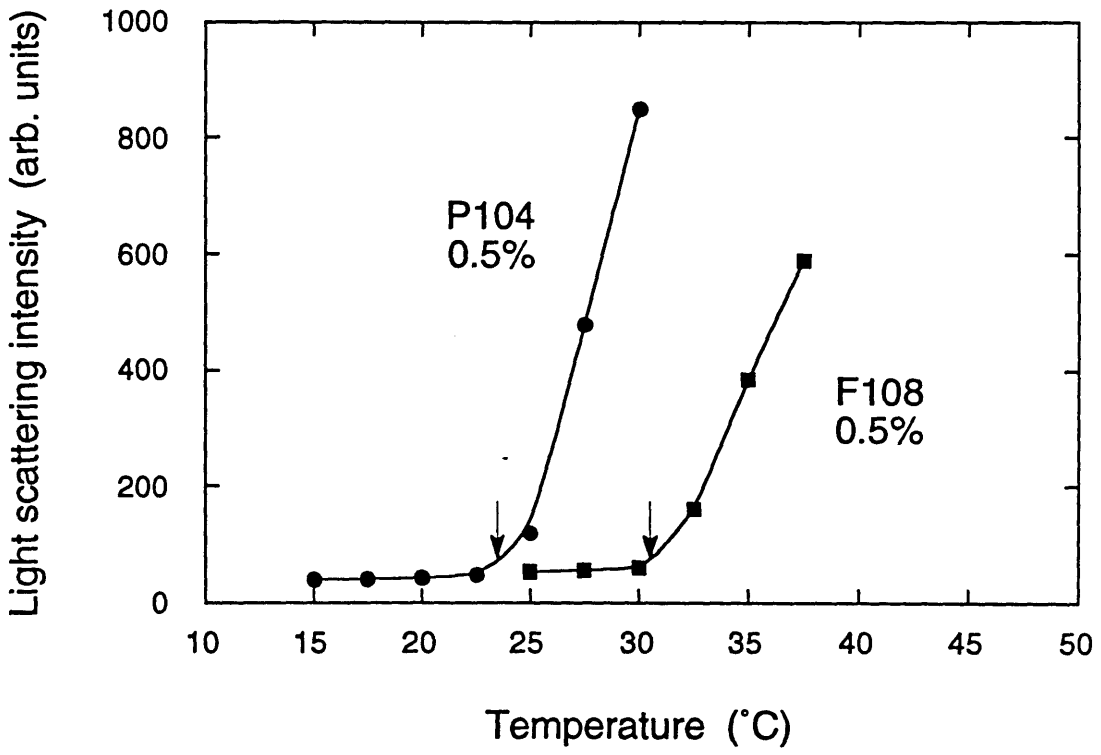

Figure 5.7 Light scattering intensity for P104 and F108 aqueous solutions (0.5% concentration), plotted as a function or temperature. The abrupt increase in the intensity is indicative of micelle growth. The arrows indicate the CMT values obtained from DPH solubilization experiments.

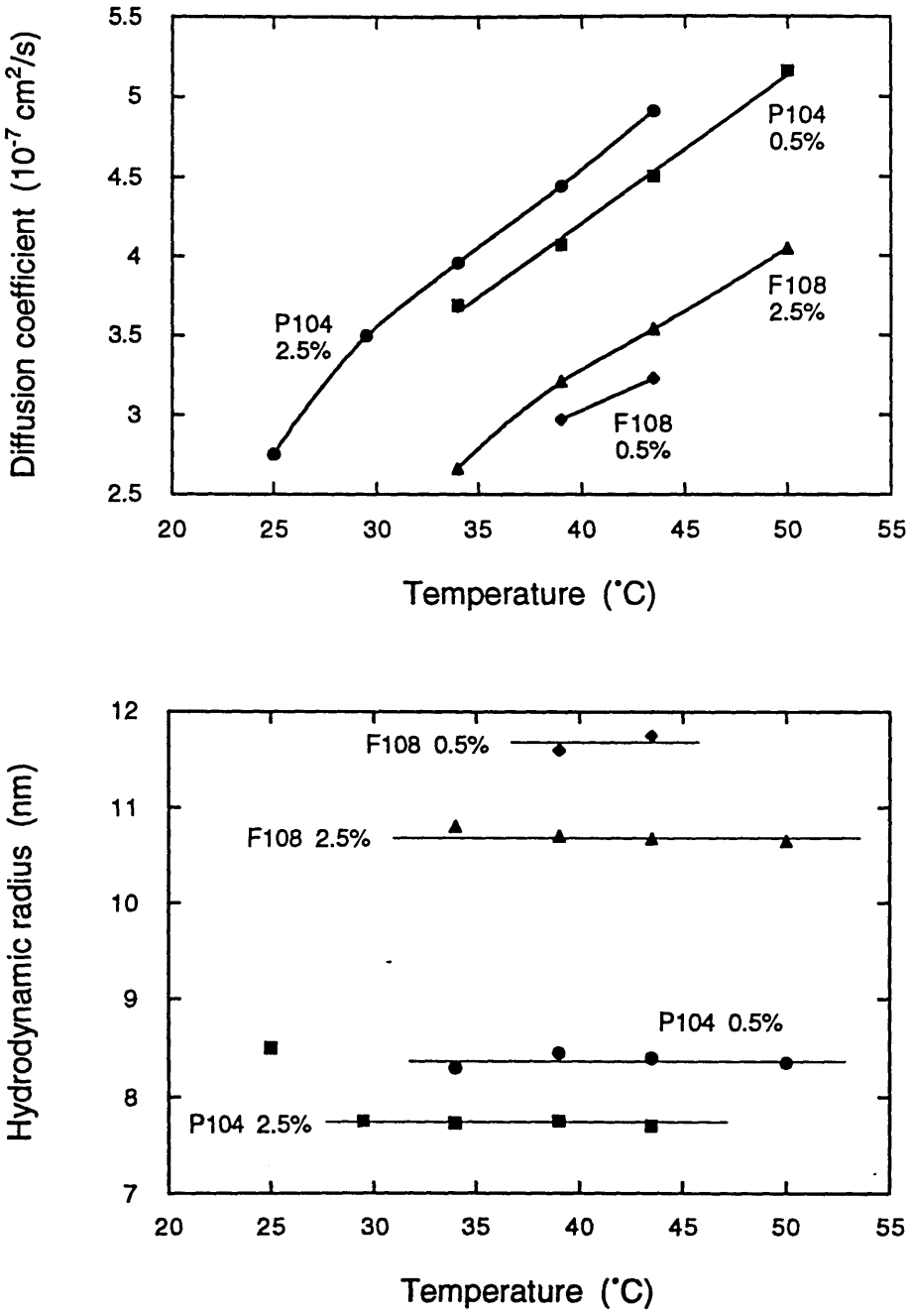

Figure 5.8 (a) Temperature dependence of the translational diffusion coefficient of P104 and F108 micelles, as determined from dynamic light scattering measurements.
(b) Micelle hydrodynamic radius as a function of temperature.

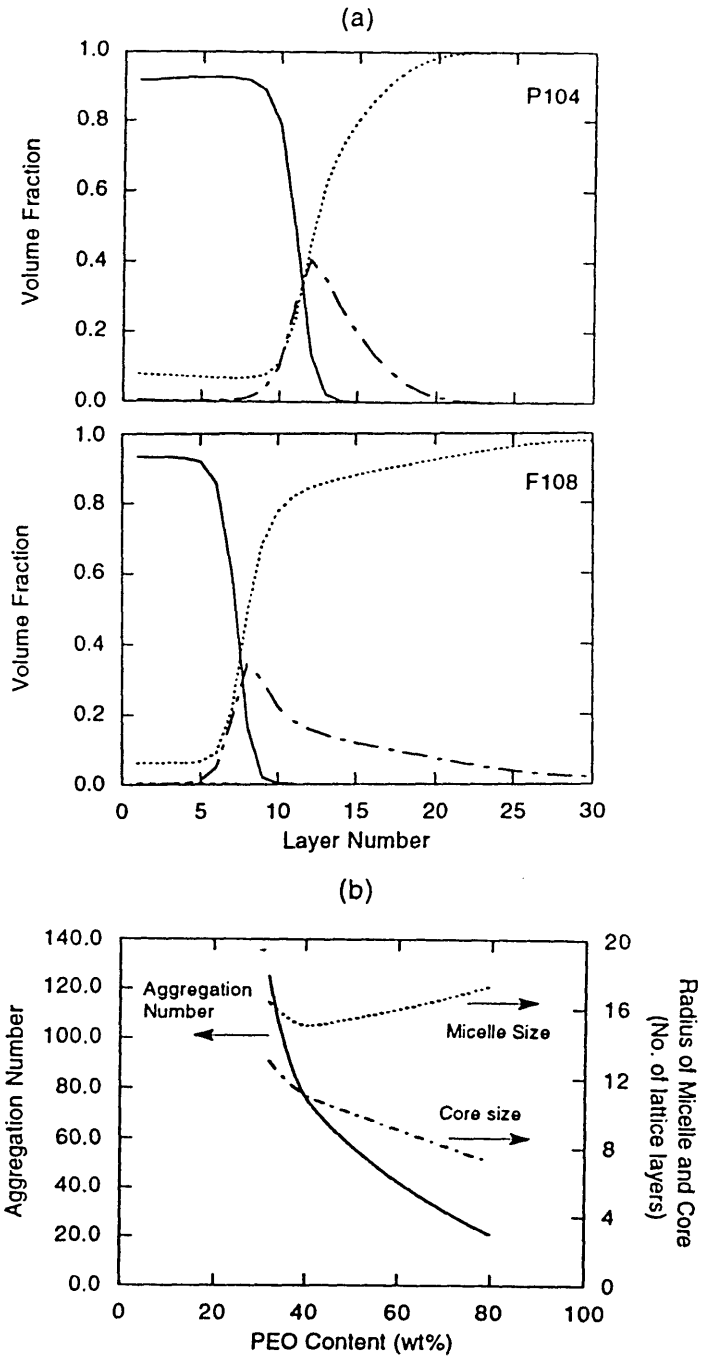

Figure 5.9 (a) Segment density profiles for EO (solid line), PO (broken line) and water (dotted line) in P104 and F108 micelles, predicted by the model of Hurter et al. [1993b]. One lattice site corresponds to approximatelly 0.4 nm.
(b) Effect of PEO content on aggregation number and core and total micelle size for Pluronic copolymers of the P103, P104, P105, F108 series, predicted by the model of Hurter et al. [1993b].

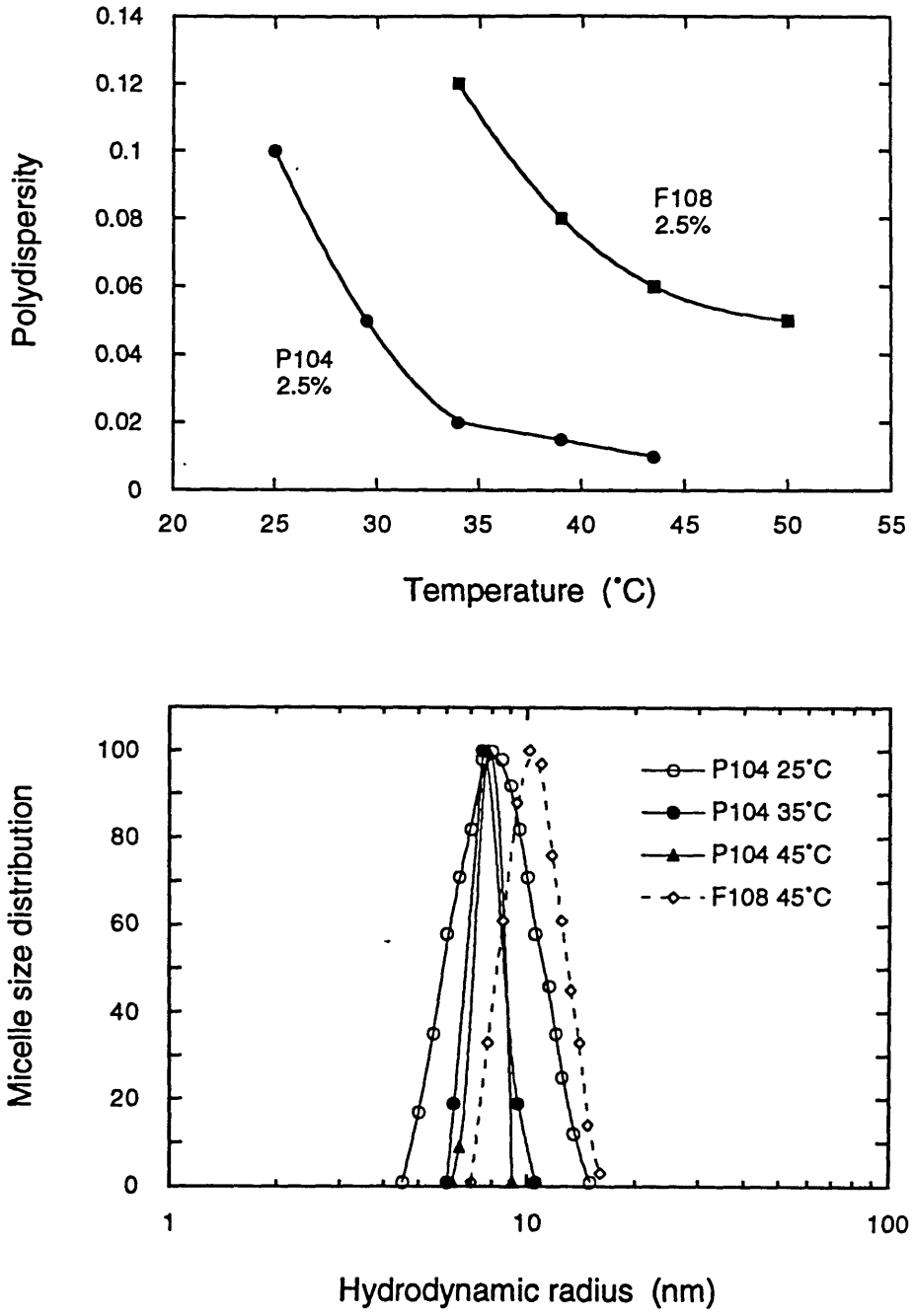

Figure 5.10 (a) Micelle polydispersity (see text for definition) as a function of temperature.
(b) Micelle size distribution for various temperatures.

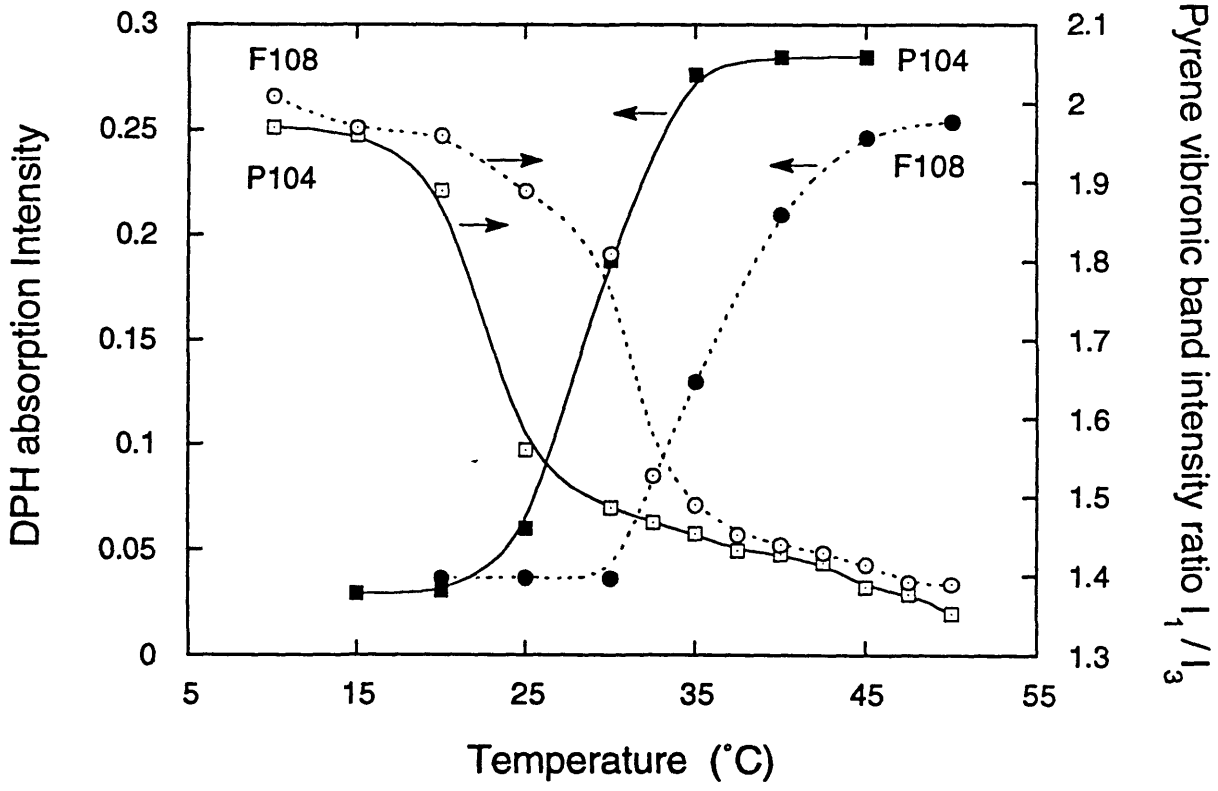

Figure 5.11 Temperature dependence of the ratio of vibronic band intensities, I_1/I_3, of pyrene (0.3 mM) in P104 and F108 aqueous solutions (open symbols). Also shown in the same graph are the DPH intensity data for the same copolymer solutions (filled symbols).

Chapter 6
Fluorescence Probe Studies on the Microenvironment in PEO-PPO-PEO Triblock Copolymer Solutions as a Function of Temperature

6.1 Introduction

Temperature effects in aqueous solutions of poly(ethylene oxide)-*block*-poly(propylene oxide)-*block*-poly(ethylene oxide) (PEO-PPO-PEO) copolymers (commercially available under the name Pluronics) have recently received increased attention due to the interesting temperature-induced micellization and gelation phenomena observed [Alexandridis & Hatton, 1994]. In a recent study that explored the potential of using PEO-PPO-PEO block copolymer micelles for the purification of water contaminated with polycyclic aromatic hydrocarbons, it was shown that solubilization efficiency depended strongly on the composition of the copolymer used and the structure of the micelles formed [Hurter & Hatton, 1992; Hurter et al., 1994]. The local environment afforded by the micelles is an important factor in determining the tendency of molecules to partition in such systems; we, therefore, undertook an investigation of the micropolarity and microviscosity in Pluronic copolymer solutions using hydrophobic fluorescent molecules as probes.

Fluorescence spectroscopy techniques have been developed and optimized over the past 15 years for the study of colloidal solutions, and many fluorescent molecules are now available for probing structural information in such systems [Thomas, 1984; Zana, 1986; Winnik et al., 1990]. Pyrene, amongst others, is a well-characterized polarity-sensitive probe. Its fluorescence emission spectrum consists mainly of five bands referred to as, I_1, I_2, ..., I_5, from shorter to longer wavelengths. The I_1/I_3 intensity ratio of this vibrational fine structure, often referred to as the "Py scale" [Dong & Winnik, 1984], strongly depends on the polarity of the medium (i.e., the larger the ratio, the more polar the

medium). Electronically excited pyrene is a reporter of the average micropolarity of the environment it visits during its lifetime (ca. 300 ns), and that renders pyrene attractive for studying restricted microenvironments such as micellar systems [Thomas, 1984; Ananthapadmanabhan et al., 1985]. Most of published studies have focused on variations of the I_1/I_3 ratio with surfactant concentration, and little is known about its temperature dependence. Turro and Kuo [1986] reported that an increase in temperature significantly decreased the values of I_1/I_3 in various PEO-PPO-PEO block copolymer solutions. This variation was attributed to a decrease in hydrophilicity of the aggregates. Zana and coworkers [Alami et al., 1993] also observed a similar trend when comparing I_1/I_3 results at 25 °C and 40 °C for solutions of polyethoxylated surfactants of relatively small molecular weight. However, in neither case was there an attempt for systematic investigation of the effect of temperature on the I_1/I_3 ratio.

The hydrophobic probe bis(1-pyrenylmethyl)ether (dipyme) shows intramolecular excimer fluorescence (intensity I_e) in competition with fluorescence from the locally excited pyrene chromophore ("monomer" emission, intensity I_1) [Georgescauld et al., 1980]. The extent of excimer emission in dipyme depends upon the rate of conformational change, the motion being restricted by the local friction imposed by the environment. As a consequence, the intensity ratio I_1/I_e provides a measure of the "microviscosity" of its environment, and is a particularly powerful means of monitoring changes in microviscosity as the system is subjected to external stimuli [Winnik et al., 1991]. Dipyme has been employed to investigate fluidity changes accompanying phase transitions in phospholipid membranes [Georgescauld et al., 1980], fluidity of polymeric micelles that exist in aqueous solutions of poly(N-isopropylacrylamide)-poly(acrylamide) copolymers [Winnik et al., 1991], and microviscosity of micelle-like cluster formation in aqueous solutions of hydrophobically modified PEO [Yekta et al., 1993].

We have used pyrene to probe the micropolarity in Pluronic copolymer solutions, by conducting a systematic investigation of the variation of the pyrene fluorescence emission intensity ratio I_1/I_3 in different media as a function of temperature. Specifically, studies were conducted in water, organic solvents, bulk poly(ethylene oxide) (PEO) and poly(propylene oxide) (PPO) homopolymers, and aqueous solutions of block PEO-PPO-PPO copolymers. The micropolarity data obtained in the PEO-PPO-PEO copolymer solutions, and their temperature dependence, were compared to those obtained in bulk

homopolymers and organic solvents. Qualitative changes in the microviscosity experienced by dipyme (and detected via the dipyme monomer/excimer fluorescence emission intensity ratio I_1/I_e) are also reported for PPO homopolymers and PEO-PPO-PEO copolymer micellar solutions, as a function of the copolymer composition and sample temperature.

6.2 Materials and Methods

Materials: The Pluronic PEO-PPO-PEO copolymers P65, P85, P105, P103, P123, P104 and F108 were obtained as a gift from BASF Corp., Parsippany, NJ (see Alexandridis et al., 1994 for information on their composition and molecular weight). UCON 50-HB-5100, a random PEO-PPO copolymer (3930 molecular weight, 50 wt % PEO) was purchased from Union Carbide Chemicals and Plastics Co., Bound Brook, NJ. Liquid PEO and PPO homopolymers of low molecular weights (300 for PEO, 425, 725, 2000, 3000, and 4000 for PPO) were obtained from Aldrich Chemical Co (Milwaukee, WI). All polymers were used as received. Pyrene (benzo[def]phenanthrene) (99% purity) was purchased from Sigma Chemical Co. (St. Louis, MO), and was recrystalized fo, r times from ethanol. A stock solution of 1 mM pyrene in acetone was prepared, from which 1 µl was added to 3 ml of sample. (1-1'-dipyrenyl)-methyl ether (dipyme) was synthesized by Dr. B. Tsao (Chemistry Dept., M.I.T.), following the procedure reported by Georgescauld et al. [1980].

Fluorescence spectroscopy: All fluorescence spectra were recorded on a SPEX FluoroMax spectrofluorometer using a 1 nm bandpass in the "s" mode (sample counts); sample PM counts were always smaller than $2x10^5$ counts/sec to ensure linear response of the detector. Wavelengths of excitation (λ_{ex}) were chosen according to the maximum intensity obtained in the excitation spectra; depending on the solution, $\lambda_{ex} \approx 335$ nm and $\lambda_{em} \approx 372$ nm. Step increments and integration times were set at 0.5 nm and 0.5 sec respectively. All samples were aerated, magnetically stirred, temperature controlled using a thermostated cuvette holder connected to a circulating water bath, and examined at right-angle geometry. Each spectrum was obtained by averaging three scans, corrected for scatter using an equivalent blank solution. In all cases the I_1/I_3 values were averaged over 4 different experiments. The reproducibility of these results was better than 3% and the

standard deviation of the I_1/I_3 values was smaller than 0.01. The pyrene concentration was $3x10^{-7}$ M in all samples; no excimer formation was observed, even in the micellar solutions.

6.3 Results and Discussion

6.3a Temperature dependence of the micropolarity "Py scale"

Typical fluorescence emission spectra of pyrene in water and bulk PPO are presented in Figure 6.1, normalized with respect to the I_1 intensity. The five distinct emission bands of the pyrene vibrational fine structure [Thomas, 1984] can be observed in both spectra shown in Figure 6.1. Note that the intensity of the I_3 band in PPO is larger than that of the I_3 band in water, reflecting a difference in polarity between the two media. The I_1/I_3 intensity ratio is smaller in bulk PPO, indicating that PPO is less polar than water.

In order to investigate the micropolarity afforded by temperature-sensitive microheterogeneous systems such as Pluronic copolymer solutions, we decided to first study the influence of temperature on the I_1/I_3 intensity ratio of pyrene in various homogeneous solvents. Results for water, acetonitrile, PEO (M_w=300), ethylacetate, PPO (M_w=3000), isopropanol, and cyclohexane are presented in Figure 6.2. A wide range of polarity was covered on the "Py scale" (Figure 6.2a), from cyclohexane (the least polar solvent studied here) to water and acetonitrile (the most polar). The I_1/I_3 ratio decreased linearly with increase of temperature. For these homogeneous solvents, the linear decrease in I_1/I_3 is attributed to temperature-induced changes in polarity. The extent of this decrease depended on the system studied as shown in Figure 6.2b where the I_1/I_3 ratios at different temperatures are plotted as a percent of the I_1/I_3 value at 10 °C. Strongest effects (i.e. larger slopes) were observed for liquid homopolymers PEO, PPO, and for ethylacetate, suggesting that polarity is highly affected by temperature for molecules subject to conformational changes. This is in accordance with the experimental and theoretical findings of PEO polarity decreasing with increasing temperature [Karlstrom, 1985; Lindman et al., 1990].

To study the effect on polarity of hydroxyl end-groups of PPO on the I_1/I_3 ratio and

its temperature dependence, we carried out pyrene fluorescence experiments in liquid PPO homopolymers of different molecular weights and consequently different hydroxyl concentrations. These results are summarized in Figure 6.3. A linear decrease of I_1/I_3 with temperature was obtained in all cases (see Figure 6.3a). As anticipated from the hydroxyl content of the polymers, the smaller the molecular weight, the larger the I_1/I_3 ratio (i.e. polarity). It is also interesting to notice that, when the I_1/I_3 values (as well as the slope representing their temperature dependence) are plotted vs the PPO molecular weight, they seem to plateau towards high molecular weights (i.e. diminishing influence of end-groups on micropolarity sensed by pyrene). Variations of I_1/I_3 and the slopes as a function of the hydroxyl number (expressed in mg of KOH necessary to titrate 1 g of polymer) are presented in Figure 6.3b. As expected, the I_1/I_3 ratio decreased with decreasing hydroxyl number; the same trend was also observed for the value of the slopes.

6.3b Micropolarity in PEO-PPO-PEO copolymer solutions

Evidence of micelle formation: I_1/I_3 ratios for 0.5% aqueous solutions of Pluronic P104 and F108 copolymers, at different temperatures, are compared to the values obtained in an equivalent aqueous solution of the UCON 50-HB-5100 random PEO/PPO copolymer in Figure 6.4. The I_1/I_3 ratio in the random copolymer solution decreased linearly over the temperature range studied (10 to 45 °C), exhibiting values that were similar to those obtained in water. It can thus be concluded that the environment sensed by the pyrene was predominantly water, and that no detectable hydrophobic microdomains were formed in the random copolymer aqueous solution (data for the UCON solution at 50 °C are not reported as this temperature corresponds to the cloud point of the polymer [Union Carbide, 1992]). A sharp decrease in I_1/I_3 was observed for P104 and F108 triblock copolymer solutions, at temperatures characteristic for each polymer, followed by a less dramatic linear decrease as temperature was further increased (Figure 6.4). This sharp decrease is attributed to the formation of micelles with a well-defined hydrophobic core into which pyrene partitions preferentially [Hurter & Hatton, 1992]. The temperature dependence of the I_1/I_3 intensity ratio can be used for the determination of the critical micellar temperature (CMT), as has been done using the I_1/I_3 vs concentration plots for the determination of the critical micellar concentration (CMC) [Thomas, 1984; Ananthapadmanabhan et al., 1985]. Excellent agreement with other techniques is obtained (see Chapter 5 of this Thesis). The smoother linear decrease observed at temperatures higher than the CMT reflects a less polar

microenvironment with increasing temperature. This can be due either to a change in composition of the core (i.e. less PEO or water) or to a temperature-induced change in the micropolarity (for the same micelle core composition); the origin of the I_1/I_3 decrease at temperatures above the CMT is discussed in Section 6.3c.

Effect of copolymer molecular weight and composition: The influence of molecular weight on the micropolarity afforded by copolymer micellar solutions is depicted in Figure 6.5 for a series of Pluronic copolymers (P105, P85, P65) having the same PPO/PEO ratio (50%). The higher molecular weight P105 exhibited the lower CMT, in accordance with the findings of Alexandridis et al. [1994]. At temperatures higher than the CMT, the I_1/I_3 ratios decreased linearly with increasing temperature for all copolymers, but their values remained in the order: I_1/I_3 (P65) > I_1/I_3 (P85) > I_1/I_3 (P105). This is an indication that micelles assembled from higher molecular weight Pluronics (maintaining constant PPO/PEO copolymer composition) exhibit more hydrophobic microdomains.

To study the effect of the PEO block on the micropolarity of copolymer micelles, we compared Pluronic copolymers having the same size PPO block but differing in the size of the PEO block. Data for P103, P105, and F108 (with 30, 50, and 80% PEO content, respectively) are summarized in Figure 6.6a. Once again, lower CMT's were observed for more hydrophobic Pluronics (lower PEO content). At temperatures higher than CMT, the values of the I_1/I_3 ratio decreased in the order: I_1/I_3 (F108) > I_1/I_3 (P105) > I_1/I_3 (P103). However, the difference in the I_1/I_3 ratios was smaller than that observed for the P65-P85-P105 series (even though the variation in copolymer M_w is larger in the P103-P105-F108 series). This suggests that the microdomains afforded by P103, P105, and F108 copolymer micelles are of comparable polarity, and provides an indication that the micropolarity in Pluronics micelles is mainly dependent on the content of PPO. The major effect of increasing the PEO content (keeping constant the size of the PPO block) is to shift the CMT towards higher temperature. These results are consistent with the representation of PEO-PPO-PEO micelles with a core presumably dominated by PPO, in which pyrene partitions preferentially, and a corona made up of hydrated PEO. The effect of the PPO block on the micropolarity of Pluronic copolymer micelles is depicted in Figure 6.6b; both P65 and P123 copolymers have the same molecular weight of PEO block but differ in molecular weights of PPO block. As anticipated from our earlier discussions, the block copolymer containing the larger PPO block has the lower CMT and the corresponding

micelles exhibit lower micropolarity. This confirms the strong influence of the PPO block on the hydrophobicity of the micelles.

For a given Pluronic, the micropolarity probed by pyrene is not affected by the concentration of the polymer, as shown in Figure 6.7. Increasing the polymer concentration from 0.5% to 5% decreased the CMT as expected [Alexandridis et al., 1994]. However, following the CMT, the I_1/I_3 values remained almost identical for all three concentrations. This is an indication that pyrene is partitioning prefentially in the interior of the micelles (and not in a fast dynamic exchange with the bulk solution) and that the probed micropolarity is an intrinsic property of the micelles and does not depend on the polymer concentraion.

It can be concluded from the data and discussion presented above, that pyrene, in addition to being a indicator of micelle formation, is also sensitive to the specific environment afforded by micelles formed from block copolymers of different composition. Indeed, as we show below, the I_1/I_3 fluorescence intensity ratio can be used to obtain information on the composition of the environment where pyrene is located.

6.3c Use of the I_1/I_3 ratio for determining the composition of the micelle core

For a binary solvent system (A and B) the calculated I_1/I_3 ratio can be approximated by [Acree et al., 1993; 1994]

$$I_1/I_3 \approx [\, x\, I_{1A} + y\, I_{1B}\,] / [\, x\, I_{3A} + y\, I_{3B}\,] \qquad (1)$$

where I_{1A}, I_{1B}, I_{3A}, and I_{3B} represent the emission intensities of the vibronic bands of pyrene in solvents A and B, and x, y are the mole fractions of A and B respectively ($x + y = 1$). If the I_3 intensity can be considered as independent of the microenvironment, Equation 1 reduces to

$$I_1/I_3 \approx x\, (I_1/I_3)_A + y\, (I_1/I_3)_B \qquad (2)$$

This assumption has been reported to be reasonable for pyrene [Nakashima et al., 1993].

We have studied the I_1/I_3 ratio in different mixtures of liquid PEO and PPO to check if the simplified linear relationship of Equation 2 could be used in the case of PEO-PPO-PEO copolymers. I_1/I_3 ratios for pyrene in PEO (M_w=300) and PPO (M_w=425) homopolymers and their mixtures are presented in Figure 6.8. In all cases, a linear decrease of I_1/I_3 with increasing temperature was observed (see Figure 6.8a). For a given temperature, the more PEO in the mixture the larger the I_1/I_3, since PEO is more polar than PPO. At a given temperature, I_1/I_3 values were calculated from Equation 2, using experimental data obtained for bulk PEO and PPO, and the appropriate weight fractions. As shown in Figure 6.8b, good agreement was obtained between predicted (open symbols) and experimental I_1/I_3 values (filled symbols), giving confidence in the use of Equation 2.

Considering the observed I_1/I_3 ratio in the PEO-PPO-PEO micellar solutions to result from a linear superposition of the corresponding emission values in PEO and PPO, we can estimate the composition of the micelle core (assuming the core to be a homogeneous mixture of PPO and PEO). Let x and y be the weight fractions of PEO and PPO in the core of the micelle respectively. One can write

$$R_{mic} = x\,R_{PEO} + y\,R_{PPO} \qquad (3)$$

where R is the I_1/I_3 ratio in the different environments. By material balance,

$$x + y = 1 \qquad (4)$$

Equations 3 and 4 can be solved for a given temperature (above the CMT) using the experimental data presented in Section 6.3b. As a first approximation we used the values obtained for bulk PPO of M_w=3000 and bulk PEO of M_w=300 to describe the core of the PEO-PPO-PEO micelles (note that the low molecular weight PEO is not really representative of the systems studied but was the only liquid PEO sample available to us). The compositions obtained from these calculations (summarized in Table 6.1), although qualitative, suggest a decrease of PPO and an increase in PEO in the micelle core as the copolymer becomes more hydrophilic. The composition ratios determined from the above set of equations did not depend much on temperature. The linear decrease in the I_1/I_3 ratio, observed in copolymer solutions at temperatures higher than the CMT, is therefore due to changes in polarity of the components of the micelle core and not to changes in its

composition.

6.3d Microviscosity in PEO-PPO-PEO copolymer micelles

As mentioned in the Introduction, the extent of excimer emission (I_e) in dipyme depends upon the rate of conformational change of the molecule, the motion being restricted by the local friction imposed by the environment. The ratio of "monomer" to excimer emission intensity bands, I_1/I_e, can thus provide a measure of the "microviscosity" that dipyme experiences: the larger the I_1/I_e ratio, the more viscous its environment (less excimer is formed as the two pyrene segments of dipyme come close less often). Typical fluorescence emission spectra of dipyme in bulk PPO are presented in Figure 6.9, where the excimer band (I_e) is shown to increase with respect to the monomer band (I_1) as temperature increases (microviscosity decreases as temperature increases).

Monomer/excimer intensity ratio (I_1/I_e) values of dipyme in bulk PPO homopolymers (M_w = 725, 2000, 3000) and Pluronic F108 micelles are shown in Figure 6.10. I_1/I_e data are reported for the 35 - 50 °C temperature range, so that micelles are present in which dipyme can be solubilized (the solubility of dipyme in water is very limited). The microviscosity decreased with temperature for all systems studied; higher microviscosity values were observed for the higher M_w PPO. The I_1/I_e values for the F108 micelles are comparable to those for bulk PPO, suggesting that the environment where dipyme is located is like bulk PPO. Note that the microviscosity that dipyme experiences in the interior of F108 micelles appears to be similar to the one sensed in low M_w (725) PPO at 35 °C, while it exceeds the microviscosity in high M_w (3000) PPO at 50 °C. This could be an indication of the micelle core becoming more compact as temperature increases. Such an observation can be related to the fact that the aggregation number of Pluronic copolymer micelles increases with temperature, while the hydrodynamic radius remains approximately constant [Alexandridis & Hatton, 1994]. A semilog plot of I_1/I_e vs temperature can be fitted to a linear relationship as seen in Figure 6.10b; activation energy (E_a) values for the microviscosity experienced by dipyme can be estimated from such a plot. E_a for F108 (=29.6 kJ/mol) was smaller than the E_a values for bulk PPO (average E_a = 37 kJ/mol).

Effect of copolymer molecular weight and composition: The influence of molecular weight on the microviscosity in PEO-PPO-PEO copolymer micelles is shown in

Figure 6.11, for a series of Pluronic copolymers (P65, P85, P105) that have the same (50%) PPO/PEO composition ratio (the temperature range for P65 was limited because of the high CMT exhibited). Larger microviscosities were observed for the higher M_w copolymer (P105), that had a PPO block of proportionally larger size. The activation energies were 28, 31.8 and 32.5 for P65, P85, and P105, respectively. Increasing the size of the PEO block, while keeping the same size PPO block, resulted in lower microviscosity values as seen in Figure 6.12a; the effect of PEO, though, is less significant than the effects of PPO (shown in Figure 6.12b) or molecular weight (Figure 6.11). These results are again consistent with the representation of PEO-PPO-PEO micelles with a core dominated by PPO, in which hydrophobic solutes partition. The difference in the microviscosity between micelles formed by various copolymers can be related to the difference in micelle size and compactness of the micelle core; Pluronic copolymers with larger size PPO block form micelles of higher aggregation number [Alexandridis & Hatton, 1994]. Change in the total copolymer concentration had almost no effect on the microviscosity of Pluronic P85 micelles as seen in Figure 6.13. The kinematic viscosity (macroscopic quantity) of bulk PPO (M_w=725) is presented in Figure 6.14 for the same temperature range used for the fluorescence data The activation energy for the kinematic viscosity temperature dependence (E_a = 34 kJ/mol) is smaller than that detected by dipyme in bulk PPO (E_a = 37 kJ/mol). The activation energies for Pluronic micelles are lower than that of PPO and higher than that of water (E_a determined from viscosity data in water is 15 kJ/mol at the 35 - 50 °C temperature range).

6.4 Conclusions

We have investigated the temperature dependence of the "Py scale" in aqueous copolymer solutions, water, homopolymers, and organic solvents. These data should allow the many researchers using pyrene as a polarity probe to decouple polarity changes in the microenvironment (in the case of microstructured systems such as micelles) from polarity changes in the macroenvironment (bulk solvent). In water, organic solvents, aqueous solutions of a random PEO-PPO copolymer, and bulk PEO and PPO homopolymers (and their mixtures), the ratio I_1/I_3 is found to decrease linearly with temperature, with a slope characteristic of the system studied.

In block copolymer solutions, a sharp decrease in I_1/I_3 over a narrow temperature range indicates the formation of micelles with a well defined hydrophobic core into which pyrene partitions preferentially; this effect can be used for the determination of the CMT. Pyrene, in addition to being an indicator of micelle formation, is also sensitive to the specific enviromnent afforded by micelles formed from block copolymers of different composition. For example, at temperatures higher than the CMT, the I_1/I_3 ratios decreased linearly with increasing temperature for copolymers of the same PPO/PEO composition and varying molecular weight, and the I_1/I_3 values remained in the order: I_1/I_3 (P65) > I_1/I_3 (P85) > I_1/I_3 (P105). This is an indication that micelles assembled from higher molecular weight Pluronics (at constant PPO/PEO copolymer composition) exhibit more hydrophobic microdomains.

The I_1/I_3 fluorescence intensity ratio was also used to obtain information on the composition of the environment where pyrene was located. The composition of the micelle cores was estimated assuming that the smoother linear decrease in the I_1/I_3 ratio above the CMT was a linear combination of the decreases observed in bulk homopolymers (this assumption was validated in the case of PEO and PPO). These qualitative results indicated a decrease in PPO and an increase in PEO in the micelle core as the copolymer becomes more hydrophilic, and point to the importance of copolymer composition in determining micellar structure and properties.

The ratio of "monomer" to excimer fluorescence emission intensity bands, I_1/I_e, of dipyme was used as a measure of the "microviscosity" that dipyme experienced: the larger the I_1/I_e ratio, the more viscous the environment. The microviscosity decreased with temperature for all systems studied. The I_1/I_e values for the F108 micelles are comparable to the ones for bulk PPO, suggesting that the environment where dipyme is located is like bulk PPO; the micelle core appeared to become more compact as temperature increased. Activation energy (E_a) values for the microviscosity experienced by dipyme were estimated. E_a for F108 (=29.6 kJ/mol) was smaller than the E_a values for bulk PPO (average E_a = 37 kJ/mol). Increase of the copolymer molecular weight at constant PPO/PEO composition, and increase of the PPO block size for constant PEO block size, resulted in increasing microviscosity and activation energies. The effect of PEO block on micelle microviscosity was less significant.

6.5 References Cited in Chapter 6

1. Acree, W. E. Jr.; Tucker, S. A.; Wilkins, D. C. *J. Phys. Chem.* **1993**, *97*, 11199.
2. Acree, W. E. Jr.; Wilkins, D. C.; Tucker, S. A.; Griffin, J. M.; Powell, J. R. *J. Phys. Chem.* **1994**, *98*, 2537.
3. Alami, E.; Kamenka, N.; Raharimihamina, A.; Zana, R. *J. Colloid Interface Sci.* **1993**, *158*, 342.
4. Alexandridis, P.; Hatton, T. A. *Colloids Surfaces A* **1994**, submitted; Chapter 1 of this Thesis.
5. Alexandridis, P.; Holzwarth, J. F.; Hatton, T. A. *Macromolecules* **1994**, 27, 2414; Chapter 2 of this Thesis.
6. Ananthapadmanabhan, K. P.; Goddard, E. D.; Turro, N. J.; Kuo, P. L. *Langmuir* **1985**, *1*, 352.
7. Dong, D. C.; Winnik, M. A. *Can. J. Chem.* **1984**, *62*, 2560.
8. Georgescauld, D.; Desmasez, J. P.; Lapouyade, R.; Babeau, A.; Richard, H.; Winnik, M. *Photochem. Photobiol.* **1980**, *31*, 539.
9. Hurter, P. N.; Hatton, T. A. *Langmuir* **1992**, *8*, 1291.
10. Hurter, P. N.; Alexandridis, P.; Hatton, T. A. in Solubilization, Christian, S. D.; Scamehorn, J. F., Eds., Marcel Dekker, 1994, in press; Chapter 7 of this Thesis.
11. Karlström, G. *J. Phys. Chem.* **1985**, *89*, 4962.
12. Lindman, B.; Carlsson, A.; Karlström, G.; Malmsten, M. *Adv. Colloid Interface Sci.* **1990**, *32*, 183.
13. Nakashima, K.; Winnik, M. A.; Dai, K. H.; Kramer, E. J.; Washiyama, J. *Macromolecules* **1993**, *26*, 7367.
14. Thomas, J. K. *The Chemistry of Excitation at Interfaces.* ACS Monograph 181. Caserio, M. C., Ser. Ed., Washington, 1984. Chapter 5.
15. Turro, N. J.; Kuo, P. L. *J. Phys. Chem.* **1986**, *90*, 4205.
16. Winnik, M. A.; Pekcan, O.; Croucher, M. D. *Scientific Methods for the Study of Polymer Colloids and their Applications*. Candau, F., Ottewill, R. H., Eds., Kluwer Academic Publishers, 1990. Pages 225-245.
17. Winnik, F. M.; Winnik, M. A.; Ringsdorf, H.; Venzmer, J. *J. Phys. Chem.* **1991**, *95*, 2583.

18. Yekta, A.; Duhamel, J.; Adiwidjaja, H.; Brochard, P.; Winnik, M. A. *Langmuir* **1993**, *9*, 881.
19. Yekta, A.; Duhamel, J.; Brochard, P.; Adiwidjaja, H.; Winnik, M. A. *Macromolecules* **1993**, *26*, 1829.
20. Zana, R., Ed. *Surfactant Solutions: New Methods of Investigation.* M. Dekker: New York, 1986.
21. *UCON Fluids & Lubricants*, Technical Information Note, Union Carbide Chemicals & Plastics Technology Corporation, 1992.

Chapter 6: List of Figures

Figure 6.7 Effect of copolymer concentration on the micropolarity of Pluronic P85 micelles.

Figure 6.8 I_1/I_3 ratios for pyrene in PEO (M_w=300) and PPO (M_w=425) homopolymers and their mixtures, plotted (a) as a function of temperature, and (b) as a function of composition (at various temperatures). The filled symbols in Figure 6.8b represent experimental data, while the open ones predictions using Equation 2.

Figure 6.9 Typical fluorescence emission spectra of dipyme in bulk PPO, showing the excimer band (I_e) increasing with respect to the monomer band (I_1) as temperature increases.

Fig. 6.10 Dipyme monomer/excimer inensity ratio (I_1/I_e) for bulk PPO homopolymers (W_w = 725, 2000, 3000) and Pluronic F108 micelles: (a) I_1/I_e vs temperature, and (b) $\log(I_1/I_e)$ vs inverse temperature.

Fig. 6.11 Effect of molecular weight on the microviscosity in copolymer micelles, for a series of Pluronic copolymers (P65, P85, P105) that have the same PPO/PEO composition ratio (50%).

Fig. 6.12 (a) Effect of PEO block on the microviscosity of copolymer micelles; the Pluronic P103, P105, and F108 copolymers have the same size PPO block but 30, 50, and 80% PEO content, respectively. (b) Effect of PPO block on the microviscosity of copolymer micelles; both P123 and P65 have the same size PEO block but differ in the molecular weights of the PPO block.

Fig. 6.13 Effect of copolymer concentration on the microviscosity of Pluronic P85 micelles.

Fig. 6.14 Viscosity (macroscopic) of bulk PPO (M_w=725).

Table 6.1 Composition of the micelle core, estimated under the assumptions in Section 6.3c.

Pluronic copolymer	PPO (wt %)	PEO (wt %)
P123	74	26
P103	73	27
P105	72	28
F108	69	31
P85	67	33
P65	63	37

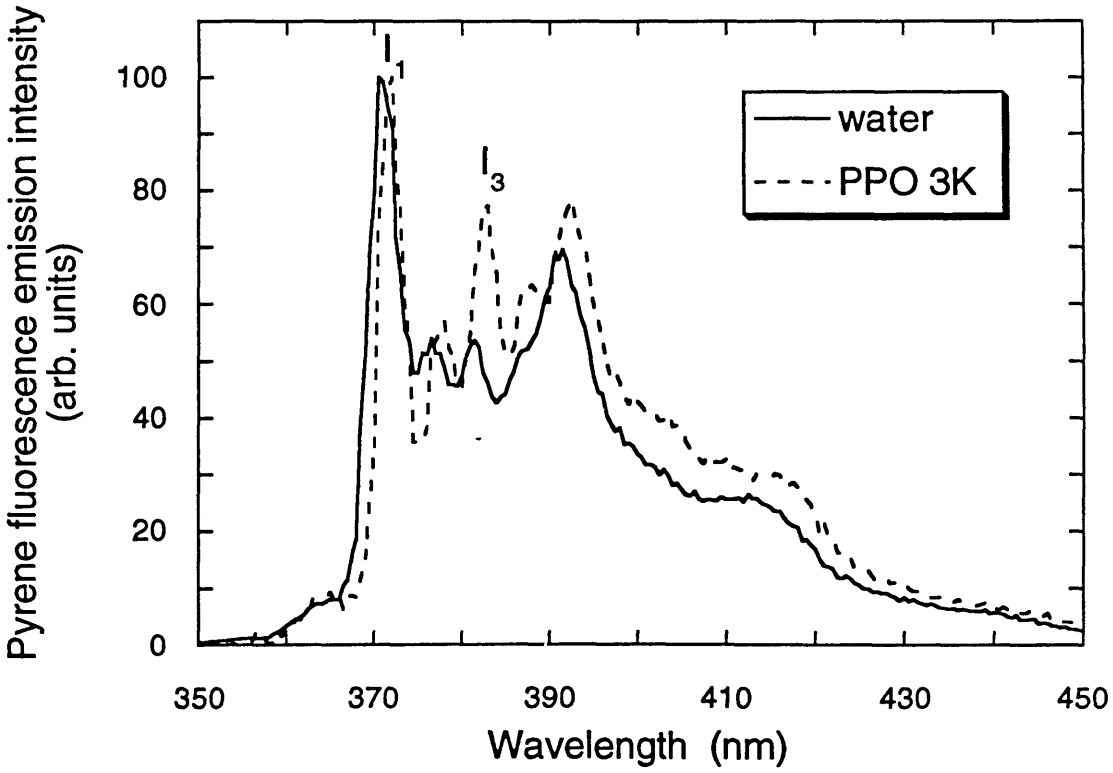

Figure 6.1 Typical fluorescence emission spectra of pyrene in water and bulk PPO.

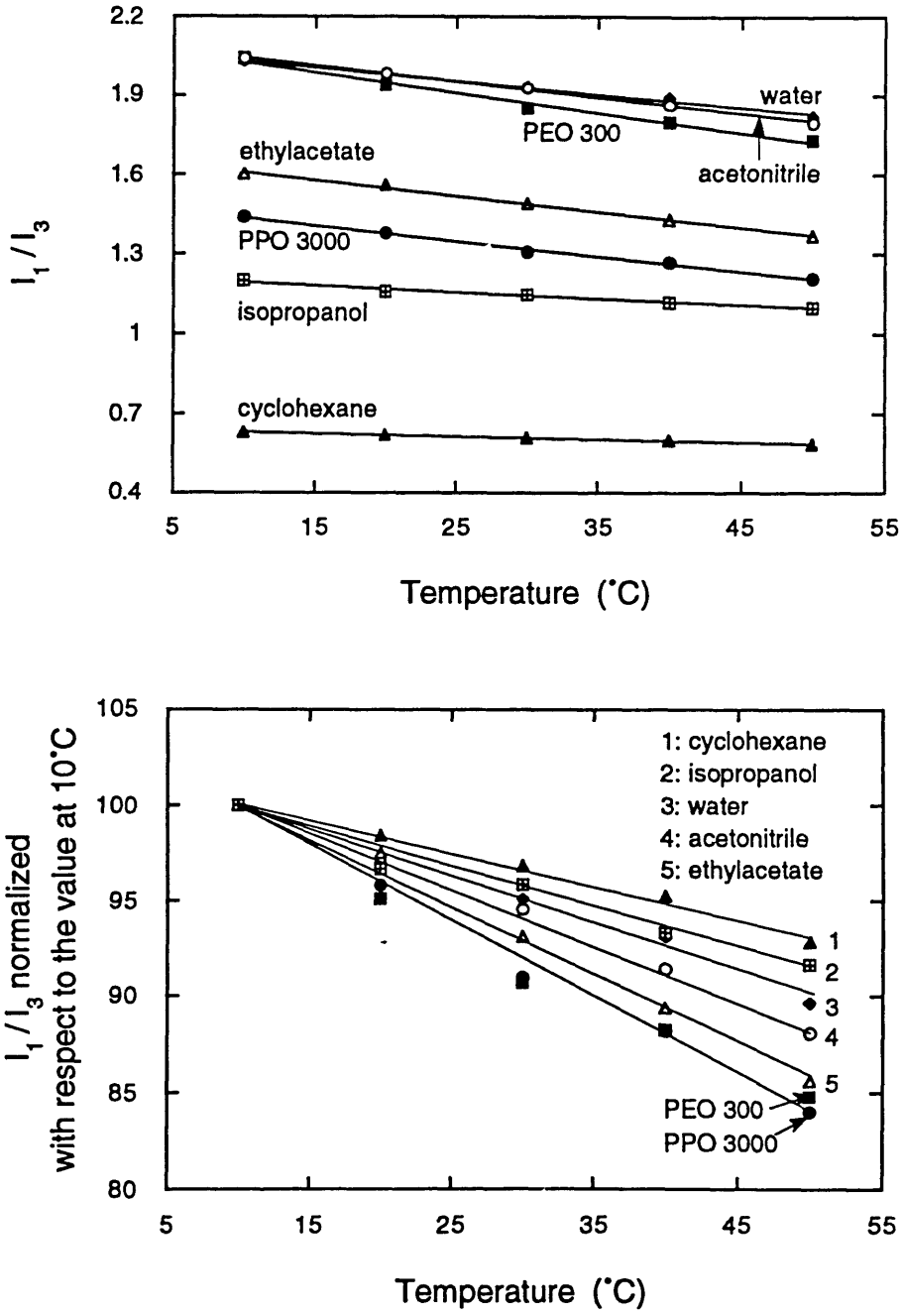

Figure 6.2 (a) I_1/I_3 fluorescence emission intensity ratio of pyrene in various homogeneous solvents. Results for water, acetonitrile, PEO (M_w=300), ethylacetate, PPO (M_w=3000), isopropanol, and cyclohexane are presented; the solid lines are linear fits to the data. (b) I_1/I_3 ratios at different temperatures, plotted as a percent of the I_1/I_3 value at 10 °C.

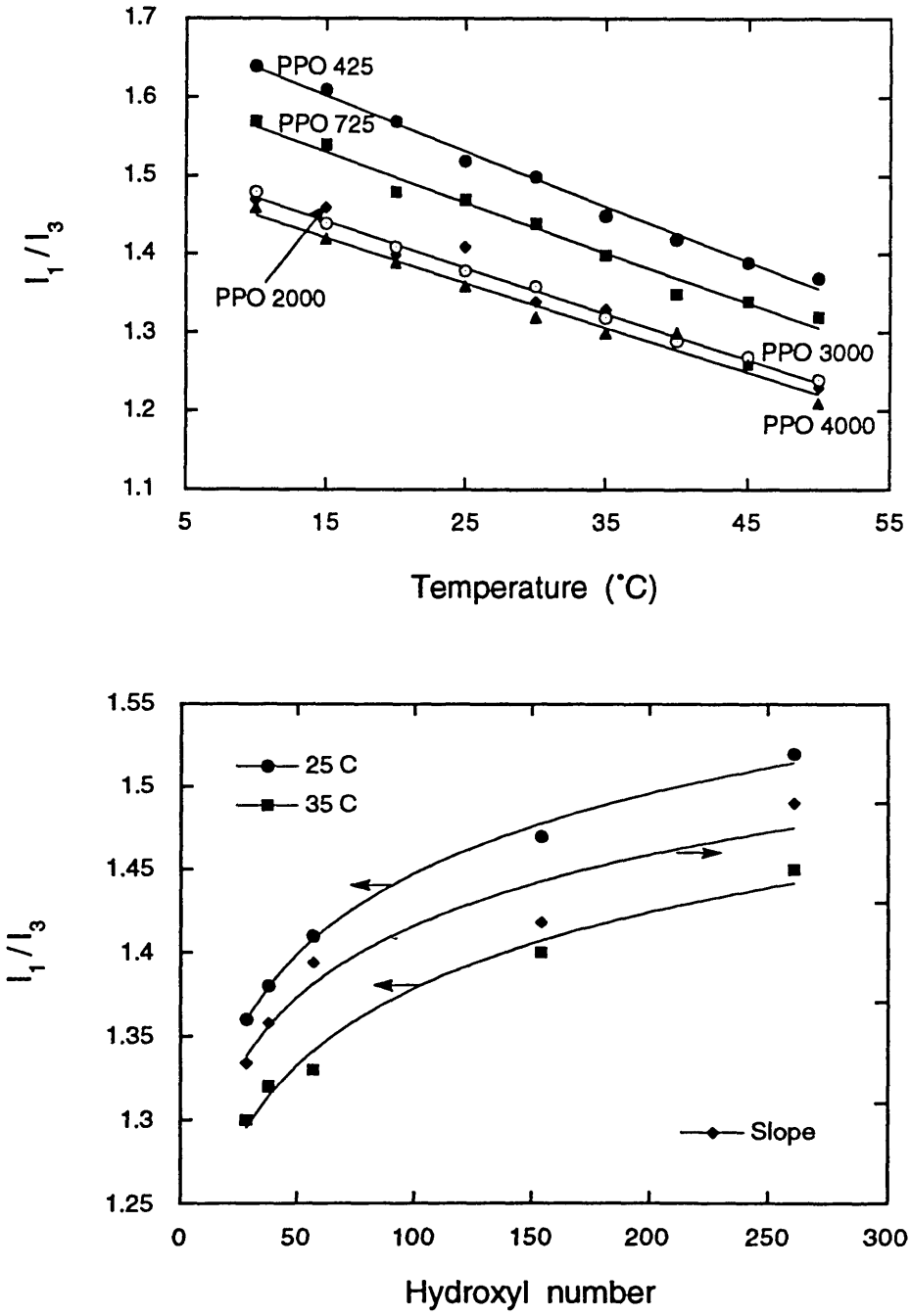

Figure 6.3 (a) Temperature dependence of the I_1/I_3 fluorescence emission intensity ratio of pyrene in bulk PPO of various molecular weights; the solid lines are linear fits to the data (for clarity, the linear fit for PPO of M_w=2000 is not shown). (b) I_1/I_3 and slope values plotted as a function of the hydroxyl number (expressed in mg of KOH necessary to titrate 1 g of polymer).

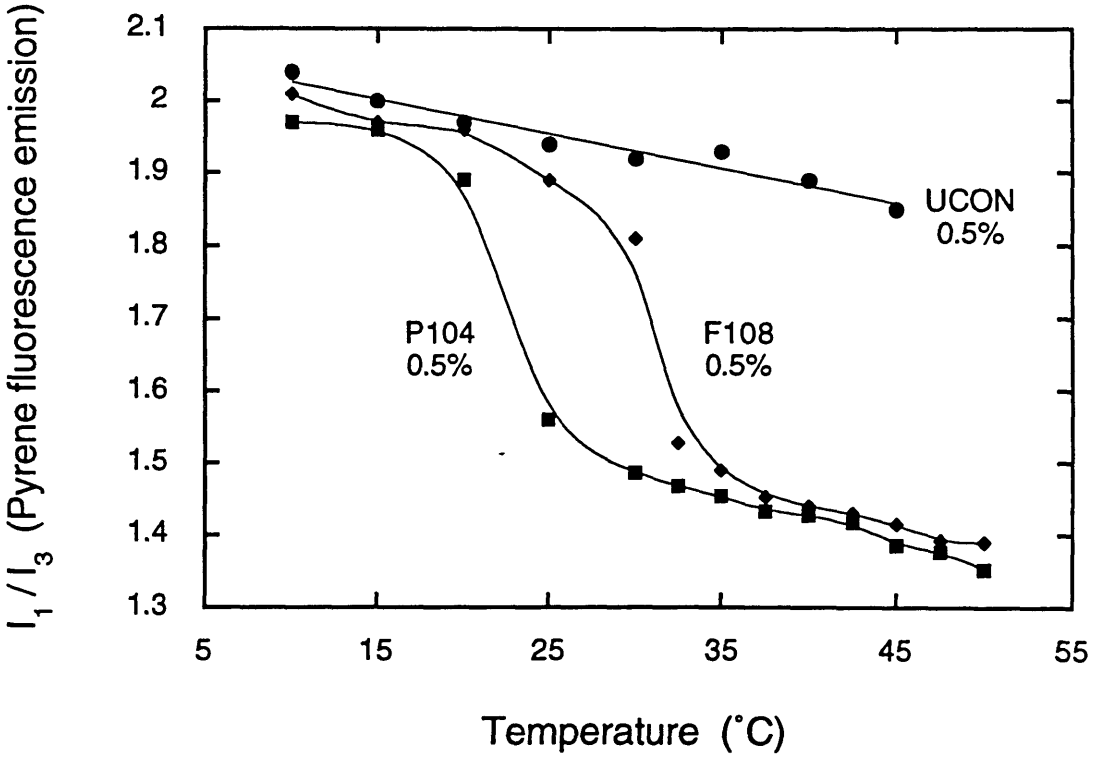

Figure 6.4 I_1/I_3 ratios for 0.5% aqueous solutions of Pluronic P104 and F108 copolymers, plotted as a function of temperature, are compared to the values obtained in an equivalent aqueous solution of the UCON 50-HB-5100 random PEO/PPO copolymer.

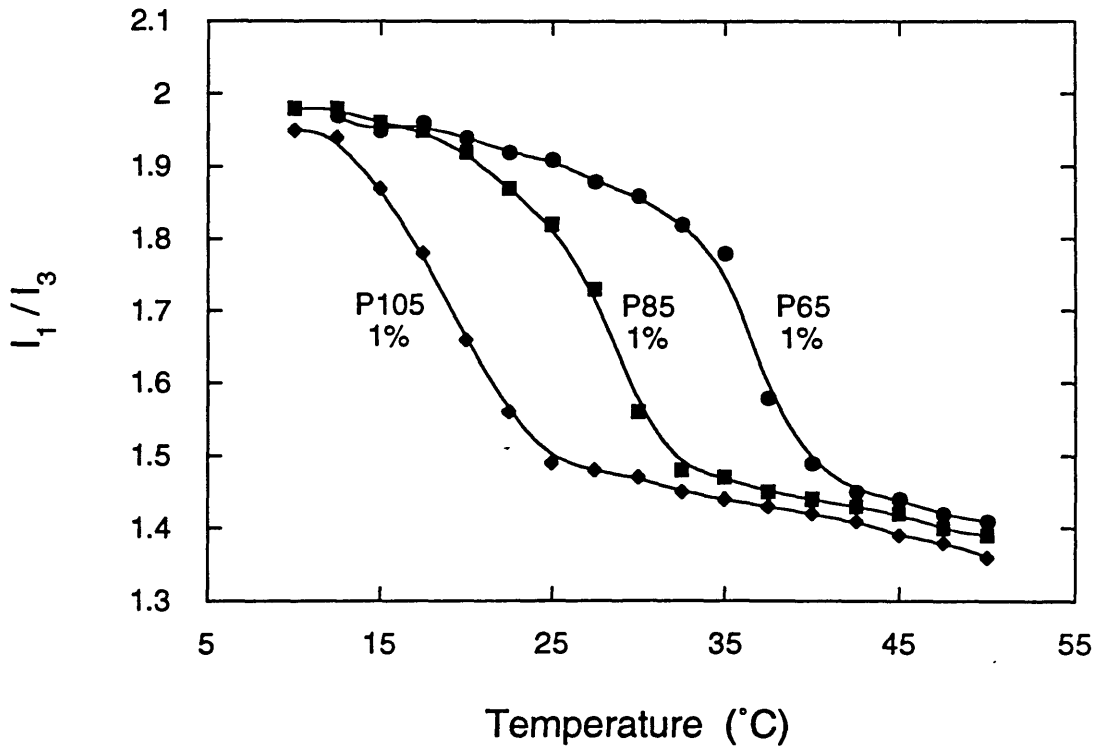

Figure 6.5 Effect of molecular weight on the micropolarity afforded by Pluronic copolymer micellar solutions, for a series of copolymers (P65, P85, P105) that have the same PPO/PEO composition ratio (50%).

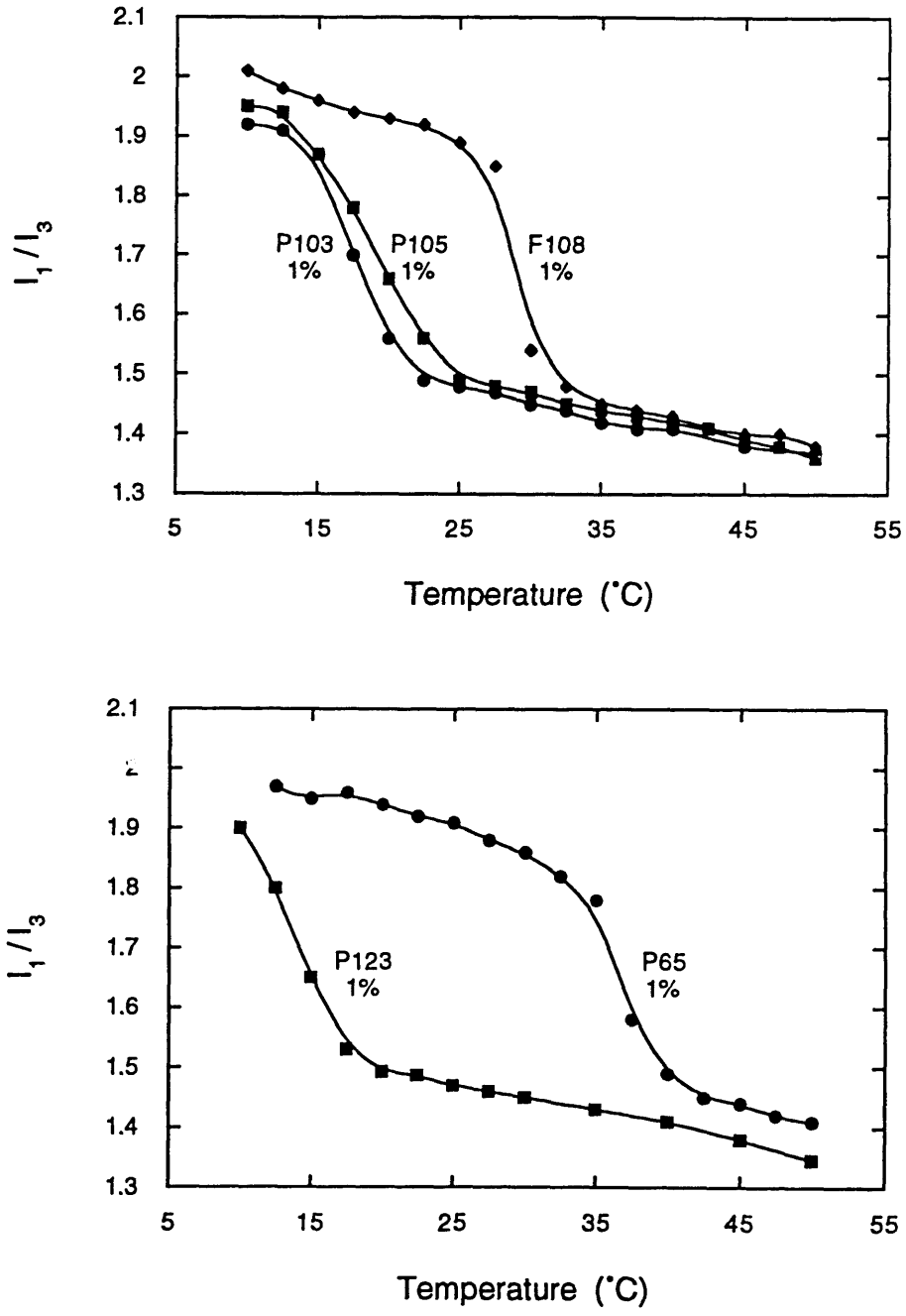

Figure 6.6 (a) Effect of PEO block on the micropolarity of copolymer micelles; the Pluronic P103, P105, and F108 copolymers have the same size PPO block but 30, 50, and 80% PEO content, respectively. (b) Effect of PPO block on the micropolarity of copolymer micelles; both P123 and P65 have the same size PEO block but differ in the molecular weights of the PPO block.

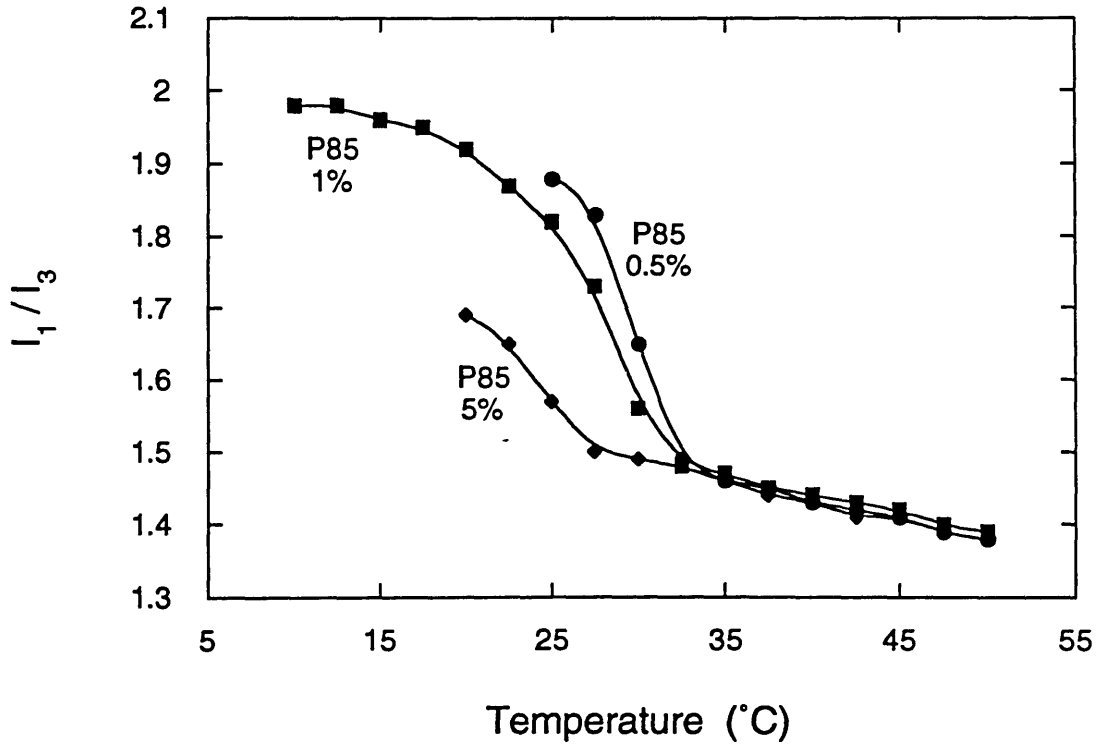

Figure 6.7 Effect of copolymer concentration on the micropolarity of Pluronic P85 micelles.

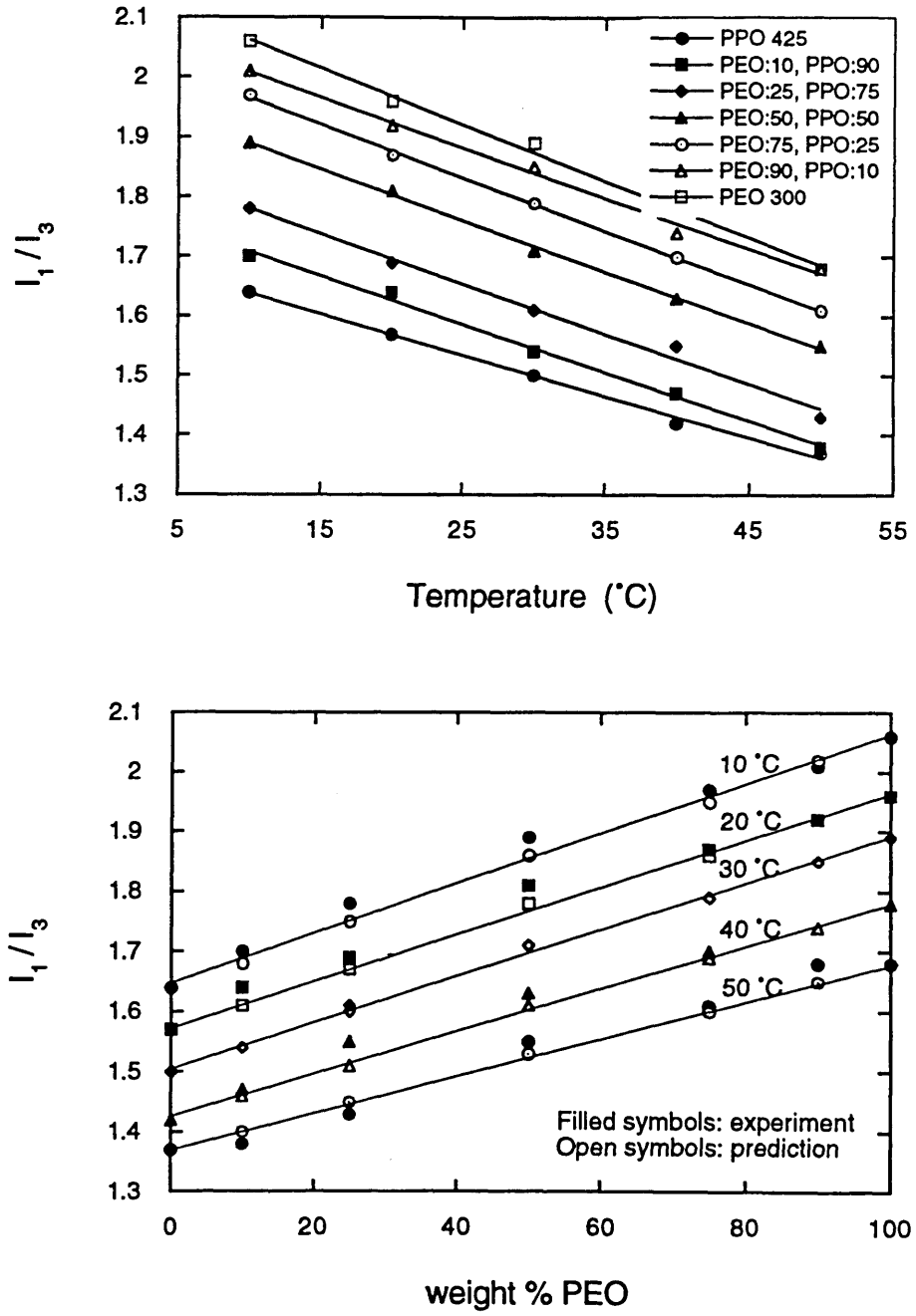

Figure 6.8 I_1/I_3 ratios for pyrene in PEO (M_w=300) and PPO (M_w=425) homopolymers and their mixtures, plotted (a) as a function of temperature, and (b) as a function of composition (at various temperatures). The filled symbols in Figure 6.8b represent experimental data, while the open ones predictions using Equation 2.

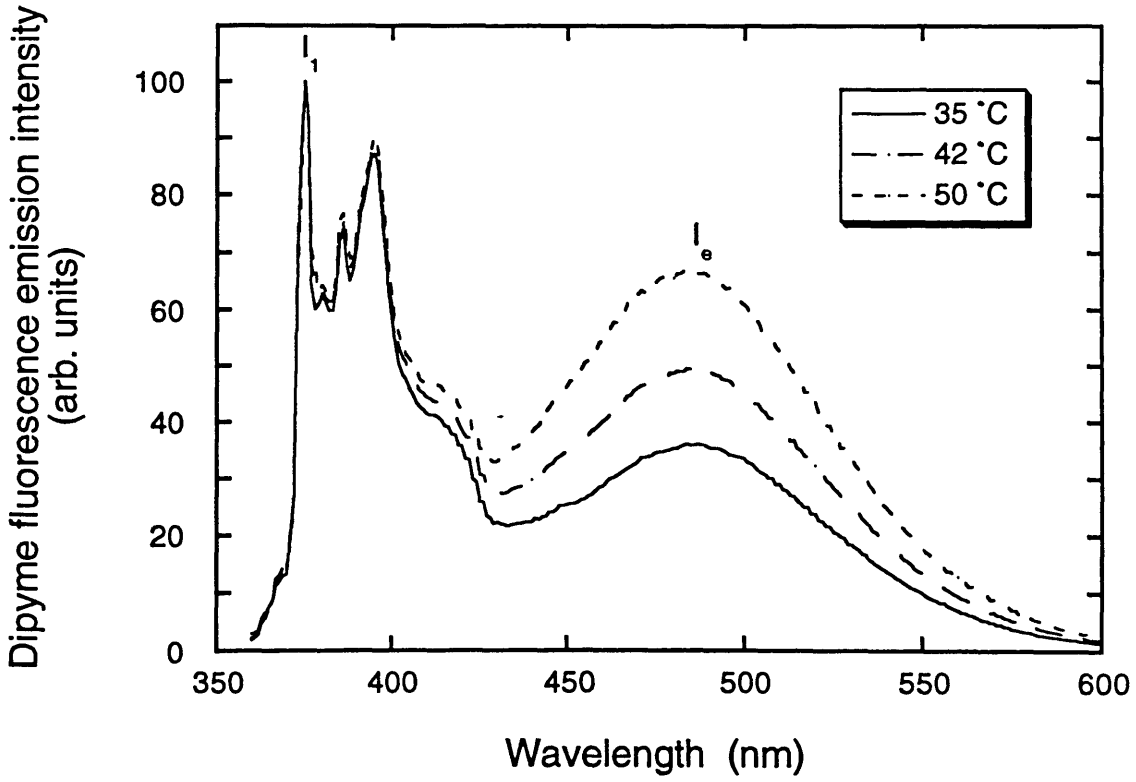

Figure 6.9 Typical fluorescence emission spectra of dipyme in bulk PPO, showing the excimer band (I_e) increasing with respect to the monomer band (I_1) as temperature increases.

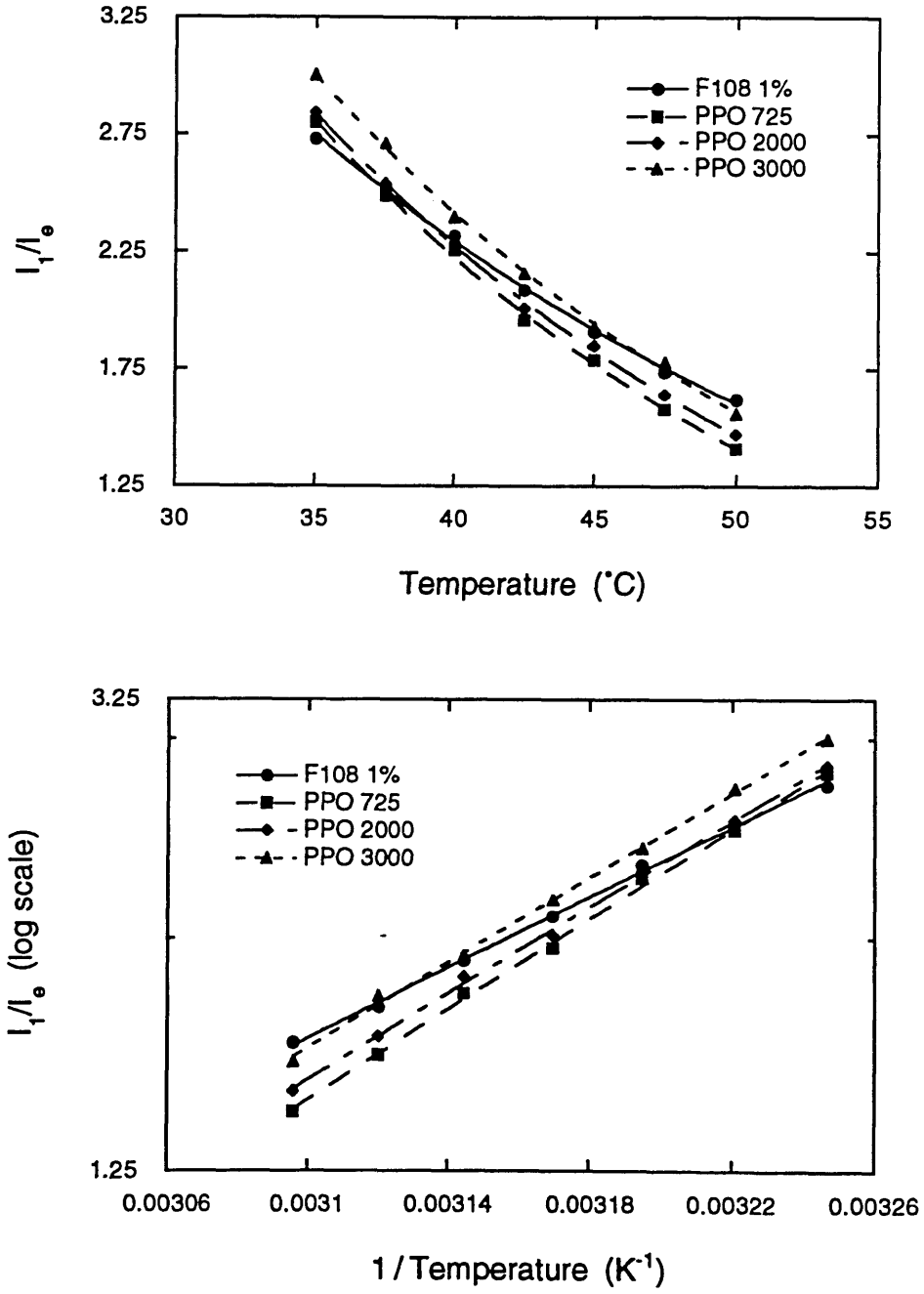

Fig. 6.10 Dipyme monomer/excimer inensity ratio (I_1/I_e) for bulk PPO homopolymers (W_w = 725, 2000, 3000) and Pluronic F108 micelles: (a) I_1/I_e vs temperature, and (b) $\log(I_1/I_e)$ vs inverse temperature.

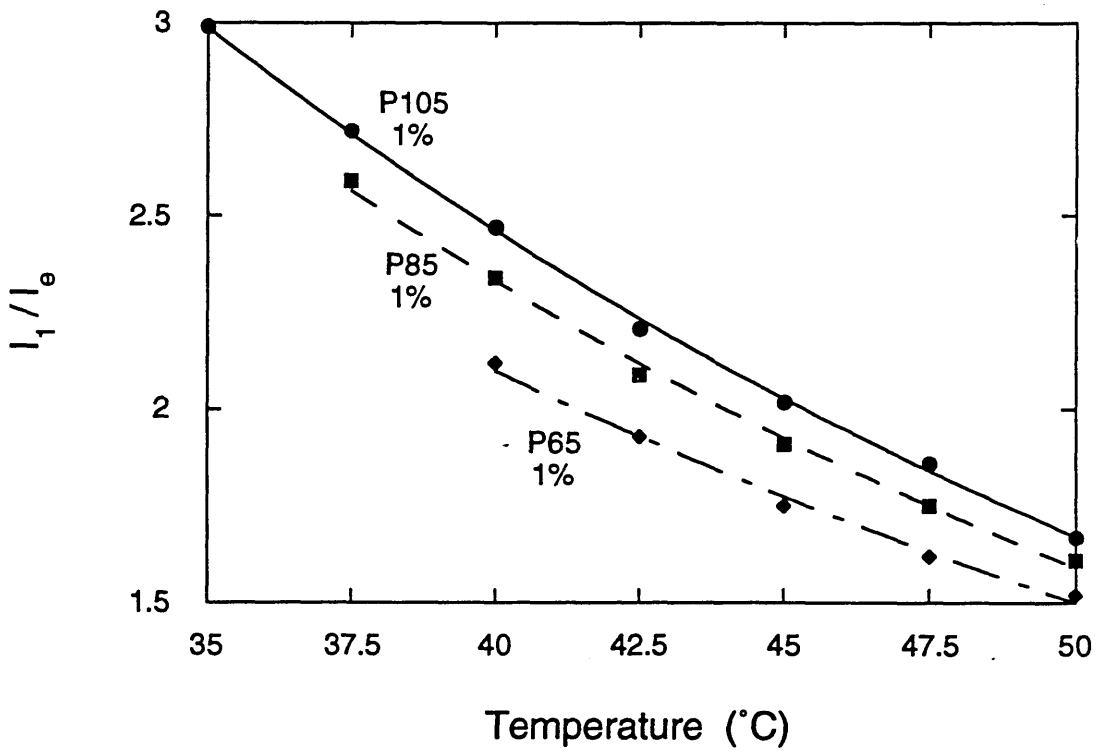

Fig. 6.11 Effect of molecular weight on the microviscosity in copolymer micelles, for a series of Pluronic copolymers (P65, P85, P105) that have the same PPO/PEO composition ratio (50%).

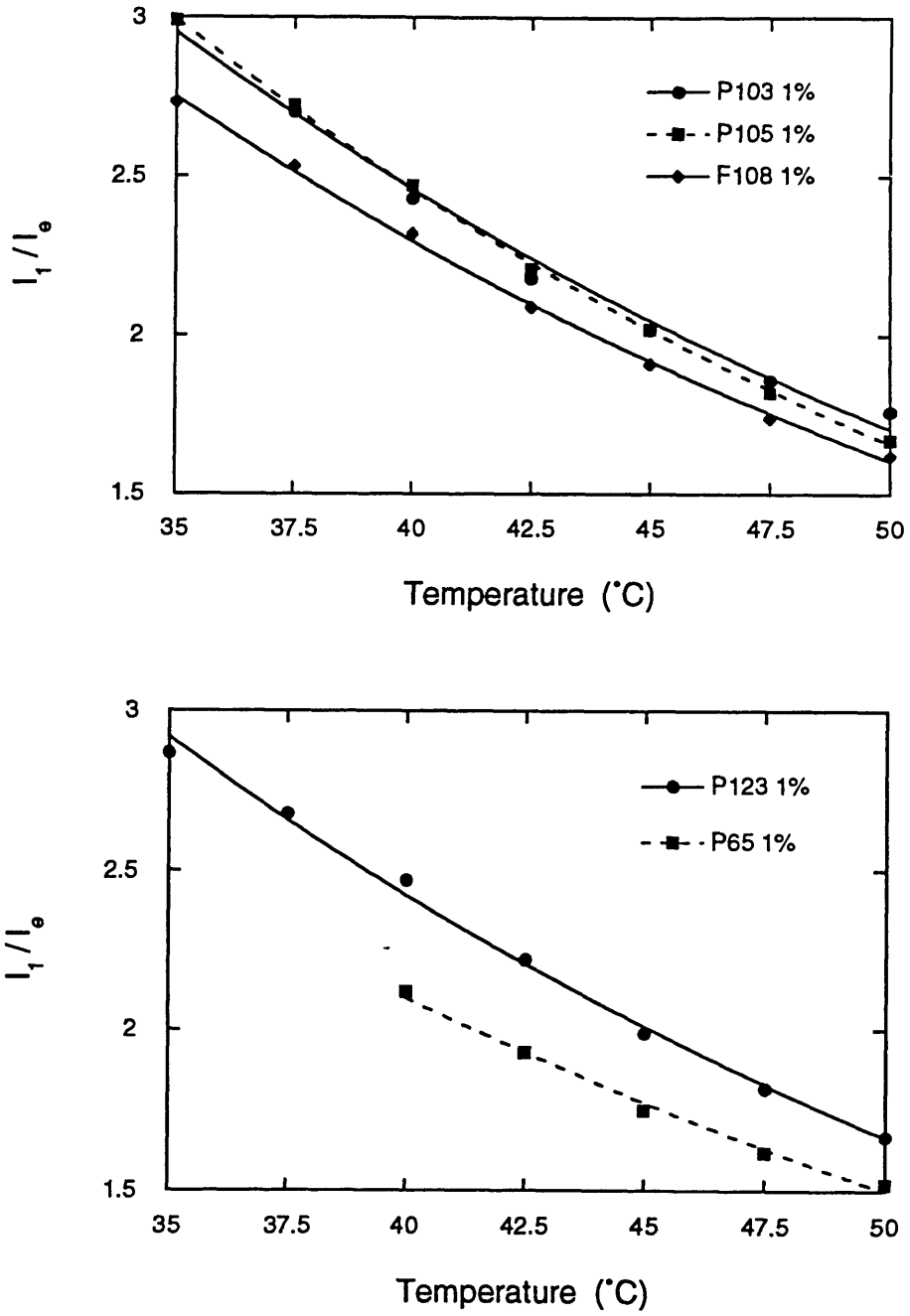

Fig. 6.12 (a) Effect of PEO block on the microviscosity of copolymer micelles; the Pluronic P103, P105, and F108 copolymers have the same size PPO block but 30, 50, and 80% PEO content, respectively. (b) Effect of PPO block on the microviscosity of copolymer micelles; both P123 and P65 have the same size PEO block but differ in the molecular weights of the PPO block.

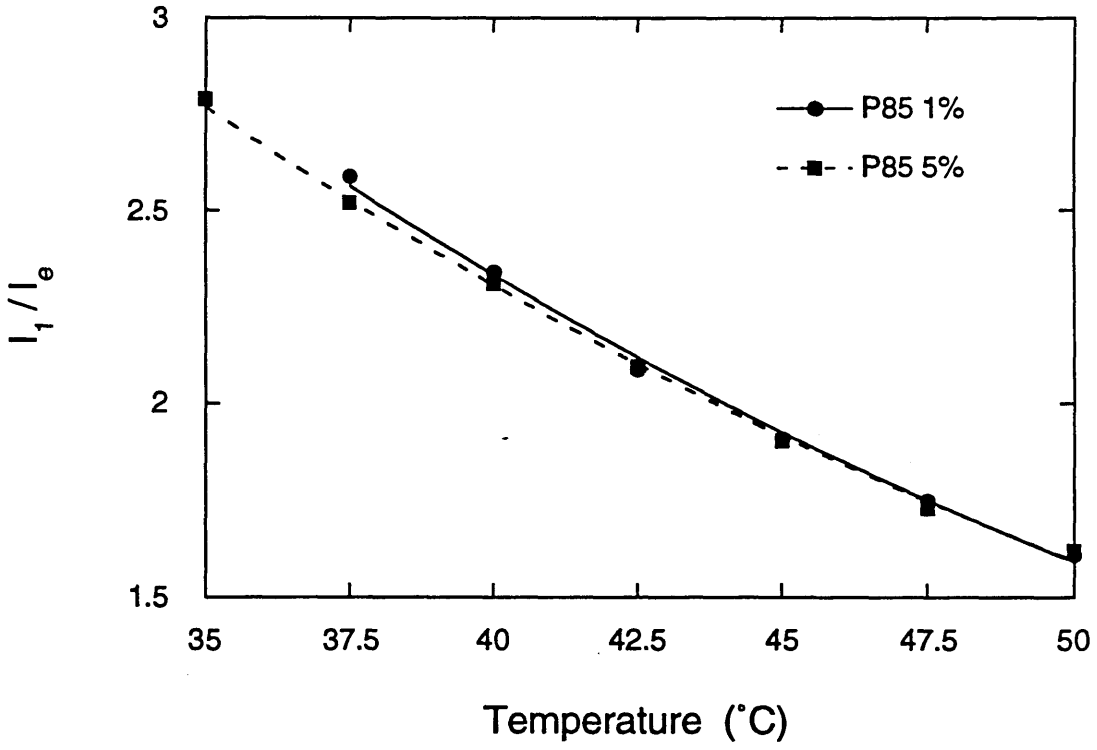

Fig. 6.13 Effect of copolymer concentration on the microviscosity of Pluronic P85 micelles.

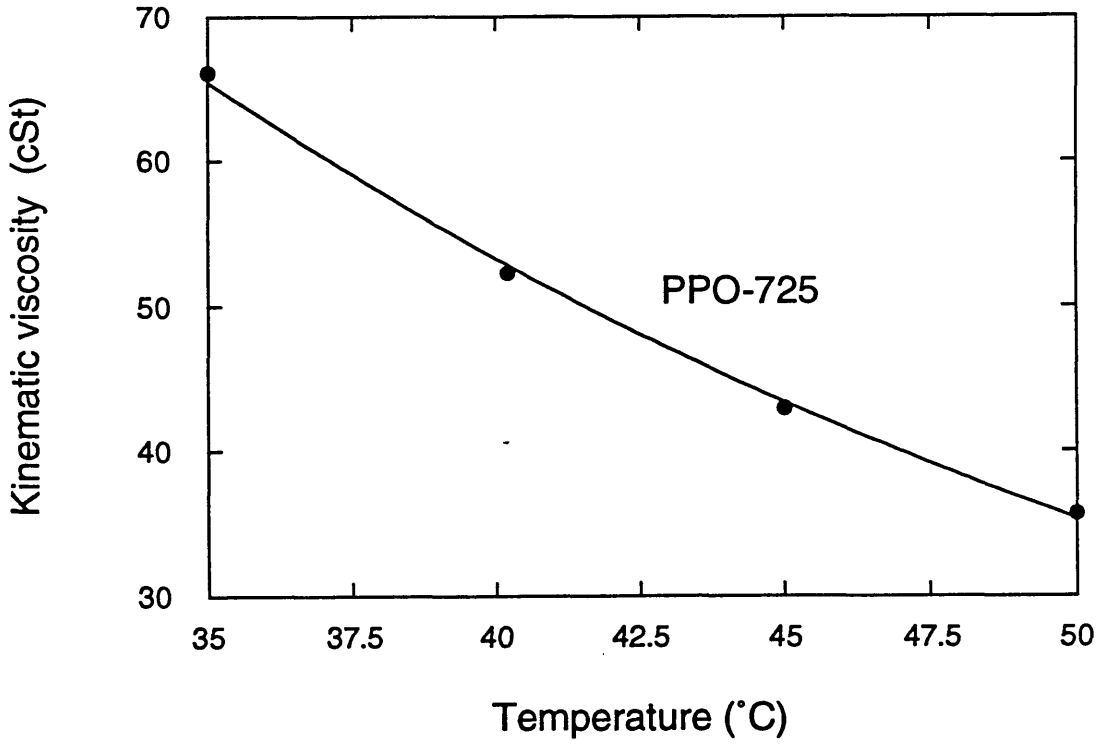

Fig. 6.14 Viscosity (macroscopic) of bulk PPO (M_w=725).

Chapter 7
Solubilization in Amphiphilic Copolymer Solutions

7.1 Introduction

Copolymers are synthesized by the simultaneous polymerization of more than one type of monomer. The result of such synthesis is called block copolymer if the monomers occur as blocks of various lengths in the copolymer molecule. The different types of blocks within the copolymer are usually incompatible with one another and, as a consequence, block copolymers self assemble in melts and in solutions. In the case of amphiphilic copolymers in aqueous solutions, the copolymers can assemble in microstructures that resemble micelles formed by low molecular weight surfactants. An interesting property of aqueous micellar systems is their ability to enhance the solubility in water of otherwise water-insoluble hydrophobic compounds. This occurs because the core of the micelle provides a hydrophobic microenvironment, suitable for solubilizing such compounds. The phenomenon of solubilization forms the basis for many practical applications of surfactants.

The enhancement in the solubility of lyophobic solutes in solvents afforded by amphiphilic copolymer micelles has shown promise in many industrial and biomedical applications. The solubility and stability of hydrophobic drugs can be improved by solubilizing the drug in an aqueous micellar solution [Lin & Kawashima, 1985; Collet & Tobin, 1979]. Nonionic surfactants (including amphiphilic block copolymers) are considered suitable for use as drug delivery agents since they are less toxic to biological systems than cationic or anionic surfactants, and their lower critical micelle concentration means that smaller concentrations are required. Photochemical reactions can be carried out in micellar systems: copolymers are used which both solubilize the molecules of interest and sensitize the photochemical reaction [Nowakowska et al., 1988]. Other promising applications are in separations: hydrophobic pollutants, such as polycyclic aromatic hydrocarbons, can be selectively solubilized in aqueous solutions of block copolymer

micelles [Nagarajan et al., 1986; Hurter, 1992].

In all these applications it is important to understand how the polymer structure, solution conditions and solute properties affect the solubilization behavior. One of the advantages of using amphiphilic copolymers over traditional surfactants is that, to a certain extent, an optimal polymer can be designed for a given application, since the polymer molecular weight, composition, and microstructure can all be varied. In this Chapter, experimental observations on the effect of polymer structure on micellar solubilization are reviewed. The effect of solute hydrophobicity and size are also discussed, as is the effect of solute uptake on the micelle structure. The effect of solution conditions, such as temperature, pH and ionic strength, on the micellar properties, e.g. size and hydrophobicity of the core, are examined. Finally, theories of micelle formation and solubilization will be described, and the predictions of these theories compared to the experimental observations.

7.2 Micelle Formation in Amphiphilic Copolymer Solutions

In addition to the well studied formation of micelles in nonionic poly(ethylene oxide)-poly(propylene oxide) (PEO-PPO) and polystyrene-poly(ethylene oxide) (PS-PEO) copolymer solutions (see Chapter 1 of this Thesis), a number of investigators probed ionic copolymer solutions. Valint and Bock [1988] synthesized poly(tert-butylstyrene-b-styrene) using anionic polymerization, and then selectively sulfonated the styrene block to make the polymer water soluble with amphiphilic properties. Block copolymers and random copolymers were synthesized, with styrene-sulfonate comprising the major component of the block to ensure water solubility. Micelle formation was inferred from viscosity measurements, and the effect of solubilization of toluene on the solution viscosity also investigated. The results indicated changes in the size, shape or aggregation numbers of the micelle, but these effects were not examined in detail. Di- and tri-block copolymers of poly(methacrylic acid) and polystyrene have also been shown to form micellar aggregates in solution [Cao et al., 1991; Prochazka et al., 1992; Tuzar et al., 1991]. The solubilization of pyrene in these micelles will be discussed below. Ikemi et al. [1981; 1982] used small-angle X-ray scattering and fluorimetric measurements to examine the structure of micelles formed by poly(ethylene oxide) and poly(2-hydroxyethyl methacrylate) (PHEMA) triblock copolymers in water. Aggregates were formed at

concentrations greater than 0.1% (w/v), and fluorescence measurements indicated the formation of hydrophobic domains. The X-ray scattering data showed that there is a large interfacial boundary region between the micellar core and corona; the width of this interface decreased with a decrease in temperature.

7.3 A Survey of Solubilization Studies in Copolymer Solutions

We include here a compilation of solubilization studies in aqueous solutions of amphiphilic copolymers. The copolymer used in each study and the compound solubilized are reported in the table. Although the list is by no means comprehensive, it certainly demonstrates the applications potential amphiphilic copolymer solutions have in solubilizing molecules that are otherwise sparingly soluble in water.

Polymer	Solute	Reference
Pluronic F68	hexane	Al-Saden et al.
Pluronics L62, L63, L64, P65, F68	p-substituted acetanilides	Collett &Tobin
Pluronics F68, F88, F108	indomethacin	Lin & Kawashima
Pluronic L64	o-xylene	Tontisakis et al.
Pluronics P103, P104, P105, F108, P123 Tetronics T904, T1304, T1504, T1107, T1307	naphthalene, phenanthrene, pyrene	Hurter & Hatton
Pluronics L64, P104, F108	pyrene	Hurter et al.
Pluronics P65, F68, P84, P85 F88, P103, P104, P105, F108,	diphenylhexatriene	Alexandridis et al.

P123, F127

Pluronic L64	diazepam	Pandya et al.
Pluronic P85	fluorescein isothiocyanate, haloperidol	Kabanov et al.
PEO-PPO-PEO	cumyl hyperoxide	Topchieva et al.
PEO-PPO (70:30), 12500 M_w poly(N-vinylpyrrolidone-styrene)	benzene, toluene, o-xylene, ethylbenzene, n-hexane, n-heptane, n-octane, n-decane, cyclohexane	Nagarajan et al.
poly(N-vinylpyrrolidone-styrene)	toluene, naphthalene, phenanthrene	Haulbrook et al.
poly(sodium styrenesulfonate-co-2-vinylnaphthalene)	anthracene, perylene, 9,10-dimethylanthracene, 9,10-diphenylanthracene, 9-methylanthracene,	Nowakowska et al.
poly(sodium styrenesulfonate-co-2-vinylnaphthalene)	2-undecanone	Nowakowska et al.
poly(sodium styrenesulfonate-co-2-vinylnaphthalene)	styrene	Nowakowska & Guilliet
poly(sodium styrenesulfonate-co-9-(p-vinylphenyl)anthracene)	perylene, tetraphenylporphine 1,3-diphenylisobenzophuran	Sustar et al.
poly(styrene)-poly(methacrylic acid)	benzene	Kiserow et al.

7.4 Effect of Polymer Type and Structure on Solubilization

The solubilization of para-substituted acetanilides in a series of Pluronic PEO-PPO-PEO triblock copolymers depended on both the polymer structure and the nature of the solubilizate [Collett & Tobin, 1979]. The more hydrophobic halogenated acetanilides showed a decrease in solubility with an increase in the ethylene oxide content, whereas the opposite trend was noted with less hydrophobic drugs such as acetanilide and the hydroxy, methoxy, and ethoxy substituted compounds. The solubility of indomethacin in aqueous solutions of Pluronic copolymers was studied by Lin and Kawashima [1985]. This hydrophobic anti-inflammatory drug was solubilized in significant amounts only above a certain threshold polymer concentration, most likely related to the CMC. The polymer concentration at the transition point was found to decrease with an increase in temperature. Furthermore, the solubilizing capacity increased with polymer molecular weight, and with temperature. Approximately 0.5 moles indomethacin per mole of copolymer could be solubilized.

An extensive study on the effect of copolymer structure on the solubilization of naphthalene in a range of PEO-PPO block copolymers has been reported by Hurter and Hatton [1992]. Enhanced solubility of naphthalene in Pluronic copolymer solutions can be achieved. As the proportion of PPO in the polymer increased, at a given total polymer concentration, the solubility of naphthalene was enhanced. The partition coefficient was found constant over the entire polymer concentration range probed For the majority of the copolymers studied by Hurter and Hatton [1992]. A linear relationship between the polymer concentration and the amount of naphthalene solubilized is an indication that the micellar structure does not change significantly in this concentration range, and that increasing the polymer concentration leads to an increase in the number of micelles rather than micellar growth. The partitioning of naphthalene was found to increase with increasing molecular weight for a series of Pluronic polymers with 40% PEO [Hurter & Hatton, 1992]. The observed dependence of the partition coefficient on polymer molecular weight could not be explained by simply considering the interaction between the polymer segments forming the core and the solutes. Clearly the molecular weight of the polymer affects the micelle structure, which has an effect on the partitioning behavior of the solute.

Theoretical studies of block copolymer micelle formation have suggested that the micelle size increases with molecular weight [Leibler et al., 1983; Noolandi & Hong, 1983; Nagarajan & Ganesh, 1989]. The effect of polymer molecular weight on micelle structure has been investigated using a self-consistent mean field lattice theory, and is discussed in more detail in section 7.8.

The partition coefficients of naphthalene in the linear Pluronic copolymers with 40% PEO was compared with those for the branched Tetronic copolymers of the same PPO/PEO composition [Hurter & Hatton, 1992]. For the same PPO content and molecular weight, the Pluronic polymers have a significantly higher capacity for naphthalene than the Tetronic polymers. This indicates that all facets of the polymer architecture play a role in determining the affinity of the solute for the block copolymer; not only are the composition and molecular weight important, but also the microstructure of the polymer. The solubilization of 1,6-diphenyl-1,3,5-hexatriene (DPH), a fluorescence dye, in Pluronic copolymer micelle solutions was investigated by Alexandridis et al. [1994] (see also Section 7.10). DPH partitioned favorably in the micellar phase, with the partition coefficient higher for P123 (a Pluronic copolymer with 70% PPO), and decreasing in the order of P123 > P103 > P104 = P105 > F127 > P84 > P85 = F108 > F88 > F68 > P65. It can be concluded from these data that the solubilization was influenced form both the relative (with respect to PEO) and absolute size of the hydrophobic PPO block.

Nagarajan et al. [1986] studied the solubilization of aromatic and aliphatic hydrocarbons in solutions of poly(ethylene oxide)-poly(propylene oxide) and poly(N-vinylpyrrolidone-styrene) (PVP-PS) copolymers. A 10 wt % solution of 12500 molecular weight PEO-PPO (70:30) copolymer, and a 20% solution of poly(N-vinylpyrrolidone-styrene) (40:60) were used. For both aromatic and aliphatic hydrocarbons, more hydrocarbon was solubilized per gram of polymer in the PVP-PS copolymer than in the PEO-PPO copolymer. This was probably due to the fact that the PEO-PPO copolymer contained only 30% of the hydrophobic PPO constituent, whereas the PVP-PS copolymer contained 60% PS, and that the polystyrene is more hydrophobic than PPO. Nagarajan et al. [1986] also noted that aromatic hydrocarbons were solubilized in larger amounts than the aliphatic hydrocarbons (see also section 7.5).

Sustar et al. [1990] have synthesized poly(sodium styrenesulfonate-co-9-

vinylphenyl anthracene) copolymers (PSSS-VPA) with 10.6 - 51 wt % VPA. The polymers containing up to 40.5% VPA were water soluble. This copolymer was believed to adopt a pseudomicellar, "hyper-coiled" structure in aqueous solution, in which the hydrophobic vinylnaphthalene groups cluster in the interior of the coil and are shielded from the solvent by a shell of carboxyl groups and counterions. The solubilizing ability of the polymer was investigated using perylene and tetraphenyl porphine as probes, both of which are extremely hydrophobic, and fluoresce negligibly in water, but very efficiently in organic solvents. The hydrophobic probes were found to be solubilized in greater amounts in the polymers with a higher VPA content, since the hydrophobicity of the polymer coil increases with an increase in the VPA fraction. The amount solubilized by a given polymer was found to depend linearly on polymer concentration, and the distribution coefficient of perylene was found to increase from $2x10^5$ for a polymer with 11% VPA to $2.6x10^6$ for a polymer with 51% VPA. Nowakowska and Guillet [1991] reported on the solubilization of styrene in aqueous solutions of poly(sodium styrene-sulfonate-co-2-vinylnaphthalene) (PSSS-VN), and found that the solubility of styrene in polymer solutions depended linearly on the polymer concentration. The distribution coefficient for styrene (which has a fairly high water solubility) between polymer and water was calculated to be 10^3.

7.5 Solute Effects on Solubilization

The phase behavior of the ternary system o-xylene/PEO-PPO-PEO/water was studied by Tontisakis et al. [1990]. The polymer was Pluronic L64, with 40 wt % PEO, and a total molecular weight of 2900. The phase diagram exhibited stable regions of both oil-in-water and water-in-oil emulsions. A region of the phase diagram consisting of polymer concentrations up to 10% with small amounts of solubilized o-xylene was investigated in detail using light scattering techniques and viscosity measurements. The aggregation number of the micelles was determined as a function of temperature and the ratio of o-xylene to polymer. The addition of o-xylene resulted in micellar growth; the aggregation numbers also increased significantly with temperature. The finding that micellar growth occurs with solute uptake is in agreement with the results of Al-Saden et al. [1982], who measured the variation in the hydrodynamic radius of Pluronic micelles with hexane uptake, and found that the micelle radius increased with an increase in solubilizate uptake (saturation loading of 0.08 gr hexane / gr polymer at 35 °C for F68). This was

postulated to result not only from the incorporation of the solutes in the micellar core, but from a simultaneous increase in the aggregation number of the micelle.

The solubilization of polycyclic aromatic hydrocarbons (PAHs) in aqueous solutions of PSSS-VN copolymers has been studied by Nowakowska et al. [1989]. Distribution coefficients between the polymer pseudophase and the aqueous phase were determined for five PAHs: perylene, 9,10 dimethylanthracene, 9,10-diphenylanthracene, 9-methylanthracene and anthracene. The average number of molecules of probe solubilized by one polymer molecule ranged from 1 (for perylene) to 10 (for 9-methylanthracene) and the distribution coefficients ranged from 10^6 to 10^{10}. The more hydrophobic PAHs had higher distribution coefficients, but the number of molecules solubilized per polymer was lower, i.e. the large increase in the distribution coefficient with an increase in solute hydrophobicity was chiefly due to the decrease in the water solubility of the PAH compounds.

This is in agreement with the results of Hurter and Hatton [1992; Hurter et al., 1993] on the solubilization of three PAHs, naphthalene, phenanthrene, and pyrene, in aqueous solutions of Pluronic block copolymers. A significant increase in the solubility enhancement for the more hydrophobic PAHs was observed, as there is a strong correlation between the octanol/water partition coefficient, K_{ow}, of the solute (a standard measure of hydrophobicity), and the micelle-water partition coefficient. Similar relationships have been found for micelle/water partition coefficients of various hydrophobic solutes in commercial surfactants such as Triton X-100 (an octylphenol polyoxyethylene surfactant) [Edwards et al., 1991], and sodium dodecyl sulfate [Valsaraj & Thibodeaux, 1989]. While the partition coefficient increased with the hydrophobicity of the solute, the concentration of solute in the micelle remained of the same order of magnitude (in fact it decreased slightly with an increase in hydrophobicity) and the dramatic increase in the partition coefficient was chiefly due to the decrease in PAH water solubility

Nagarajan et al. [1986] found that the solubilization of aliphatic hydrocarbons in copolymer micelles was negligible in comparison to that of aromatics. A Flory-Huggins type interaction parameter between the solubilizate and the polymer block constituting the core, χ_{sc}, was estimated using Hildebrand-Scatchard solubility parameters. It was found that the aromatic hydrocarbons, which had smaller values of χ_{sc}, were solubilized to a

greater extent than the aliphatic molecules, which had larger values of χ_{sc}. However there was not a direct correlation between χ_{sc} and the amount solubilized, particularly for the aliphatic molecules which had large χ_{sc} values. For binary mixtures of benzene and hexane, it was shown that the micelles selectively solubilized the aromatic benzene.

7.6 Temperature Effects on Solubilization

Experimental results suggested that raising the temperature of the solution could induce micelle formation in polymers that are relatively hydrophilic, either due to their low molecular weight or to a high PEO content [Alexandridis & Hatton, 1994]. The phase diagrams of both ethylene oxide and propylene oxide in water exhibit a lower critical solution temperature [Malcolm & Rowlinson, 1957], indicating that raising the temperature causes water to become a poorer solvent for these polymers. The decreased solubility of ethylene oxide could be due to the breaking of hydrogen bonds between the ether oxygen and water, or to conformational changes in the ethylene oxide chain structure as temperature is increased [Karlstrom, 1985; Samii et al., 1991]. Thus, while these hydrophobic polymers might not aggregate at room temperatures, an increase in the temperature could induce aggregation as water becomes a poorer solvent. The formation of micelles should lead to enhanced solubilization, resulting from the hydrophobic environment afforded by the micelle core, which is attractive to organic solutes such as naphthalene. These observations indicate that solution temperature could have a significant effect on solubilization.

Tontisakis et al. [1990] studied the solubilization of o-xylene in an aqueous solution of L64. The aggregation number of the micelles was determined as a function of temperature, and of the o-xylene/polymer ratio. The addition of o-xylene resulted in micellar growth, and the aggregation numbers also increased significantly with temperature. For the pure polymer in water, the aggregation number increased from 14 to 90 as the temperature was increased from 30 °C to 42 °C. Similar increases in the aggregation number with temperature were observed for the copolymer systems with solubilized o-xylene. While the aggregation number increased monotonically with temperature, the hydrodynamic radius of the micelle initially decreased, passed through a minimum, and then increased with further increase in temperature [Tontisakis et al., 1990].

This was attributed to exclusion of water from the micelle, as water became a poorer solvent for both PEO and PPO at higher temperatures. As temperature was raised even further, a point was reached where effectively all the water was excluded from the micelle; since the micelle aggregation number continued to increase, the micelle radius started increasing.

In section 7.4, it was reported that P104 significantly enhanced the solubility of naphthalene in water at 25 °C, and that the micelle-water partition coefficient was not dependent on polymer concentration. The light scattering results of Wanka et al. [1990] indicate that P104 forms micelles with an aggregation number of around 50 at 25 °C. In Figure 7.1, the solubilization of naphthalene as a function of temperature is compared for 10% solutions of Pluronics P104, L64 and F108 [Hurter, 1992]. The solubility of naphthalene in both F108 and P104 appears to increase rapidly at first, and then above a transition temperature of 21 °C for P104 and 26 °C for F108, the solubility enhancement with temperature becomes less significant. It can be shown that the solubility enhancement at higher temperatures is chiefly due to the increase in the naphthalene water solubility; the normalized naphthalene concentration becomes independent of temperature above the transition point. The results for L64 show a monotonic increase in solubility with temperature. It is possible that the saturation phenomenon would occur at a higher temperature than that investigated, but the solution of L64 became turbid above 41.5 °C. Similar trends were observed in the solubilization of 1,6-diphenyl-1,3,5-hexatriene in various Pluronic copolymer solutions [Alexandridis et al., 1994].

The results in Figure 7.1 for Pluronics P104 and F108 seem to indicate that the micelles become saturated with naphthalene at higher temperatures. It is possible that for P104 and F108, micellar growth occurs up to the transition temperature, and that above this temperature the micelle size no longer increases, resulting in no further increase in the partition coefficient between the micelles and water. McDonald and Wong [1974] showed that the aggregation number of L64 aggregates was unity at 24 °C, 5.9 at 30 °C, and 29.9 at 35 °C, i.e. that micellar growth occurs with an increase in temperature. An alternative explanation, or contributing factor, could be that the hydrophobicity of the micellar core (or the polymer coil, in the case of unimolecular "micelles") increases with an increase in temperature. Al-Saden et al. [1982] measured the hydrodynamic radius of L64 aggregates in an 8% solution as a function of temperature, and found that the radius initially decreased,

and then increased above 40 °C. They suggested that as temperature was increased, the polymer chains contract, squeezing out water, as the latter became a poorer solvent for both PEO and PPO. As the temperature approaches the cloud point, no more contraction is possible (if effectively all the water has already been excluded) and the increase in aggregation leads to an increase in the hydrodynamic radius. The transition temperature observed for P104 and F108 could be the temperature at which the micelle has become as hydrophobic as possible, owing to the exclusion of virtually all water from the core. Raising the temperature further cannot significantly alter the hydrophobicity of the core, so that the normalized naphthalene concentration no longer increases with temperature. The transition temperature for L64 would be approximately 41 °C, which is above the range of these experiments, so that the saturation phenomenon was not fully observed, though Figure 7.1 does show that the increase in solubility with temperature becomes less pronounced above 35 °C.

7.7 Effect of Solution Ionic Strength and pH on Solubilization

Amphiphilic block copolymers with a polyelectrolyte comprising the hydrophilic portion can also be effective at solubilizing organic molecules. Since polyelectrolytes have a high affinity for water, highly nonpolar polymers, such as polystyrene, can be used for the hydrophobic block in larger proportions, while still maintaining water solubility. The chain conformation of the polyelectrolyte constituent of the copolymer is obviously strongly affected by factors such as the ionic strength and pH of the solution, which leads to some interesting effects on the micelle structure, and on the solubilization behavior.

Kiserow et al. [1992] have synthesized diblock copolymers of polystyrene (PS) and polymethacrylic acid (PMAA), and studied the solubilization of benzene in aqueous micellar solutions of these polymers. The polymers had molecular weights from 45 000 to 70 000 and molar fraction of PS varying from 46 to 60%. The micelle aggregation numbers ranged from 53 to 290. While most of the benzene was solubilized within the PS core of the micelle, some benzene was solubilized in hydrophobic domains in the shell, particularly at low pH where hydrophobic hypercoiling of the MAA occurred. At high pH, the PMAA segments are ionized, resulting in an extended shell region and a more stable micelle. In fact, viscosity measurements indicated that the mutual repulsion of these highly

charged micelles resulted in some structural organization in the micellar solution. The solubilization of benzene was found to increase with increasing pH, with mass ratios of benzene to PS of up to 5:1 being obtained in these systems.

Nowakowska et al. [1989] have synthesized a high molecular weight random copolymer of poly(sodium styrenesulfonate) and poly(2-vinylnaphthalene) (PSSS-PVN) and studied the conformation of this polymer in water. The polymer had a molecular weight of 310 000, and contained 60 mol % of the hydrophobic PVN. In aqueous solution these polymers adopt a pseudomicellar, "hypercoiled" structure. It has been shown [Nowakowska et al., 1990] that 2-undecanone is effectively solubilized in aqueous solutions of PSSS-PVN. The distribution coefficient was maximized at neutral pH and at high ionic strength, where the coil was determined to be in a more expanded form. This is in contrast to the solubilization behavior observed using more hydrophobic solutes such as PAHs [Hurter & Hatton, 1992], which favor a more compact coil conformation, as will be discussed below.

Photochemical reactions of PAHs solubilized in aqueous solutions of these PSSS-PVN copolymers have been studied by Nowakowska et al. [1989]; the effect of polymer composition, pH and ionic strength on the solubilization behavior has also been investigated. Perylene was found to be solubilized more effectively in polymers with a lower number of sulfonate groups. The decrease in repulsive interactions in the coil resulted in a more compact conformation, which probably led to a more hydrophobic environment, and consequently favored solubilization of PAHs. Similarly, maximum solubilization occurred at acidic and alkaline pH, where the coil is most compact. With an increase in the ionic strength, solubilization was initially enhanced, however at higher ionic strengths the amount solubilized decreased. Sustar et al. [1990] investigated the solubilization of tetraphenyl porphine in poly(sodium styrenesulfonate-co-9-vinylphenyl)anthracene copolymers (PSSS-VPA) as a function of ionic strength. The results were similar to those obtained for PSSS-VN, with the solubilization increasing up to an ionic strength of 0.5, and then decreasing at higher ionic strengths. It was suggested that the extremely compact conformation formed at high ionic strengths limited the number of molecules that could be solubilized.

7.8 Modelling of Solubilization in Block Copolymer Micelles

Theories of micelle formation in solutions of block copolymers have been advanced by a number of researchers over the past decade. Leibler et al. [1983], Noolandi and Hong [1983], Munch and Gast [1988], and Nagarajan and Ganesh [1989] computed the free energy of micelle formation assuming uniform copolymer concentrations in the core and corona regions, respectively. Scaling theories for polymeric micelles with an insoluble core and an extended corona were developed by Halperin [1987], Marques et al. [1988], Semenov [1985], and Zhulina and Birsthein [1986]. In a third approach, Van Lent and Scheutjens [1989] used a self-consistent field theory to determine the detailed segment density profiles within a micelle, making no a priori assumptions as to the locations of the micellar components. The micelle structures determined from this model have been confirmed recently by Monte Carlo simulations [Wang et al., 1993] and show that the interfacial region between the core and corona of the micelle is diffuse, and not sharp as is assumed in the other modelling approaches.

7.8a Phenomenological theory of solubilization in block copolymer micelles

Nagarajan and Ganesh [1989] extended their theory of micellization to describe solubilization in A-B diblock copolymer micelles. A spherical micelle was assumed, with a core consisting of solvent-incompatible A-blocks and solute, and a corona which contained solvent and the solvent-compatible B-blocks. No allowance was made for solute molecules in the corona of the micelle, which lead trivially to their conclusion that "almost all" of the solute was confined to the core. Constant compositions of all components were assumed in both the core and the corona. The interfacial free energy was related to the interfacial tension between the core components and water, assuming a sharp interface between them, and neglecting the presence of the B-blocks in the corona. The total free energy of solubilization was assumed to be due to contributions from the change in the state of dilution and deformation of the A blocks in the core, and of B blocks in the corona, the localization of the joints between the blocks at the interface, and the free energy of the core-corona interface.

On the basis of this free energy model, the CMCs, the size and composition

distribution of the micelles containing solubilizates, the aggregation number of the micelles, the maximum extent of solubilization and the core radius and the shell thickness of the micelles, were able to be predicted. Illustrative calculations showed that, in general, the micelles were practically monodispersed both in their size and in the extent of solubilization. The solubilization behavior of the micelles and their geometrical characteristics were found to be influenced significantly by the interactions between the solubilizate and the solvent-incompatible A-block of the copolymer as well as by the solubilzate-solvent interfacial tension. The various free energy contributions were analyzed as a function of the volume fraction of the solubilizate in the micelle core. The (negative) free energy contribution provided by the change in state of dilution of block A decreased with an increase in the volume fraction of the solubilizate, thus favoring the uptake of the solubilizate within the micelle. The magnitude of this contribution was larger if the solubilizate - core block interaction parameter χ_{AJ} was lower and if the molecular size of the solubilizate was smaller. The free energy contributions arising from the deformation of block A and the core - solvent interfacial energy restricted the swelling of the micellar core by the solubilizate, and, consequently, the extent of solubilization. The increase in the positive interfacial free energy accompanying the uptake of solubilizates by the micelles was also dependent on the solubilizate-solvent interfacial tension σ_{SJ}; the micellar capacity would be larger for solubilizates with lower σ_{SJ}. The micellar structural parameters were affected also by the interactions between the solvent S and the solvent-compatible B block of the copolymer though to a lower degree when compared to the corresponding solubilizate-free systems. The solubilization process was found to decrease the CMC and increase the micellar core radius substantially. The larger the solubilization capacity, the more significant are the changes in the radius and CMC. The increase in the core radius resultsed not only from the incorporation of the solubilizate but also because of the increasing number of block copolymer molecules that are accommodated within the micelle. The ratio of shell thickness to micelle radius was found to decrease with increasing solubilization capacity of the micelles, while the shell thickness was not very much affected by solubilization.

The predictions of this theory have been compared against the earlier experimental data of Nagarajan and coworkers [1986] on the solubilization of hydrocarbons in aqueous solutions of diblock copolymers. These measurements suggested that the extent of solubilization was dependent on the nature of interactions between the solubilizate and the

block that constitutes the core of the micelle. More interestingly, the measurements revealed unusual selectivity in the solubilization behavior when mixtures of hydrocarbons were solubilized; aromatic molecules were found to be solubilized preferentially compared to aliphatic hydrocarbons. In general, the agreement between the experimental and theoretically predicted values of solubilization capacities was satisfactory for all solubilizates studied (aromatic hydrocarbons and straight chain alkanes). Generalized scaling relations have also been developed that explicitly relate the micelle core radius, the shell thickness, and the volume fraction of the solubilizate within the micelle core to the molecular features of the copolymer, the solvent, and the solubilizate. The domain of the existence of spherical micelles (on the basis of the Nagarajan and Ganesh theory) for the system PEO-PPO copolymer (M_w: 12 500, 50% PEO) - water - benzene was determined. The theory predicted micelles forming in benzene for up to 20% water (with respect to benzene-water mixture) and micelles forming in water for up to 5% benzene (with respect to benzene-water mixture). The effect of temperature on micelle size, structure, and solubilization (very important for copolymers containing PEO) was not considered in the theory of Nagarajan and Ganesh.

7.8b Self-consistent mean-field lattice theory of solubilization in block copolymer micelles

Another approach in modelling block copolymer micelles has been through the Scheutjens-Fleer theory, an extension of the Flory-Huggins analysis of homogeneous polymer solutions [Flory, 1953], in which the polymer chains are allowed to assume different conformations on a lattice. In the Flory-Huggins analysis, a first-order Markov approximation is used, so that the position of a segment depends only on that of the preceding segment in the chain, the result being that the chain conformation follows the path of a random walk. In addition, a mean field assumption is invoked to describe the interactions between unlike segments. The free energy of the system is minimized in order to calculate the equilibrium thermodynamic properties of the polymer solution. For spatially inhomogeneous systems such as those containing interfaces, Scheutjens and coworkers [Scheutjens & Fleer, 1979; van Lent & Scheutjens, 1989; Leermakers et al., 1989] restricted the mean field approximation to two dimensions, i.e., within parallel or concentric lattice layers, and applied a step-weighted random walk to account for the inhomogeneities normal to the layers. The polymer and solvent molecules are assumed to

be distributed over a lattice, such that solvent molecules and polymer segments occupy one lattice site each. Each polymer chain can assume a large number of possible conformations, defined by the layer numbers in which successive segments are found. There can be many different arrangements for each conformation; If the number of polymer chains in each conformation is specified, the configurational entropy contribution to the system free energy can be evaluated, the other contributions to this free energy being due to the interactions between the polymer molecules, solvent molecules and the surface, which are characterized by Flory-Huggins χ-parameters. If the free energy of the system is minimized with respect to the number of polymer chains in each conformation, it is possible to calculate the equilibrium segment density profiles.

The self-consistent field theory can be used to calculate the segment density profiles in a micelle once the aggregation number of the micelle is known [van Lent & Scheutjens, 1989; Leermakers et al., 1989; Leermakers & Scheutjens, 1989]. To find this aggregation number, small system thermodynamics can be used [Hall & Pethica, 1967; Hill, 1963; Hill, 1964], in which the change in the free energy due to the change in the number of micelles (at constant temperature, pressure and number of molecules) must be zero at equilibrium. This "excess free energy" is the sum of the energy required to create micelles, and the energy due to the translational entropy of the micelles. Since the segment density profiles are required in order to calculate the energy of micelle formation, an iterative process is required.

The self-consistent mean field lattice theory of Scheutjens and Fleer [1979] has been used to study many colloidal systems, including homopolymer and block copolymer adsorption on surfaces [Evers et al., 1990], interactions between adsorbed polymer layers [Scheutjens & Fleer, 1985] and the formation of micelles [Leermakers et al., 1989], vesicles [Leermakers & Scheutjens, 1989] and membranes [Scheutjens et al. 1989]. For aggregation structures, the detailed segment density profiles are obtained, and macroscopic quantities such as critical micelle concentration, aggregation number and micelle size can be calculated. Cogan et al. [1992] applied the Scheutjens and Fleer theory to describe spherical block copolymer micelles in the presence of two solvents, each selective for one of the blocks. In particular, they performed calculations describing their earlier experimental results of PEO-PS block copolymers in cyclopentane with trace amounts of water. The size of the core block (in their case PEO) was found to dominate the micelle

solubilization capacity. However the coronal block size can be an important factor if the size change is large enough to significantly modify the copolymer symmetry [Cogan et al., 1992].

Recently, the Scheutjens and Fleer theory has been extended to study the formation of micelles by linear and branched, star-like amphiphilic block copolymers, and the solubilization of naphthalene in these micelles has been analyzed as a function of polymer structure, composition and molecular weight [Hurter et al., 1993]. The micellar solubilization of PAHs was investigated, by modelling the PAHs as chains of benzene molecules. The segment density profiles for naphthalene solubilized within a micelle formed by P104 showed the naphthalene to be confined mainly to the micelle core. The theory reproduced the experimental finding of a strong correlation between the PPO content of the polymer and the micelle/water partition coefficient, K_{mw}. The effect of molecular weight on solubilization was reproduced qualitatively by the theory, but the experimental results showed a far larger dependence of K_{mw} on polymer size. The theoretical predictions showed that, for both the Pluronic and Tetronic molecules, the PPO content of the polymer has a strong effect on the micelle-water partition coefficient, in agreement with experiments. The theory also confirmed the experimental finding that naphthalene partitions more favorably into the linear Pluronic polymers than into the branched Tetronic molecules. The Tetronic molecules form micelles with a lower concentration of PPO in the core, resulting in a less hydrophobic core environment, which would inhibit naphthalene solubilization. In addition, the Tetronic molecules formed smaller micelles, which would result in a lower micelle-water partition coefficient, as discussed above.

7.8c Lattice Theory for Monomers with Internal Degrees of Freedom

The simple lattice theory for flexible chain molecules outlined in Section 7.8b cannot capture effects such as the phase behavior of PEO and PPO in water, where a lower critical solution temperature is observed. To predict such behavior, the gauche and trans bond orientations of the polymer chain must be accounted for. Leermakers [1988] used the rotational isomeric state scheme, which accounts for the gauche-trans orientations in a chain, and eliminates backfolding, combined with the self-consistent field theory, to predict the formation of lipid bilayer membranes and lipid vesicles. An approach which is computationally more simple than the rotational isomeric state scheme, but which accounts

for the temperature and composition dependence of the interaction parameter χ in a physically acceptable manner, has recently been presented by Karlstrom [1985]. This model recognized that certain sequences of the gauche-trans orientations in a EO monomer would lead to a polar conformation, while others will be essentially nonpolar, and was successful in reproducing the solubility gap in PEO-water and PPO-water phase diagrams.

A model for solubilization in block copolymer micelles has been developed [Hurter et al., 1993], which incorporated Karlstrom's ideas to account for the conformational distribution in PEO and PPO. Using this model, the effect of temperature and the solubilization of naphthalene on the micelle structure have been investigated, and the results compared to experimental observations. An increase in temperature caused the model-predicted micelle aggregation number to increase, and the CMC to decrease. The conformation of the polymer was affected by both the temperature and the composition of the surrounding solution; both PEO and PPO had a lower fraction of polar segments in the core of the micelles, and the polar fraction decreased with an increase in temperature. The micelle aggregation number was found to increase with an increase in the solute bulk concentration; in agreement with the experimental results of Al-Saden et al. [1982].

The presence of free (unmicellized) polymer in the bulk solution enhanced the solubility of naphthalene in this region, indicating that the copolymer associated with the naphthalene to some degree [Hurter et al., 1993]. The polymer bulk (unmicellized) concentration decreases with increasing solute concentration, probably because the addition of a hydrophobic solute increases the aggregating tendencies of the polymer, resulting in a higher aggregation number, and a lower concentration of polymer in the bulk solution. The fact that the polymer bulk concentration changed with solute concentration was one of the contributing factors leading to the nonlinear relationship between the overall solute concentration, and the equilibrium concentration of naphthalene in water. This nonlinear relationship indicates that the partition coefficient between water and the micelles changes with the solute concentration, and aspect of the problem that has yet to be investigated experimentally. Again, the theory reproduced the experimental finding that there is a strong correlation between the PPO content of the polymer and its propensity to solubilize naphthalene, although it overpredicts the magnitude of the PPO effect.

7.8d Effect of copolymer molecular weight on solubilization

It was shown experimentally that the molecular weight of the polymer has a significant effect on the partitioning behavior of naphthalene in Pluronic and Tetronic polymers. The lattice theory for flexible chain molecules [Hurter et al., 1993b] significantly underpredicted the magnitude of the molecular weight effect. The modified lattice theory [Hurter et al., 1993a] improved upon this prediction. In addition to showing that naphthalene solubilization increases with polymer molecular weight, the theory was able to reproduce the nonlinear relationship between the naphthalene solubilized and the polymer concentration for low molecular weight polymers, observed experimentally in both Pluronic and Tetronic polymers. An analysis of the theoretical results shows that the polymer bulk concentration is not constant for the low molecular weight polymers. The bulk polymer concentration was higher for lower molecular weight polymers, which meant less of the polymer aggregating to form micelles and less naphthalene solubilized, thus providing a partial explanation for the molecular weight effect.

7.9 Conclusions

The solubilization of hydrophobic solutes in block copolymer micelles depends strongly on the structure of the micelle-forming polymers, whether they are linear or branched, the chemical nature of the constituents, and on the hydrophobic to hydrophilic balance in the copolymer. Linear triblock copolymers are more accommodating than branched polymers, which is attributed to their ability to form tighter micelles. It is believed that the configurational constraints on branched polymers in micellar solutions leads to the formation of looser aggregates which do not provide as apolar an environment in the core as found in the case of the linear copolymers. As could be expected, the partitioning of hydrophobic solutes to the micelles is enhanced as the hydrophobic content of the block copolymers increases. Polymer molecular weight is important, with higher molecular weight polymers forming larger micelles, and having a higher solubilizing capacity. The partitioning behavior also correlates well with the octanol-water partition coefficient of the solute, K_{ow}. Varying solution conditions such as ionic strength, pH and temperature all have a signigicant effect on the micelle structure, and consequently affect the solubilization behavior.

A self-consistent field theory [Hurter et al., 1993] was able to elucidate the solubilization behavior of hydrophobic solutes in block copolymer micelles, by providing detailed information on the microstructure of the micelles formed by linear and branched copolymers. The calculations showed qualitative agreement with experimental predictions on the effect of hydrophobicity and molecular weight of the polymer, and quantitative agreement was remarkably good considering that all parameters were obtained from independent experiments. Modifying the simple lattice theory for flexible chain molecules to allow for polar and nonpolar conformations of the PEO and PPO chains [Hurter et al., 1993a] enables the theory to successfully reproduce the anomalous phase behavior of these polymers, and improves the ability of the theory to predict more subtle effects such as the molecular weight dependence of naphthalene solubilization in block copolymer micelles.

The theory shows that, as the temperature is increased, the fraction of segments in the nonpolar conformation increases, thus increasing the hydrophobicity of the polymer and creating an environment which is attractive to organic solutes. This is in agreement with the experimental results, which show an increase in solubilization of naphthalene with temperature. Comparing the segment density profiles of naphthalene-saturated micelles formed by block copolymers of differing composition shows that the micelle structure is strongly dependent on the composition of the polymer. Polymers with a higher proportion of the hydrophilic block, PEO, tend to form smaller micelles, with a lower concentration of PPO and a higher concentration of water in the core, which results in less naphthalene being solubilized. The amount of naphthalene solubilized is thus not simply dependent on the amount of PPO in the solution, but depends on the polymer structure and composition. Similarly, polymers of low molecular weight form micelles with a less hydrophobic core environment, and are not as efficient at solubilizing naphthalene.

These interesting results on solubilization in block copolymer micelles show that the solubilization is affected by the detailed microstructure of the aggregates, which in turn depends on both polymer and solute structure, and solution conditions. This allows a great deal of flexibility in designing novel solvents which can be used as extractants and solubilizers in a variety of pharmaceutical, biological and industrial applications.

7.10 Appendix: Partitioning of 1,6-diphenyl-1,3,5-hexatriene in PEO-PPO-PEO Micelles: Effect of Temperature and Polymer Composition

A measure of the effectiveness of a particular surfactant in solubilizing a given hydrophobic molecule is the Molar Solubilization Ratio (MSR), defined as the number of moles of hydrophobic compound solubilized per mole of surfactant added to solution [Edwards et al., 1991]. In the presence of excess hydrophobic compound, the MSR can be obtained from the slope of the curve that results when the solubilizate concentration is plotted against surfactant concentration. The MSR can be calculated as follows:

$$MSR = (S_{mic} - S_{cmc}) / (C_{surf} - CMC) \quad (A.1)$$

where S_{cmc} is the apparent solubility of a hydrophobic compound (expressed in mol/L) at the CMC, S_{mic} is the total apparent solubility of the hydrophobic compound in a micellar solution at a particular surfactant concentration greater than CMC, and C_{surf} is the surfactant concentration at which S_{mic} is evaluated.

An alternative approach in quantifying solubilization is based on characterizing the partitioning of the hydrophobic compound between micelles and unimer solution with a mole-fraction micelle-phase / aqueous-phase partition coefficient, K_m, defined as the ratio of the mole fraction of the compound in the micellar pseudophase, X_m, to the mole fraction of the compound in the aqueous phase, X_a. The mole fraction of the hydrophobic compound in the micellar pseudophase, X_m, can be calculated as

$$X_m = (S_{mic} - S_{cmc}) / (C_{surf} - CMC + S_{mic} - S_{cmc}) \quad (A.2)$$

or in terms of the MSR, as

$$X_m = MSR / (1 + MSR) \quad (A.3)$$

The mole fraction of the hydrophobic compound in the aqueous phase, X_a, is approximated for dilute solutions by $X_a = S_{cmc} V_m$, where V_m is the molar volume of water (L/mol). An

expression for K_m is thus

$$K_m = (S_{mic} - S_{cmc}) / \{ (C_{surf} - CMC + S_{mic} - S_{cmc}) (S_{cmc} V_m) \} \quad (A.4)$$

or

$$K_m = MSR / \{ (1 + MSR) (S_{cmc} V_m) \} \quad (A.5)$$

Solubilization of 1,6-diphenyl-1,3,5-hexatriene was used for the determinatcn of the onset of micelle formation in PEO-PPO-PEO copolymers present in aqueous solutions (see Chapter 2 of this Thesis). In the course of these experiments, the absorption intensity of the solution (due to DPH) was recorded as a function of temperature and copolymer concentration, allowing the MSR for solubilization of DPH in PEO-PPO-PEO micelles to be determined from plots of optical absorption intensity at 356 nm (proportional to the DPH concentration) vs the copolymer concentration. The partition coefficient was subsequently calculated from Equation A.5. Micelle/water partition coefficients for DPH in PEO-PPO-PEO micelles are presented for a number of copolymers in Figure 7.2, plotted as a function of inverse temperature. DPH partitioned favorably in the micellar phase, with the partition coefficient higher for Pluronic P123 (a PEO-PPO-PEO copolymer with 70% PPO), and decreasing in the order of P123 > P103 > P104 = P105 > F127 > P84 > P85 = F108 > F88 > F68 > P65 (see Chapter 2 of this Thesis for molecular weights and composition of these copolymers). It can be concluded from these data that the solubilization was influenced by both the relative (with respect to PEO) and absolute size of the hydrophobic PPO block.

The standard free energy of partitioning, ΔG°_{part}, can be obtained from the partition coefficient through the relationship: $\Delta G^\circ_{part} = - RT \ln K_m$, [Katz & Diamond, 1974] where R is the gas law constant and T the absolute temperature. The enthalpy and entropy of partitioning are related to the partition coefficient through the following expression [Katz & Diamond, 1974]:

$$\ln K_m = - \Delta G^\circ_{part} / RT = - \Delta H^\circ_{part} / RT + \Delta S^\circ_{part} / R \quad (A.6)$$

Equation A.6 indicates that a graph of lnK against 1/T should give a straight line with a slope of $- \Delta H^\circ_{part} / R$ and intercept on the ordinate of $\Delta S^\circ_{part} / R$. The only assumption involved in fitting a straight line through the experimental points is that ΔH°_{part} may be

considered independent of temperature, over the temperature range considered [Katz & Diamond, 1974]. The enthalpy of partitioning values for DPH in various copolymer micelles were obtained from the partition coefficient data shown in Figure 7.2. Note that ΔH°_{part} is positive (endothermic) and the partitioning of DPH in the micelles is driven by entropy, just like in the micellization phenomenon (see Chapter 2 of this Thesis).

The lnK data are linear with respect to 1/T for most copolymers; for the most hydrophobic copolymers, there appears to be a change in slope (enthalpy) in the lnK vs 1/T data at ~ 35 °C, reminiscent of phase transitions observed in phospholipid membranes [Katz & Diamond, 1974]. It is not clear at this time whether there is a change ("phase transition") in the micelle core, or whether the partition coefficient depends on the total copolymer concentration (the copolymer concentrations used to measure the MSR were lower at the higher temperatures). The ΔH°_{part} values discussed here were obtained before the break (at 35 °C) in the lnK vs 1/T curve. The change in slope of the lnK vs temperature curve (seen in Figure 7.2) is reminiscent of the results of Hurter [Hurter, 1992; Hurter et al., 1993] for partitioning of naphthalene in Pluronic P104 and F108 copolymer micelle (see, e.g., Figure 7.1). for Pluronics P104 and F108 seem to indicate that the micelles become saturated with naphthalene at higher temperatures. This behavior was attributed to either halting of micellar growth or to the exclusion of virtually all water from the core at the transition temperature. Raising the temperature further cannot significantly alter the size or hydrophobicity of the core, so that the normalized naphthalene concentration no longer increased with temperature.

ΔH°_{part} values (expressed as kJ per mol DPH) are presented in Figure 7.3a, plotted as a function of copolymer molecular weight. ΔH°_{part} increases with increasing molecular weight for groups of Pluronics that have the same PPO/PEO composition (P84-P104, P65-P85-P105, F68-F108). The highest ΔH°_{part} values were observed for the relatively hydrophobic Pluronics P104 and P105. Since DPH partitions in the hydrophobic PPO core of the micelles, we also considered appropriate to examine ΔH°_{part} with respect to the size of the PPO block in the copolymers. Enthalpy of partitioning values for DPH in PEO-PPO-PEO micelles are presented in Figure 7.3b, plotted as a function of the number of PO segments, N_{PO} in the copolymer. When plotted in this manner, the ΔH°_{part} values appear to fall on the same line for all copolymer studied here. ΔH°_{part} increases with increasing

N_{PO}, however, ΔH°_{part} normalized with respect to N_{PO} decreases with increasing N_{PO}. The effects of PPO and PEO block sizes on the enthalpy of partitioning are also shown in Figure 7.4, where ΔH°_{part} values are plotted as a function of the copolymer PPO/PEO composition. ΔH°_{part} is higher for groups of Pluronics with larger PPO block (i.e., P103-P104-P105-F108), and appears to increase with decreasing PEO block size for groups of copolymers with the same size PPO block. Finally, a good correlation can be seen between enthalpy of partitioning for DPH in PEO-PPO-PEO micelles and the enthalpy of micellization for PEO-PPO-PEO copolymers in aqueous solutions (Figure 7.5). This is an interesting result, and it is probably a manifestation a driving force (entropy on the water side) which is the same in both solubilization and micellization phenomena.

7.11 References cited in Chapter 7

1. Alexandridis, P.; Hatton, T. A. *Colloids Surfaces A* **1994**, submitted for publication; Chapter 1 of this Thesis
2. Alexandridis P.; Holzwarth, J. F.; Hatton, T. A. Manuscript in preparation, 1994.
3. Al-Saden, A. A.; Whateley, T. L.; Florence, A. T. *J. Colloid Interface Sci.* **1982**, *90*, 303.
4. Cao, T.; Munk, P.; Ramireddy, C.; Tuzar, Z.; Webber, S. E. *Macromolecules* **1991**, *24*, 6300.
5. Cogan, K. A.; Leermakers, F. A. M.; Gast, A. P. *Langmuir* **1992**, *8*, 429.
6. Collett, J. H.; Tobin, E. A. *J. Pharm. Pharmacol.* **1979**, *31*, 174.
7. Edwards, D. A.; Luthy, R. G.; Liu, Z. *Environ. Sci. Technol.* **1991**, *25*, 127.
8. Evers, O. A.; Scheutjens, J. M. H. M.; Fleer, G. J. *Macromolecules* **1990**, *23*, 5221.
9. Flory, P. *Principles of Polymer Chemistry*; Cornell University : Ithaca, NY, 1953.
10. Hall, D. G.; Pethica, B. A., Chapter 16 in *Nonionic Surfactants*, Schick, M. J. (Ed.), Marcel Dekker, 1967.
11. Halperin, A. *Macromolecules* **1987**, *20*, 2943.
12. Hill, T. L. *Thermodynamics of Small Systems, Vol. 1*, Benjamin, 1963.
13. Hill, T. L. *Thermodynamics of Small Systems, Vol. 2*, Benjamin, 1964.
14. Haulbrook, W. R.; Feerer, J. L.; Hatton, T. A.; Tester, J. W. *Environ. Sci. Technol.* **1993**, *27*, 2783.

15. Hurter, P. N. *Ph.D. Thesis*, Massachusetts Institute of Technology, Cambridge, MA, 1992.
16. Hurter, P. N.; Hatton, T. A. *Langmuir* **1992**, *8*, 1291.
17. Hurter, P. N.; Anger, L. A.; Vojdovich, L. J., Kelley, C. A.; Cohen, R. E.; Hatton, T. A. in *Solvent Extraction in the Process Industries*; Logsdail, D. H., Slater, M. J., Eds., Elsevier Applied Science: London, 1993, Vol. 3, p 1663.
18. Hurter, P. N.; Scheutjens, J. M. H. M.; Hatton, T. A. *Macromolecules* **1993**, *26*, 5592.
19. Hurter, P. N.; Scheutjens, J. M. H. M.; Hatton, T. A. *Macromolecules* **1993**, *26*, 5030.
20. Ikemi, M.; Odagiri, N.; Tanaka, S.; Shinohara, I.; Chiba, A. *Macromolecules* **1981**, *14*, 34.
21. Ikemi, M.; Odagiri, N.; Tanaka, S.; Shinohara, I.; Chiba, A. *Macromolecules* **1982**, *15*, 281.
22. Kabanov, A. V.; Batrakova, E. V.; Melik-Nubarov, N. S.; Fedoseev, N. A.; Dorodnich, T. Yu.; Alakhov, V. Yu.; Chekhonin, V. P.; Nazalova, I. R.; Kabanov, V. A. *J. Controlled Rele. se* **1992**, *22*, 141.
23. Karlstrom, G. *J. Phys. Chem.* **1985**, *89*, 4962.
24. Kiserow, D.; Prochazka, K.; Ramireddy, C.; Tuzar, Z.; Munk, P.; Webber, S. E. *Macromolecules* **1992**, *25*, 461.
25. Katz, Y.; Diamond, J. M. *J. Membrane Biol.* **1974**, *17*, 101.
26. Leermakers, F. A. M. *Ph.D. Thesis*, Wagenigen Agricultural University, Wagenigen, 1988.
27. Leermakers, F. A. M.; van der Schoot, P. P. A. M.; Scheutjens, J. M. H. M.; Lyklema, J. in *The Equilibrium Structure of Micelles* Mittal, K. L. (Ed.), Plenum, 1989.
28. Leermakers, F. A. M.; Scheutjens, J. M. H. M. *J. Phys. Chem.* **1989**, *93*, 7417.
29. Leibler, L.; Orland, H.; Wheeler, J.C. *J. Chem. Phys.* **1983**, *79*, 3550
30. Lin, S.-Y.; Kawashima, Y. *Pharm. Acta Helv.* **1985**, *60*, 339.
31. Malcolm, G. N.; Rowlinson, J. S. *Trans. Faraday Soc.* **1957**, *53*, 921.
32. Marques, C. M. *Macromolecules* **1988**, *21*, 1051.
33. McDonald, C.; Wong, C. K. *J. Pharm. Pharmac.* **1974**, *26*, 556.
34. Munch, M. R.; Gast, A. P. *Macromolecules* **1988**, *21*, 1360.
35. Nowakowska, M.; White, B.; Guillet, J. E. *Macromolecules* **1988**, *21*, 3430.

36. Nagarajan, R.; Barry, M.; Ruckenstein, E. *Langmuir* **1986**, *2*, 210.
37. Nagarajan, R.; Ganesh, K. *J. Chem. Phys.* **1989**, *90*, 5843.
38. Nagarajan, R.; Ganesh, K. *Macromolecules* **1989**, *22*, 4312.
39. Noolandi, J.; Hong, K. M. *Macromolecules* **1983**, *16*, 1443.
40. Nowakowska, M.; White, B.; Guillet, J. E. *Macromolecules* **1989**, *22*, 2317.
41. Nowakowska, M.; White, B.; Guillet, J. E. *Macromolecules* **1989**, *22*, 3903.
42. Nowakowska, M.; White, B.; Guillet, J. E. *Macromolecules* **1990**, *23*, 3375.
43. Nowakowska, M.; Guillet, J. E. *Macromolecules* **1991**, *24*, 474.
44. Pandya, K.; Bahadur, P.; Nagar, T. N.; Bahadur, A. *Colloids Surf. A* **1993**, *70*, 219.
45. Prochazka, K.; Kiserow, D.; Ramireddy, C.; Tuzar, Z.; Munk,. P.; Webber, S.E. *Macromolecules* **1992**, *25*, 454.
46. Samii, A. A.; Karlstrom, D.; Lindman, B. Langmuir **1991**, *7*, 1065.
47. Scheutjens, J. M. H. M., Fleer, G. J. *J. Phys. Chem.* **1979**, *83*, 1619.
48. Scheutjens, J. M. H. M.; Fleer, G. J. *Macromolecules* **1985**, *18,* 1882.
49. Scheutjens, J. M. H. M.; Leermakers, F. A. M.; Besseling, N. A. M.; Lyklema, J. in *Surfactants in Solution, Vol 7,* Mittal, K. L. (Ed.), Plenum, 1989.
50. Semenov, A. N. *Sov. Phys. JETP* **1985**, *61*, 733.
51. Sustar, E.; Nowakowska, M.; Guillet, J. E. *J. Photochem. Photobiol. A: Chemistry* **1990**, *53*, 233.
52. Tontisakis, A.; Hilfiker, R.; Chu, B. *J. Colloid Interface Sci.* **1990**, *135*, 427.
53. Topchieva, I. N.; Osipova, S. V.; Polyakov, V. A. *Colloid J. USSR* **1990**, *52*, 347.
54. Tuzar, Z.; Webber, S. E.; Ramireddy, C.; Munk, P. *Polym. Prepr.* **1991**, *32*, 525.
55. Wang, Y.; Mattice, W. L.; Napper, D. H. *Langmuir* **1993**, *9*, 66.
56. Wanka, G.; Hoffmann, H.; Ulbricht, W. *Colloid Polym. Sci.* **1990**, *266*, 101.
57. Valint Jr., P. L.; Bock, J. *Macromolecules* **1988**, *21*, 175.
58. Valsaraj, K. T.; Thibodeaux, L. J. *Water Res.* **1989**, *23*, 183.
59. van Lent, B.; Scheutjens, J. M. H. M. *Macromolecules* **1989**, *22*, 1931.
60. Zhulina, Y. B.; Birshtein, T. M. *Polym. Sci. USSR (Engl. Transl.)* **1986**, *12*, 2880.

Chapter 7: List of Figures

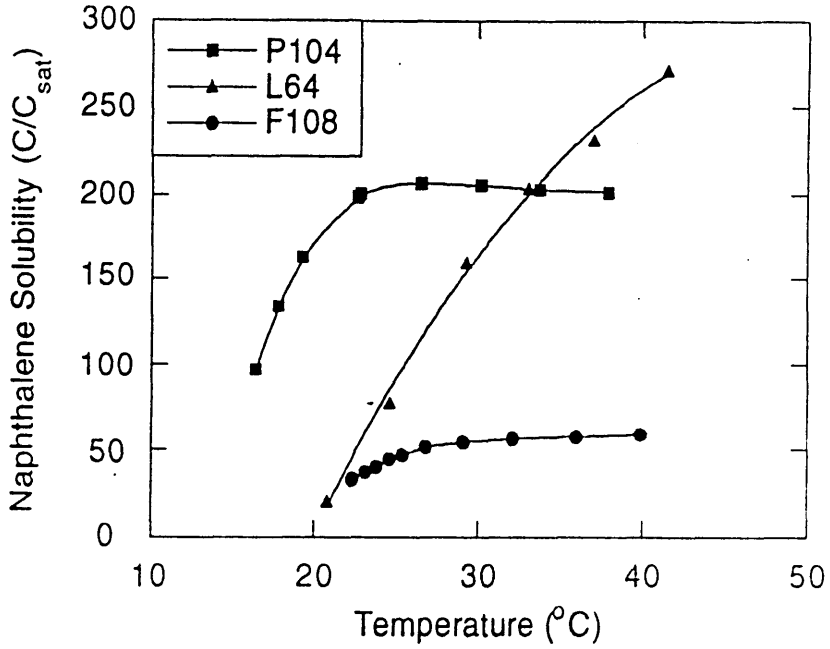

Figure 7.1 The temperature effect on the concentration of naphthalene in 10% aqueous solutions of P104, L64, and F108. The naphthalene concentration has been normalized by the solubility of naphthalene in water at the appropriate temperature.

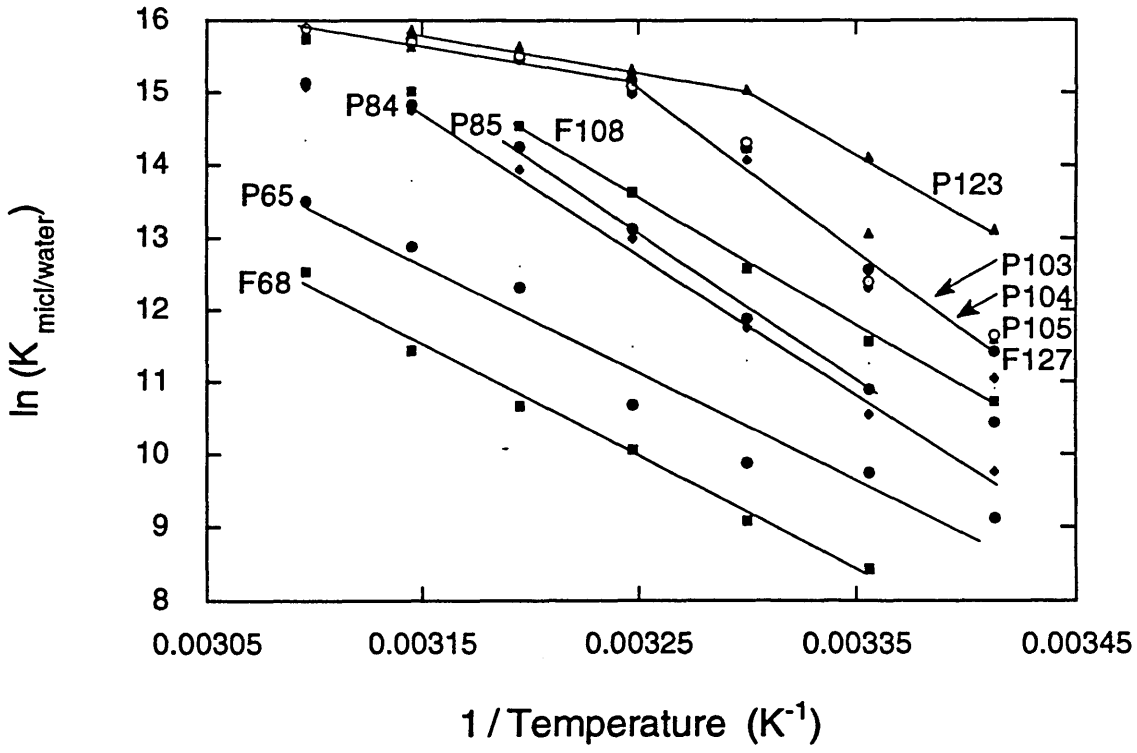

Figure 7.2 Micelle/water partition coefficient for DPH in PEO-PPO-PEO micelles plotted as a function of inverse temperature.

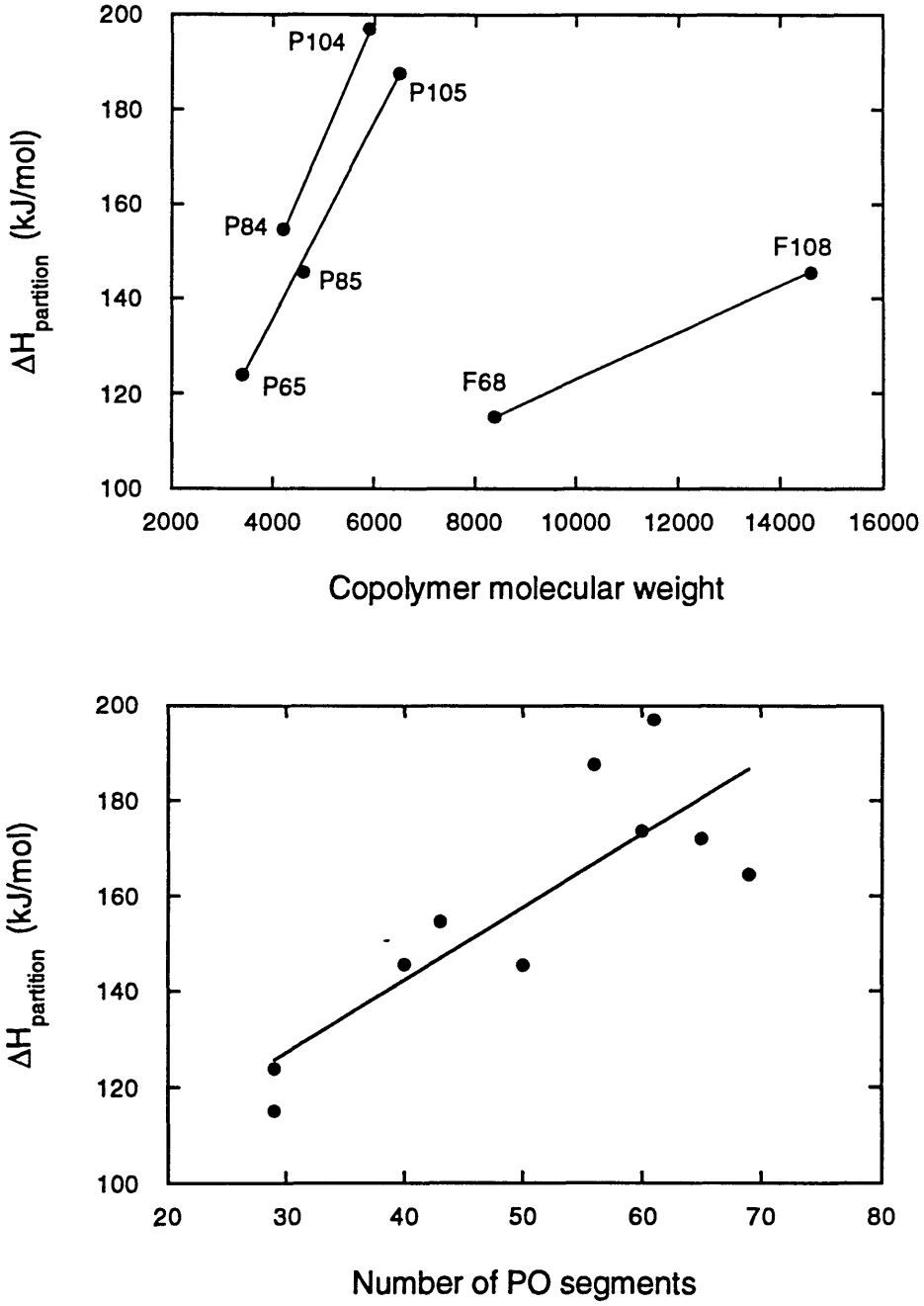

Figure 7.3 Enthalpy of partitioning for DPH in PEO-PPO-PEO micelles plotted as a function of (a) copolymer molecular weight, and (b) the number of PO segments in the copolymer.

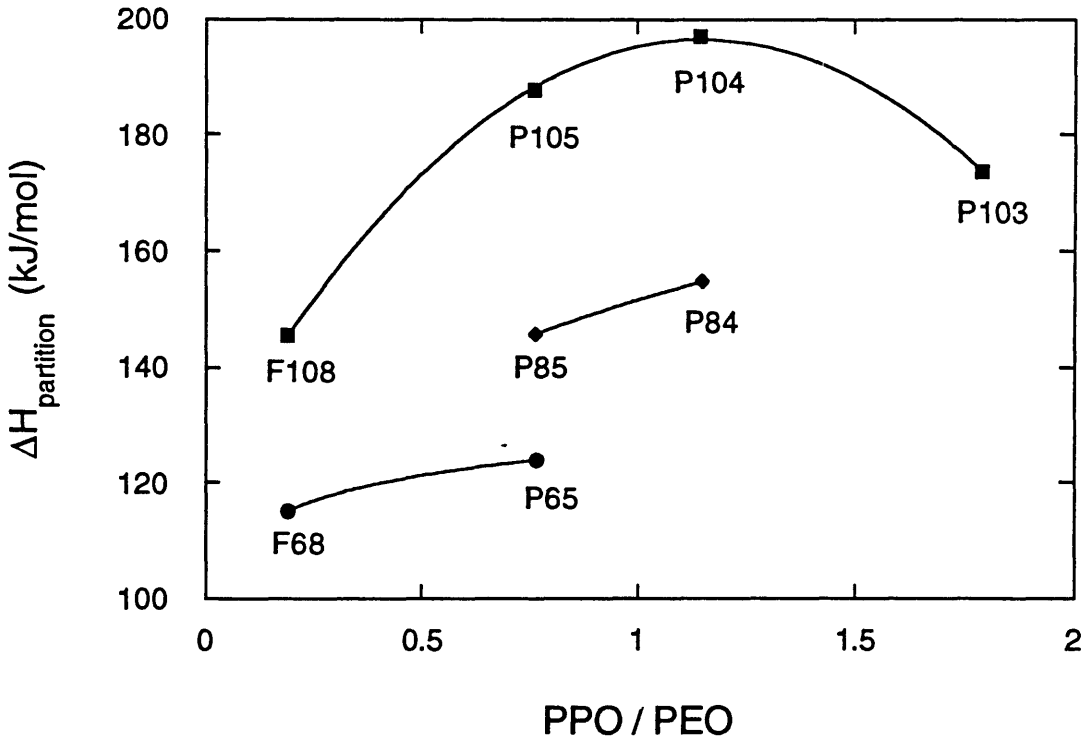

Figure 7.4 Enthalpy of partitioning for DPH in PEO-PPO-PEO micelles, plotted as a function of the copolymer PPO/PEO composition ratio.

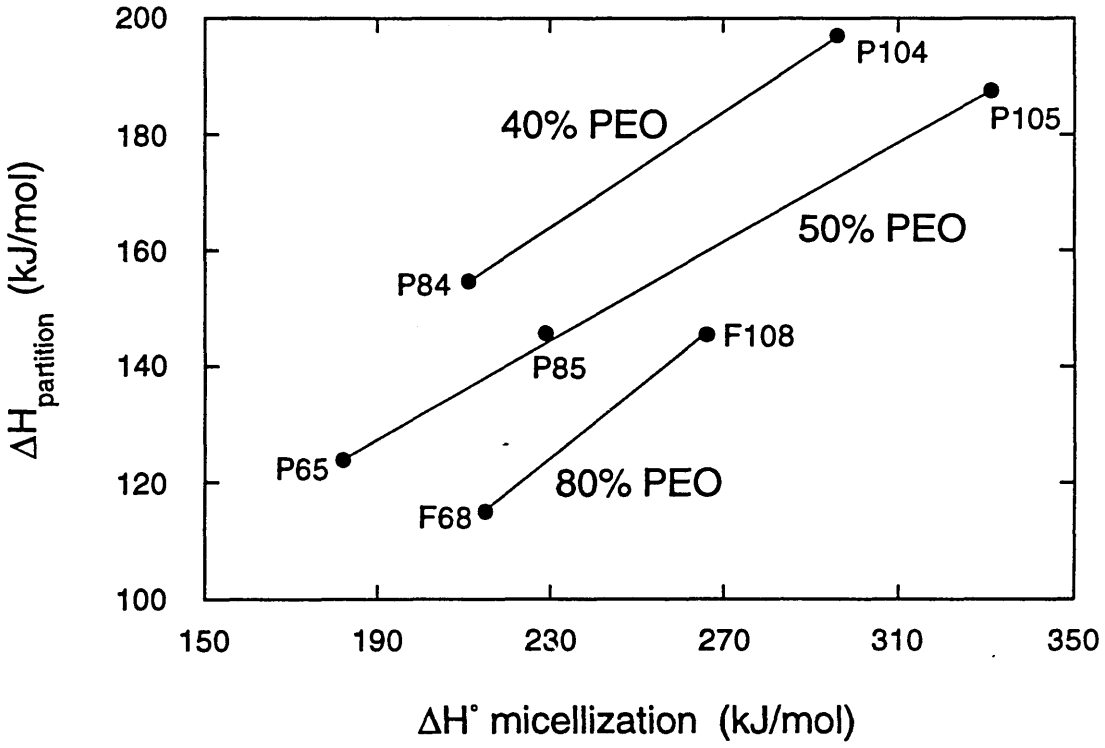

Figure 7.5 Enthalpy of partitioning for DPH in PEO-PPO-PEO micelles plotted vs the enthalpy of micellization for PEO-PPO-PEO copolymers in aqueous solutions.

Chapter 8
Micellization and Solubilization Kinetics in Block-Copolymer Micellar Systems

8.1 Introduction and Literature Review

The existence of two relaxation processes related to micellar equilibria in aqueous solutions of ionic detergents is generally accepted [Aniansson et al., 1976; Aniansson, 1978; Hoffmann, 1978; Kahlweit & Teubner, 1980]. These processes are characterized by the relaxation times τ_1 and τ_2, differing by as much as two to three orders of magnitude ($\tau_1<\tau_2$). The fast process τ_1 (on the order of 10^{-6} s) has been assigned to the association-dissociation (exchange) equilibrium of amphiphilic molecules to/from micelles. The slow process τ_2 (ranging between 10^{-3} - 1 s) has been attributed to the micelle assembly-dissociation equilibrium. Relaxation techniques [Bernasconi, 1976], such as temperature jump [Kresheck et al., 1966; Bennion & Eyring, 1979] or concentration jump [Yasunaga et al., 1973], have been used to measure the characteristic times τ_1 and τ_2 for micellar solutions [Note 1].

The study of the kinetics of polymeric micelles, which has attracted insufficient attention, is important both from fundamental and applications points of view. In particular, it may improve the understanding of the kinetics of solubilization by such micelles, which are relevant to the use of copolymers in dispersion polymerization and in the formulation of lubricants; the micellar life-time has been related to the bubble dynamics and the rates of solubilization and detergency in ionic surfactant solutions by Shah and coworkers [Oh et al., 1992; Oh & Shah, 1993]. The consideration of micellar kinetics also involves questions concerning the desorption dynamics of polymeric surfactants [Alexander & Halperin, 1989]. The large molecular weight and chain-like structure of block copolymer molecules is expected to complicate the processes of micelle formation and exchange of copolymer molecules between micelles and the bulk solution; disentanglement of copolymer molecules from the micelles should result in time scales slower than the ones observed in conventional, low-molecular weight, surfactants.

From the dynamic point of view, three types of molecular processes take place in copolymer micellar solutions [Tian et al., 1993]: (i) assembly of new micelles from unimers and disassociation of existing micelles, (ii) fission of existing micelles into two multimolecular parts and fusion of two existing micelles, and (iii) escape of individual unimers from micelles and their reentry. The rate of assembly of new micelles depends on a high power of the unimer concentration, and decreases sharply with decreasing CMC [Aniansson et al., 1978]. The assembly / disassociation process may become significant in nonequilibrium situations, e.g., when the unimer concentration is inappropriately high after a sudden jump in temperature or in the composition of the mixed solvent. The micellization then becomes a nucleation process driven by the supersaturation of the unimers in the solution. Once the supersaturation is relieved, the assembly of new micelles may be stopped for all practical purposes [Tian et al., 1993]. As Halperin and Alexander [1989] pointed out, the free energy penalty of fission or fusion of large micelles would often be too high and this process may be kinetically hindered or fully frozen.

Association and dissociation rates of poly(styrene)-*block*-poly(hydrogenated isoprene) and poly(styrene)-*block*-poly(hydrogenated butadiene)-*block*-poly(styrene) copolymer micelles were studied by Bednar et al. [1988] using a stopped flow technique with light scattering detection. The formation of micelles was induced by mixing a solution containing copolymer in a thermodynamically good solvent (60 vol. % 1,4-dioxane, 40 % heptane) with the same amount of pure dioxane; dissociation of the micelles was achieved by mixing a dioxane solution containing micelles with an equal volume of heptane. Relaxation times on the order of 50 ms were estimated by fitting the normalized relaxation decay curves to an exponential function. Bednar et al. [1988] noted that these relaxation times pertained to major changes (from only micelles to only unimers or vice versa) and could not be interpreted in terms of a step-wise association mechanism used in relaxation studies of surfactant micelles. The first step in the dissociation process would be a rapid influx of solvent molecules into the micelle core, separating the core blocks. The dissociation process was found to be very fast for the diblock copolymer ($\tau < 1$ ms) and slower ($\tau = 137$ ms) for the triblock copolymer micelles. It was proposed that the association process involved the formation of small aggregates that merged to form micelles with a higher aggregation number. Exchange of unimers or rearrangement of the chain conformation within the micelles could go on for a rather long time, but was not detected,

as it would not affect the observed scattered light intensity.

Wang et al. [1992] used a fluorescence method for the measurement of the rate of exchange of labeled-chains between micelles formed by poly(styrene)-poly(ethylene oxide) diblock copolymers in aqueous solutions. The rate constant at 60 °C, deduced from the time dependence of the fluorescence intensity, was on the order of 10^{-5} s^{-1}. No exchange could be detected at ambient temperature, presumably because of the difficulty of extraction of poly(styrene) segments from the glassy micelle core. Similar experiments with fluorescence-probe-labeled copolymer micelles having poly(styrene) core and poly(hydrogenated isoprene) coronas in aliphatic solvents were performed by Prochazka et al. [1991]; the relaxation time of the unimer exchange was on a time scale of 10^3 s. Tian et al. [1993] followed the rate of micelle hybridization when two solutions containing micelles formed from two different poly(methacrylic acid)-poly(styrene) copolymers were mixed. The rate of hybridization, determined from sedimentation velocity measurements, varied from 0.5 hours to 20 days (!). Generally, the rate decreased when the size of either block of either copolymer increased. The rate controlling process was apparently the escape of the unimers from the micelles that was slowed down both by increasing size of the insoluble block extricating itself from the micelle core and by the increasing width of the corona. Transfer of unimers from the large micelles to the small ones dominated the transfer in the opposite direction, irrespective of the diblock or triblock nature of the copolymers. Halperin and Alexander [1989] analyzed theoretically the dynamics of unimers in micellar solutions and developed scaling relations for the unimer transfer. A mechanism allowing the micellar size distribution to adjust in steps consisting of single-chain insertion / expulsion was found to have the lowest activation free energy.

Studies on the kinetics of entry and exit of hydrophobic solute molecules in block copolymer micelles have been reported by Cao et al. [1991] and Hruska et al. [1993]. The solubilization and release properties of polymer micelles formed by triblock poly(methacrylic acid)-poly(styrene)-poly(methacrylic acid) in aqueous solutions was examined by Cao et al. [1991] using pyrene as a fluorescence probe. The rate of pyrene intermicellar exchange was monitored by the change of excimer fluorescence [Birks, 1970] when pyrene-loaded micelles were mixed with pyrene-free micelles. A relatively rapid change in monomer / excimer fluorescence intensity ratio occurred at early times (10 - 20 min), with a much slower approach to equilibrium at longer times (on the order of a week).

This process was limited by diffusion of the probe into and out of the micelles, since stirring the solution did not change the time dependence. The exit and entry rate constants for 4-bromo-1-acetonaphthone (BAN) in poly(styrene)-poly(ethylene oxide) block copolymer micelles were investigated by Hruska et al. [1993] using phosphorescence quenching experiments. The exit rate constant, approximately $8x10^3$ s^{-1}, was found to be independent of the micelle size, whereas the entry rate constant increased linearly with the micelle core radius; under the experimental conditions of Hruska et al. [1993], BAN molecules always reentered the same micelle from which they had departed to enter the aqueous phase. Transfer of relatively short polycation chains from their polyelectrolyte complex with a relatively long polyanion to another polyanion of the same chemical structure and chain length but tagged with a fluorescent group has been investigated by Bakeev et al. [1992] with a luminescence quenching technique.

To the best of our knowledge, no study of micellization and solubilization kinetics in aqueous poly(ethylene oxide)-*block*-poly(propylene oxide)-*block*-poly(ethylene oxide) (PEO-PPO-PEO) Pluronic copolymer micellar systems has been reported to date. The only relevant information, outlined below, was inferred through steady-state observations. Linse and Malmsten [1992] and Malmsten and Lindman [1992a] followed the temperature dependence of the micellization process in Pluronic F127 solutions by performing gel-permeation chromatography experiments at different temperatures. The micelle fraction appeared as a separate peak in the chromatogram; this led the authors to the conclusion that the residence time of the polymer molecules in the F127 micelles is extremely long (~hours). On the other hand, Fleischer [1993] reported that the lifetime of a copolymer molecule within the micelle was shorter that the minimum observation time of the experiments (≈ 3 ms). He reached this conclusion from Pulsed-Field-Gradient NMR measurements of Pluronic F127 self-diffusion: since unimers and micelles coexist in the solution, Fleischer expected to observe two self-diffusion coefficients, one for the unimers, and one for the micelles, if there were no exchange of the molecules between the two states within the diffusion time. A single diffusion coefficient was observed, and thus Fleischer [1993] inferred that the copolymer solution was in the dynamic range of fast exchange.

It becomes obvious from the above review that kinetic studies on block copolymer micellar systems are limited and, in the case of Pluronic copolymers, nonexistent. Preliminary data on kinetics of micelle formation / disassociation and solubilization / release

of a hydrophobic solute in aqueous solutions of Pluronic copolymers are reported here. Temperature jump and concentration jump experiments were performed to induce micelle formation or dissociation and solute uptake or release, and the dynamic response of the system was observed with light scattering intensity or absorption spectroscopy. The characteristic relaxation times were estimated, and the mode of micelle growth (diffusion vs reaction limited) was examined.

8.2 Materials and Methods

The PEO-PPO-PEO Pluronic copolymers P104 and F108 studied here have been described by Alexandridis et al. [1994]. Both P104 and F108 have a PPO block of similar size (M_w~3000); P104 has 40 % and F108 80% PEO. Sample preparation was similar to that of Alexandridis et al. [1994]. The UV-vis spectrophotometer and the light scattering apparatus used have been described previously in Chapters 2 and 5, respectively.

Three kinds of kinetic experiments are reported here: (i) temperature jumps of copolymer solutions, (ii) temperature jumps of copolymer solutions containing diphenylhexatriene (DPH), and (iii) concentration jumps of copolymer solutions containing DPH. The light scattering intensity was used as a probe for the temperature jumps of case (i): the copolymer solution was equilibrated in the thermostated cell holder of a light scattering apparatus, the thermostat temperature was changed, and the scattering intensity of the sample was measured and recorded every minute. Approximately 3 minutes were needed to achieve the new temperature, for jumps of 2.5 K. The time dependence of the UV-vis absorption (at 356 nm) of copolymer solutions that contained DPH was recorded as a function of time in cases (ii) and (iii); DPH served as an indicator for the "fate" of the micelles during the experiment.

For the temperature jump experiments in the presence of DPH, the cuvette containing the sample was equilibrated (both with respect to temperature and composition) at the desired temperature; the cuvette was then placed in a UV-vis spectrophotometer cell holder that was thermostated at a temperature higher (up-jump) or lower (down-jump) than the cuvette temperature (20 or 30 °C). The time required for the cuvette to reach the new temperature was less than 3 minutes for a 10 K jump; however, composition equilibration

required longer times, thus allowing us to observe it with the aid of a spectrophotometer. In the concentration jump experiments, the sample concentration was altered by adding copolymer solution or water at a given temperature; the cuvette containing the sample was placed in the spectrophotometer cell holder immediately after mixing (~30 s) and the sample absorption recorded as a function of time. Fluorescence emission intensity was also used to follow the kinetics in block copolymer solutions containing DPH. The relaxation kinetics were generally the same for both UV-vis absorption and fluorescence emission detection; however, photobleaching of DPH over time complicated the observation over long (30 min) time scales.

The times characteristic for the changes observed in the temperature and concentration jump experiments were obtained by fitting the data to an exponential relationship of the form

$$(I_t - I_\infty) / (I_0 - I_\infty) = \exp(-t/\tau)$$

for the down-jump, and

$$(I_t - I_\infty) / (I_0 - I_\infty) = 1 - \exp(-t/\tau)$$

for the up-jump, where I_t is the intensity at time t, I_0 the initial intensity, I_∞ the intensity at the new equlibrium (infinite time), and τ is the characteristic relaxation time. The up- and down-temperature jumps were reversible and the equilibrium, I_∞, values were attained over the time of observation in all experiments reported here.

8.3 Results and Discussion

8.3a Temperature jump with light scattering detection

The static light scattering intensity (originating from concentration fluctuations) is directly proportional to the weight-average aggregation number of the micelles, $\langle N_w \rangle$, for sufficiently dilute solutions [Hiemenz, 1986]. A large increase in the intensity of scattered light would, therefore, indicate an increase in $\langle N_w \rangle$, provided critical fluctuations are not

significant. Light scattering intensity for 0.5% P104 and F108 aqueous solutions is plotted in Figure 8.1 as a function or temperature. The abrupt increase in the intensity is indicative of micelle size and/or number growth upon heating past the critical micellization temperature. It is generally accepted that, following micellization, the micelles exist in the solution in equilibrium with unimers of concentration equal to the CMC. In the experiment shown in Figure 8.1, the total copolymer concentration remained constant, while the CMC decreased with increasing temperature [Alexandridis et al., 1994], thus leaving more copolymer molecules available to associate in micelles. The number of micelles is expected, based on this mechanism, to increase with temperature. At the same time, the aggregation number of Pluronic copolymer micelles would increase with temperature [Alexandridis & Hatton, 1994]. The strong dependence of light scattering intensity on temperature was used for observing the kinetics of micelle formation and growth. The arrows in Figure 8.1 indicate the temperature jumps, performed at 27.5 - 30, and 35 - 37.5 °C intervals, for P104 and F108 solutions, respectively.

The normalized scattering intensity values for up- and down- temperature jumps of 0.5% P104, and F108 copolymer solutions are plotted in Figure 8.2 as a function of time. The relaxation times characteristic for the intensity increase (shown in Table 8.1) were estimated to be 4.5 and 5.8 min for P104 and F108, respectively. It is expected that, when the unimer concentration is inappropriately high after a sudden jump in temperature, the micellization becomes a nucleation process driven by the supersaturation of the unimers in the solution [Tian et al., 1993] and may involve fusion of existing micelles or pre-micellar aggregates. The slower relaxation time for the F108 system (compared to the one of P104) may indicate that the association of unimers and/or pre-micellar aggregates to form micelles is hindered by the EO segments (the lag time observed in the F108 relaxation may also be related to this), and is despite the fact that the temperature-jump for F108 was done at a higher temperature where unimer and micelle diffusion is faster [Alexandridis et al., 1994b]. The relaxation times characteristic for the intensity decrease were 4.0 and 3.6 min for P104 and F108, respectively. The faster relaxation time for F108 was probably due to the higher temperature (compared to the temperature-jump for P104) and/or a smaller aggregation number that allowed for "easier" break-up of the micelles [Alexandridis et al., 1994b]. The hydrophobic (PPO) block, making up the micelle core, is of comparable size for both P104 and F108 copolymers.

The type of "aggregation" mechanism during micelle growth due to temperature increase can be tested by utilizing the relationship between the micelle size and the light scattering intensity. For diffusion-limited aggregation, the logarithm of the particle size scales linearly with the logarithm of time, while for reaction-limited aggregation, the logarithm of the particle size scales linearly with time [Lin et al., 1989]. The data for temperature jumps resulting in increase of intensity are presented in Figure 8.3a using double logarithmic axes. Linearity is observed at the 2 - 10 min time range when the data are plotted in this way, suggesting that micelle growth is diffusion limited, rather than reaction limited. This implies that for the experimental conditions employed, most of the collisions between particles were effective [Probstein, 1989]. The solid lines in Figure 8.3a are the fit to a power law expression; the power-law exponents are listed in Table 8.1. Figure 8.3b shows a semi-logarithmic intensity vs time plot for down- temperature jumps; the solid lines are the fit to an exponential decay expression, exhibiting a behavior typical for relaxation kinetics.

8.3b Temperature jump with DPH UV-vis absorption detection

Temperature jumps were also conducted in copolymer solutions in the presence of DPH, a hydrophobic solute with a characteristic UV-vis spectrum that allows for easy detection. The solubilization of DPH in micellar solutions has been employed by Alexandridis et al. [1994] for the determination of the onset of micelle formation. Figure 8.4 shows the UV-vis absorption intensity of P104 Pluronic copolymer solutions (of varying concentration) containing DPH. The absorption intensity due to DPH is low when there are no micelles in solution; DPH molecules are presumably in some form of an aggregate suspended in the solution. Upon increasing the temperature, copolymer micelles are formed, DPH is solubilized in a hydrophobic environment and the absorption intensity increases, as seen in Figure 8.4. The plateau reached at high concentration and temperature indicates that all DPH has been solubilized. The temperature jumps were performed between 20 (no micelles and little solubilization) and 30 °C (micelles present in solution). The kinetic events probed with these temperature jump experiments include the rate of incorporating DPH in the micelles, in addition to the micelle formation / growth rate. The solubilization of DPH into the micelles would involve movement of DPH molecules out of microcrystalline aggregates, via the aqueous solution, through the hydrated PEO micelle corona, and into the PPO hydrophobic core. Such would be the case in 2.5% P104

solutions, where some micelles already exist at 20 °C. In the case where micelles are formed at the same time that solubilization occurs, some of the steps outlined above may not be in effect, with micellization and solubilization occurring in a single step. The presence of DPH may thus complicate the analysis of the temperature jump experiments reported here; nevertheless, the combined phenomenon of micellization / solubilization is of importance in various applications of Pluronic copolymers [Alexandridis & Hatton, 1994].

The normalized intensities for up- and down-temperature jumps of P104 copolymer solutions in the presence of DPH are plotted in Figure 8.5. A log-time scale is used to allow inspection of both short and longer time ranges. Attainment of equilibrium upon increase of temperature was achieved in 10 - 50 minutes; the relaxation times (listed in Table 8.1) for up-temperature jumps behaved in a nonmonotonic way with respect to polymer concentration. The values for relaxation times in the presence of DPH were slower than the temperature-jumps with light scattering detection; implying that the process observed in the case of UV-vis absorption detection is the solubilization of DPH in the copolymer micelles. It is not easy to rationalize the dependence of relaxation time on the copolymer concentration, given that the temperature jump range was rather broad; more experiments are needed to draw definite conclusions. A maximum was observed in the slow relaxation time (τ_2) for sodium dodecyl sulfate (SDS) micelles at a certain SDS concentration; the rate of solubilization of benzene and a hydrophobic dye in SDS solutions was also maximum at this concentration [Oh & Shah, 1993]. The relation of the relaxation times to DPH can also be seen in the down-temperature jumps. A trend of increasing relaxation time with increasing copolymer concentration was observed (see Table 8.1); indeed, it took approximately two days for the absorption to decrease (and DPH to exit the micelles) when the 2.5% P104 solution was cooled down from 20 to 30 °C. This was probably due to some short of stabilization (emulsification) of the solubilized DPH by copolymer molecules, at the time that micelles were not thermodynamically stable.

To elucidate the mechanism of DPH solubilization, the intensity vs time data for up-temperature jumps are plotted on different scales in Figure 8.6. A log intensity vs log time plot (Figure 8.7) was the most adequate representation for the data in the 0.5 - 8 min time range, suggesting that DPH solubilization is diffusion limited, rather than reaction limited. It is not clear from this analysis, though, what exactly is the rate limiting step (diffusion of DPH out of the microcrystalline aggregates or through the hydrated PEO micelle corona).

It is interesting to note that the power law exponent obtained from fitting the data was approximately equal to 1 for the 0.05 - 1% solutions, and dropped to 0.7 for the 2.5% P104 solution (Table 8.1). Figure 8.8 shows intensity vs time data for down-temperature jumps, plotted in different scales. A log intensity vs time plot (exponential decay) was the more adequate representation for the data in the 1 - 10 min time range (Figure 8.9).

8.3c Concentration jump with DPH UV-vis absorption detection

Three concentration jump experiments are described here: (i) a small amount of DPH solution in methanol was injected into a 5% P104 micellar solution at 20 °C (Figure 8.10a); (ii) a 5% P104 solution containing DPH was diluted 1:1 with water, taking the resulting 2.5% copolymer solution below CMC at 20 °C (Figure 8.10b); (iii) a 10% P104 solution was mixed 1:1 with water containing DPH (Figure 8.10c). In all cases, (macroscopic) mixing was achieved in less than 30 s, and the UV-vis absorption intensity due to DPH was recorded over time. In experiment (i), the DPH molecules were added in a molecularly dispersed form and the diffusion of DPH in the water for a distance equal to that between two micelles was faster than the mixing time. It is thus expected that experiment (i) would provide information on the rate of DPH incorporation in the micelles through the PEO corona; as seen in Figure 8.10a, this process was completed in less than 10 minutes (see also Figure 8.10c). De-solubilizing DPH upon reducing the copolymer concentration below the CMC in experiment (ii) took much longer, as seen in Figure 8.10b. This result resembles that obtained from a 30 to 20 °C temperature jump in 2.5% P104 solution (2 days were required for reequilibration), and indicates again that DPH molecules or microcrystals can be stabilized as a suspension by adsorbed copolymer (or that DPH induces aggregation of copolymers around it), even when micelles are not thermodynamically stable.

8.4 Conclusions

Preliminary data on kinetics of micelle formation / disassociation and solubilization / de-solubilization of a hydrophobic solute in aqueous solutions of Pluronic copolymers are reported here. Temperature jump and concentration jump experiments were performed to induce micelle formation or dissociation and solute uptake or release, and the dynamic

response of the system was observed with light scattering intensity or absorption spectroscopy.

In the light scattering intensity experiments, the relaxation time observed for the up-temperature jump in the F108 system was slower than that of P104, indicating that the association of unimers or pre-micellar aggregates to form micelles may be hindered by the EO segments, despite the fact that the temperature-jump for F108 was done at a higher temperature (than P104) where unimers and micelles diffuse faster. The data for temperature jumps resulting in increase of intensity were linear over the 2 - 10 min time range when plotted in a double logarithmic way, suggesting that micelle growth was diffusion limited. The down-temperature jumps were described well by an exponential decay expression. The characteristic relaxation times for these experiments were on the order of 5 minutes.

Temperature jumps were also conducted in copolymer solutions in the presence of DPH, a hydrophobic solute. The rate of incorporating DPH in the micelles was generally slower that the micelle formation / growth rate. Attainment of equilibrium upon increase of temperature was achieved in 10 - 50 minutes; the relaxation times for up-temperature jumps behaved in a nonmonotonic way with respect to polymer concentration. A trend of increasing relaxation time with increasing copolymer concentration was observed in the down-temperature jumps. This was probably due to some short of stabilization (emulsification) of the solubilized DPH by copolymer molecules, at the time that micelles were not thermodynamically stable. Concentration jumps were performed, providing information on the rate of DPH incorporation in copolymer micelles and the rate of DPH de-solubilization. The characteristic time for the former process was less than 5 minutes, while the latter was not completed even after 80 minutes.

In summary, the following conclusions can be drawn from the above experiments: the copolymer micelle association and dissociation process has a relaxation time of 5 minutes; solubilization of molecularly dispersed solute in the micelles takes place in the same time range; dissolution of DPH microcrystalline aggregates can take longer and can be the rate limiting step in the solubilization process; DPH that has been solubilized in micelles can remain long in solution, even below the CMC.

8.5 References and Notes Cited in Chapter 8

1. Alexandridis, P.; Hatton, T. A. *Colloids Surfaces A*, **1994**, submitted; Chapter 1 of this Thesis.
2. Alexandridis, P.; Holzwarth, J. F.; Hatton, T. A. *Macromolecules*, **1994**, *27*, 2414; Chapter 2 of this Thesis.
3. Alexandridis, P.; Nivaggioli, T.; Hatton, T. A. *Colloids Surfaces A*, **1994b**, submitted; Chapter 5 of this Thesis.
4. Aniansson, E. A. G.; Wall, S. N.; Almgren, M.; Hoffmann, H.; Ulbricht, W.; Zana, R.; Lang, J.; Tondre, C. *J. Phys. Chem.* **1976**, *80*, 905.
5. Aniansson, G. E. A. *J. Phys. Chem.* **1978**, *82*, 2805.
6. Bakeev, K. N.; Izumrudov, V. A.; Kuchanov, S. I.; Zezin, A. B.; Kabanov, V. A. *Macromolecules* **1992**, *25*, 4249.
7. Bednar, B.; Edwards, K.; Almgren, M.; Tormod, S.; Tuzar, Z. *Makromol. Chem., Rapid Commun.* **1988**, *9*, 785.
8. Bennion, B. C.; Eyring, E. M. *J. Colloid Interface Sci.* **1970**, *32*, 286.
9. Bernasconi, C. F. *Relaxation Kinetics*, Academic Press, 1976.
10. Birks, J. B. *Photophysics of Aromatic Molecules*; Wiley-Interscience: New York, 1970; Chapter 7.
11. Cao, T.; Munk, P.; Ramireddy, C.; Tuzar, Z.; Weber, S. E. *Macromolecules* **1991**, *24*, 6300.
12. Fleischer, G. *J. Phys. Chem.* **1993**, *97*, 517.
13. Halperin, A.; Alexander, S. *Macromolecules* **1989**, *22*, 2403.
14. Hiemenz, P. C. *Principles of Colloid and Surface Chemistry*; Marcel Dekker: New York, 2nd ed., 1986.
15. Hoffmann, H. *Ber. Bunsenges. Phys. Chem.* **1978**, *82*, 988.
16. Hruska, Z.; Piton, M.; Yekta, A.; Duhamel, J.; Winnik, M. A.; Riess, G.; Croucher, M. D. *Macromolecules* **1993**, *26*, 1825.
17. Kahlweit, M., Teubner, M. *Adv. Colloid Interface Sci.* **1980**, *13*, 1.
18. Kresheck, G. C.; Hamori, E.; Davenport, G.; Scheraga, H. A. *J. Am. Chem. Soc.* **1966**, *88*, 246.
19. Lin, M. Y.; Lindsay, H. M.; Weitz, D.; A.; Ball, R. C.; Klein, R.; Meakin, P. *Nature*, **1989**, *339*, 360.

20. Linse, P.; Malmsten, M. *Macromolecules* **1992**, *25*, 5434.
21. Malmsten, M.; Lindman, B. *Macromolecules* **1992**, *25*, 5440.
22. Oh, S.-G.; Klein, S. P.; Shah, D. O. *AIChE Journal* **1992**, *38*, 149.
23. Oh, S. G.; Shah, D. O. *J. Am. Oil Chem. Soc.* **1993**, *70*, 673.
24. Probstein, R. F. *Physicochemical Hydrodynamics*; Butterworths; Boston, 1989.
25. Prochazka, K.; Bednar, B.; Svoboda, P.; Trnena, J.; Mukhtar, E.; Almgren, M. *J. Phys. Chem.* **1991**, *95*, 4563.
26. Tian, M.; Qin, A.; Ramireddy, C.; Webber, S. E.; Munk, P.; Tuzar, Z.; Prochazka, K. *Langmuir* **1993**, *9*, 1741.
27. Wang, Y.; Batalj, R.; Quirk, R. P.; Mattice, W. L. *Polym. Bull.* **1992**, *28*, 333.
28. Yasunaga, T.; Takeda, K.; Harada, S. *J. Colloid Interface Sci.* **1973**, *42*, 457.

Note 1 The techniques employed for measuring events in a chemical system at a short time scale can be classified into two groups, flow and relaxation techniques. In relaxation techniques, the equilibrium state of a system is perturbed through a step change, or "jump", in an intensive property of the system, such as temperature, pressure, or electric charge. The approach of the system to the equilibrium state at the new value of the system property is recorded as a function of time. There are two conditions for the application of a relaxation method to be appropriate: (i) the system must attain a state of equilibrium before and after the relaxational jump (the fast event cannot be irreversible), and (ii) the change of the intensive parameter must cause a measurable change in the system; in the case of temperature jump, the event must possess a sizable free energy of activation $\Delta H^{\ddagger}$.

Chapter 8: List of Tables and Figures

Figure 8.8 Intensity vs time data for 30 to 20 °C (down-) temperature jumps: (a) linear intensity - linear time, (b) linear intensity - square root of time, and (c) log intensity - log time scales.

Figure 8.9 Log intensity vs time plot for 30 to 20 °C (down-) temperature jumps, showing the fit to an exponential decay expression.

Figure 8.10 Absorption intensity as a function of time, following (a) injection of a small amount of DPH to a 5% P104 micellar solution at 20 °C, (b) dilution of a 5% P104 solution (containing DPH) below CMC upon the addition of water, and (c) mixing a 10% P104 solution with water containing DPH.

Table 8.1 Characteristic relaxation times and exponents of power law (when applicable) for the temperature jump experiments.

Polymer	Concentration (%)	Temperature range (°C)	Relaxation time (min)	Power-law exponent
P104	0.5	27.5 -> 30	4.46	1.06
P104	0.5	30 -> 27.5	4.04	
F108	0.5	35 -> 37.5	5.76	2.16
F108	0.5	37.5 -> 35	3.58	
P104	0.05	20 -> 30	21.6	0.99
P104	0.05	30 -> 20	0.97	
P104	0.1	20 -> 30	4.35	1.16
P104	0.1	30 -> 20	5.25	
P104	0.5	20 -> 30	16.4	1.17
P104	0.5	30 -> 20	-	
P104	1.0	20 -> 30	4.24	0.91
P104	1.0	30 -> 20	60.2	
P104	2.5	20 -> 30	16.9	0.68

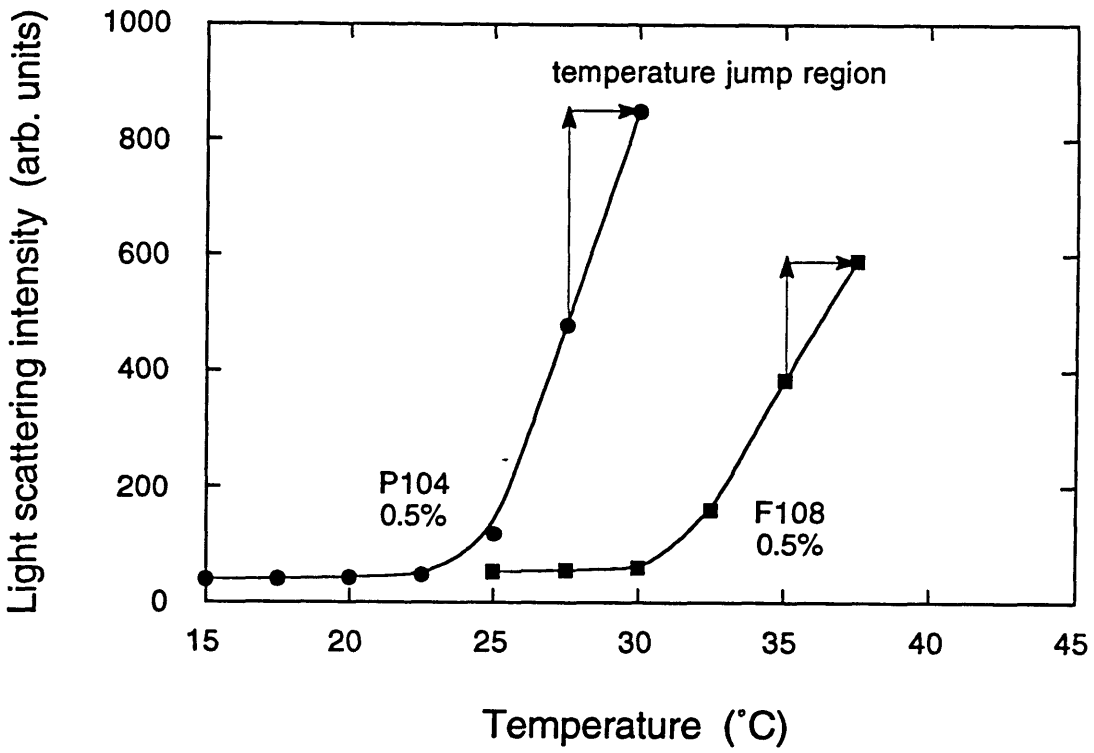

Figure 8.1 Light scattering intensity of P104 anf F108 Pluronic copolymer solutions; the temperature jumps were performed at 27.5 - 30, and 35 - 37.5 °C intervals, for P104 and F108, respectively.

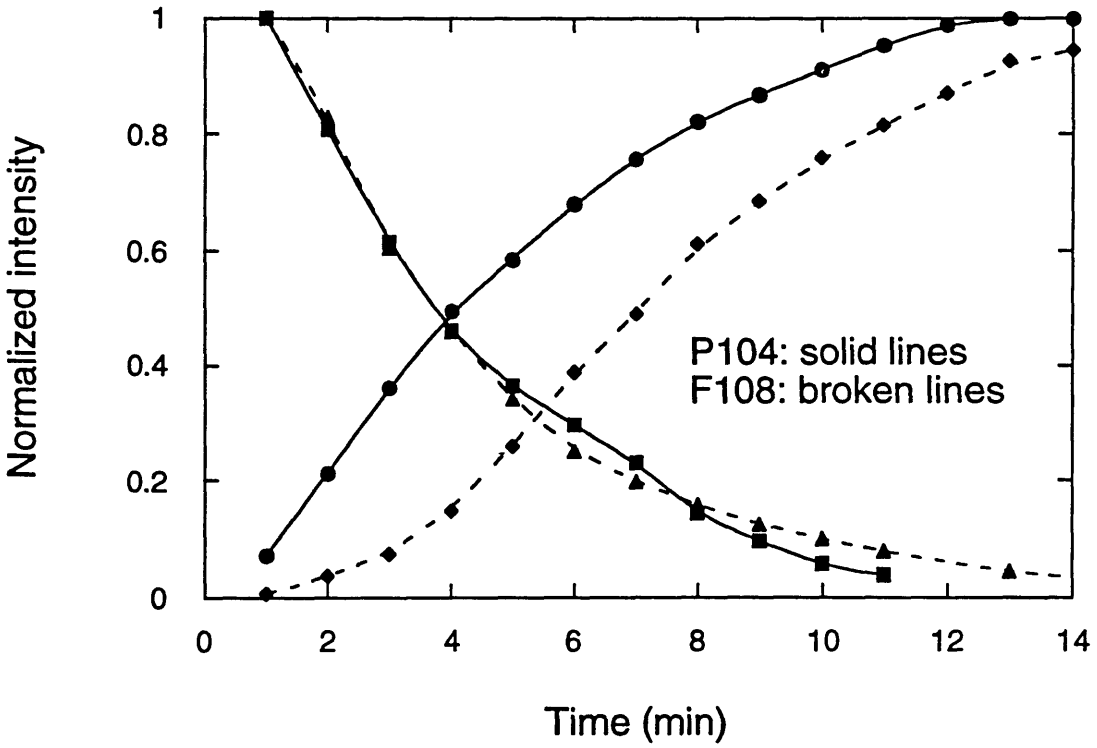

Figure 8.2 Normalized intensity plotted as a function of time for up- and down-temperature jumps of 0.5% P104, and F108 copolymer solutions.

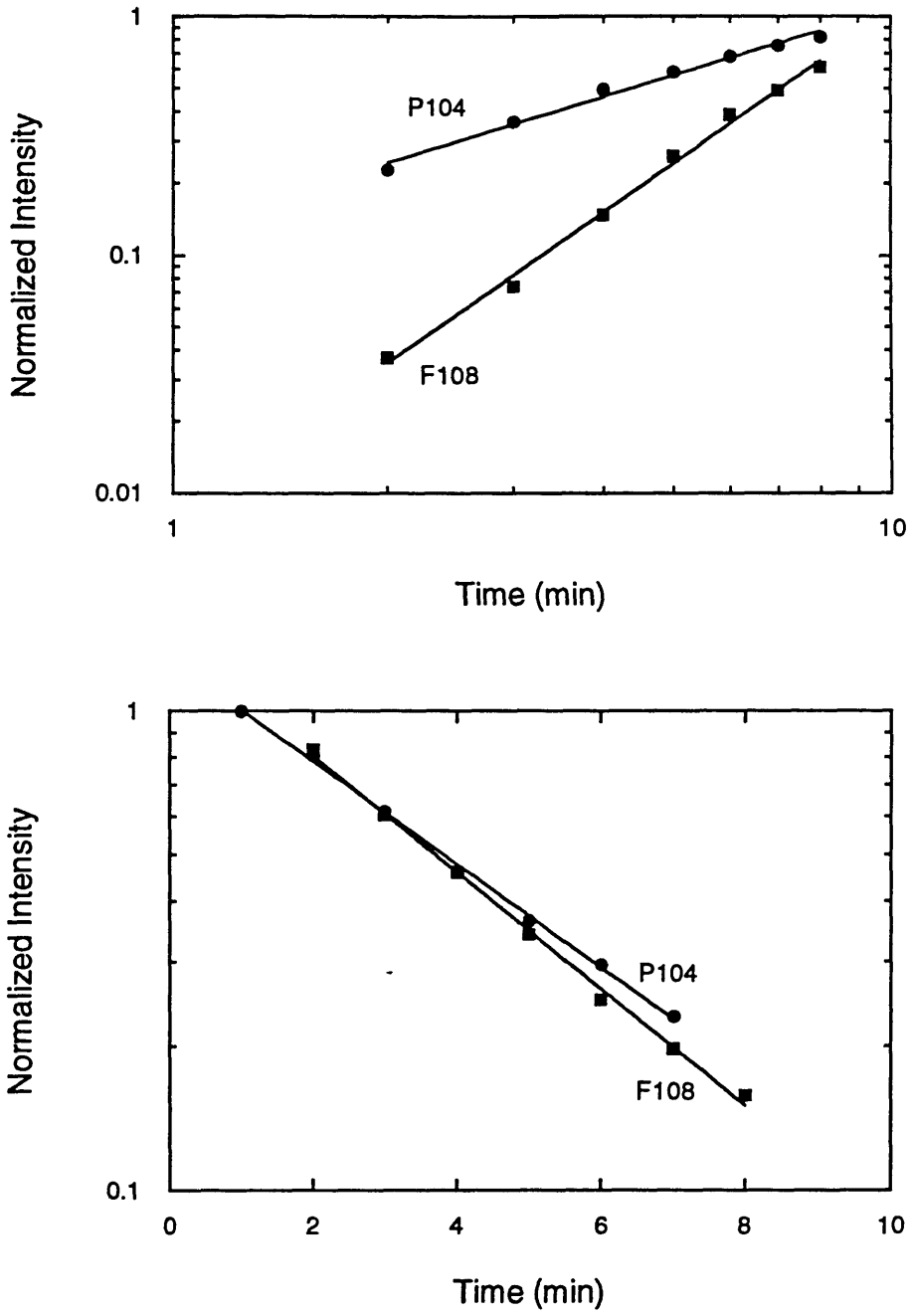

Figure 8.3 (a) Log intensity vs log time plot for up-temperature jumps, showing the fit to a power law expression.
(b) Log intensity vs time plot for down- temperature jumps, showing the fit to an exponential decay expression.

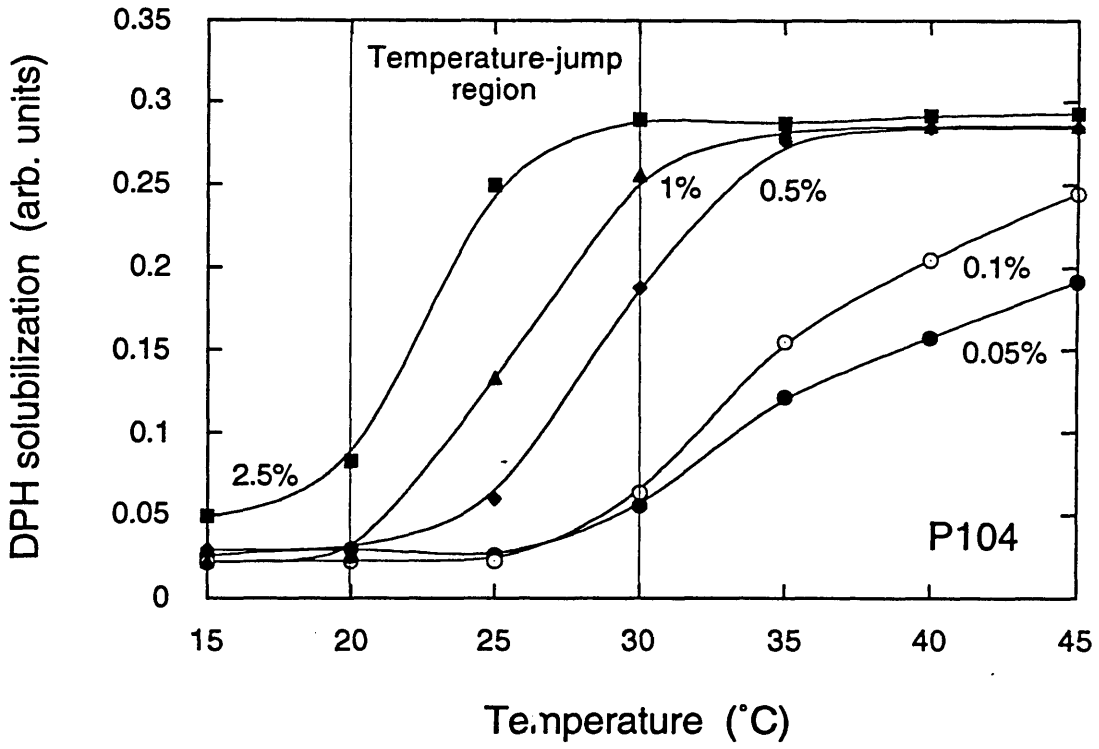

Figure 8.4 UV-vis absorption intensity of P104 Pluronic copolymer solutions containing DPH; the temperature jumps were performed between 20 and 30 °C for samples of copolymer concentrations shown in the graph.

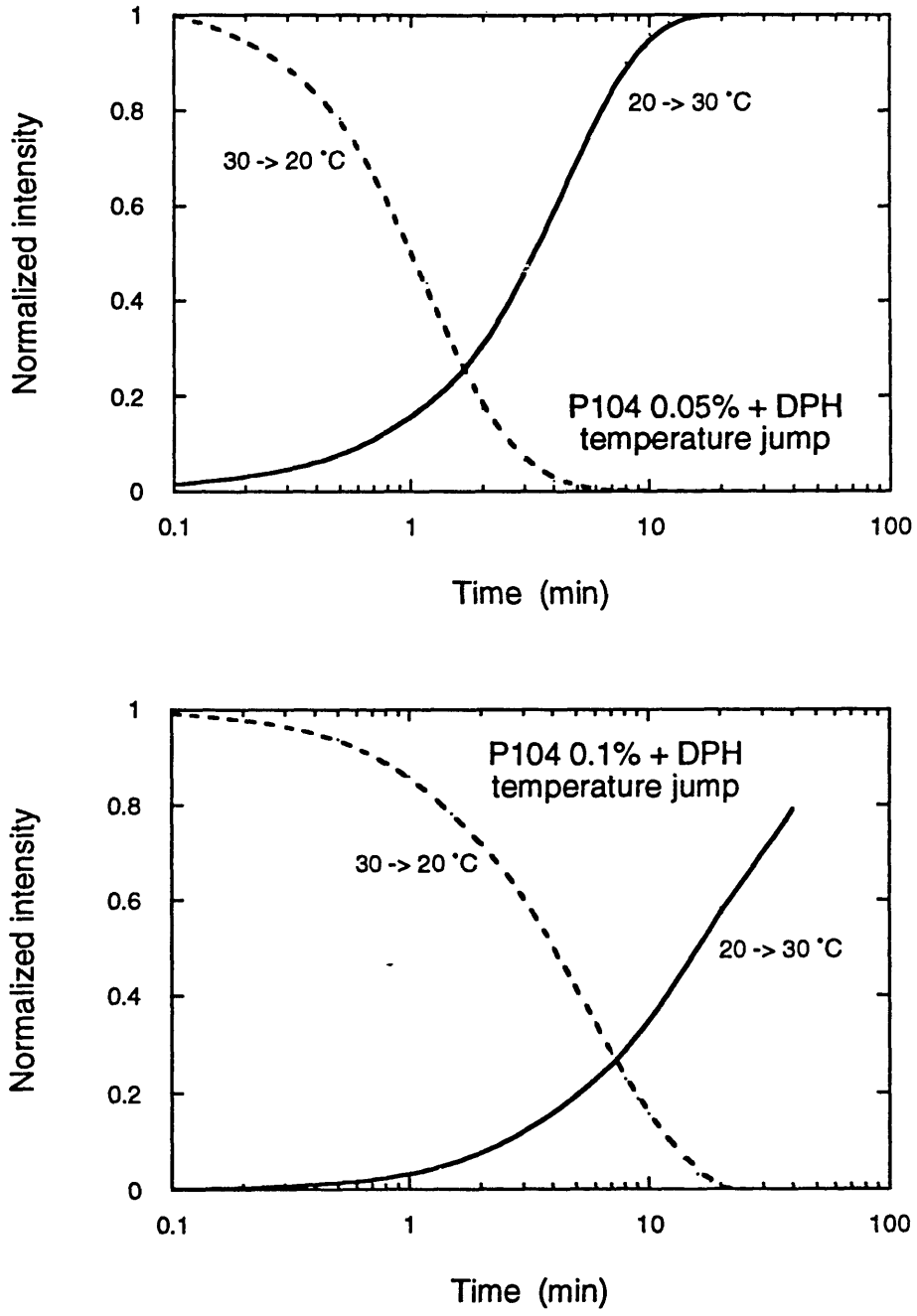

Figure 8.5 Normalized intensity plotted as a function of time (log scale) for up- and down- temperature jumps of (a) 0.05, (b) 0.1, (c) 0.5, (d) 1, and (e) 2.5% copolymer solutions.

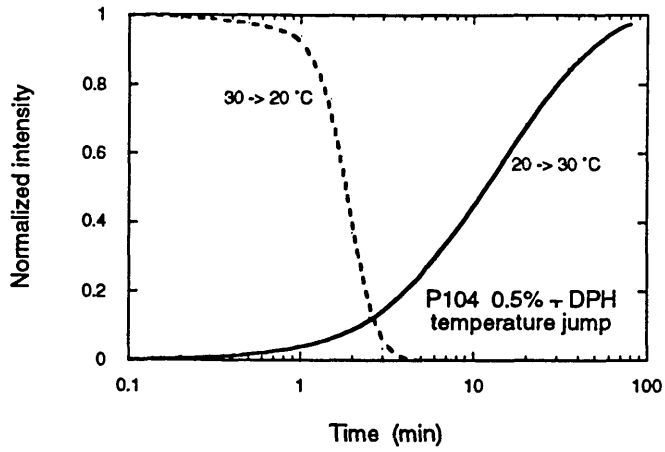

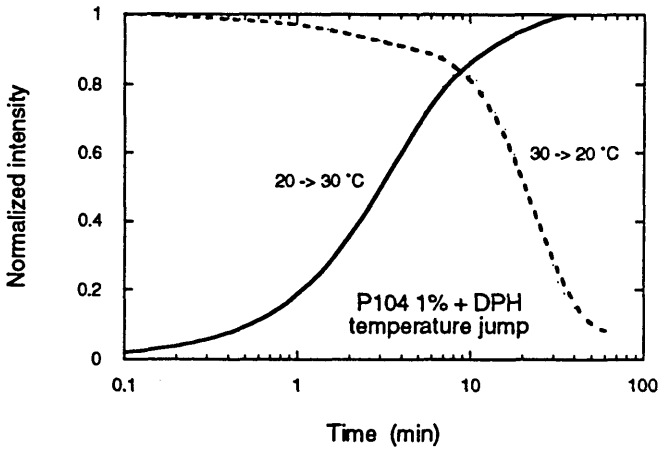

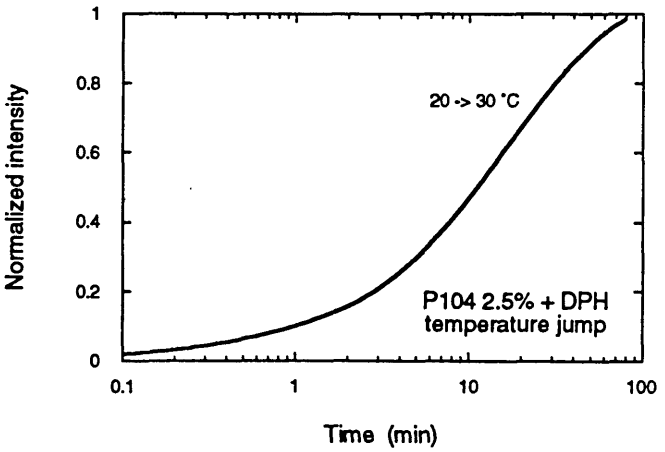

Figure 8.5 Continued.

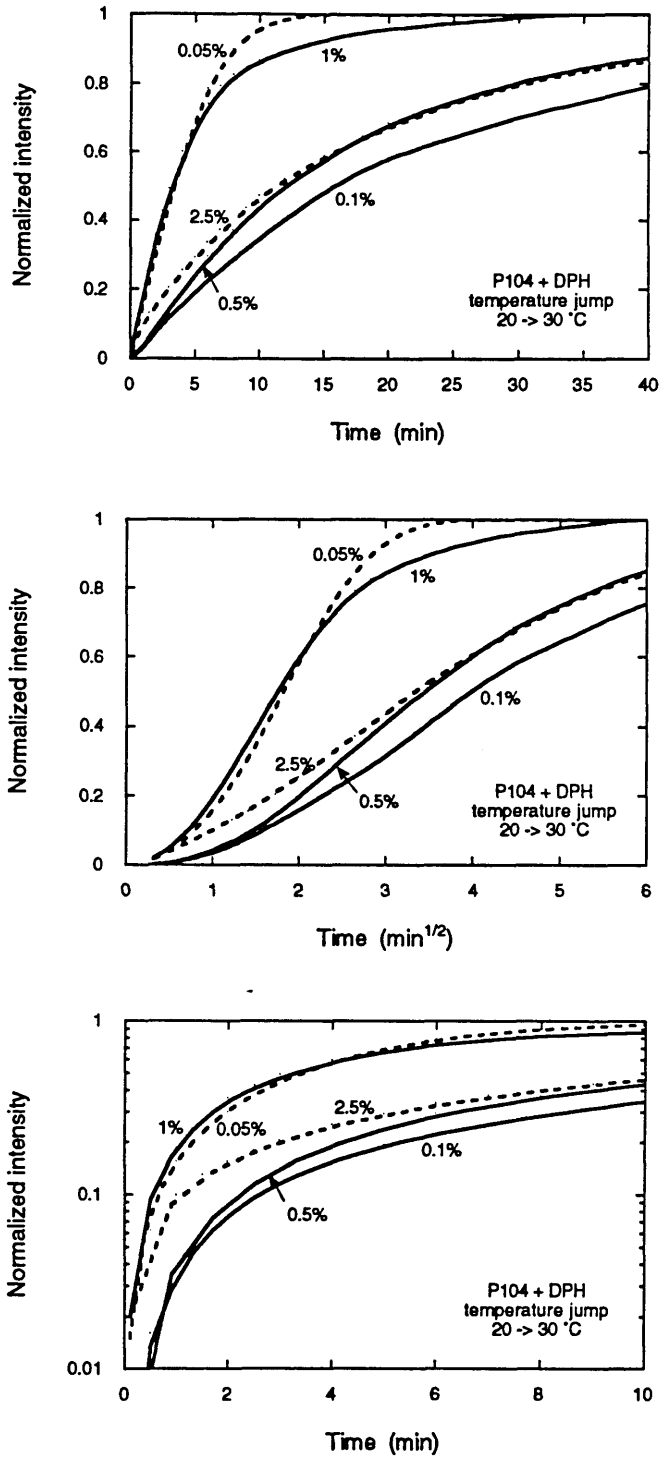

Figure 8.6 Intensity vs time data for 20 to 30 °C (up-) temperature jumps: (a) linear intensity - linear time, (b) linear intensity - square root of time, and (c) log intensity - linear time scales.

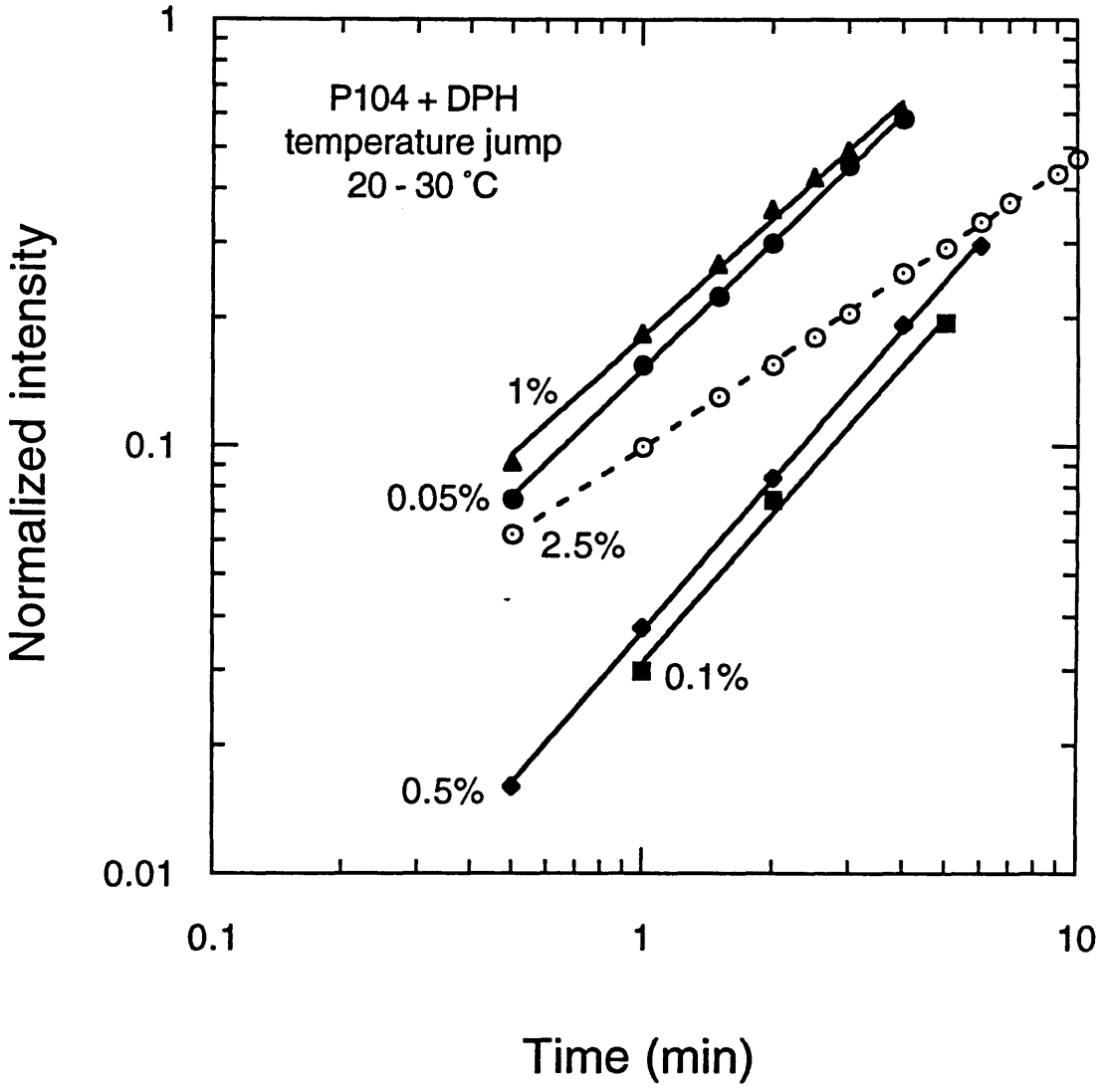

Figure 8.7 Log intensity vs log time plot for 20 to 30 °C (up-) temperature jumps, showing the fit to a power law expression.

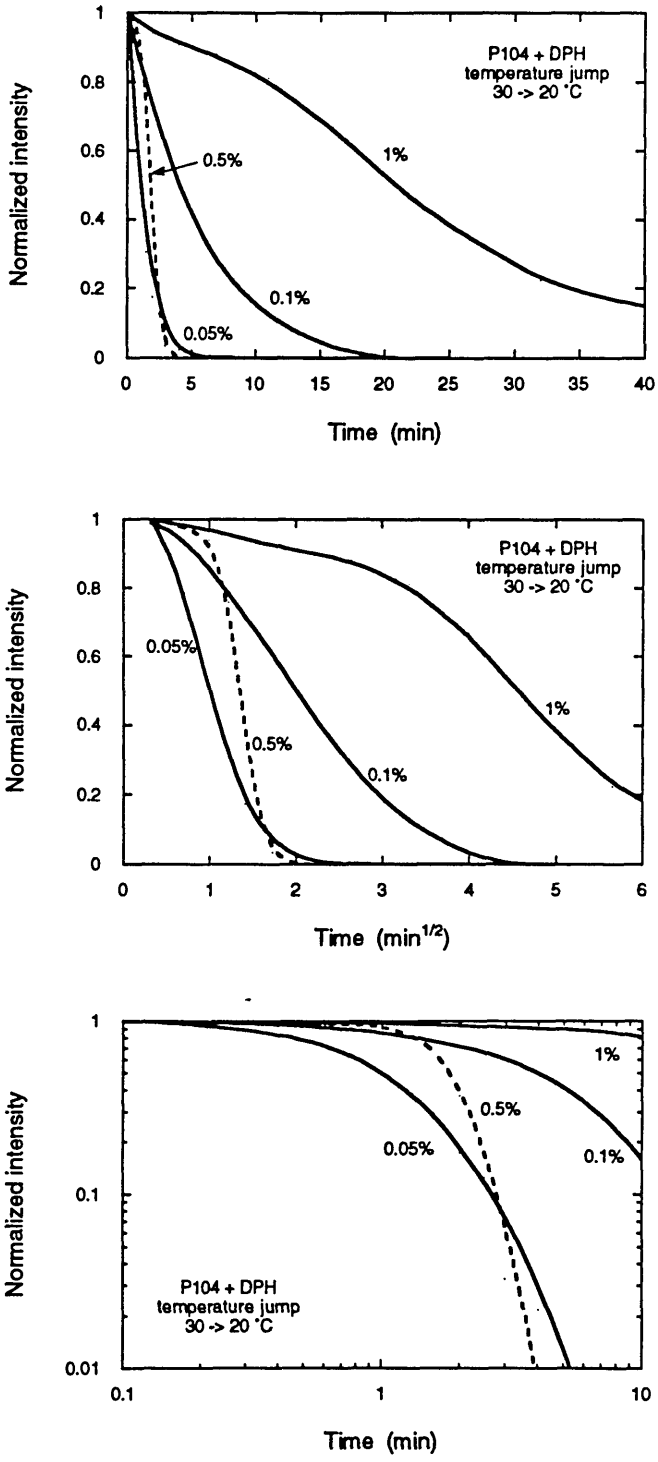

Figure 8.8 Intensity vs time data for 30 to 20 °C (down-) temperature jumps: (a) linear intensity - linear time, (b) linear intensity - square root of time, and (c) log intensity - log time scales.

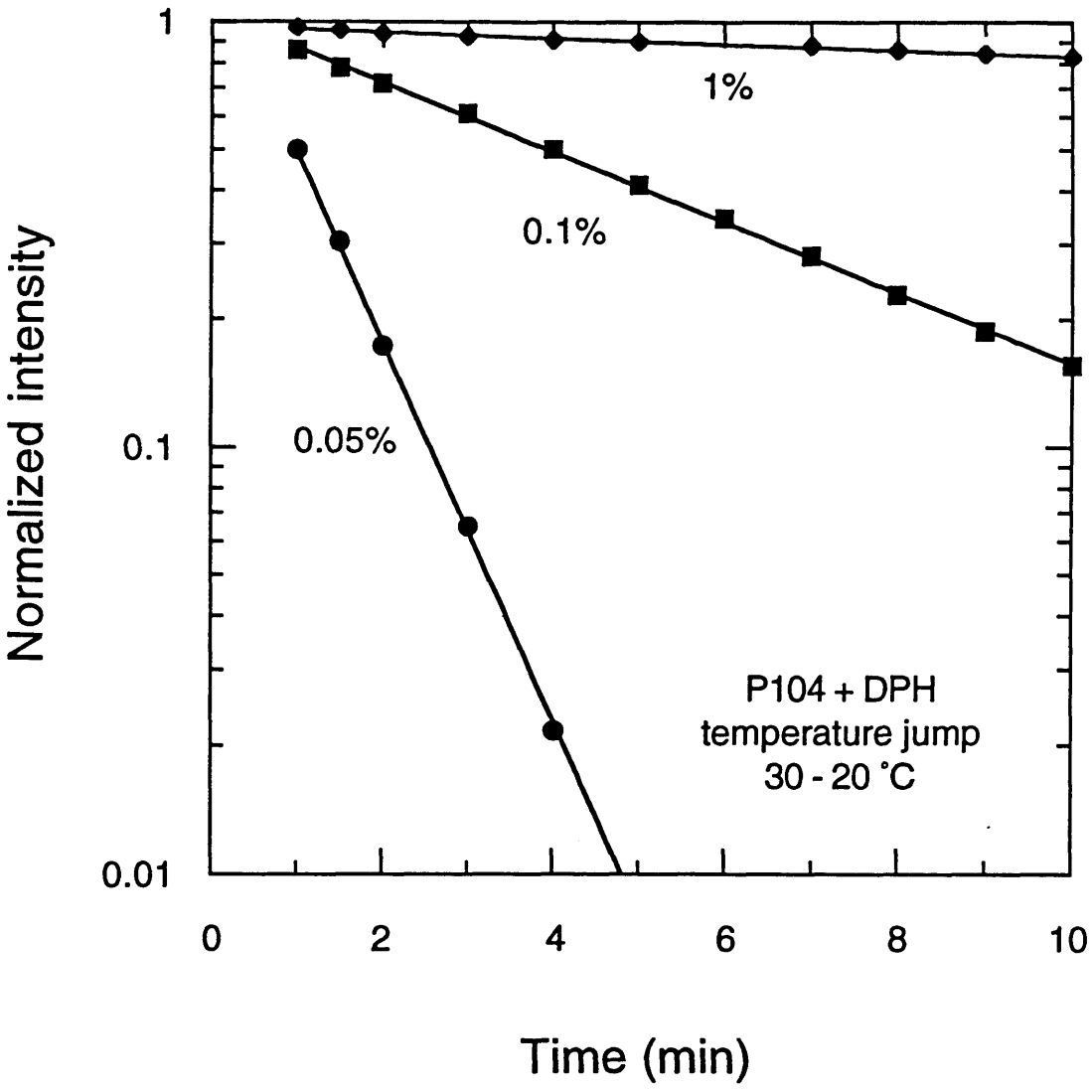

Figure 8.9 Log intensity vs time plot for 30 to 20 °C (down-) temperature jumps, showing the fit to an exponential decay expression.

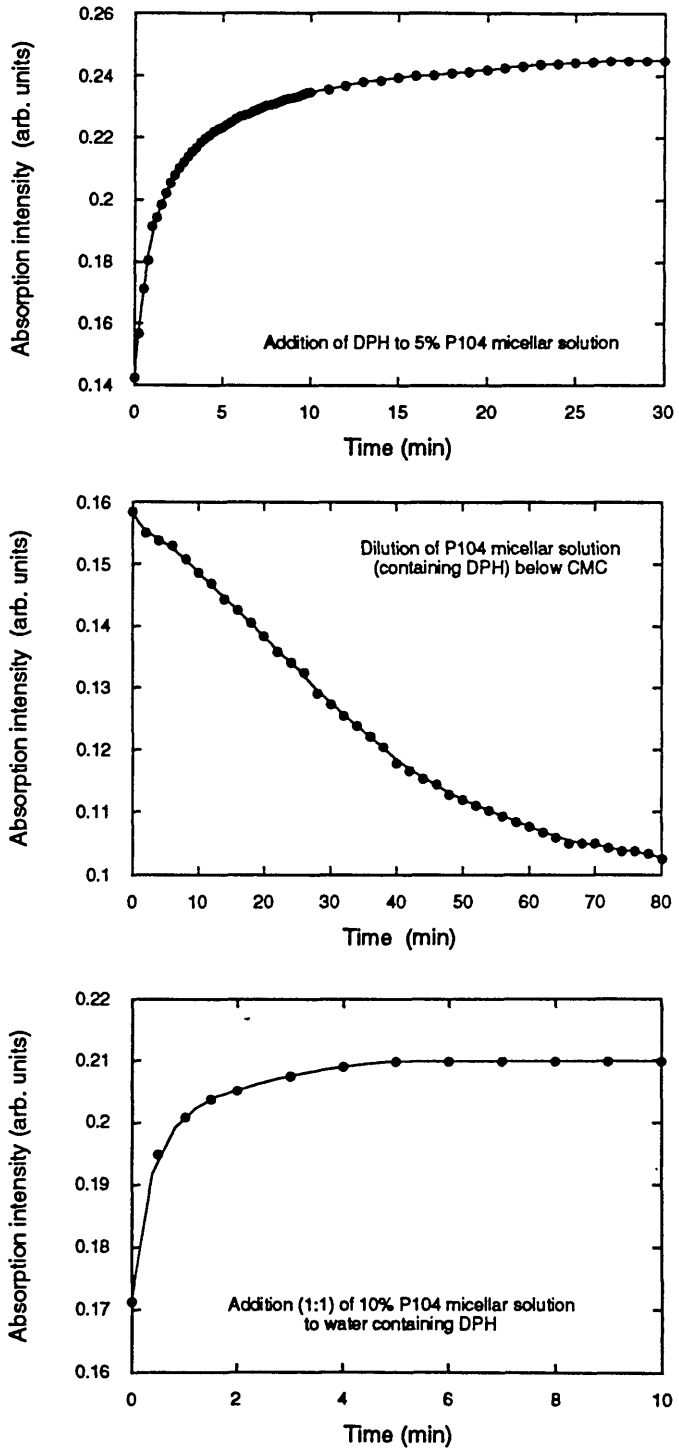

Figure 8.10 Absorption intensity as a function of time, following (a) injection of a small amount of DPH to a 5% P104 micellar solution at 20 °C, (b) dilution of a 5% P104 solution (containing DPH) below CMC upon the addition of water, and (c) mixing a 10% P104 solution with water containing DPH.

Chapter 9
Summary and Future Work on Block Copolymer Micellar Systems

Water-soluble triblock copolymers of poly(ethylene oxide) (PEO) and poly(propylene oxide) (PPO), often denoted PEO-PPO-PEO, are commercially available nonionic macromolecular surface active agents. Variation of the molecular characteristics (PPO/PEO ratio, molecular weight) of the copolymer during the synthesis allows the production of molecules with optimum properties that meet the specific requirements in different areas. As a result, PEO-PPO-PEO block copolymers are an important class of surfactants and find widespread industrial applications in detergency, dispersion stabilization, foaming, emulsification, lubrication, etc., along with more specialized applications in, e.g., pharmaceutics (drug solubilization and controlled release), bioprocessing (protecting microorganisms against mechanical damage), and separations (solubilization of organics in aqueous solutions). Commercial names for these surfactants are Poloxamers and Pluronics. [Chapter 1]

Prompted by the potential of PEO-PPO-PEO Pluronic block copolymer micellar solutions as extractants of organic contaminants in water [Hurter & Hatton *Langmuir* **1992**, *8*, 1291]), the many applications of industrial importance in which these copolymers find use, and the insufficient and often conflicting information published in the literature, we undertook a systematic investigation of micellization, structural and surface-active properties, and micelle-solute interactions for a number of PEO-PPO-PEO block copolymers. A summary of our major observations and conclusions is presented below. Significant progress has been achieved on determining the phase behavior, micellization thermodynamics, surface activity, effect of temperature on structural properties, micelle microenvironment, solubilization thermodynamics, and micellization and solubilization kinetics of aqueous Pluronic copolymer solutions, and in understanding the mechanisms underlying such behavior.

At low temperatures and/or concentrations the PEO-PPO-PEO copolymers exist in

aqueous solution as individual coils (unimers). The copolymers associate and form micelles with increasing copolymer concentration and/or solution temperature, as revealed by e.g., light scattering and dye solubilization experiments. The unimer-to-micelle transition is not sharp, but spans a concentration decade or 10 °C. The critical micellization temperature (CMT) and critical micellization concentration (CMC) values (onset of micelle formation) of twelve Pluronic PEO-PPO-PEO block copolymers, covering a wide range of molecular weights (2900 - 14600) and PPO/PEO ratios (0.19 - 1.79), were determined employing a dye solubilization method. The CMCs and CMTs decrease with increase in the copolymer PPO content or molecular weight. A closed association model was found to describe adequately the copolymer micellization process for the majority of the Pluronics, and used to obtain the standard free energies (ΔG°), enthalpies (ΔH°), and entropies (ΔS°) of micellization. It was determined that the micellization process has an endothermic micellization enthalpy and is driven by the entropy gain in water when unimers aggregate to form micelles (hydrophobic effect) and by the decrease in polarity of ethylene oxide (EO) and propylene oxide (PO) segments as temperature increases. The CMC dependence on temperature and size of headgroup (PEO) of Pluronics follows a similar trend with lower-molecular weight C_iE_j nonionic surfactants, the effect of temperature being more pronounced with the Pluronics. The PEO-PPO-PEO block copolymers were compared to PPO-PEO-PPO block and PEO-PPO random copolymers, in an attempt to probe the effect of molecular architecture in the formation of micelles. No micelles were observed in aqueous PPO-PEO-PPO block copolymer solutions with increasing temperature, up to the cloud point. [Chapter 2]

A correlation is presented for the estimation of CMC and CMT values for PEO-PPO-PEO copolymers in aqueous solutions. CMCs and CMTs are expressed as a function of copolymer molecular weight and PPO/PEO composition, and solution temperature (for CMC determination) or concentration (in the case of CMT). The correlation was developed from experimental CMT data for a set of twelve Pluronic PEO-PPO-PEO triblock copolymers (studied in Chapter 2), and is based on a simple expression for the standard free energy of micellization (ΔG°). The latter is discussed in the light of Flory-Huggins free energy of mixing and phenomenological theories of block copolymer micellization. The theory of Nagarajan [Nagarajan & Ganesh *J. Chem. Phys.* **1989**, *90*, 5843], developed for diblock copolymers, succeeds in predicting qualitatively the contributions of the copolymer composition and molecular weight on the micellization

of triblock copolymers; however, the theory overpredicts the experimentally obtained free energies of micellization by a factor of four. Modification in the Nagarajan theory to account for triblock copolymers [Prochazka et al., *Polymer* **1991** *32*, 3038] is not sufficient to reduce the discrepancy between the experimental data and theoretical predictions. [Chapter 3]

The surface tension of aqueous solutions of seven PEO-PPO-PEO copolymers, covering a wide range of molecular weights (3400 - 14600) and PPO/PEO ratios (0.19 - 1.79), was determined over the 10^{-5} - 10 % w/v concentration range, at two temperatures (25 and 35 °C). Two breaks (changes in slope) were observed in the surface tension vs log concentration curve for most of the copolymers. The low-concentration break, occurring at bulk copolymer concentrations of approximately 10^{-3} %, is believed to originate from rearrangement of the copolymer molecules on the surface at complete coverage of the air/water interface. The breaks in the high-concentration part of the surface tension curve occurred at concentrations that correspond to the critical micellization concentration (CMC) values as determined by a dye solubilization technique. The surface area per copolymer molecule, A, increased as a function of the number of EO units, N_{EO}, obeying a scaling law ($A \sim N_{EO}^{1/2}$) similar to that of lower molecular weight C_iE_j nonionic surfactants. The surface activity of PEO-PPO-PEO block copolymers was compared to that of a PPO-PEO-PPO block copolymer, a PEO-PPO random copolymer, and literature values for PEO and PPO homopolymers, in an attempt to probe the effect of molecular architecture on the orientation of the copolymer at the air-water interface. The presence of the PPO block in the center of the copolymer molecule resulted in a copolymer headgroup (PEO) surface area smaller than that of PEO homopolymer of comparable molecular weight, indicating desorption of PEO segments from the air/water interface and/or tightly packed segments. [Chapter 4]

The effects of temperature on the micellization properties and the structure of the micelles for two PEO-PPO-PEO copolymers (Pluronic P104 and F108), having similar size hydrophobic (PPO) block and different size hydrophilic (PEO) blocks (P104 has 40% PEO, and F108 80%), are reported. CMC and CMT data for aqueous copolymer solutions, obtained from a dye solubilization method, were corroborated with differential scanning calorimetry, surface tension, density, light scattering intensity, and fluorescence spectroscopy experiments; very good agreement among the different techniques has been

observed. The hydrodynamic radii of the copolymer micelles, determined using dynamic light scattering, remained constant over the temperature range investigated; the polydispersity of the micelle size decreased with temperature. The micelles have hydrodynamic radii of approximately 10 nm and aggregation numbers on the order of 50. A decrease in micelle size with increase in copolymer concentration was observed for both P104 and F108. A self-consistent mean-field lattice model [Hurter et al., *Macromolecules* **1993**, *26*, 5030, 5592] for the formation of micelles can capture qualitatively the trends observed experimentally, and provide information on the distribution of the EO and PO segments in the micelle. [Chapter 5]

The micropolarity and microviscosity in aqueous PEO-PPO-PEO micellar solutions were probed utilizing hydrophobic fluorescent molecules which partition preferentially in the micelle interior and are sensitive to the specific enviromnent afforded by the micelles. The micropolarity was probed as a function of temperature using the I_1/I_3 intensity ratio of the pyrene vibrational fine structure recorded in fluorescence emission spectra. The decreasing values for the intensity ratio, following the formation of micelles, were considered to be a linear combination of the temperature effects on polarity observed in bulk PEO and PPO homopolymers. The composition of the micelle core was estimated using these data, suggesting approximately 30% PEO content. Micelles assembled from higher molecular weight PEO-PPO-PEO copolymers (at constant PPO/PEO copolymer composition) exhibit more hydrophobic microdomains. The ratio of "monomer" to excimer fluorescence emission intensity bands, I_1/I_e, of dipyme was used as a measure of the "microviscosity" that dipyme experienced. The microviscosity decreased with temperature for all systems studied. The I_1/I_e values for the F108 micelles are comparable to the ones for bulk PPO, suggesting that the environment where dipyme is located is like bulk PPO; the micelle core appeared to become more compact as temperature increased. Increase of the copolymer molecular weight at constant PPO/PEO composition, and increase of the PPO block size at constant PEO block size, resulted in increasing microviscosity and activation energies. The effect of PEO block on micelle microviscosity was less significant. [Chapter 6]

The solubilization of 1,6-diphenyl-1,3,5-hexatriene (DPH), a fluorescence dye, in Pluronic copolymer micelle solutions was investigated. DPH partitioned favorably in the micellar phase, with the partition coefficient higher for P123 (a Pluronic copolymer with

70% PPO), and decreasing in the order of P123 > P103 > P104 = P105 > F127 > P84 > P85 = F108 > F88 > F68 > P65. It can be concluded from these data that the solubilization was influenced by both the relative (with respect to PEO) and absolute size of the hydrophobic PPO block. Standard free energies (ΔG°), enthalpies (ΔH°), and entropies (ΔS°) of solubilization were estimated. The solubilization process is also entropy-driven and has an endothermic enthalpy. [Chapter 7]

Temperature jump and concentration jump experiments were performed to induce micelle formation or dissociation and solute uptake or release, and the dynamic response of the system was observed with light scattering intensity or absorption spectroscopy. The following conclusions can be drawn from the above experiments: the copolymer micelle association and dissociation process has a relaxation time of 5 minutes; solubilization of molecularly dispersed solute in the micelles takes place in the same time range; dissolution of DPH microcrystalline aggregates can take longer and can be the rate limiting step in the solubilization process; DPH that has been solubilized in micelles can remain long in solution, even below the CMC. [Chapter 8]

In addition to the phase behavior, micellization thermodynamics, surface activity, fluorescence, and solubilization studies outlined above, a number of other related investigations have been initiated or are in progress. The effect of urea on the micellization properties of Pluronic P104 (in progress), the enthalpy of dilution for a number of PEO-PPO-PEO copolymers and the enthalpy change upon solubilization or emulsification of apolar solvents in aqueous copolymer solutions, both measured using titration calorimetry (initiated) were examined. The investigation on urea should provide more information on the mechanism (polymer-polymer or polymer-solvent interactions) responsible for micellization; urea is considered a "structure breaker" that decreases the hydrophobic effect in water, thus altering polymer-solvent interactions. Enthalpy of dilution values for PEO-PPO-PEO copolymer solutions would allow us to relate the enthalpy change measured from differential scanning calorimetry to the standard enthalpy of micelle formation obtained from the association model. Dissolution rates of solid (or paste) copolymer in water could also be measured with titration calorimetry.

Some of the topics discussed in this Thesis could also be extended. In particular, the relationships between micellization thermodynamic parameters and copolymer

composition (Chapter 2) along with the correlation for predicting CMC and CMT (Chapter 3) deserve more analysis, the aim being a model of micellization for the PEO-PPO-PEO copolymers with predictive capabilities. A very interesting area for future investigation is that of micellization and solubilization kinetics. The information presented in Chapter 8 could be expanded and further rationalized. In terms of future developments, it is worth pointing out the medical applications of PEO-PPO-PEO copolymers as micelles, gels, and adsorbed at surfaces. Gels are formed by certain PEO-PPO-PEO block copolymers at high concentrations, while the micelles remain apparently intact in the form of a "crystal". There are a few studies available on the application of copolymer micelles and gels as controlled release agents, and there is definitely need for a better understanding of the phenomena involved. Our contributions on thermodynamics and kinetics of micellization and solubilization constitute a very sound basis for further work in the various applications that PEO-PPO-PEO copolymers find.

Part B

Thermodynamics of Micelle Clustering, and Interfacial Dynamics in Reverse Micellar (Water-in-Oil Microemulsion) Systems

Chapter 10
Dynamic Processes in Reverse Micellar Systems

10.1 Reverse Micellar or Water-in-oil Microemulsion Systems

10.1a Introduction to reverse micelles

Certain surfactant molecules form thermodynamically stable reverse micelles when dissolved in apolar solvents. The polar groups ("heads") of the amphiphilic molecules are directed towards the interior of the spheroidal aggregates, forming a polar core in which water and various hydrophilic molecules can be solubilized. The aliphatic surfactant chains ("tails") are directed towards the apolar solvent. In the case of significant water solubilization inside the polar core, the reverse micelles can be envisaged as distinct, nanometer-scale water droplets, maintained in solution with the aid of the surfactant monolayer which reduces unfavorable oil-water contact. These solutions of "swollen" reverse micelles are thermodynamically stable, and are often called "water-in-oil microemulsions".

Reverse micelles are only one possible aggregate structure among an extremely rich variety of structures observed in systems composed of surfactant, cosurfactant, oil, water and salt [Ekwall et al., 1970; Israelachvili et al., 1976; Tamamushi & Watanabe, 1980; Friberg, 1985; Israelachvili, 1986; Shinoda & Friberg, 1975; 1986]. Still, reverse micellar solutions have attracted particular attention over the past twenty years. This can be attested to by a growing number of review papers on surfactant aggregation and micellization in nonpolar solvents [Kertes & Gutman, 1976; Shinoda & Friberg, 1986; Shinoda & Lindman, 1987; Eicke, 1980; Eicke, 1987], on the application of various sophisticated analytical methods in the study of reverse micelles [Eicke, 1980; Eicke, 1987; Kitahara, 1980; Luisi & Magid, 1986; Luisi et al., 1988; Zana, 1987; Vos et al., 1987], and on the study of solubilization, catalysis and enzymology in reverse micelles [Kitahara, 1980; Shinoda & Friberg, 1986; Shield et al., 1986; O'Connor, 1987; Luisi et al., 1988; Khmelnitski et al., 1989].

10.1b Applications of the reverse micellar systems

Reverse micelles attracted the interest of technologists and engineers because of their important practical applications in oil recovery [Sharma & Shah, 1985; Miller & Qutubuddin, 1987], lubrication, cosmetics, and the food industry [Eicke & Parfitt, 1987]. Biologists have considered micelles as useful membrane-mimetic systems for a long time [Fendler, 1982]. Reverse micellar systems can be used by chemists as microreactors, in which guest molecules are brought together to react, often showing reactivities that differ markedly from those observed in pure solvents [Fendler, 1982; Atik et al., 1985; Shield et al., 1986; O'Connor, 1987; Luisi et al., 1988; Khmelnitski et al., 1989; Bommarius, 1989]. Biotechnologists became interested in these systems when it was shown that many proteins and other biopolymers can be solubilized in reverse micelles without significant losses in biological activity [Luisi et al., 1988; Luisi & Magid, 1986; Martinek et al., 1986; Khmelnitski et al., 1989]. The separation potential of micellar liquid-liquid extraction for complex systems has been studied by Hatton and coworkers [Göklen and Hatton, 1985, 1987; Woll et al., 1989], and Dekker et al. [1986].

An increased interest in reverse micellar systems has been observed in recent years, as the feasibility of novel applications of these systems is investigated. More specifically, reverse micellar solutions have been proposed as media for polymerization reactions [Candau et al., 1984; Candau & Carver, 1989; Voormans & de Schryver, 1989; Menger & Tsuno, 1990], for reactions producing colloidal microparticles [Kandori et al., 1988; Robinson et al., 1989; Barnickel & Wokaun, 1990] and semiconductor particles [Lianos & Thomas, 1987; Steigerwald et al., 1988; Steigerwald & Brus, 1989; Petit & Pileni, 1988; Petit et al. 1990, and for enzymatic reactions [Luisi & Magid, 1986; Luisi et al., 1988; Martinek et al., 1986; Khmelnitski et al., 1989]. The possible uses of reverse micelles in supercritical organic solvents have also attracted much attention recently [Johnston & Penninger, 1989; Smith et al., 1990; Yazdi et al., 1990].

10.1c The interfacial region in reverse micellar systems

Two of the most interesting features of reverse micellar (water-in-oil microemulsion) phases are the availability of an extensive surfactant interface between oil and water, and the compartmentalization property. Each water-in-oil microemulsion

droplet consists of two distinct regions with widely different properties: (i) the water pools, and (ii) the surfactant interface. The surfactant "heads" are located in an intermediate fuzzy region separating the polar core from the apolar tails. This has often been considered as a third important region with properties that differ from those of the water pools, since water can be highly structured in the proximity of the surfactant interface. It is generally believed that the surfactant molecules adsorb in the form of a monolayer on the curved oil-water interface in the microemulsion droplets [Prince, 1977; Eicke, 1987]. A slightly different picture was put forward by Maitra [1984] who suggested that some surfactant molecules "remain outside the interface and thereby increase the effective thickness of the AOT monolayer to a value of about 15 Å". However, this interpretation has not been supported by many investigators. Usually the surfactant interface is viewed as a monolayer, whose apparent thickness may increase because of fluctuations of the surfactant molecules about their mean position.

The molecular interfaces of supramolecular surfactant aggregates possess considerable fluidity, a phenomenon that has attracted theoretical interest in the past few years (see the discussions by Schneider et al. [1984], Helfrich [1986], and Faucon et al., [1989], on the fluidity of vesicles and biological membranes, and the discussion by Aniansson et al. [1976], Ljunggren and Eriksson [1984], and Halle et al. [1988] on the fluctuations of normal micelles). The significant shape fluctuations of microemulsion droplets have been examined theoretically by Safran [1983], Milner and Safran [1987], and Borkovec et al. [1989]. An experimental study by Carlström and Halle [1989] indicated that a substantial shape polydispersity may exist. The interface fluidity affects the presence of water and oil in the interfacial region; available experimental results suggest that water (and probably ions) can penetrate the surfactant sheath [Bardez et al., 1986]. Molecular dynamics simulations by Brown and Clarke [1988], as well as similar calculations by Jönsson et al. [1986] in normal micelles, indicated that water can penetrate into the surfactant monolayer. Another important issue is the ability of the organic solvent to penetrate the surfactant tail region. Longer alkanes are generally less able to penetrate into the tail region; more penetrating solvents, like cyclohexane and toluene increase the tendency of the interface to bent towards the aqueous side. The region were reverse micelles are stable occupies a much larger area of the phase diagram when penetrating organic solvents are used. To date there is no realy satisfactory explanation of the interaction of the organic solvent with the surfactant tails [Leodidis, 1990].

10.2 Microemulsion Dynamics

10.2a Dynamics at the molecular level

The dynamic processes occurring in surfactant-containing system on a molecular level are a unifying theme in the kinetics of surfactant association, reverse-micelle coalescence, and solubilizate exchange. Experimental techniques such as fluorescence spectroscopy, NMR, neutron and light scattering, and ultrasounds, have been used in an attempt to shed light on the microscopic-level interaction mechanisms. Lindman and Stilbs [1988] reviewed molecular diffusion processes in microemulsions, and methods for measuring diffusion, such as nuclear spin-echo, tracer techniques, transient optical grating methods, and dynamic light scattering. Grieser and Drummond [1988] discussed many of the molecular spectroscopic probe techniques that have been used to determine the apparent microviscosity and other physicochemical properties of micellar systems. Vos et al. [1987], reviewing techniques employed to obtain structural information about surfactant aggregates, cover magnetic resonance and optical methods by which the dynamics of micellar systems can be investigated on a molecular level.

D'Arrigo et al. [1989] measured the ultrasonic absorption and sound velocity in the water/AOT/n-heptane microemulsion system as a function of the [water]/[AOT] molar concentration ratio, Wo, and temperature. The ultrasonic relaxation spectra in the frequency range 15 - 250 MHz were described by a single time relaxation equation. The investigators attributed the relaxation process observed in the composition range $0<Wo<20$ to the exchange of water molecules between bulk and bonded aqueous domains inside the droplet core. In the $20<Wo<40$ range, in addition to the fast process described above, a slower process with relaxation times that increase with Wo has been identified and assigned to thermal shape fluctuations of the reversed micelles. Relaxation processes related to collisional and diffusional modes occur at a frequency range below that explored by the ultrasonic technique. Sound velocity results showed that water-filled micelles are more "floppy" than bulk water. Fletcher et al. [1986] used quasi-elastic neutron scattering to investigate the mobility of surfactant and water molecules in w/o microemulsions stabilized by AOT. They found that addition of benzyl alcohol (which is absorbed at the interface) or

toluene effected little change in the lateral translational diffusion of AOT within the interface. Replacing the water by glycerol resulted in a two-fold reduction in surfactant mobility.

10.2b Kinetics of surfactant association

The existence of two relaxation processes related to micellar equilibria in aqueous solution of ionic detergents is generally accepted [Aniansson, 1978; Hoffmann, 1978; Kahlweit & Teubner, 1980]. These processes are characterized by the relaxation times τ_1 and τ_2 differing by as much as two to three orders of magnitude ($\tau_1<\tau_2$). The fast process τ_1 (on the order of 10^{-6} s) has been assigned to the association-dissociation (exchange) equilibrium of amphiphilic ions to/from micelles; τ_1 has been detected by means of ultrasonic absorption, temperature-jump, and/or shock tube method. The slow process τ_2 (ranging between 10^{-3} - 1 s), which has been detected by pressure-jump and/or temperature-jump, is attributed to the micellization-dissolution equilibrium.

Aniansson et al. [1976] presented a theory for the micelle kinetics which accounted for the complex concentration, temperature, hydrophobic tail length, and counterion dependence of the relaxation times that have been observed in solutions of sodium alkyl sulfates. Uehara [1976], and Almgren et al. [1978] studied the effect of alcohols on the slow relaxation constant (τ_2) using pressure-jump. The lower alcohols decreased τ_2, and the higher ones increased it. Yiv et al. [1981] used chemical relaxation methods to probe the dynamics of micellar solutions of long chain surfactants (TTAB and CTAB) and medium chain length alcohols (butanol to hexanol). They found that the rate constant for the dissociation of a surfactant from a mixed micelle and the relaxation time for the surfactant exchange between micelles and surrounding solution decreased with the addition of alcohol, and they attributed this to micelle charge density dilution due to alcohol solubilization.

10.2c Bending of interface

Particularly important in understanding the behavior of microemulsions are the fluidity and flexibility of the oil-surfactant-water interface. Indeed, these properties reflect the ease with which the film rearranges upon a constraint, and thus its dynamics. The

fluctuations of the interface have been investigated in so-called "birefringent microemulsions" using spin labels [Di Meglio et al., 1983]. The characteristic times for such fluctuations, which correspond to the local reorganization of the film, appeared to be longer than 0.1 μs. In a transient birefringence study of various water-in-oil microemulsions, a negative birefringence component observed was attributed to such film fluctuations and found to have a characteristic time of about 1 μs [Guering & Cazabat, 1984], in agreement with the conclusion of the spin label study.

An important parameter in describing surfactant interfaces in microemulsions and related systems is the bending modulus or bending elasticity / rigidity constant [Helfrich, 1973], defined as twice the amount of energy required to bend a unit area of surface by a unit of curvature. Attempts have been made to measure the surfactant monolayer rigidity κ by analyzing shape fluctuations of microemulsion droplets in the three-component AOT-water-alkane system. Neutron spin-echo techniques revealed that the monolayer rigidity does indeed control the fluctuations of the interface [Huang et al., 1987]. The bending elasticity constant was estimated to be about 5 kT. Kotlarchyk et al. [1988] estimated the bending energy of an AOT microemulsion interface to be 0.4 kT (from SANS data) using a polydispersity relationship that is based on a microemulsion fluctuation model proposed by Safran [1983]. The Safran model provided the basis for an analysis of Kerr effect measurements on AOT microemulsions by Borkovec and Eicke [1989], from which a bending monolayer rigidity of 0.5 kT was estimated.

10.2d Kinetics of coalescence and solubilizate exchange

Reverse micelles are colloidal aggregates; because of their size (in the 1 - 10 nm range) these aggregates are subject to Brownian motion, colliding continually and sometimes coalescing to form short-lived dimers that redisperse again to form new micelles. It should be noted that such a phenomenon is not observed with normal micelles, because the charged surfactant headgroups pointing outward to the aqueous continuum lead to Coulombic repulsions between the micelles. As a result of the coalescence and decoalescence sequence, probe molecules solubilized in the water pools are redistributed over the micelle population at a rate that can be characterized in terms of a second-order reaction constant k_{ex}. A reverse micellar system cannot be observed directly during collisions or in the state of the transient dimer, and, therefore, indicator reactions between

probe molecules must be used to obtain information about the coalescence process. In order to investigate solubilizate exchange between micellar cores, it is desirable that the probe molecules partition exclusively in the water-pools; otherwise other (e.g. interfacial transport processes may dominate the exchange.

There are five sequential elementary steps associated with coalescence and reaction processes in reverse micellar systems [Bommarius et al., 1990]: (i) diffusional approach of the micellar aggregates, (ii) opening of the surfactant interface, (iii) diffusion of the indicator ions inside the temporary dimeric aggregate, (iv) chemical reaction of the indicator ions, and (v) decoalescence of the temporary dimeric aggregate. The observed overall time constant for the reaction can be expressed in terms of the individual time constants for each of the independent steps in this sequence. Collision between micellar aggregates is governed by diffusion which is the fastest process by which two species can approach and encounter each other. The rate constant for the diffusional encounter of aggregates, $k_{diff,agg}$, is thus an important upper bound for second order processes such as reverse micellar coalescence. The latter depends on the concentration or number density N of reversed micelles, and has a time constant of $1/k_{ex}N$. With typical values of N approximately 10^{-3} M, and k_{ex} of approximately 10^{7} $(M\ s)^{-1}$ [Zana and Lang, 1988], the order of magnitude of this time constant is 10^{-4} s.

The study of dynamics of both oil-in-water and water-in-oil microemulsions has witnessed rapid progress in recent years [Zana & Lang, 1988]. Eicke et al. [1976] demonstrated that solubilizate exchange must involve reversed micellar collisions and at least partial merging on a fast time scale. More recently, the problem of quantifying the exchange rate constant kex has been addressed, mostly with the system AOT/hydrocarbon/water [Fletcher & Robinson, 1981, 1984; Atik & Thomas, 1981a, 1981b; Pileni et al., 1984; Fletcher et al., 1987; Lang et al., 1988]. Atik and Thomas [1981] used pulsed-laser flash-photolysis to measure an exchange rate constant k_{ex} of 1.7 x 10^{7} $(M\ s)^{-1}$ for the AOT/n-heptane system in the absence of additives. The type of solvent used can change k_{ex} by an order of magnitude. In an extensive study, Fletcher et al. [1987] found similar k_{ex} values and the surfactant layer opening to be the rate limiting step in the coalescence process. Although there has been some agreement as to the magnitude of the exchange constant reported in a number of different studies, this is not a universal result and much higher exchange rate constants have been obtained in some cases [Lang et.

al., 1988]. The values reported by Lang et. al. [1988] were close to the diffusion limit of reaction and thus solubilizate exchange may no longer have been rate limiting. Compared to AOT stabilized microemulsions, less work has been done on other surfactant systems [Clark et al., 1990; Fletcher & Parrot, 1989; Jada et al., 1990; Lang et al., 1990; Atik & Thomas, 1981; Bommarius et al, 1990].

These reported studies on micellar exchange rates show that there is still no clear consensus as to the precise nature of the interactions between reversed micelles and the actual rates of the micelle-micelle fusion process. Indeed some of the results may have been influenced by experimental artifacts associated with the localization of probes within the reversed micellar water pools and consequent non-coalescence-related interchange of micellar contents. Moreover, it is still not clear what role the structure and composition of the surfactant interface layer play in determining the facility with which the micelles fuse and solubilizate exchange occurs. Additional information regarding microemulsion droplet interactions and droplet content exchange can be obtained through conductivity percolation experiments (see Chapters 11 and 12 of this Thesis).

10.3 Adsorption at and Diffusion through Interfaces

Different approaches have been developed in the theoretical modelling of the interfacial transport processes. Physical scientists treated transport as a chemical reaction-like process in a "pseudophase", and coupled it to absorption in and desorption from the interface; electrochemists, studying the transfer of ions through interfaces between two immiscible electrolyte solutions, developed a stochastic approach; engineers started from the three-dimensional continuum transport equations and modified them down to the two-dimensional interface. A potential energy barrier, that the diffusing solute has to overcome on its way through the interface, is a unifying theme in all three approaches.

10.3a Interfacial transport models

Brenner and Leal [1978; 1981] have published a series of papers establishing the fundamental processes leading to behavior that can be represented by a mass transfer coefficient. They examined the interfacial transport process as a continuous motion of

solute over a small region of finite thickness, rather than as a discontinuous jump in either concentration or its gradients across a two-dimensional surface. By taking the limit as the thickness of the interfacial region becomes infinitesimal (relative to the length scale of observation), Brenner and Leal determined appropriate expressions for the macroscopically observed "jump" in properties. The solute molecules were modelled as noninteracting Brownian spheres, influenced by spatially varying physicochemical forces (as well as the enhanced hydrodynamic resistance) in the immediate vicinity of the interface. These forces were presumed to be derived from a potential energy function which varied smoothly from one bulk-phase to the other. Under these conditions, the solute flux was shown to be related to the concentration profile via a one-dimensional steady-state Smoluchowski equation. Integration of this equation provided an expression for the overall resistance to mass transfer in terms of an integral over local properties of the system:

$$R = \int_{-\infty}^{0} [\exp(E(x)-E_1^{\infty})-1]\,[D(x)]^{-1}\,dx + \int_{0}^{\infty} [\exp(E(x)-E_2^{\infty})-1]\,[D(x)]^{-1}\,dx$$

where E_1^{∞}, E_2^{∞} are the potential energy of the solute in bulk phases 1 and 2 respectively, D(x) and E(x) are the diffusion coefficients and potential energy profiles applying throughout the interfacial region, and K is the partition coefficient between the phases, $K = \exp[-(E_1^{\infty}-E_2^{\infty})]$.

The analysis of Brenner and Leal has been extended to studies of more complex two-phase systems [Shaeiwitz & Raterman, 1982; Larson, 1982; Larson and Lam, 1986; Borwankar and Wasan, 1986], relaxing some of the assumptions used in the initial works. The consensus amongst these workers is that, in their generality and fundamental basis, the above equation and succeeding expressions are extremely powerful, but that to date little is known about the actual form of the diffusion coefficient and energy profiles in the vicinity of interfacial regions. Shaeiwitz and Raterman [1982] have attempted to calculate physical interfacial resistances assuming various energy profiles and hindered diffusivities. Their study examined first several idealized profiles to check the effect of their shapes on resistance, and then employed a calculated profile based on dispersion energies [Mahanty and Ninham, 1973]. However this latter energy profile led to results having no physical significance, a fact that the authors ascribed to limitations of the model upon which it was based.

Borwankar and Wasan [1986] studied the interfacial resistance to transfer of solute (assumed to have negligible surface activity) due to the presence of a soluble surfactant at equilibrium distribution in the system. The interfacial region was treated as a microcontinuum, and the surfactant and the solvents regarded as a "composite" solvent with local-average position-dependent properties. In a study of surfactant adsorption at fluid-fluid interfaces, Borwankar and Wasan [1988] represented activation energy barriers to solute exchange between the bulk and the interface using kinetics of a reversible reaction. In their conclusion, Borwankar and Wasan [1986] remarked: "an a priori calculation of the interfacial resistance is currently ruled out for solute transport across interfaces with adsorbed surfactant because of the lack of detailed knowledge regarding the structure and composition of the interfacial region". The form that the energy profiles take in the interfacial region, and their impact on the observed resistance, is clearly one of great interest.

10.3b Diffusion and association in amphiphilic membranes

Ketterer et al. [1971] proposed that the transport of lipid-soluble ions through bilayer membranes occurs in three distinct steps: (i) adsorption to the membrane solution interface; (ii) passage over an activation barrier to the opposite interface; and (iii) desorption into the aqueous solution. From relaxation experiments, Ketterer et al. [1971] found the desorption into the aqueous phase to be the rate limiting step. Jordan and Stark [1979] expanded the above model and treated the coupling of diffusion, adsorption and translocation processes in an exact manner. Honig et al. [1986] reviewd electrostatic interactions in membranes and proteins, and enumerated the contributions to the total potential energy profile that a charged molecule has to overcome when moving through a bilayer. The free energy for small charged molecules, as a function of their position in the membrane, can be written as the sum of electrical and nonelectrical terms: the Born, image and dipole energy contributions contain all of the dominant electrical interactions of a charged molecule with the membrane, while the neutral energy term includes all the other contributions to the free energy such as hydrophobic, van der Waals, steric, and specific chemical interactions. The free energy of transfer in moving a charged body to a region of a different dielectric constant is given by the Born expression and, for the case of lipid bilayers, poses the most significant barrier to ion transport across bilayers. The neutral energy contribution is the free energy of transfer for moving a small molecule from the

aqueous phase to the membrane, apart from electrical contributions.

10.3c Ion transfer through liquid-liquid interfaces

The transfer of heavy particles (ions) through the interface of two non-conducting condensed media was investigated theoretically by Gurevich and Kharkats [1986] in the framework of a stochastic approach. Samek et al. [1986; 1988] modified this approach, taking into account the reorganization of the solvent around the ion transferred, and studied transfer kinetics across the interface between two immiscible electrolyte solutions. The stochastic approach was based on the Langevin equation of motion and the assumptions that the fluctuations in the condensed medium are statistically independent, and their duration is small compared with the characteristic period of time of the system evolution. Applying the Maxwell-Boltzmann equilibrium distribution for the distribution of particle velocities, the solution of a Fokker-Plank equation resulted in the particle flux expression. The microscopic diffusion coefficient $\underline{D}$ used in this expression is, in general, not identical with the phenomenological diffusion coefficient D appearing in the second Fick's law. Specifically, for the ion transport in solids, in which case the potential energy of the ion has a fixed profile, the two quantities can be related to each other through the equation: $D = \underline{D} \exp[-\Delta U_{ion}/(kT)]$, where ΔU_{ion} is the activation energy of the ion motion. In liquids D and $\underline{D}$ are similar, this being related to the absence of a fixed profile of a potential energy of an ion, the motion of which does not consist of a sequence of jumps over activation barriers as in solids, but in a large number of small stochastic displacements. Comparing their experimental results (for transfer of tetraalkylammonium ions across the water/nitrobenzene interface) to the model, Samek et al. [1986] concluded that ΔU_{ion} is comparable with the activation energy for the ionic motion in solids. Such a barrier was attributed to the short range interactions between an ion and the solvent molecules in the vicinity of the interface.

10.4 Relaxation Techniques

10.4a Theory

The techniques employed for measuring events in a chemical system at a

microsecond level can be clasified into two groups, flow and relaxation techniques. In relaxation techniques, the equilibrium state of a system is perturbed through a step change, or "jump", in an intensive property of the system, such as temperature, pressure, or electric charge. The approach of the system to the equilibrium state at the new value of the system property is recorded as a function of time. There are two conditions for the application of a relaxation method to be appropriate: (i) the system must attain a state of equilibrium before and after the relaxational jump (the fast event cannot be irreversible), and (ii) the change of the intensive parameter must cause a measurable change in the system; in the case of temperature jump, the event must possess a sizable free energy of activation $\Delta H^{\ddagger}$, while a pressure jump method necessitates a measurable volume of activation $\Delta V^{\ddagger}$.

Flow methods are based on the measurement of rate events after rapid mixing of components. In the stopped-flow method, two streams (containing the reactive species) are mixed by simultaneous acceleration via two syringes (acting as pistons) and subsequent deceleration in the mixing chamber. The stopped-flow technique is limited by the dead-time of mixing, approximately 5 ms. This problem is reduced in the continuous flow method, in which two streams are continuously mixed at the entry of a plug-flow reactor. The fast event occurs within the residence time of the fluid element. Again, the limit of this method is reached when the timescale of the preceding mixing event becomes dominant. Since turbulent conditions, i.e. high flow rates, have to be maintained in the tube, and since all material is discarded at the end of the tube, the material consumption during continuous flow experiments tends to exceed those of other methods; this can constitute a drawback to this method.

Chemical relaxation methods are more suitable for the study of interfacial transport in reverse micellar systems, since the high flow rates needed to investigate phenomena with very small time constants using the continuous flow method could cause structural changes in the aggregates. The kinetics of transport across the surfactant layer separating the water pools from the organic continuum has been investigated by the group of Schelly [Tamura and Schelly, 1979; 1981; Harada and Schelly, 1982]. Stopped flow, concentration jump, and pressure jump methods were used to investigate the solubilization rates of picric acid in dry (0.03% w/w water) AOT/benzene reversed micelles; Schelly et al. reported relaxation times of ms, but they also noted that at least one more process was too fast to allow observation by the stopped-flow apparatus. Harada and Schelly [1982] used pressure-

jump to study the solubilization of 7,7,8,8,-tetracyanoquinodimethane in dry reversed micelles of dodecylpyridium iodide in benzene. A laser temperature-jump apparatus was employed by Brock et al. [1981] for the study of ion transport through planar lipid membranes; among the solutes used was 2,4,6-trinitrophenol. Gruenhagen [1975] applied electric field jump relaxation to cetylpyridinium iodide micelles above, but close to, the critical micellization concentration. The rise and fall time of the pulse was in the order of 10^{-8} s. Candau et al. [1990] used temperature-jump by means of discharging a capacitor to study elongated micelles of cetyltrimethylammonium bromide; the rise time of the T-jump was approximately 1 μs. A number of applications of relaxation techniques in aqueous micellar solutions can be found in Kahlweit and Teubner [1980].

10.4b Iodine Laser Temperature Jump (ILTJ)

Among the relaxation techniques [Bernasconi, 1976] such as pressure-jump, electrical-field-jump and ultrasonic absorption, the temperature-jump method is most widely used because almost every chemical equilibrium exhibits a variation with temperature. In commercially available instruments, a high-voltage capacitor is discharged through an electrolyte solution, causing resistance heating of the system; the decoupling of the electric field and temperature effects on the kinetics investigated, however, can be difficult. Salt concentrations of approximately 0.1 M are necessary in order to reduce the electrical resistance of the sample and make the capacitor discharge possible.

Direct optical heating of the solution or the solvent, however, is not limited by the electrical resistance of the discharge circuit and the sample. The heating time in this case would be governed by the emission of the pulsed light source and the lifetime of the excited states. While pulsed microwave sources and flashlamps have been successfully used in the μs range, only mode-locked lasers are able to emit an energy of about 1 joule at a suitable wavelength in a time below 1 ns. The laser pulse energy can be transferred in the solution as thermal energy either via the solute or the solvent. A dye or a colored transition metal complex was initially used to absorb the energy and transmit it to the solvent, because of the limitations of some laser systems. A serious problem in these experiments was the interference of the energy-transferring substance with the reaction under investigation via the excited electronic states and the long lifetime of these excited electronic states (in most cases 10^{-6} - 10^{-8} s). A more elegant method is available with direct absorption of laser

pulse energy by vibrational or rotational states of the solvent (lifetimes of approximately 10^{-12} s) [Holzwarth et al., 1977].

Holzwarth et al. [1977] (see also Frisch et al. [1979]) built an iodine laser with an emission wavelength of 1315 nm; the water -OH bonds are preferentially excited at this frequency. Their laser system has an energy output of 1 - 20 J, characteristic pulse lengths of 2.4 μs or 3 ns, and has been used successfully in many applications [Holzwarth, 1979, 1989; Bannister et al., 1984; Groll, 1986; Jobe et al., 1989; Fletcher & Holzwarth, 1991]. The Iodine Laser is a photochemical gas laser; its chemical principles are described by Andrews [1986], and Brederlow et al. [1983]. Perfluoroisopropyliodide (i-C_3F_7I) gas is flashed by UV-light resulting in electronically excited iodine atoms; their stimulated emission produces laser pulses. The main part of the initial compound is regenerated after deexcitation of iodine atoms and the C_3F_7-radicals. In the case of the laser apparatus built by Holzwarth, a low inductance capacitor (2 F), charged up to 40 kV, is discharged over linear Xenon flash lamps. The flash lamps (rise time 2 μs) are placed inside an aluminum reflector that surrounds the laser tube. The laser tube, made from quartz suprasil, is filled with pure C_3F_7I; its gas pressure is controlled by a thermostat filled with liquid C_3F_7I. The oscillator is connected to a gas recycling system which removes iodine molecules and replaces the decomposed part of the laser gas by circulating C_3F_7I through a thermostat held at 260 K. This ensures that the output energy remains constant from shot to shot. This laser oscillator emits 2 J in a characteristic time of 2.4 μs. The energy output shows a simple exponential decay with time. Pulses with a duration of 0.7 to 3 ns can be produced when the very intense spike appearing in the first 100 ns of the oscillator emission is actively mode-locked.

A Krypton ion laser is used as the detection light source; the detection laser can operate in the 337.5 - 799.3 nm band with an output of up to 4.6 W. The signals from the photomultiplier tube (RCA 1P28) are fed into an amplifier circuit connected to a Tektronix 7904 oscilloscope equipped with a 7A22 amplifier of 1MHz bandwidth and a 7B92A timebase. The analog signal from the oscilloscope is connected to a Biomation 8100 transient digitizer used in the dual timebase mode for digitizing and recording the relaxation signals. The digitizer is linked through a IEEE bus to a HP Vectra computer. Further data processing involves sampling and averaging of the signals as well as calculating the relaxation times by appropriate fitting of the signal to the relaxation kinetics equations [Jobe

et al., 1989]. A schematic of the the ILTJ system is shown in Figure 10.1.

The advantages of the fast temperature jump with the iodine laser are [Holzwarth, 1979; Bannister et al., 1984]: (i) the T-jump is independent of ionic concentration and electrical conductivity; no additives are required; (ii) there are no electric field effects; (iii) reaction rates from second to sub-nanosecond levels can be measured; (iv) sample volumes from 10 μl to 1 ml can be used; (v) uniform excitation avoids temperature gradient problems; (vi) the apparatus is compatible with a wide variety of reaction monitoring techniques (fluorescence, optical absorbance, electrical conductivity, turbidity).

10.5 References cited in Chapter 10

1. Almgren, M., Grieser, F., Thomas, J. K. *J. Chem. Soc. Faraday Trans. 2* **1978**, *74*, 1674.
2. Andrews, D. L. *Lasers in Chemistry*, Springer-Verlag, 1986.
3. Aniansson, G. E. A. *J. Phys. Chem.* **1978**, *82*, 2805.
4. Aniansson, G. E. A., Wall, S. N., Almgren, M., Hoffmann, H., Kielmann, I., Ulbricht, W., Zana, R., Lang, J., Tondre, C. *J. Phys. Chem.* **1976**, *80*, 905.
5. Atik, S., Kuczynski, J., Milosavljevic, B. H., Chandrasekaran, K., Thomas, J. K. in Shah, D. O., (ed.), *Macro-and Microemulsions, ACS Symp. Ser.* **1985**, *272*, 303.
6. Atik, S. S., Thomas, J. K. *Chem. Phys. Let.* **1981a**, *79*, 351.
7. Atik, S. S., Thomas, J. K. *J. Am. Chem. Soc.* **1981b**, *103*, 3543.
8. Bannister, J. J., Gormally, J., Holzwarth, J. F., King, T. A. *Chemistry in Britain*, March 1984, 227.
9. Bardez, E., Monnieur, E., Valeur, B. *J. Colloid Interface Sci.* **1986**, *112*, 200.
10. Barnickel, P., Wokaun, A. *Mol. Phys.* **1990**, *69*, 1.
11. Bernasconi, C. F. *Relaxation Kinetics*, Academic Press, 1976.
12. Bommarius, A. S. *Enzymatic Reactions and Transport in Reversed Micellar Systems*, PhD Thesis, M.I.T., Cambridge, MA, 1989.
13. Bommarius, A. S., Holzwarth, J. F., Wang, D. I. C., Hatton, T. A. *J. Phys. Chem.* **1990**, *94*, 7232.
14. Borkovec M.; Eicke, H.-F. *Chem. Phys. Lett.* **1989**, *157*, 457.

15. Borkovec, M., Eicke, H.-F., Ricka, J. *J. Colloid Interface Sci.* **1989**, *131*, 366.
16. Borwankar, R. P., Wasan, D. T. *Ind. Eng. Chem. Fundam.* **1986**, *25*, 662.
17. Borwankar, R. P., Wasan, D. T. *Chem. Engng Sci.* **1988**, *43*, 1323.
18. Brederlow, G., Fill, E., Witte, K. J. *The High-Power Iodine Laser*, Springer-Verlag, 1983.
19. Brenner, H., Leal, L. G. *AIChE J.* **1978**, *24*, 246.
20. Brenner, H., Leal, L.G. *J. Colloid Interface Sci.* **1982**, *88*, 136.
21. Brock, W., Stark, G., Jordan, P. C. *Biophys. Chem.* **1981**, *13*, 329.
22. Brown, D., Clarke, J. H. R. *J. Phys. Chem.* **1988**, *92*, 2881.
23. Candau, F., Carver, M. in Pileni, M. P., (ed.), *Structure and Reactivity in Reverse Micelles*, Elsevier, Amsterdam, Holland, 1989.
24. Candau F., Leong, Y. S., Pouyet, G., Candau, S. *J. Colloid Interface Sci.* **1984**, *101*, 167.
25. Candau, S. J., Merikhi, F., Waton, G., Lemarechal, P. *J. Phys. France* **1990**, *51*, 977.
26. Carlström, G., Halle, B. *J. Phys. Chem.* **1989**, *93*, 3287.
27. Clark, S., Fletcher, P. D. I., Ye, X. *Langmuir* **1990**, *6*, 1301.
28. Cazabat, A.-M.; Langevin, D. *J. Chem. Phys.* **1981**, *73*, 3148.
29. D'Arrigo, G., Paparelli, A., D'Aprano, A., Donato, I. D., Goffredi, M., Turko Liveri, V. *J. Phys. Chem.* **1989**, *93*, 8367.
30. Dekker, M., Van'T Riet, K., Weijers, S. R., Baltussen, J. W. A., Laane, C., Bijsterbosch, B. H. *Chem. Eng. J.* **1986**, *33*, B27.
31. Di Meglio, J.-M.; Dvolaitzky, M.; Ober, R.; Taupin, C. *J. Phys. Lett.* **1983**, *44*, L229.
32. Eicke, H.-F. *Topics Cur. Chem.* **1980**, *87*, 85.
33. Eicke, H.-F. in Eicke, H.-F., Parfitt, G. D., (eds), *Interfacial Phenomena in Apolar Media*, Marcel Dekker, N.Y., 1987.
34. Eicke, H.-F., Parfitt, G. D. *Interfacial Phenomena in Apolar Media*, Marcel Dekker, N.Y., 1987.
35. Ekwall, P., Mandell, L., Fontell, K. *J. Colloid Interface Sci.* **1970**, *33*, 215.
36. Evans, D. F., Mitchell, D. J., Ninham, B. W. *J. Phys. Chem.* **1986**, *90*, 2817.
37. Faucon, J. F., Mitov, M. D., Meleard, P., Bivas, I., Bothorel, P. *J. Phys. France* **1989**, *50*, 2389.
38. Fendler, J. H. *Membrane Mimetic Chemistry*, Wiley, N.Y., 1982.

39. Fletcher, P. D. I., Holzwarth, J. F. *J. Phys. Chem.* **1991**, *95*, 2550.
40. Fletcher, P. D. I., Howe, A. M., Robinson, B. H. *J. Chem. Soc., Faraday Trans. 1* **1987**, *83*, 985.
41. Fletcher, P. D. I., Parrott, D. in W. Knoche and R. Schomaecker (Eds.), *Reactions in Compartmentalized Liquids*, Springer-Verlag, 1989.
42. Fletcher, P. D. I., Robinson, B. H. *Ber. Bunsenges. Phys. Chem.* **1981**, *85*, 863.
43. Fletcher, P. D. I., Robinson, B. H., Tabony, J. *J. Chem. Soc., Faraday Trans. 1* **1986**, *82*, 2311.
44. Friberg, S. E. *J. Disp. Sci. Tech.* **1985**, *6*, 317.
45. Frisch, W. Schmidt, A., Holzwarth, J. F., Volk, R. in W.J. Gettins, E. Wyn-Jones (Eds.), *Techniques and Applications of Fast Reactions in Solutions*, Reidel, 1979.
46. Göklen, K. E., Hatton, T. A. *Biotech. Progr.* **1985**, *1*, 69.
47. Göklen, K. E., Hatton, T. A. *Sep. Sci. Tech.* **1987**, *22*, 831.
48. Grieser, F., Drummond, C. J. *J. Phys. Chem.* **1988**, *92*, 5580.
49. Groll, R. *Struktur und Lynamik von Phospholipid-Doppelschichten mit rekonstituierten biologischen Einheiten*, Inaugural-Dissertation, Freie Universität, Berlin, Germany, 1986.
50. Gruenhagen, H. H. *J. Colloid Interface Sci.* **1975**, *53*, 282.
51. Guering, P.; Cazabat, A.-M. *J. Phys. Lett.* **1984**, *44*, L601.
52. Gurevich, Yu. Ya., Kharkats, Yu. I. *J. Electroanal. Chem.* **1986**, *200*, 3.
53. Halle, B., Landgren, M., Jönsson, B. *J. Phys. France* **1988**, *49*, 1235.
54. Harada, S., Schelly, Z. A. *J. Phys. Chem.* **1982**, *86*, 2098.
55. Helfrich, W. *J. Phys. France* **1986**, *47*, 321.
56. Hoffmann, H. *Ber. Bunsenges. Phys. Chem.* **1978**, *82*, 988.
57. Holzwarth, J. F. "Fast Continuous Flow" in W. J. Gettins, E. Wyn-Jones (Eds.), *Techniques and Applications of Fast Reactions in Solutions*, Reidel, 1979.
58. Holzwarth, J. F. "Laser Temperature Jump" in W. J. Gettins, E. Wyn-Jones (Eds.), *Techniques and Applications of Fast Reactions in Solutions*, Reidel, 1979.
59. Holzwarth, J. F. in A. Cooper, J. L. Houben, L. C. Chien (Eds.), *The Enzyme Catalysis Process*, Plenum, 1989.
60. Holzwarth, J. F., Schmidt, A., Wolff, H., Volk, R. *J. Phys. Chem.* **1977**, *81*, 2300.

61. Honig, B. H., Hubbell, W. L., Flewelling, R. F. *Ann. Rev. Biophys. Biophys. Chem.* **1986**, *16*, 163.
62. Huang, J. S.; Milner, S. T.; Farago, B.; Richter, D. *Phys. Rev. Lett.* **1987**, *59*, 2600.
63. Israelachvili, J. in Mittall, K. L., Bothorel, P., (eds), *Surfactants in Solution*, Vol. 4, Plenum Press, N.Y., 1986.
64. Israelachvili, J. N., Mitchell, D. J., Ninham, B. W. *J. Chem. Soc. Faraday Trans. 2* **1976**, *72*, 1525.
65. Jada, A., Lang, J., Zana, R., Makhloufi, R., Hirsch, E., Candau, S. J. *J. Phys. Chem.* **1990**, *94*, 378.
66. Jobe, D., Dunford, H. B., Pickard, M., Holzwarth, J. F. in W. Knoche, R. Schomäcker (Eds.), *Reactions in Compartmentalized Liquids*, Springer, 1989.
67. Johnston, K.P., Penninger, J. M. L., (eds), *Supercritical Fluid Science and Technology*, ACS Symp. Ser. 406, Washington DC, 1989.
68. Jönsson, B., Edholm, O., Teleman, O. *J. Chem. Phys.* **1986**, *85*, 2259.
69. Jordan, P. C., Stark, G. *Biophys. Chem.* **1979**, *10*, 273.
70. Kahlweit, M., Teubner, M. *Adv. Colloid Interface Sci.* **1980**, *13*, 1.
71. Kandori, K., Kon-No, K., Kitahara, A. *J. Colloid Interface Sci.* **1988**, *122*, 78.
72. Kandori, K., Kon-No, K., Kitahara, A. *J. Disp. Sci. Tech.* **1988**, *9*, 61.
73. Kertes, A. S., Gutman, H. in Matijevic, E., (ed.), *Surface and Colloid Science*, Vol. 8, Wiley, N.Y., 1976.
74. Ketterer, B., Neumcke, B., Läuger, P. *J. Membrane Biol.* **1971**, *5*, 225.
75. Khmelnitski, Y. L., Kabanov, A. V., Klyachko, N. L., Levasov, A. V., Martinek, K. in Pileni, M. P., (ed.), *Structure and Reactivity in Reverse Micelles*, Elsevier, Amsterdam, Holland, 1989.
76. Kitahara, A. *Adv. Colloid Interface Sci.* **1980**, *12*, 109.
77. Kotlarchyk, M.; Stephens, R. B.; Huang, J. S. *J. Phys. Chem.* **1988**, *92*, 1533.
78. Lang, J., Mascolo, G., Zana, R., Luisi, P. L. *J. Phys. Chem.* **1990**, *94*, 3069.
79. Larson, R. S. *J. Colloid Interface Sci.* **1982**, *88*, 487.
80. Larson, R. S., Lam, D. K. *Ind. Eng. Chem. Fundam.* **1986**, *25*, 148.
81. Leodidis, E. B. *Solubilization of Ions and Amino Acids in AOT Reversed Micellar Solutions*, PhD Thesis, M.I.T., Cambridge, MA, 1990.
82. Lianos, P., Thomas, J. K. *J. Colloid Interface Sci.* **1987**, **117**, 505.
83. Lindman, B., Stilbs, P. in S.E. Friberg, P. Bothorel (Eds.), *Microemulsions:*

Structure and Dynamics, CRC Press, 1988.

84. Ljunggren, S., Eriksson, J. C. *J. Chem. Soc. Faraday Trans. 2* **1984**, *80*, 489.
85. Luisi, P. L., Magid, L. J. *CRC Crit. Rev. Biochem.* **1986**, *20*, 409.
86. Luisi, P. L., Giomini, M., Pileni, M. P., Robinson, B. H. *Biochim. Biophys. Acta* **1988**, *947*, 207.
87. Mahanty, J., Ninham, B. W. *J. Chem. Phys.* **1973**, *59*, 6157.
88. Maitra, A. N. *J. Phys Chem.* **1984**, *88*, 5122.
89. Martinek, K., Levasov, A. V., Klyachko, N., Khmelnitski, Y. L., Berezin, I. V. *Eur. J. Biochem.* **1986**, *155*, 453.
90. Menger, F. M., Tsuno, T. *J. Am. Chem. Soc.* **1990**, *112*, 1263.
91. Miller, C. A., Qutubuddin, S. in Eicke, H.-F., Parfitt, G. D., (eds), *Interfacial Phenomena in Apolar Media*, Marcel Dekker, N.Y., 1987.
92. Milner, S. T., Safran, S. A. *Phys. Rev. A* **1987**, *36*, 4371.
93. O'Connor, C. J. in Eicke, H.-F., Parfitt, G. D., (eds.), *Interfacial Phenomena in Apolar Media*, Marcel Dekker, N.Y., 1987.
94. Petit, C., Pileni, M. P. *J. Phys Chem.* **1988**, *92*, 2282.
95. Petit, C., Lixon, P., Pileni, M. P. *J. Phys. Chem.* **1990**, *94*, 1598.
96. Pileni M. P., Brochette, P., Hickel, B., Lerebours, B. *J. Colloid Interface Sci.* **1984**, *98*, 549.
97. Prince, L. M. in Prince, L.M., (ed.), *Microemulsions. Theory and Practice*, Academic Press, N.Y., 1977.
98. Robinson, B. H., Khan-Lodi, A. N., Towey, T. in Pileni, M. P., (ed.) *Structure and Reactivity in Reversed Micelles*, Elsevier, Amsterdam, Holland, 1989.
99. Safran, S. A. *J. Chem. Phys.* **1983**, *78*, 2073.
100. Samec, Z. *Chem. Rev.* **1988**, *88*, 617.
101. Samec, Z., Gurevich, Yu. Ya., Kharkats, Yu. I. *J. Electroanal. Chem.* **1986**, *204*, 257.
102. Schneider, M. B., Jenkins, J. T., Webb, W. W. *J. Phys. France* **1984**, *45*, 1457.
103. Shaeiwitz, J. A., Raterman, K. T. *Ind. Eng. Chem. Fundam.* **1982**, *21*, 154.
104. Sharma, M. K., Shah, D. O. in Shah, D. O., (ed.), *Macro- and Microemulsions. Theory and Applications, ACS Symp. Ser.* **1985**, *272*, 149.
105. Shield J. W., Ferguson, H. D., Bommarius, A. S., Hatton, T. A. *Ind. Eng. Chem. Fundam.* **1986**, *25*, 603.
106. Shinoda, K., Friberg, S. *Adv. Colloid Interface Sci.* **1975**, *4*, 281.

107. Shinoda, K., Friberg, S., *Emulsions and Solubilization*, Wiley, N.Y., 1986.
108. Shinoda, K., Lindman, B. *Langmuir* **1987**, *3*, 135.
109. Smith, R. D., Fulton, J. L., Blitz, J. P., Tingey, J. M. *J. Phys. Chem.* **1990**, *94*, 781.
110. Steigerwald, M. L., Alivisatos, A. P., Gibson, J. M., Harris, T. D., Kortan, R., Muller, A. J., Thayer, A. M., Duncan, T. M., Douglass, D. C., Brus, L. E. *J. Am. Chem. Soc.* **1988**, *110*, 3046.
111. Steigerwald, M. L., Brus, L. E. in Pileni, M. P., (ed.) *Structure and Reactivity in Reversed Micelles*, Elsevier, Amsterdam, Holland, 1989.
112. Tamamushi, B., Watanabe, N. *Colloid Polym. Sci.* **1980**, *258*, 174.
113. Tamura, K., Schelly, Z. A. *J. Am. Chem. Soc.* **1979**, *101*, 7643.
114. Tamura, K., Schelly, Z. A. *J. Am. Chem. Soc.* **1981**, *103*, 1018.
115. Uehara, H. *J. Sci. Hiroshima Univ., Ser. A* **1976**, *40*, 305.
116. Voormans, G., de Schryver, F. C. in Pileni, M.P., (ed.) *Structure and Reactivity in Reversed Micelles*, Elsevier, Amsterdam, Holland, 1989.
117. Vos, K., Laane, C., Visser, A. J. W. G. *Photochem. Photobiol.* **1987**, *45*, 863.
118. Yazdi, P., McFann, G. J., Fox, M. A., Johnston, K. P. *J. Phys. Chem.* **1990**, *94*, 7224.
119. Yiv, S., Zana, R., Ulbricht, W., Hoffmann, H. *J. Colloid Interface Sci.* **1981**, *80*, 224.
120. Zana, R., (ed.), *Surfactant Solutions: Various Analytical Methods of Investigation*, Marcel Dekker, N.Y., 1987.
121. Zana, R., Lang, J. in S. E. Friberg, P. Bothorel (Eds.), *Microemulsions: Structure and Dynamics*, CRC Press, 1988.
122. Woll, J. M., Hatton, T. A., Yarmush, M. L. *Biotech. Progr.* **1989**, *5*, 57.

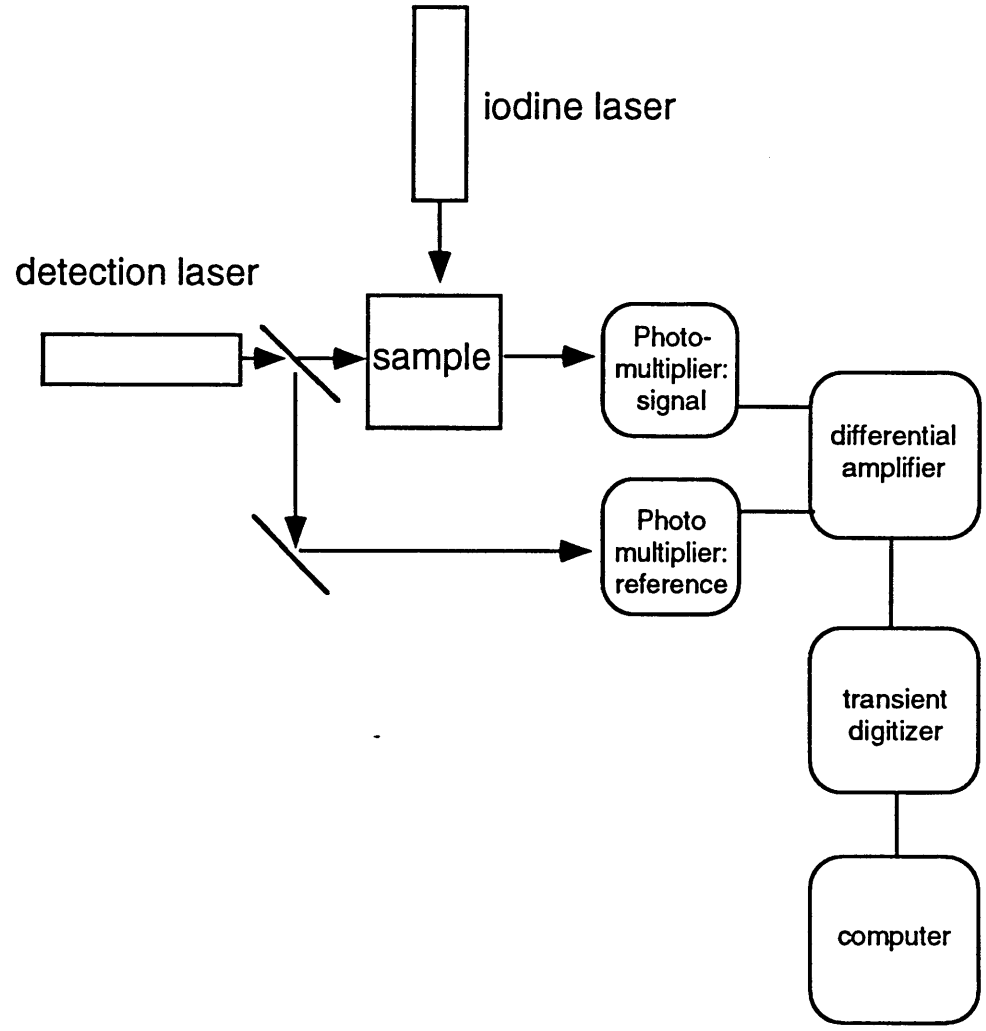

Figure 10.1 Iodine Laser Temperature Jump Apparatus schematic.

Chapter 11
Heating-Induced Conductivity Percolation in AOT Water-in-Oil Microemulsions

11.1 Introduction and Literature Review

Water-in-oil microemulsions or reverse micelles are thermodynamically-stable complex fluids that can be envisaged as distinct, nanometer-size water droplets maintained dispersed in an apolar solvent with the aid of a surfactant monolayer that reduces unfavorable oil-water contact. The microemulsions are highly dynamic systems, whose components rearrange over time and space. Studies on the dynamics of microemulsions can be broadly divided into four groups [Zana & Lang, 1988]: (i) internal motions of the surfactant and cosurfactant molecules [Lindman & Stilbs, 1988]; (ii) dynamics of the surfactant film separating oil and water [Safran, 1983; Borkovec & Eicke, 1989; Huang et al., 1987]; (iii) dynamics of processes involving whole microemulsion droplets, e.g., droplet diffusion or clustering [Cazabat & Langevin, 1981]; and (iv) the exchange of contents when microemulsion droplets coalesce [Fletcher & Robinson, 1981; Bommarius et al., 1990].

Particularly important in understanding the behavior of microemulsions are the fluidity and flexibility of the oil-surfactant-water interface, manifested in the dynamic processes (ii), (iii), and (iv) mentioned above. Recently, we interpreted [Alexandridis et al., 1993] the dynamic response of microemulsion droplets to perturbations caused by rapid energy transfer in terms of the surfactant film bending modulus [Helfrich, 1973]. Conductivity is employed here for the study of AOT water-in-oil microemulsions, addressing some of the issues concerning dynamics of droplet clustering and exchange of contents upon coalescence. As discussed below, the phenomena of high conductivity, droplet coalescence, and bending of the surfactant interface are related to each other.

Conductivity has been used to assess microemulsion formation, investigate the structural changes leading to their occurrence, and probe the exchange of some of the

microemulsion components (e.g., water, ions) when microemulsion droplets coalesce. Many studies are available regarding the electroconductive behavior of water-surfactant-oil systems, but no general criteria for its interpretation have been fully established as yet. Two typical situations can be depicted, depending on the components (and experimental conditions) selected [Chittofrati et al., 1992]: (i) the emergence of a bicontinuous structure (open water channels) [Borkovec et al., 1988], and (ii) the dynamic percolation [Note 1] of a phase of spherical water globules present in the oil continuum [Grest et al., 1986]. The dynamic percolation approach applies to systems where the basic assumption of constant dimension of the droplets is valid even as the droplet concentration changes upon dilution with the continuous phase. Such a condition can be approximated when the partitioning of surfactant does not vary significantly upon change of the water volume fraction, thus ternary systems such as AOT/water/alkane are favorable cases to clarify percolative behavior and its origin [Borkovec et al., 1988; Jada et al., 1990a].

Kim and Huang [1986] proposed a surfactant anion hopping model with a temperature dependent hopping range to describe the effect of temperature on the percolation threshold ϕ_c. Percolation occurred when the effective droplet volume (as defined by the hopping range) exceeded the hard-sphere close-packing limit of 0.65 so that charge transfer could occur between clusters of droplets. The sensitivity of the range of interaction to temperature reflected the combined effect of increased probability of the surfactant to be ionized and the increased range of ion diffusion as the mobility of the ion increases with increasing temperature. Maitra et al. [1990] inferred from measurements of water self-diffusion coefficients in AOT water-in-isooctane microemulsions that the percolative conduction arose form hopping of charge carriers across the surfactant monolayer of the droplets, and that the aggregates open up only at the onset of formation of bicontinuous microemulsions. Although the percolation threshold temperature was considerably lowered by the addition of gramicidin (a channel forming protein) and was significantly increased by the addition of cholesterol (a membrane rigidifying agent), the water self-diffusion coefficient in these systems was found not to change at the threshold temperatures indicating that the droplets maintain their "closed" shell structure.

Zana and coworkers [Zana et al., 1991; Jada et al., 1989; Jada et al., 1990b] have studied the rate of exchange of droplet contents in ternary microemulsion systems and showed that the rate constant for droplet collision with exchange of material must reach a

value of at least 10^9 M^{-1} s^{-1} for percolative behavior to occur, irrespective of the parameter varied to induce percolation. They concluded, therefore, that the electrical conductivity of water-in-oil microemulsions above the percolation threshold is due to motion of surfactant counterions within transient water channels arising in droplet clusters upon opening of surfactant layers. Hamilton et al. [1990] found in a quaternary microemulsion system the percolation thresholds determined by conductivity to occur at the same or slightly higher water volume fraction as those determined using NMR, indicating that conduction involved movement of ions in channels connecting droplets and not via the surfactant interface or by a charge-hopping mechanism. It was also proposed that the onset of percolation occurs in microemulsions when the interdroplet attraction exceeds a critical value of 2kT.

Dielectric spectroscopy and other techniques [van Dijk, 1985] supported the notion that clustering of water droplets, occurring in water/AOT/isooctane microemulsions due to short range attractive interactions, cause the observed high conductivity. While phase separation could be clearly distinguished from the percolation phenomena, van Dijk et al. [1985; 1986] noted that the interactions involved in the clustering of the droplets may be the same that finally, at higher temperatures, cause phase separation. Attractive interactions accounted for a decrease in the droplet volume fraction needed for a certain level of conduction [Safran et al, 1987], while dynamic effects of droplet motion and rearrangement were suggested as being responsible for the change in critical exponents that describe the percolation transition [Lagües et al., 1978; Safran et al, 1987]. Mukhopadhay et al. [1990] studied heating-induced percolation behavior of AOT water-in-decane microemulsion in the presence of alkanols, cholesterol, benzyl alcohol, and a crown ether. The percolation threshold temperature was increased by the additives, except for benzyl alcohol and the crown ether; the latter exhibited a less sharp conductance-temperature profile and a lower threshold temperature. Addition of alkanols offered softness or flexibility to the interface with easier charge fluctuations and thereby enhanced conductance. The addition of cholesterol and its esters had, on the other hand, a decreasing effect on the intrinsic conductance of the microemulsion; the sterols caused more compact interfaces and reduced the effective excess charges on the droplets by restricting the charge fluctuations thereby lowering conductivity. Estimates of activation energies for conduction supported the mechanism of heating-induced percolation transition by efficient transport of Na+ counter-ions through water channels formed in clusters of droplets upon collision, rather than hopping of the AOT ions between droplets [Mukhopadhay et al., 1990]. Dutkiewicz and

Robinson [1988] favored a transient merging of droplets based on analysis of the effects of toluene and benzyl-alcohol on an AOT/water/dodecane system. It becomes obvious from the above that interdroplet attractions and droplet coalescence and decoalescence (controlled by the surfactant film elasticity) influence the percolative behavior in microemulsions. These processes would be modulated by such factors as temperature, droplet size and concentration, and the nature of the apolar medium in which droplets are present.

Percolative behavior has been observed in ternary microemulsion systems having spherical droplet structure under suitable experimental conditions (typically at constant Wo, molar [water]/[surfactant] ratio), while no percolation was observed when size and concentration of droplets were varied at constant [surfactant]/[oil] (1/So) ratio [Hilfiker & Eicke, 1987; Carver et al., 1989]. High conductivities, up to 1 Sm^{-1}, were generally observed above the percolation threshold, whereas conductivities on the order of 10^{-3} Sm^{-1} or less have been explained by migration of statistically charged droplets; the quantitative charge fluctuation model [Eicke et al., 1989; Hall, 1990; Kallay & Chittofratti, 1990; Halle, 1990; Pan, 1991] accounted for the non-monotonic variation of conductivity observed experimentally at low Wo values [Note 2].

Most of the percolation data in the microemulsion literature concern increase of conductivity following addition of water. The earliest reports on heating-induced percolation in water-in-oil microemulsions are from van Dijk et al. [1985; 1986], Huang and coworkers [Battacharya et al., 1985; Kim & Huang, 1986], and Moha-Ouchane et al. [1987]. More recent studies include those by Maitra et al. [1990], Mukhopadhay et al. [1990], and Ray et al [1993]. Although all of the investigations referred to above concern AOT microemulsions, the range of compositions for which percolation was studied is limited and information on the percolation mechanism fragmented. We therefore undertook a comprehensive experimental study of heating-induced percolation in AOT water-in-oil microemulsions and related our results to the mechanisms responsible for this phenomenon. More specifically, we examined systematically the effect that microemulsion droplet size and concentration have on conductivity for microemulsions formulated with four different alkanes as the continuous phase, and probed the effect of added salt for one microemulsion system.

11.2 Materials and Methods

Materials: AOT (Sulfosuccinic acid bis[2-ethylhexyl] ester, sodium salt) of purity 99% was purchased from Sigma Chemical Co., (St. Louis, MO) and used as received. Isooctane, n-hexane, n-decane, and n-dodecane (AR grade) were obtained from Mallinckrodt (Paris, KY). All salts were of analytical grade or better. The water used was triple-distilled.

Microemulsion system: Conductivity experiments were performed on AOT / water / alkane microemulsion systems, for the alkanes n-hexane, isooctane, n-decane, and n-dodecane. The formulation of the microemulsions is given in terms of Wo, the ratio of water to surfactant molar concentrations, and So, the ratio of oil to surfactant molar concentrations. Microemulsions of compositions So = 5, 13, and 20, and Wo = 0 - 50 were investigated. In the AOT system, Wo essentially determines the radius of the water droplets and So their concentration in the oil phase [van Dijk et al., 1986]. As the critical micellar concentration of AOT in both oil and water is low in comparison with the concentrations used here, it can be assumed that all the surfactant is localized at the interface between water and oil [Moha-Ouchane et al., 1987]. The temperature range for the conductivity measurements was generally 10 - 62 °C; for some microemulsions the upper temperature limit was that of phase separation. The microemulsions were prepared using the injection method, by mixing an appropriate quantity of aqueous solution with an AOT solution in oil. The resulting microemulsions were placed in Teflon-stoppered test tubes, and left to equilibrate at room temperature for approximately one day before the conductivity experiment. We worked inside the L2 phase boundary, where the structure of the aggregates is spheres [Kotlarchyk et al., 1985; Robertus et al., 1989; Hilfiker et al., 1990]. This droplet structure has been found fairly insensitive to both the concentration of the droplets and the temperature [Kim & Huang, 1986].

Conductivity measurements: The conductivity of the microemulsions was measuring at different temperatures with a CDM 83 Conductivity Meter and a CDC 344 Electrode (constant: 3.191 cm), both from Radiometer Copenhagen (Copenhagen, Denmark). The electrode was inserted in the test tube containing the microemulsion, and the test tube placed in a thermostated water bath. We started monitoring the conductivity of the microemulsion sample at a low temperature and went up in temperature in regular

temperature intervals. Conductivity values were recorded every 4 °C or less; sufficient time (at least 10 mins [Mukhopadhay et al., 1990]) for equilibration was allowed between conductivity measurements at different temperatures. The sample temperature was monitored with a T801 temperature probe from Radiometer Copenhagen. All samples were one-phase and optically transparent under the conditions of the conductivity measurements.

11.3 Results and Discussion

11.3a Effect of temperature

The effect of temperature on conductivity is presented in Figure 11.1 for water-in-hexane microemulsions of varying droplet radii (Wo) and concentrations (~1/So), and in Figure 11.2 for So=13 microemulsions formulated with isooctane, decane, and dodecane. For each conductivity curve of Wo=constant the radius of the microemulsion droplets remains approximately constant, independent of temperature [Kim & Huang, 1986]. For Wo values less than or equal to 10, the logarithm of the microemulsion conductivity increased linearly with temperature for all droplet concentration and solvents studied, and did not suggest a percolation process. The conductivity values in this Wo region also increased as the droplet concentration increased for a given solvent, and as the solvent molecular weight increased for a given droplet concentration. The conductivity at low Wo values is believed to originate from fluctuations in the ion content of the microemulsion droplets which create charged droplets that can conduct electricity [Eicke et al., 1989]. An increase in temperature may increase the frequency of the charge fluctuations and thus increase the conductivity. Note, that the coalescence of microemulsion droplets followed by exchange of their content, a process facilitating the charge fluctuations, is known to increase with temperature [Fletcher et al., 1987; Bommarius et al., 1990]. The high conductivity observed at Wo=10 will be discussed in Section 11.3b (Figures 11.4, 11.5).

For Wo > 15 the logarithm of the microemulsion conductivity exhibited a characteristic sigmoidal behavior as the temperature increased; this increase of conductivity over 4 orders of magnitude is indicative of percolation. Both charge hopping and coalescence percolation mechanisms can explain well the influence of temperature on conductivity. The percolation temperature, defined as the point at which the conductivity

vs temperature curve has an inflection, decreased with increase in the size of the droplets (at constant droplet concentration). This effect can be attributed to enhanced interdroplet interaction with increasing micelle size, as the overlap volume of the surfactant tails when two droplets approach each other increases, and to an increased flexibility of the surfactant interface (see Section 11.3c). The percolation temperature decreased with increase in the molecular weight of the solvent, for droplets of the same size and concentration; this can again be attributed to enhanced interdroplet interaction as the solvent penetrates less into the surfactant monolayers (see also Section 11.3c). Wo=15 appears to be an intermediate case in terms of percolation since the transition from low to high conductivity is less pronounced, especially for high So. Note, that the Wo range probed in the case of dodecane is limited because the phase boundary was reached.

The percolation temperatures for microemulsions of given droplet size (Wo) can be plotted as a function of the volume fraction of the dispersed phase (water plus AOT) to form a phase diagram showing the regions of percolating and nonpercolating behavior. This has been done in Figures 11.3a, 11.3b, and 11.3c, for hexane, isooctane, and decane microemulsions, respectively. Note that the percolation boundary moves towards the low temperature - low dispersed volume fraction corner of the phase diagram as the solvent molecular weight increases. The percolation temperature for microemulsions of small droplet size (i.e., Wo=25) depended more strongly on the volume fraction of the dispersed phase, compared to higher Wo values.

The temperature dependence of the conductivity σ and dielectric constant ε at two frequencies for an AOT water-in-decane microemulsion of Wo=40 and 8% volume fraction of dispersed phase was reported by Bhattacharya et al. [1985]. Both σ and ε increased markedly as temperature increased towards the phase-separation temperature of 34 °C; the dielectric constant reached a peak while the conductivity continued to rise. It was suggested that the critical exponents governing the conductivity percolation when temperature was varied should be the same as those obtained by varying ϕ, provided that the percolation threshold, ϕ_c, is analytic in T. Indeed, the scaling exponents for σ=f(T) were in agreement with those obtained from a variation of ϕ at a fixed temperature in the same system. In a recent investigation, Ray et al. [1993] reported that the heating-induced percolation in AOT/water/heptane microemulsions at constant Wo obeyed the scaling law $\sigma \sim (T - T_c)^n$, but the derived n values were not 2 as previously reported but ranged between

1.85 and 4.25, depending on Wo.

As mentioned in the Introduction, the percolation phenomenon has been linked [Zana et al., 1991; Jada et al., 1989; Jada et al., 1990b] to the coalescence rate of microemulsion droplets. Fletcher et al. [1987] found the exchange rate of aqueous solubilizates between droplet in an AOT microemulsion to be slowest at the low-temperature boundary, and increasing as the upper-temperature boundary was approached. Similar trends were observed in the dodecyl-trimethylammonium chloride / hexanol / n-heptane / water microemulsion system [Bommarius et al., 1990]. The mechanism of solubilizate exchange is thought to involve the formation of short-lived dimers, followed by their separation [Fletcher et al., 1987; Bommarius et al., 1990]. For the dimer to form, the surfactant monolayer has to deform (or break), a process governed by the bending elasticity of the interface [Fletcher & Horsup, 1992]. The slow exchange rates indicate more stable droplets (higher bending moduli of the surfactant monolayer) at temperatures close to the low-temperature boundary, where the actual AOT monolayer curvature is equal to its natural curvature. As the natural curvature becomes less negative with increase in temperature, the discrepancy between the natural and actual curvature increases [Note 3]. Based on the above discussion, one would expect to observe a decrease of the surfactant monolayer bending elasticity with increasing temperature for a given droplet size. That would correspond to an increase in the frequency of droplets coalescing and exchanging material and an increase in the electrical conductivity of the microemulsion, but the variation of bending elasticity alone cannot account for the sharp increase of conductivity at the percolation threshold.

11.3b Effect of droplet size and concentration

The effects of droplet size on conductivity for water-in-isooctane and water-in-decane microemulsions are reported in Figures 11.4 and 11.5, respectively, at various temperatures. In the So = 20 and 13 cases, the conductivity values remained below 1 μS/cm for temperatures lower that ~ 25 °C. For this range of droplet concentrations, and for temperatures greater that 30 °C, there was a Wo value at which the conductivity started increasing by 2 to 4 orders of magnitude, indicative of percolation. Increase of droplet interactions with droplet size is probably the cause for the percolation observed under the above conditions. Although it spans 4 orders of magnitudes, the increase in conductivity

effected by increasing the droplet size appears to be more gradual than the conductivity increase due to temperature. This can be attributed to the fact that temperature increases both droplet interactions and diffusion rates of ions (if the ion hopping phenomenon is in effect), whereas increase of droplet size would affect mainly droplet interactions.

A very interesting aspect of Wo effects on conductivity is a pronounced local maximum in the conductivity vs Wo curve, observed at Wo=10 for So=5. The dielectric properties of AOT/water/isooctane microemulsions far below the percolation threshold have been interpreted in terms of the polarizability of clusters of water droplets in an aggregation equilibrium [van Dijk et al., 1986]. Water-in-oil microemulsion conductivities on the order of 10^{-3} Sm^{-1} or less have been explained by migration of statistically charged droplets in terms of the charge fluctuation model, according to which, charged droplets are formed by spontaneous number fluctuations of the ions residing in the droplets [Eicke et al., 1989; Hall, 1990; Kallay & Chittofratti, 1990; Halle, 1990; Pan, 1991]. This explained the experimentally observed fact that the conductivity of water-in-oil microemulsions is approximately proportional to the volume fraction of the droplets for a wide range of compositions. Consideration of the discrete nature of the electrical charges accounted for the non-monotonic variation of conductivity observed experimentally (see Figures 4, 5) at low Wo values [Hall, 1990; Kallay & Chittofratti, 1990].

For relatively low temperatures the conductivity decreased after the maximum at Wo=10, and no percolation was observed with further increase of Wo. At intermediate temperatures the conductivity values exhibited a maximum at Wo=10, decreased, and passed through a minimum, before increasing monotonically for the higher Wo values, whereas, for high temperatures the conductivity increased steeply at Wo = 5 - 10 and continued to increase with increasing Wo. An upper limit in conductivity values was apparent at ~ 5000 μS/cm; an increase in Wo would either lead to conductivity of comparable magnitude or phase separation. The solvent had a significant effect on both the upper Wo for a stable one-phase microemulsion over the temperature range that we studied (e.g., for decane and So=5, the maximum Wo was 35; for dodecane and So=5, 13, the maximum Wo was 25), and the magnitude of the conductivity maximum observed at low Wo values.

A maximum and a minimum in the log conductivity vs P_w (~Wo) plots for

AOT/water/undecane and AOT/water/isooctane microemulsions at different values of P_{oil}/P_{AOT} (~So), where P_i is the content of component i by weight, were also observed by Peyrelasse and Boned [1990]. The position of the first maximum was at the same P_w for both oils, whereas the point at which the final plateau conductivity value was reached appeared at lower P_w values for the higher molecular weight oil; the conductivity values were in general higher for the higher molecular weight oil. According to Peyrelasse and Boned [1990] the maxima and minima did not correspond to structural changes but were linked to $|\phi - \phi_c(Wo)|$, where $\phi_c(Wo)$ is the volume fraction of water and AOT at the percolation threshold.

As shown in Figure 11.1, increasing the droplet concentration (decreasing So) resulted in decreasing the percolation threshold temperatures. The effect of droplet concentration on conductivity is also shown in Figure 11.6, where conductivity is plotted as a function of So for water-in-oil microemulsions of Wo=10 at various temperatures. Increase in droplet concentration (decrease in So) resulted in increasing conductivity for all Wo values; the increase was more pronounced at Wo=10, plotted in Figure 11.6. While water-in-hexane microemulsions of So=20 and So=13 had conductivity values which were almost identical, the difference between So=20 and So=13 conductivity values increased with increasing solvent molecular weight, as seen in Figure 11.6. Given that conductivity in this Wo range is a result of fluctuations in the number of ions residing in the droplets, it becomes apparent that such fluctuations are modulated by the solvent, in addition to being concentration dependent.

11.3c Effect of apolar solvent

We showed above that increasing the molecular weight of the alkane solvent, which formed the microemulsion continuous phase, resulted in decreasing the temperature, droplet size and concentration required for percolation (see Figures 11.2 - 11.6). The effect of solvent on microemulsion phase behavior and droplet interactions can be understood by invoking the work of Shah and coworkers [Hou & Shah, 1987] who studied the effects of the continuous oil phase and molecular structure of the interface on the solubilization capacity of water in water-in-oil microemulsions. In considering the thermodynamic stability of microemulsion systems, Hou and Shah have shown the growth of droplets during the solubilization process to be limited either by the spontaneous

curvature of the interface or by the attractive interaction between the microemulsion droplets. For microemulsion systems formulated with small oil molecules (e.g., benzene, toluene, hexane) the penetration of oil in the interfacial layer is large and the attractive interactions small. As a result, the solubilization capacity of water in such systems tends to be limited by the value of the radius of the spontaneous curvature; the latter increases with increasing molecular volume of oil, and decreasing salinity and cosurfactant chain length. Heptane was found to have the higher solubilization capacity for water [Note 4]. As the molar volume of the oil is increased (isooctane, decane, tridecane) the large attractive interaction among droplets plays the major role in limiting the solubilization capacity of water by limiting the actual radius to smaller values than the critical droplet radius; the latter decreases with increasing molecular volume of oil, and decreasing salinity and cosurfactant chain length. Hou et al. [1988] studied the droplet size and interdroplet interaction in AOT water-in-oil microemulsions using light scattering, and found a small droplet size increase, whereas the interdroplet attraction increased significantly with increasing oil chain length.

Hamilton et al. [1990] studied the water / sodium 1-(4'-heptylnonyl) benzenesulfonate (SHBS) / isobutyl alcohol / C8 - C16 alkanes microemulsion system and found the water percolation thresholds to decrease as the alkane chain length decreased. Small-angle neutron scattering experiments showed the microemulsion droplets to be spherical and of roughly the same size and the magnitude of the attractive interaction between the droplets to increase with increasing alkane chain length (from 0.1 kT for octane to ~6 kT for hexadecane). The interaction potential normalized with the droplet radius at the percolation had a value of approximately 2kT for all oils used. This observation lead Hamilton et al. [1990] to propose several predictions about the general behavior of microemulsions. As the difference between the surfactant and cosurfactant tail length is increased, the interaction strength increases, and percolation occurs at a lower droplet radius. As the droplet radius is increased, the overlap volume (when two droplets come close to each other) increases, the interaction potential increases, and percolation eventually occurs. The water droplet radius can be changed by the addition of water without the addition of surfactant, which requires that droplets grow at constant total surface area; by the addition of salt, which decreases the head-group area and thus decreases the droplet radius; and by changing the oil in the continuous phase. A penetrating oil (short chain or cyclic) increases the area required for the surfactant tails and thus decreases the droplet radius. A non-penetrating oil decreases the surfactant tail area

and increases the droplet radius.

While droplet attractions play an important role in causing percolation, the nature of the interface of the individual droplets also has an effect; for percolation to occur, droplets must exchange contents and so the droplet interface must rupture. Jada et al. [1989; 1990b] have studied the rate of exchange of droplet contents in ternary microemulsion systems made with AOT and with a series of cationic single-tailed surfactants with varying surfactant chain length. As the thickness of the interface was increased (by increasing the surfactant chain length), the droplet exchange rate decreased and the percolation threshold increased. Thickening of the interface results in a greater energy requirement for rupture of the droplet interface. In the AOT systems, the exchange rate increased as the oil chain length increased, and the percolation threshold decreased. This behavior is consistent with the model proposed by Hamilton et al. [1990].

The solvents we used in our conductivity studies are such that the microemulsions formed fell in the range where attractive interactions were important. Increasing the molecular weight of the alkane solvent constituting the microemulsion continuous phase increased the interdroplet attractions and the droplet content exchange rate, phenomena that were manifested in the decrease of temperature, droplet size, and droplet concentration needed for percolation to occur.

11.3d Effect of added salt

In addition to microemulsions formed by injecting water, conductivity experiments were carried out with microemulsions formed by injecting aqueous solutions of salts and buffer. It is known that water-in-oil microemulsions of AOT in nonpolar solvents are profoundly affected by the addition of small amounts of electrolyte [Kunieda & Shinoda, 1979]; however, the compositions we used allowed us to operate in the one-phase (L2) region. Figure 11.7 is an example of the influence of salt on the conductivity of microemulsions. Conductivity vs temperature data for a water-in-isooctane microemulsion (So=5 and Wo=10) formulated with NaCl added in the aqueous pools are shown in Figure 11.7a. Replacing the water with 0.5 M NaCl aqueous solution decreased the conductivity of the microemulsion by two orders of magnitude. Microemulsions formed with 0.1 M NaCl aqueous solution showed behavior intermediate between that of [NaCl] = 0 and 0.5

M, whereas microemulsions formed with 0.01 M NaCl aqueous solution behaved similarly to microemulsions with no added salt. Note that there is a finite concentration of Na^+ ions in the water pool (even when there is no NaCl added) due to AOT counterions, although most are tightly adsorbed to the negatively charged AOT headgroups. Assuming that 10 % of Na^+ counterions are "free" (not bound), their concentration in a droplet of Wo=10 is approximately 1 Na^+ per 100 water molecules. This is to be compared to the concentration of added Na^+ ions, which for 0.5 M NaCl solution is 1 Na^+ per 100 water molecules. This explains why added [NaCl] = 0.01 M has little effect on conductivity: it does not alter significantly the Na^+ concentration in the microemulsion droplets. The effect on the conductivity of forming a microemulsion with $[CaCl_2]$ = 0.05 and 0.25 M is the same as the effect of [NaCl] = 0.1 and 0.5, respectively (data not shown). This would indicate that the ionic strength of the cation (rather than the molar concentration) is responsible for the conductivity decrease.

Figure 11.7b shows conductivity data as a function of temperature for water-in-isooctane microemulsions of So=13 and Wo=15 and 30, formulated with buffer tris(hydroxymethyl)-aminomethan / HCl (pH=8) of 0.08 M in the aqueous pools. The buffer-containing microemulsion of Wo=30 exhibited a percolation temperature approximately 5 °C lower than the percolation temperature of a microemulsion formed with tri-distilled water. For the Wo=15 microemulsion, addition of buffer decreases the conductivity value by a factor of approximately 5 (as compared to a microemulsion formed with tridistilled water). For the Wo=5 microemulsion (data not shown), addition of buffer had no major effect in the conductivity of the microemulsion.

As mentioned in Section 11.3c, the solvents that we used in our conductivity studies were such that, as the molar volume of the oil was increased, large attractive interactions between droplets limited the actual droplet radius to values smaller than the critical droplet radius; the latter decreased with decreasing salinity. Such an increase of salinity (through the addition of NaCl) would bring the droplet radius farther away from the critical radius and should then reduce the attractive interactions between microemulsion droplets; this could explain the large decrease in conductivity afforded to by the addition of salt. From light scattering experiments, Bedwell and Gulari [1984] and Hou et al. [1988] found that NaCl in the water pools diminished the magnitude of attraction between reverse micelles. These results were ascribed to a decrease of the interfacial area per polar head of

the surfactant molecules with increasing salinity, that made the interface more rigid (implying a larger bending elasticity) and less penetrable, and decreased the strength of the attractive interaction between droplets. Eicke and Shepherd [1974] measured the dielectric increment due to micelles and water-in-oil microemulsions as a function of water content and electrolyte added to the water. They found that water increased the magnitude of the dipole moment generated in an aggregate by an external electric field, while electrolyte added to the system decreased the magnitude of the dipole moment generated in a microemulsion droplet.

11.4 Conclusions

We investigated the effect of temperature on conductivity of AOT water-in-oil microemulsions (oil: n-hexane, i-octane, n-decane, or n-dodecane) of varying droplet size and concentration. The microemulsions exhibited a sharp increase in electrical conductivity with increasing temperature at constant Wo (for Wo values greater than 15) indicative of a percolation phenomenon. It is believed that conductivity percolation takes place when microemulsion droplets come close enough so that ions can hop from one to another and/or when droplets coalesce and exchange material. An increase in temperature would result in increasing the effective (with respect to ion hopping) diameter of the droplets, the droplet coalescence rate, and the exchange of material after coalescence, and would thus facilitate percolation. The temperature at which the percolation occurred decreased with increasing Wo (and corresponding microemulsion droplet size), and with decreasing So (increasing droplet concentration); in other words, the larger the droplet and the closer they are together the "easier" percolation happened. For Wo values smaller than 15 the logarithm of the microemulsion conductivity increased linearly with temperature.

The microemulsions were also found to exhibit a percolation point with increasing droplet size (increasing Wo) at constant droplet concentration and temperature, for temperatures > 30 °C. This phenomenon is thought to originate from an increase in interdroplet interaction as the droplet size increases. The Wo value at which percolation occurred decreased with increasing tempereature, and with decreasing So. For T < 30 °C, the conductivity passed through a maximum at Wo=10 (more pronounced at So=5), dropped to lower values, and then increased again at higher Wo's. The observed

conductivity maximum was interpreted in terms of the charge fluctuation model. Increase in the molecular weight of the alkane solvent shifted the percolation threshold to lower temperatures and dispersed volume fraction values; this was attributed to the influence of the solvent on attractive interactions between the microemulsion droplets.

The effect of salt in the aqueous phase of the microemulsions was investigated for a isooctane water-in-oil microemulsion of So=5 and Wo=10 that exhibited an unusually high conductivity. Addition of 0.1 N Na^+ or Ca^{+2} in the water pools decreased the conductivity of the microemulsion by two orders of magnitude, probably by decreasing droplet interactions or making the surfactant interface more compact and less amenable to breakage (leading to material exchange).

12.5 References and Notes Cited in Chapter 11

1. Alexandridis, P.; Holzwarth, J. F.; Hatton, T. A. *Langmuir* **1993**, *9*, 2045; Chapter 13 of this Thesis.
2. Bedwell, B.; Gulari, E. *J. Colloid Interface Sci.* **1984**, *102*, 88.
3. Bhattacharya, S.; Stokes, J. P.; Kim, M. W.; Huang, J. S. *Phys. Rev. Lett.* **1985**, *54*, 2253.
4. Bommarius, A. S.; Holzwarth, J. F.; Wang, D. I. C.; Hatton, T. A. *J. Phys. Chem.* **1990**, *94*, 7232.
5. Boned, C.; Peyrelasse, J.; Saidi, Z. *Phys. Rev. E* **1993**, *47*, 468.
6. Borkovec, M.; Eicke, H.-F.; Hammerich, H.; Gupta, B. D. *J. Phys. Chem.* **1988**, *92*, 206.
7. Borkovec M.; Eicke, H.-F. *Chem. Phys. Lett.* **1989**, *157*, 457.
8. Carver, M. T.; Hirsch, E.; Wittmann, J. C.; Fitch, R. M.; Candau, F. *J. Phys. Chem.* **1989**, *93*, 4867.
9. Cazabat, A.-M.; Langevin, D. *J. Chem. Phys.* **1981**, *73*, 3148.
10. Chen, V.; Evans, D. F.; Ninham, B. W. *J. Phys. Chem.* **1987**, *91*, 1823.
11. Chittofrati, A.; Sanguineti, A.; Visca, M.; Kallay, N. *Colloids Surfaces* **1992**, *63*, 219.
12. Dutkiewicz, E.; Robinson B. H., *J. Electroanal. Chem.* **1988**, *251*, 11.
13. Eicke, H.-F.; Borkovec, M.; Das-Gupta, B. *J. Phys. Chem.* **1989**, *93*, 314.

14. Eicke, H.-F.; Shepherd, J. C. W. *Helv. Chim. Acta* **1974**, *57*, 1951.
15. Fletcher, P. D. I.; Robinson, B. H. *Ber. Bunsenges. Phys. Chem.* **1981**, *85*, 863.
16. Fletcher, P. D. I.; Howe, A. M.; Robinson, B. H. *J. Chem. Soc., Faraday Trans. 1* **1987**, *83*, 985.
17. Fletcher, P. D. I.; Horsup, D. I. *J. Chem. Soc., Faraday Trans.* **1992**, *88*, 855.
18. Grest, G. S.; Webman, I.; Safran, S. A.; Bug, A. L. R. *Phys. Rev. A* **1986**, *33*, 2842.
19. Hall, D. G. *J. Phys. Chem.* **1990**, *94*, 429.
20. Halle, B. *Progr. Colloid Polym. Sci.* **1990**, *82*, 211.
21. Hamilton, R. T.; Billman, J. F.; Kaler, E. W. *Langmuir* **1990**, *6*, 1696.
22. Helfrich, W. *Z. Natur.* **1973**, *C28*, 693.
23. Hilfiker, R.; Eicke, H.-F. *J. Chem. Soc., Faraday Trans. 1* **1987**, *83*, 1621.
24. Hilfiker, R.; Eicke, H.-F.; Sager, W.; Steeb, C.; Hofmeier, U.; Gehrke, R. *Ber. Bunsenges. Phys. Chem.* **1990**, *94*, 677.
25. Hou, M.-J.; Shah, D. O. *Langmuir* **1987**, *3*, 1086.
26. Hou, M. J.; Kim, M.; Shah, D. O. *J. Colloid Interface Sci.* **1988**, *123*, 398.
27. Huang, J. S.; Milner, S. T.; Farago, B.; Richter, D. *Phys. Rev. Lett.* **1987**, *59*, 2600.
28. Jada, A.; Lang, J.; Zana, R. *J. Phys. Chem.* **1989**, *93*, 10.
29. Jada, A.; Lang, J.; Zana, R. *J. Phys. Chem.* **1990**, *94*, 381.
30. Jada, A.; Lang, J.; Zana, R.; Makhioufi, R.; Hirsch, E.; Candau, S.-J. *J. Phys. Chem.* **1990**, *94*, 387.
31. Kallay, N.; Chittofrati, A. *J. Phys. Chem.* **1990**, *94*, 4755.
32. Kim, M. W.; Huang, J. S. *Phys. Rev. A* **1986**, *34*, 719.
33. Kotlarchyk, M.; Huang, J. S.; Chen, S.-H. *J. Phys. Chem.* **1985**, *89*, 4382.
34. Kunieda, H.; Shinoda, K. *J. Colloid Interface Sci.* **1979**, *70*, 577.
35. Lagües, M.; Ober, R.; Taupin, C. *J. Physique Lett.* **1978**, *39*, L487.
36. Lagües, M. *J. Physique Lett.* **1979**, *40*, L331.
37. Lagües, M.; Sauteray, C. *J. Phys. Chem.* **1980**, *84*, 3503.
38. Lindman, B.; Stilbs, P. in *Microemulsions: Structure and Dynamics*, Friberg, S.E.; Bothorel, P. (Editors), CRC Press, **1988**.
39. Maitra, A.; Mathew, C.; Varshney M. *J. Phys. Chem.* **1990**, *94*, 5290.
40. Mathew, C.; Patanjani, P. K.; Nabi, A.; Maitra, A. N. *Colloids Surfaces* **1988**,

30, 253.

41. Moha-Ouchane, M.; Peyrelasse, J.; Boned, C. *Phys. Rev. A* **1987**, *35*, 3027.
42. Mukhopadhay, L.; Bhattacharya, P. K.; Moulik S. P. *Colloids Surfaces* **1990**, *50*, 295.
43. Pan, H.-Y. *Chem. Phys. Lett.* **1991**, *185*, 344.
44. Peyrelasse, J.; Boned, C. *Phys. Rev. A* **1990**, *41*, 938.
45. Ray, S.; Bisal, S. R.; Moulik, S. P. *J. Chem. Soc. Faraday Trans.* **1993**, *89*, 3277.
46. Robertus, C.; Philipse, W. H.; Joosten, J. G. H.; Levine, Y. K. *J. Chem. Phys.* **1989**, *90*, 4482.
47. Safran, S. A. *J. Phys. Chem.* **1983**, *78*, 2073.
48. Safran, S. A.; Grest, G. S.; Bug, A. L. R.; Webman, I. in *Microemulsion Systems*, H. Rosano and M. Clausse (Eds), Marcel Dekker, NY, **1987**, p.235.
49. van Dijk, M. A. *Phys. Rev. Lett.* **1985**, *55*, 1003.
50. van Dijk, M. A.; Casteleijn, G.; Joosten, J. G. H.; Levine, Y. K. *J. Chem. Phys.* **1986**, *85*, 626.

51 Zana, R.; Lang, J. in *Microemulsions: Structure and Dynamics*, Friberg, S.E.; Bothorel, P. (Editors), CRC Press, **1988**.

52 Zana, R.; Lang, J.; Candau, D. *J. Phys. Chem.* **1991**, *95*, 3364.

Note 1 A conducting microheterogeneous dispersion in a very weakly conducting or nonconducting medium may show a rapid rise in conductane above a threshold concentration; this phenomenon is called percolation (Landauer, R. *J. Appl. Phys.* **1952**, *23*, 779; Kirpatrick, S. *Rev. Mod. Phys.* **1973**, *45*, 574; Bernasconi, J. *Phys. Rev. B* **1973**, *7*, 2252; **1974**, *9*, 4575).

Note 2 Hall [1990] gave a modified version of Eicke's model [Eicke et al., 1989] in which he sonsidered the disceteness of electric charge and achieved even better agreement with experiment that the original Eicke model where continuity of electric charge is supposed. Meanwhile, Kallay and Chittofrati [1990] published a note in which they distinguish the Born radius from the Stokes radius of a droplet and improved the agreement between theory and experiment, especially for small microemulsion droplets. Pan [1991] showed that Hall's model may be based on the thermodynamic fluctuation theory in a quite rigorous and general way, and that the two-droplet equilibrium mechanism introduced by Hall is unnecessarily restrictive.

Note 3 Increase of temperature for an AOT-water-oil system of given composition is

associated with changing the surfactant monolayer curvature from that of a water-in-oil aggregate structure (negative curvature) to that of an oil-in-water aggregate structure (positive curvature); for the AOT microemulsions studied in this paper the actual curvature as determined by Wo shows only a small variation with temperature [Kim & Huang, 1986].

Note 4 In a recent study McFann and Johnston [McFann, G. J.; Johnston, K. P. *Largmuir* **1993**, *9*, 2942] reported data for water solubilization in AOT microemulsions that are in agreement with the data of Hou & Shah [1987] for the solvents octane, nonane, and decane, but are not in agreement for pentane, hexane and heptane. McFann and Johnston found maximum solubilization for pentane; the solubilization capacity dropped as the molecular weight of the alkane increased. Our data show a monotonic trend from hexane to dodecane and agree with the trend seen by McFann and Johnston.

Chapter 11: List of Figures

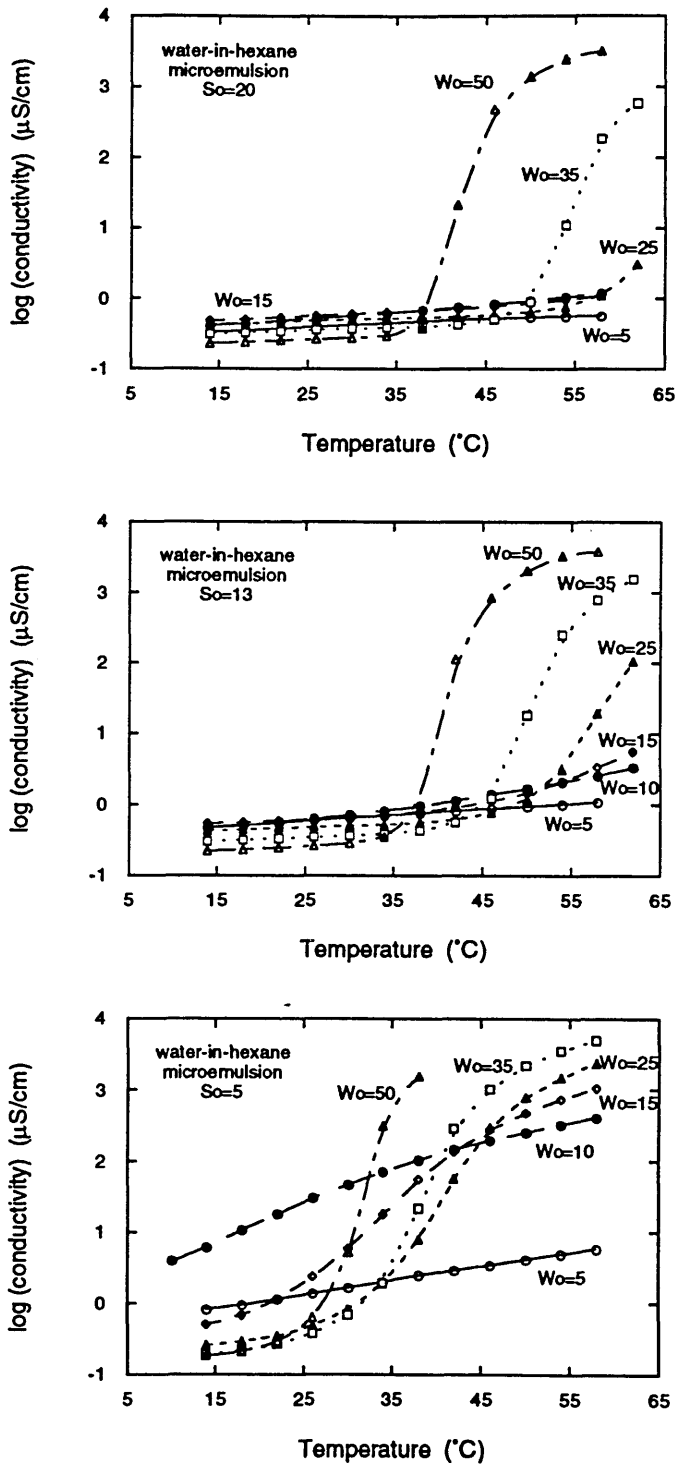

Figure 11.1 Conductivity as a function of temperature for water-in-hexane microemulsions of various Wo (=[water]/[AOT]) values at given So (=[oil]/[AOT]) ratios.

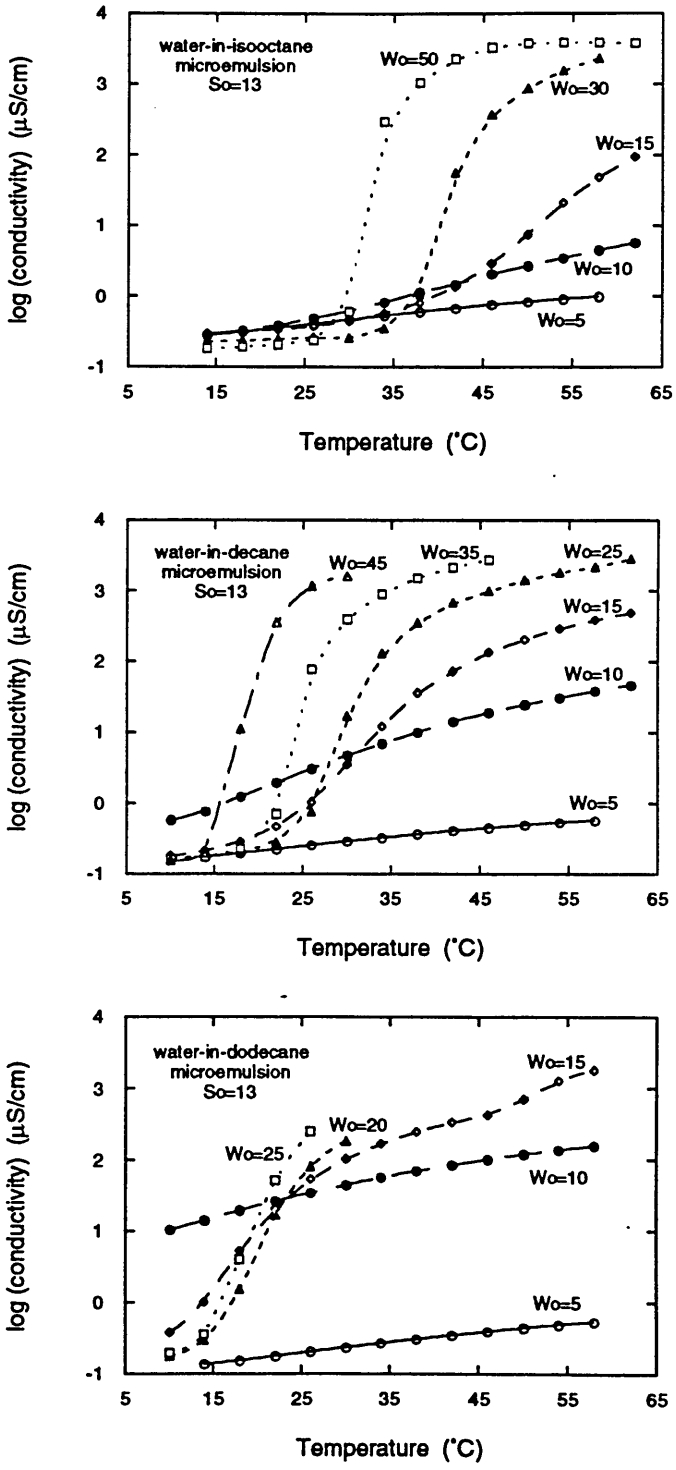

Figure 11.2 Conductivity as a function of temperature for water-in-oil microemulsions of So =13 formulated with isooctane, decane, and dodecane.

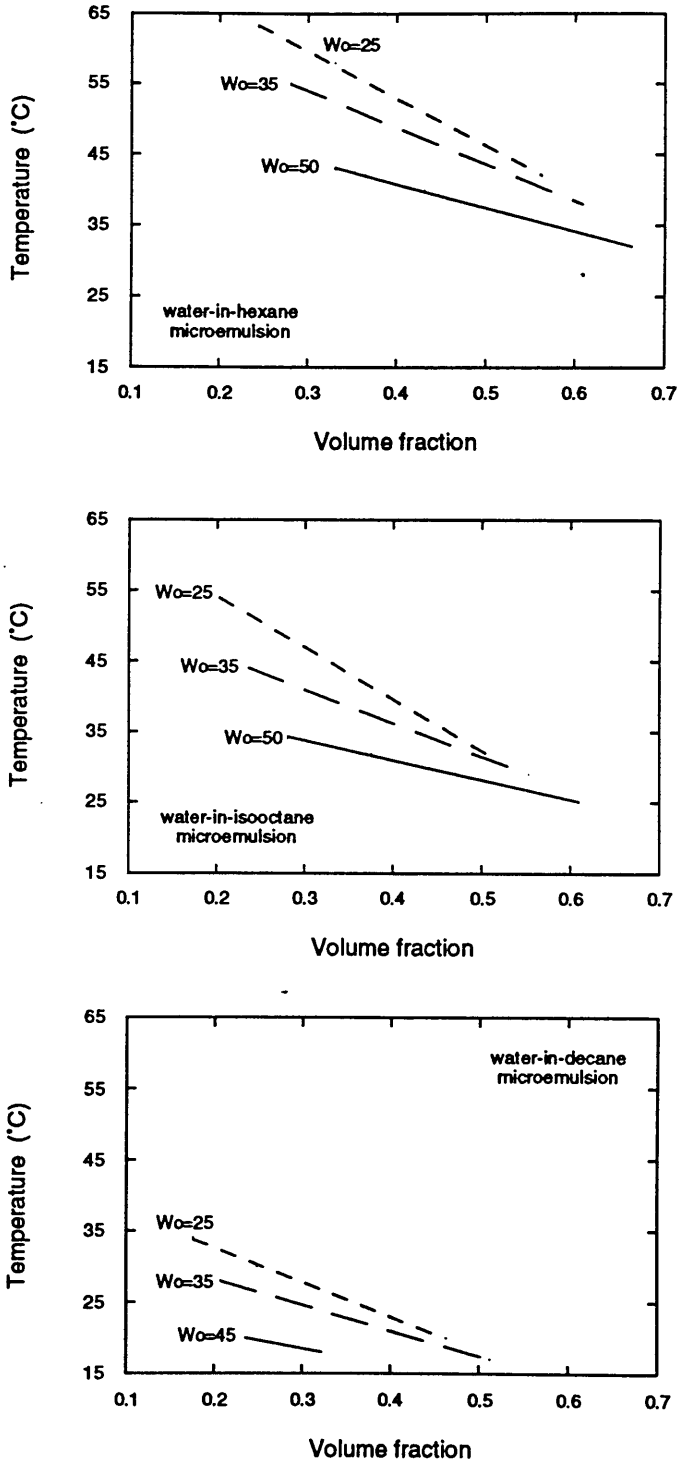

Figure 11.3 Percolation boundary on temperature vs dispersed volume fraction diagram: (a) water-in-hexane, (b) water-in-isooctane, and (c) water-in-decane microemulsions.

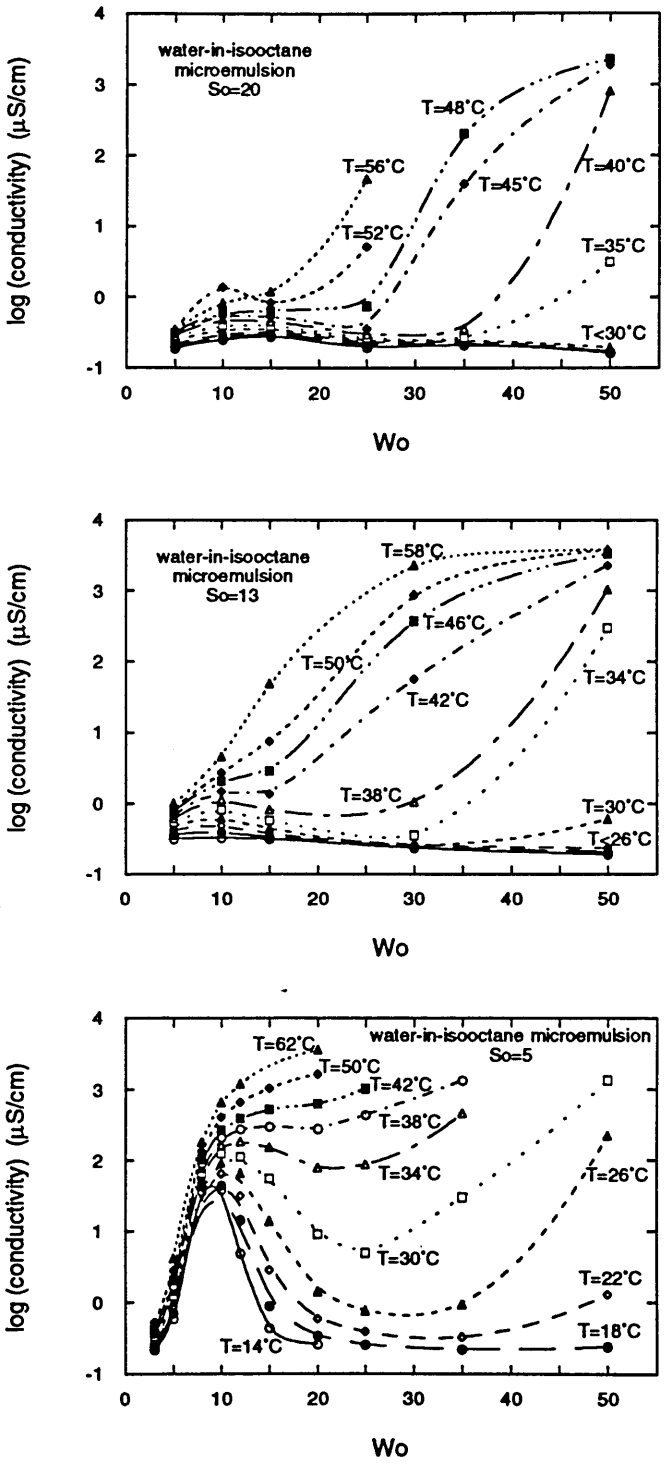

Figure 11.4 Conductivity as a function of the Wo (=[water]/[AOT]) ratio (~ micelle size) for water-in-isooctane microemulsions at various temperatures.

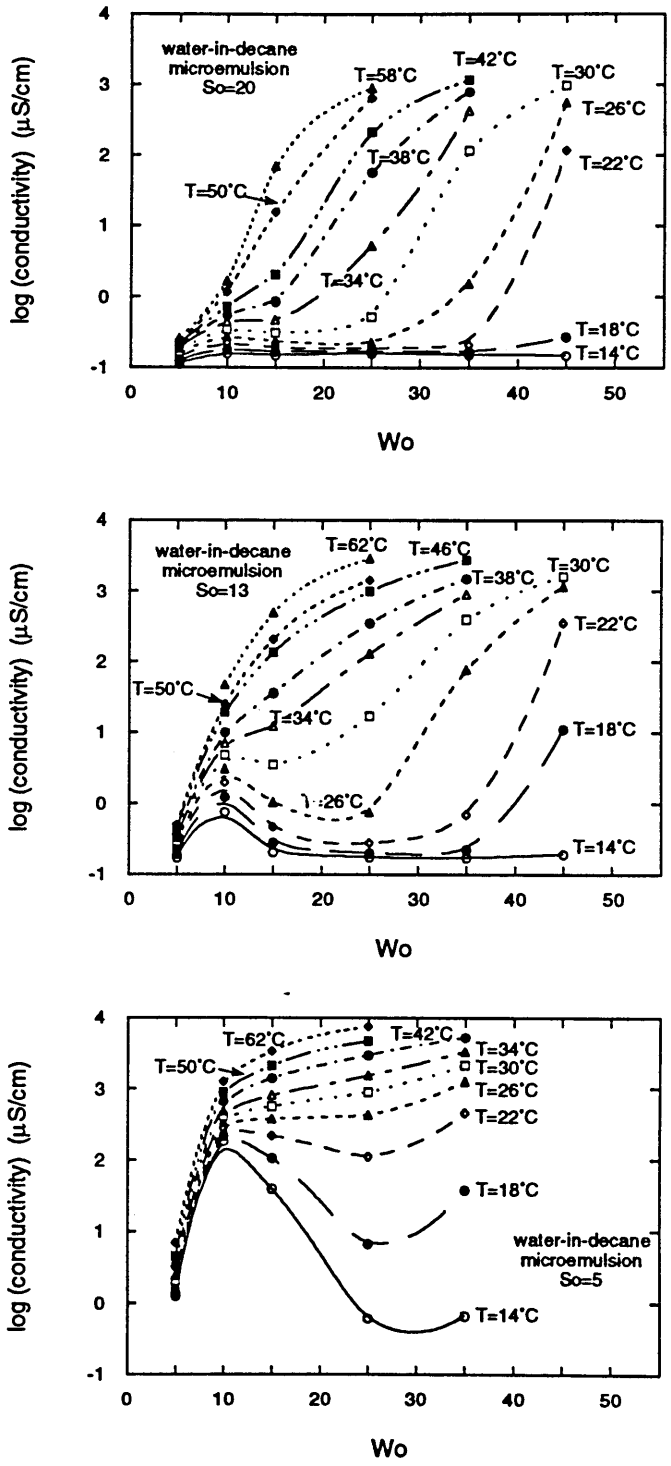

Figure 11.5 Conductivity as a function of the Wo (=[water]/[AOT]) ratio (~ micelle size) for water-in-decane microemulsions at various temperatures.

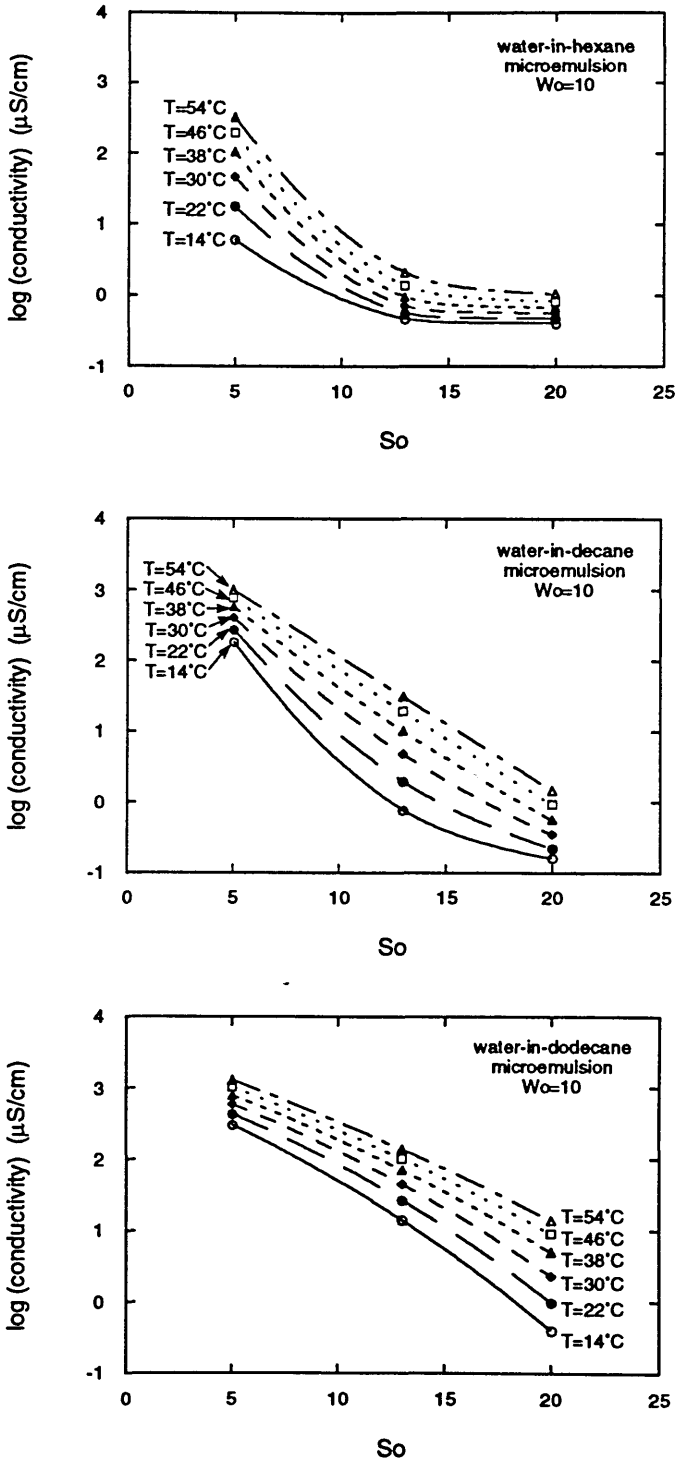

Figure 11.6 Conductivity as a function of the So ratio (inversely proportional to the micelle concentration) for water-in-oil microemulsions of Wo=10 at various temperatures: (a) water-in-hexane, (b) water-in-decane, and (c) water-in-dodecane microemulsions.

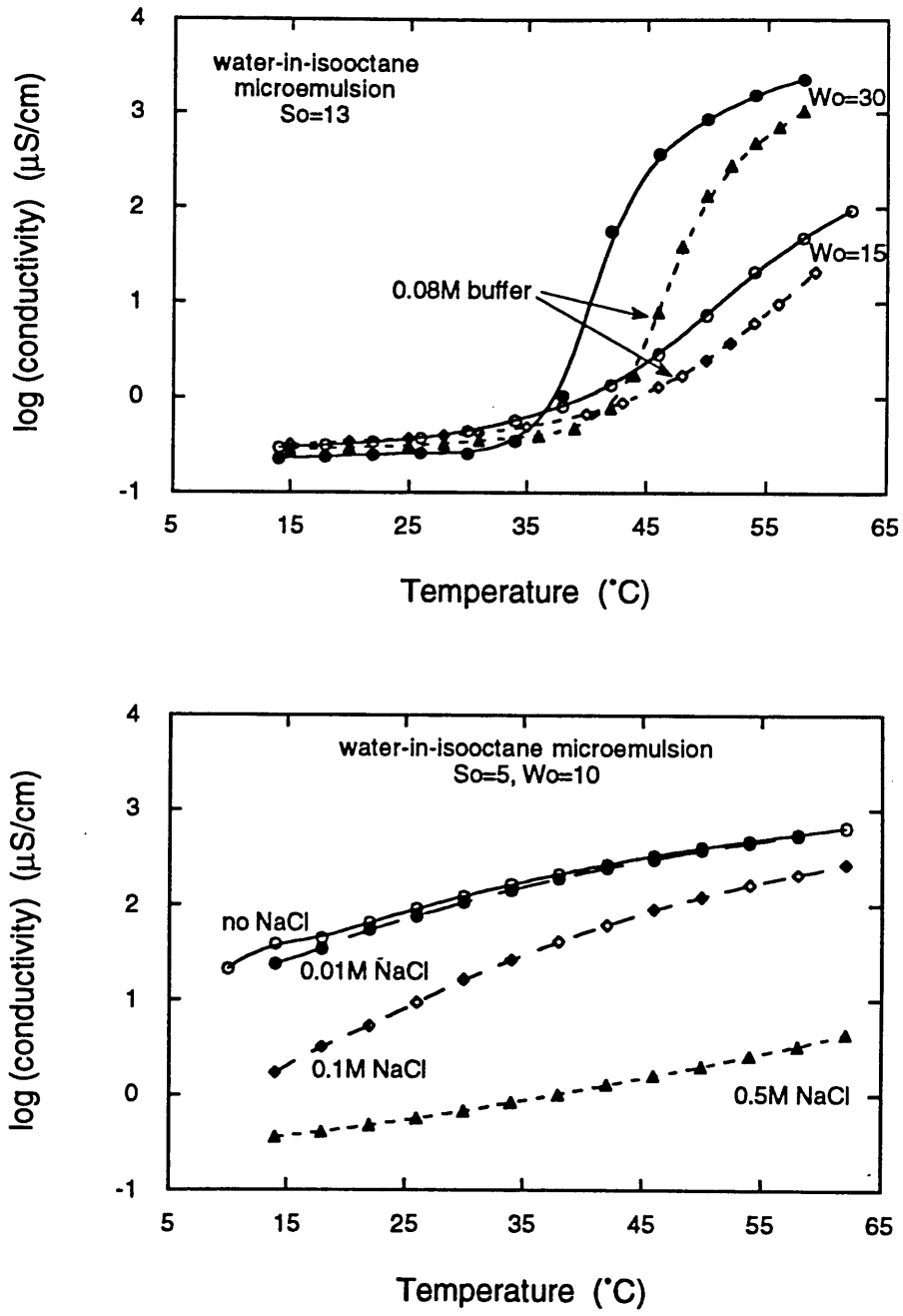

Figure 11.7 Effects of salt on microemulsion conductivity: (a) conductivity vs temperature for water-in-isooctane microemulsion of So=5 and Wo=10, formulated with [NaCl] = 0, 0.01, 0.1, and 0.5 M in the aqueous phase, (b) conductivity vs temperature for water-in-isooctane microemulsions of So=13 and Wo=15, 30, formulated with 0.08M buffer of in the aq. phase.

Chapter 12
Thermodynamics of Droplet Clustering in Percolating AOT Water-in-oil Microemulsions

12.1 Introduction

Water-in-oil microemulsions or reverse micelles are thermodynamically-stable complex fluids that can be envisaged as distinct, nanometer-size, water droplets maintained dispersed in an apolar solvent with the aid of a surfactant monolayer that reduces unfavorable oil-water contact [Zana & Lang, 1988; Lindman & Stilbs, 1988]. One of the parameters used to assess microemulsion formation, investigate the structural changes leading to their occurrence, and probe the exchange of microemulsion components (such as water and ions) when microemulsion droplets coalesce, is electrical conductivity. The sharp increase in conductivity (over orders of magnitude) observed in water-in-oil microemulsion systems with spherical droplet structure has been characterized as a percolation [Note 1] of identical conducting objects, randomly distributed in an insulating medium. It is generally considered that, during percolation, water microdroplets come in close contact and charge carriers propagate by hopping between droplets [Grest et al., 1986] and/or by exchange of the droplet contents when droplets coalesce. High conductivity values, up to 1 Sm^{-1}, are observed above the percolation threshold, however, conductivities on the order of 10^{-3} Sm^{-1} have been explained by migration of statistically charged droplets; the quantitative charge fluctuation model [Eicke et al., 1989; Hall, 1990; Kallay & Chittofrati, 1990] accounted for the non-monotonic variation of conductivity observed experimentally at low Wo (=[water]/[AOT]) values. Ternary microemulsion systems, such as AOT/water/alkane that maintain constant droplet size when the droplet volume fraction varies (i.e., upon dilution with the continuous phase), can be used as model systems in clarifying percolative behavior and its origin [Borkovec et al., 1988; Jada et al., 1990a].

A surfactant anion hopping model with a temperature dependent hopping range was proposed by Kim and Huang [1986] to describe the effect of temperature on the percolation

threshold ϕ_c. According to this model, percolation would occur when the effective droplet volume (as defined by the hopping range) exceeded the hard-sphere close-packing limit of 0.65 so that charges could be transferred between clusters of droplets. The range of interaction depended on temperature, reflecting the combined effects of increased probability of the surfactant ionization and increased range of ion diffusion effected by increasing temperature. Maitra et al. [1990] inferred from measurements of water self-diffusion coefficients in AOT/water/isooctane microemulsions that the percolative conduction arose due to the hopping of charge carriers across the surfactant monolayer of the droplets, and that the aggregates opened up only at the onset of formation of bicontinuous microemulsions. However, Jada et al. [1989; 1990b] reached the conclusion that the electrical conductivity in water-in-oil microemulsions above the percolation threshold was due to motion of surfactant counterions within transient water channels (arising in droplet clusters upon opening of the surfactant layers). The exchange of droplet contents was studied in ternary microemulsion systems [Jada et al., 1989; Jada et al., 1990b; Zana et al., 1991] and it was showed that, for percolative behavior to occur, the rate constant for droplet collision with exchange of material must reach a value of at least 10^9 M^{-1} s^{-1}, irrespective of the parameter varied to induce percolation.

In a quaternary microemulsion system, Hamilton et al. [1990] found the percolation thresholds determined from conductivity measurements to occur at the same or slightly higher water volume fraction as those determined from NMR, indicating that conduction involved movement of ions in channels connecting droplets and not through the surfactant interface or by a charge-hopping mechanism. It was also proposed that the onset of percolation occurred in microemulsions when the interdroplet attraction exceeded a critical value of 2kT [Hamilton et al., 1990]. Dielectric spectroscopy and other techniques [van Dijk, 1985] supported the notion that clustering of water droplets, occurring in water/AOT/isooctane microemulsions due to short range attractive interactions, are causing the observed high conductivity. The effect of additives (i.e., alkanols, cholesterol, crown ether) on temperature induced percolation in AOT/decane microemulsions was interpreted by Mukhopadhay et al. [1990] in terms of modulations of the surfactant interface effected by the additives. Estimates of activation energies for conduction supported the mechanism of temperature-induced percolation transition by efficient transport of Na^+ counterions through water channels formed in the clusters of water microdroplets upon collision, rather than hopping of the AOT ions from one droplet to another [Mukhopadhay et al., 1990]. It

becomes obvious from the above that clusters of droplets are responsible for the percolative behavior in microemulsions. Cluster formation will be influenced by such factors as temperature, droplet size and concentration, and the nature of the apolar medium in which droplets are dispersed.

Most of the percolation data in the water-in-oil microemulsion literature concern increase of conductivity upon addition of water [Lagues, 1979; Lagues & Sauteray, 1980]. Reports on percolation induced by increasing temperature have been published from van Dijk et al. [1985; 1986], Huang and coworkers [Kim & Huang, 1986; Bhattacharya et al., 1985], Moha-Ouchane et al. [1987], Maitra et al. [1990], and Moulik and coworkers [Mukhopadhay et al., 1990; Ray et al., 1993]. We recently undertook a comprehensive experimental study of temperature induced percolation in AOT water-in-oil microemulsions and related our results to the mechanisms responsible for this phenomenon (Chapter 11 of this Thesis). The effect of microemulsion droplet size and concentration on conductivity was examined systematically in microemulsions formulated with various alkanes as continuous phase. In this Chapter we analyze the percolation temperature vs concentration data of Chapter 11 to estimate the energy parameters associated with the formation of percolation clusters. The remainder of the paper is organized as follows. The derivation of the free energy, enthalpy, and entropy of clustering values from an "association" model of droplet clustering is described. The effects of microemulsion droplet size and concentration on droplet clustering energetics are then presented, followed by a discussion on the effect of apolar solvent. The droplet clustering phenomenon is then contrasted to the formation of micelles and the flocculation of sterically stabilized colloidal particles, and discussed in the light of the attractive interactions known to exist between microemulsion droplets. Other approaches in obtaining energy parameters for droplet clustering are also presented and compared to the "association" model used here.

12.2 Materials and Methods

AOT (Sulfosuccinic acid bis[2-ethylhexyl] ester, sodium salt) of 99% purity was purchased by Sigma Chemical Co. (St. Louis, MO) and used as received. N-hexane, isooctane, and n-decane (AR grade) were obtained from Mallinckrodt Inc. (Paris, KY). The water used was triple-distilled. Conductivity experiments were performed in AOT

water-in-alkane microemulsions, for the alkanes n-hexane, isooctane, and n-decane. We worked inside the L2 phase boundary, where the structure of the aggregates is spheres [Kotlarchyk et al., 1985; Robertus et al., 1989; Hilfiker et al., 1990]; the droplet shape and size has been found fairly insensitive to both the concentration of the droplets and the equilibrium temperatures [Kim & Huang, 1986]. The composition of the microemulsions is given here in terms of Wo, the ratio of water to surfactant molar concentrations, and So, the ratio of oil to surfactant molar concentrations; in the AOT system Wo essentially determines the radius of the water droplets, and So their concentration in the oil phase [van Dijk et al., 1986]. The microemulsions were prepared using the injection method, by adding an appropriate quantity of water to an AOT solution in oil [Alexandridis et al., 1993]. The resulting microemulsions were placed in Teflon-stoppered glass test tubes, and left to equilibrate at room temperature for approximately one day before the conductivity experiment. The conductivity of microemulsions was measured as a function of temperature with a CDM 83 Conductivity Meter and a CDC 344 Electrode (constant: 3.191 cm), both from Radiometer Copenhagen (Copenhagen, Denmark). The electrode was inserted in the test tube containing the microemulsion, and the test tube placed in a thermostated water bath. The temperature of the sample was monitored with a T801 temperature probe from Radiometer Copenhagen. Sufficient time (at least 10 mins [Mukhopadhay et al., 1990]) was allowed for equilibration between conductivity measurements at different temperatures. All microemulsion samples were single-phase and optically transparent under the conditions of the conductivity measurements reported here.

12.3 Results and Discussion

12.3a Energetics of droplet clustering during percolation: "association" model

The effect of temperature on conductivity for AOT microemulsions of varying droplet radii and concentration, formulated with four different alkane solvents, has been reported in Chapter 11. For Wo values smaller than 10, the logarithm of the microemulsion conductivity increased linearly with temperature for all droplet concentrations and solvents studied. The conductivity for these Wo values is believed to originate from fluctuations in the ion content of the microemulsion droplets, resulting in

charged droplets, able to conduct electricity [Eicke et al., 1989]. For Wo > 15, the logarithm of the microemulsion conductivity exhibited a characteristic sigmoidal behavior as the temperature increased; this increase of conductivity over 4 orders of magnitude, was indicative of percolation [Note 1]. Figure 12.1 shows conductivity data plotted as a function of temperature, for AOT water-in-oil microemulsions of constant droplet size (Wo=35) at various droplet concentrations (So is inversely proportional to droplet concentration). The percolation temperature, T_p, is defined here as the point at which a change in slope (break) in the conductivity vs temperature curve occurs, indicating the transition from a non-percolating state to a percolating state. T_p decreased with increase in the droplet size (for constant droplet concentration) and with increasing droplet concentration at constant Wo (in other words, the larger the droplets and the closer they are together the "easier" percolation takes place). This has been attributed to an increase in interdroplet attactive interactions (that enhance cluster formation) as the microemulsion droplet size and concentration increase (see Chapter 11).

It is generally accepted, as mentioned in the Introduction, that conductivity percolation in microemulsions with spherical droplet structure is a result of microemulsion droplet clustering; a schematic of a percolating droplet cluster is shown in Figure 12.2. Ray et al. [19] estimated the energetics of the droplet clustering process utilizing the values of dispersed-phase (AOT plus water) volume fraction (ϕ_d) at the percolation threshold for different temperatures. It was postulated that the threshold of electrical percolation corresponded to the formation of the first open structure of an infinite cluster [Ray et al., 1993]. The microemulsion droplets above the percolation threshold, aggregated in clusters, were considered to be a phase different than that of non-percolating droplets, with distinct physical properties such as conductivity. This is comparable to the pseudophase concept used for modelling the micelle formation in solutions of amphiphilic molecules (association model) [Hunter, 1987]. Diluting a clustered (percolating) microemulsion system upon addition of apolar solvent at constant droplet size (~Wo) would lower the conductivity rapidly until the clusters dissociate into individual droplets below the threshold ϕ_d; this phenomenon is comparable to the process of demicellization occurring when the surfactant concentration is lowered below the CMC (critical micellization concentration [Hunter, 1987]). In the light of the concept of droplet "association", the Gibbs free energy of droplet clustering (standard free energy change for the transfer of 1 mol of droplets from solution to the percolating cluster), ΔG°_{cl}, was calculated from the relationship [Atwood &

Florence, 1983; Hunter, 1987; Ray et al., 1993]

$$\Delta G^{\circ}_{cl} = R\,T\,\ln X_p \qquad (1)$$

where R is the gas law constant, T is the absolute temperature, and X_p is the mole fraction of the microemulsion droplets corresponding to the percolation threshold ϕ_d at temperature T and at constant droplet size (Wo). Another way of arriving at Equation 1 is to assume an equilibrium between individual droplets and droplet clusters [Hunter, 1987; Alexandridis et al., 1994]. Application of the Gibbs-Helmholtz equation allows the standard enthalpy of cluster formation, ΔH°_{cl}, to be expressed as [Hunter, 1987; Atwood & Florence, 1983]

$$\Delta H^{\circ}_{cl} = -R\,T^2\,[\,\partial \ln(X_p) / \partial T\,] = R\,[\,\partial \ln(X_p) / \partial (1/T)\,] \qquad (2)$$

Finally, the standard entropy of cluster formation per mol of droplets, ΔS°_{cl}, can be obtained from:

$$\Delta S^{\circ}_{cl} = (\Delta H^{\circ}_{cl} - \Delta G^{\circ}_{cl}) / T \qquad (3)$$

It has been shown for micellization of surfactants and block copolymers ([Alexandridis et al., 1994] and references cited therein) that, within experimental error,

$$\partial \ln(X_p) / \partial (1/T) = \partial \ln(X) / \partial (1/T_p) \qquad (4)$$

where X is the droplet concentration expressed in mol fraction, and T_p is the percolation temperature for a given ϕ_d; thus Equation 2 becomes

$$\Delta H^{\circ}_{cl} = R\,[\,\partial \ln(X) / \partial (1/T_p)\,] \qquad (5)$$

In accordance with Equation 5, the natural logarithm of droplet concentration is plotted in Figure 12.3 as a function of inverse percolation temperature for various solvents and Wo values. For a given microemulsion system, the percolation temperatures increased as the droplet concentration (X) or size (Wo) decreased. Increasing the molecular weight of the apolar solvent resulted in a shift to lower percolation temperatures for comparable

Wo and X. The solid lines in Figure 12.3 are linear fits from which ΔH°_{cl} can be calculated using Equation 5; the linear fit seems satisfactory, although, admittedly, in a few cases the data are limited. As evidenced from the slopes in the graphs of Figure 12.3, the standard enthalpy of cluster formation, ΔH°_{cl}, is positive for all cases studied here, indicating that the transfer of microemulsion droplets from solution to the percolating cluster is an enthalpically-unfavorable endothermic process. The free energy, ΔG°_{cl}, is negative, since the clusters are formed spontaneously. It is clear, therefore, that a positive entropy contribution must be the driving force for clustering during conductivity percolation; ΔS°_{cl} can be derived from Equation 3, of from the slope of graphs similar to that shown in Figure 12.4.

Movement of ions and/or water during percolation (through "breaking" of the droplet surfactant interface during coalescence and/or diffusion via the nonconducting solvent) could involve an activation energy barrier leading to positive ΔH°_{cl}. For example, if an AOT surfactant should exit the droplet leaving the Na^+ counterion in the water core, the static electric energy is of the order of 17 kT [Kim & Huang, 1986] or 42 kJ/mol at 298 K; the activation energy for opening the surfactant layer can be 50 - 100 kJ/mol. The positive entropy observed can be related to the attractive interactions that are known [Hamilton et al., 1990] to exist between microemulsion droplets (see discussion in Section 12.3c). Furthermore, ions and water that are localized ("restricted") in individual droplets in a non-percolating system can move within a percolating cluster thus gaining entropy. The dependence of ΔG°_{cl}, ΔH°_{cl} and ΔS°_{cl} values on microemulsion droplet size and concentration are discussed below.

12.3b Effect of droplet size and concentration on droplet clustering energetics

Free energy values for the droplet clustering process, calculated from Equation 1, are plotted in Figure 12.5 as a function of So (inversely proportional to the surfactant concentration or total surface area in the microemulsion) for various droplet sizes (~Wo); the ΔG°_{cl} values were estimated at the percolation temperature for microemulsions of given composition. For a given droplet size, the free energy took more negative values as the droplet concentration decreased (this is a result of both T_p and $\ln X_p$ increasing). For a

given So, the free energy became more negative as the droplet size increased. This is despite the fact that percolation temperatures decrease with increasing Wo, and is due to X_p becoming smaller (and $\ln X_p$ more negative) when the droplet size increases at constant So. Increase of the molecular weight of the apolar solvent (for the same So and Wo) resulted in less negative ΔG°_{cl}.

Values for the enthalpy of droplet clustering are presented in Figure 12.6a, plotted as a function of Wo for various apolar solvents. As discussed in Section 12.3a, the clustering process is endothermic (positive ethalpy); the values for ΔH°_{cl} ranged form 45 to 125 kJ/mol. The clustering enthalpy increased with droplet size, and was higher for the microemulsion formulated with decane. The entropy of clustering ΔS°_{cl} behaved in a similar fashion to ΔH°_{cl} (see Figure 12.6b); ΔS°_{cl} was found to increase with Wo and with increasing solvent molecular weight. The ΔH°_{cl} and ΔS°_{cl} reported by Ray et al. [1993] for AOT/heptane microemulsions also increased with Wo.

12.3c Effect of apolar solvent on droplet clustering energetics

Increase in the molecular weight of the alkane solvent from hexane to decane shifted the percolation threshold to lower temperatures for comparable Wo and So; this has been attributed to the influence of the solvent on attractive interactions between the microemulsion droplets. The effect of solvent on microemulsion phase behavior and droplet interactions can be understood by invoking the work of Shah and coworkers [Hou & Shah, 1987] who showed that large attractive interaction between droplets is the major factor limiting the solubilization capacity of water as the molar volume of the oil is increased beyond pentane or heptane [Note 2]. Hou et al. [1988] found (using light scattering) the interdroplet attractive interaction in AOT water-in-oil microemulsions to increase significantly with increasing Wo and chain length of the oil. Small-angle neutron scattering experiments in quaternary microemulsion systems [Hamilton et al., 1990] also showed the magnitude of the attractive interaction between the microemulsion droplets to increase as the alkane solvent chain length increased. Increase in the droplet radius would increase the overlap volume between two droplets (formed when they come close to each other) and, consequently, the interaction potential [Lemaire et al., 1983]; percolation can thus be facilitated.

While droplet attractions play an important role in percolation, the nature of the interface of the individual droplets also has an effect; for percolation to occur, droplets must exchange contents and so the droplet interface must rupture. Jada et al. [1989; 1990b] found the exchange rate of droplet contents to increase and the percolation threshold to decrease as the apolar solvent chain length increased in AOT microemulsion systems. This was attributed to reduction in solvent penetration into the interface with increasing solvent molecular weight, resulting in greater interdroplet attraction and lower percolation threshold. Johannsson et al. [1991] observed large clusters forming in AOT/dodecane microemulsions already rather far from critical point, while only small clusters (or dimers) were present in microemulsions formed by isooctane; cluster formation increased with the concentration of micelles.

Increasing the molecular weight of the apolar solvent (for the same So and Wo) resulted in less negative ΔG°_{cl} values; the change was more pronounced at low droplet concentrations. Note that, while increasing either microemulsion droplet size or solvent molecular weight effected changes in percolation temperature in the same direction, more negative ΔG°_{cl} values were obtained by increasing Wo. The enthalpy of droplet clustering is plotted in Figure 12.7 as a function of the apolar solvent density for various Wo values. ΔH°_{cl} increased significantly with increasing density (and molecular weight) of the alkanes; the rate of increase was lower at the higher Wo value. ΔS°_{cl} was also found to increrase from hexane- to decane-based microemulsions. It can thus be concluded that the energy barier (or entropy gain) related to the percolation phenomenon is higher for the higher molecular weight solvent. It can also be conjectured that the favorable-to-percolation interdroplet attractions discussed in the previous paragraph are of entropic nature.

12.3d Origin of enthalpic and entropic contributions to clustering energetics

The positive enthalpy and entropy observed in percolating microemulsions are reminiscent of the behavior of these thermodynamic parameters in the phenomenon of micelle formation taking place in aqueous surfactant and amphiphilic block copolymer solutions (see [Alexandridis et al., 1994] and references cited therein). When hydrophobic residues aggregate in aqueous solution, the water entropy increases as hydrogen bonding is restored (hydrophobic effect); this overcomes the loss of entropy due to the localization of the hydrophobic chains in the micelles. The entropy contribution usually dominates the

micellization process in aqueous surfactant solutions, with the enthalpy playing a minor role. Despite the parallels drawn between association of amphiphilic molecules into micelles and microemulsion droplets into clusters in modelling the latter phenomenon, it seems unlikely that entropy gain from the side of the apolar solvent is behind the positive entropy contribution observed experimentally in the case of droplet clustering, since no effect such as the hydrophobic is expected to occur. Note, that the micellization of copolymers in apolar solvents originates from enthalpic interactions between the copolymer segments and the solvent, and is not favored entropically [Price, 1983].

An interesting connection can be made between microemulsion droplet clustering and flocculation of sterically stabilized colloidal particles. Such flocculation is usually reversible and may occur either upon heating or cooling, or both, depending on the colloidal system [Napper, 1983; Piirma, 1992]. Three different types of steric stabilization can be identified: enthalpic, entropic, and combined enthalpic-entropic stabilization [Hunter, 1987]. In enthalpic stabilization, the enthalpy change on close approach of the particles promotes stabilization (ΔH_f positive), whereas the corresponding entropy change promotes flocculation (ΔS_f positive). For a dispersion that flocculates on heating (similar to the heating-induced droplet clustering at percolation) ΔS_f is positive and the stabilization is enthalpic. In entropic stabilization, the roles of the enthalpy and entropy terms are reversed. Entropic stabilization is more common in non-aqueous dispersion media, while enthalpic stabilization is typical in aqueous dispersions; however, both stabilization types have been observed in both aqueous and non-aqueous dispersion media [Hunter, 1987]. Using the terminology advanced in this paragraph, the water-in-oil microemulsion droplets are "enthalpically stabilized".

The Flory-Huggins free energy of mixing expression can be used to shed some light on the microscopic origins of the enthalpic stabilization observed in microemulsion droplet clustering [Hunter, 1987]. The (combinatorial) entropy of mixing is higher when the surfactant tail is mixed with the solvent, rather than the surfactant layer of another droplet, and is thus in favor of stabilization; consequently, the positive entropy contribution observed in droplet clustering cannot be due to mixing (note though, that, as the molecular weight of the solvent increases and becomes comparable to that of the surfactant tail, the mixing entropy term will be less significant). The enthalpy of mixing (contact dissimilarity) term can be either positive or negative but is usually small [Hunter, 1987].

This leaves the free volume dissimilarity enthalpy and entropy terms [Hunter, 1987] to contribute in the "right" direction (positive ΔH and ΔS) for droplet clustering. The free volume dissimilarity terms arise from the fact that the free volume of the apolar solvent increases with temperature, while the surfactant molecules are "restricted" at the droplet interface. Furthermore, the partial molar volume of oil molecules associated with surfactant tails in normal micelles is larger compared to that in the pure liquid phase [Lemaire et al., 1983].

One of the first attempts to interpret and model the short-range attractive interactions between microemulsion droplets was by Lemaire et al. [1983], who generalized Hamaker's treatment to estimate the internal energy of the overlapped region between two micelles. Their results indicated that slight increase in the specific volume of CH_2 segments in the surfactant layer induced a sharp variation of the attractive part of the interaction potential in the overlapping region, resulting in a more attractive potential [Lemaire et al., 1983]. The importance of the specific volume of $-CH_2-$ segments agrees with the conclusions of the previous paragraph regarding the free volume dissimilarity enthalpy and entropy terms. Pincus and Safran [1987] proposed that short-range attractions between micelles are induced by the perturbations of the dilute surfactant solution which coexists with the surfactant incorporated in the micelles; the attraction strength, A, is of the order of the attractive interactions between surfactant molecules in the particular solvent. However, the enthalpic or entropic components of A or their origin were not discussed. Denkov et al. [1991] expressed the potential energy of two interacting droplets as a superposition of the deformation energy due to expansion of the interfacial layer (soft repulsion) and the energy due to van der Waals attractions; the latter becomes more important when the droplets deform as they approach each other. Bedeaux et al. [1993] noted that the sticky hard sphere (SHS) model (used by Robertus et al. [1989] and others to interpret SAXS experiments in microemulsions) does not predict the observed temperature dependence, and proposed a modification to it, by introducing a repulsive barrier preceding the minimum of the SHS potential. The modified potential accounted for the increase in the fraction of "bound" (clustered) droplets with increasing temperature but the origin of the various contributions to the interaction potential was not discussed.

It can be concluded from the above discussion that the activation energy barrier (ΔH°_{cl}) restricting movement of charges during percolation can be overcome by a positive

ΔS originating from free volume dissimilarity phenomena. The latter arise from the fact that the free volume of the apolar solvent increases with temperature, while the surfactant molecules are "restricted" at the droplet interface. A slight increase in the specific volume of CH_2 segments in the surfactant layer was found to induce a sharp variation of the attractive part of the interaction potential in the overlapping region, resulting in a more attractive potential [Lemaire et al., 1983]. The treatment of Lemaire et al. [1983] could be a good starting point for a theory that takes temperature effects in droplet interactions into account.

12.3e Other approaches for obtaining energy parameters in droplet clustering

In addition to the droplet "association" model, other methods for deriving energy parameters for the percolation process have also been reported in the literature. Van Dijk and coworkers [1986] interpreted the temperature dependence of the volume fraction of the dispersed matter ϕ_d needed for percolation with a model for dielectric permittivity that involved the polarizability of a single AOT-water droplet and the activation energy E_a for the clustering of two droplets. The model was based on the presence of an aggregation equilibrium for the AOT water droplets in the microemulsion (shifting to the formation of larger aggregates - clusters as the temperature was raised) that causes anisotropy and increase in the polarizability of the medium. Fitting model parameters to experimental data for an AOT/isooctane microemulsion led to values for the activation energy per "bond" in the clusters, E_a, of 80 and 120 kJ/mol at Wo = 25 and 35, respectively [van Dijk et al., 1986]. These E_a values are to be compared with ΔH°_{cl} = 50 and 70 kJ/mol (at Wo = 25 and 35, respectively) obtained from the droplet association model used here.

Mathew et al. [1988] related the conductivity (σ) in microemulsions to the mobility and self-diffusion coefficient of the charge carriers (Na^+ ions), and considered the diffusion of the ions in terms of permeation across the surfactant monolayer in the microemulsion droplets. The activation jump of the charge carrier was then described in terms of an activation energy (ΔE) using an Arrhenius-type equation. The following relationship was obtained:

$$d \ln(\sigma) / d (\Delta E) = - 1 / (RT) \qquad (6)$$

Mukhopadhay et al. [1990] used Equation 6 (without, though, justifying it or referring to the derivation of Mathew et al. [1988]) to evaluate the activation energy, E_a, for conduction in the percolation region. The estimated E_a for the AOT/decane microemulsion ranged from 700 kJ/mol (in the absence of additives) down to 300 kJ/mol (in the presence of additives such as butanol). Activation energies for conduction in microemulsion systems preceding and following the percolation transition were 5 and 50 kJ/mol, respectively. According to Mukhopadhay et al. [1990], since these energies roughly fell in the range of activation energies for ions, the systems exhibited a "normal" (not percolating) mode of conduction.

The approaches of both van Dijk and coworkers [1986] and Mathew et al. [1988] for the estimation of activation energies for the percolation phenomenon are reasonable, however, the assumption of a specific (and different in each reference) mechanism for percolation may a shortcoming. The droplet association/clustering model used here is more general, the main assumption being the existence of two phases, percolating and non-percolating, in equilibrium with each other.

Johannsson and Almgren [1993] monitored the structure of droplet clusters with increasing temperature (20 - 50 °C range) for AOT microemulsions formulated with dodecane and octane as solvents using time-resolved fluorescence and phosphorescence, and observed a decrease in droplet fusion rate and an increase of activation energy, E_a, with increase in the droplet size. The activation energies ranged from 25 kJ/mol at Wo=8.5 to 47 kJ/mol at Wo=30; both the trend and the E_a value at Wo=30 are in agreement with the findings of the present study. Increase in activation energy with Wo has also been observed in a study by Fletcher et al. [1987], where apparent enthalpies and entropies of activation for the microemulsion droplet coalescence and solubilizate exchange process were determined by a stopped flow technique. No difference in clustering activation energy was observed between droplets in octane and dodecane by Johannsson and Almgren [1993], contrary to the results of the present study. Bommarius et al. [1990] studied droplet coalescence and solubuilizate exchange in a quaternary microemulsion system and found lower activation energy and higher activation entropy compared to ternary AOT microemulsions; this was attributed to AOT microemulsions being more ordered and stable. The values for ΔH°_{cl} estimated from the association model (in the order of 100 kJ/mol) are comparable to the activation energies observed in microemulsion

droplet coalescence and solubilizate exchange [Fletcher et al., 1987][Bommarius et al., 1990], providing evidence that the latter process is taking place during percolation.

12.4 Conclusions

Free energy, enthalpy, and entropy values related to the cluster formation of microemulsion droplets undergoing percolation were estimated from an association model. The microemulsion droplets above the percolation threshold, aggregated in clusters, were considered to be a phase different than that of non-percolating droplets, with distinct physical properties such as conductivity. This is comparable to the pseudophase concept used for modelling the micelle formation in solutions of amphiphilic molecules. For a given microemulsion system, the percolation temperatures increased as the droplet concentration or size decreased. The standard enthalpy of cluster formation, ΔH°_{cl}, was thus positive, indicating that the transfer of microemulsion droplets from solution to the percolating cluster is an enthalpically-unfavorable endothermic process. The free energy, ΔG°_{cl}, was negative, since the clusters are formed spontaneously. A positive entropy contribution was thus the driving force for clustering during conductivity percolation. The free energy of cluster formation became more negative as the droplet size increased, at constant droplet concentration; increase of the molecular weight of the apolar solvent resulted in less negative ΔG°_{cl} values. For constant droplet size, the free energy became less negative with increasing droplet concentration. The enthalpy and entropy of clustering were found to increase with droplet size and molecular weight of the apolar solvent.

Movement of ions and/or water through the surfactant droplet interface and the apolar continuum during percolation involves apparently an activation energy barrier; following the terminology of steric stabilization, the microemulsion droplets are subject to "enthalpic stabilization". The positive entropy observed in droplet clustering can be related to the attractive interactions known to exist between microemulsion droplets, and most likely originates from free volume dissimilarity phenomena. The latter arise from the fact that the free volume of the apolar solvent increases with temperature, while the surfactant molecules are "restricted" at the droplet interface. Simple conductivity experiments can thus provide insight, and even quantitative estimates, on interdroplet interactions in microemulsion systems. The values for ΔH°_{cl} estimated from the association model (in the

order of 100 kJ/mol) are comparable to the activation energies observed in microemulsion droplet coalescence and solubilizate exchange, providing evidence that the latter process occurs during percolation.

12.5 References and Notes Cited in Chapter 12

1. Alexandridis, P.; Holzwarth, J. F.; Hatton, T. A. *Langmuir* **1993**, *9*, 2045; Chapter 13 of this Thesis.
2. Alexandridis, P.; Holzwarth, J. F.; Hatton, T. A. *Macromolecules* **1994**, *27*, 2414; Chapter 2 of this Thesis.
3. Attwood, D., Florence, A. T. *Surfactant Systems: Their Chemistry, Pharmacy and Biology*; Chapman and Hall: London, 1983.
4. Bedeaux, D.; Koper, G. J. M.; Smeets, J. *Physica A* **1993**, *194*, 105.
5. Bhattacharya, S.; Stokes, J. P.; Kim, M. W.; Huang, J. S. *Phys. Rev. Lett.* **1985**, *54*, 2253.
6. Bommarius, A. S.; Holzwarth, J. F.; Wang, D. I. C.; Hatton, T. A. *J. Phys. Chem.* **1990**, *94*, 7232.
7. Borkovec, M.; Eicke, H.-F.; Hammerich, H.; Gupta, B. D. *J. Phys. Chem.* **1988**, *92*, 206.
8. Denkov, N. D.; Kralchevsky, P. A.; Ivanov, I. B.; Vassilieff, C. S. *J. Colloid Interface Sci.* **1991**, *143*, 157.
9. Eicke, H.-F.; Borkovec, M.; Das-Gupta, B. *J. Phys. Chem.* **1989**, *93*, 314.
10. Fletcher, P. D. I.; Howe, A. M.; Robinson, B. H. *J. Chem. Soc., Faraday Trans. 1* **1987**, *83*, 985.
11. Grest, G. S.; Webman, I.; Safran, S. A.; Bug, A. L. R. *Phys. Rev. A* **1986**, *33*, 2842.
12. Hall, D. G. *J. Phys. Chem.* **1990**, *94*, 429.
13. Halle, B. *Progr. Colloid Polym. Sci.* **1990**, *82*, 211.
14. Hamilton, R. T.; Billman, J. F.; Kaler, E. W. *Langmuir* **1990**, *6*, 1696.
15. Hilfiker, R.; Eicke, H.-F.; Sager, W.; Steeb, C.; Hofmeier, U.; Gehrke, R. *Ber. Bunsenges. Phys. Chem.* **1990**, *94*, 677.
16. Hou, M.-J.; Shah, D. O. *Langmuir* **1987**, *3*, 1086.
17. Hou, M. J.; Kim, M.; Shah, D. O. *J. Colloid Interface Sci.* **1988**, *123*, 398.

18. Hunter, R. J. *Foundations of Colloid Science*; Oxford University Press: New York, 1987; Vol. 1.
19. Jada, A.; Lang, J.; Zana, R. *J. Phys. Chem.* **1989**, *93*, 10.
20. Jada, A.; Lang, J.; Zana, R. *J. Phys. Chem.* **1990b**, *94*, 381.
21. Jada, A.; Lang, J.; Zana, R.; Makhioufi, R.; Hirsch, E.; Candau, S.-J. *J. Phys. Chem.* **1990a**, *94*, 387.
22. Johannsson, R.; Almgren, M.; Alsins, J. *J. Phys. Chem.* **1991**, *95*, 3819.
23. Johannsson, R.; Almgren, M. *Langmuir* **1993**, *9*, 2879.
24. Kallay, N.; Chittofrati, A. *J. Phys. Chem.* **1990**, *94*, 4755.
25. Kim, M. W.; Huang, J. S. *Phys. Rev. A* **1986**, *34*, 719.
26. Kotlarchyk, M.; Huang, J. S.; Chen, S.-H. *J. Phys. Chem.* **1985**, *89*, 4382.
27. Lagües, M. *J. Physique Lett.* **1979**, *40*, L331.
28. Lagües, M.; Sauteray, C. *J. Phys. Chem.* **1980**, *84*, 3503.
29. Lemaire, B.; Bothorel, P.; Roux, D. *J. Phys. Chem.* **1983**, *87*, 1023.
30. Lindman, B.; Stilbs, P. in *Microemulsions: Structure and Dynamics*, Friberg, S. E.; Bothorel, P. (Editors), CRC Press, 1988.
31. Maitra, A.; Mathew, C.; Varshney M. *J. Phys. Chem.* **1990**, *94*, 5290.
32. Mathew, C.; Patanjali, P. K.; Nabi, A.; Maitra, A. *Colloids Surfaces* **1988**, *30*, 253.
33. Moha-Ouchane, M.; Peyrelasse, J.; Boned, C. *Phys. Rev. A* **1987**, *35*, 3027.
34. Mukhopadhay, L.; Bhattachārya, P. K.; Moulik S. P. *Colloids Surfaces* **1990**, *50*, 295.
35. Napper, D. H. *Polymeric Stabilization of Colloidal Dispersions*, Academic Press: London, 1983.
36. Piirma, I. *Polymeric Surfactants (Surfactant Science Series, Vol. 42)*, Marcel Dekker: New York, 1992.
37. Pincus, P. A.; Safran, S. A. *J. Chem. Phys.* **1987**, *86*, 1644.
38. Price, C. *Pure Appl. Chem.* **1983**, *55*, 1563.
39. Ray, S.; Bisal, S. R.; Moulik, S. P. *J. Chem. Soc. Faraday Trans.* **1993**, *89*, 3277.
40. Robertus, C.; Philipse, W. H.; Joosten, J. G. H.; Levine, Y. K. *J. Chem. Phys.* **1989**, *90*, 4482.
41. van Dijk, M. A. *Phys. Rev. Lett.* **1985**, *55*, 1003.
42. van Dijk, M. A.; Casteleijn, G.; Joosten, J. G. H.; Levine, Y. K. *J. Chem. Phys.*

1986, *85*, 626.

43. van Dijk, M. A.; Broekman, E.; Joosten, J. G. H.; Bedeaux, D. *J. Physique* **1986**, *47*, 727.

44. Zana, R.; Lang, J. in *Microemulsions: Structure and Dynamics*, Friberg, S. E.; Bothorel, P. (Editors), CRC Press, 1988.

45. Zana, R.; Lang, J.; Candau, D. *J. Phys. Chem.* **1991**, *95*, 3364.

Note 1 A conducting microheterogeneous dispersion in a very weakly conducting or nonconducting medium may show a rapid rise in conductane above a threshold concentration; this phenomenon is called percolation (Landauer, R. *J. Appl. Phys.* **1952**, *23*, 779; Kirpatrick, S. *Rev. Mod. Phys.* **1973**, *45*, 574; Bernasconi, J. *Phys. Rev. B* **1973**, *7*, 2252; **1974**, *9*, 4575).

Note 2 In a recent study McFann and Johnston [McFann, G. J.; Johnston, K. P. *Langmuir* **1993**, *9*, 2942] reported data for water solubilization in AOT microemulsions that are in agreement with the data of Hou and Shah [1987] for the solvents octane, nonane, and decane, but are not in agreement for pentane, hexane and heptane. McFann and Johnston found maximum solubilization for pentane; the solubilization capacity dropped as the molecular weight of the alkane increased. Our data show a monotonic trend from hexane to dodecane and agree with the trend observed by McFann and Johnston.

Chapter 12: List of Figures

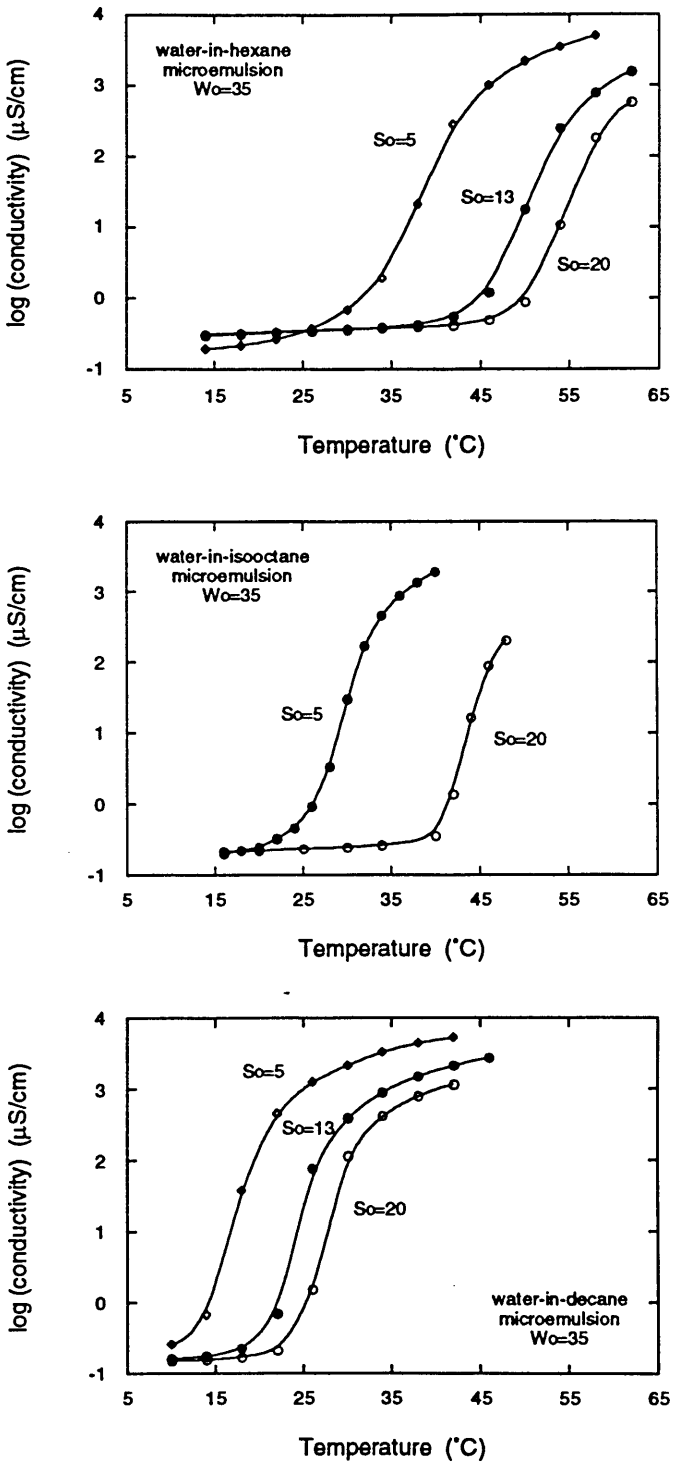

Figure 12.1 Conductivity as a function of temperature for water-in-oil microemulsions of various So (=[oil]/[AOT]) values at Wo=35: (a) water-in-hexane, (b) water-in-isooctane, and (c) water-in-decane microemulsions.

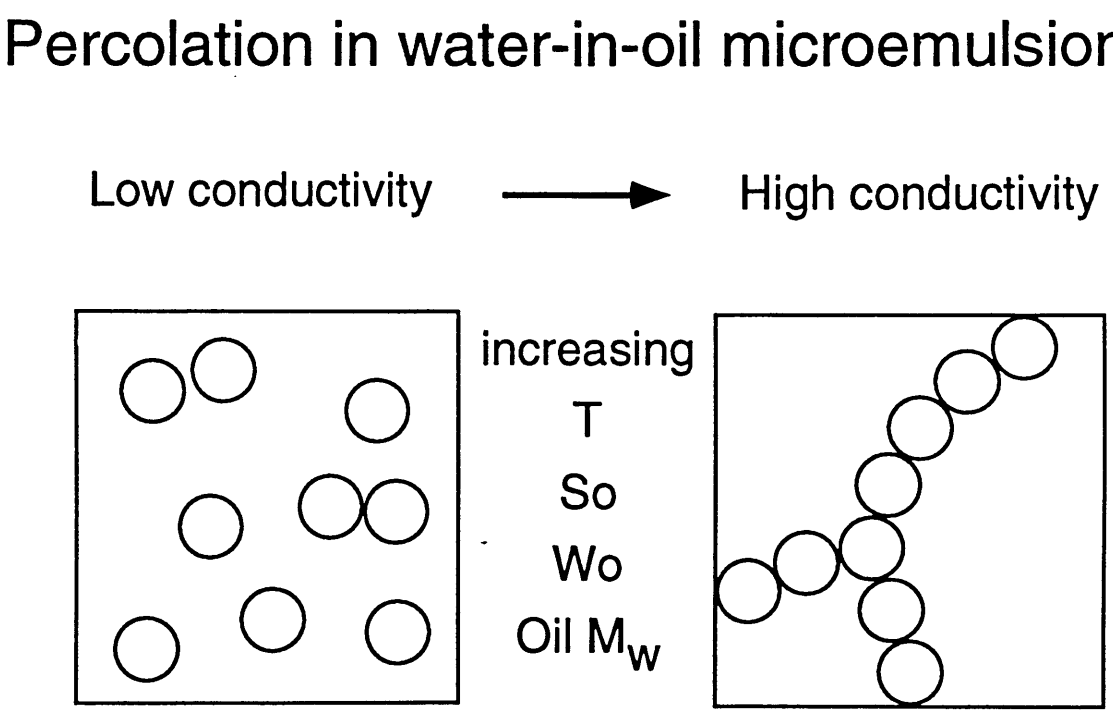

Figure 12.2 Schematic of percolation in water-in-oil microemulsion systems.

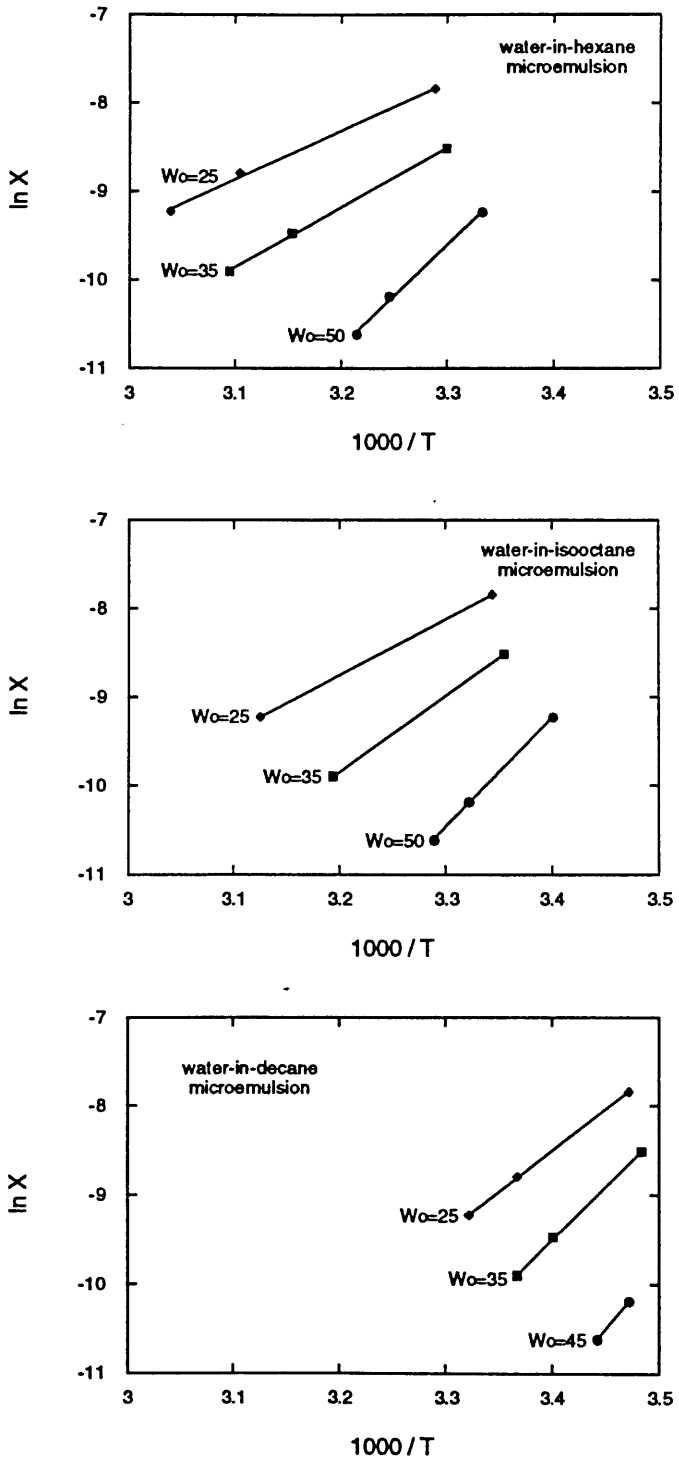

Figure 12.3 Natural logarithm of droplet concentration plotted as a function of inverse percolation temperature for various Wo values: (a) water-in-hexane, (b) water-in-isooctane, and (c) water-in-decane microemulsions.

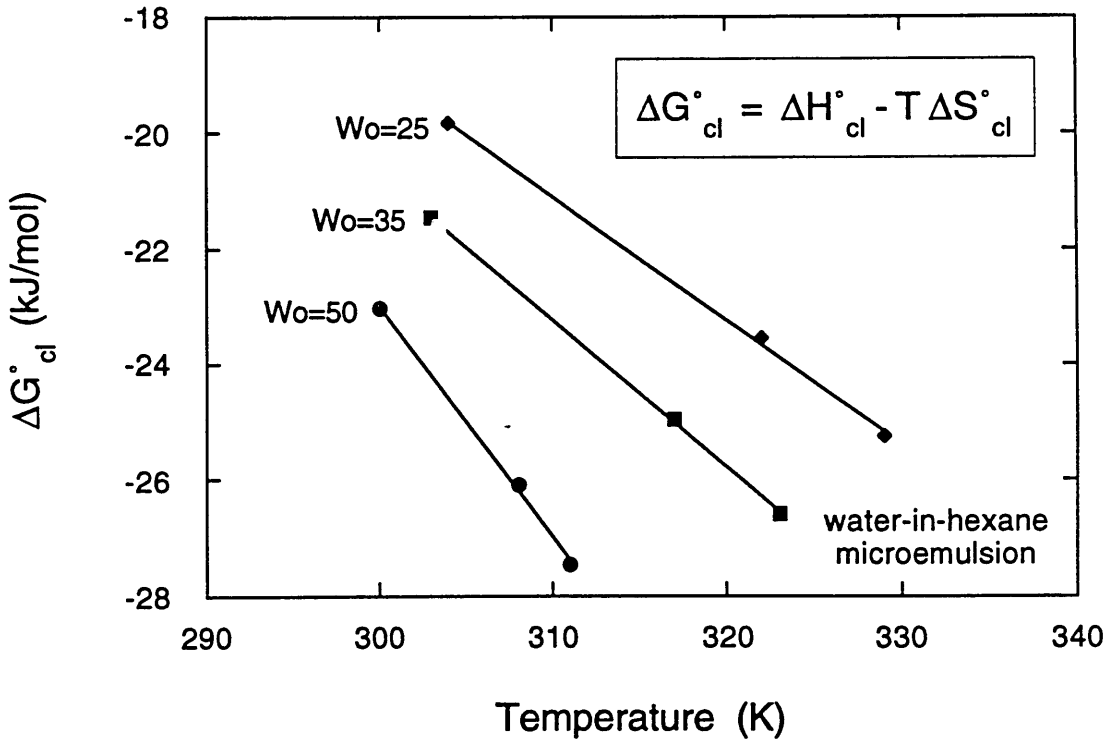

Figure 12.4 Free energy of droplet clustering plotted as a function of temperature for various Wo values (water-in-hexane microemulsion).

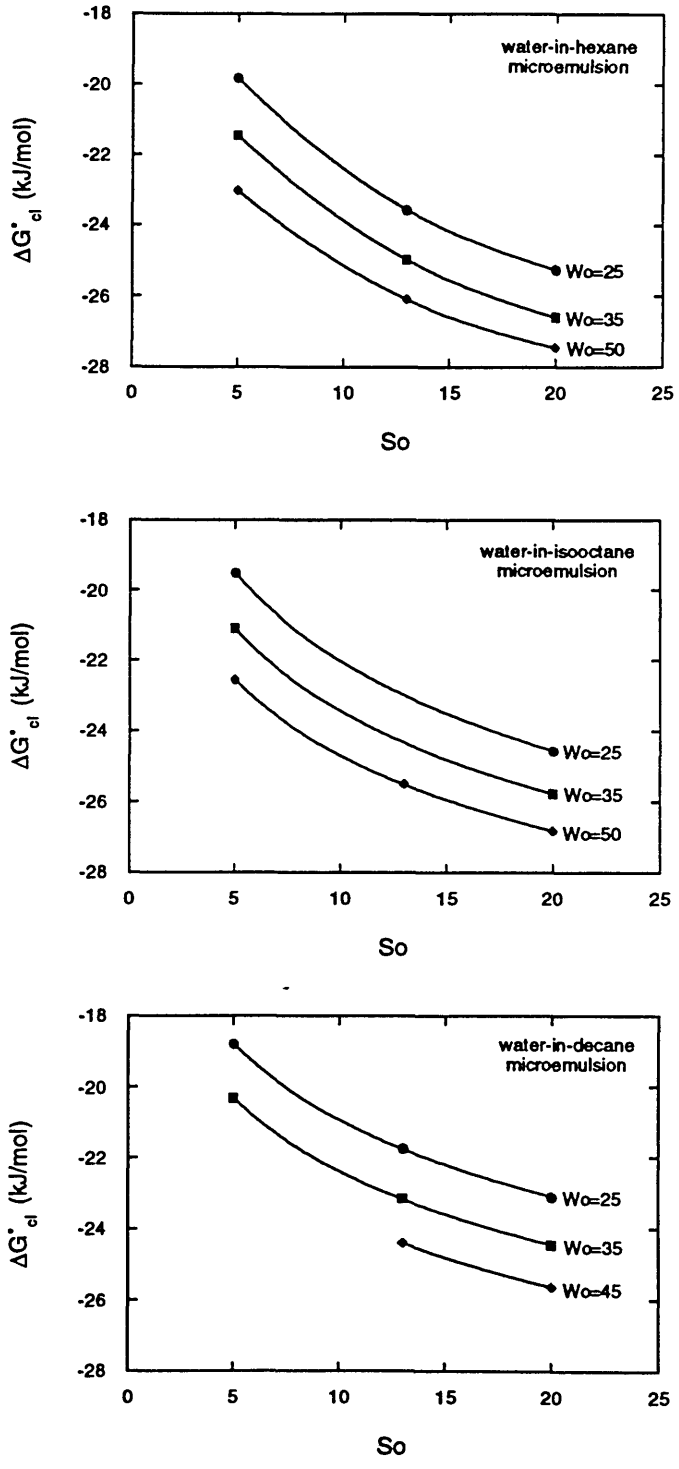

Figure 12.5 Free energy of droplet clustering plotted as a function of So for various droplet sizes (~Wo): (a) water-in-hexane, (b) water-in-isooctane, and (c) water-in-decane microemulsions.

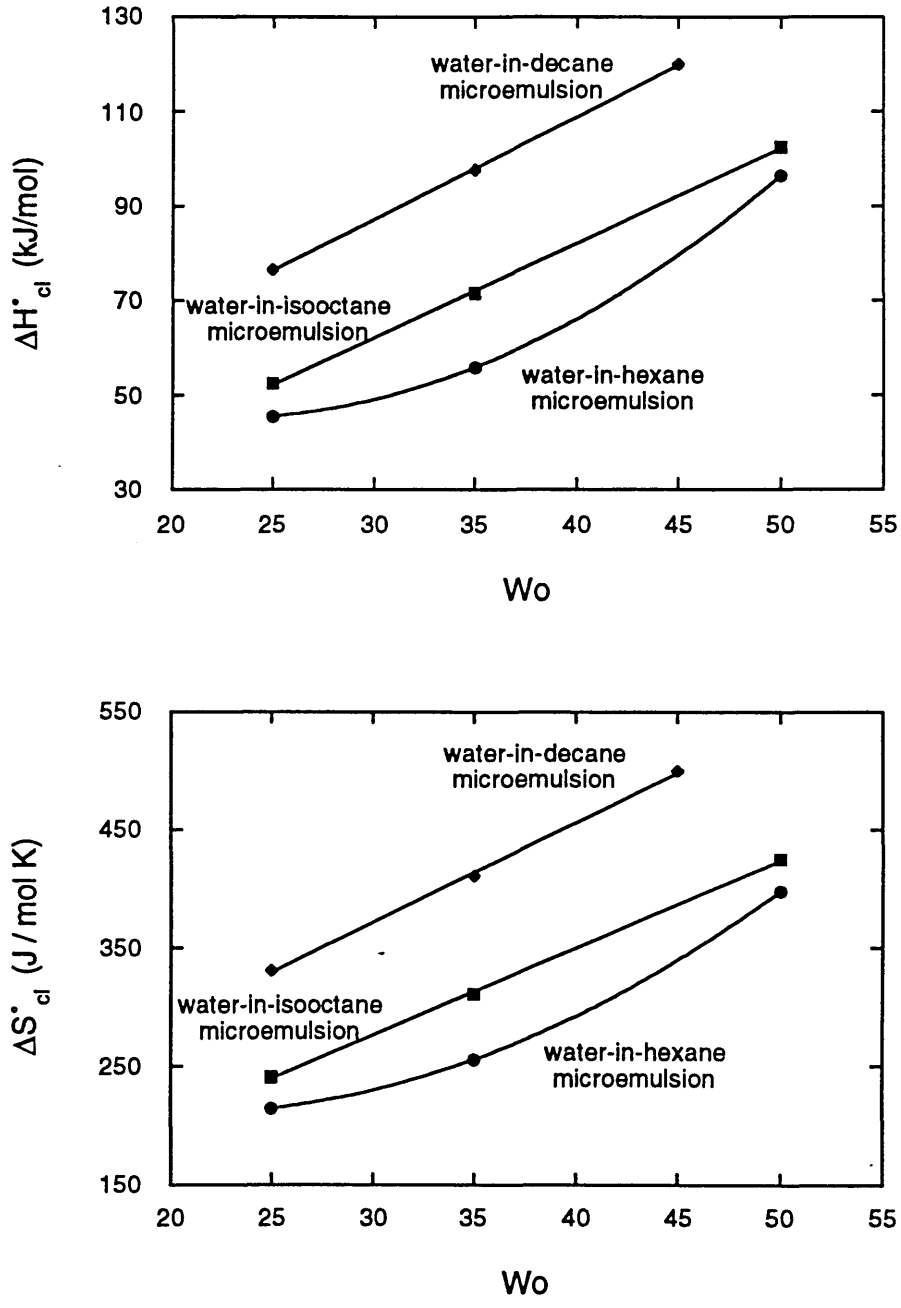

Figure 12.6 (a) Enthalpy of droplet clustering, and (b) entropy of droplet clustering, both plotted as a function of Wo for various solvents.

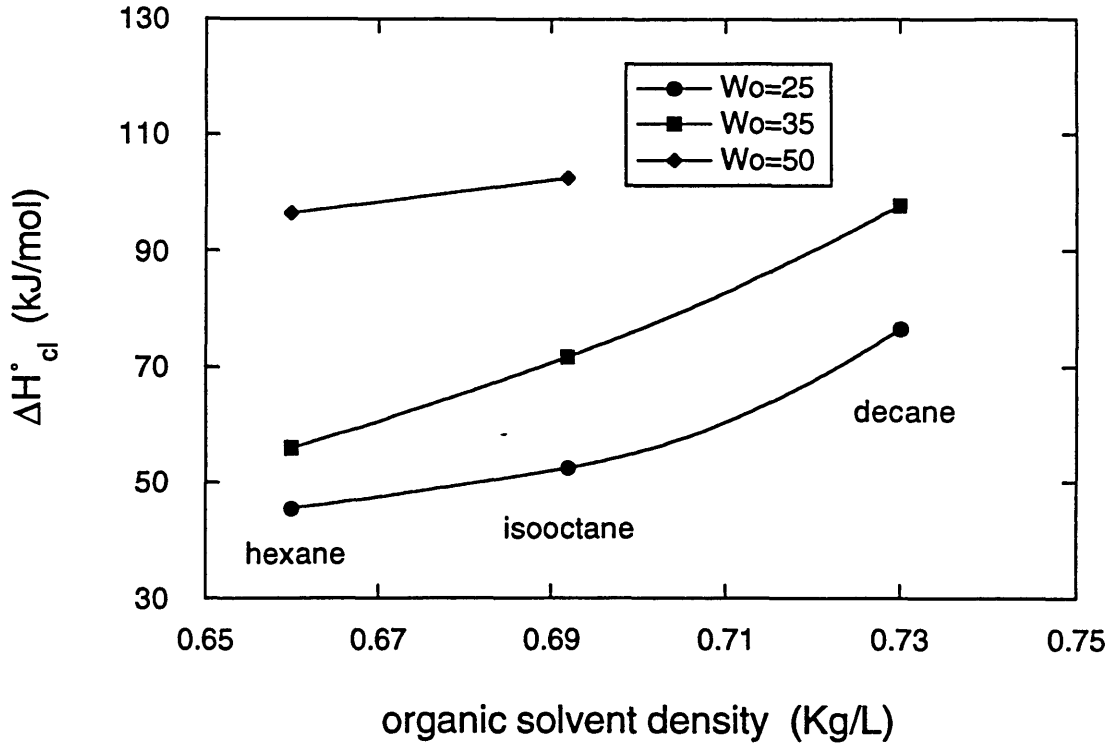

Figure 12.7 Enthalpy of droplet clustering plotted as a function of solvent density for various Wo values.

Chapter 13
Interfacial Dynamics of Water-in-Oil Microemulsion Droplets: Determination of the Bending Modulus

13.1 Introduction

Particularly important in understanding the behavior of microemulsions are the fluidity and flexibility of the oil-surfactant-water interface. Indeed, these properties reflect the ease with which the film rearranges upon a constraint, and thus its dynamics. The fluctuations of the interface have been investigated in so-called "birefringent microemulsions" using spin labels [Di Meglio et al., 1983]. The characteristic times for such fluctuations, which correspond to the local reorganization of the film, appeared to be longer than 0.1 μs. In a transient birefringence study of various water-in-oil microemulsions, a negative birefringence component observed was attributed to such film fluctuations and found to have a characteristic time of about 1 μs [Guering & Cazabat, 1984], in agreement with the conclusion of the spin label study. An important parameter in describing surfactant interfaces in microemulsions and related systems is the bending modulus or bending elasticity / rigidity constant [Helfrich, 1973], defined as twice the amount of energy required to bend a unit area of surface by a unit of curvature. Attempts have been made to measure the surfactant monolayer rigidity κ by analyzing shape fluctuations of microemulsion droplets in the three-component AOT-water-alkane system. Neutron spin-echo techniques revealed that the monolayer rigidity does indeed control the fluctuations of the interface [Huang et al., 1987]. The bending elasticity constant was estimated to be about 5 kT. Kotlarchyk et al. [1988] estimated the bending energy of an AOT microemulsion interface to be 0.4 kT (from SANS data) using a polydispersity relationship that is based on a microemulsion fluctuation model proposed by Safran [Safran, 1983]. The Safran model provided the basis for an analysis of Kerr effect [Note 1] measurements on AOT microemulsions by Borkovec and Eicke [1989], from which a bending monolayer rigidity of 0.5 kT was estimated.

While the studies outlined above constitute important contributions in characterizing the dynamics of the interface, more work needs to be done in this direction. Use of an "active" technique that perturbs the interface in a reversible way, as opposed to a "passive" method that observes the spontaneous fluctuations of the interface, could be advantageous when one considers real applications such as emulsion and foam stability, and phase transitions, in which the interface is subjected to stresses induced by differences in chemical potential or temperature. We used the Iodine Laser Temperature Jump (ILTJ) method [Holzwarth et al., 1977], a chemical relaxation technique, to identify and quantify the relaxation of a water-in-oil microemulsion system upon a rapid but small increase of its temperature. The sensitive detection system we used allowed time resolution of 10^{-7} s, with the capability to observe the whole 10^{-7} - 10^{0} s time range in a single measurement. We attributed the relaxation observed in the ILTJ experiments to the disturbance and reorganization of the oil-surfactant-water interface after the temperature rise in the water pools.

13.2 Experimental Procedure

Materials: AOT (Sulfosuccinic acid bis[2-ethylhexyl] ester, sodium salt) was purchased from Sigma (purity 99%) and used as received. Isooctane (Uvasol, spectroscopy grade) was from Merck (Darmstadt). The water used was triple-distilled. Sodium Chloride (NaCl) was obtained from Mallinckrodt (Analytical Reagent grade). The microemulsions were prepared using the injection method and were single-phase and stable during the ILTJ experiments. Their composition is given in terms of W_o, the ratio of water-to-surfactant molar concentrations, and S_o, the ratio of oil-to-surfactant molar concentrations. The experiments presented here were conducted for S_o values of 5 and 13, and W_o values (proportional to the reversed micelle radii) ranging from 5 to 50.

Iodine Laser Temperature Jump (ILTJ) technique: The ILTJ technique uses the photon emission of an Iodine laser in the near IR (1315 nm) to create a very fast temperature rise in aqueous solutions. This occurs by photon absorption of overtone vibrations of the OH bonds of water molecules. Very homogeneous temperature-jumps in layers up to 3 mm can be achieved, and no additional molecules or ions beside the solvent

water are necessary [Note 2]. The rise time of the temperature-jump can be as short as $2x10^{-10}$ s, constituting the short-time limit in dynamic investigations (the typical rise time for the present experiments was 1 μs). The longer time operational range is limited by the cooling of the sample back to its thermostatically controlled original temperature (5 - 10 sec). An INNOVA-100-K3 Krypton Ion CW-Laser (Coherent, Palo Alto, CA) was used to detect the effects of the temperature perturbation on the sample scattering intensity. The detection laser could operate in the 337.5 - 799.3 nm band with an output of up to 4.6 Watts; the 406.7 nm line was used in the present experiments. The emission of the Krypton laser was stabilized by an LIS 100 Laser Intensity Stabilizer (S.M.V., Munich), improving in this way the signal-to-noise ratio to approximately 10^3 in a single experiment. The iodine laser beam and the detection laser beam were perpendicular to each other, and both on the horizontal plane. The iodine laser was focused to a 10 mm (width) X 3.5 mm (height) X 5 mm (depth) volume in the cuvette that contained the sample (cuvette dimensions: 10 mm (width) X 30 mm (height) X 5 mm (depth)). The detection laser beam (with a 2 mm diameter) was adjusted on the horizontal plane to enter the sample cuvette near the entry side of the iodine laser beam, and on the vertical plane to pass within the 3.5 mm height of the iodine-laser-beam-heated sample volume. The signals from the photomultiplier tube (RCA 1P28) were fed into the amplifier circuit of a Tektronix 7904 oscilloscope equipped with a 7A22 amplifier of 1MHz bandwidth and a 7B92A timebase. The analog signal from the oscilloscope's "signal out" port was connected to two Tektronix 390AD transient digitizers, used in the dual timebase mode for digitizing and recording the relaxation signals in 8192 channels. The digitizer was linked through an IEEE bus to an HP Vectra computer. Further data processing involved sampling and averaging of the signals as well as calculating the relaxation times by appropriate fitting of the signal to the relaxation kinetics equations.

For the ILTJ experiment, approximately 1.5 ml of the microemulsion were placed in a 5 X 10 mm quartz cuvette, and sealed with a teflon cap. The cuvette was placed in the temperature controlled holder of the ILTJ detection chamber, and allowed to equilibrate at the desired temperature (controlled by a Haake F3C thermostat). ILTJ experiments were performed in the 10 - 50 °C range. The microemulsion systems under study were single-phase and stable during the ILTJ experiments. Care was taken to avoid loss of solvent due to evaporation, especially for experiments at higher temperatures. Recording of the sample scattering intensity at 180° started 5μs before the temperature-jump and covered the time

range up to 1 ms. Six relaxation signals were averaged at each experimental condition. Every precaution was taken to avoid artifacts due to the optics and electronics interfering with our experimental results. Distilled water and AOT-isooctane solutions were subjected to iodine laser temperature-jump to test whether thermal lens effects and/or laser induced light scattering interfered with our measurements; no such phenomena were observed. In fact, we used the temperature-jump relaxation for water to adjust the vertical (up-down) alignment of the detection beam before we did any measurements, ensuring that the detection laser beam passed through the homogeneously heated area of the sample.

13.3 Results and Discussion

In a typical ILTJ measurement, an iodine-laser pulse of 1315 nm wavelength, carrying energy of approximately 1 Joule in 1 μs, was focused on a 10 mm (width) X 3.5 mm (height) area in the microemulsion system. The energy thus added to the water pools was rapidly (within 1 μs) dissipated to the whole microemulsion in this region, resulting in a temperature increase of the scattering volume of approximately 0.5 - 1 °C. The response of the microemulsion to this energy input was reflected by a change in the sample scattering intensity with a single characteristic relaxation time of 2 - 10 μs. Long-time monitoring of the signal (up to 1 ms) indicated the absence of any other significant relaxation processes. Figure 13.1 shows typical ILTJ relaxation traces in AOT water-in-oil microemulsions. The ordinate represents the scattering intensity of the sample detected at 406.7 nm (arbitrary units), and the abscissa the time elapsed during and after the temperature-jump. The relaxation of the scattering intensity was characterized in terms of the relaxation amplitude (change of scattering intensity due to the temperature-jump), and the relaxation time, denoted here as τ. The latter was obtained by fitting the data to a single-exponential curve calculated according to

$$I_t = (I_o - I_\infty)e^{-t/\tau} + I_\infty \qquad (1)$$

where I_t, I_0, and I_∞ are the measured scattered light intensities at times t, zero, and infinity, respectively. The measured trace appears to be well-described by a single-exponential curve.

13.3a ILTJ relaxation amplitudes

The relaxation amplitudes of both S_o=5 and S_o=13 microemulsions passed through a maximum in the vicinity of W_o=15 with increasing micelle size (increasing W_o), took on a negative value at W_o=30 and then became positive again at W_o=50. In Figure 13.2 we present the ILTJ relaxation amplitudes as a function of W_o, for different temperatures and for the two different isooctane-to-AOT ratios.

The ILTJ relaxation amplitude variations with W_o can be ascribed to light scattering from the reversed micelles, which is caused by differences in the refractive indices of the domains in the system. More specifically, the scattered light intensity from particles small compared to the wavelength of light is proportional to the square of the refractive index increment (dn/dc) [Tanford, 1961]. The refractive index of microemulsions can be calculated satisfactorily assuming a dispersion of spherical, polarizable particles of refractive index n_{disp} in a host medium of refractive index n_{cont}. Furthermore, the dispersed phase can be considered to be a homogeneous mixture of surfactant (AOT) and water [Rebbouch & Lalanne, 1990]. Due to the ordering of the refractive index values of the microemulsion components ($n_{AOT}>n_{iC8}>n_{water}$), optical matching phenomena are observed when the refractive index of the droplets (AOT + water mixture) and the host medium (isooctane) are the same. When this happens, the refractive index increment of the microemulsion approaches zero, and the light intensity scattered from the system is minimal [Zulauf & Eicke, 1979; Eicke & Kubik, 1980]. As a result, the plot of scattering intensity vs. W_o for an AOT water-in-oil microemulsion passes through a minimum at a certain W_o value.

Zulauf and Eicke [1979] found the refractive index match for AOT-isooctane microemulsion to occur at W_o=30 for a temperature of 25 °C. As the refractive indices of the microemulsion components decrease with increasing temperature, the W_o at which optical matching occurs also depends on the temperature. Ricka et al. [1991] modeled dilute water-in-oil microemulsions as polydispersed suspensions of spherical droplets coated with surfactant, and derived analytical expressions for the refractive index increment, the average scattering intensity, the apparent hydrodynamic radius, and the second cumulant of dynamic light scattering. They fitted experimental data from the AOT-hexane microemulsion to the W_o dependance of the above quantities, and derived the

values for the model free parameters, surfactant layer thickness (1 nm), and radius polydispersity (12%).

We used the analytical relationships of Ricka et al. [1991], together with data for the refractive indices of isooctane, water, and AOT-in-solution as a function of temperature [Johnson & Smith, 1972], to predict the refractive index increment and average scattering intensity for the AOT-isooctane microemulsion. Figure 13.3a shows the logarithm of the reduced average scattering power of the microemulsion droplets [Note 3] as a function of W_o for different temperatures. Note the maximum in the scattering intensity at a W_o value of 10 - 15, the minimum at 25 - 30 due to the refractive index match, and the high scattering intensity as the droplet size increases beyond W_o=30. This behavior, which parallels the maxima and minima observed in the ILTJ relaxation amplitudes (shown in Figure 13.2), is similar to the findings of the Fletcher and Holzwarth [1991] ILTJ investigation of oil-in-water microemulsions. It should be recognized that the magnitude of the scattering intensity, which increases almost exponentially with W_o (for W_o>30), is the result of idealized scattering at infinite dilution, with no micellar interactions. In reality, droplet interactions tend to decrease the light scattered by suspensions [Penders & Vrij, 1993], which is probably the cause of the small difference between the relaxation amplitudes at W_o=15 and W_o=50; our microemulsions have high dispersed volume fractions (up to 50%) and the reversed micelles are expected to interact with each other [Huang, 1985].

Of particular relevance is the behavior of scattering intensity with respect to temperature at a certain W_o value, since our experimental method perturbs the temperature of the system. Increasing temperature results in an increase in the W_o value required for refractive index match. This effectively shifts the scattered intensity vs. W_o curves to the right (Figure 13.3a). The scattering intensity, calculated using the Ricka et al. model [Ricka et al., 1991], increases with temperature for W_o values of 5, 10, and 15, whereas for W_o=30 it decreases with increasing temperature. This is consistent with observations in our ILTJ experiments: the ILTJ relaxation amplitudes for W_o = 5, 10, and 15, are positive, indicating an increase in the sample scattering intensity with increasing temperature, while for W_o values of 30 or 35, the relaxation amplitudes are negative, evidence of decreasing scattering intensity of the microemulsion after the temperature increase. To emphasize this point, we plot the derivative (rate of change) of the average

microemulsion scattering power with respect to temperature (dI/dT) as a function of W_o for different temperatures in Figure 13.3b; it is these results that should be compared with the experimental results in Figure 13.2. Positive dI/dT values correspond to increase in the calculated scattering intensity with increasing temperature. Good agreement between the temperature behavior of the calculated scattering intensity and the ILTJ experimental relaxation amplitudes was not observed for the microemulsions with W_o=50, probably because we did not allow for an increase in the radius polydispersity value we used in the model (an increase in radius polydispersity is expected for microemulsions with a high water content). This discrepancy could also be due to percolation in the microemulsion [see Chapters 11 & 12 of this Thesis] that would alter its scattering behavior.

The above agreement between the scattering intensity of the microemulsion droplets, and the ILTJ relaxation amplitudes indicated that the relaxations observed in ILTJ experiments were a result of the microemulsion structure, and, more specifically, of the temperature-dependent properties of the spherical, surfactant-coated water droplets.

13.3b ILTJ relaxation times

The ILTJ relaxation times for the AOT microemulsions were found to be in the range of 2 to 10 μs, as shown in Figure 13.4. The heating of the water pools via the iodine-laser pulse was completed in-approximately 1 μs, thus precluding the detection of any faster processes. The ILTJ relaxation times were generally larger for the high AOT-volume-fraction (low S_o = [isooctane] / [AOT]) microemulsions. The error associated with the evaluation of the relaxation times was approximately ±1 μs.

To interpret the relaxation process observed, one must consider what happens to an individual water droplet due to the temperature-jump. The photons emitted from the iodine laser are immediately absorbed by the overtone vibrations of the OH bonds of water molecules, leading to an increase of the water pool temperature within the rise-time of the iodine-laser pulse (1 μs). Subsequently the volume of the water pools increases (thermal expansion) and the surfactant interface is "pushed out", resulting in deformation of its equilibrium (space- and time-averaged) shape, followed by relaxation of the spheroidal shape of the droplets towards their equilibrium spherical form [note 4]. A scaling relationship for the droplet shape relaxation characteristic time can be derived by drawing

parallels with polymer physics [de Gennes, 1979; de Gennes & Taupin, 1982]. The microemulsion droplet surface is associated with a certain elastic energy $F_{el} = {}^1/_2 kR^2$ (the spring constant k being equal to κ/R^2, where κ is the bending modulus of the surfactant layer surrounding the nanodroplet [Helfrich, 1973], and R the droplet characteristic length), and a certain friction constant ζ [de Gennes, 1979]. The friction force on the surface is $\zeta\, \partial R/\partial t$ and this balances the elastic force: $\zeta\, \partial \mathbf{R}/\partial t = - k\mathbf{R}$. This leads to a characteristic relaxation time for surface deformation $\tau = \zeta/k$. If we incorporate backflow effects (for which $\zeta \propto 6\pi\eta R$ [de Gennes, 1979]) and substitute $\kappa = kR^2$, the expression for the relaxation time becomes:

$$\tau \propto \frac{6\pi\eta R^3}{\kappa} \tag{2}$$

The characteristic time τ for the droplet shape relaxation is thus inversely proportional to the bending rigidity of the surfactant layer surrounding the nanodroplet, and proportional to the viscosity, η, and to the third power of the droplet characteristic length R.

The interplay of the bending and viscous forces on the microemulsion interface can be analyzed in more detail by using a mechanics model. The rate of the droplet shape relaxation depends on the conditions for the velocity fields of the fluids near the surface of the particle [Milner & Safran, 1987]. The motion of the surface of the droplet is overdamped and consequently the forces that drive the surface to its equilibrium form are balanced by the viscous forces arising from the induced fluid motion. In general $du_{\lambda m}/dt = - \tau_\lambda^{-1} u_{\lambda m}$, where $u_{\lambda m}$ is the deformation amplitude [Note 5], and τ_λ (the characteristic relaxation time) is given by [Linden et al., 1991]:

$$\tau_\lambda = \eta_o R_w^3 \beta \frac{E(2\lambda^3+3\lambda^2-5) + (2\lambda^3+3\lambda^2+4)}{\lambda(\lambda^2-1)(\lambda+2)\left[\kappa\beta\lambda(\lambda+1) - \frac{1}{8\pi\sigma^2}\right]} \tag{3}$$

κ is the bending modulus, $\beta = 1/k_B T$, k_B Boltzmann's constant, T the absolute temperature, $\sigma^2 = \langle R_w^2\rangle/\langle R_w\rangle^2 - 1$, $E = \eta_i/\eta_o$, η_i and η_o the viscosities of the fluid inside (water) and outside (isooctane) the droplet, respectively, and $(8\pi\sigma^2)^{-1} = 2\kappa\beta(3 - 2R_w/R_s)$ following Milner and Safran [1987] (R_w is the equilibrium radius of the water core of the micelle, R_s

is the natural radius of curvature). Applying such a model for the dynamics of a microemulsion droplet, van der Linden et al. [1991] described the relaxation of electrically induced birefringence (dynamic Kerr effect) in AOT-decaline microemulsion droplets. The relaxation times they observed were in the 1 - 5 μs range, which is essentially the same as in our ILTJ relaxation times. Using an average relaxation time of 3 μs from the ILTJ experiments and solving Equation 3 for κ, we obtained bending modulus values of 0.4 (±25%) kT, assuming a droplet polydispersity of 12% [Eicke & Kubik, 1980]. This κ value is in agreement with the result of van der Linden et al. [1991], and with static Kerr effect measurements [Borkovec & Eicke, 1989].

In addition to the dynamics of the surfactant film separating oil and water that appear to be responsible for the relaxation that we observed in AOT water-in-oil microemulsions with the ILTJ experiments, other dynamic processes take place on the timescale of our observation. Such mechanisms that may cause a change in the microemulsion scattering intensity could involve variation of micelle concentration (due to thermal and/or density gradients or Brownian motion of the microemulsion droplets) and/or micelle size (droplet coalescence) in the scattering volume. To resolve the effects of such phenomena in the context of our ILTJ measurements, we examine them in the Appendix.

13.3c Effect of temperature on ILTJ relaxation times and microemulsion bending moduli

In principle it should be possible to predict the temperature dependence of the bending modulus (and the corresponding relaxation time) if the variation of the surfactant monolayer "natural" curvature could be predicted from the microemulsion phase boundaries [Fletcher & Horsup, 1992]. Single-phase microemulsions are stable over a restricted temperature range which depends on their composition and temperature. For the single-phase AOT microemulsion systems, decreasing the temperature below the lower temperature boundary produces a reduced water-content microemulsion phase (i.e. lower W_o value) in equilibrium with a (almost pure) water phase (Winsor II system). Increasing the temperature beyond the upper temperature stability limit results in separation of an oil-in-water microemulsion and a conjugate oil phase, Winsor I system (observed in mixtures containing comparable volumes of oil and water), or a liquid crystalline phase (containing AOT and water) with a conjugate oil phase (for water-in-oil microemulsion phases

containing smaller amounts of water) [Fletcher et al., 1987]. Increase of temperature for an AOT-water-oil system of given composition is associated with changing the surfactant monolayer curvature from that of a water-in-oil aggregate structure (negative curvature) to that of an oil-in-water aggregate structure (positive curvature).

A distinction must be made between "natural" and actual curvature of the surfactant film. Natural curvature is the observed surfactant film curvature when the droplet phase is in equilibrium with a conjugate phase of the dispersed component (e.g. in Winsor I and II systems) [Fletcher et al., 1987]. The actual surfactant film curvatures observed in single-phase microemulsions are dictated by the microemulsion composition. For the AOT microemulsion studied in this paper the actual curvature (the inverse of the reversed micelle radius) is determined by W_o (the radius has been found to vary linearly with W_o for AOT microemulsions) and shows only a small variation with temperature [Kotlarchyk et al., 1982; 1984]. At the lower temperature boundary the actual curvature is equal to the natural curvature. As the natural curvature becomes less negative with increase in temperature, the discrepancy between the natural and actual curvature increases as the upper phase boundary is approached.

Fletcher et al. [1987] measured exchange rates of aqueous solubilizates between reversed micelles in a AOT water-in-oil microemulsion. They found the exchange rate to be slowest at the low-temperature boundary, and increasing as the upper-temperature boundary was approached. Similar trends were observed for rates of solubilizate exchange at the dodecyl-trimethylammonium chloride / hexanol / n-heptane / water microemulsion system by our group [Bommarius et al., 1990]. The mechanism of solubilizate exchange is thought to involve the formation of short-lived dimers, followed by their separation [Bommarius et al., 1990; Fletcher et al., 1987]. For the dimer to form, the surfactant monolayer has to deform (or break), a process governed by the bending modulus value of the interface [Fletcher & Horsup, 1992]. The slow exchange rates indicate more stable droplets (higher bending moduli of the surfactant monolayer) at temperatures close to the low-temperature boundary, where the actual AOT monolayer curvature is equal to its natural curvature.

Based on the discussion of the previous paragraph, one would expect to observe a decrease of the surfactant monolayer bending modulus (corresponding to increase in ILTJ

relaxation times) with increasing temperature, for a given droplet size. The ILTJ relaxation times for the S_o = 5, W_o = 5 and 35 microemulsions increased with increasing temperature (Figure 13.4b), following the expected trend. For the microemulsions formulated with water+NaCl (see Figure 13.5 and the following section for related discussion) the relaxation times generally increased with increasing temperature, again in agreement with the decrease of the surfactant monolayer bending modulus with increasing temperature (for W_o = 5 the relaxation times showed no variation within the experimental error). For the S_o = 13, W_o = 5, 15, and 50 microemulsions the values of relaxation time at different temperatures fell within the experimental error (±1 μs).

It becomes apparent that the ILTJ experimental data tend to support the expected [Fletcher & Horsup, 1992; Fletcher et al., 1987] temperature dependence of the bending modulus (decrease of κ with increasing temperature) given the variation of the "natural" surfactant monolayer curvature, known from the phase boundaries. However, the uncertainty in some of our relaxation time data make it difficult to make solid conclusions at to the effect of temperature on the bending modulus of the AOT monolayer.

13.3d Effect of salt on ILTJ relaxation times and microemulsion bending moduli

The ILTJ results discussed above were obtained in the absence of added salt in the aqueous phase of the microemulsions. It is known that water-in-oil microemulsions of AOT in nonpolar solvents are profoundly affected by the addition of small amounts of electrolyte [Kunieda & Shinoda, 1979]. The effect of salt was investigated by carrying out ILTJ experiments in S_o=13 microemulsions formulated with [NaCl] = 0.01, 0.05, and 0.1 M in the aqueous phase. Higher salt concentrations reduced greatly the microemulsion L2 monophasic region in which we could operate [Kunieda & Shinoda, 1979]. The ILTJ relaxation times for S_o=13, [NaCl] = 0.05 M microemulsions are presented in Figure 5 as a function of W_o for different temperatures. Note that the microemulsion relaxation times in the presence of NaCl were larger than those in microemulsions formulated without added salt in the aqueous phase, indicating a decrease in the interfacial bending modulus κ with increasing salinity.

The dependence of κ on the addition of salt has been predicted theoretically by

Ninham and coworkers [Mitchell & Ninham, 1989; Fogden et al., 1990], Lekkerkerker [1989], Kozlov et al. [1992], Ennis [1992], and Barneveld [1991]. Ninham et al. [1989; 1990] found the electrostatic free energy of bending to vary with the square of the surface charge density. According to their theory, an increase in salt concentration results in a lower surface charge density and a decrease in the bending modulus. Lekkerkerker [1989] and Kozlov et al. [1992] derived the same dependance of the electrostatic bending free energy on the square of the surface charge density. In Figure 13.6 we plot the theoretical electrostatic contribution to the bending modulus as a function of electrolyte concentration, based on data from Table 1 by Lekkerkerker [1989]. Note that the theoretical bending modulus decreased approximately by a factor of two (from 0.67 kT to 0.29 kT) when the electrolyte concentration increased from 0.01 M to 0.05 M. This is in agreement with the decrease in bending modulus that we observed experimentally when we added 0.05 M NaCl solution as the aqueous phase of the AOT microemulsions; we obtained $\kappa = 0.2$ (±25%) kT based on a τ–value of 6 μs, as shown on Figure 13.6. We did not take the AOT sodium counterions into account in reporting the salt concentration for our experimental bending modulus values in Figure 13.6, because we had no information on their effective concentration in the microemulsion water pools.

Although there is good agreement between the theoretical predictions of Ninham [1989; 1990] and Lekkerkerker [1989] and our experimental data, it should be emphasized that there is no clear consensus on the effect of salinity on the bending modulus of surfactant interfaces. Ennis [1992], using a mean-field model for monolayers of short chain surfactants, predicted that the bending modulus increases very slightly as the salt concentration increases; he nevertheless noted that the results were limited by numerical error. Barneveld [1991] calculated the bending elasticity moduli of equilibrium bilayers and monolayers of surfactants using a self-consistent field lattice model extended to incorporate ionic interactions. His model predicted that screening of the electric double layer by salt had two opposing effects on the rigidity of monolayers and bilayers of ionic surfactants: the contribution of the double layer diminished but the surfactant layer became thicker. The latter effect was dominant and resulted in increase of the predicted bending modulus with salt concentration. From light scattering experiments, Bedwell and Gulari [1984] and Hou et al. [1988] found that NaCl in the water pools diminished the magnitude of attraction between reversed micelles. These results were ascribed to a decrease of the interfacial area per polar head of the surfactant molecules with increasing salinity, that made

the interface more rigid (implying a larger bending modulus) and less penetrable, and decreased the strength of the attractive interaction between droplets. It becomes apparent from the discusion in the preceding paragraph that screening of electrostatic interactions in the headgroup area will cause the interface to be less rigid (decrease the bending modulus) thus making the interpretation of the light scattering results mentioned above ambiguous.

Binks et al. [1991] varied the organic solvent in systems containing AOT + aqueous NaCl solution + normal alkane, and concluded that the values of bending moduli depended on the penetration of the organic solvent into the surfactant tail region, and that the bending modulus was independent of salt concentration. One should keep in mind though, that Binks et al. have studied flat, macroscopic interfaces in a three-phase system. We investigated microscopic, highly curved interfaces in a single-phase water-in-oil microemulsion system. The contributions of surfactant head (electrostatic) and tail effects to the magnitude of the bending modulus should be different for interfaces of flat and curved geometries. A stronger influence of the electrostatic interactions between the surfactant headgroups (as observed in our experiments by altering the ionic strength in the vicinity of the headgroups) would be no surprise in a curved interface like in a reverse micelle, where the headgroups are constrained and the area per headgroup is smaller than in a flat interface. The differences between our experimental system and the one Binks et al. studied, our system focusing more on the surfactant headgroup, may account for the different conclusions reached.

13.4 Conclusions

We have shown that the effects of water pool size, temperature and salt content on the dynamic response of water-in-oil microemulsions to small perturbations from equilibrium can be investigated using the Iodine Laser Temperature Jump (ILTJ) technique. The relaxations observed in the experiments were concluded to be the response of the system to perturbations in the microemulsion structure caused by changes in the shape / size of the spherical, surfactant-coated water droplets induced by rapid changes in the temperature of the microemulsion. The observed characteristic relaxation times of 2 to 10 μs were in agreement with published results obtained using other techniques. Interfacial bending rigidities of approximately 0.4 kT were estimated from these characteristic

relaxation times using published models [Milner & Safran, 1987; Linden et al., 1991] for the relaxation of perturbed interfaces to their equilibrium spherical shapes; these extracted bending moduli were in agreement with literature values using both static (SANS) and dynamic (Kerr effect) techniques, pointing to the validity of the ILTJ technique as an effective probe for microemulsion interfacial properties. The dependence of the ILTJ relaxation times on temperature tended to support the expected [Fletcher & Horsup, 1992; Fletcher et al., 1987] bending modulus decrease with increasing temperature, given the variation of the "natural" surfactant monolayer curvature with temperature. Addition of NaCl to the aqueous pools resulted in an increase in the relaxation times, or a decrease in the bending modulus, in agreement with theoretical predictions [Mitchell & Ninham, 1989; Lekkerkerker, 1989; Kozlov et al., 1992]. Thus, it can be concluded that the ILTJ technique is a useful addition to the range of methods that can be used for the probing of dynamic and static interfacial properties of curved, surfactant-laden interfaces.

13.5 Appendix

Change of micelle concentration could result from thermal and/or density gradients or Brownian motion of the microemulsion droplets, and potentially affect the scattering intensity changes that we observed in the present ILTJ experiments. Homogeneous heating of the water in the scattering volume can be achieved in an ILTJ experiment [Holzwarth et al., 1977], but the heat has to be transferred first to the other components (AOT, isooctane) in the scattering volume, and then to the rest of the sample. We can estimate the timescales characteristic to these processes from the thermal diffusivities ($\alpha = k/\rho c_p$) of the microemulsion components ($\alpha = 1.5 \times 10^{-4}$ cm^2/s for water and 0.8×10^{-4} cm^2/s for octane) [Perry & Green, 1984]. The characteristic lengths within the scattering volume are: 1 nm for AOT (surfactant monolayer thickness), 10 nm for water (reversed micelle radius), and 10 nm for isoctane (distance between two micelles). The corresponding timescales, characteristic for heat transfer, are 1×10^{-10} s, 0.7×10^{-8} s, and 1.1×10^{-8} s, respectively. These are two orders of magnitude faster than our ILTJ relaxation times, and it can thus be concluded that heat transfer at the individual micelle length scale should not interfere with the relaxation processes of interest. The timescales characteristic for diffusive heat transfer from the scattering volume to other parts of the cuvette (typical size of 1mm) are 70 s for water and 120 s for octane, so that such heat transfer is slow relative to the timescale of our

ILTJ measurements. We do not expect any convective heat transfer (which should be faster than heat diffusion) to occur during our experiment, since the Rayleigh ratio [Chandrasekhar, 1961] is below the thermal instability value.

Brownian motion of the microemulsion droplets could also be a cause of fluctuations in the micelle concentration, and change in the scatering intensity. For spherical particles of radius r the characteristic time for Brownian diffusion is $\tau = r^2/D_{Br}$, where D_{Br} is the diffusion coefficient of the micelles [Probstein, 1989]. We obtained the apparent diffusion coefficients of AOT reverse micelles for different W_o and temperature values, based on data for the micelle hydrodynamic radius [Ricka et al., 1991]. From these we calculated the characteristic times for Brownian diffusion. Varying W_o from 5 to 50 resulted in a four-orders-of-magnitude increase in the Brownian diffusion characteristic times. We have observed no such strong dependance on W_o in our ILTJ relaxation times, indicating no significant interference from Brownian motion. In addition, no important change over the time of observation was seen in the microemulsion scattering intensity in the absence of temperature-jumps. It should be noted at this point that, apart from coefficients, the scaling expression for the deformation relaxation time τ (Equation 2) coincides with the relaxation time associated with rotation of a solid Brownian sphere of radius R [Tanford, 1961; de Gennes, 1979]. Thus rotation and deformation have the same characteristic times in solution. Nevertheless it is unlikely that droplet rotation interfered with the relaxation times that we measured, since the temperature perturbation caused by the ILTJ should not affect the rotational diffusion of the reversed micelles.

Changes in the micelle size and/or shape in the scattering volume could originate from droplet coalescence / decoalescence. Reversed micellar coalescence is a second-order process, dependent on the concentration or number density N of reversed micelles, and has a characteristic time constant of $1/(k_{ex}N)$, k_{ex} being the collision rate constant [Bommarius et al., 1990]. With typical values of N of about 10^{-3} M, and k_{ex} of approximately 10^7 $(Ms)^{-1}$ [Zana & Lang, 1988; Fletcher et al., 1987; Atik & Thomas, 1981; 1981; Pileni et al. 1984] the order of magnitude for this time constant is 10^{-4} s, or 100 μs. This time is 10 to 50 times longer than the ILTJ relaxation times. Furthermore, comparing relaxation times between S_o=5 and S_o=13 microemulsions, the latter having half the micelle concentration of the former, we do not see the N dependance on relaxation times we would expect from a second-order coalescence process.

13.6 References and Notes cited in Chapter 13

1. Atik, S. S.; Thomas, J. K. *J. Am. Chem. Soc.* **1981**, *103*, 3543;
2. Atik, S. S.; Thomas, J. K. *Chem. Phys. Lett.* **1981**, *79*, 351;
3. Barneveld, P. A. *PhD Thesis*, Wagenigen Agricultural University, p. 91, 1991.
4. Bedwell, B.; Gulari, E. *J. Colloid Interface Sci.* **1984**, *102*, 88.
5. Binks, B. P.; Kellay, H.; Meunier, J. *Europhys. Lett.* **1991**, *16*, 53.
6. Bommarius, A. S.; Holzwarth, J. F.; Wang, D. I. C.; Hatton, T. A. *J. Phys. Chem.* **1990**, *94*, 7232.
7. Borkovec M.; Eicke, H.-F. *Chem. Phys. Lett.* **1989**, *157*, 457.
8. Chandrasekhar, S. in *Hydrodynamic and Hydromagnetic Instability*, p. 508, Oxford University Press, 1961.
9. De Gennes, P.-G.; Taupin, C. *J. Phys. Chem.* **1982**, *86*, 2294.
10. De Gennes, P.-G. *Scaling Concepts in Polymer Physics*, p. 180, Cornell University Press, 1979.
11. Di Meglio, J.-M.; Dvolaitzky, M.; Ober, R.; Taupin, C. *J. Phys. Lett.* **1983**, *44*, L229.
12. Eicke, H.-F.; Kubik, R. *Ber. Bunsenges. Phys. Chem.* **1980**, *94*, 36.
13. Ennis, J. *J. Chem. Phys.* **1992**, *97*, 663.
14. Fletcher, P. D. I.; Holzwarth, J. F. *J. Phys. Chem.* **1991**, *95*, 2550.
15. Fletcher, P. D. I.; Howe, A. M.; Robinson, B. H. *J. Chem. Soc., Faraday Trans. 1* **1987**, *83*, 985.
16. Fletcher, P. D. I.; Horsup, D. I. *J. Chem. Soc., Faraday Trans.* **1992**, *88*, 855.
17. Guering, P.; Cazabat, A.-M. *J. Phys. Lett.* **1984**, *44*, L601.
18. Helfrich, W. *Z. Natur.* **1973**, *C28*, 693.
19. Holzwarth, J. F.; Schmidt, A.; Wolff, H.; Volk, R. *J. Phys. Chem.* **1977**, *81*, 2300.
20. Hou, M. J.; Kim, M.; Shah, D.O. *J. Colloid Interface Sci.* **1988**, *123*, 398.
21. Huang, J. S. *J. Chem. Phys.* **1985**, *82*, 480.
22. Huang, J. S.; Milner, S. T.; Farago, B.; Richter, D. *Phys. Rev. Lett.* **1987**, *59*, 2600.
23. Johnson, B. L.; Smith, J. in *Light Scattering from Polymer Solutions*, Huglin, M.

B. (Editor), p. 27, Academic Press, 1972.
24. Kotlarchyk, M.; Chen, S. H.; Huang, J. S. *J. Phys. Chem.* **1982**, *86*, 3273;
25. Kotlarchyk, M.; Chen, S. H.; Huang, J. S.; Kim, M. W. *Phys. Rev. A* **1984**, *29*, 2054.
26. Kotlarchyk, M.; Stephens, R. B.; Huang, J. S. *J. Phys. Chem.* **1988**, *92*, 1533
27. Kozlov, M. M.; Winterhalter, M.; Lerche, D. *J .Phys. II France* **1992**, *2*, 175.
28. Kunieda, H.; Shinoda, K. *J. Colloid Interface Sci.* **1979**, *70*, 577.
29. Lekkerkerker, H. N. W. *Physica A* **1989**, *159*, 319.
30. Linden, E. v. d.; Bedeaux, D.; Hilfiker, R.; Eicke, H.-F. *Ber. Bunsenges. Phys. Chem.* **1991**, *95*, 876.
31. Milner, S. T.; Safran, S. A. *Phys. Rev. A* **1987**, *36*, 4371.
32. Mitchell, D. J.; Ninham, B. W. *Langmuir* **1990**, *6*, 159.
33. Mitchell, D. J.; Ninham, B. W. *Langmuir* **1989**, *5*, 1121; Fogden, A.;
34. Penders, M. H. G. M.; Vrij, A. *J. Chem. Phys.* **1993**, *93*, 3704.
35. Perry, R. H.; Green, D. (Editors) *Perry's Chemical Engineer's Handbook*, 6th Edition, McGraw Hill, 1984.
36. Probstein, R. F. *Physicochemical Hydrodynamics*, p. 237, Butterworths, 1989.
37. Rebbouch, N.; Lalanne, J. R. *J. Chem. Phys.* **1990**, *90*, 1175.
38. Ricka, J.; Borkovec, M.; Hofmeier, U. *J. Chem. Phys.* **1991**, *94*, 8503.
39. Safran, S. A. *J. Phys. Chem.* **1983**, *78*, 2073.
40. Tanford,C. *Physical Chemistry of Macromolecules*, p. 275, J. Wiley & Sons, 1961.
41. Zulauf, M.; Eicke, H.-F. *J. Phys. Chem.* **1979**, *83*, 480.

Note 1 The Kerr effect is the optical anisotropy induced by an electric field. Permanent dipole moments and the electrical polarizabilities of the dispersed particles govern the interaction of the particles with the applied electrical field. This leads to an alignment and/or deformation of the particles, whose optical polarizabilities determine a detectable optical anisotropy. The response of the anisotropy to the functional behavior of the field provides information about rotational diffusion and the deformation kinetics of the particles.

Note 2 Laser temperature-jump can also be achieved via laser excitation of dye molecules that subsequently transmit the energy to the solvent. A serious problem in such an experiment can be the interference of the energy transferring substance with the system under investigation via the excited electronic states and their long lifetime.

In commercially available instruments a high-voltage capacitor is discharged through an electrolyte solution, causing temperature-jump by resistance heating of the system; the decoupling of the electric field and temperature effects, however, may be difficult. High salt concentrations are needed to achieve fast heating times; stable reversed micelles could not be formed under such conditions.

Note 3 The ordinate of Figure 13.3a is the "average reduced scattering power of a particle, i.e. the average square polarizability per average droplet volume" [Ricka et al., 1991]. This is proportional to the Rayleigh ratio (R) of the suspension (microemulsion) [Ricka et al., 1991] which, in term, is proportional to $1+\cos^2\theta$ for small particles (Jansen, J. W.; De Kruif, C. G.; Vrij, A. *J. Colloid Interface Sci.* **1986**, *114*, 492). The Ricka et al. derivation was done for 90^0; multiplication of the numbers in Figure 13.3a with the constant factor $2 = [1+\cos^2(180°)]/[1+\cos^2(90°)]$ will make them correspond to our measurements (done at 180°).

Note 4 Our data and related analysis strongly suggest deformation of the interface as causing the relaxation observed in the ILTJ experiments with AOT microemulsions; however, we cannot pinpoint the exact mechanism of this relaxation at the molecular level. More data from extensive experiments (e.g. by varying the organic solvent) are needed to distinguish between the possible mechanisms (such as interfacial shear or dilation) causing the deformation.

Note 5 To derive Equation 3 the shape of a microemulsion droplet was described by expressing the distance $r(\theta,\phi)$ of the droplet surface to some conveniently chosen interior point as a function of the direction given by θ and ϕ in polar coordinates. It is assumed that $r(\theta,\phi,t)$ is a single valued function. Expanding this shape function in spherical harmonics ($Y_{\lambda m}$) one has: $r(\theta,\phi,t) = R_w [1 + \sum_{\lambda m} u_{\lambda m}(t) Y_{\lambda m}(\theta,\phi)]$ where the summation is over $\lambda=0,1,2,...$ and $-\lambda \le m \le \lambda$, R_w is the equilibrium radius of the water core of the micelle. The spheroidal deformation of the droplet is described by the ellipsoidal ($\lambda=2$) shape fluctuation. Fluctuations with $\lambda=0$ (polydispersity) or $\lambda>2$ have small amplitudes [Safran, 1983], while $\lambda=1$ describes the displacement of the reverse micelle.

Chapter 13: List of Figures

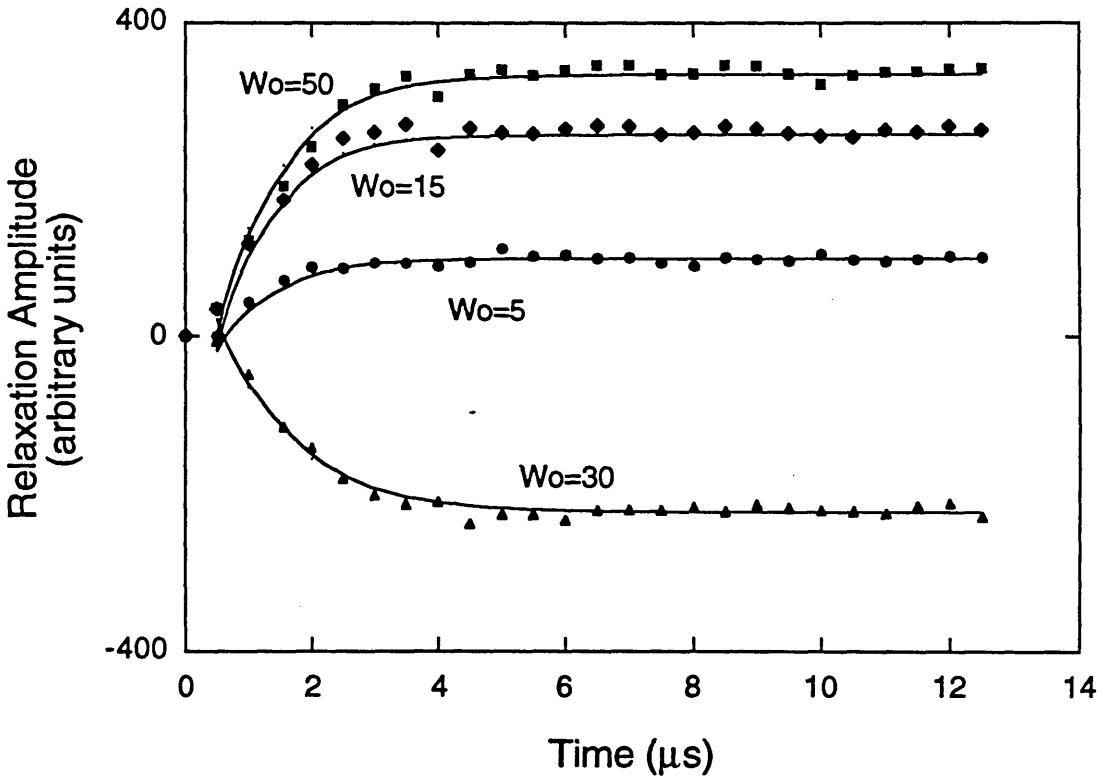

Figure 13.1 Typical ILTJ relaxation traces in AOT water-in-oil microemulsions (S_o=13, T=10 °C). The solid lines indicate exponential curve fits.

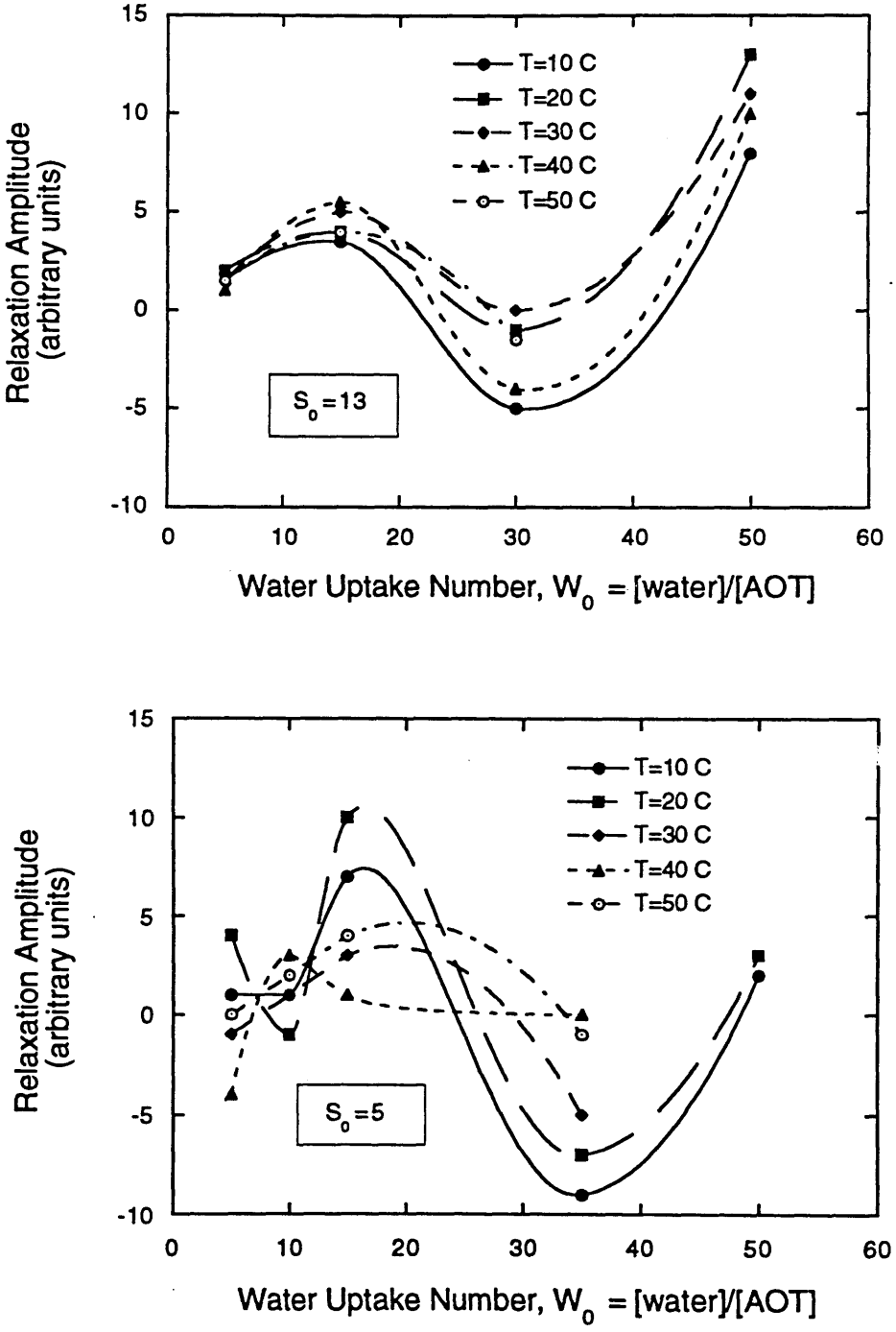

Figure 13.2 ILTJ relaxation amplitude as a function of W_o for different temperatures (a) S_o=13, and (b) S_o=5. One relaxation amplitude unit corresponds to approximately 2 mV; the uncertainty in the relaxation amplitude values is less than 15%; the lines connecting the experimental points are plotted for purposes of guiding the eye.

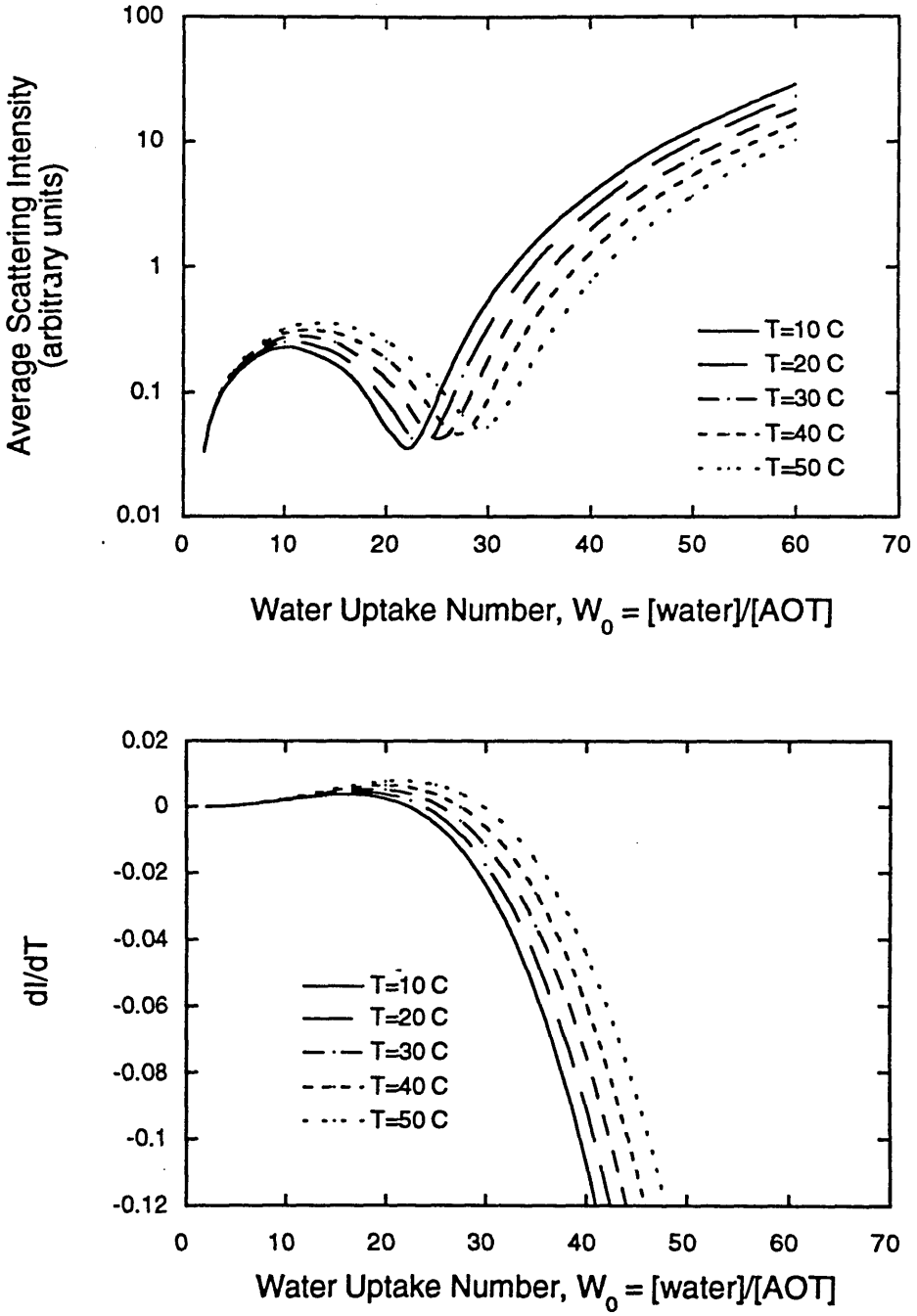

Figure 13.3 Effect of water content of microemulsion droplets and temperature on (a) reduced average scattering intensity, and (b) temperature derivative of the average microemulsion scattering power.

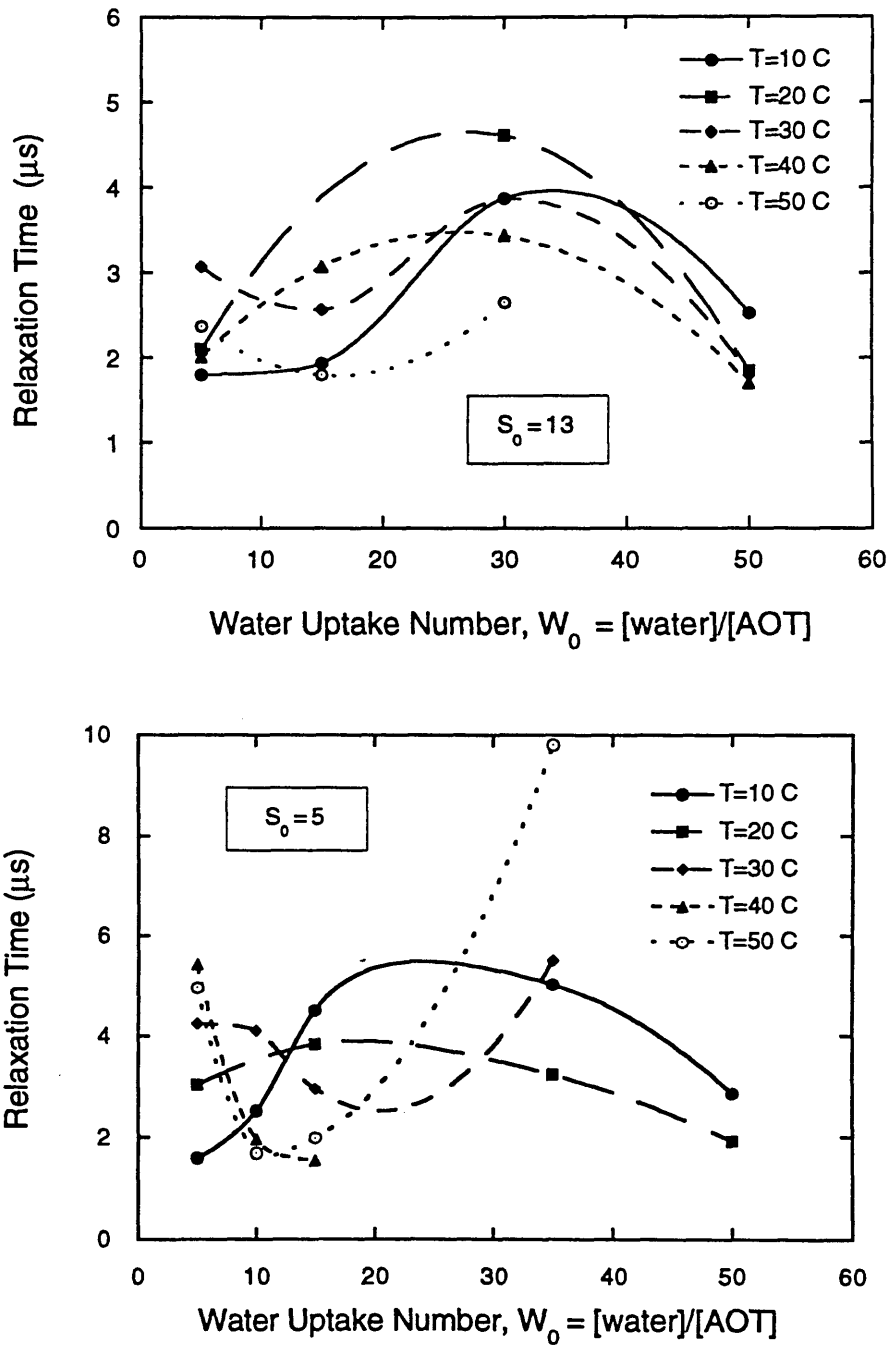

Figure 13.4 ILTJ relaxation time as a function of W_o for different temperatures; (a) S_o=13 and (b) S_o=5 (the lines connecting the experimental points are plotted for purposes of guiding the eye).

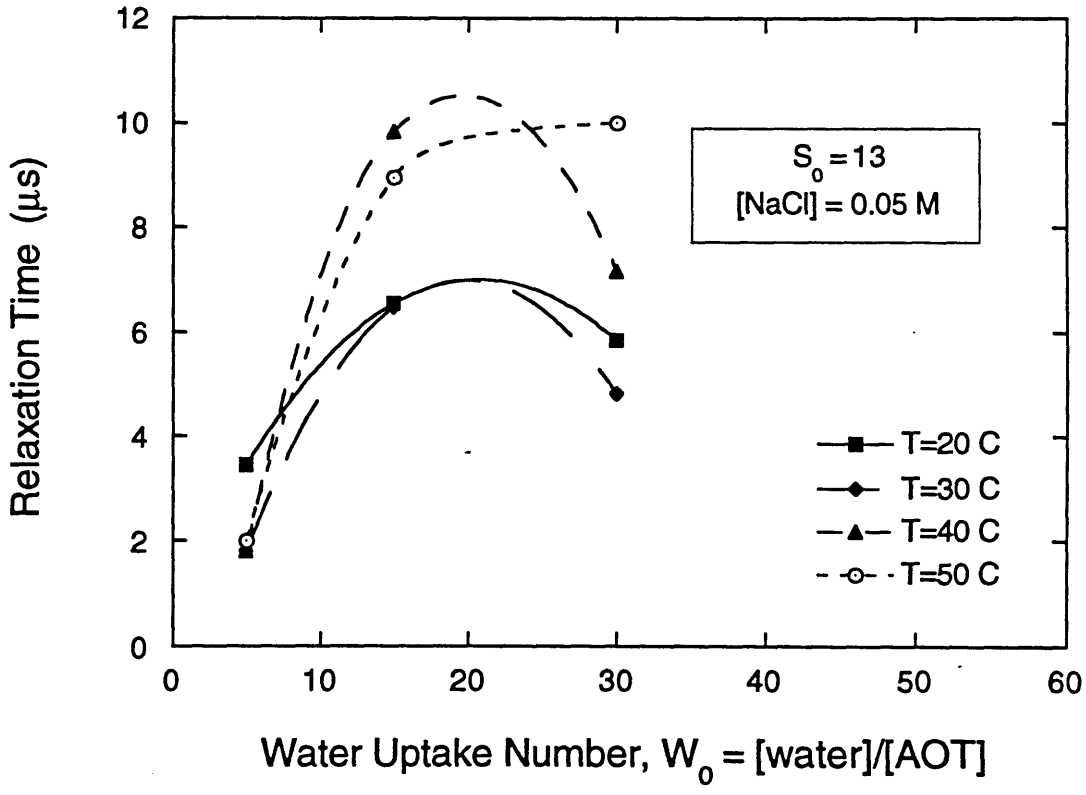

Figure 13.5 ILTJ relaxation time as a function of W_o, for S_o=13, [NaCl]=0.05 M, and different temperatures (the lines connecting the experimental points are plotted for purposes of guiding the eye).

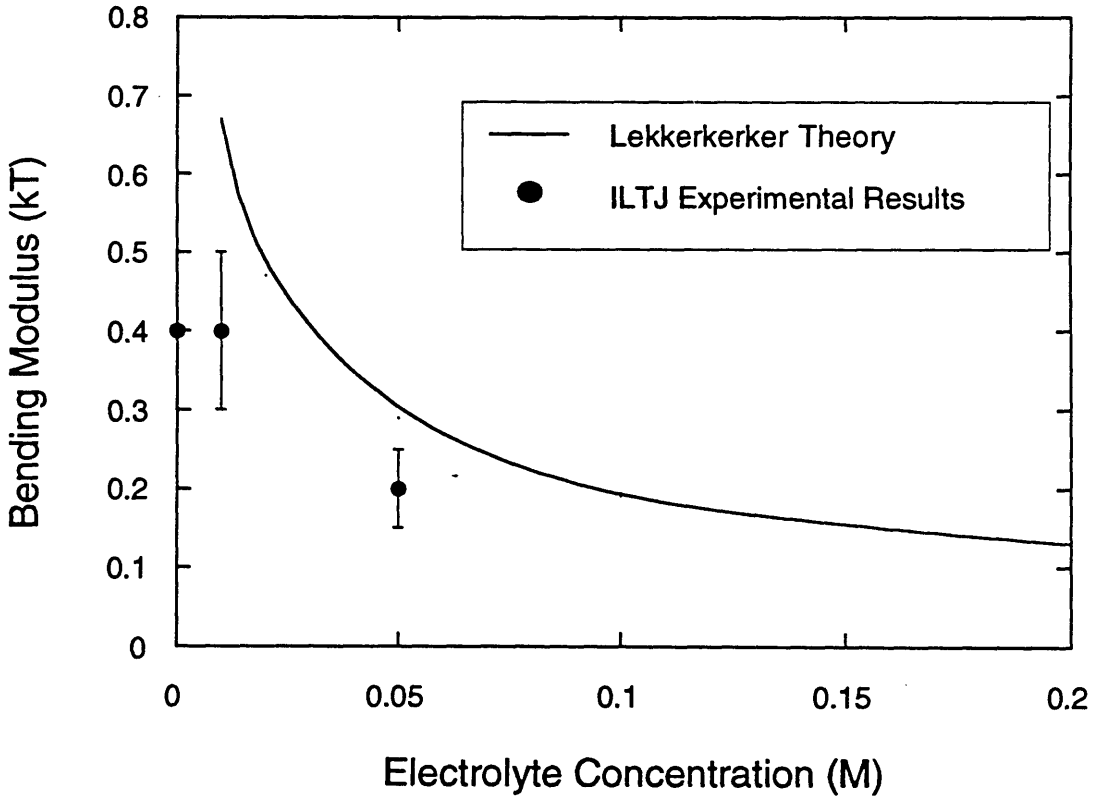

Figure 13.6 Effect of electrolyte concentration on the electric contribution to the bending modulus. Theoretical curve (solid line) based on the results tabulated by Lekkerkerker [1989].

Chapter 14
Dynamics of Interfacial Association and Transport Processes for p-Nitrophenol in an AOT Water-in-oil Microemulsion

14.1 Introduction

There are many technological reasons for interest in the water-in-oil microemulsion systems, many of which rely on the ability of microemulsions to solubilize hydrophilic and amphiphilic compounds in bulk organic phases in which these compounds would normally exhibit no or very slight solubility. Water-in-oil microemulsions can be exploited in areas such as selective separation processes, biocatalytic synthesis of a range of important pharmaceuticals, and enhanced and selective drug delivery, to name but a few. The thermodynamic equilibrium distribution of solubilizates over the various regions of the microemulsion (water pool, surfactant interface and bulk organic continuum) is important and has been well-studied [Leodidis & Hatton, 1990]. The rates at which solutes redistribute over these regions following some perturbation to the system, e.g. transport of lipophilic substrates across the surfactant barrier to enable them to participate in enzymatically-catalyzed synthesis reactions, have been substantially less well-investigated, however. A better understanding of the dynamic processes (such as transport through the curved surfactant interfaces and material exchange between the oil and water microphases) in water-in-oil microemulsion systems could lead to better mechanistic descriptions of such diverse phenomena as phase transitions, emulsion and foam stability, transport in cell and membrane-mimetic media, biocatalysis in reverse micellar systems and transport resistances in large-scale extraction separation processes, where surfactants are often present at the interfaces.

The dynamics of processes that involve exchange of material between reverse micelles have been probed by chemical relaxation methods [Bernasconi, 1976], such as stopped and continuous flow concentration jump measurements and fluorescence lifetime

studies, by the groups of Thomas [Atik & Thomas, 1981], Robinson [Fletcher & Robinson, 1981; Fletcher et al., 1987], Lang and Zana [Lang et al., 1988; Jada et al., 1989; Jada et al., 1990], and de Schryver [Verbeeck & de Schryver, 1987; Verbeeck et al, 1989], among others. Continuous flow methods, with analysis in terms of a population balance model for the determination of the exchange constants [Hatton et al., 1993], have been used in our group [Bommarius et al., 1990]. However, to the best of our knowledge, the kinetics of transport across the surfactant layer that separates the microemulsion water pools from the organic continuum have been investigated only by the group of Schelly [Tamura & Schelly, 1979; 1981; Harada & Schelly, 1982]; they used stopped flow concentration jump and pressure jump methods to investigate the solubilization rates of picric acid in dry (0.03% w/w water) AOT/benzene reverse micelles, and of 7,7,8,8,-tetracyano-quinodimethane in reversed micelles of dodecylpyridium iodide in benzene. The time resolution of their detection system was limited to 10^{-3} - 10^{-4} s, comparable to that of virtually all the concentration and temperature jump methods used in the literature, but not adequate to resolve all the phenomena involved.

In this Chapter, we report results on microemulsion dynamics using the Iodine Laser Temperature Jump (ILTJ) technique to identify and quantify the interfacial association and transport time scales of p-nitrophenol (pNP) at the curved surfactant interface in the AOT water-in-oil microemulsion system. The location of pNP was monitored spectrophotometrically, after a temperature perturbation of the system shifted the partitioning of pNP between the water and oil phases (see Figure 14.1 for a schematic of the processes occurring). The sensitive detection system used allowed time resolution of 10^{-7} s, and the capability to observe the whole 10^{-7} - 10^{0} s time range in a single experiment.

The Iodine Laser Temperature Jump (ILTJ) technique developed by Holzwarth and coworkers [1977], which can capture events in the 10^{-9} - 10^{0} sec range, has been used to explore the dynamics of organized molecular assemblies such as phase transitions in lipid vesicles [Holzwarth, 1989], the kinetics of azide binding to chloroperoxidase in reversed micelles [Jobe et al., 1989], and the aggregation kinetics of oil-in-water microemulsions [Fletcher & Holzwarth, 1991]. The choice of pNP was guided by the fact that its protonated (uncharged) form (denoted here as pNPH) partitions both in the oil and water phase. The pNP protonation-deprotonation equilibrium is shifted by temperature and that

will alter the partitioning of pNPH between oil and water (Figure 14.1). Furthermore, pNP is a chromophore used in the preparation of a wide variety of synthetic esterase substrates employed in enzymatic activity assays. The considerable difference in spectral properties between the substrate (ester) and the nitrophenol product facilitate simple spectrophotometric determination of enzyme activities [Hartley & Kilby, 1952]. Carboxylic acid esters of pNP have been used for the assay of lipases and other enzymes in water-in-oil microemulsion systems by the group of Robinson [Fletcher et al., 1985; Oldfield et al., 1990]. pNP was also employed by Kabanov et al. [1988] to track the kinetics of establishing equilibrium in the formation of protein-containing AOT microemulsions.

14.2 Materials and Methods

Materials: AOT (Sulfosuccinic acid bis[2-ethylhexyl] ester, sodium salt) was purchased by Sigma (purity 99%) and used as received. Although the presence of acidic contaminants in AOT may influence acid-base behavior in microemulsions, Oldfield et al. [1990] concluded that the AOT supplied by Sigma was the highest quality commercially available and relatively free of acidic impurities. Isooctane (Uvasol, spectroscopy grade) was from Merck. p-Nitrophenol (crystalline, for spectroscopy) was from Sigma. All salts used for buffer preparation were of analytical grade or better. The water used was triple-distilled.

Microemulsion system: The AOT water-in-isooctane microemulsion system used in this study has been well characterized. The anionic AOT has a number of attractive properties: (i) it does not need a cosurfactant; a three-component system of oil, water (or aqueous salt solution), and surfactant forms reversed micelles readily; (ii) it can take up a large amount of water per amount of surfactant added; and (iii) AOT can be handled very easily when preparing the microemulsions. P-nitrophenol (pNP) was used as a probe molecule. The aqueous solution of its protonated form (pNPH) is colorless, but when ionized (pNP(-)) (pK of 7.15 at 25 °C [CRC Handbook, 1985]) p-nitrophenol takes on a distinct yellow color and has a strong optical absorption peak at 400 nm. To ensure the existence of both the protonated and the unprotonated form of pNP in detectable quantities, it was necessary to work in the pH range of 6.2 to 8.2, by buffering the solutions

accordingly. The buffers used were potassium dihydrogenphosphate / sodium hydroxide, and tris(hydroxymethyl)-aminomethan / hydrochloric acid. The microemulsions were prepared using the injection method, by mixing an appropriate quantity of buffered aqueous solution (with or without the solute pNP) to an AOT solution in isooctane. The resulting microemulsions were put in teflon-stoppered glass vials, and left at room temperature for one to three hours to equilibrate.

Partition coefficients: The partition coefficient of pNP between isooctane and water as a function of temperature was determined by mixing equal volumes of aqueous pNP solution of low pH (so that [pNP(-)] = 0) and isooctane in teflon-stoppered test tubes, equilibrating the mixtures at the desired temperature for three days, and measuring the pNPH concentration spectrophotometrically at 315 nm for the aqueous phase, and 285 nm for the organic phase. To convert absorption intensity to pNP concentration we used extinction coefficients from Oldfield et al. [1990].

Spectroscopic Investigation: The spectra of aqueous solutions and microemulsions containing pNP were recorded in the UV-Vis range, at different system compositions and temperatures. The UV-Vis absorption intensities at the characteristic peaks of pNPH and pNP(-) were used to determine their concentrations and protonation-deprotonation equilibria. The isosbestic point observed in the spectra, when a parameter (e.g. temperature, pH, microemulsion composition) varied while the overall solute concentration remained constant, was an indication of attainment of equilibrium conditions in the solutions. UV-Vis spectra were also used before and after the ILTJ experiments to check if any irreversible changes occurred in the system studied (no such changes were observed). A thermostated Shimadzu UV 2100 spectrophotometer was used.

Iodine Laser Temperature Jump: The ILTJ technique [Holzwarth et al., 1977] uses the photon emission of an Iodine laser in the near IR (1315 nm) to create a very fast temperature rise in aqueous solutions. This occurs by photon absorption of overtone vibrations of the OH bonds of water molecules. Very homogeneous temperature-jumps in layers up to 3 mm can be achieved, and no additional molecules or ions beside the solvent water are necessary [Holzwarth et al., 1977]. The rise time of the temperature-jump can be as short as 2×10^{-10} s, constituting the short-time limit in dynamic investigations (the typical rise time for the present experiments was 1 μs). The longer time operational range is

limited by the cooling of the sample back to its thermostatically controlled original temperature (5 - 10 sec). An INNOVA-100-K3 Krypton Ion CW-Laser (Coherent, Palo Alto, CA) was used to detect the effects of the temperature perturbation on the sample turbidity. The specifics of the instrument setup we employed for these experiments are presented in Alexandridis et al. [1993] (see Chapter 13 of this Thesis).

For the ILTJ experiments, approximately 1 ml of the microemulsion was placed in a 5x10mm cuvette, sealed with a teflon cup. The cuvette was placed in the temperature controlled holder of the ILTJ detection chamber, and allowed to equilibrate at the desired temperature. ILTJ experiments were generally performed in the 10 - 40 °C range. The microemulsions systems under study were monophasic and stable during these runs. Care was taken to avoid loss of solvent due to evaporation, especially for experiments at higher temperatures. Recording of the absorbance of the sample at 406.7 nm started 5 μs before the temperature-jump and covered the time range up to 1 s. The absorbance of the microemulsion at 406.7 nm was mainly due to the unprotonated p-nitrophenol, pNP(-), although it must be recognized that the microemulsion droplets also scatter some light at this wavelength [Alexandridis et al., 1993]. The characteristic response of the sample absorbance at 406.7 nm, due to the temperature perturbation, was recorded immediately after the Iodine laser shot. Six relaxation signals were averaged at each experimental condition. The relaxation times were calculated by fitting an exponential to the averaged curve. Every precaution was taken to avoid artifacts due to the optics and electronics interfering with our experimental results.

14.3 Results and Discussion

14.3a Experiments

Energy added to the water pools by absorption of the iodine laser pulse was distributed rapidly over the whole microemulsion in the sample volume so that it can be assumed that the microemulsion was uniformly heated on the time scales of interest [Alexandridis et al., 1993]. Figure 14.2 shows typical ILTJ relaxation traces in pNP-containing AOT water-in-isooctane microemulsions. The ordinate (logarithmic scale) represents the absorbance of the sample at 406.7 nm (arbitrary units), and the abscissa the

time elapsed during and after the temperature-jump.

Two relaxation times were observed: the first at 2 - 10 μs, and the second at 0.1 - 1 ms. The first relaxation was the response of the microemulsion to the energy input by the Iodine laser pulse. Also observed in the absence of pNP, the first relaxation results in an increase or decrease in the detected light intensity, depending on the sample parameters. This relaxation was attributed to fluctuations of the oil-surfactant-water interface due to the temperature-jump. A complete investigation of this fast relaxation and its implications in the microemulsion dynamics is presented in Chapter 13 of this Thesis [Alexandridis et al., 1993].

The second relaxation was observed only when the indicator molecule pNP was present in the microemulsion. The time constant of this relaxation, 0.1 - 1 ms, was consistent with the diffusion regime. The amplitude change in the second relaxation (see, e.g., Figure 14.2) was always negative (decrease of absorbance with respect to the baseline) and its direction was independent of the amplitude change of the first relaxation (at 2 - 10 μs). This suggests that the second relaxation were caused by a decrease in [pNP(-)] and not any physical disturbance of the microemulsion caused by the temperature-jump.

To identify the mechanism responsible for this relaxation, one must consider the physicochemical processes taking place after the temperature-jump and the first (fast) relaxation of the microemulsion: (i) the volume of the aqueous phase increases with temperature (above 4 °C), which tends to dilute the pNPH and pNP(-) concentrations inside the water pool; (ii) the pH (maintained by the buffer) in the water pool changes with temperature as the chemical equilibrium of the buffer species is altered [Dawson et al.], with subsequent redistribution of the pH-sensitive pNP protonation-deprotonation equilibrium; (iii) the equilibrium constant of the pNP protonation-deprotonation is temperature-dependent resulting in increase of the pNP(-) concentration with increasing temperature; and (iv) the partitioning of pNP between the organic phase, the surfactant interface, and the water pools will change as a result of the temperature increase. Of these four processes, the first three take place only in the aqueous phase. The fourth process (iv) involves partitioning of pNP between oil (isooctane) and water, and association of pNP with the surfactant (AOT) interface. The former is mainly controlled by the hydrophobic

effect, whereas the latter involves electrostatic interactions with the surfactant headgroups in addition to hydrogen bonding.

To decouple the aqueous phase effects from the combined effects in the microemulsions, we examined the "dynamics" (kinetics) and "thermodynamics" (equilibrium) of aqueous buffered pNP solutions. The kinetics of the protonation-deprotonation reaction in aqueous pNP solution buffered at pH 7.5 were measured using ILTJ. The absorption intensity at 406.7 nm, corresponding to pNP(-), increased after the temperature-jump; the time-scale of the response (faster than 1μs, the heating time of the solution) verified that the establishment of the pNP protonation-deprotonation equilibrium was very fast and did not interfere with the relaxation observed in the 0.1-1 ms time scale. UV-Vis scans of aqueous solutions of p-nitrophenol at two different pH and equilibrated at various temperatures (see Figure 14.3) showed an increase in the absorbance at 400 nm (corresponding to pNP(-)) and a decrease in the absorbance at 310 nm (corresponding to pNPH) with increasing temperature. The spectra exhibited a good isosbestic point, indicative of equilibrium. It can be concluded, therefore, that the result of processes (i) - (iii) should be an increase in [pNP(-)] with increasing temperature.

The overall equilibrium effect of the temperature on [pNP(-)] in the microemulsions was obtained from UV-Vis scans of AOT-isooctane water-in-oil microemulsions with pNP at different initial aqueous-phase pH, Wo=[water]/[AOT], and temperatures (see Figure 14.4). We found that the absorbance at 400 nm (due to pNP(-)) decreased, and the absorbance at 310 nm (due to pNPH) increased with increasing temperature, a behavior opposite that observed in the aqueous solution. Furthermore, variation of the temperature for the same microemulsion sample, and variation of the Wo value for the same overall pNP concentration, gave spectra that exhibited a well-defined isosbestic point, indicative of thermodynamic equilibrium (this is important considering the fact that temperature-jump is a relaxation technique that works in the vicinity of an equilibrium position). Since the overall result of (i) - (iii) has been demonstrated to be an increase in [pNP(-)] and decrease in [pNPH] with increasing temperature, the opposite trends observed in microemulsions must be the result of process (iv), change in the distribution of pNP between the organic phase, the surfactant interface, and the water pools as a result of the temperature increase. This change in the location of pNP after the temperature increase can be attributed either to transport of pNP between oil (isooctane) and water, or to pNP association with the

surfactant (AOT) interface, or to both. We examine these possibilities below.

The partition coefficient of the protonated pNP between isooctane and aqueous acidic (HCl) solution was measured as a function of temperature, to investigate the driving force for transfer of pNP from the aqueous to the organic phase of the microemulsion. pNPH partitions favorably towards the aqueous phase, but the pNPH quantity partitioning to the isooctane phase increases significantly with increasing temperature (water/oil pNPH partition coefficients: 365 at 6 °C, 196 at 21 °C, 142 at 35 °C). Therefore, a temperature increase in a water-isooctane two-phase system would result in decrease of [pNP(-)] in the aqueous phase; this is consistent with what was observed in the ILTJ experiments.

For the transport of pNP from the aqueous to the oil phase to occur, the solute has to pass through the surfactant interface. A preliminary indication of pNP association with the AOT interface was provided by Menger and Saito [1978]; they observed an increase in the pKa of the pNP protonation-deprotonation equilibrium in the water pools of an AOT microemulsion, and attributed this to pNP adsorption at the AOT interface [Note 1]. Oldfield et al. [1990] reached similar conclusions. Quantitative information on the pNP interfacial association came from Magid et al. [1981]. They measured binding constants for a series of phenols (among them pNP) to AOT inverted (dry) micelles in isooctane. The binding of pNP was found to depend on the total pNP concentration, and for pNP concentration of $6x10^{-5}$ (the closest to the value used in our experiments) the ratio of AOT-bound pNP to free pNP (disolved in isooctane) was 3670 times the AOT (molar) concentration (this value is basically a pNP AOT-isooctane partition coefficient). For the AOT concentration in our system (400 mM) the value of AOT-bound pNP to free pNP would be approximately 1500. It should be noted however that our system contains water as well, whereas the binding constant reported by Magid et al., [1981] applies to dry micelles. Magid et al. [1981] did not examine the effect of water in the pNP binding AOT-isooctane, but they did so for phenol. The binding constant (as defined above) for phenol decreased from 350 when Wo=0 to 180 at Wo=15 (one half of the Wo=0 value) and remained steady for higher Wo values. Similarly one would expect the ratio of AOT-bound pNP to free pNP in the microemulsion to be significantly lower than 1500, especially if part of the pNP is in its charged (pNP(-)) form [Note 2]. The studies of Menger [1978] and Magid [1981] were performed at a constant temperature (25 °C). The effect of temperature on the association of pNP to the interface can be inferred from data on the

distribution of substituted phenols into lipid (dimyristoyl-phosphatidylcholine, DMPC) vesicles by Davis et al. [1986]. The liposome-water partition coefficient increased with temperature ($\log_{10}K$ was equal to 3.8 at 6 °C and 4.1 at 22 °C). Although the oil-AOT-water interface is different than the water-liposome interface and the pH used in the Davis et al. [1986] study was not mentioned, one may expect the interfacial partition coefficient of pNP in the AOT interface to behave in a similar way with temperature. It can thus be concluded from the above that there is significant association of pNP with the AOT interface, and that the extent of association increases with temperature. Increase in pNP association with temperature will have a decrease in [pNP(-)] as a consequence; this is consistent with what we observed in the ILTJ experiments.

It becomes clear from the evidence presented above, that the decrease in [pNP(-)] with increasing temperature observed in the spectrophotometric and ILTJ experiments results from a change in the distribution of pNP between the organic phase, the surfactant interface, and the water pools. Table 14.1 presents the relaxation times derived from fitting the experimental relaxation trace to an exponential decay. These values are consistent with order of magnitude estimates based on typical values of 10^5 - 10^6 s/m for the interfacial transport resistance, R [Aunins, 1991], offered by a planar surfactant layer of characteristic thickness $\delta = 10^{-9}$ m at the interface between two immiscible bulk phases; i.e., $\tau \sim R\delta \sim 10^{-4}$ - 10^{-3} s.

14.3b Model

The kinetics of this redistribution and the contribution of the water-surfactant partitioning driving force can be deduced from the ILTJ relaxation times with the help of a model that accounts for mass-transfer between the water-surfactant-oil regions. Let A represent the concentration of protonated pNP (pNPH) and A^- the concentration of deprotonated pNP (pNP(-)) in the water pools of the microemulsion ($A = K_{assn}A^-$, $K_{assn} = 10^{pK-pH}$), B the pNP concentration at the surfactant monolayer, and C the pNP concentration in the oil phase. The relationships for transfer of pNP from the aqueous phase to the surfactant monolayer and from there to the oil phase can be written as

$$V_{water}\, d(A + A^-)/dt = k_{L1}\, S\, (B - H_1 A) \qquad (1)$$

$$V_{AOT}\, dB/dt = - k_{L1}\, S\, (B - H_1 A) \quad (2)$$

$$V_{AOT}\, dB/dt = k_{L2}\, S\, (B - H_2 C) \quad (3)$$

$$V_{water}\, d(A + A^-)/dt + V_{AOT}\, dB/dt + V_{oil}\, dC/dt = 0 \quad (4)$$

where V_i, is the volume of phase i (note that the surfactant layer is treated as a macroscopic phase), S is the total surface area (afforded by the surfactant); k_{L1} and k_{L2} are mass transfer coefficients for pNP moving from the aqueous phase to the surfactant phase, and from the surfactant phase to the oil phase, respectively; $H_1 = B/A$ and $H_2 = B/C$ at equilibrium (partition coefficients).

As a first approximation, we neglect transport of pNP from the surfactant to the oil phase, as the pNP AOT/oil partition coefficient is very large. Relating dA and dB, from Equations 1 and 2, respectively, and defining $B' = B/(H_1\, K_{assn})$, we get

$$dB' / dA^- = - V_{water}\, (1 + K_{assn})\, (V_{AOT}\, H_1\, K_{assn})^{-1} \quad (5)$$

Integrating Equation 5 we obtain

$$B' = (B_o' - q\, A_o^-) + qA^- \quad (6)$$

where B_o' and A_o^- are integration constants, and $q = V_{water}\, (1 + K_{assn}) / (V_{AOT}\, H_1\, K_{assn})$. Substituting Equation 6 in Equation 1 we get

$$d(A^-)/dt = \gamma\, (\delta - A^-) \quad (7)$$

where

$\delta = (B_o' - qA_o^-)/(1-q)$. By integration of Equation 7, we can derive an expression for A^- as a function of time:

$$A^- = \delta - (\delta - A_o^-)\, \exp(-\gamma t) \quad (8)$$

where

$$\gamma = k_{L1} S H_1 \{V_{water}(1+K_{assn}^{-1})\}^{-1} \{ 1 - V_{water} (1 + K_{assn}^{-1}) (V_{AOT} H_1)^{-1} \}$$

The characteristic relaxation time measured from ILTJ experiments is related to $1/\gamma$, when association with the interface is the dominant process taking place. $1/\gamma$ is proportional to V_{water} and inversely proportional to K_{assn} (when $K_{assn}<1$ or $A^- \rightarrow A$), the mass transfer coefficient k_{L1}, surface area S (proportional to the amount of AOT in the microemulsion), and AOT/water partition coefficient H_1. For a microemulsion of constant composition (V_{water} and S), increase in temperature will decrease K_{assn}, and increase H_1 and k_{L1}. Apparently there are two competing effects when temperature increases, that of K_{assn} which would tend to increase the relaxation time (τ), and that of H_1 and k_{L1} that would decrease the relaxation time. The ILTJ relaxation times listed in Table 14.1 exhibit a maximum at T = 25 °C, providing an indication that the decrease in K_{assn} may result in an increase of τ at the 15 - 25 °C temperature range, and that the increase in H_1 and k_{L1} may result in a decrease of τ at temperatures above 25 °C. Increase in Wo at constant AOT concentration (effectively an increase in V_{water}) should result in increasing relaxation time, provided the other parameters do not change much. Again, the ILTJ relaxation times listed in Table 14.1 show a trend of increase with increasing Wo, suggesting that the model described above can capture the phenomena affecting the rate of association of pNP at the AOT interfaces in water-in-oil microemulsions.

14.4 Conclusions

The spectrum of dynamic phenomena ranging from 1 μs to 100 ms in a microemulsion has been explored using the Iodine Laser Temperature technique. We are unaware of other results at curved interfaces against which our preliminary results for association of pNP from the aqueous to the surfactant pseudophase and transport to the oil can be compared, although they are consistent with estimates based on reported results for interfacial resistance offered by surfactants at planar interfaces. The transport time was measured to be in the range 0.1 to 1 ms. A simple model described here can capture the phenomena contributing to the rate of association of pNP with the AOT interfaces in water-

in-oil microemulsions. The dynamic phenomena observed in the μs time range, attributed to the bending of the oil-surfactant-water interface due the temperature rise in the water pools, are discussed elsewhere [Alexandridis et al., 1993].

14.5 References and Notes cited in Chapter 14

1. Alexandridis, P.; Holzwarth J. F.; Hatton, T. A. Langmuir **1993**, *9*, 2045; Chapter 13 of this Thesis.
2. Atik, S. S.; Thomas, J. K. *Chem. Phys. Lett.* **1981**, 79, 351.
3. Atik, S. S.; Thomas, J. K. *J. Am. Chem. Soc.* **1981**, *103*, 3543.
4. Aunins, A. H. *Solute Transport Across Surfactant-laden Interfaces*, PhD Thesis, Massachusetts Institute of Technology, Cambridge, MA, 1991.
5. Bernasconi, C. F. *Relaxation Kinetics*, Academic Press, **1976**.
6. Bommarius, A. S.; Holzwarth, J. F.; Wang, D. I. C.; Hatton, T. A. *J. Phys. Chem.* **1990**, *94*, 7232.
7. Davis, S. S.; James, M. J.; Anderson, N. H. *Faraday Discuss. Chem. Soc.* **1986**, *81*, 313.
8. Dawson, R. M. C.; Elliott, D. C.; Elliott, W. H.; Jones, K. M. *Data for Biochemical Research*, 3rd Edition, Clarendon Press, Oxford, p. 436.
9. Fletcher, P. D. I.; Robinson, B. H. *Ber. Bunsenges. Phys. Chem.* **1981**, *85*, 863.
10. Fletcher, P. D. I.; Robinson, B. H.; Oldfield, C.; Freedman, R. B. *J. Chem. Soc., Faraday Trans. 1* **1985**, *81*, 2667.
11. Fletcher, P. D. I.; Howe, A. M.; Robinson, B. H. *J. Chem. Soc., Faraday Trans. 1* **1987**, *83*, 985.
12. Fletcher, P. D. I.; Holzwarth J. F. *J. Phys. Chem* . **1991**, *95*, 2550.
13. Harada, S.; Schelly, Z. A. *J. Phys. Chem.* **1982**, *86*, 2098.
14. Hartley, B. S.; Kilby, B. A. *Biochem. J.* **1952**, *50*, 672.
15. Hatton, T. A.; Bommarius, A. S.; Holzwarth, J. F. *Langmuir* **1993**, *9*, 1241.
16. Holzwarth, J. F.; Schmidt, A.; Wolff, H.; Volk, R. *J. Phys. Chem.* **1977**, *81*, 2300.
17. Holzwarth, J. F. in *The Enzyme Catalysis Process*, Cooper, A.; Houben, J. L.; Chien, L. C. (Editors), Plenum Publishing Corporation, 1989.

18. Jada, A.; Lang, J.; Candau, S.-J.; Zana, R. *Colloids and Surfaces* **1989**, *38*, 251.
19. Jada, A.; Lang, J.; Zana, R.; Makhloufi, R.; Hirsch, E.; Candau, S.J. *J. Phys. Chem.* **1990**, *94*, 378.
20. Jobe, D.; Dunford, H. B.; Pickard, M.; Holzwarth, J. F. in *Reactions in Compartmentalized Liquids*, Knoche, W.; Schomacher, R. (Edrs), Springer Verlag, 1989.
21. Kabanov, A. V.; Nametkin, S. N.; Matveeva, E. G.; Klyachko, N. L.; Martinek, K.; Levashov, A. V. *Molecular Biology* **1988**, *22*, 382.
22. Lang, J.; Jada, A.; Malliaris, A. *J. Phys. Chem.* **1988**, *92*, 1946.
23. Leodidis, E. B.; Hatton, T. A. *J. Phys. Chem.* **1990**, *94*, 6400.
24. Magid, L. J.; Kon-no, K.; Martin, C. A. *J. Phys. Chem.* **1981**, *85*, 1434.
25. Menger, F. M.; Saito, G. *J. Am. Chem. Soc.* **1978**, *100*, 4377.
26. Oldfield, C.; Robinson, B. H.; Freedman, R. B. *J. Chem. Soc., Faraday Trans.* **1990**, *86*, 833.
27. Tamura, K.; Schelly, Z. A. *J. Am. Chem. Soc.* **1979**, *101*, 6743.
28. Tamura, K.; Schelly, Z. A. *J. Am. Chem. Soc.* **1981**, *103*, 1081.
29. Verbeeck, A.; de Schryver, F. C. *Langmuir* **1987**, *3*, 494.
30. Verbeeck, A.; Voortman, G.; Jackers, C.; de Schryver, F. C. *Langmuir* **1989**, *5*, 766.
31. *CRC Handbook of Chemistry and Physics*, 66th Edition, CRC Press, Boca Raton, Florida, **1985**, p. D-162.

Note 1 It should be noted that the apparent pK of the pNP in the AOT microemulsion is higher than the pK of pNP in aqueous solutions, as determined from the relative magnitudes of the absorbance of the protonated-unprotonated pNP in aqueous buffer solutions and microemulsions prepared with the same buffer. This is mostly due to the negative surface charge of the AOT interface [Drummond, C. J.; Grieser, F.; Healy, T. W. *J. Chem. Soc., Faraday Trans. 1* **1989**, *85*, 521, 537; Karpe, P.; Ruckenstein, E. *J. Colloid Interface Sci.* **1990**, *137*, 408]. The apparent pK depends on the Wo, the difference from the aqueous pK becoming smaller as the water pool size in the microemulsion increases.

Note 2 Kozarac et al. [Kozarac, Z.; Cosovic, B.; Gasparovic, B.; Dhathathreyan, A.; Moebius, D. *Langmuir* **1991**, *7*, 1076] found no adsorption of pNP(-) to the air-water interface, slight adsorption to mercury-water interface and no adsorption to neutral phospholipid (DPPC) monolayers at the air-water interface.

Chapter 14: List of Tables and Figures

Table 14.1 ILTJ relaxation times related to the association of pNP at the surfactant interface in AOT water-in-oil microemulsions.

Temperature (°C)	Relaxation time (ms)		
	[AOT]=400mM Wo=5	[AOT]=400mM Wo=15	[AOT]=400mM Wo=30
15	0.07	0.9	0.43
20	0.13	0.22	0.52
25	0.56	0.54	0.85
30	0.27	0.29	0.73
35	0.12	0.09	0.26

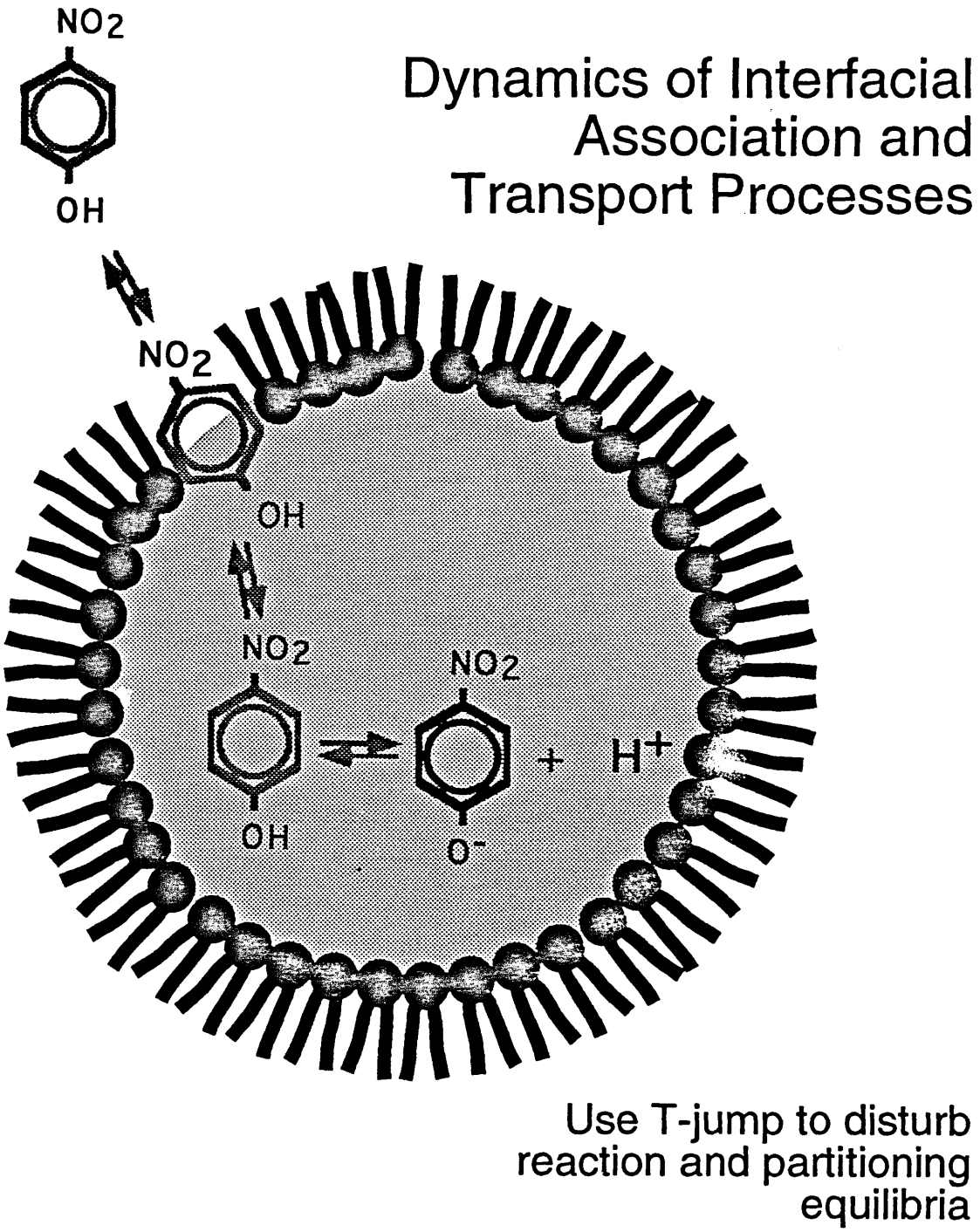

Figure 14.1 Schematic of the processes pertinent to the distribution of pNP between water, surfactant interface, and oil.

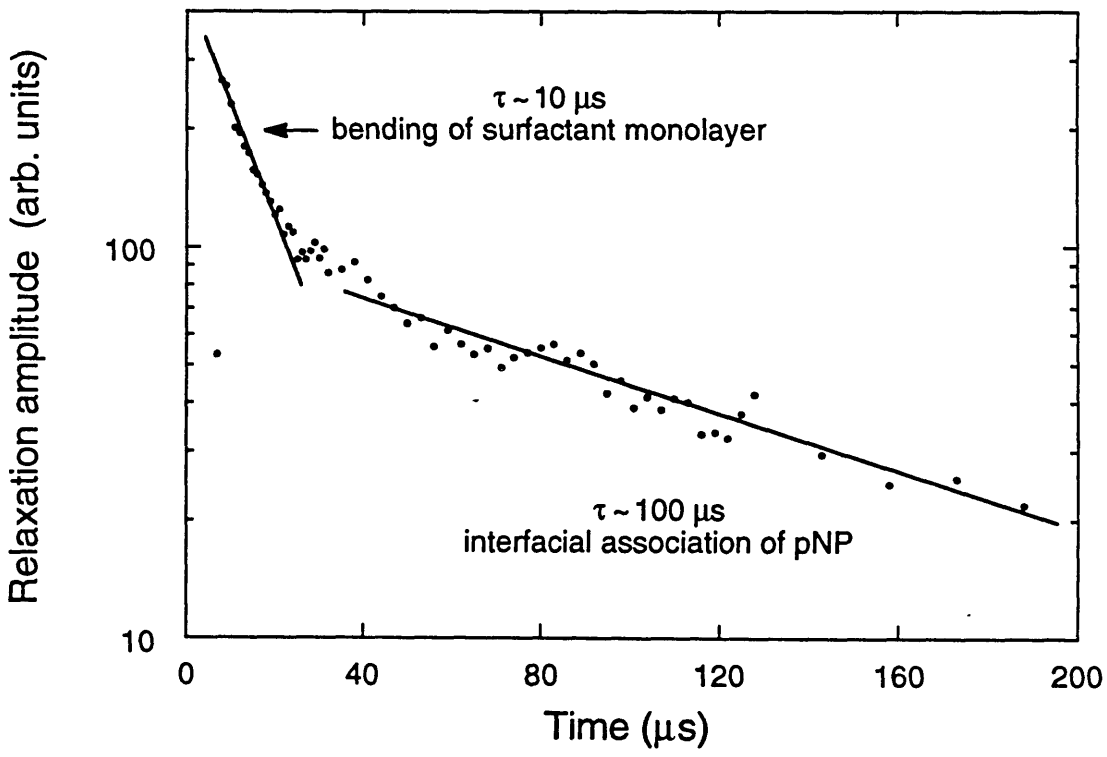

Figure 14.2 ILTJ relaxation amplitude vs time, for microemulsions containing pNP.

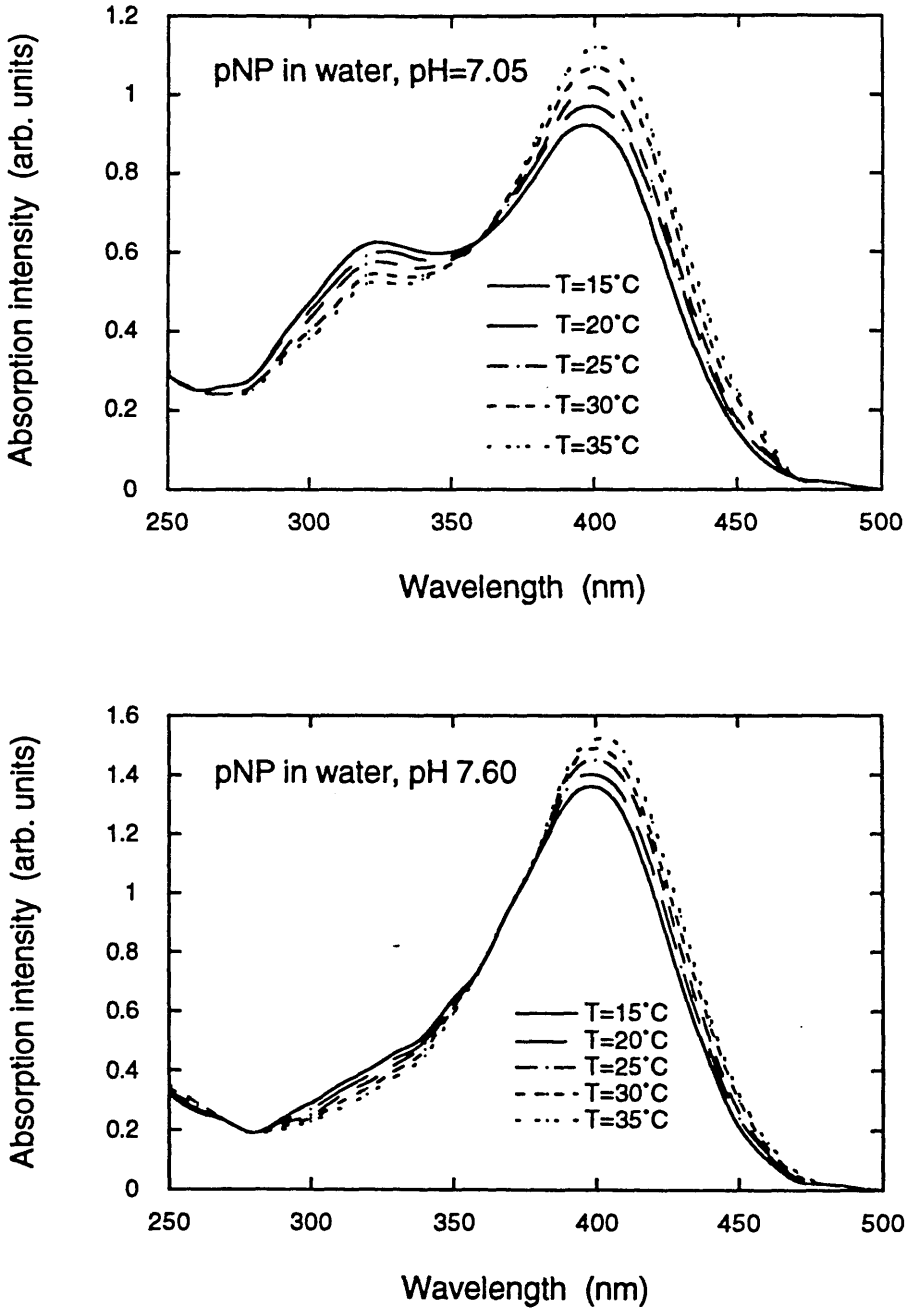

Figure 14.3 UV-Vis scans of aqueous solutions of p-nitrophenol (pNP) at pH of 7.05 (a) and 7.60 (b), and various temperatures.

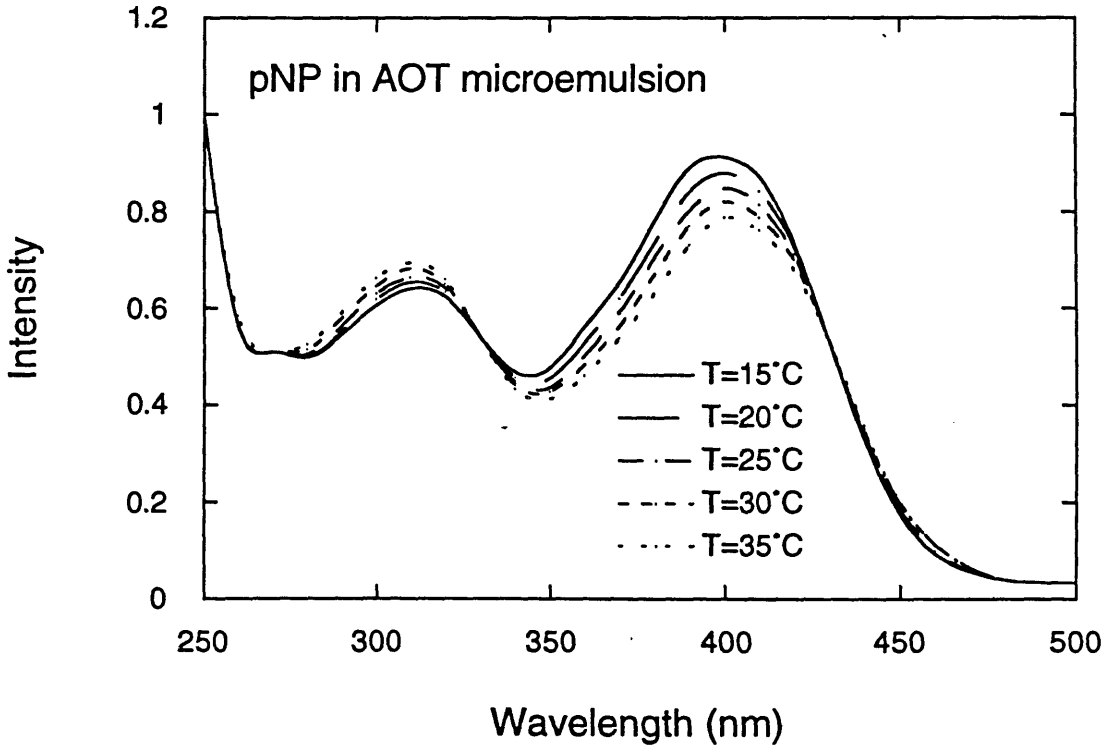

Figure 14.4 UV-Vis scans of AOT water-in-isooctane microemulsion with pNP at pH of 8.0, and various temperatures (Wo = 30).

Chapter 15
Summary and Future Work on Dynamics in Reverse Micellar Systems

Reverse micelles or water-in-oil microemulsions are thermodynamically-stable complex fluids that can be envisaged as distinct, nanometer-size water droplets maintained dispersed in an apolar solvent with the aid of a surfactant monolayer that reduces unfavorable oil-water contact. The microemulsions are highly dynamic systems, and their components rearrange over time and space. A better understanding of the dynamic processes in microemulsion systems can lead to better mechanistic descriptions of such diverse phenomena as, e.g., emulsion and foam stability, phase transitions, transport in cell and membrane-mimetic media, and biocatalysis in reverse micellar systems. Studies on the dynamics of microemulsions can be broadly divided into four groups: (i) internal motions of the surfactant and cosurfactant molecules; (ii) dynamics of the surfactant film separating oil and water; (iii) dynamics of processes involving whole microemulsion droplets, e.g., droplet diffusion or clustering; and (iv) the exchange of contents when microemulsion droplets coalesce.

Particularly important in understanding the behavior of microemulsions are the fluidity and flexibility of the oil-surfactant-water interface, manifested in the dynamic processes (ii), (iii), and (iv) mentioned above. Conductivity has employed here for the study of water-in-oil microemulsions formulated with dioctyl sulfosuccinate (AOT) in various alkanes, in order to address some of the issues concerning dynamics of droplet clustering and exchange of contents upon coalescence. The dynamics of the surfactant layer separating the water droplets from the oil phase were studied by perturbing the system with rapid heat transfer, and the interfacial bending elasticity was estimated. As discussed in this Thesis, the phenomena of high conductivity, droplet coalescence, and bending of the surfactant interface are related to each other. [Chapter 10]

The conductivity of AOT water-in-oil microemulsions (oil: n-hexane, isooctane, n-decane, or n-dodecane) was investigated for a wide composition and temperature range.

While log-conductivity increased linearly with temperature for microemulsions of Wo (= [water]/[AOT]) < 15, a sharp increase in electrical conductivity with increasing temperature was exhibited for Wo > 15, indicative of a percolation phenomenon. The temperature at which the percolation occurred decreased with increasing Wo (and corresponding microemulsion droplet size) and with decreasing So (= [oil]/[AOT]). The microemulsions also exhibited a percolation point with increasing droplet size (increasing Wo) at constant temperature; the Wo value at which percolation occurred decreased with increasing temperature, and with decreasing So. For T < 30 °C, the conductivity passed through a maximum at Wo=10 (more pronounced at So=5), dropped to lower values, and then increased again at higher Wo's. The observed conductivity maximum was interpreted in terms of the charge fluctuation model. Increase in the molecular weight of the alkane solvent shifted the percolation threshold to lower temperatures and dispersed volume fraction values; this was attributed to the influence of the solvent on attractive interactions between the microemulsion droplets. The effect of salt in the aqueous phase of the microemulsions was investigated for a water-in-isooctane microemulsion of So=5 and Wo=10 that exhibited an unusually high conductivity. Addition of 0.1 N Na^{+} or Ca^{+2} in the water pools decreased the conductivity of the microemulsion by two orders of magnitude. [Chapter 11]

The free energy, enthalpy, and entropy associated with the formation of droplet clusters in percolating water-in-oil microemulsions were estimated utilizing an association model, similar to that used in describing the micellization of amphiphiles. Microemulsions formulated with AOT in hexane, isooctane, and decane, were investigated. While the microemulsion droplets assembled spontaneously into clusters during percolation (the standard free energy of clustering, ΔG°_{cl}, was negative), the enthalpy of cluster formation, ΔH°_{cl}, values were found positive, indicating that the transfer of microemulsion droplets from solution to the percolating cluster was an enthalpically-unfavorable endothermic process. A positive entropic contribution, ΔS°_{cl}, was thus the driving force for clustering. Movement of ions and/or water through the droplet surfactant interface and the apolar solvent during percolation confronted an activation energy barrier; the microemulsion droplets were subject to "enthalpic stabilization". The positive entropy observed in droplet clustering could be related to the attractive interactions known to exist between microemulsion droplets. Both ΔH°_{cl} and ΔS°_{cl} increased with droplet size and molecular weight of the apolar solvent constituting the continuous phase. Increase of the molecular

weight of the apolar solvent (for the same droplet size and concentration) resulted in less negative ΔG°_{cl} values; ΔG°_{cl} became also less negative as the droplet concentration increased at constant droplet size. The values for ΔH°_{cl} (on the order of 100 kJ/mol) estimated from the association model are comparable to the activation energies observed in microemulsion droplet coalescence and solubilizate exchange, providing evidence that the latter process is occurring during percolation. [Chapter 12]

The dynamic response of AOT water-in-oil microemulsion droplets to perturbations caused by rapid energy transfer has been interpreted in terms of the surfactant interface bending rigidity. The Iodine Laser Temperature Jump technique was used to increase the microemulsion temperature rapidly (within 1 μs) and thus disturb the system equilibrium. The dynamic relaxation to the new equilibrium position was monitored by measuring the scattering intensity at 180° of the microemulsion over a 1 ms time interval immediately after the temperature jump. The rate and direction of the scattering intensity change depended on the initial temperature, size and salt content of the water droplets. The observed characteristic relaxation times of 2 to 10 μs were attributed to the relaxation of the surfactant interface. A bending modulus of approximately 0.4 kT was derived for the AOT monolayer, based on published models for the shape perturbation of a spherical interface. Addition of NaCl to the aqueous pools resulted in a decrease of the bending modulus, in agreement with published theoretical predictions. [Chapter 13]

The time scales for the association of p-nitrophenol (pNP) with the curved surfactant interface in a AOT water-in-oil microemulsion system were identified and quantified using the Iodine Laser Temperature Jump (ILTJ) technique. The location of pNP was monitored spectrophotometrically as a function of time, after a temperature perturbation of the system shifted the partitioning of pNP between the water and oil phases. The characteristic time assigned to association was measured to be in the range 0.1 to 1 ms. The equilibrium distribution of pNP was determined and used to identify the mechanism responsible for this relaxation time. Our preliminary results for association of pNP from the aqueous phase to the curved surfactant interface and transport to the oil are consistent with estimates based on reported results for interfacial resistance offered by surfactants at planar interfaces. A simple model was proposed to describe the rate of association of pNP at the surfactant pseudophase and used to analyze the experimental characteristic times. [Chapter 14]

Modelling the interaction between surfactant tails at the molecular level would be well suited as a continuation and extension of the work on microemulsion clustering presented in this Thesis. Experimentally, the pertinent trends are established, however a comprehensive theoretical description of the attractive interactions observed in microemulsion systems is still not available. The Iodine Laser Temperature Jump (ILTJ) technique would be very useful in elucidating micellization kinetics in block copolymer solutions of the kind described in Part A of this Thesis; the light scattering intensity of such solutions is a strong function of temperature and will thus be affected by a sudden temperature increase. The dynamics of association at surfactant-laden interfaces is another interesting area for future work; fluorescence-recovery-after-photobleaching experiments (the experimental setup is currently under development in our lab) can be used to expand the information on interfacial association obtained from the ILTJ technique.